AD-A052 862 ADVISORY GROUP FOR AEROSPACE RESEARCH AND DEVELOPMENT--ETC F/G 17/7
APPLICATIONS OF ADVANCES IN NAVIGATION TO GUIDANCE AND CONTROL.(U)
FEB 78

UNCLASSIFIED AGARD-CP-220 NL

1 OF 3
AD A052862

AGARD-CP-220

AGARD

ADVISORY GROUP FOR AEROSPACE RESEARCH & DEVELOPMENT

7 RUE ANCELLE 92200 NEUILLY SUR SEINE FRANCE

AGARD CONFERENCE PROCEEDINGS No. 220

Applications of Advances in Navigation to Guidance and Control

NORTH ATLANTIC TREATY ORGANIZATION

DISTRIBUTION AND AVAILABILITY
ON BACK COVER

NORTH ATLANTIC TREATY ORGANIZATION

ADVISORY GROUP FOR AEROSPACE RESEARCH AND DEVELOPMENT

(ORGANISATION DU TRAITE DE L'ATLANTIQUE NORD)

AGARD Conference Proceedings No.220

APPLICATIONS OF ADVANCES IN NAVIGATION TO GUIDANCE AND CONTROL

Papers presented at the 24th Technical Meeting of the Guidance and Control Panel, held in Stuttgart, Germany, 10–13 May 1977.

THE MISSION OF AGARD

The mission of AGARD is to bring together the leading personalities of the NATO nations in the fields of science and technology relating to aerospace for the following purposes:

- Exchanging of scientific and technical information;
- Continuously stimulating advances in the aerospace sciences relevant to strengthening the common defence posture;
- Improving the co-operation among member nations in aerospace research and development;
- Providing scientific and technical advice and assistance to the North Atlantic Military Committee in the field of aerospace research and development;
- Rendering scientific and technical assistance, as requested, to other NATO bodies and to member nations in connection with research and development problems in the aerospace field;
- Providing assistance to member nations for the purpose of increasing their scientific and technical potential;
- Recommending effective ways for the member nations to use their research and development capabilities for the common benefit of the NATO community.

The highest authority within AGARD is the National Delegates Board consisting of officially appointed senior representatives from each member nation. The mission of AGARD is carried out through the Panels which are composed of experts appointed by the National Delegates, the Consultant and Exchange Program and the Aerospace Applications Studies Program. The results of AGARD work are reported to the member nations and the NATO Authorities through the AGARD series of publications of which this is one.

Participation in AGARD activities is by invitation only and is normally limited to citizens of the NATO nations.

A large part of the content of this publication has been reproduced
directly from material supplied by AGARD or the authors;
the remainder has been set by Technical Editing and Reproduction Ltd.

Published February 1978

ISBN 92-835-0211-6

Printed by Technical Editing and Reproduction Ltd
Harford House, 7–9 Charlotte St, London, W1P 1HD

FOREWORD

Positioning and navigation systems provide essential information to guide and control any aircraft, weapon or reconnaissance system on a required trajectory to accomplish the prescribed mission phases. Within the last decade there have been significant advances in positioning and navigation techniques making possible great improvements in guidance and control systems and hence in the resulting mission performance and capabilities. It was the objective of the symposium to promote constructive ideas and discussions on the application of these recent advances in navigation to guidance and control.

The users and the engineers are fully aware of the new advances in positioning and navigation destined for application to guidance and control. On the other hand, the problem of cost-effectively applying these techniques seems not to have been conclusively solved until now. The cost of aircraft and systems, in real terms, has steadily risen and NATO countries are compelled to have fewer aircraft. Cost is the reason for the very real and continuous struggle between complexity (with increased capability) and simplicity (with reduced capability, but larger numbers). There is a tendency to add a new piece of equipment to aircraft systems – another box – without removing anything, thus resulting in further increasing complexity and cost. It was the purpose of the symposium to consider advanced positioning and navigation systems related to guidance and control which perform functions that can replace other pieces of equipment. It was intended to stimulate thinking for the avoidance of proliferation, looking for more elegant, simpler and less costly systems which give the same or even better performance.

The aims which led to the decision to hold this meeting were:

(1) to review the increased technical capabilities of those guidance and control systems which would benefit from advances in positioning and navigation;

(2) to discuss whether these increased capabilities derived from the advances in positioning and navigation will lead to more cost-effective solutions to guidance and control systems.

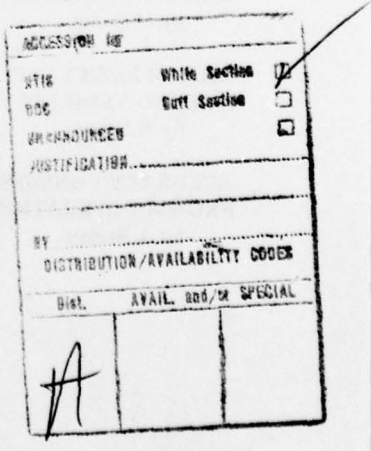

CONTENTS

* Not available for publication.

AN OPERATIONAL OVER-VIEW ON WHERE ADVANCES IN NAVIGATIONAL TECHNIQUES SHOULD LEAD TO SIGNIFICANT IMPROVEMENTS IN MISSION EFFECTIVENESS

by

Air Commodore D.F.H.Grocott, CBE, AFC, FRIN, RAF
Ministry of Defence, UK

INTRODUCTION

I wonder how many of you have travelled through the beautiful West Country of England and asked one of the natives the way to some strange sounding place like Penwithickstents? The probability is fairly high that you will have been told "If I were you, I wouldn't start from here. I would go to St Austell and start from there". The dilemma facing Air Force Commanders in Europe is not unlike that of the tourist and the native. He knows where he would like to go in the sense that he knows what he is trying to achieve operationally in the next decade. He would also like to be able to start from another place and another time, but he is constrained by having an inventory of aircraft, navigation and attack systems and weapons, and a pot of gold that shows no sign of growing in a period of detente and slack economies. These constraints, I would suggest, will force all NATO nations to spend a great deal of time and effort evaluating those advances in navigational techniques which appear to offer significant improvements in mission effectiveness, carefully weighing the promised improvements in operational effectiveness against the projected cost. In most cases these evaluation studies will, in my judgement, lead to step by step improvements in existing sytems with only the exceptional quantum jump into new and novel systems. There are very few panaceas in our business and as Juvenal said in the first century 'No man ever reached the climax in one step'.

In my address I want to cover navigation in the land/air environment in Central Europe and then to touch upon navigation in the maritime/air environment of the EASTLANT area and I shall not attempt to assess the relative priority of each environment. Suffice to say that the only certainty in defence is its uncertainty or, as Field Marshal Count Von Moltke said "The enemy has three courses of action open to him. Of these, he will choose the fourth". History suggests that whatever scenario we write for a period 15 years ahead is most likely to be wrong. For instance, if we take 1975 as the datum year, planners of that period were writing scenarios based on flexible response and they poured scorn on papers advocating the nuclear tripwire. Yet 15 years earlier in 1960, we thought only in terms of the nuclear tripwire. Going back a further 15 years to 1945, no member of the public had even heard of a nuclear weapon, and I would be very surprised to learn that air forces of that period wrote scenarios centred on the nuclear tripwire philosophy. If we go back a further 15 years to 1930, the planners of that day, no doubt carrying out their continuation flying training on biplanes, should have been thinking of operations involving large concentrations of four engined bombers capable of conducting precision attacks by day and night; I wonder if they were? So, what conclusion do I draw from this brief look at recent history? It is that we should have air forces capable of coping with the unforeseen. They should inherently possess great flexibility, ideally being capable of operating in more than one role, in both the land/air and the maritime/air environments and at both low and medium level. In other words, a general purpose force equipped with a multi-purpose navigation and attack system. I do not rule out specialist aircraft, but I feel strongly that the number of such aircraft should be kept to an absolute minimum.

Let me start my tour d'horizon with a look at a possible scenario for the Central Region of Allied Command Europe.

LAND/AIR

A possible, if not very probable, scenario in the Central Region is one predicated on increasing political tension over say the access routes to Berlin, this tension rising to such a level that the Warsaw Pact decide to seize the area of Western Germany covering these routes. From a Warsaw Pact planning viewpoint speed would be of the essence and the plan would no doubt have the aim of seizing territory as quickly as possible. To achieve this aim, the Warsaw Pact have at their disposal a large number of tank divisions and motor rifle divisions, practised in operating 24 hours a day, and I would not be surprised to learn that one of their plans was to concentrate these highly mobile forces along axes favourable to speedy advance – such as the North German Plain or the Fulda Gap, rather than through say the Harz Mountains. But while concentration would favour the attacking forces while attempting to break through the NATO defences, the Warsaw Pact would have to be careful not to offer target densities favourable to nuclear weapons or even to cluster weapons. Hence one possible tactic that the Warsaw Pact could employ would be a series of concentrations to penetrate areas offering a significant measure of resistance, followed by a spreading out of the armoured forces across the mean line of advance, and then regrouping when the advance is held up.

The Warsaw Pact tank and motor rifle divisions employed in the advance would have integral air defence systems, effective at both low and medium level, and would be supported by the Tactical Air Forces. With the introduction of highly mobile SAM Systems such as the SA6 and SA8, coupled with the existing area defence and point defence SAM and gun systems, NATO aircraft would face a density of ground based air defence systems not hitherto seen in Western Europe. Unless these defences are avoided or suppressed electronically or physically, attrition levels will be such as to question the role of the aircraft in stemming the Warsaw Pact armoured forces. And dare I remind this erudite audience that with an attrition level of 20% and flying three sorties per day, an air force is reduced to a quarter of its starting strength by the end of the second day and will have lost virtually all of its aircraft by the end of the fifth day. Even with attrition levels around 10%, that same air force would be down to 50% of its starting strength by the end of the second day and down to the 20% level by the end of the fifth day. To say the least, an attrition level in excess of 10% would pose a NATO commander with a number of very difficult decisions, especially if he wished to retain a credible nuclear option. It is possible of course that there would be no warning of the Warsaw Pact attack or we might not recognise the signs of the impending attack. Is it inconceivable that the Warsaw Pact might use one of their regular exercises to get themselves into a position to launch a surprise attack? If such an attack came, who else but the air forces of NATO stand any chance of stemming the Warsaw Pact forces in the first 24 hours? So let us then using this hypothetical scenario examine where advances in navigational techniques should lead to significant improvements in mission effectiveness.

The NATO reaction to the massive Warsaw Pact blitzkreig and steamroller tactics must be to stop the armoured forces as far east as possible. If the attack is a genuine surprise, it could well be that NATO would have only light covering forces forward and the task of destroying the Warsaw Pact armour at this phase of the war would fall primarily to the NATO tactical air forces – at least until the NATO armies had deployed forward to meet the threat. The position facing NATO in this scenario is somewhat similar to that facing the Israelis on the Golan Heights. No matter what the NATO air force commanders might want to do to counter the Warsaw Pact air forces, I would suggest that the politico-military directive would accord the anti-armour task first priority.

Present generation aircraft in the NATO tactical air forces have no difficulty in navigating from their bases to the general scene of operations. They are flying over friendly territory which they know like the back of their hand and most of the aircraft are equipped with a navigation and attack system capable of determining position to an accuracy of about one nautical mile per hour. It is when the aircraft arrive in the battle area that the real problems begin. Even though NATO may have only light covering forces forward, there is clearly a need for tactical aircraft to be integrated into the firepower plan of the ground forces and this generally means that aircraft must be able to talk to the ground forces without the enemy being able to gain intelligence from the communication. It would certainly simplify the target location problem if the ground and air forces engaged in close support operations had a common reference system of equal accuracy. It is one thing to make this simple statement and quite another to meet this requirement, bearing in mind that whatever system is chosen must operate in a dense electronic environment and with the Warsaw Pact doing their best or worst to interfere with our communication and navigation systems. Add to this the hostile air defence environment, and the need to identify friend from foe, and you have the seed corn to keep the avionics industry going for at least a decade.

The key in the battle area is the suppression of the Warsaw Pact ground based air defence systems. If these can be suppressed, aircraft attrition levels will be reduced and hence NATO would be able to mount more offensive support sorties in a given time and could attack the Warsaw Pact armour at will with cluster weapons or more sophisticated anti-armour weapons. Advances in navigational techniques that would allow NATO aircraft to locate the ground based air defence systems and then to stay outside the lethal envelopes of the SAMs while weapons were launched capable of homing on the SAM radar transmissions, or navigating to the precise locations of the SAM systems would certainly be welcomed by airmen. Similarly, decoys launched from the aircraft or by the ground forces would confuse the SAM systems and their commanders and this would reduce attrition and so lead to an increase in mission effectiveness. Given all of these advances, it would be necessary to co-ordinate the attacks very carefully and this naturally leads on to a debate whether these defence suppression missions should be fully orchestrated campaigns with the conductor positioned in say an AWACS aircraft or whether the local commander can achieve his aim by hanging defence suppression weapons and an ECM pod on aircraft in the first wave and then put in waves of anti-armour aircraft. I think there is a case for looking at electronic warfare across the entire Central Region and there may be a case to orchestrate some of the defence suppression attacks in the major thrust areas, but the mind boggles at the thought of conducting one gigantic defence suppression operation across the entire Central Region or, indeed, of eating up the lion's share of the budget developing sophisticated defence suppression forces which may only work where the density of radars is low and the radars are radiating.

The next area to examine is how best to attack the Warsaw Pact armour. If the armour is concentrated and the integral ground based air defence systems are either intact or not yet reduced to a level that would result in an acceptable attrition level to NATO aircraft, then any navigational development that would allow NATO aircraft to stand off and launch weapons capable of homing on to armour or of putting down a good lethal carpet guaranteed to avoid our troops on the ground in typical European weather conditions would certainly improve mission effectiveness. Whether this is a guidance development within a weapon or a navigational development within the aircraft would depend on cost-effectiveness studies. And if RPVs could replace aircraft in this role I do not think that many airmen would object. Where the Warsaw Pact achieve a breakthrough and are rushing westwards at high speed the NATO air forces may well be tasked to carry out counter-penetration missions along the most probable axes of advances to find and destroy these forces. With the high speed of modern aircraft and the problem of acquiring armour targets in the fog of war it is quite probable that on a number of occasions the pilot will spot the enemy armour in a position not lending itself to a first pass attack. Any

navigational development that would allow the pilot to mark the enemy force and instruct the weapon to go to that point would avoid the necessity of a second pass attack against an alerted enemy. This would increase his chance of survival and so enable NATO to fly more offensive support sorties.

In summary then, the areas where advances in navigational techniques should lead to significant improvements in effectiveness in close support and interdiction operations are those which would enable the aircraft to locate SAM systems, to launch weapons against these systems from outside their lethal envelopes, to stand off and launch anti-armour weapons and to launch anti-armour weapons against targets spotted outside the cone associated with first pass attacks.

I will now turn to offensive counter air attacks, an emotive topic which is not fully understood by either the airman or the soldier. And the first question we should ask ourselves is why do we want to carry out counter air missions when the politico-military directive in my scenario is to stop the enemy armour as far east as possible? Are we attacking the Warsaw Pact airfields to keep the enemy air off the backs of our troops? If so, we have set ourselves a very difficult task. The Warsaw Pact tactical aircraft are normally housed in hardened aircraft shelters and to destroy these we must first penetrate through the area defence SAM systems in the satellite countries and then face the formidable point defence SAM and gun systems at the airfield itself. The aircraft that succeed in penetrating to the airfield then have the unenviable task of carrying out precision attacks against the hardened shelters or, alternatively, immobilizing the airfield by attacking the operating surfaces with some kind of runway or airfield denial weapons. Attacks against hardened shelters are complicated by the need to avoid or suppress the enemy ground based air defence systems. If carried out at very low level, below the effective minimum operating height for the low level air defence systems, there is the very real problem of how to acquire the shelter target quickly and, having acquired, how to release and guide the weapon to the target to an accuracy of a few feet without exposing the aircraft unduly. If the attack is carried out at medium level, where the aircraft would be illuminated by a large number of SAM systems, it would be essential to have a supporting force of aircraft equipped to suppress the enemy SAM systems. Having penetrated to the target area at medium level, how does one acquire the target in average European weather conditions? If by radar, are there any navigational developments on the horizon that will enable a weapon to be guided to an accuracy of a few feet? Given target coordinates to a high order of accuracy we could perhaps think in terms of releasing a guided weapon attack from a set of coordinates outside the target area. And taking it one step further, the weapon could be an RPV and taking it one step further the aircraft could have stayed at home. But would such weapons be cost-effective and would they be as flexible as aircraft? If they proved cost-effective, there is nothing more final than the physical destruction of an aircraft in a shelter. The Warsaw Pact can replace aircraft but there is no way that hardened aircraft shelters can be replaced overnight.

Weapons designed to deny the airfield to the enemy have one thing in common. They do not in general destroy aircraft. They will, indeed, stop the enemy from operating from that airfield until the airfield denial devices have been removed and any craters in the runways filled, but once the airfield has been reopened the enemy can catch up on the sorties lost. So I come back to my basic question – why attack enemy airfields? The reason I would suggest is quite complex. If NATO shows that it has a credible counter air option, then the Warsaw Pact must deploy ground based air defence systems around all airfields and must keep a large number of dual role aircraft in the air defence role. NATO has the initiative of when to carry out the attacks against the Warsaw Pact airfields and, bearing in mind the inherent flexibility of aircraft, there is no reason why NATO should not operate this option selectively, linked to what is happening in the land battle. For instance, counter air attacks linked to a major NATO counter attack or to NATO forces deploying to forward positions, could well result in a large number of Warsaw Pact aircraft being held on the ground during the critical phases of these operations.

The navigational improvements one would like to see in the counter air field are linked entirely to the target phase of the operation. I mentioned the application of advances in navigational techniques to defence suppression when I discussed close support and interdiction operations – they are equally true for defence suppression on counter air operations. Other advances that should lead to improvements in mission effectiveness are connected with the target complex. The aircraft shelters and operating surfaces are fixed point targets and their positions should be known to a high order of accuracy. Given a navigation system of similar accuracy one has the possibility of developing a spectrum of options involving aircraft, decoys and RPVs leading to significant improvements in mission effectiveness. Let us hope that if and when such a navigation system comes along we take a very hard look at cost-effectiveness and the possibility of simplifying aircraft systems.

I should now like to spend just a few minutes talking about navigation in the maritime/air environment.

MARITIME/AIR

Aircraft play a significant role in three types of maritime operations, namely anti-ship, anti-submarine warfare and air defence. From a navigational viewpoint, there is much common ground between the three roles and although it will mean some other simplification I shall look at the maritime/air environment in a rather different way from the land/air environment. In essence, I shall be discussing navigation and guidance under the broad headings of detection, tracking and interception, and attack. And before I do so, I want to say a few words on the maritime scene itself. Whereas in the land/air environment the Threat was measured in terms of thousands of tanks and aircraft concentrated into a small area, in which radar and visual attacks are often confused with ground returns, in the maritime/air environment almost the

converse is true. A relatively small number of enemy ships, submarines and aircraft pose a threat in the EASTLANT area, but these will generally be operating alone or in very small groups scattered across a very large area of ocean, and will present themselves as very good radar echoes against the sea background.

Detection of an enemy aircraft, ship or submarine in the EASTLANT area may be determined from a variety of ground based, shipborne and aerospace borne radar and more esoteric sensors, and the accuracy of the detection can vary from a few feet to many miles. Any significant error in detection will increase the area of search and, at least in the case of ships and submarines, may lead to the enemy craft not being intercepted. If a cost-effective high accuracy navigation system could be developed to cover the EASTLANT area and units of this system located at every detection sensor, then the resulting common reference system would lead to a significant improvement in the Commander's ability to position his forces to counter the threat. Such a system need give relative positions only within the area of operation and, if units within this system were required to radiate, it may prove possible to adapt these radiations to convey secure speech or command and control data and to identify friends within the system.

Moving on to the subject of tracking and interception, this often involves a great deal of cooperation between shore based units and craft located on, above and below the surface of the sea. The operational requirement for tracking accuracy of enemy craft varies considerably, being highest in the case of a friendly craft laying a pattern of sonobuoys and perhaps lowest for an aircraft or SAM equipped ship in direct radar contact with an enemy aircraft. Any improvements to the navigation system which would allow an aircraft to lay a pattern of sensors to a high order of accuracy and then to navigate precisely within the sensor coverage area would lead to a significant improvement in mission effectiveness.

Finally, I want to mention the attack phase. In the case of an aircraft carrying out a final attack on a submerged submarine, the key factors are the relative positions of hunter and hunted, the accuracy of the assessed submarine track and speed, and the accuracy of the interception vector. These requirements are similar to those discussed under the tracking phase and I shall say no more.

Final attacks against Soviet warships, bristling with shipborne SAM and gun systems, involve cooperation between widely spaced units, for example between aircraft and an AEW aircraft and/or EW support group, and both timing and relative position are vital to the success of the operation. Any improvements in navigation and attack systems and in navigational reference systems that would enable an attack aircraft to proceed passively until the last possible moment and to arrive at the radar switch-on point at the right time and heading in the right direction would lead to a reduced attrition level. Such a navigational system would enable the task force commander to marshal all elements connected with this complex operation and to deploy units such as defence suppression and electronic warfare support units to maximum effect.

SUMMARY

To summarise, and perhaps to oversimplify, navigation and guidance developments that would appear to offer significant improvements in mission effectiveness in the land/air environment are those connected with the attack phase of close support, defence suppression, interdiction and counter air operations. In the maritime/air environment the developments that would appear most significant are those connected with the provision of a common reference navigation and command and control system for all craft, and navigation and guidance developments associated with the tracking and attack phases of anti-submarine and anti-ship operations.

CHALLENGES IN RESEARCH AND DEVELOPMENT

by

Major General Edwin A.Coy
Director of SPACE, USAF
Pentagon, Washington, D.C.

Today I would like to share with you some thoughts, concerns and perceived opportunities regarding the impacts of advancing technology on operational systems for communications, position, navigation and weapon delivery. My viewpoint is one of a current member of the corporate R&D management. As many of the sessions of this conference will demonstrate, we are applying our scientific knowledge to achieve economic, operational, and performance improvements. We are striving to eliminate or at least minimize the general confusion that pervades the combat areas. Military history provides us with numerous examples of battles, campaigns, and even wars that have been lost due to confusion caused by not being able to talk to our fellow combatants, not knowing where we are and as a result losing coordination among forces.

We in R&D are taking positive action to improve mission success with programs under development that will provide the operators with reliable and high quality information in a timely manner. We are also striving to reverse the trend toward proliferation of special purpose systems and equipments, i.e. each designed to meet unique, limited requirements, by taking advantage of emerging technologies to develop low-cost, multi-purpose systems that meet the broad requirements of our land, sea, and air forces. The conduct of military operations today dictates that our forces must have available to them the means to go anywhere, at any time, day or night in all weather conditions to conduct coordinated military operations in a wide range of battlefield scenarios, to deliver weapons more effectively and efficiently, and to do all this with minimum delay. This translates into a real need for improved communications, positioning and navigation systems and for processing all available information to enhance the effectiveness of our forces. We also recognize that the users must be freed of time consuming rituals when getting information. To this end we have turned to advancements in digital equipment (both hardware and software), signal processing, information management, and navigation and communication subsystems.

For example, recognizing that flexible and secure communications (in the face of hostile jamming) is mandatory to conduct smooth operations, we are developing the Joint Tactical Information Distribution System (JTIDS). JTIDS is an L-band, jam resistant, time shared and secure system with features such as identification, relative positioning and communication. JTIDS allows, on demand, a force element to find out the status of any other element. This information dispels uncertainties and allows a new degree of flexibility during combat, changes to the prebriefed or planned operation are more easily accommodated. As such JTIDS will be a significant enhancement in the real time coordination of combat activities.

Like communication, accurate operator knowledge of position is necessary to avoid confusion. I am sure that each of you can appreciate the situation a combatant experiences when he realizes that he does not know where he is or if his lost position is deteriorating. Knowing position and velocity are necessary to those on, above and below the surface of the earth. Even more critical is the need to enhance force effectiveness through the ability to deliver weapons precisely. The NAVSTAR Global Positioning System is designed to provide 24 hour, all weather, three dimensional position and velocity data in a common grid to an unlimited number of users. NAVSTAR is a space-based L-band radio navigator system featuring high jam resistance, accurate determination of the user position while allowing the user to remain passive, and highly accurate system time for use in enhancing on-board weapon delivery system capabilities.

We see these programs improving the performance of our combat elements and doing so with an economic advantage. These new systems will eventually replace older equipments and provide cost avoidance by improved reliability and a commonality of equipments across many platforms. These aspects (reliability and commonality) allow cost avoidance in the areas of logistic support, training and acquisition. Logistic costs are impacted due to fewer failures, fewer unique items in supply lines, similarity of maintenance instructions and extensive use of built-in-test functions. Training for both operational and maintenance personnel is impacted by similar and common equipments allowing those people to spend less time in school and more time on the job. Acquisition costs are impacted by high volume procurements and capitalizing on past designs. JTIDS, NAVSTAR, the ARC-164 radio and our standard Inertial Navigation System efforts are all structured to meet operational needs while accruing cost benefits through using common or multiapplication equipments. These subsystems exemplify the tremendous increase in technology we have achieved in the past decade.

Television, satellite communication and hand calculators have changed the life style of our civilian communities. Similarly, systems like JTIDS and NAVSTAR will reshape many of our fundamental defense concepts. Right now we have precision guided munition whose delivery error are within the weapons lethal range. NAVSTAR lets the pilot put his aircraft over a fixed target so accurately that blind deliveries will be effective. And JTIDS provides necessary information to the operator with a minimum of ritual. Data concerning any other element is generated continuously as opposed to past systems where data was generated only after it was requested. In the past, a pilot would ask another fellow where he was – he would read his instruments and then answer the question. JTIDS will provide that information without bothering the other fellow. I would speculate that we are going to experience substantial changes in planning, equipping and conducting military operations.

These phenomenal increases in capability are achieved by focusing technology on specific subsystem applications. Specifically, the use of digital circuitry (MSI and LSI), controlled computer programming methods, microprocessing and multiplex allow packing many interacting functions into a small volume at a price we can afford. Our current LSI chips now have about 15,000 functions per square centimeter and this figure will double in the near future. Computer memory density is currently about two hundred fifty thousand bits per square centimeter at a cost of about three tenths of a cent per bit; in a few years we expect the density to double while the cost drops to one hundredth of a cent per bit. The initial design of these elements is labor intensive and is a high cost item.

In the software area we have increased the productivity of the programmers by the use of higher order languages. We are experiencing five to ten times more instructions being generated per manhour now, as opposed to the method of programming in assembly language. Software design and test, like LSI design, is labor intensive. I believe we have turned the corner on managing software design, test, and maintenance. The use of higher order language, structured programming techniques and managerial awareness are responsible for keeping software production costs in line. Thus we are able to bring about system changes by issuing magnetic tapes as opposed to the method of buying expensive hardware and paying a premium price for installation.

The microprocessor is having a profound impact on our subsystem design. These devices allow large amounts of processing to be done at the sensor. The size and low power of microprocessors often allow redundant installations which increase the probability of mission success. These devices are finding application in the built-in-test functions that ease the maintenance of digital systems. I believe that we have just scratched the surface of applying microprocessors to military equipment.

Several of our new aircraft use multiplex for routing information between sensors and computers. Multiplex was introduced into our aircraft as a weight saving measure. A pair of twisted wires with a shielding jacket now carry the same information that would otherwise require several hundreds and occasionally thousands of single purpose wires. It is estimated that by use of multiplex on the B1 Electrical Power Control System we were able to save over 1500 pounds that represents just under four miles of wire. Similar savings were realized in the avionics and central test systems.

Currently we have a tri-service multiplex standard that will foster greater commonality of interfacing as well as allowing one service to use a sensor developed by another with a minimum of change. The existing standard for multiplex specifies a one megabit data rate with a 400 hertz bandwidth. This capacity allows us to address over 90% of all signals on board an aircraft. We are currently investigating the higher data rate buses for the integration of high speed information as found in audio and video systems. The technique of fiber optics appears to be a high payoff solution to the high speed data transfer problem. Not only is the fiber optic bus capable of handling data rates in excess of 100 megabits per second; but the bus exhibits immunity to the electromagnetic disturbances that may distort electrical signals transmitted by wire.

In spite of these modern day digital "miracles", we still do not have enough resources to explore, develop, and produce all of the applications that we can earnestly say would enhance our performance and yield a payoff on investment. The question facing us is "how do I choose which subsystems will reach production and which technologies do I explore?".

Looking ahead we may conservatively predict that we will continue to meet the future user needs; but, the funding and manpower required will become a more critical factor. The technologies will be available to solve just about any problem that we can postulate. But simply stated . . . can we afford it? . . . . We are meeting the problem head on; the fundamental issue as we see it is to better manage our technical resources. We are examining the selection criteria for which systems are to be produced and we are rethinking the methods used in specification and design of a system.

We are developing a method of analyzing the individual requirements and subsequent designs that fulfill user needs. What we believe to be the key is found in the very successful management of subsystem designs. Today's subsystems show a great deal of commonality from user to user, they exhibit many common modules within the subsystem, they have efficient interfacing between elements of the subsystem and they occasionally satisfy more than one operational requirement. We propose to step back and look at the weapon system design and satisfaction of requirements in the same light as the subsystem designer does.

If common modules are good for subsystems, they should be great for the weapon system as a whole. If efficient interfaces ease the task of the subsystem design, they should also serve the system designer. If one computer

programming language and one programming discipline pays off for the subsystem designer, It should also benefit the system designer. And if the subsystem designer has control and display problems the system designer must have tremendous problems.

As I see the design cycle of a future weapon system being done in an integrated manner, the process would proceed as follows: First we begin with the user requirements. We look at these needs not as individual entities but as elements of a system, and in so doing, we usually can identify some overlap in the requirements. There is another category of user needs that must be considered; that is, those needs that are not formally stated and in some cases not even informally stated. The requirements for a new weapon system must specify sufficient growth and flexibility to allow expansion of the design at a later time to meet additional user needs, while keeping costs down.

From the requirements and anticipated requirements, we can specify what type of sensors are required to perform the missions. From the list of candidate groupings of sensors we may form several initial system designs. In each case the method of design is the same. The mission segments are collectively viewed with respect to three basic functions, i.e. control and display information, transfer, and processing.

Consider segments such as mission and traffic control, weapon delivery, flight control, stores manangement, and navigation. Each of these segments is individually assessed for its need for processing of data, its need to communicate with other sensors, and its control and display demands.

By viewing each mission segment or subsystem in this manner during the same analysis it is possible to determine those areas where commonality of design across the entire weapon system can come about. By applying the element of time to the analysis we can reduce the amount of equipment in the system by selective resource sharing. Having the several candidate designs in hand we may examine each one in detail for expected performance and cost attributes.

There is nothing really new about this approach to system design. Each of us has probably been exposed to the idea that there is money to be made if we could all march to the same tune. The fallacy has been of course that we each have different musical preferences. This stumbling block is being removed by developing a method of system design that can be used in many applications. We start by considering all aircraft avionics needs and then descend from that large abstract case to several specific designs. Using a common origin for each individual design, resource sharing and sameness of equipment is more easily attained. It is necessary to verify that the total systems approach to avionics designs is viable and can be institutionalized. This verification is being done by an ongoing laboratory program called the Digital Avionics Information System (DAIS). We have designed and fabricated a set of core avionics for multiple mission aircraft. The core consists of avionics computers, modular software, multiplex and controls and displays. These elements are now configured in a ground test bed, to serve an adverse weather close air support mission. Following test and analysis of that configuration, the core elements will be reconfigured into an avionics suite for a night air superiority mission. The effort expended to make the reconfiguration, the degree of commonality achieved and the cost benefits will be determined and documented. The DAIS effort will provide specifications, standards and a design methodology that will enhance resource sharing across subsystems and across weapon systems. It will provide a common framework for all avionics system designers.

We are taking other positive measures to make reuse of past efforts more attractive. These efforts include establishing a software control agency and a multiplex control agency.

Each of these agencies are in their formative stages now. These offices will perform a control function; that is, assuring that system designers adhere to existing directives. Even more important, however, they will serve as technical experts to assist system designers in the details of design. One important function of the control agencies is maintaining a library of designs and applications. That information will be available to all avionics designers and will promote reuse of past design efforts. Efforts like DAIS and the control agencies demonstrate that we are investing resources in technical management as well as technology.

Some of this influence will be seen in the fine presentations you will receive in the sessions that follow. The concepts of mutiapplication, operator satisfaction and ease of maintenance are reflected in many of the program descriptions.

The systematic approach from the subsystem level upward, that I have attempted to describe, offers a large potential for major benefits in terms of reliability, maintainability, logistical supportability, investment protection, sensible product improvement and cost avoidance. I thank you for your kind attention and the opportunity to share with you my notions concerning the corporate management of our R&D.

FUTURE APPLICATIONS OF LOW COST STRAPDOWN LASER INERTIAL NAVIGATION SYSTEMS

by
James B. Matthews
Division Staff Technical Planning
Raytheon Company
528 Boston Post Road
Sudbury, Massachusetts 01776
and
Davis R. Bates, Jr.
Manager, SSD Marketing

SUMMARY

The laser gyro has the potential to play a decisive role in lowering the cost of future guidance and navigation systems. This role is comparable to the impact which the crystal oscillator has had on current systems. Fundamental principles of the laser gyro are reviewed, briefly, to identify characteristics of this new means of measuring direction. The review of the development progression from Sagnac's Ring Interferometer through Multibeam Ring Resonator to Regenerative Ring Resonator is concise in order to emphasize considerations important in the comparison of the various laser gyro mechanization approaches. The treatment is intended to be augmented by reference material carefully selected and recommended for deeper study. Laser gyros based on dithered approaches to lock-in circumvention are compared to the Raytheon Multioscillator Laser Gyro in terms of performance requirements for precision pointing and high bandwidth versus navigation applications. A description of the Raytheon Multioscillator approach is presented together with performance and physical data on current instruments. Projected system physical characteristics are presented.

The gyroscope has enjoyed, in the realm of instrumentation, a position of glamour rivaled only by the clock. Because of the importance of time measurement in navigation, there was a period, probably in the eighteenth century, when navigation symposia would have featured clocks in the program. Since the development of the crystal oscillator, precision time measurement in vehicles has become so commonplace that the clock has been absorbed into the digital processors of most systems, losing its traditional identity with instrumentation. For most applications the time measurement problem has been solved, and the glamour is gone. Today the measurement of direction lacks an adequate solution. The spinning wheel supported by ingenious mechanical systems has, like the mechanical clock, both served and fascinated man. Almost a year ago, Dr. H. W. Sorg of the University of Stuttgart in a paper presented before the Internation Navigation Congress in Boston, Massachusetts presented a fine survey of the interesting history of gyroscope development (Reference [1]). The survey, covering the two centuries of classical gyro development, ends in the present with the projection that better and better conventional gyros will be developed in answer to ever increasing accuracy requirements for space and military navigation needs. Is this the future? Perhaps. Today, we from Boston are here in Stuttgart. We are here to talk about the laser gyroscope and that future. We offer this thesis: the laser gyro will be to the measurement of <u>direction</u> as the crystal oscillator clock has been to the measurement of <u>time</u>. The laser gyro is not just another step in the continuing saga of better and better gyro development. It is the quantum jump in gyro technology that will initiate the third century of gyro development.

For this reason, the impact on future systems of the type shown in Figure 1 is difficult to estimate. The effect may be analogous to the adaptation of digital systems resulting from the development of precision oscillators. In fact, the impact may be so great that we may look forward to future navigation symposia that include no papers on either clocks or gyros.

This new approach to the measurement of direction has become possible as the result of two separate scientific discoveries of the twentieth century. The first has been attributed to Sagnac (Reference [2]) who demonstrated in 1913 the capability of measuring the state of rotation of a frame of reference using an optical interferometer (see

Figure 2). In his experiment the rotation was detected by a fringe shift (ΔZ) given by the relation:

$$\Delta Z = \frac{4A \cdot \Omega}{\lambda C}$$

in which A is the area enclosed by the light path, λ is the vacuum wavelength and C is the free space velocity of light. The scalar product $A \cdot \Omega$ expresses the important dependence of the fringe shift on the cosine of the angle between the normal to the enclosed area and the axis of rotation of the optical system.

At optical frequencies the denominator is of the order of 10^2 so that even relatively large interferometers of say one meter on a side would yield a fringe shift of less than 1/25 per radian/second of rotation rate (Ω). Also since intensities of the fringes have a $\cos^2$ form the ability to resolve fringes is quite limited making measurement of low rates difficult with small devices (see Figure 2). Michelson and Gale measured earth rotation using such an interferometer; however, it required one about 450 meters on a side to produce a fringe shift of less than 1/4.

The significance of this discovery is not therefore in the direct application of the interferometer, but in the important implication that was derived relative to the dependence of the cavity resonance of such a closed optical path (References [2] and [3]). In the interferometer (Figure 3) the frequency is determined by the source (f_i). The counter-directed beams (f_{CW}) and f_{CCW}) are therefore of the same frequency. As the system rotates the time required for each of the counter-directed beams to traverse their respective paths becomes different so that the energy recombined at the output of the beam splitter will have a phase difference dependent on the rotation rate of the system. In the lower figure the beam splitter is replaced by a high reflecting mirror so that energy injected into the cavity can circulate. Such a cavity (similar to a Fabry-Perot type resonator) will have minimum loss at frequencies determined by the cavity resonant modes. The resonant frequency of an optical path enclosing an area must be dependent on $A \cdot \Omega$. That is, the resonant frequencies for counter-directed electromagnetic waves for the same cavity (optical path) are shifted symmetrically up and down as a function of $A \cdot \Omega$ according to the formula:

$$\Delta f = \frac{4A \cdot \Omega}{L\lambda}$$

where Δf is the difference in the resonant frequencies of the counter-directed waves and L is the optical pathlength of the circuit. The significance of this discovery should be emphasized. Since the counter-directed traveling waves share the same optical path, the effects of the mechanical instabilities which change the resonant frequency of the one, change the other by the same amount. The configuration is therefore primarily sensitive to only the rotation of the system Ω. This matter is treated in more detail in References [2] and [3].

The second important element is, of course, the success in demonstrating the feasibility of sustaining a population inversion in a Helium-Neon gas plasma (1961, Reference [4]). This was the final step to realizing the long sought for means to provide coherent gain at optical frequencies using stimulated emission in gases. (Light Amplification by Stimulated Emission of Radiation "LASER".) This provided the means of adding gain to an optical resonant cavity, thus making it a regenerative oscillator (see Figure 4). The gain can be used to significantly enhance the cavity Q (Reference [5]). Low loss optical resonant cavities may be designed using state-of-the-art dielectric multilayer mirrors to obtain line widths of the order of $\Delta\nu = 5 \times 10^5$ hertz. With the addition of a laser gain medium, the cavity can become a regenerative oscillator having exceedingly narrow line width. The result is an optical cavity sensitive to rotation with frequency stability of the beat frequency between the counter-directed beams that can be estimated to be of the order of $\Delta f = 10^{-4}$ Hz or better. The ring resonator and the regenerative ring resonator were first suggested by Rosenthal in 1961 as an instrument for use in studying light propagation effects. The first regenerative ring resonator was constructed and operated by Macek and Davis, 1963 (Reference [6]). From this early beginning, the laser gyro has emerged as a prime contender for the future.

Why laser gyros? Listed below are all of the reasons -- all of the factors required in inertial systems and as yet unattained to the degree desired in low cost systems:

- Inertial grade performance, but low cost
- Mechanical simplicity and small size

- Digital output
- High dynamic range
- Instant reaction
- Low power
- Flexible form factor
- High "g" high dynamic environment
- Reliability - low life cycle cost.

The need for a reliable, small and low cost unit can be satisfied by the development of instrumentation technology which eliminates the complex mechanical mechanisms peculiar to current systems. Recent inertial technology developments are leading to this capability. Through the development of strapdown inertial techniques, mechanical gimbals of inertial platforms will be replaced by computer computations. Accelerometers are being improved and simplified. Finally, and more importantly, the promising advances of laser gyro technology make it apparent that a strapdown inertial measurement unit (IMU) can be developed with performance comparable to conventional, gimballed inertial platform systems. Thus, the inherent simplicity of the laser gyro promises breakthroughs in both cost and reliability. The development of a laser gyro with size, cost and performance comparable to mechanical instruments would, therefore, have a decisive effect on the realization of a low cost inertial system for many applications.

Since the laser gyro is basically a solid state device its advantages are many. Being inherently a digital device, it is ideally suited to strapdown applications. In addition, since it has no moving parts and its insensitivity is derived from rotating light, it has essentially no "g" sensitivity thereby avoiding the necessity for complicated computational g-related unbalance compensations. This "g" insensitivity minimizes a major error source in computing "miss distance" in any navigation or guidance system.

The laser gyro also has a wide dynamic range, being essentially linear from 0 to greater than 600 degrees per second, and may provide both angle and angular rate outputs. These characteristics make it suitable for multipurpose use on missiles, such as midcourse guidance, head stabilization and autopilot functions, thereby replacing several other conventional instruments normally required for these separate functions.

Other key features of the laser gyro are its low power and low thermal environment sensitivity. The need for temperature control elements is eliminated. This fact, coupled with the gyro's low operating power, reduce power supply requirements which further reduces system size, weight and cost. The elimination of any thermal control for the gyro means that it is essentially an "instant on" device, providing useful output information immediately, making it ideally suited for fast reaction time applications.

At Raytheon, a continuing research and development effort is being conducted to develop a laser gyro with wide application potential. Our goal is to produce instruments and systems to satisfy the low cost system needs for the next decade. This work involves topics of both gyro development and system studies to apply the new gyro to specific applications. The results of system studies are reported separately in References [7], [8], and [9]. These studies have emphasized:

1. demonstration of the navigation potential of ring laser gyros in a strapdown system;
2. development and verification of system error models pertinent to this and future ring laser gyro systems;
3. demonstration of the use of modern filter techniques with a ring laser gyro navigation system.

This work involved formulation of system concepts, analysis, system laboratory and mobile tests and, finally, analysis of test results. This work covers consideration of the more obvious application of the laser gyro to guidance and navigation. The results indicate the differences between this instrument and its more classical counterpart. Since this subject has been treated before, we will concentrate in this paper on the important low noise characteristics of the Raytheon laser gyro and the potential impact on future application in precision pointing of the space telescope (References [10], [11], and [12]).

As stated previously, a laser gyroscope consists of a medium with gain located in a ring resonator, as described in Figure 5. Such a combination can oscillate with a traveling wave going around the ring in a counterclockwise (CCW) direction. In the absence of rotation of the structure, these two waves oscillate at identical frequencies. When the structure rotates around an axis perpendicular to the figure, the two frequencies become different, the difference being proportional to the rotation rate.

At low frequency differences the two waves tend to remain locked at a common frequency because the system behaves as two coupled oscillators. This phenomenon is usually referred to as lock-in. It causes loss of information at low rotation rates and departure from linearity outside the range of lock-in (see Figure 6).

There are two common practices used to avoid this lock-in. One is to angularly dither the gyro cavity about the input axis relative to the case. The second is to optically bias the gyroscope in such a way that the two frequencies are unequal in the absence of rotation. In this second approach any drift in bias will be interpreted as a rotation rate, and it is necessary to switch (periodically dither) between two bias points (+B and -B in Figure 6). If this switching takes place in a completely symmetric way any drifts in the bias average out to zero as they do in the mechanically dithered case above (see Reference [13] and [14]). Because of the transition through "lock-in" required by both approaches some information is lost, causing a noise source in the output (Reference [14]).

The gyro output is usually obtained by simply counting the output beat frequency. Since this is essentially a process of integration each cycle represents an incremental change in input angle, and the sum will represent the angle the instrument has been rotated through since the counting process was initiated. The relationship of a cycle of the output frequency to a change in angle is the instrument's "scale factor" and may be derived from the expression in Figure 5. Frequency jitters or pulses lost due to transition through lock-in will therefore be interpreted as angular disturbances.

The importance of this noise source is at first not obvious, but if considered, reveals that a laser gyro mechanized in a way that requires such transitions through this region, in which the signal is lost, results in an instrument incapable of realizing the potential of the very narrow line width (or high beat frequency stability) of the laser cavity (see Figure 4). As stated previously, it is possible to construct a gyro cavity having a Power Spectral Density of beat frequency fluctuations of the order of 1×10^{-6} Hz^2/Hz (References [5], [15], and [16]) whereas dithering the same cavity will induce noise resulting from transition through lock-in that is typically of the order of 1×10^{-2} Hz^2/Hz or greater (Reference [14]).

This wide band noise phenomenon increases with the square as the size of the gyro diminishes. This is primarily true because the output pulse size (angular quantization) is inversely proportional to the ring size thus changing both the effective size of the deadband and the value of the pulse. The effect of the noise on navigation, alignment and gyrocompassing is treated further in Reference [8]. This limitation becomes important in applications requiring low noise and high resolution.

In Figure 7 these considerations are illustrated. The figure represents "gyro drift" in terms of the standard deviation an estimate of gyro output rate derived by simply summing output cycles for a period of time and computing:

$$\dot{\theta} = \frac{1}{\Delta T} \Sigma \Delta\theta$$

where $\dot{\theta}$ is the rate estimate, ΔT is the sample time, $\Sigma \Delta\theta$ is the sum of the gyro output pulses. The curves can apply equally well to a dynamic situation in which the actual rate is zero or some known rate. The usefulness of the figure is to relate the various types or sources of gyro drift are considered:

- Wide Band Noise, with $1/\sqrt{T}$ behavior typical of the dithered gyro, and also other frequency fluctuations.
- Pulse Quantization Noise, with $1/T$ behavior.
- Long term drift, with $\sqrt{T}$ behavior due to thermal and other long term drift sources (see Reference [14]).

Shown also are the curves representing the requirement for one nautical mile per hour performance, and the requirement for precision pointing of the Large Space Telescope (LST).

At Raytheon we have proven the feasibility of an alternate mode of operation, in which the application of a fixed bias leads to oscillation at four different frequencies. These oscillations occur in traveling waves of two mutually orthogonal polarizations, one frequency at each polarization traveling around the ring in a clockwise direction, and one of each traveling in a counterclockwise direction.

With the appropriate read-out system a signal can be obtained from this four-frequency gyroscope, the frequency of which is proportional to rotation rate. This frequency is also insensitive to bias instabilities and bias drifts, making the switching of bias polarity as used in two-frequency gyroscopes unnecessary.

Figure 8 compares the relative performance of the Raytheon four-frequency (multi-oscillator) gyroscope with the performance of the two-frequency dithered instrument for various configurations. The figure is based on actual laboratory testing indicates that the Raytheon instrument is limited by the gyro output quantization (a design parameter) and not be dither-generated noise, as is the case for the two-frequency instruments. This low noise feature of the Raytheon instrument not only promises high accuracy in navigation application but makes the Raytheon multioscillator a potential competitor to the so-called third generation mechanical gyro in precision pointing applications such as the Large Space Telescope (LST).

A description of the device as it was first implemented follows. We start with a ring laser geometry which places no constraints on the polarization of the traveling waves which can oscillate. Such a structure is shown in Figure 9. Its frequency spectrum is also indicated. In the absence of any bias or rotation all polarizations are equivalent, and only one frequency can oscillate.

Then we place an element in the ring which has rotary birefringence, such as properly oriented crystalline quartz, Figure 10. This means that the ring now had a different length for a wave of right-hand circular polarization (RHCP) than left-hand circular polarization (LHCP). The result is that the ring can now sustain oscillation of circularly polarized modes only, the frequencies of RHCP and LHCP being different by an amount determined by the birefringence and size of the quartz.

Subsequently a Faraday rotator is added to the ring as shown in Figure 11. Its function is to remove the frequency degeneracy between the circular polarization traveling CW and CCw. With a fixed magnetic field applied, the frequency spectrum now consists of four frequencies as indicated. We now monitor the frequency

$$\Delta f = (f_4 - f_3) - (f_2 - f_1)$$

It can be readily be proven that this frequency can be expressed as

$$f = \frac{8A}{\lambda L} \cdot \omega$$

The attractive feature of this approach is that neither the bias provided by the rotary birefringence nor the bias introduced by the Faraday rotator enter into this quantity, and bias drifts are of no importance. Furthermore, lock-in which exists in two-frequency laser gyros will occur when $(f_4 - f_3)$ and $(f_2 - f_1)$ approaches zero. With proper choice of components this can be made to occur at very high rotation rates.

A typical embodiment of the gyro device is shown in Figure 12. Similar laboratory units have been used to demonstrate that output noise is significantly lower than in the classic dithered approaches to lock-in avoidance. Analysis and data have shown that the gyro noise is (as predicted) proportional to 1/t (where t is the sampling or summing interval), is limited by quantization. This quantization limitation can be reduced by external electronics to meet special system requirements such as for a high performance stabilization system. This data is summarized in Figure 8. The dashed lines in the lower left hand corner represent quantization recently achieved.

The Raytheon Multioscillator Gyro output frequency versus input rotation rate data is compared to data from a typical two-frequency gyro cavity at low rotation rates, Figure 13. The superior linear performance of the multioscillator through zero rate should be noted. The rectangle near zero rotation rate is expanded in Figure 14. Here data is presented showing that this fine linearity is maintained down to rates as low as 1/3 degrees per hour. The data taken in the region marked by the dashed lines (i.e., below one degree per hour) is limited in accuracy by the test table. No deadband has ever been observed at these low rates.

Another advantage of the avoidance of dithered lock-in prevention methods, and of the minimization of wide band noise problems, is to make it possible to construct smaller gyro cavities maintaining satisfactory performance. Raytheon is currently fabricating a gyro (RB-25) having a ring length of 25 centimeters and a quantization of approximately 1.5 arc seconds per output pulse. In a single axis configuration, this gyro occupies about 50 in^3 including electronics, Figure 15. The ring size can probably be reduced to 15 centimeters and with other design modifications we feel it is possible to develop a version that would occupy about 25 in^3 including electronics. This means that a three-axis IMU with these gyros and a small accelerometer triad could be developed in the 60 - 75 in^3 size range. The possibility of such small units with navigation grade performance should be considered for the potential impact on future systems.

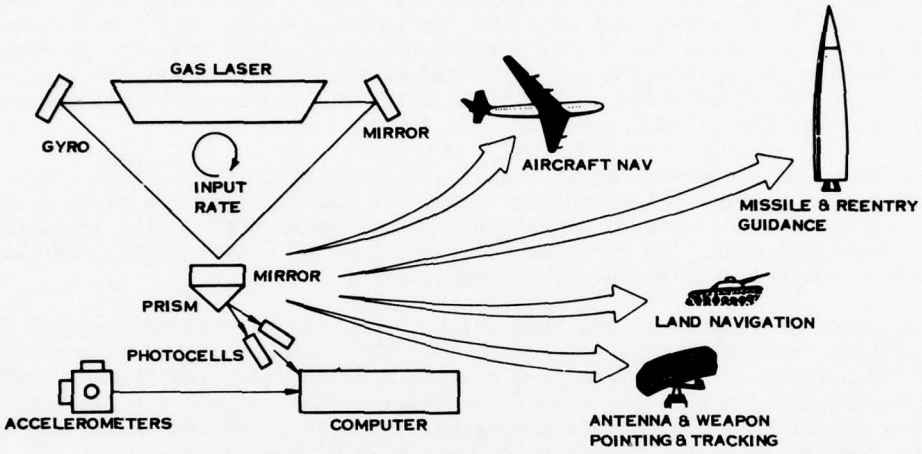

ADVANTAGES

- DORMANCY
- STRAPPED-DOWN CONFIGURATION
  - COST
  - *RELIABILITY*
  - MAINTAINABILITY
- EQUIVALENT PERFORMANCE

Figure 1. Strapped-Down Laser Inertial System

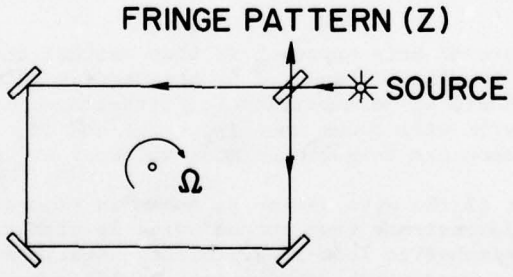

$$\Delta Z = \frac{4A \cdot \Omega}{C\lambda} \approx 1.5 \times 10^{-6}$$

A = 1 METER SQUARED
Ω = EARTH ROTATION RATE
λ = 0.6328 μm

Figure 2. Ring Interferometer

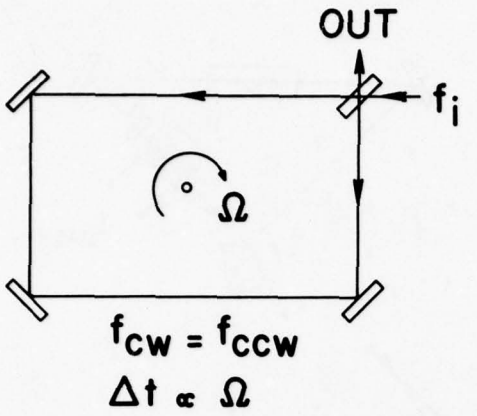

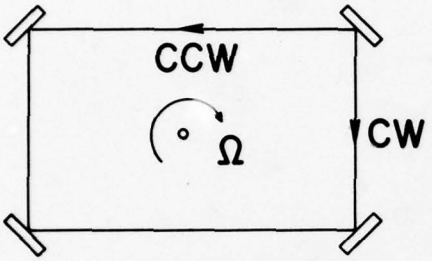

$$f_{cw} - f_{ccw} = \frac{4A \cdot \Omega}{\lambda L}$$

Figure 3. From Ring Interferometer to Ring Resonator

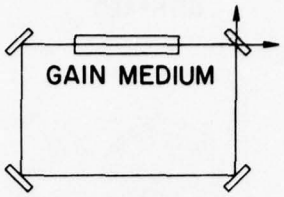

LINE WIDTH NARROWING

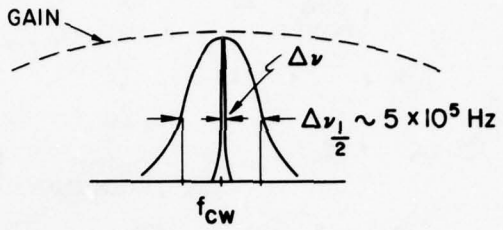

$$\Delta\nu = \frac{K}{P}(\Delta\nu_{\frac{1}{2}})^2 \approx 10^{-4}\ \text{Hz} \rightarrow 10^{-4}\ \text{DEG/HR}$$

Figure 4. Regenerative Ring Resonator

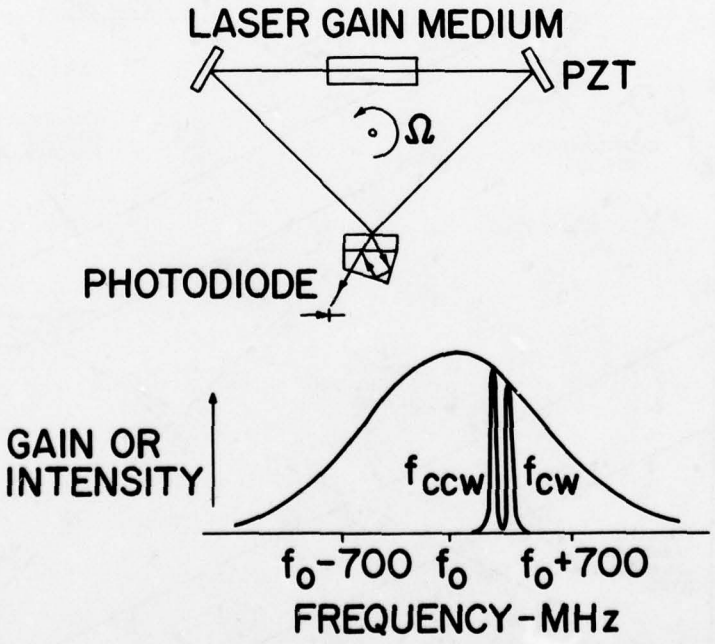

$$\Delta f = f_{cw} - f_{ccw} = \frac{4A\Omega}{L\lambda}$$

Figure 5. Two-Frequency Laser Gyro

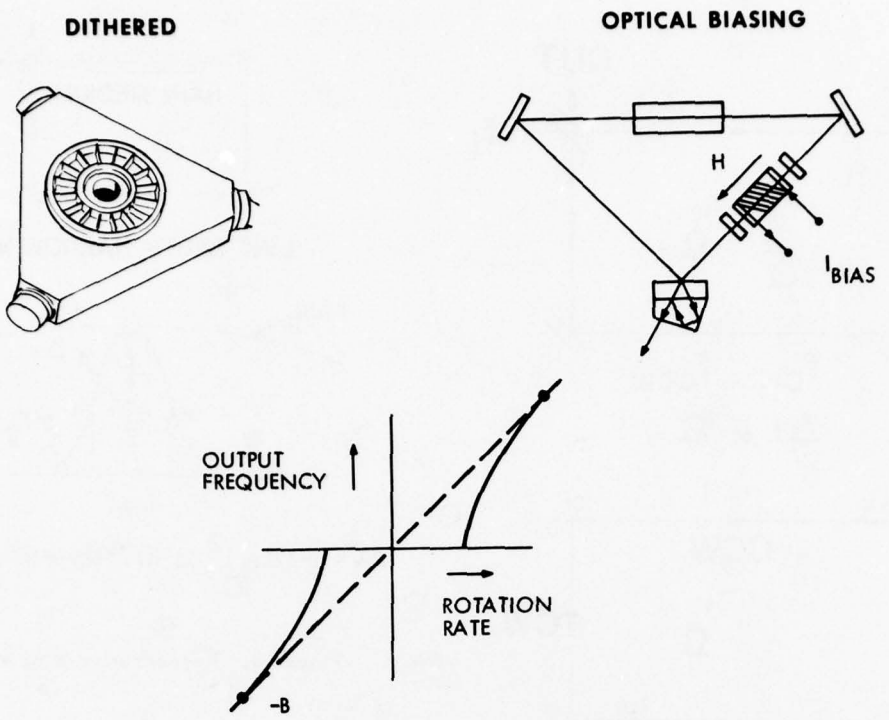

Figure 6. Lock-in Circumvention Techniques

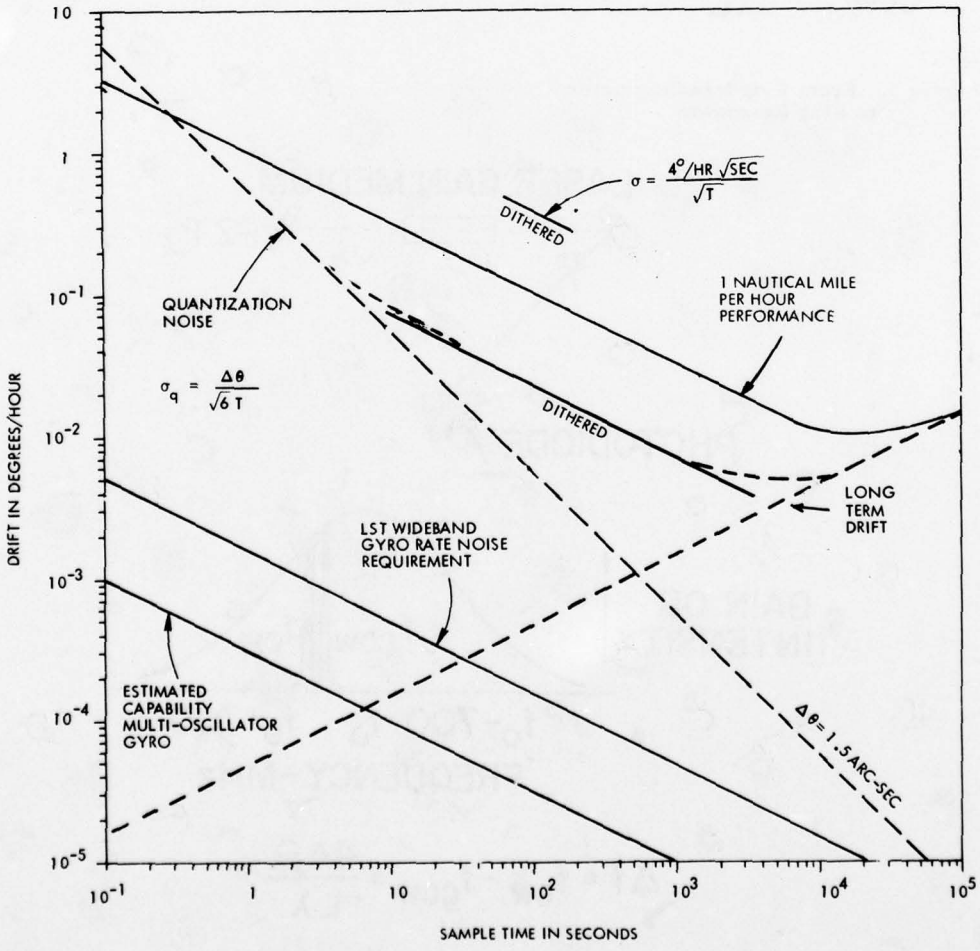

Figure 7. Standard Deviation of Rate Measurement as a Function of Sample Time

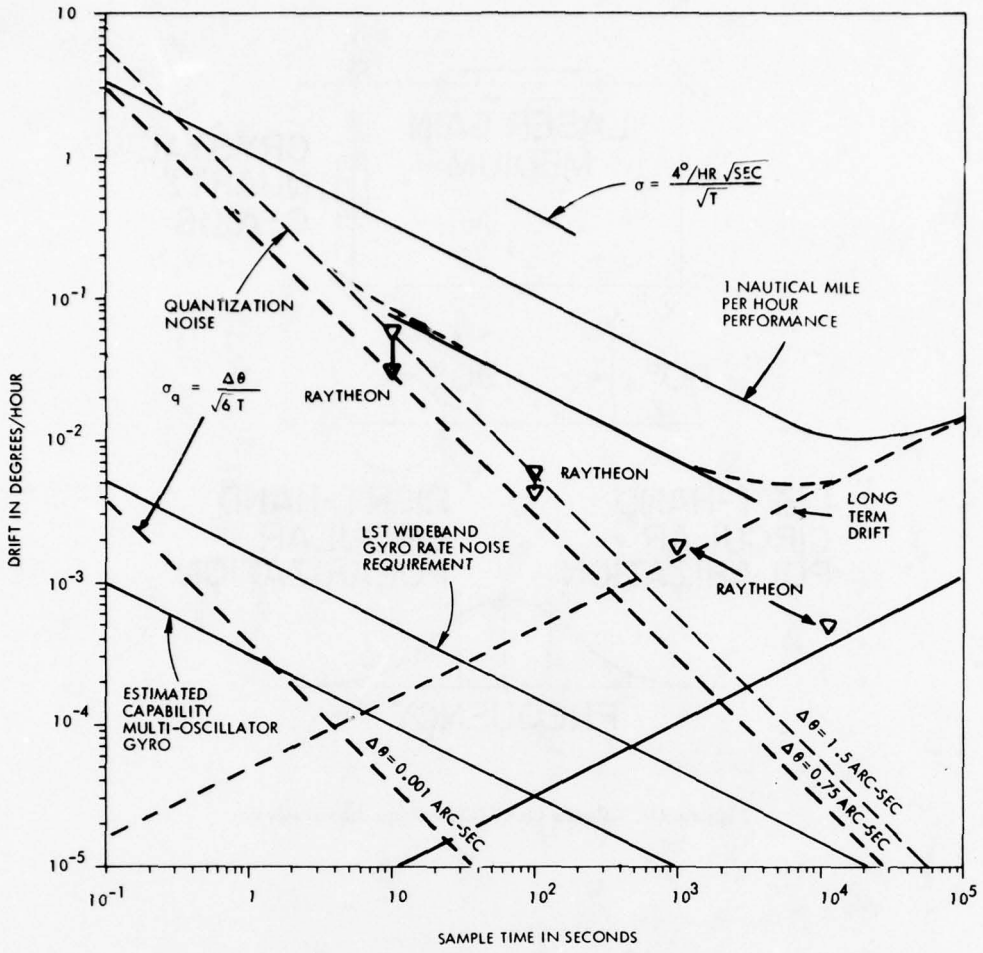

Figure 8. Standard Deviation of Rate Measurement as a Function of Sample Time

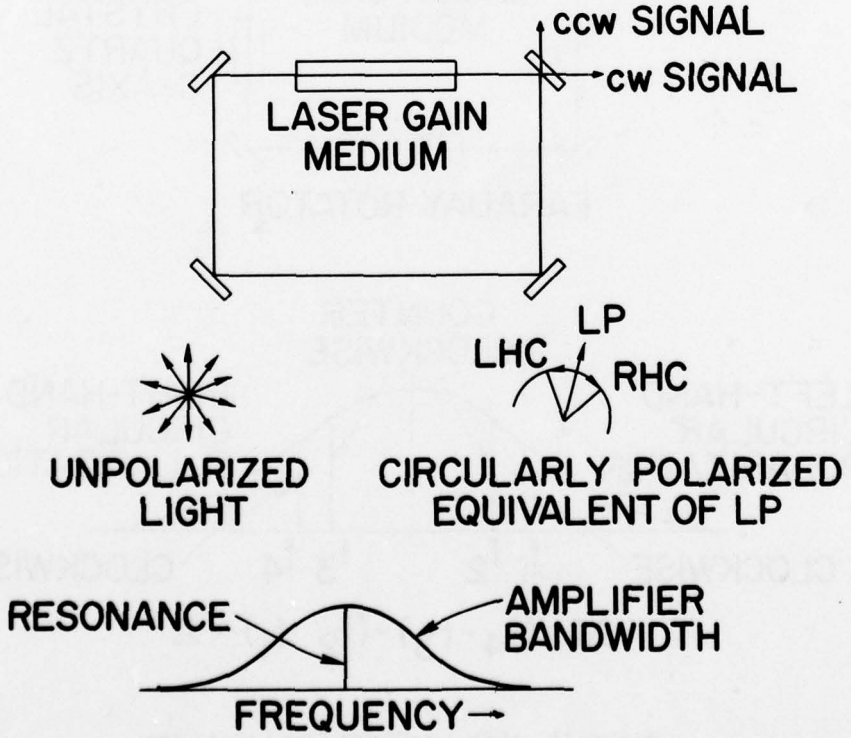

Figure 9. Multi-Oscillator Ring Laser Gyro

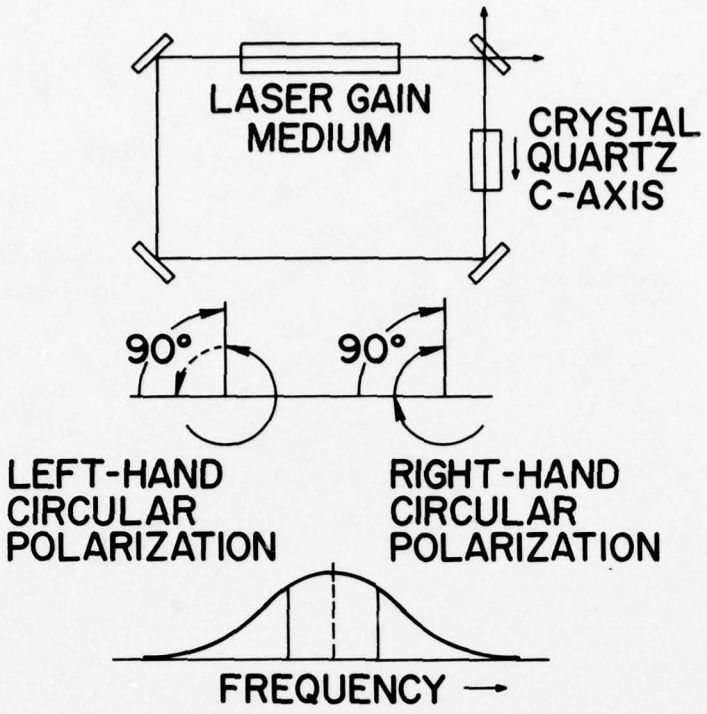

Figure 10. Multi-Oscillator Ring Laser Gyro

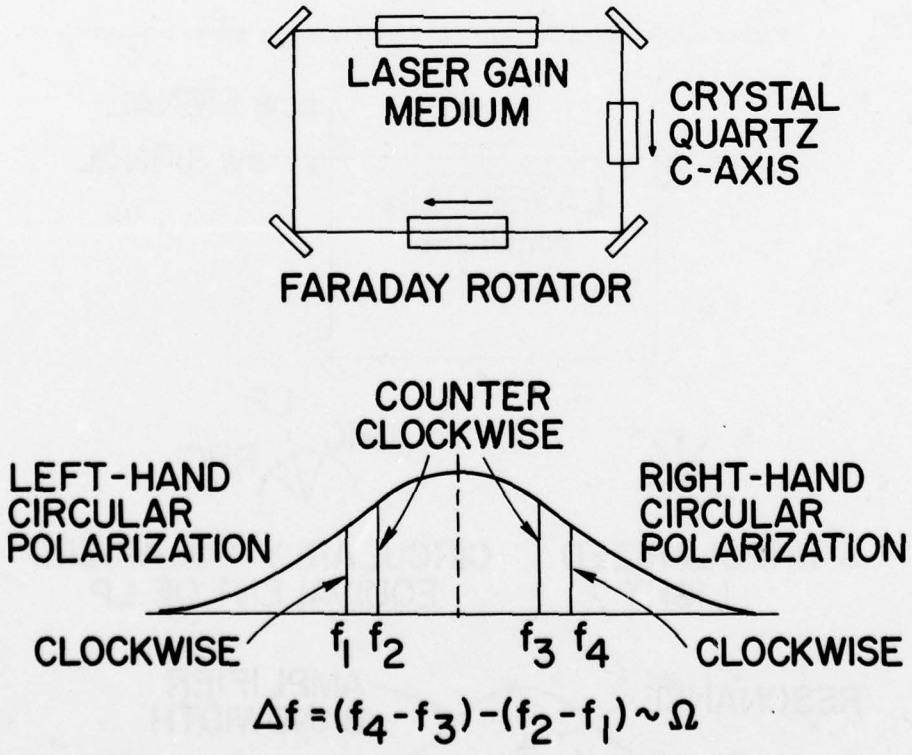

Figure 11. Multi-Oscillator Ring Laser Gyro

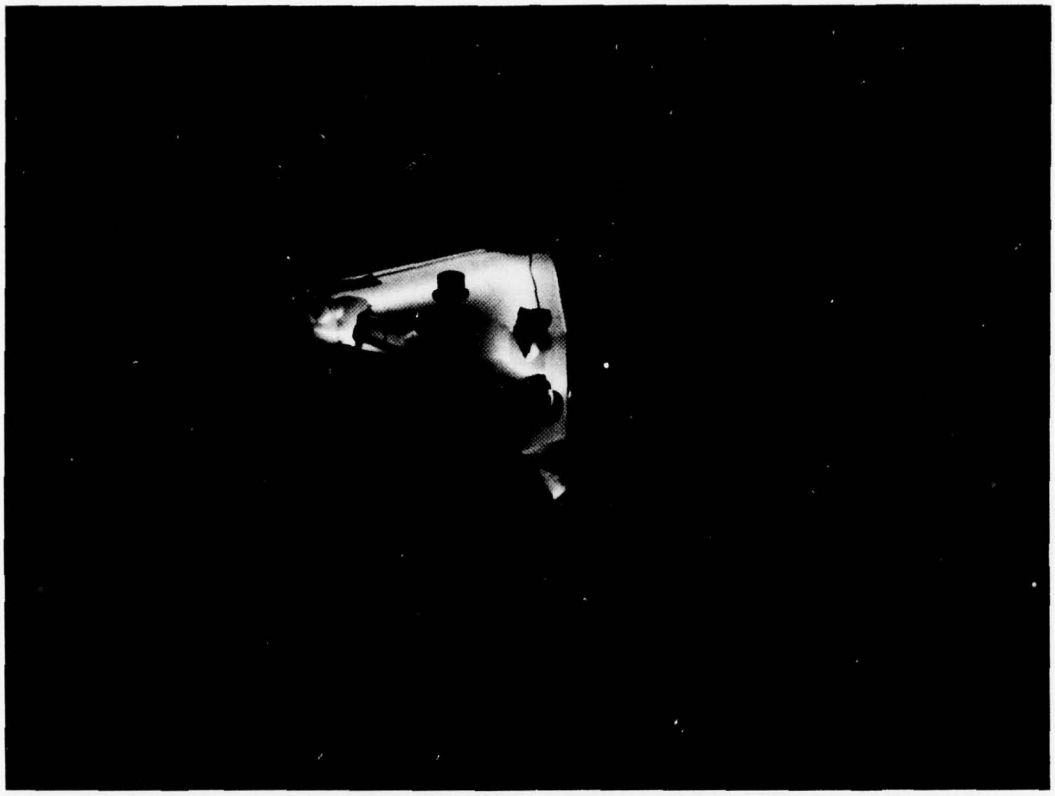

Figure 12. Multi-Oscillator Ring Laser Gyro Cavity

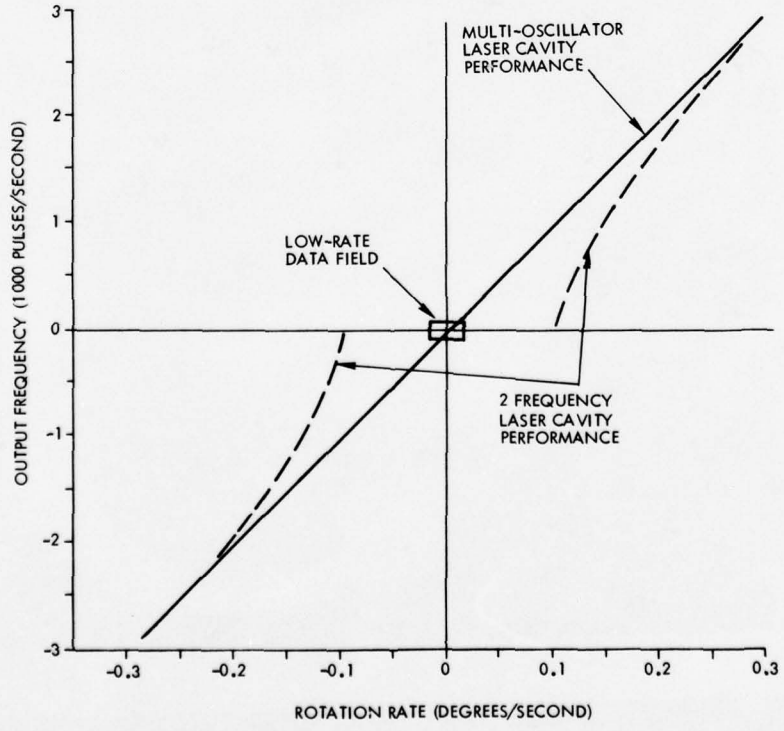

Figure 13. Output Frequency vs Rotation Rate

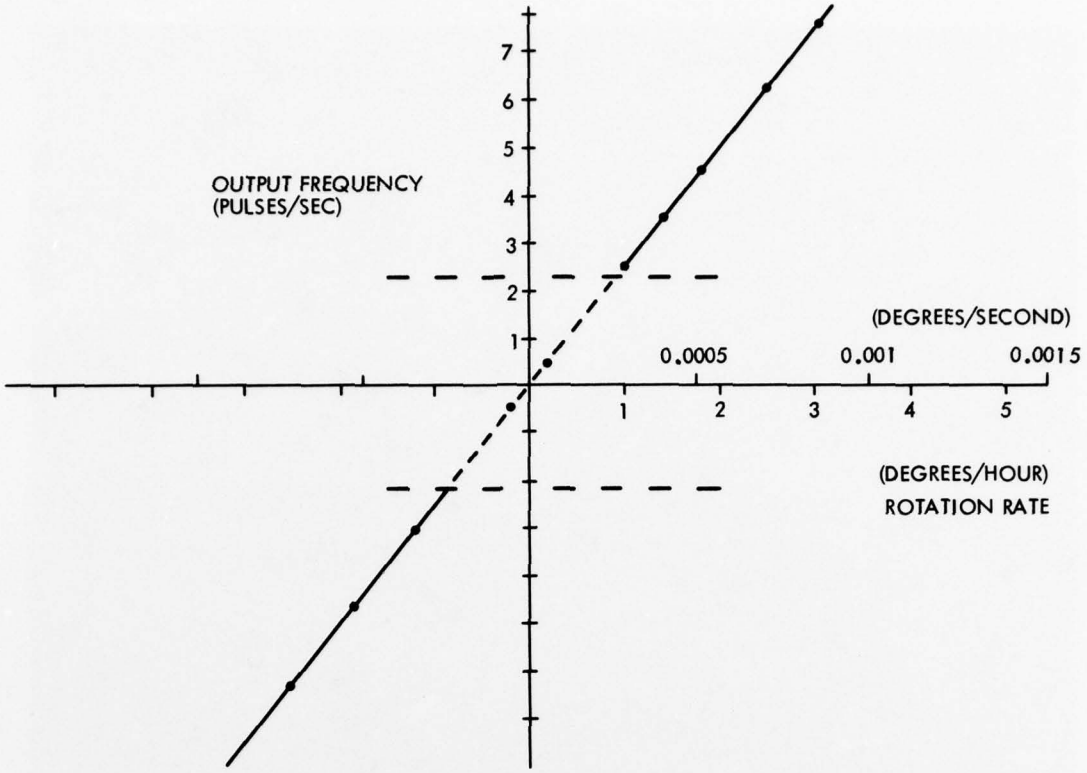

Figure 14. Low Rate Scale Factor Data Multi-Oscillator Laser Cavity

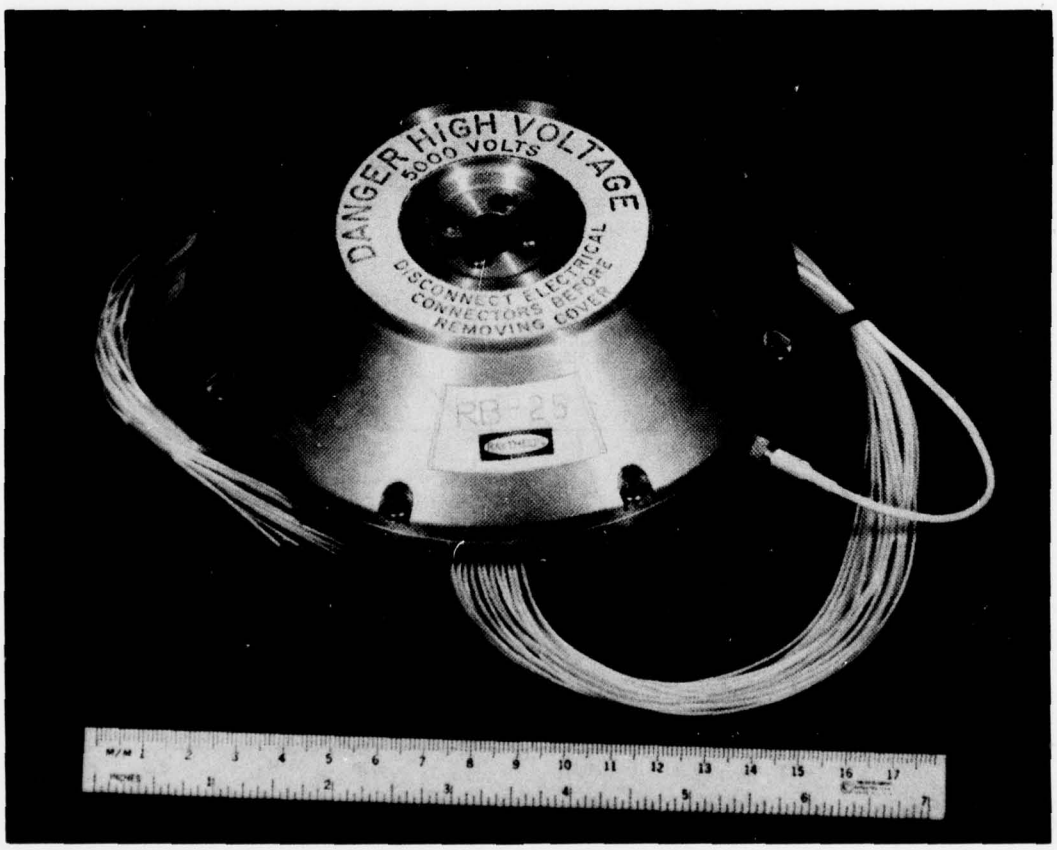

Figure 15. Multi-Oscillator Ring Laser Gyro RB-25

REFERENCES

[1] Sorg, H. W., "From Serson to Draper - Two Centuries of Gyroscopic Development", Navigation: Journal of the Institute of Navigation, Volume 23, No. 4, pp. 313-324, Winter 1976-77.

[2] Post, E. J., "Sagnac Effect", Reviews of Modern Physics, Vol. 39, No. 2, pp. 475-493, April 1967.

[3] Rosenthal, A. H., "Regenerative Circulatory Multiple-Beam Interferometry for the Study of Light-Propagation Effects", Journal of the Optical Society of America, Vol. 52, No. 10, pp. 1143-1148, October, 1962.

[4] Bennett, W. R., "Gaseous Optical Masers" Applied Optics, Supplement 1 (Optical Masers), pp. 24-61, 1962.

[5] Statz, H., Bass, M., deMars, G. A., "Suppression of Close-Lying Modes in Ring Lasers and Related Devices", Journal of Applied Physics, Vol. 39, 4045 (1968).

[6] Macek, W., Davis, D. and Olthuis, D. T. M., "Ring Laser Rotation Rate Sensor", from Schneider, J. R. and White, G. R., (Optical Masers), pp. 199-207, Polytechnic Institute of Brooklyn Press, Brooklyn, N. Y., 1963.

[7] Matthews, J. B., Gneses, M. I., Pasik, D. J., and Taylor, G. R., "Results of the Developmental Testing of the First Ring Laser Gyro Inertial Navigation System", Proceedings of the Seventh Biennial Guidance Test Symposium, Central Inertial Guidance Test Facility, Holloman Air Force Base, New Mexico, May 1975.

[8] Pasik, D. J., Gneses, M. I., and Taylor, G. R., "A Ring Laser Gyro Strapdown Inertial Navigation System: Performance Analysis and Test Results", AIAA Paper No. 75-1095, presented at AIAA Guidance and Control Conference, Boston, Massachusetts, August 20-22, 1975.

[9] Taylor, G. R., Pasik, D. J., and Fish, J. W., "Calibration and Field Testing of a High-Quality Strapped Down Inertial Navigation System", The Eighth Biennial Guidance Test Symposium, Holloman Air Force Base, New Mexico , May 11-13, 1977.

[10] Lucus, W. R., "The State of the Center - 1976", a Message to Employees of George C. Marshall Space Flight Center, National Aeronautics and Space Administration, Huntsville, Alabama, February 1977.

[11] Glaese, J. R., Kennel, H. F., Nurre, G. S., Setzer, S. M., and Shelton, H. L., "A Low Cost LST Pointing Control System", AIAA Paper No. 75-1057, presented at AIAA Guidance and Control Conference, Boston, Massachusetts, August 20-22, 1975.

[12] Jacot, A. D. and Emsley, W. W., "Assessment of Fine Stabilization Problems for the LST", AIAA Paper No. 73-881, presented at AIAA Guidance and Control Conference, Key Biscayne, Florida, August 20-22, 1973.

[13] Aronowitz, F. and Collins, R. J., "Lock-In and Intensity-Phase Interaction in the Ring Laser", Journal of Applied Physics, Vol. 41, No. 1, pp. 130-141, January 1970.

[14] Savage, P. G., "Laser Gyros in Strapdown Inertial Navigation Systems", presented at IEEE Position Location and Navigation Symposium, San Diego, California, November 1-3, 1976.

[15] Egorov, Y. P., "Measurements of the Natural Line Width of the Emission of a Gas Laser with Coupled Modes", JETP Letters, Vol. 8, No. 10, pp. 320-322, 20 November 1968.

[16] Yariv, Amnon, "Introduction to Optical Electronics", Holt, Rinehart and Winston, Inc., New York, 1971.

[17] Clarke, D. and Grainger, J. F., "Polarized Light and Optical Measurement", Pergamon Press, Oxford, 1971.

Also, see U.S. and foreign Raytheon laser gyro patents.

NEW TECHNIQUES FOR LOW COST STRAPDOWN INERTIAL SYSTEMS

by
P.M. Brodie
C.R. Giardina
The Singer Company
Kearfott Division
Little Falls, New Jersey 07424
USA

SUMMARY

Due to recent developments in low cost inertial sensors and airborne processors, strapped-down inertial reference systems have matured to the point of multi-purpose application. Specifically, moderate cost and performance applications such as flight control, weapon delivery and aided navigation are ideal candidates for highly reliable modular strapped-down inertial configurations. Typically for these applications, the key parameter is reliability and an overall measure of performance. Traditionally, reliability in flight control systems has been achieved through the use of "brickwall" or independent instrument packages. Now with current technology, redundant sensor packages can be economically configured for this task. The concept of designing systems where repeatability of sensors and system reliability is equally or more important than navigational accuracy is relatively new. This paper will discuss the system approaches and techniques applicable to achieving these goals.

INTRODUCTION

Although interest in strapdown inertial technology is now relatively prominent, this technology has been under study and development for at least fifteen years. Early strapdown efforts were often concerned with the problems of computation. The difficulty in performing attitude matrix computations in digital processors of that era led to most of the literature on computational algorithms. It is only recently that airborne computer technology has permitted the real time calculation of direction cosines by direct integration without undue computer burden. Chronologically, the modelling of inertial component errors was next to be pursued as the dynamic strapdown environment propagates component errors that are of little concern to stable platform mounted sensors. This point is just as applicable today as newer, non rotating inertia gyroscopes are being developed and must be modelled. Early strapdown inertial sensors were primarily designed from the standpoint of achieving the primary performance requirements of low random drift and high torquing rates (to follow vehicle motions). Today as these problems are largely in hand, efforts have been turned to secondary performance areas. Thus sensor efforts are now concerned with designing instruments which exhibit lower strapdown environment propagated errors such as anisoinertia, coning, cross coupling, etc. Hopefully, the newer non-inertia based sensors (e.g., laser gyroscopes) will demonstrate intrinsically lower environmental propagated errors, thereby providing the basis for high performance systems.

Current strapdown developments have effectively branched into two distinct areas. The first is concerned with following the goal of high performance gimballed navigators i.e. one nautical mile per hour or better. At present the most promising candidates appear to be non rotating inertia sensors such as the Laser Gyro and the Magnetic Resonance Gyro. This approach will permit the advantages of strapdown inertial systems (simpler construction, fewer components, potentially lower cost, etc.) and the performance goal of high accuracy gimballed inertial systems. The second approach is concerned with inertial system applications with less stringent performance requirements. Actually there are many such applications, for example, tactical weapon guidance and flight control fall into this category as do aided inertial navigation systems. Radio navigation systems such as GPS (Global Positioning System) and JTIDS (Joint Tactical Information Distribution Systems) naturally fall into this group of aided navigation. While requiring less accuracy (typically 2 to 10 nautical miles per hour) from the inertial system, they often concurrently require greater reliability due to use in unmanned or critical systems.

With recent developments in electronic circuit reliability, particularly in LSI (Large Scale Integration) logic and airborne processors, the inertial sensors have become the key elements in strapdown system reliability. As part of the production cycle of these components, literally years are spent after development, improving accuracy and reliability. Thus for applications such as flight control where reliability is paramount, it makes good sense to extrapolate proven inertial hardware. At Kearfott, the Gyroflex* gyro, a flexure hinged tuned rotor gyro has had this kind of reliability improvement over the years. Kearfott has installed more than 11,000 Gyroflex gyros in inertial platforms. Over 5 million field operating hours have been achieved. Figure 1 shows a MTBF growth curve (for Gyroflex gyros for the A-7 aircraft system) which approaches 20,000 hours.

Therefore the development of these components with proven performance into lower cost strapdown versions becomes highly desirable. HIREX and CONEX are two such lower cost derivations of the Gyroflex gyro at Kearfott (Figure 2). As these inertial sensors are lower cost than their more accurate gimballed platform relatives, they are a natural choice for use in redundant configurations where Fail Operational or Fail-Safe requirements are dictated. For the first time, these redundant configurations can be developed for moderate cost applications based upon a strapdown mechanization utilizing proven gyro technology.

* Registered in U.S. Patent Office

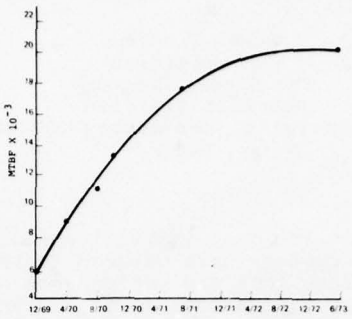

Fig. 1 Gyroflex Gyro MTBF Growth Curve

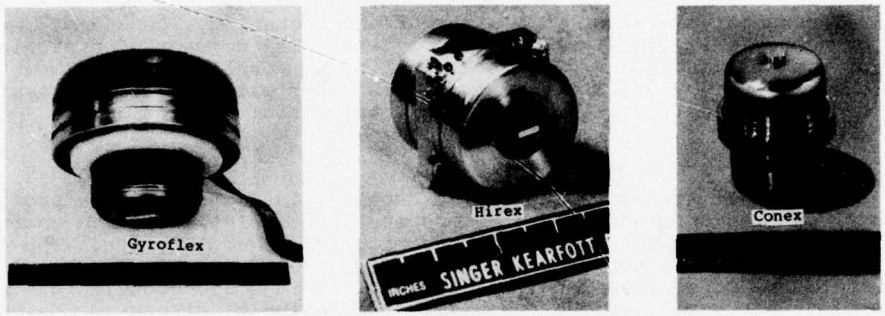

Fig. 2 Kearfott Gyro Development

The Kearfott SKN-3000 Strapdown Inertial Navigator is a good example of a departure point for redundant design as it is based precisely upon the technology discussed above. Figure 3 shows this strapdown system packaged in a standard ATR case.

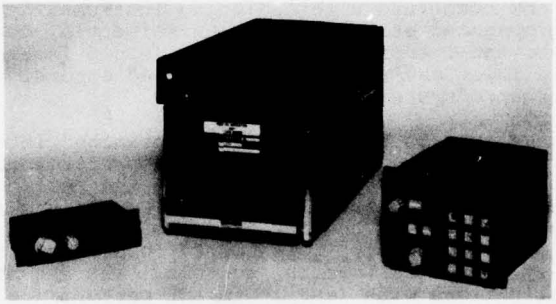

Fig. 3 SKN-3000 Strapdown Inertial Navigator

This paper will address a number of techniques which can be employed to make a redundant strapdown configuration feasible.

CONCEPT OF SELF CONTAINED REDUNDANCY

Most current redundant inertial systems can be classified as Brickwall Systems. For reasons of overall system reliability, a Brickwall system provides both physical and electrical isolation between sensing channels. Often this isolation extends through the downstream control system e.g., in each channel of an autoland flight control system. While supplying total isolation, this approach does add considerable cost, weight, and volume due to complete subsystem redundancy. The use of Duplex or Triplex Brickwall systems leads readily to the concept of fail operational and fail safe systems. In a fail operational system, a failure in a subsystem in one channel, still leaves two completely untouched channels i.e., in a Triplex system. A failure in a Duplex system would usually be classified as fail safe as the system cannot tolerate a second failure. These definitions are typical of flight control systems and do vary somewhat between applications. While this approach does yield the required system redundancy, it is also a costly and complex solution. An alternate approach to this problem of redundant inertial sensing is through modular redundancy. It is the advent of strapdown inertial technology which has permitted this concept to really become feasible. Using redundant elements in an inertial system is certainly not a new idea. Redundant platform gyros or "fourth" gyro concepts for example, have seen many applications over the years. However, in a stable, gimbal isolated platform, complete redundancy is not very practical. The addition of redundant elements to an inertial system should really be looked upon as a means of improving the probability of mission success. Thus the

redundant system must be capable of providing adequate system performance even after a failure has occurred. A modular, redundant, strapdown system provides precisely this kind of redundancy. Figure 4 shows an example of such a configuration. In this case three, two-degrees-of-freedom sensors are orthogonally mounted with their input axes skewed. This is an effective configuration, but is only one of many that is possible.

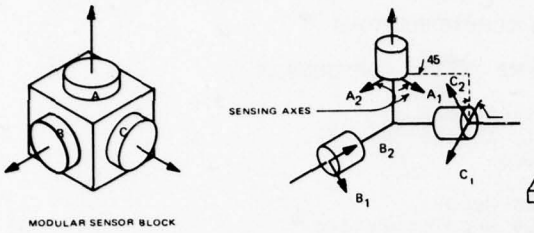

Fig. 4 Modular Redundant System

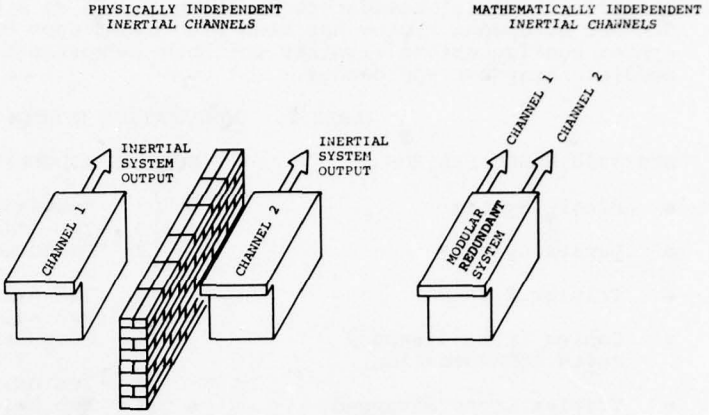

Fig. 5 Fail-Safe Inertial Ref. System

The principle advantage of a modular redundant strapdown system is indicated in Figure 5. Savings in system cost due to a simple system with fewer but modularly replaceable elements are apparent. The strapdown system must, of course, be equivalent to the brickwall approach not only in accuracy but in the vital areas of isolation and reliability. Techniques for achieving this system independence will now be described.

As each sensor (A, B or C) represents a two-axis inertial sensor, redundancy is afforded to each axis of a sensing triad. This redundancy is achieved by skewing the sensing axes of each sensor as previously shown (Figure 4).

In a system data processing sense, the redundant inertial system is as indicated in Figure 6. Both accelerometer and gyro data is supplied in six component vectors (for the three, 2-axis sensors indicated in Figure 4). Instead of complete separation as in a brickwall system, this sensor data is "cross-strapped" to each redundant processor. In terms of processing, the six instrument axes (per sensor type) are divided

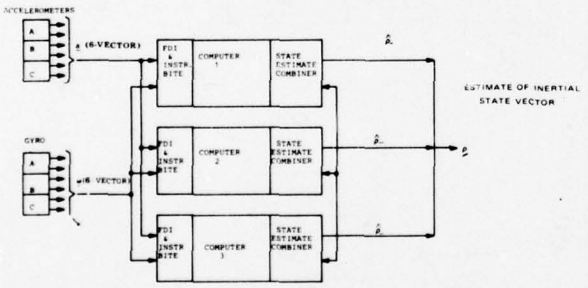

Fig. 6 System Interconnection Block Diagram

COMPUTER CHANNEL	INSTRUMENTS & AXES	IF...		
		A-FAILS	B-FAILS	C-FAILS
1	A1-A2-B1-B2	Use C1 & C2	Use C1 & C2	No Effect
2	C1-C2-A1-A2	Use B1 & B2	No Effect	Use B1 & B2
3	B1-B-2-C1-C-2	No Effect	Use A1 & A2	Use A1 & A2

Table 1 Fail-Op Sensor Axis Organization

into three groups of three that share a sensor and have a common axis. One such arrangement has been shown in Figure 6. Here, all instrument axes are available to all computers. For example, from Table 1 below, Computer channel 1 utilizes instrument axes A1, A2, B1, B2. Channel 2; C1, C2, A1, A2 and Channel 3; B1, B2, C1, C2 as indicated in the table, a failure in one instrument axis pair effects a replacement with an unused pair (for that axis) thereby permitting continuous operation in the presence of a failure. If all systems are functional, a voting process does not take place, but all data is utilized to form the best estimates of inertial system variables indicated on Figure 6 as a "State Estimator Combiner." If one sensor fails, the sensing axis triad is mathematically rearranged to delete the failed axis and use a remaining functional sensor in its place. Computationally, the navigational calculations are reinitialized from a channel unaffected by the instrument failure.

MODULAR RELIABILITY COMPARISONS

As previously stated, a key attribute of a modular redundant strapdown system is the achievement of true fail-operational or fail safe characteristics while retaining the reliability of more complex duplex and triplex individual sensing systems. In order to appreciate the magnitude of reliability improvement achieveable, it is useful to perform a comparative analysis. For purposes of analysis, the Kearfott SKN-3000 strapdown inertial navigators has been chosen as a baseline. Similarly, a modular redundant strapdown system has been also based upon SKN-3000 components. Table 2 indicates system configurations examined for both independent strapdown systems and redundant modular strapdown approaches.

TABLE 2. COMPARATIVE SYSTEM CONFIGURATIONS

SKN-3000 BASED SYSTEMS	MODULAR REDUNDANT SYSTEM COMPONENTS
• Single System	
• Duplex System	• 3 Two-Axis Gyros, 3 Two Axis Accelerometers, 2 Computers
• Triplex System	
• Duplex Cross Strapped (with communication)	• 3 Two Axis Gyros, 3 Two Axis Accelerometers, 3 Computers
• Triplex Cross Strapped	• 4 Two Axis Gyros, 4 Two Axis Accelerometers, 3 Computers

As this analysis is being performed for comparative purposes only, just the key redundant elements (sensors and processors) are included. Thus the resulting system reliability values will be somewhat higher than a complete system due to higher parts count for electronics, connectors, etc. Figure 7 gives the result of this analysis. Note that Mean Time Between Failures (MTBF) has been calculated rather than application of mission reliabilities. Mission values could be misleading as for most applications, they are close to unity, thereby affording little differentiation between cases.

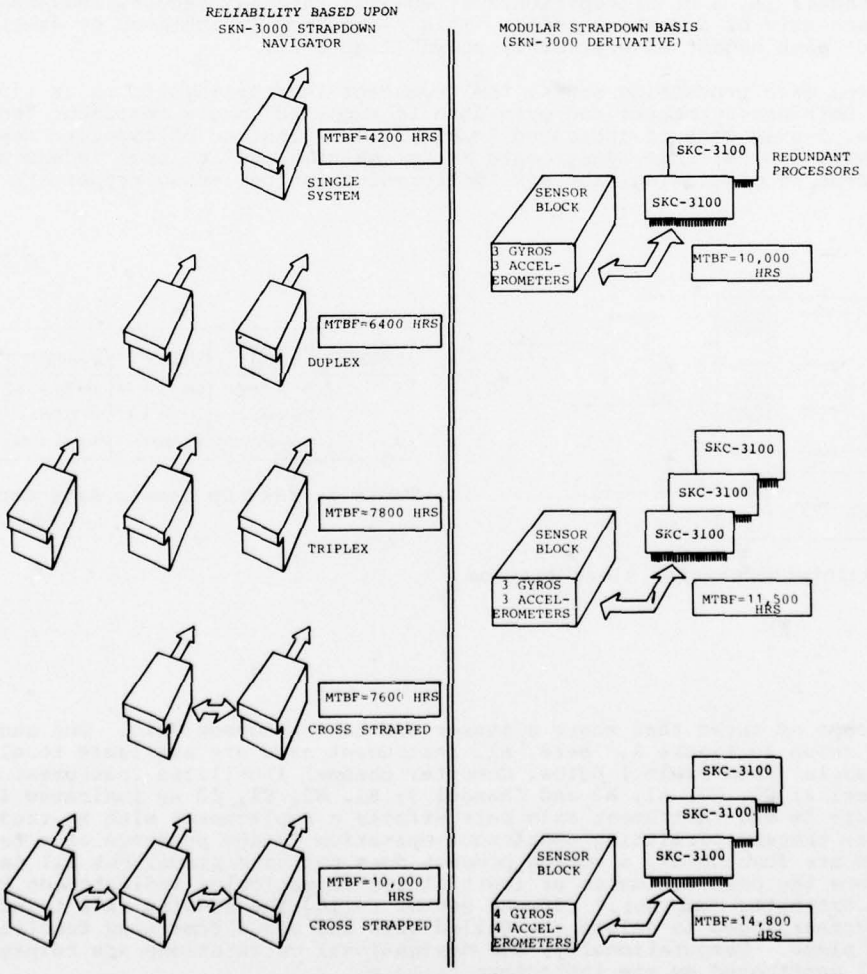

Fig. 7 Comparative Reliability

Although cross-strapped redundant systems are naturally more reliable than brickwalled systems as shown, in each case the modular redundant systems are much higher in reliability than their brickwalled counterparts. In fact, the greatest reliability margin is exhibited by the fail-operational system with four gyros and accelerometers. Figure 8 graphically indicates the reliability advantages of a modular approach.

Note that no single instrument failure affects all three channels. In operation, each computer receives navigation states from the other two and averages these outputs. Computer failure is detected by built-in test features or BITE on both processor software and hardware. When these BITE tests indicate a computer failure, its own static computation is deleted from the average and its outputs inhibited.

There are several key advantages to this technique. A computer failure cannot cause a sensor to become effectively inoperative as no instrument is dedicated to a particular channel. As all computer outputs are combined or averaged, using multiple sensors actually supplies a system accuracy advantage. Additionally, a channel is not lost when a sensor failure occurs. What is lost is a measure of statistical independence between channels. Failures can occur in two distinct categories, hard and soft. Hard or complete failures are the easiest to detect with the appropriate BITE circuitry. Soft or partial failures (such as gross shifts in performance), are more difficult to detect. Techniques for detecting this kind of failure are referred to as FDI (Failure Detection and Isolation) and are discussed in a latter part of this paper. It should be noted, however, that undetected soft failures are reduced essentially by a factor of three by the channel averaging process previously described.

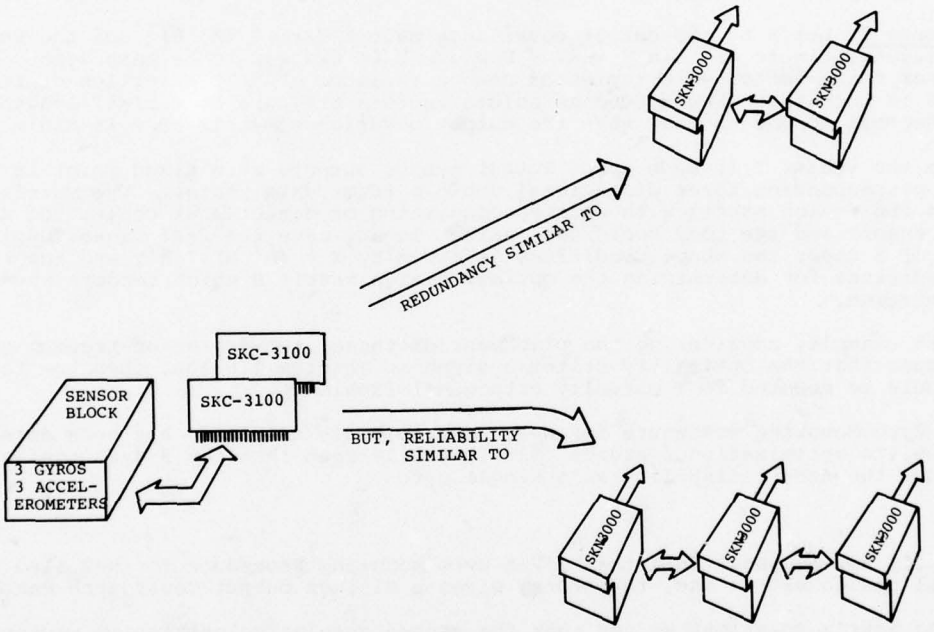

Fig. 8 Reliability Advantage of Modular Redundant Approach

Failure rates used in the calculation of MTBF figures displayed in Figure 7, have been verified at Kearfott by exhaustive tracking of operating units. These failure values are:

$\lambda_{Computer} = 75$ failures/10^6 hours

$\lambda_{Gyro} = 50$ failures/10^6 hours

$\lambda_{Accelerometer} = 20$ failures/10^6 hours

The mathematics of the computation of comparative reliability can be found in the Appendix to this paper.

DATA PROCESSING REDUNDANCY ADVANTAGES

In addition to advantages of higher reliability given by redundant strapdown systems, overall system accuracy can also be improved by appropriately filtering the sensed inertial data. The filtering process can be conducted at different stages in the system data processing flow. Specifically, total sensor data from n sensing axes can be condensed into vehicle body frame related information by least squares or other estimation procedures for subsequent use in attitude matrix calculations. This method of preprocessing is called pre-attitude filtering. Alternately, post-attitude filtering can be performed. There are advantages to both approaches. In the post-attitude case, non-redundant sensor data is used in calculating an attitude matrix and filtering is performed on the transformed data in each channel. In all cases, redundancy and appropriate modeling and filtering will improve the overall accuracy of the system. It can be shown that the output variance of instrument errors decreases with the addition of properly modeled sensors.

An optimal configuration for the sensors can be determined in many cases. For example, when pre-attitude filtering is used, an optimal configuration based on the Best Linear Unbiased Estimation Procedure (Ref 1) can be derived. Theorem 1 given below is employed in establishing an optimal orientation for the sensors.

> Theorem 1 Let R be the output covariance matrix $R = \sigma^2 (H' H)^{-1}$ of the Best Linear Unbiased Estimate of X in $Y = HX + U$ where U is assumed to be mean zero uncorrelated sensor noise vector with tuples of common variance σ^2. If selection of the column of H is such that when viewed as column vectors they are of maximal length and orthogonal to one another then the output covariance matrix of R is minimal.

Here the vector Y is made up of actual sensor outputs at a fixed point in time, X is the corresponding three dimensional vehicle frame data vector. The matrix H is called the design matrix with entries consisting of directional cosines of angles between sensors and the body coordinate axis. In any case the Best Linear Unbiased Estimate of X under the above conditions is given by $X = (H' H)^{-1} H'Y$ and the theorem gives conditions for determining the optimal design matrix H which renders the corresponding orientation.

As an example, considering the placement of three, two-degree-of-freedom gyros A, B, C such that the optimality criteria given in Theorem 1 holds, then the three gyros should be mounted in a mutually orthogonal fashion.

The Gyro Mounting Procedure for N=3, as previously outlined, has been determined based upon its optimization features. It is easily seen that the 3 gyro configuration gives about the same reliability as a single gyro.

It will now be shown that this given Gyro Mounting Procedure for N=3 also gives an optimal design matrix and, therefore, gives a minimum output Covariance Matrix.

Using matrix notation, we see that the sensed angular velocities in vector form Y equals the design matrix H times the angular velocity vector x, namely $Y = H x$ where,

$$Y = \begin{vmatrix} A_1 \\ A_2 \\ B_1 \\ B_2 \\ C_1 \\ C_2 \end{vmatrix} \qquad x = \begin{vmatrix} p \\ q \\ r \end{vmatrix}$$

The Design Matrix H specifies the orientation of the 3 gyros.

$$H = \begin{vmatrix} \cos\alpha & A_1 & \cos\beta & A_1 & \cos\gamma & A_1 \\ \cos\alpha & A_2 & \cos\beta & A_2 & \cos\gamma & A_2 \\ \cos\alpha & B_1 & \cos\beta & B_1 & \cos\gamma & B_1 \\ \cos\alpha & B_2 & \cos\beta & B_2 & \cos\gamma & B_2 \\ \cos\alpha & C_1 & \cos\beta & C_1 & \cos\gamma & C_1 \\ \cos\alpha & C_2 & \cos\beta & C_2 & \cos\gamma & C_2 \end{vmatrix}$$

It can now be shown that

$$H = \begin{vmatrix} 1 & 0 & 0 \\ 0 & 1 & 0 \\ 0 & 1 & 0 \\ 0 & 0 & 1 \\ 0 & 0 & 1 \\ 1 & 0 & 0 \end{vmatrix}$$

is an optimal design matrix for this problem. Note that in practice the sensors do not sense the exact projections of roll, pitch, and yaw rates, consequently, the equation $Y = Hx$ is not exactly true; there is noise present which has not been taken into consideration. These errors in the sensors shall be modeled by the equation $Y = Hx + u$, where u is a 6 x 1 random noise vector such that it has mean zero and the entries are uncorrelated with common variance $\sigma 2$. Thus $E(u)=0$ and the input covariance matrix Q is a scaler matrix as follows: $Q = \sigma^2 I$.

Notice that each sensor is assumed as good as the next and the random errors in any two sensors (even from the same gyro) are uncorrelated. A simple application of the Gauss Markov Theorem gives the best minimum variance linear unbiased estimate $\hat{x}$ of the true rate vector X and $\hat{X} = (H' H)^{-1} H'Y$ with output covariance matrix $R = \sigma^2 (H'H)^{-1}$.

Observing that the output covariance matrix is a function of the input variances and the Design Matrix H, it will be shown that the gyro orientation chosen with N=3 "minimizes the variances in R."

In this application

$$H_o = \begin{vmatrix} 1 \\ 0 \\ 0 \\ 0 \\ 0 \\ 1 \end{vmatrix} \quad H_1 = \begin{vmatrix} 0 \\ 1 \\ 1 \\ 0 \\ 0 \\ 0 \end{vmatrix} \quad H_2 = \begin{vmatrix} 0 \\ 0 \\ 0 \\ 1 \\ 1 \\ 0 \end{vmatrix}$$

and $H_o' H_1 = H_1' H_2 = H_1' H_2 = 0$. Furthermore, $H_o' H_o = H_1'H_1 = H_2' H_2 = 2$.

Here, $\hat{x} = (H'H)^{-1} H'Y$ and best estimates of roll, pitch and yaw $\hat{p} = 1/2 (A_1 + C_2)$, $\hat{q} = 1/2 (A_2 + B_1)$, and $\hat{r} = 1/2 (C_1 + B_2)$. The output covariance matrix for this particular design is $R = \sigma^2 (H 'H)^{-1}$. Hence,

$$R = \begin{vmatrix} \sigma^2/2 \\ 0 \\ 0 \end{vmatrix} \quad \begin{vmatrix} 0 \\ \sigma^2/2 \\ 0 \end{vmatrix} \quad \begin{vmatrix} 0 \\ 0 \\ \sigma^2/2 \end{vmatrix}$$

Thus, the output noise on each channel has been reduced by about 1/3, that is the output standard deviation equals 0.707 .

Similar examples can be given for 4, 5 or greater sensor situations.

It should be emphasized that the Pre-Filtering algorithm serves a dual function as it transformed the observations from sensor coordinates into body coordinates. Simultaneously the data was smoothed in some optimal statistical manner. In the post-filtering operation, usually only the latter function is performed and the data processing algorithms are generally simpler.

FAILURE DETECTION AND ISOLATION

FDI deals with the detection and isolation of both hard and soft failures. Soft failures are defined as partial failures such as component performance shifts while a hard failure is a complete or total failure of a device. As the sensor block previously described is usually a key item of failure concern, sensor FDI techniques lend a unique redundancy characteristic to this approach. With this technique it will be possible to continue uninterrupted operation without subsystem or higher level redundancy.

There is a sizable history of the application of FDI techniques to inertial sensing systems (since about 1964 at Kearfott for example). This early work was concerned with the skewing of redundant strapdown sensor triads. In addition to sensor error detection, this concept also provided the means for failure isolation by virtue of the fact that an instrument failure propagates an error vector with its own spatial orientation.

Extension of this work to cover non-orthogonal sensor configurations was next accomplished, particularly the dodecahedron configuration which has received much attention in the literature. This led directly to Kearfott's FDI extension to gimballed IMU's in 1969 (Ref. 2). Practically, in a gimballed application, the technique was a direct extension of earlier vector FDI studies. This approach has been granted a U.S. patent and will see its flight application when the Space Shuttle makes its first navigation flight. The effect will be the detection, isolation and possible replacement of soft-failed sensors in a redundant IMU system. Here, the sole interest is in the increased

reliability required for a space mission. FDI makes most sense, however, for a modular strapdown system as it affords both increased reliability and reduced system cost. This could for example make practical the application of inertial systems to most all commercial airliners, supplying reasonable flight control sensing and navigation.

FDI as defined, acts at the instrument level, detecting and isolating both soft and hard failures before they have had chance to propagate through the system. This is accomplished by having each sensor placed in a skewed orientation. A required orthogonal sensing triad is then formed mathematically from the sensed set of variables. Thus if a sensor fails, its output can be replaced by the composite output of other sensors. By skewing, the greatest degree of redundancy is obtained. In Figure 9, the direction of the sensing axes for the previously described sensor block is shown.

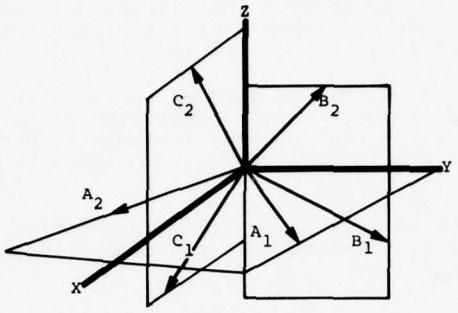

Fig. 9 Sensing Axes Spatial Orientation

Referring back to Figure 4, the sensors (gyros, accelerometers) in this particular configuration are mounted in orthogonal directions with their sensing axes skewed 45 degrees. As given in Figure 9, these sensor directions A's, B's, C's fall within a basic orthogonal triad. There is then a matrix H which transforms the sensed data into this orthogonal frame or:

$$\underline{X} = H\,\underline{Y}$$

where $\underline{Y}$ is the sensing frame and $\underline{X}$ is the orthogonal body computational frame. When a sensor failure occurs, the H matrix is restructured so that the components of the $\underline{Y}$ or sensor vector are not coupled into the $\underline{X}$ or measurement vector. Both acceleration and body rates are coupled into an orthogonal frame by the H matrix. As this sensor data is redundant, there are really two different measures of the $\underline{X}$ vector. By forming a difference vector where

$$\underline{\epsilon} = \underline{X}_1 - \underline{X}_2$$

a sensor failure can be observed by noting when this failure vector $\underline{\epsilon}$ is not zero. When a failure has occurred, $\underline{\epsilon}$ is non-zero and its vector direction falls in a plane of the failed sensor's input axes. For this technique to function properly, the skewed sensor axes must be chosen in such a way that they span the measurement space. This isolation of a failed sensor can be observed by transforming the error vector back to sensor coordinates as

$$\underline{Y} = H^{-1}\,\underline{X}$$

thereby directly indicating the faulty instruments.

This simple technique supplies a powerful method for the utilization of redundant sensors in a failure tolerant system. Of particular importance is the ability to detect both soft and hard failures. Soft failures such as caused by shifts in basic instrument parameters have heretofor been undetectable. Hard or complete instrument failures are still detectable by more ordinary BITE techniques but of course show up graphically with this FDI method. As might be expected, the level of fault detection does add some complexity. Actually, the failure vector ϵ will usually have some small value as no two sensors are really identical. Also, calibration and alignment variations, readout errors, etc. all add to a normal finite value for ϵ. Practical use of this type of sensor FDI then requires the setting of appropriate threshold tests. If such a threshold is set too low, then the probability of detection false alarms becomes a concern. False alarms are naturally to be avoided as they usually result in the removal of a properly operating sensor from the modular system. Thus this sensor is no longer available for system error improvement and redundancy uses. Effectively it is as if the sensor has failed. However, setting the threshold too high also presents difficulty as the probability of missed failures can become high. Figure 10 demonstrates this error threshold set on the error vector $\underline{\epsilon}$.

Here the failure threshold is shown as the radius ℓ of a sphere. In terms of the two failure vectors shown, vector ϵ_1 has exceeded this threshold. This constitutes error detection. Isolation will then be performed by resolving components of the vector $\underline{\epsilon}$. Failure vector ϵ_2 is a more typical case, of finite value but below the detection threshold ℓ.

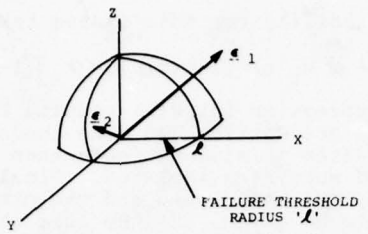

Fig. 10 FDI Error Threshold

Another way to look at this detection process is in terms of Gaussian distributed sensor errors. As no instrument is truly error free, this distribution exists with or without a failure. Figure 11 demonstrates these error distributions.

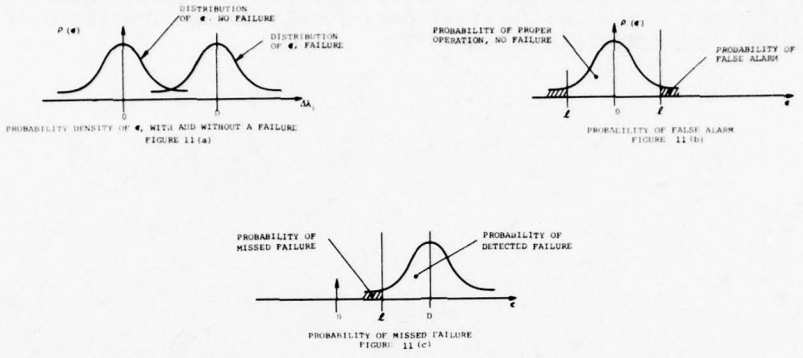

Fig. 11 Error Distribution

A failure in one of the modular sensors appears in the error vector $\underline{\epsilon}$ as a shift in the distribution. This is denoted by a new mean, D. As shown in 11-b, selecting a threshold level determines the area of proper FDI function i.e., no detection. The cross hatched area indicates the condition of false alarm i.e., in proper error indication. Adding a sensor failure to the system results in the shifted error distribution of Figure 11-c. Errors between the threshold 'ℓ' and the distribution 'D' are properly detected. However errors falling in the crosshatched area represent undetected failures. An obvious solution is the lowering of the FDI threshold 'ℓ'. This unfortunately also results in an increase in FDI false alarms. For a particular modular sensor application it is then necessary to first choose a threshold 'ℓ', and then calculate typical probabilities of detection.

These probabilities can be summarized in the following Table:

	NO FAILURE	FAILURE OCCURRED
Use instrument	$1 - \alpha$ II	β
Isolate and remove	I α	$1 - \beta$

TABLE 3. SYSTEM USE AND ISOLATION PROBABILITIES

Here, α is defined as the probability of a false alarm i.e., no failure has occurred but the sensing element is taken off-line. β is defined as the probability that a subsystem has failed but has not been properly isolated i.e., the failed element has not been removed.

For purposes of this discussion, it has been assumed that if A or B system fails and isn't isolated, the introduction of contaminated information into the total system would cause system failure. However, in general, the above statement is a simplification. Actually, where the threshold boundaries are set for the FDI, the specifics of the subsystems involved are the determining factors. Consequently the effect of system reliability with a failed redundant sensor must also be accounted for.

To evaluate system reliability, appropriate values of α and β should be given for each subsystem. These values are of course directly dependent upon the probability of detection and isolation. Once this is accomplished, total reliability can be formed using the theory of conditional probabilities. As an illustration, for the identical instrument X with reliability $R_x(t)$ positioned such that both are working but only one is needed for system success. Let α_x and β_x be the corresponding Type I and II

probabilities. Then the reliability for this system taking into account the FDI in

$$R(t) = R^2_x(t)\,[1-\alpha_x]^2 + 2\,R_x(t)\,[1-R(t)]\,[1-\alpha_x][1-\beta_x] + 2\,R^2_x(t)\,\alpha_x\,[1-\alpha_x]$$

The first term in the expression for R(t) results from the fact that the system is reliable when both subsystems are working and none isolated as a failure. The second term comes about since the system is also reliable when one subsystem has failed, the other working, and the failed subsystem isolated. Finally the system is working when both subsystems are operable, one being used and the other isolated due to a false alarm. Further examples could be given, but the idea should be clear, that total system reliability does depend on FDI effectiveness.

REFERENCES

(1) C.R. Giardina "Optimal Gyro Mounting Configurations for a Strapdown System" IEEE National Aerospace Electronics Conference (NAECON), Dayton, Ohio 1974.

(2) E.G. Solov and F.J. Pasquariello, "Unique Approach to Failure Detection and Isolation for Redundant Gimballed Inertial Measurement Units" Institute of Navigation (ION) National Space Meeting March 1972.

APPENDIX - COMPARATIVE RELIABILITIES

This Appendix includes the derivation of some of the comparative reliabilities for brickwall SKN-3000 type systems and modular derivatives as discussed in this paper.

SKN-3000 TYPE SYSTEM

SINGLE SYSTEM

This system consists of two 2-axis gyroscopes and 3 single-axis accelerometers, and one computer. Figure A-1 indicates this pictorially.

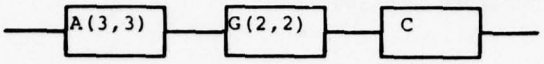

Fig. A-1 Single System, A(3,3) G(2,2)C

The notation used in the figure will be used throughout this section. A (n,m) will denote the condition of n accelerometer axes out of a total of m, remaining operating. Thus A(3, 3) denotes the condition of no axis failures. System reliability can then be written as:

$$R_S(t) = R_A^{\,3}(t)\, R_G^{\,2}(t)\, R_C(t)$$

Assuming exponential reliability,

$$R_S = e^{-(3\lambda_A + 2\lambda_G - \lambda_C)\, t}$$

Thus:

$$MTBF = \frac{1}{3\lambda_A + 2\lambda_G + \lambda_C}$$

DUPLEX SYSTEM

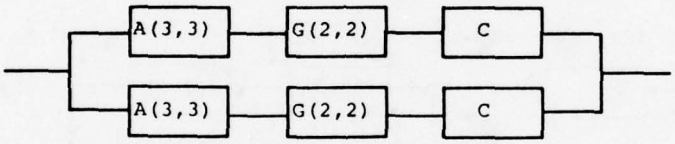

Fig. A-2 Two SKN-3000 in Parallel

The reliability of this configuration is:

$$R(t) = 1-(1 - R_S(t))^2$$

or

$$R(t) = 2R_A^{\,3}(t)\, R_G^{\,2}(t)\, R_C(t) - R_A^{\,6}\, R_G^{\,4}\, R_C^{\,2}$$

using exponential reliability:

$$R(t) = 2e^{-(3\lambda_A + 2\lambda_G + \lambda_C)\, t}\, e^{-(6\lambda_A + 4\lambda_G + 2\lambda_C)\, t}$$

thus:

$$MTBF = \frac{9\lambda_A + 6\lambda_G + 3\lambda_C}{(3\lambda_A + 2\lambda_G + \lambda_C)\,(6\lambda_A + 4\lambda_G + 2\lambda_C)}$$

TRIPLEX SYSTEM 3 C A (3,3) G (2,2)

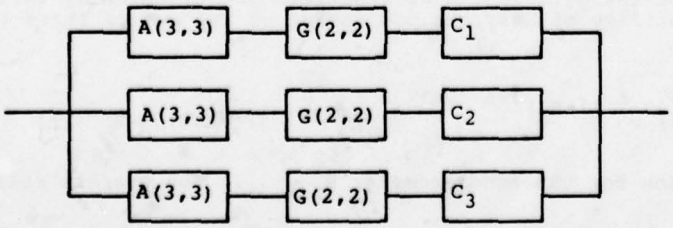

Fig. A-3 Triple Redundant SKN-3000

Therefore, for the triple redundant system the reliability is:

$$R(t) = 1 - (1 - R_S(t))^3$$

$$R(t) = 3R_A^3 R_G^2 R_C - 3R_A^6 R_G^4 R_C^2 + R_A^9 R_G^6 R_C^3$$

Assuming exponential reliabilities:

$$R(t) = 3\, e^{-(3\lambda_A + 2\lambda_G + \lambda_C)t} - 3e^{-(6\lambda_A + 4\lambda_G + \lambda_C)\, t} + e^{-(9\lambda_A + 6\lambda_G + 3\lambda_C)}$$

and

$$MTBF = \frac{3}{(3\lambda_A + 2\lambda_G + \lambda_C)} - \frac{3}{(6\lambda_A + 4\lambda_G + 2\lambda_C)} + \frac{1}{(9\lambda_A + 6\lambda_G + 3\lambda_C)}$$

DOUBLE REDUNDANT CROSS STRAPPED SKN-3000's

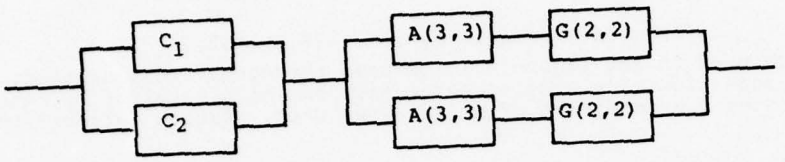

Fig. A-4 2C2 A(3,3) G(2,2)

For a configuration consisting of two computers in parallel in series with two orthogonal IMU's as in Figure A-4, the reliability is given below.

The reliability equals:

$$R(t) = (2R_C(t) - R_C^2(t))\ (2R_A^3 R_G^2 - R_A^6 R_G^4)$$

CROSS STRAPPED TRIPLE REDUNDANT SKN-3000

For the configuration of two computers in parallel in series with three IMU's as in Figure A-5. The reliability R(t) equals:

$$R(t) = (2R_C - R_C^2)\ (3R_A^3 R_G^2 - 3R_A^6 R_G^4 + R_A^9 R_G^6)$$

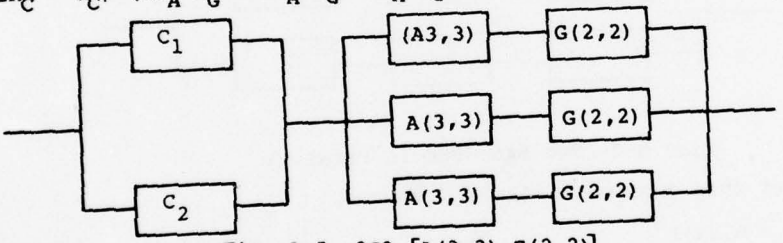

Fig. A-5 2C3 [A(3,3) G(2,2)]

MODULAR STRAPDOWN 2CG(2,3)A(2,3)

The configuration of Figure A-6 consists of two computers in parallel and in series with three TDF gyros of which two or mroe are needed in series with three accelerometers of which two are needed.

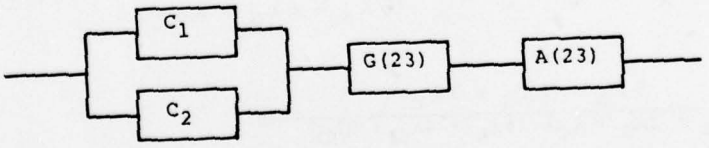

Fig. A-6 2CG(2,3) A(2,3)

The reliability of the gyros and accelerometers are binominally distributed. For example, the reliability of a system consisting of two out of three remaining operating is:

$$R_{G(2,3)} = \sum_{K=2}^{3} \binom{3}{K} R_G^K\ (1-R_G)^{3-k} = 3\ R_G^{\ 2}\ (t)\ (1-R_G(t) + R_G^{\ 3}\ (t)$$

and a similar expression for the accelerometer $R_{A(2,3)}$. The overall reliability can then be written as:

$$R(t) = (2R_C(t) - R_C^2(t))(3R_G^2 - 2R_G^3)(3R_A^2 - 2R_A^3)$$

MODULAR STRAPDOWN 3CG(2,4)A(2,4)

The reliability of the configuration in Figure A-7 consisting of three computers in parallel and in series with a (2,4) gyro configuration and a (2,4) accelerometer configuration is:

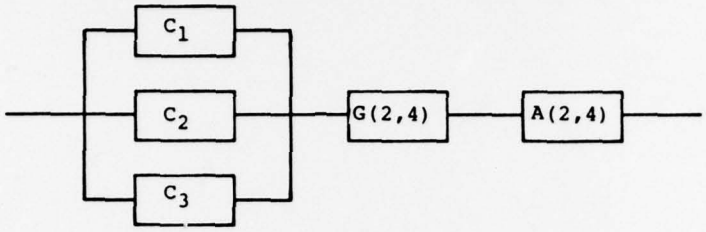

Fig. A-7 3CG(2,4)A(2,4)

The reliabilities for the gyro and accelerometers can be calculated binominally for the gyros and accelerometers. For example, the gyro reliability can be written as:

$$R_{G(3,4)} = \sum_{K=3}^{4} \binom{4}{K} R_G^{K} (1-R_G)^{4-K}$$

$$= 3R_G^4 (t) - 8R_G^3(t) + 6R_G^2 (t)$$

The accelerometer reliability is handled in a similar fashion.

Overall reliability can then be written as:

$$R(t) = (3R_C - 3R_C^2 + R_C^3)\ (3R_G^4 - 8R_G^3 + 6R_G^2).\ (3R_A^4 - 8R_A^3 + 6R_A^2)$$

DOUBLE REDUNDANT SYSTEM (FAIL-OP) WITH THREE COMPUTERS

The configuration is given below in Figure A-8.

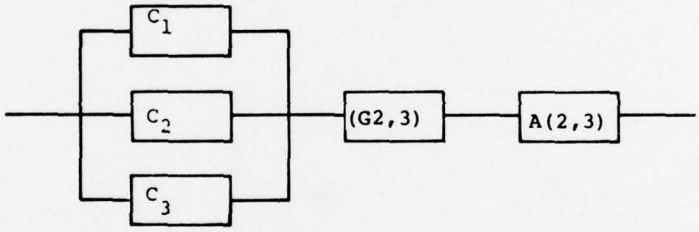

Fig. A-8 3CG(2,3)A(2,3)

The reliability of this configuration, consisting of three computers connected in parallel, all in series with three gyros and accelerometers each in a (2,3) configuration is:

$$R(t) = (3R_C - 3\ R_C^2 + R_C^3)\ (3R_A^2 - 2R_A^3)\ (3R_G^2 - 2R_G^3)$$

LISSAGE ET EXTRAPOLATION INERTIELS DE FAISCEAUX ILS

Application à l'AIRBUS A.300.B

par

J. IRVOAS et D. BUISSON
S.N.I.Aérospatiale
316, route de Bayonne, TOULOUSE, FRANCE

P. LLORET et X. LAGARDE
S.A.G.E.M.
6, avenue d'Iéna, PARIS, FRANCE

SUMMARY

One of the problems of automatic approach and landing is the accuracy of aircraft guidance as the aircraft flies along the ILS Beams. If the beam is noisy, or disturbed by undesirable reflections of the emitted signal on natural obstacles or on an aircraft which is flying over the localizer transmitter during its take-off, the lateral displacement and the roll movements of the aircraft could be very large. As far as ILS transmitter or receiver failures are concerned, they increase go-around probability, which is undesirable as far as the airlines are concerned. The system studied here can smooth the Loc data and ensure continuation of aircraft guidance in the event of a Localizer failure. This system only needs complementary speed information from an inertial sensor system in order to provide the auto-pilot with a filtered Loc signal instead of the raw signal. The final system, based on Kalman filtering, was implemented by means of a digital computer, then flight tested on the AIRBUS A.300.B.Certification of this system with reduced operational visibility minima is expected in the Spring of 1978.

NOTATIONS

y : écart latéral métrique de l'avion par rapport à l'axe de la piste.

η : écart angulaire entre la droite émetteur Loc-avion et l'axe de la piste, transformé en micro-ampères.

D : distance de l'avion à l'émetteur "localizer".

h : altitude de l'avion (ft) dans des axes liés à la piste d'atterrissage.

V : vitesse de l'avion.

$\Delta V_N, \Delta V_E$: erreurs constantes de vitesse de l'INS selon les axes respectivement Nord, Est, Transversal, longitudinal.
$\Delta V_T, \Delta V_L$

γ_N, γ_E : variations avec le temps des erreurs de l INS.
γ_T, γ_L

$\hat{x}$: estimation de la variable x par le filtre LIS.

S_ℓ, S_{ℓ_F} : sensibilité d'écart du faisceau Loc ($\mu A/_{deg}$) respectivement réelle et affichée dans le calculateur.

R, R_I : route, route indiquée par l'INS.

Ψ_{set} : cap géographique de la piste.

$\delta R_o = R_{I_o} - \Psi_{set}$: erreur de route à t = 0 (initialisation du Filtrage).

LIS : Loc-Inertiel Système.

LISS : Loc-Inertiel Statistique Système.

1 INTRODUCTION

L'utilisation de termes inertiels pour améliorer les modes de guidage de l'avion sur les faisceaux ILS (Instrument Landing System) a déjà été étudié, en particulier aux Etats-Unis. (réf. (1)). On peut ainsi espérer utiliser l'avion dans les conditions d'un atterrissage en Catégorie II alors que le faisceau lui-même n'est que de catégorie I.

En France, sous contrat des Services Officiels (Service Technique Aéronautique : STAé), et à la suite d'une demande de la Compagnie Air Inter, la SNIAS (Société Nationale des Industries Aérospatiales) et SAGEM (Société d'Applications Générales d'Electricité et de Mécanique) ont étudié un système qui permet une diminution du taux de remises de gaz jugées trop fréquentes sur certaines pistes équipées de faisceaux Loc (localizer) trop bruités ou brouillés par des phénomènes parasites.

Les objectifs du système ont donc été précisés en trois points :

1 - Lissage des informations "ILS" de catégorie II ou III afin de diminuer le taux d'approches manquées dues aux imperfections de l'ILS.

2 - Survie du système à une panne des émetteurs ILS à basse altitude lors d'approches en Catégorie II ou III, et, à plus long terme, en catégorie III sans hauteur de décision.

3 - Lissage des informations ILS de catégorie I en vue d'améliorer la qualité du guidage aussi bien en approche manuelle au directeur de vol qu'en approche automatique.

Les problèmes rencontrés par Air Inter concernent essentiellement l'axe latéral de guidage de l'avion ; le faisceau "localizer" est donc le principal intéressé. L'étude a été conduite en l'appliquant à l'avion AIRBUS A.300.B et à son pilote automatique latéral SFENA (Société Française d'Equipements pour la Navigation Aérienne) qu'on s'est efforcé de ne pas modifier. Le système est cependant universel et pourrait être appliqué au guidage en approche d'un avion quelconque.

Le système de filtrage a été défini à l'aide d'une simulation numérique de la boucle de guidage de l'avion sur ordinateur, puis programmé dans le calculateur SAGEM UTD avant d'être essayé sur le simulateur de vol "Airbus" en laboratoire, puis en vol sur l'Airbus n° 3 équipé d'une installation d'essais en vol adéquate.

2 PRESENTATION SUCCINTE DE LA SIMULATION SUR ORDINATEUR

Le schéma général de la simulation numérique est présenté figure 2.1. Il fait apparaître plusieurs sous-ensembles :

- mécanique du vol de l'avion, sous l'aspect des mouvements latéraux seulement

- pilote automatique latéral, qui élabore les ordres de commande à appliquer aux gouvernes de gauchissement et de direction (en particulier les modes MAINTIEN de LOC, puis ALIGNEMENT).

- les différents détecteurs placés à bord de l'avion sont :

  . un récepteur ILS (Localizer et glide) fournissant un courant proportionnel à l'écart angulaire entre l'avion et le faisceau : η_{mes} (μA) pour le faisceau LOC et ε_{glide} (μA) pour le faisceau glide.

  . un radio-altimètre fournissant l'altitude de l'avion $h_{R.A}$, différente de l'altitude réelle dans le repère d'axes liés à la piste à cause du profil du terrain survolé.

  . une centrale à inertie qui permet d'avoir dans le repère géographique local la vitesse de l'avion : V_{NI}, V_{EI} sont ses composantes selon les axes Nord et Est.

- le filtre LIS (Loc Inertiel Système), qui, à partir des informations ILS (η_{mes}, ε_{glide}), de l'altitude $h_{R.A}$ et des vitesses inertielles V_{NI} et V_{EI} reconstitue la position de l'avion $\hat{\eta}$ qu'on transmet au P.A. (position (2)) à la place de la sortie brute du récepteur Loc (position (1)).

Les différentes perturbations, qui agissent comme entrées de la simulation sont les suivantes :

- vent latéral et turbulences atmosphériques associées, selon la réglementation F.A.A. précisée dans la circulaire AC 20-57 A. Deux types de vent ont été utilisés :

  . V_Y = 10 KT (vent de face nul)

  . V_Y = 15 KT, vent de face V_X = 20 KT (total 25 KT)

  Les turbulences associées ont un spectre équivalent à celui d'un bruit blanc filtré par un filtre passe-bas du 1er ordre.

- bruits du faisceau Localizer.

  L'annexe 10 de la réglementation OACI (Organisation de l'Aviation Civile Internationale) donne les spécifications en ce qui concerne les coudes d'alignement des faisceaux "Localizer".

  La figure 2.2 présente la valeur maximum à ne pas dépasser avec une probabilité de 95 %. Toutefois ce document ne précise pas le spectre des bruits. Après l'étude de quelques faisceaux Loc français vérifiés en vol par le Service Technique Français de la Navigation Aérienne (S.T.N.A.), de même que quelques faisceaux américains (réf. (2)), le modèle de bruits aléatoires choisi est porté figure 2.3. Il correspond à un bruit blanc filtré par un passe-bas de constante de temps variable avec la distance de l'avion au seuil de piste. Le niveau du bruit est également variable avec la distance. Il est possible de superposer à ce bruit aléatoire une distorsion spatiale du faisceau de telle sorte que le niveau maximum toléré par l'OACI soit effectivement atteint.

- profil du terrain. L'altitude mesurée par une radio-sonde va servir à reconstituer la distance à l'émetteur Loc. Le profil du terrain influence donc le calcul. On peut donc simuler soit un terrain en moyenne plat, soit une pente positive ou négative du terrain. Des perturbations aléatoires représentant les accidents du terrain sondé ou les bruits de mesure, s'ajoutent au profil moyen.

- bruits du faisceau "glide". Nous supposons que, dans le plan vertical, l'avion est parfaitement stabilisé sur la trajectoire théorique de descente définie par le faisceau glide. Le bruit du faisceau glide n'est donc présent dans la simulation que comme perturbation du calcul de la distance à l'émetteur Loc. C'est à nouveau un bruit aléatoire généré par filtrage d'un bruit blanc.

- erreurs de vitesse de la centrale à inertie.

La centrale MGC 30 de SAGEM, choisie pour équiper (optionnellement) l'AIRBUS est du type à cardans, la mécanisation choisie étant du type "azimuth libre". On peut donc considérer que les erreurs sur chacun des axes Nord et Est sont indépendantes. Etant donné que le temps d'utilisation des vitesses par le système hybride est faible devant la période de Schüler (84 mn.), les erreurs de vitesse peuvent être approchées par une erreur constante et une dérive au cours du temps :

$$V_{N_{INS}} = V_{N_{vraie}} + \Delta V_N + \gamma_N . t$$

$$V_{E_{INS}} = V_{E_{vraie}} + \Delta V_E + \gamma_E . t$$

où ΔV_N , ΔV_T , γ_N , γ_E sont des constantes au cours d'une approche donnée.

3 DESCRIPTION DE LA VERSION CLASSIQUE DU FILTRE LIS 1 (VERSION N° 1)

SAGEM a initialement proposé une architecture classique pour le filtrage entre les informations localizer et les vitesses inertielles.

Ce filtre déterministe est à l'origine des premières études, puis des tout premiers essais en vol au CEV (Centre d'Essais en Vol) de BRETIGNY et ainsi a permis de vérifier les principes de base du système.

3.1 Principe.

Ce filtre utilise la technique du filtre complémentaire.

La position estimée de l'avion va être reconstituée à partir des informations radio-électriques du localizer et des informations de vitesse par rapport au sol de la centrale à inertie.

Les informations délivrées par le récepteur LOC sont disponibles sous forme d'écart angulaire entre la droite avion-émetteur localizer et l'axe piste.

On obtient l'écart métrique par rapport à l'axe piste grâce à la connaissance de la distance avion-émetteur et de la sensibilité du faisceau localizer.

$$y_{mes} = \eta_{mes} \cdot \frac{\hat{D}}{S\ell_F}$$

A partir des vitesses Nord et Est fournies par la centrale et du cap de la piste, on élabore la vitesse inertielle transversale de l'avion $\dot{y}_I$ (cf. figure 3.1).

Ces deux informations sont entachées d'erreurs de types différents :

- $y_{mes} = y_{vrai} + y_{bruit\ LOC}$

où $y_{bruit\ LOC}$ comprend les bruits radio-électriques et les distorsions de faisceau.

- $\dot{y}_I = \dot{y}_{vrai} + \Delta V_T$

où ΔV_T est la dérive constante (ou variant lentement) de la centrale à inertie.

ΔV_T comprend la dérive propre de la centrale à inertie et l'erreur due à la projection des vitesses Nord et Est sur une direction de référence légèrement distincte du cap géographique de la piste.

Cette dernière erreur est constante tant que la vitesse longitudinale de l'avion ne varie pas.

On forme alors le filtre complémentaire :

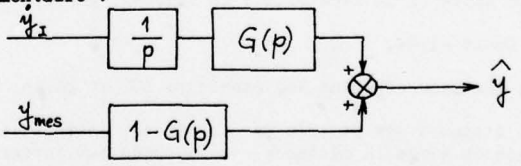

avec $G(p) = \dfrac{p^2}{p^2 + ap + bp}$

On obtient ainsi :

$$\hat{y} = y_{vrai} + \frac{p}{p^2 + ap + b}\ \Delta V_T + \frac{ap + b}{p^2 + ap + b}\ y_{bruit\ LOC}$$

Le bruit LOC est donc filtré par le filtre $\dfrac{ap + b}{p^2 + ap + b}$ tandis que les erreurs inertielles seront résorbées par le filtre dérivateur, à savoir : $\dfrac{p}{p^2 + ap + b}$

Le schéma d'un tel filtre est présenté figure 3.2

3.2 Réalisation.

Le bloc-diagramme du filtre complet est donné figure 3.4

Ce schéma comprend, outre l'élaboration d'un écart latéral, un filtrage inertiel de la distance

avion-émetteur localizer, nécessaire à la transformation des écarts angulaires en écarts métriques.

3.2.1 - Elaboration de l'écart latéral filtré.

Le système fournit deux estimations de l'écart latéral filtré, qui sont élaborées à partir de deux boucles similaires constituant deux filtres complémentaires de fréquence de coupure différentes :

La vitesse inertielle transversale est corrigée par la somme des sorties d'un passe-bas et d'un intégrateur de contre-réaction. Cette vitesse corrigée est intégrée pour donner l'écart calculé par rapport à l'axe de piste.

a) Boucle lente.

La pulsation de coupure de cette boucle diminue au cours du temps pour atteindre o,1 rd/s en fin d'approche.

L'erreur de position est filtrée afin d'obtenir une estimation de la variation de dérive de l'inertie.

b) Boucle rapide.

Sa pulsation de coupure est plus élevée : 0,55 rd/s.

L'erreur de position est redressée puis filtrée, elle permet d'obtenir une estimation du bruit recueilli sur le signal localizer.

c) Pondération.

L'écart latéral final est le résultat d'une double pondération :

- pondération des écarts calculés dans la boucle lente et dans la boucle rapide. D'une manière générale, plus le bruit ILS sera important, plus la boucle "lente" aura d'importance dans la pondération et réciproquement, plus la variation de dérive inertielle sera importante, plus la part de la boucle "rapide" sera grande.

- pondération pour transférer progressivement les informations d'écart latéral du signal LOC brut η_{mes} au signal LOC filtré $\hat{\eta}$; ceci afin d'éviter une discontinuité dans l'information transmise au pilote automatique.

d) Mise en inertie pure.

Lors d'une perte du faisceau LOC, l'écart latéral est calculé par l'intégration de la vitesse inertielle corrigée de l'estimation de dérive de la boucle lente.

3.2.2 - Elaboration de la distance émetteur LOC-avion.

Le principe est le même que pour le filtrage de l'écart latéral de l'avion par rapport à l'axe de la piste.

La distance métrique à l'émetteur localizer est calculée à partir des mesures glide et radio-sonde (figure 3.3):

$$D_{mes} = \frac{h_{RA}}{\gamma_g + S_g \cdot \varepsilon_{glide}} + d_{gl}$$

où h_{RA} est la hauteur radio-sonde,

γ_g, S_g sont la pente et la sensibilité du faisceau glide,

ε_{glide} est l'écart glide,

d_{gl} est la distance séparant les émetteurs LOC et glide.

Cette distance est filtrée par la vitesse inertielle longitudinale. En cas de perte des informations radio-sonde ou glide la distance est calculée par intégration de la vitesse inertielle.

3.2.3 - Initialisations.

Le filtrage de l'écart latéral est initialisé à la fin de la capture du faisceau localizer, lorsque l'avion est resté pendant 10 secondes au moins à l'intérieur du domaine défini par un écart localizer inférieur à 15 μA.

Le filtrage de la distance est initialisé lors de la capture du faisceau glide. Avant cette initialisation, qui intervient généralement après celle du filtrage latéral, on utilisera la distance brute dans les équations d'élaboration de l'écart latéral filtre, distance qui sera faussée par le fait que le récepteur glide donne un signal non proportionnel à l'écart angulaire réel.

3.3 Enseignements tirés de l'optimisation du filtre classique LIS 1.

Le filtre classique a fait l'objet des simulations décrites au paragraphe 2 et d'essais en vol au CEV. L'avantage de ces essais a été de procurer un moyen de trajectographie précise de l'avion, grâce au système à laser STRADA, permettant d'analyser finement les performances obtenues au cours de vols réels. Par ailleurs, le CEV de BRETIGNY s'est donné les moyens de "rejouer" à postériori les approches effectuées

à l'aide des enregistrements des données d'entrée du calculateur LIS.

Ces simulations se sont révélées un outil d'analyse très efficace, grâce à la possibilité de faire varier les paramètres de filtrage.

Les principaux enseignements tirés, aussi bien des simulations que des essais en vol, ont été les suivants :

- dans sa fonction de lissage, le filtre LIS 1 atténue significativement (division dans un rapport supérieur à 3) les distorsions du faisceau LOC situées dans une bande de fréquence supérieure à 0,03 Hz (périodes inférieures à 30 sec.). Cette atténuation est particulièrement nette au niveau des mouvements de roulis et de lacet de l'avion réduits dans un rapport 1/3 même en présence de faisceaux ILS réputés peu bruités.

- dans sa fonction de survie à une panne ILS à basse altitude ($h \leqslant 100$ ft), le filtre LIS 1 assure un bon guidage de secours : la précision à l'impact est de l'ordre de 3 m (à 1σ) dans les cas défavorables, résultat homogène avec la précision de l'estimation des erreurs inertielles en fin d'approche.

Le paragraphe 7 rend compte des principaux résultats obtenus. Cependant, il a été jugé souhaitable de poursuivre les efforts en vue d'éliminer certaines limitations inhérentes au filtre classique LIS 1. Voici les principales limitations rencontrées :

- si on cherche à obtenir une atténuation des distorsions du faisceau LOC dans les fréquences inférieures à 0,03 Hz, on obtient en contre-partie une erreur statique ("trainage") du filtre qui devient vite prohibitive et dégrade la précision d'impact obtenue sans ce nouveau système. Le réglage final fait apparaître une diminution de la précision d'impact de 3 % seulement (elle passe de 2,94 m à 1σ en guidage LOC à 3,03 m avec le guidage LIS 1), mais le lissage de la trajectoire est médiocre.

- un terrain montant ou descendant en amont de la piste entraîne des erreurs dans l'évaluation de l'écart métrique y_{mes} à partir de l'écart angulaire η_{mes}. Un effet similaire découle du fait qu'on utilise une valeur moyenne de la sensibilité du faisceau (75 μA/deg) alors que la valeur réelle peut varier de 55 à 110 μA/deg selon la longueur de la piste et la position respective des émetteurs. Ces différentes causes conduisent à une diminution de la durée de survie du système à une panne LOC, et même à la divergence de la boucle de guidage dans un cas extrême.

- enfin, la formulation classique ne permet pas d'estimer l'erreur entre la direction de référence pour la projection des vitesses et le cap géographique de la piste. Ce terme, peu important lorsqu'on ne se préoccupe que du guidage de l'avion à vitesse constante, intervient à chaque variation de vitesse et en particulier à la décélération sur la piste. Pour éviter ce problème avec la formulation LIS 1, la seule solution est l'introduction du cap de la piste sur laquelle on va atterrir dans le calculateur. Dans une formulation statistique, on a la possibilité d'évaluer ce terme pourvu que l'avion décélère suffisamment en cours d'approche.

La formulation statistique (filtre de Kalman) a donc été choisie pour les versions suivantes. Elle apporte d'ailleurs plus de souplesse dans la mesure où elle prend en compte les différentes possibilités d'initialisation qui dépendent de la procédure utilisée pour l'approche, alors que la formulation classique est optimisée pour une approche "standard".

4 DESCRIPTION DU FILTRE STATISTIQUE LISS

4.1 Principe - version n° 2 (LISS 2).

Afin d'avoir un filtrage optimal entre informations LOC et vitesses inertielles, il a semblé intéressant d'utiliser les équations du filtre de Kalman-Bucy. Pour cela, il faut écrire les équations d'état du système, en tenant compte, de plus, de l'évolution avec le temps de l'erreur de vitesse inertielle. Il vient :

$$\dot{y} = \dot{y}_I + \Delta V_T + \gamma_T \cdot t \qquad (4.1)$$

où ΔV_T et γ_T sont des constantes.

Le récepteur LOC fournit la position angulaire de l'avion, à la sensibilité près (observations du système) :

$$y_{mes} = \frac{\hat{D}}{S_{\ell_f}} \eta_{mes} = y + y_{bruit\ Loc} \qquad (4.2)$$

Nous supposerons ici que $y_{bruit\ LOC}$ est un bruit blanc. La méthode du filtre récursif de Kalman-Bucy, où les observations sont continues, nous permet d'évaluer les trois variables y, ΔV_T et γ_T à partir des mesures $\dot{y}_I$ et η_{mes}. Par rapport à la version classique du filtre LOC-Inertie, on a donc ajouté une boucle supplémentaire qui permet de fournir la dérive au cours du temps de l'erreur de vitesse de la centrale inertielle. Ce terme était cependant estimé dans la version LIS 1 par filtrage de l'erreur statique $\hat{y}$ - ymes.

4.2 Principe de la version n° 3 (LISS 3).

Les difficultés rencontrées avec la première version du filtre statistique viennent du fait que les erreurs du rapport $\frac{\hat{D}}{S_{\ell_f}}$ agissent de façon différente selon qu'il est sur ou sous-estimé par rapport au rapport de transformation réel $\frac{D}{S_\ell}$. Les recalages des estimations, compte tenu de l'indication du récepteur LOC, sont alors faussées.

Afin de reporter les erreurs dues à la mauvaise estimation de la distance non plus sur l'équation d'observation (4.2), mais sur l'équation d'état (4.1), une nouvelle formulation a été essayée. Elle consiste à utiliser comme variable d'état l'écart angulaire η au lieu de l'écart métrique y. Les nouvelles équations du système s'écrivent donc :

$$\dot{\eta} = \frac{S_\ell}{D}\left(\dot{y}_I - \Delta V_T - \gamma_T \cdot t\right) + \frac{V}{D}\eta \qquad (4.3)$$

$$\eta_{mes} = \eta + \eta_{bruit\ LOC} \qquad (4.4)$$

Toujours en supposant que $\eta_{bruit\ LOC}$ est un bruit blanc, nous pourrons écrire les équations du filtre de Kalman-Bucy pour évaluer les 3 variables $[\eta, \Delta V_T, \gamma_T]$.

Afin de diminuer l'influence des erreurs sur S_{ℓ_F} et $\hat{D}$, on utilise la technique de l'epsilon (ref. (3)) : elle permet de pondérer le calcul des 3 gains de recalage de la confiance placée dans les calculs par la méthode de Kalman.

4.3 Principe de la version n° 4 (LISS 4).

Les équations écrites jusqu'ici supposaient que la vitesse longitudinale de l'avion restait sensiblement constante pendant toute l'approche, depuis l'initialisation jusqu'à l'impact. Or, la sortie du train ou des volets hyper-sustentateurs nécessite une réduction de la vitesse de l'avion. Ces évolutions de vitesse provoquent des écarts de trajectoire au moment où elles surviennent, écarts provoqués par la différence entre la route de l'avion indiquée par la centrale à inertie au moment de l'initialisation du filtrage et le cap géographique réel de la piste. En prenant un modèle plus compliqué des erreurs de vitesse transversale, on peut espérer évaluer cette erreur de route, pourvu cependant que la vitesse de l'avion évolue pendant le temps de filtrage.

Le nouveau modèle de l'erreur de vitesse inertielle sera donc :

$$\dot{y}_I = \dot{y} + \Delta V_T + \gamma_T \cdot t + \delta R_o \left(V_{L_o} - V_{L_n}\right) \qquad (4.5)$$

où ΔV_T, γ_T et δR_o sont des constantes.

Les quatre variables d'état estimées par le filtre seront alors $\hat{x}^T = [\hat{\eta}, \Delta\hat{V}_T, \hat{\gamma}_T, \delta\hat{R}_o]^T$
La présence du terme $(V_{Lo} - V_{Ln})$ dans l'équation (4.5) rend le système non linéaire et l'évolution des covariances des différentes erreurs d'estimation dépend donc de l'évolution de la vitesse longitudinale de l'avion.

4.4 Intégration de la boucle élémentaire dans le schéma complet.

Les équations analogiques décrites ci-dessus ne sont pas programmables directement dans un calculateur numérique. D'autre part, les entrées issues des récepteurs radio sont des entrées analogiques qu'il convient donc de convertir numériquement pour les utiliser. Par ailleurs, la centrale à inertie transmet les composantes de la vitesse sol de l'avion au moyen d'une ligne BUS du type ARINC 571 à la fréquence de rafraîchissement de 5 Hz. Le pas de calcul choisi est donc de 0,2 sec. Il faudra calculer les différents gains de recalage à partir des diverses covariances des erreurs d'estimation selon la programmation discrète du filtre de Kalman-Bucy (réf. (3)).

L'organigramme général des calculs complets de filtrage est resté le même que pour la version classique (LIS 1) : il comporte la boucle d'évaluation de la distance de l'avion à l'émetteur "localizer", qui n'est active qu'à partir de l'apparition du signal logique indiquant que la capture du faisceau glide est terminée. La boucle d'estimation de l'écart latéral à transmettre au pilote automatique, telle qu'elle est décrite ci-dessus dans ses différentes versions, remplace les deux boucles lente et rapide et le calcul de pondération entre ces deux boucles d'estimation. L'initialisation du filtrage de l'écart latéral de l'avion par rapport à la piste a toujours lieu dès que la capture du faisceau LOC de l'ILS est terminée, à la commutation en mode "LOC-TRACK".

5 RESULTATS OBTENUS AVEC LE FILTRE STATISTIQUE EN SIMULATION

5.1 Statistiques de l'écart latéral à 100 ft, 15 ft et à l'impact.

Afin de vérifier l'avantage de la version n° 3 du filtre LISS par rapport aux versions n° 1 ou 2, 200 approches ont été simulées dans chaque cas :

- 100 en cas de pistes longues ($\bar{S}_\ell \approx 100\ \mu A/deg$), avec un terrain qui descend quand on s'éloigne de la piste de telle sorte que l'altitude mesurée soit de 2.000 ft alors que l'altitude comptée dans des axes liés à la piste d'atterrissage n'est que de 1.500 ft.

- 100 en cas de pistes courtes ($\bar{S}_\ell \approx 60\ \mu A/deg$), avec un terrain montant quand on s'éloigne de la piste (hvraie = 1.500 ft ; h mesurée = 1.000 ft).

Le vent traversier moyen étant toujours dans le même sens, les moyennes de l'écart latéral du centre de gravité de l'avion ne sont pas nulles. Pour avoir l'écart quadratique moyen pour un vent nul en moyenne il faut combiner le nombre d'approches simulées avec un nombre identique d'approches mais avec un vent latéral opposé. L'écart type du total sera alors $\sqrt{m^2 + \sigma^2}$. Nous avons porté sur le tableau 5.1 les statistiques dans les divers cas de guidage :

- LOC : à partir du signal LOC brut

- LIS 1 : à partir du signal hybride du filtre classique (n° 1)

- LISS 2 : à partir du signal hybride fourni par le filtre statistique ; version n° 2, de variables d'état (y, ΔV_T, γT)

- LISS 3 : à partir du signal du filtre statistique; version n° 3, de variables (η , ΔV_T, γT)

L'avantage des deux versions du filtre statistique sur le filtre classique est visible. Cependant, on voit que, en cas de guidage LISS 2, et pour une piste courte, le gain est très faible par rapport au guidage LOC. La version n° 3 du filtre statistique résoud ce problème, mais, par contre, les dispersions ont légèrement augmenté quand l'avion atterrit sur une piste longue. C'est cependant la version LISS 3 qui a été retenue pour la programmation définitive du filtrage LOC-Inertiel, car elle aplanit les différences rencontrées avec les autres versions pour les divers types de piste d'atterrissage.

- 400 nouvelles approches ont été simulées avec le filtre LISS 3, afin de combiner les diverses possibilités de vent (vent fort - vent faible) et de pistes (pistes moyennes - longues - courtes). Au total, en ajoutant les 600 approches obtenues avec un vent opposé, il s'agit de 1.200 approches dont les statistiques sont portées tableau 5.2. L'apport du filtre statistique sur le lissage de la trajectoire est net puisque l'écart-type de l'écart latéral aux passages à 100 ft, à 15 ft et à l'impact a diminué de 5% à 8% par rapport au guidage LOC alors qu'on perdait de 3 à 7 % dans le cas du guidage hybride à l'aide du filtre classique. Le paramètre lambda de trajectoire entre 700 ft et l'impact a également beaucoup diminué (- 30 %).

- Enfin 200 approches ont été simulées en considérant que les erreurs de vitesse de la centrale sont divisées par 2. Leurs résultats sont portés tableau 5.3 par comparaison aux résultats du guidage hybride mais avec les performances de la centrale nominales. On ne constate pas de différences sensibles, si ce n'est sur les valeurs maximum, c'est-à-dire que la qualité de la centrale inertielle n'a pratiquement pas d'influences sur le résultat final.

5.2 Exemples de trajectoire.

Avec un exemple de bruit de faisceau et de turbulence atmosphérique comme définis au paragraphe 2, les trajectoires en cas de guidage LIS 1, puis en cas de guidage LISS 2 ou 3 sont comparées à celles obtenues avec le guidage LOC pur. Ce sont les figures 5.4 et 5.5. La trajectoire est aussi perturbée avec le filtre classique LIS 1, puis devient meilleure avec le filtre statistique. La sensibilité aux bruits de faisceau est plus importante dans les premiers instants du filtrage avec la version LISS 3 qu'avec la version LISS 2. A partir de la capture glide, la trajectoire est identique quelle que soit la version du filtre statistique.

Pour la même approche, nous avons porté les corrections apportées par le filtre à la vitesse transversale calculée à partir des indications de vitesse inertielles. Nous voyons qu'avec le filtre classique (figure 5.6), les bruits de faisceau ont beaucoup plus d'influence qu'avec le filtre statistique (figure 5.5)

5.3 Mouvements autour du centre de gravité de l'avion. Agitations des gouvernes.

Les mouvements autour du centre de gravité de l'avion, traduits par les paramètres de dérapage (β), d'assiette latérale ($\phi 1$), de cap ($\Delta\psi$), de route (ΔR_Y) ou d'accélération latérale (a_{y_1}), de même que l'assiette latérale commandée par le pilote automatique (- ϕc) et les braquages des gouvernes de gauchissement (δ_{p_Y}) et de direction (δr_j) sont provoqués par les bruits de faisceau LOC et par les turbulences atmosphériques. Vis-à-vis des perturbations de l'atmosphère, le comportement de l'avion n'est pas modifié car on s'est imposé de ne pas toucher au pilote automatique en mode "maintien de LOC". Quant aux bruits de faisceau, ce sont leurs hautes fréquences qui agissent sur ces paramètres si bien que la présence d'un filtrage LOC-Inertiel devrait être très bénéfique. Les écarts-type de ces différentes variables sont portées sur le tableau 5.8. Ils sont calculés tout au long d'une seule approche, celle déjà utilisée pour les exemples de trajectoire au paragraphe 5.2. Le filtre classique apportait déjà un gain appréciable, mais le filtre statistique est encore meilleur.

5.4 Pannes du faisceau LOC : disparition avec drapeau de panne à h = 100 ft.

Le système de guidage hybride radio-inertie doit être capable de guider l'avion en cas de panne de l'émetteur "localizer" entraînant la disparition du faisceau et l'apparition d'un signal d'alarme sur le récepteur à bord de l'avion. Nous supposerons ici qu'il existe un système de confirmation de la position de l'avion, alors que ce dernier suit le faisceau glide et atteint l'altitude de 100 ft. Ce système, étudié par le SENA, permet, en fournissant la position latérale de l'avion, de savoir si les derniers moments de l'approche se sont bien ou mal passés, et, par conséquent si le faisceau LOC était correct ou pas. Nous supposons que l'émetteur tombe en panne aussitôt après ce test. Afin de bien situer les performances de la survie du système à cette panne, nous avons simulé 200 approches dans ce cas, dont 100 avec une piste moyenne où distance et sensibilité sont bien évaluées et 100 dans le cas contraire (piste courte). Les statistiques de l'écart latéral sont portées sur le tableau 5.9.

Deux remarques peuvent être formulées :

- pour les pistes moyennes, les deux filtres LIS 1 et LISS 3 ont des performances comparables : avec le filtre statistique il se produit une diminution de l'écart type, mais une petite augmentation des valeurs maximum.

- pour les pistes courtes, le filtre statistique permet de beaucoup mieux guider l'avion à partir des informations inertielles seulement. Les corrections à apporter à la vitesse transversale de l'avion ($\dot{y}_I$) sont donc beaucoup plus justes.

La durée de survie du filtre statistique ne dépend donc pas du type de piste sur lequel l'avion va atterrir. Elle est, au minimum, de 16 à 20 sec., c'est-à-dire que quand la panne a lieu au passage à 100 ft, le guidage de l'avion jusqu'à l'impact est correct, même si celui-ci est tardif dans le cas d'un arrondi plus long que la normale. La version LISS 4, permet de plus, pourvu que la procédure d'approche fasse apparaître une variation de vitesse de l'avion pendant le filtrage, un guidage correct jusqu'à des vitesses très faibles, de telle sorte que la catégorie IIIB d'atterrissage puisse être envisagée, même en cas de panne définitive du LOC.

5.5 Anomalies détectées de faisceau LOC (créneaux - rampes).

Nous supposons ici que l'axe du faisceau LOC se décale brutalement de 20 μA (créneau) ou lentement avec une vitesse constante (rampe). Le moniteur placé au seuil de piste surveille l'alignement du centre du faisceau : dès que celui-ci dépasse une distance correspondant à $\pm$ 8,5 μA (valeur valable pour les faisceaux de catégorie III), pendant plus de 2 secondes, le mauvais alignement est détecté et nous supposons que le premier ensemble d'émission est mis hors série et est remplacé par le second ensemble en moins de 1 sec. L'émission correcte reprend donc au bout de 3 sec. au maximum.

L'écart de trajectoire varie en fonction de l'altitude de l'avion au moment de l'anomalie LOC. Les figures 5.10 et 5.11 présentent le comportement de l'avion dans 3 cas de créneaux (h = 1.000 ft, 500 ft et 100 ft) et dans 2 cas de rampes (h = 1.000 ft, dérive du faisceau de 0,1 μA/sec. et h = 500 ft, dérive de 2 μA/sec.). En ce qui concerne les anomalies brutales du faisceau, l'apport du filtre statistique est très net, tandis que pour les divergences lentes du faisceau, il n'y a aucune amélioration, quel que soit le type du filtre qui assure le guidage de l'avion.

5.6 Anomalies non détectées du faisceau LOC.

Ce paragraphe concerne les anomalies spatiales ou temporelles du faisceau LOC que le moniteur placé à l'entrée de piste ne peut pas détecter car elles ne provoquent pas de dépassement du seuil de détection. Il s'agit d'abord d'un saut brutal de l'axe du faisceau d'un bord à l'autre du seuil ($\pm$ 8,5 μA) alors que l'avion est à h = 500 ft, puis d'une courbure en forme de sinusoïde à une période de 50 sec. (V $\simeq$ 70 m/s) qui commence alors que l'avion termine son palier à 1.500 ft et passe en descente le long du faisceau glide, et enfin d'une seule période de sinusoïde décalée de l'axe de la piste (figure 5.12).

Pour toutes ces perturbations, le guidage hybride apporte une très légère amélioration, mais les périodes de ces phénomènes sont importantes, et dans ce cas, il est très difficile de filtrer : le filtrage devient plus net pour des périodes inférieures à 50 secondes.

5.7 Interférences dues à un avion survolant l'émetteur LOC.

Le Royal Aircraft Establishment (R.A.E.) anglais a étudié ce phénomène (réf. 4) provoqué par un avion qui survole l'émetteur LOC au cours de son décollage alors que l'avion considéré commence son approche. On obtient, par exemple, un bruit ramené au niveau de la sortie du récepteur LOC tel que celui présenté sur la figure 5.13 (a). Les planches 5.13 (b) et (c) donnent le comportement de l'avion sans guidage LOC ou avec les filtres classique (LIS 1) et statistique (LISS 3). La trajectoire est nettement lissée, en même temps que les mouvements de roulis et de cap sont réduits dans un rapport de 3 à 4 selon le paramètre considéré.

5.8 Comportement du filtre en présence de bruits de faisceau LOC réels (enregistrés en vol).

Les faisceaux LOC enregistrés en vol, qui nous ont déjà servi pour trouver un modèle représentatif des bruits de faisceau afin de les reconstituer, ont été également utilisés en simulation. Leur inconvénient est cependant qu'ils sont limités en temps total et que le temps de filtrage n'est pas assez important pour que le lissage soit net. La figure 5.14 montre les trajectoires obtenues sur trois faisceaux LOC américains. Pour celui de LOS ANGELES (fig. 5.14 c), nous avons considéré que le bruit était nul avant l'enregistrement réel pour augmenter le temps de filtrage. Nous avons alors un meilleur lissage que dans le cas où l'initialisation est tardive (fig. 5.14 b).

5.9 Influence du mouvement longitudinal de l'avion.

Du fait d'une variation de vitesse à la capture glide par exemple (au moment de la sortie du train et de l'affichage de VREF à l'automanette) la version LISS 3 du filtre statistique entraîne des écarts de trajectoire qui se résorbent ensuite et n'ont aucune conséquence sur l'écart latéral à l'impact. Afin de réduire ces écarts latéraux, la version LISS 4 a été implémentée. On voit très nettement cette réduction figure 5.15. Cette dernière version permet donc de diminuer les effets de changements de vitesse sol obtenus en cas de gradient de vent ou d'approches volontairement décélérées et a l'avantage de permettre le guidage automatique de l'avion au freinage sur la piste au cas où une panne LOC survient en fin d'approche. De plus, les résultats obtenus quand la vitesse de l'avion est constante ne sont pas changés.

6 DESCRIPTION DU LOC-INERTIEL SAGEM - LIS 30 :

6.1 Intégration dans l'avion.

Le système numérique LOC-Inertiel a été conçu pour être transparent au pilote automatique, c'est-à-dire qu'il s'insère dans le câblage avion entre les récepteurs ILS et les calculateurs du pilote automatique, sans modification de ces derniers.

Il reçoit les informations d'écart du récepteur de l'ILS, les informations de vitesses Nord et Est de la centrale inertielle et l'information de hauteur de la Radio-Sonde.

Il restitue vers le pilote automatique des informations d'écart, électriquement analogues à celles du réceptuer ILS, mais lissées par la centrale inertielle.

Il assure la survie du guidage en cas de perte ILS ; d'autre part, en cas d'anomalie, le système se met fonctionnellement en court-circuit et le pilote automatique se trouve alors couplé directement au récepteur ILS.

6.2 Description du système.

- Caractéristiques physiques : La taille du système est $\frac{1}{2}$ ATR conforme à la norme ARINC 404 A. Sa masse est de 12 kg maximum, sa consommation ne dépassant pas 150 W.

- Organisation du système : Le système est organisé autour d'une unité de traitement digital, l'UTD. La totalité des traitements d'information, ainsi que la plus grande partie des tests de surveillance sont effectués dans l'UTD par le programme.

Des systèmes d'entrée-sortie permettent l'acquisition des grandeurs d'entrée par l'UTD et la conversion des grandeurs de sortie en un format assimilable par l'utilisateur.

- L'UTD : C'est un calculateur universel, à organisation parallèle sur 16 bits et dont l'unité de contrôle est microprogrammée.

Les principales caractéristiques sont résumées dans le tableau 6.1.

Pour le calculateur du LIS 30, la mémoire implantée sera de 4 K mots programme et 1 K mots de mémoire travail.

- Mémoire reprogrammable : La mémoire programme est du type effaçable et reinscriptible, ceci directement sur les cartes mémoires, ce qui confère au calculateur une grande souplesse pour les modifications du programme.

- Le codeur : Il permet l'acquisition des grandeurs analogiques (signaux LOC, glide et radio-sonde) et la conversion de l'information de sortie (LOC filtré) dirigée vers le pilote automatique.

résolution : 12 bits
précision : $\pm \frac{1}{2}$ LSB

- Les entrées-sorties numériques : Elles permettent l'acquisition et l'émission des signaux discrets, des données numériques en provenance des centrales inertielles par l'intermédiaire d'une ligne BUS, et enfin le dialogue inter-systèmes dans le cas d'une architecture à deux voies de calcul.

6.3 Fonctionnement en Mono et bicalculateur.

L'installation de base des pilotes automatiques de l'AIRBUS a un niveau de redondance particulièrement élevé pour obtenir la catégorie III grâce à l'utilisation :

- de 2 jeux de détecteurs auto-surveillés (ILS et Radio-Sonde)

- de 4 voies de calcul dans les pilotes automatiques.

Ce niveau est plus faible pour la catégorie II (2 voies de calcul sur un jeu de détecteurs auto-surveillés).

Afin de s'intégrer à l'architecture actuelle de l'AIRBUS, le système LISS 30 est capable des deux configurations suivantes :

- Mono-calculateur : Utilisation d'un seul calculateur en association avec un seul côté du pilote automatique.

- Bi-calculateur : Utilisation de deux calculateurs, l'un étant associé au côté 1, l'autre au côté 2.(figure 6.2).

Une ligne numérique permet le dialogue entre les deux calculateurs afin de réaliser des tests de vraisemblance entre les deux chaînes.

6.4 Détection de panne.

- Mise en "court-circuit" : Du fait que le système LISS 30 s'intercale entre le récepteur ILS et le pilote automatique on lui demande de se mettre en court-circuit sur une panne détectée : c'est-à-dire que par un jeu de relais on restitue le signal localizer brut à l'entrée du pilote automatique (système transparent).

- Autotests du système : Un résultat négatif de l'un de ces tests entraîne une mise en court-circuit du système :

  - test calculateur (microprogramme)
  - contrôle de l'exécution du logiciel (matériel)
  - test des mémoires mortes (logiciel)
  - test des mémoires vives (logiciel)
  - test des opérations (logiciel)
  - test du codeur (logiciel)

- Tests de vraisemblance intercalculateurs : Ces tests sont réalisés dans le cas de l'architecture bi-calculateurs. Si une différence apparaît entre les deux chaînes, les deux systèmes LISS 30 sont mis en court-circuit.

- Panne du senseur inertiel auto-détectée : Le système devient transparent.

- Panne localizer : Lorsqu'une panne localizer intervient on assure une survie inertielle du guidage pendant un délai dépendant de la convergence du filtre. Ce délai passé on met le système en court-circuit.

En-dessous de 100 ft, la survie inertielle est assurée jusqu'au sol.

- Panne glide ou radio-sonde : Les informations glide et radio-sonde permettent d'évaluer la distance à l'émetteur localizer. Cette distance est filtrée à l'aide de la vitesse inertielle et en cas de panne de l'un des deux senseurs radio, une survie inertielle est assurée pendant un délai dépendant du temps de filtrage. Ce délai de filtrage passé, on met le système en court-circuit.

En-dessous de 250 ft, la distance est calculée à l'aide des vitesses inertielles seulement, le signal glide n'ayant plus aucune signification dès que l'arrondi est commencé.

6.5 Sortie pour enregistrements.

Les calculateurs prototypes sont équipés d'une sortie numérique pour enregistrements, qui se présente sous forme d'une ligne BUS à 2 fils.

Cette sortie émet 17 mots de 24 bits tous les cycles de calcul (paramètres d'entrée, sortie, signaux internes de logique et paramètres internes de filtrage). Elle permet une analyse rapide des phénomènes rencontrés en vol.

7 ESSAIS EN VOL AU C.E.V. :

7.1 Historique.

C'est au C.E.V. (Centre d'Essais en Vol) de BRETIGNY qu'eurent lieu les toutes premières évaluations du LOC inertiel.

Ces essais se sont déroulés durant 1975. Les calculs de filtrage étaient effectués en temps réel par un calculateur industriel embarqué à bord d'un NORD 262.

Le filtre proposé par SAGEM était de structure très simple : il était composé d'une boucle élémentaire de la version classique (LIS 1).

Cependant, les résultats obtenus ont été très encourageants et ont permis de confirmer la faisabilité du système.

Au début de 1976 l'évaluation du LOC-Inertiel a été poursuivie par des simulations au sol réalisées à partir de données enregistrées en vol.

Cette technique a permis une première étude de la version classique du filtre (LIS 1).

Toutefois ces essais étant réalisés hors de la boucle de pilotage avion, ils n'ont pu mettre en évidence les performances du système couplé à un pilote automatique.

7.2 Essais en vol du calculateur SAGEM LIS 30.

Un calculateur LIS 30 programmé dans la version classique a été essayé en vol au C.E.V. de BRETIGNY en décembre 1976 sur un NORD 262 puis à nouveau à partir de Mars 1977 sur un Mystère 20.

Dans les deux cas le LIS 30 était couplé au Pilote automatique de l'avion.

Le programme d'essais en vol se compose d'une étude statistique à BRETIGNY (50 à 60 approches) et d'une série d'explorations de terrains aux ILS réputés mauvais.

A BRETIGNY, la trajectographie STRADA (à base de télémétrie LASER) a permis d'évaluer les performances du système.

Sur les terrains extérieurs la trajectographie est déterminée par des moyens embarqués (inertie recalée avec une caméra).

Ces essais doivent se poursuivre avec un calculateur programmé dans la version statistique d'ordre 4. Pour tous ces essais, la centrale inertielle utilisée est une centrale SAGEM MGC 30.

7.3 Premiers résultats du filtre classique LIS 1.

Les essais du système LIS 30 se poursuivent au C.E.V. A ce jour, une cinquantaine d'approches réalisées à BRETIGNY avec la version classique sur l'avion NORD 262 ont pu être exploitées. Grâce au système de trajectographie STRADA, les performances du système ont pu être évaluées, tant pour la restitution de la position de l'avion que pour l'évaluation des erreurs inertielles.

A l'aide des enregistrements des données d'entrée du système LIS 30, une vingtaine d'approches ont pu être simulées en introduisant le cap géographique vrai de la piste comme direction de référence. Le tableau 7.1 donne les performances de filtrage dans le cas normal (utilisation de la route inertielle au moment de l'initialisation) comparées au cas de l'utilisation du cap piste réel. De la même façon, le tableau 7.2 donne les performances de guidage de l'avion dans le cas d'une mise en inertie pure à 100 ft. On notera l'amélioration très nette qu'apporte l'utilisation du cap piste réel sur le guidage de l'avion après l'impact. Une approche a été effectuée avec un fort gradient de vent entraînant une variation de vitesse de 50 KTS Ce cas avait donné une erreur importante à l'impact dans le cas normal (8 m). Avec l'introduction du cap piste, ce cas extrême disparaît.

En résumé, les essais en vol permettent de conclure que le filtre classique permet sans introduction du cap piste, une survie inertielle jusqu'à l'impact, pourvu que l'approche s'effectue à vitesse sol constante.

Si l'on introduit le cap piste réel, la survie est assurée au roulage et l'approche peut être

effectuée avec des variations de vitesse.

8 ESSAIS A LA S.N.I.AEROSPATIALE

8.1 Essais au simulateur de vol.

Après les essais en vol au C.E.V. de la version classique du système LOC-Inertiel, les nouvelles équations de filtrage (LISS.3) ont été programmées dans un second calculateur numérique SAGEM. Avant de le monter sur l'avion, ce calculateur a été placé au laboratoire de simulation du vol de l'Aérospatiale à TOULOUSE-BLAGNAC, couplé aux équipements réels de l'AIRBUS. Les essais ont permis de mettre à jour quelques petites fautes de programmation ou de câblage de l'avion. Les corrections ont été rapidement exécutées, en particulier à l'aide des mémoires reprogrammables. De nouveaux essais, dans les mêmes conditions que la simulation sur ordinateur, ont permis de retrouver exactement les résultats obtenus auparavant.

8.2 Essais sur l'AIRBUS A.300.B n° 3.

Le calculateur LISS 30 a été ensuite mis à la disposition des essais en vol de AIRBUS-INDUSTRIE. Un premier vol (25.3.77) a permis de vérifier le bon fonctionnement du système, aussi bien en mode de filtrage normal qu'en cas de panne simulée du signal localizer. La modification du programme de filtrage pour passer de la version LISS 3 (où seulement 3 variables sont estimées) à la version LISS 4, qui comporte quatre estimations a été opérée en une semaine. Un bref passage au simulateur de vol a permis de vérifier le fonctionnement du système, puis, de nouveau les essais en vol ont repris. Grâce au système d'enregistrement en vol des paramètres de l'avion et des paramètres internes du système, il a été possible de comparer les estimations du système réel avec les estimations obtenues par le programme de simulation. La précision moins importante du calculateur réel (32 bits pour les paramètres critiques) n'a pas entraîné d'erreurs supérieures à 1 %, même après un temps de filtrage important.

L'AIRBUS n° 3 est allé ensuite explorer quelques faisceaux localizer bruités. L'amélioration du confort pour l'équipage a été très nette : trois approches étaient accomplies sur chaque terrain, l'une sans le système LISS (boucle ouverte), la seconde avec le système dans la boucle de guidage (boucle fermée), puis la dernière toujours en boucle fermée, mais avec une panne du signal LOC à 100 ft. Le comportement du système a été satisfaisant, même en cas de freinage sur la piste, jusqu'à l'arrêt de l'avion, alors qu'avec la version précédente (LISS 3), le pilote était obligé de déconnecter le Pilote Automatique dès que la vitesse commençait à diminuer fortement ($V \leq 100$ KTS).

9 CONCLUSIONS

Le guidage hybride radio-inertie que nous venons de vous présenter permet donc :

- le lissage de la trajectoire de l'avion au cours d'une approche automatique le long des faisceaux ILS, en particulier dans sa phase finale ($h \leq 700$ ft).

- une très nette réduction des mouvements latéraux de l'avion autour de son centre de gravité et des agitations des gouvernes dus aux bruits du faisceau LOC.

- la survie du guidage au cas où une panne apparaît sur le récepteur LOC. Si cette panne commence alors que l'avion passe à 100 ft, la durée de survie est de 20 à 25 secondes, c'est-à-dire que l'impact est assuré, même dans le cas d'un atterrissage long. Pourvu qu'il y ait eu une variation de vitesse au cours du filtrage, la survie quand l'avion freine sur la piste est également assurée.

- Au cas où des anomalies importantes et brutales (de période inférieure à 50 sec.) perturbent le guidage de l'avion, le système LISS permet de ne plus tenir compte du signal LOC et réduit les mouvements de l'avion.

- Le système ne nécessite qu'une centrale inertielle de performances relativement faibles (CEP $\leq 2{,}5$ NM/h), une centrale meilleure améliorant légèrement les choses.

Ce système devrait ainsi permettre d'opérer sur une piste d'atterrissage dans les conditions météorologiques de la catégorie supérieure à celle du terrain envisagé, tout en assurant un meilleur confort pour les passagers. Quant au taux de remises de gaz dues aux pannes ou aux anomalies du faisceau "localizer", il devrait être diminué par la présence de ce système pour le guidage de l'avion.

REFERENCES :

1 R.J. BLEEG, H.F. TISDALE, R.M. VIRCKS (Boeing Company) "Inertially augmented automatic landing system (A/P performances with imperfect ILS Beams)"
F.A.A. Contract RD-72-22 (April 1972).

2 Bendix Corporation - Eclipse - Pioneer Division "Analytical study of ILS Beam Characteristics"
F.A.A. Contract ARDS-451 (August 31, 1962).

3 P. FAURRE "Navigation inertielle optimale et filtrage statistique"
Collection "Méthodes mathématiques de l'Informatique" - Ed. DUNOD - PARIS (1971).

4 N.H. HUGHES, M.A. "The effects on Automatic Landing Lateral Performance of interference to the ILS localizer by reflection from an aircraft taking off"
R.A.E. Technical Report 68156 (june 1968).

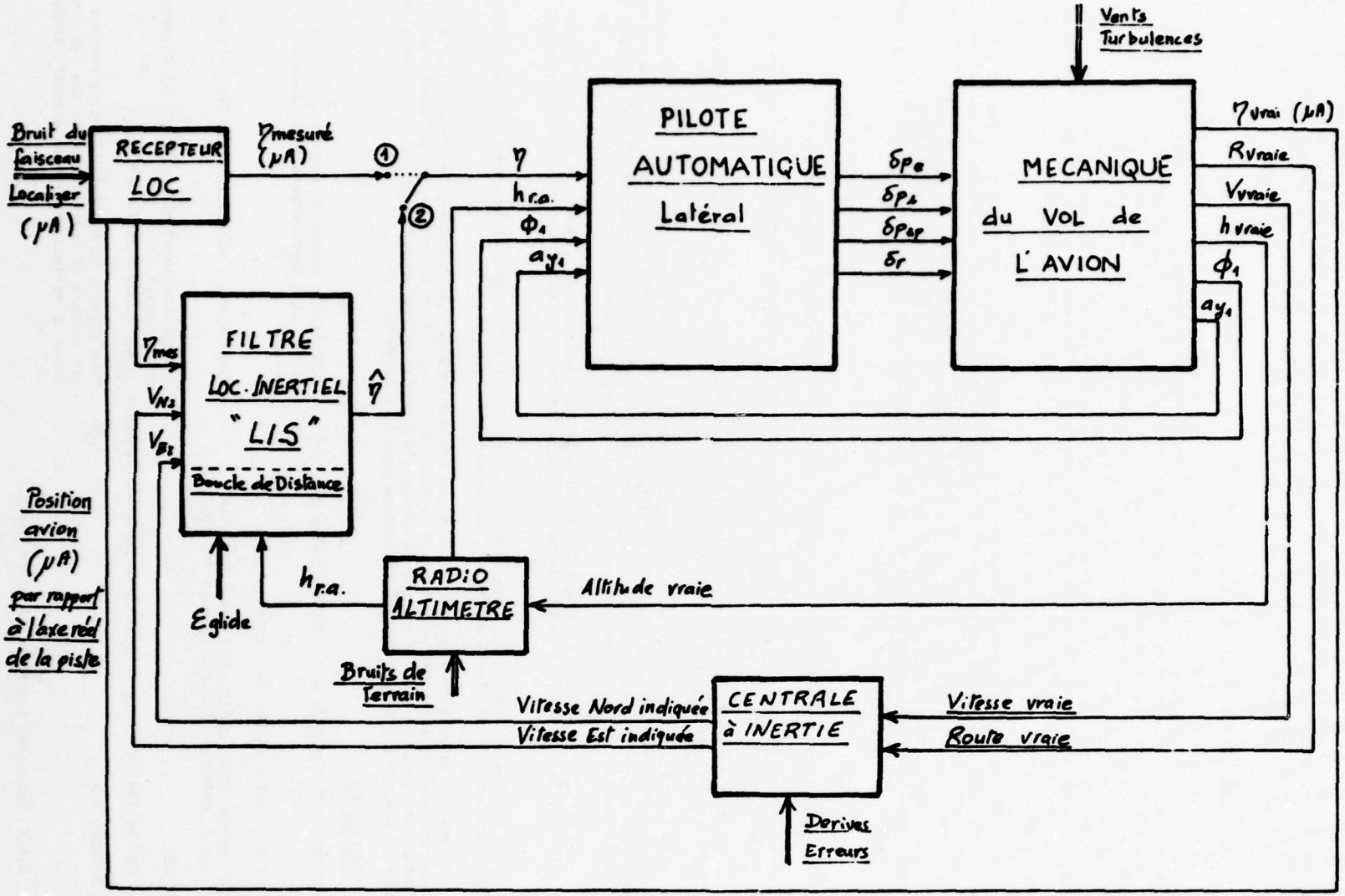

SCHEMA de la SIMULATION

Figure 2.1

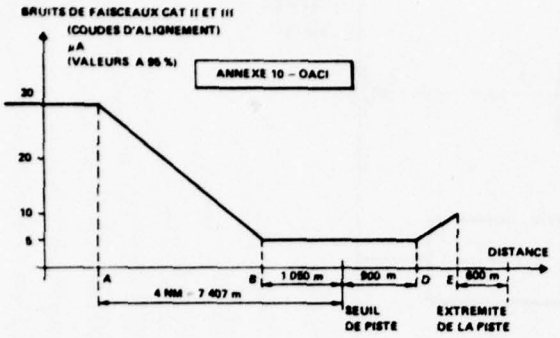

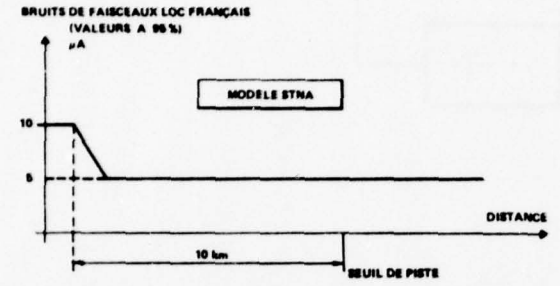

MODELES DE BRUITS DE FAISCEAUX LOC

Figure 2.2

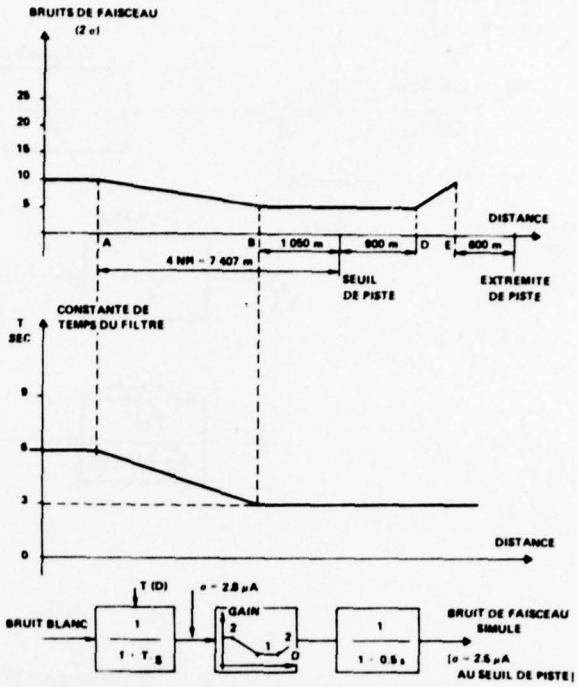

MODELE DE BRUITS DE FAISCEAUX PROPOSE

Figure 2.3

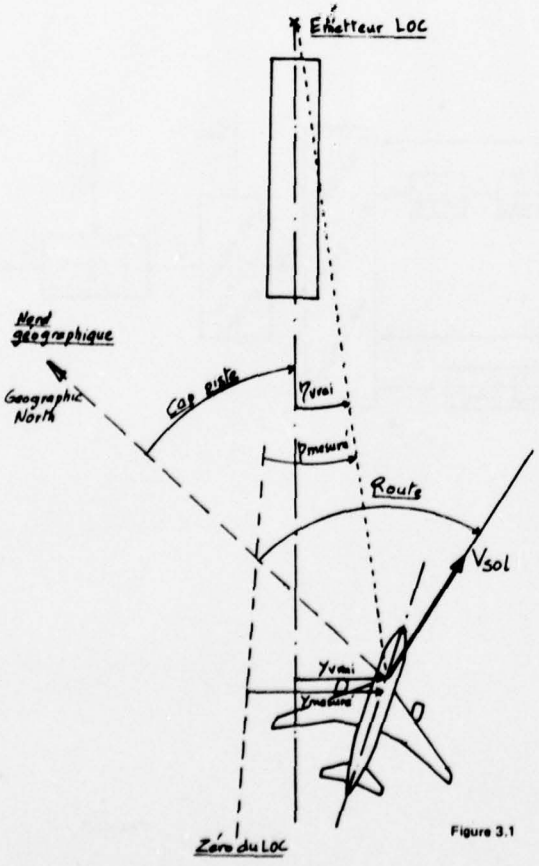

Figure 3.1

Reconstitution de la Distance à l'émetteur LOC

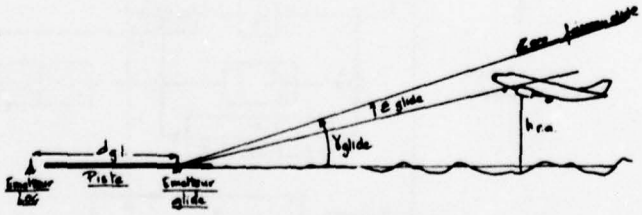

$$D = \frac{h_{r.a}}{\gamma_{glide} + \delta_g . E_{glide}} + d_{gl}$$

d_{gl} : distance entre les emetteurs loc et glide

γ_{glide} : pente du faisceau glide (rad)

δ_g : sensibilité du faisceau glide (rad/µa)

E_{glide} : Sortie du récepteur glide (µa)

Figure 3.2

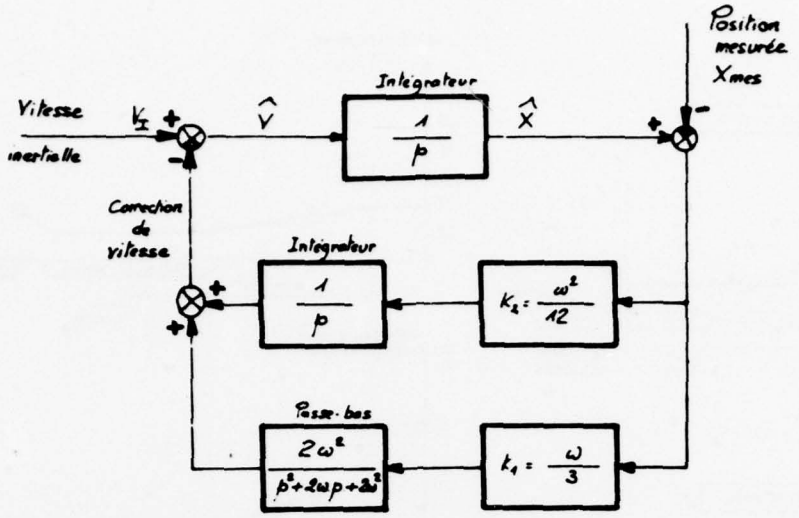

Figure 3.3 CELLULE ELEMENTAIRE de FILTRAGE - Version classique (LIS1)

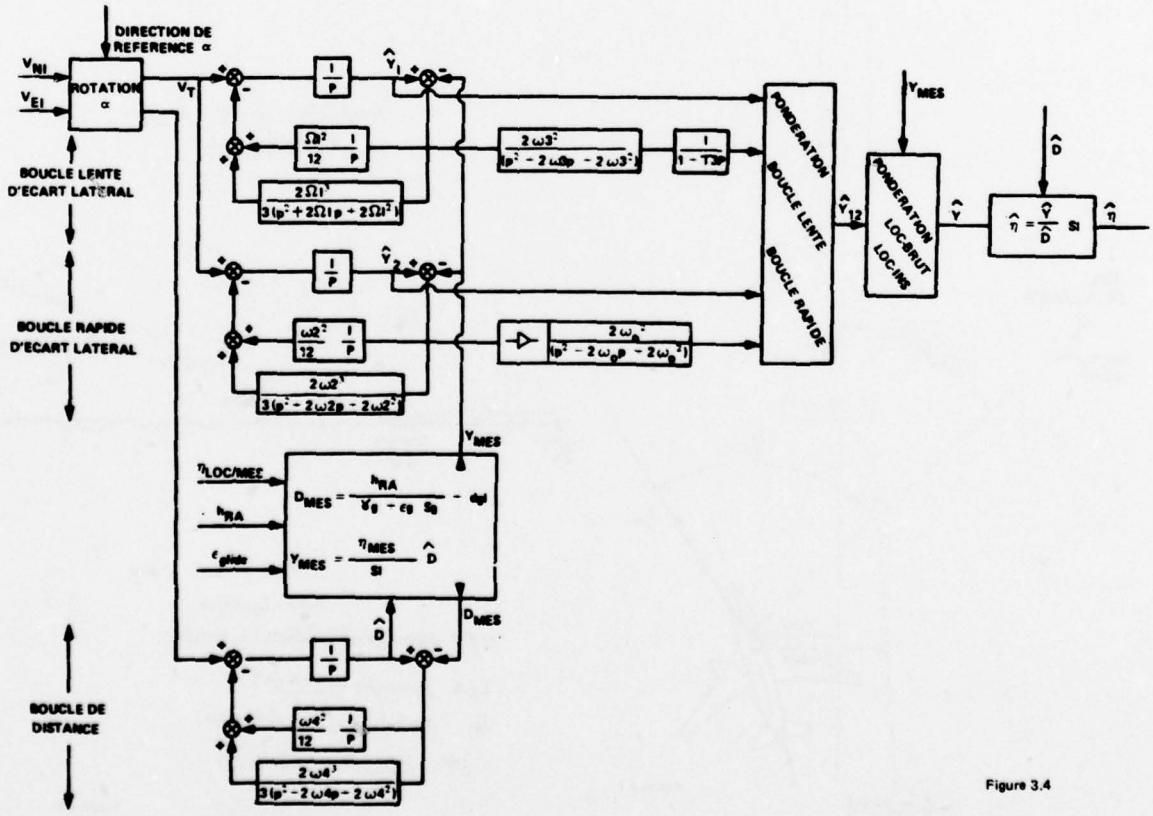

Figure 3.4

ECARTS . TYPES			GUIDAGE LOC	GUIDAGE LIS 1	GUIDAGE LISS 2 $(\eta, \Delta V_T, \dot{V}_T)$	GUIDAGE LISS 3 $(\eta, \Delta V_T, \dot{V}_T)\varepsilon \neq 0$
PISTE LONGUE VENT FORT (100 APPROCHES)	$Y_{CG_{100ft}}$	σ	2,54	2,70	2,04	2,17
		$\sqrt{m^2+\sigma^2}$	3,36	3,55	3,13	3,17
	$Y_{CG_{15ft}}$	σ	2,06	2,23	1,66	1,84
		$\sqrt{m^2+\sigma^2}$	3,39	3,30	2,99	3,12
	$Y_{CG_{impact}}$	σ	2,34	1,87	1,48	1,56
		$\sqrt{m^2+\sigma^2}$	3,07	3,04	2,80	2,88
PISTE COURTE VENT FAIBLE (100 APPROCHES)	$Y_{CG_{100ft}}$	σ	2,60	2,59	2,47	2,01
		$\sqrt{m^2+\sigma^2}$	3,37	3,38	3,03	2,78
	$Y_{CG_{15ft}}$	σ	2,25	2,40	2,12	1,90
		$\sqrt{m^2+\sigma^2}$	2,70	3,02	2,70	2,60
	$Y_{CG_{impact}}$	σ	1,95	2,14	1,81	1,63
		$\sqrt{m^2+\sigma^2}$	2,34	2,56	2,32	2,22

RESULTATS STATISTIQUES

COMPARAISON DES DEUX VERSIONS DU FILTRE STATISTIQUE

Figure 5.1

$Y_{CG_{100\ ft}}$ (m)		σ	RAPPORT	VALEUR MAX.	APPROCHES REJETEES (CONFIRMEUR)*
GUIDAGE	LOC	3,18	1	8,54	0
	LIS	3,36	1,056	9,74	6 (DONT 1 DIVERGENCE)
	LISS	2,97	0,934	9,12	1

$Y_{CG_{15\ ft}}$ (m)		σ	RAPPORT	VALEUR MAX.	APPROCHES REJETEES (ECARTS EXCESSIFS LOC) *
GUIDAGE	LOC	2,95	1	8,61	0
	LIS	3,15	1,068	9,11	1 (DIVERGENCE)
	LISS	2,80	0,949	7,09	0

$Y_{TP\ impact}$ (m)		σ	RAPPORT	VALEUR MAX.
GUIDAGE	LOC	2,94	1	9,24
	LIS	3,03	1,030	8,41
	LISS	2,71	0,922	7,23

BRUITS LOC : MODELE AS

TURBULENCES

600 APP. : V_y = 10 KT

600 APP. : V_y = 15 KT

* SUR 600 APPROCHES SEULEMENT

STATISTIQUES SUR 1 200 APPROCHES

Figure 5.2

Y_{CG} 100 FT	σ	MAX.
LOC	2.63	7.61
LIS INS NOMINALE	2.57	7.75
LIS ERREUR INS/2	2.53	6.85

15 FT	σ	MAX.
LOC	2.61	7.83
LIS INS NOMINALES	2.39	6.89
LIS INS/2	2.31	5.71

$$\lambda_{vrai} = \sqrt{\frac{\sum_{i=1}^{n} max\,(\gamma_{mes})^2}{2\pi}}$$

Y_{CG} IMPACT	σ	MAX.	λ vrai
LOC	2.76	8.76	5.81
LIS	2.34	6.07	4.49
LIS INS/2	2.31	5.26	4.27

400 APPROCHES

Tableau 5.3

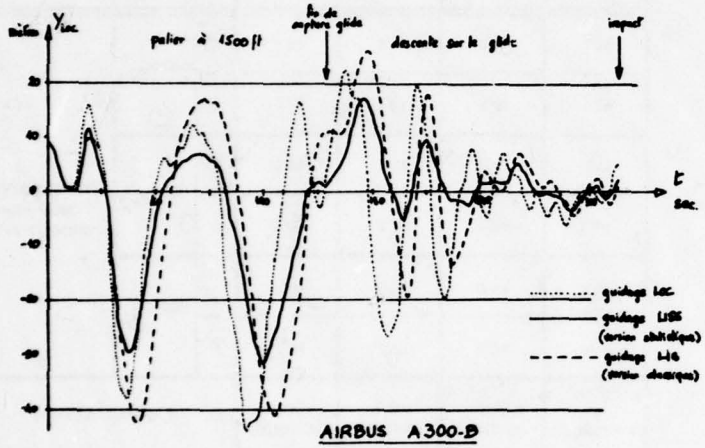

Figure 5.4

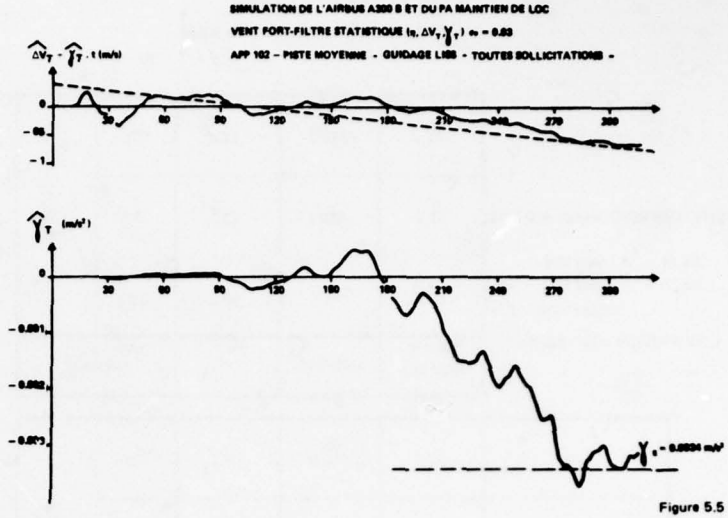

Figure 5.5

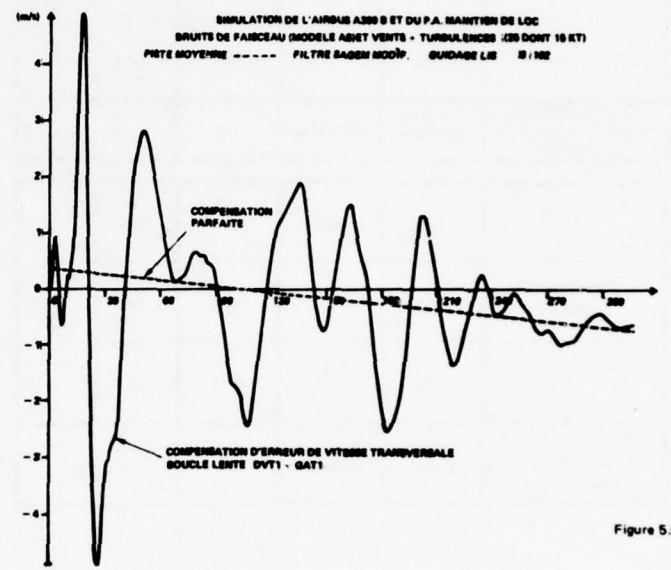

Figure 5.6

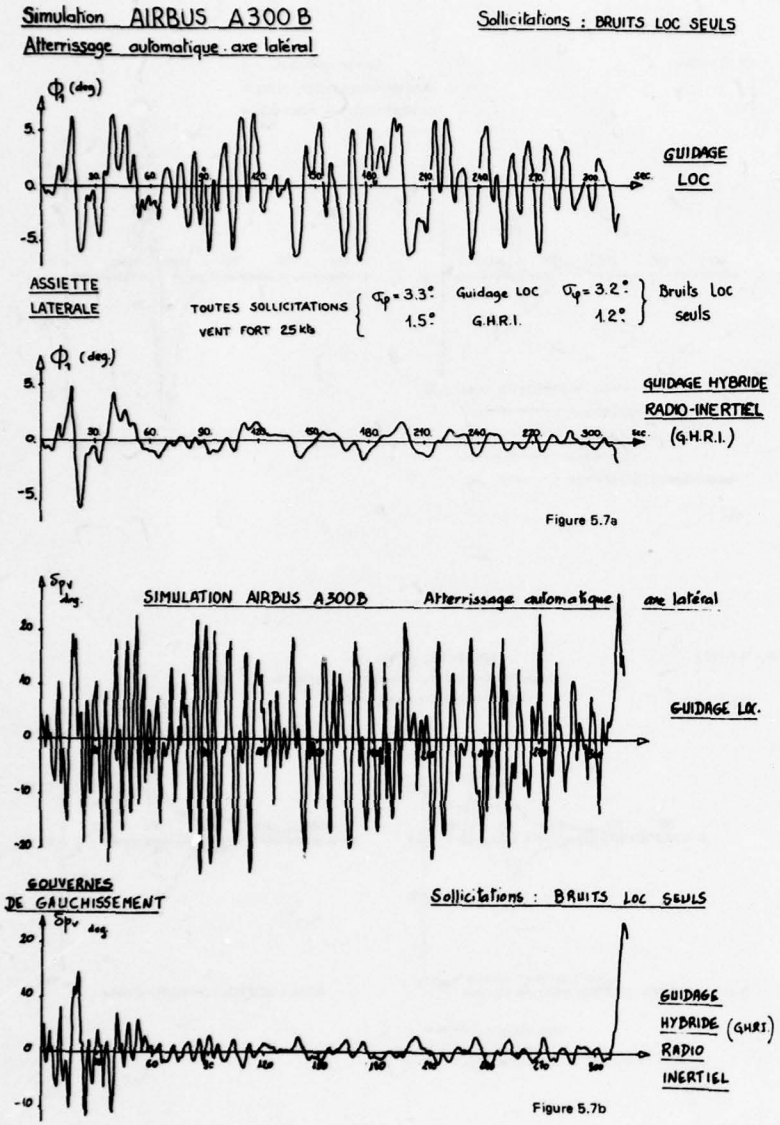

Figure 5.7a

Figure 5.7b

MOUVEMENTS AUTOUR DU CENTRE DE GRAVITE
AGITATIONS DES GOUVERNES

	BRUIT LOC SEUL			BRUIT LOC + TURBULENCES		
GUIDAGE	LOC	LIS 1	LISS 3	LOC	LIS 1	LISS 3
δ deg	0.79	0.48	0.47	1.13	0.91	0.91
θ deg	3.24	1.73	1.21	3.34	2.04	1.47
$\Delta\psi$ deg	1.85	1.81	1.08	2.11	1.87	1.41
ΔR_V deg	2.04	1.81	1.12	2.03	1.88	1.66
σ_{γ_1} m/s²	0.071	0.045	0.039	0.110	0.085	0.082
θ_c deg	3.73	1.88	1.38	3.73	2.03	1.47
δp_v deg	10.07	4.06	3.60	10.84	6.47	6.89
δr_g deg	1.80	0.88	0.81	1.96	0.83	0.79

Tableau 5.8

	PISTES MOYENNES VENT FORT					PISTES COURTES VENT FORT				
	LOC *	LIS1 *	LIS 1	LISS 3 *	LISS 3	LOC SANS PANNE	LIS 1 SANS PANNE	LIS 1	LISS 3 SANS PANNE	LISS 3
Y_{cg} 100 FT σ	2.31	2.61		1.88		2.46	2.04		2.39	
Y_{cg} 100 FT MAX.	7.70	8.98		7.30		7.87	9.06		9.12	
Y_{cg} 15 FT σ	2.38	2.49	2.47	1.84	1.65	2.39	2.37	3.11	1.86	2.83
Y_{cg} 15 FT MAX.	8.61	9.11	8.48	6.70	9.35	7.39	8.71	10.39	6.17	7.88
Y_{cg} IMPACT σ	2.77	2.11	2.89	1.72	2.35	2.66	2.36	4.82	1.61	2.83
Y_{cg} IMPACT MAX.	6.89	7.48	8.32	6.88	9.88	6.33	8.97	16.07	5.88	9.46

*SANS PANNE

PANNES DE L'EMETTEUR LOC
DISPARITION FAISCEAU A 100 FT

Tableau 5.9

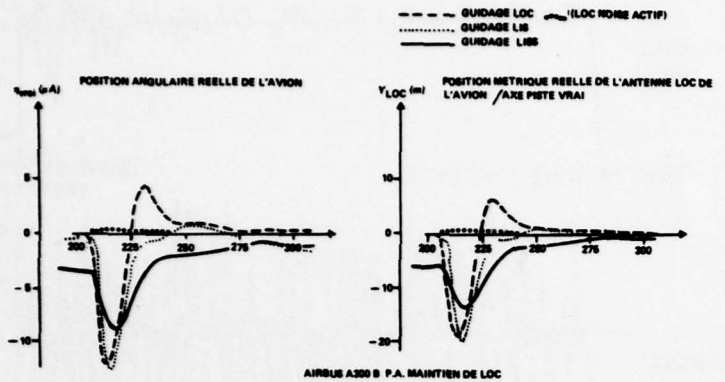

AIRBUS A300 B P.A. MAINTIEN DE LOC
CRENEAUX SUR LE SIGNAL LOC DE 20 µA PENDANT 3 SEC.
H = 1 000 FT GUIDAGE LISS

Figure 5.10a

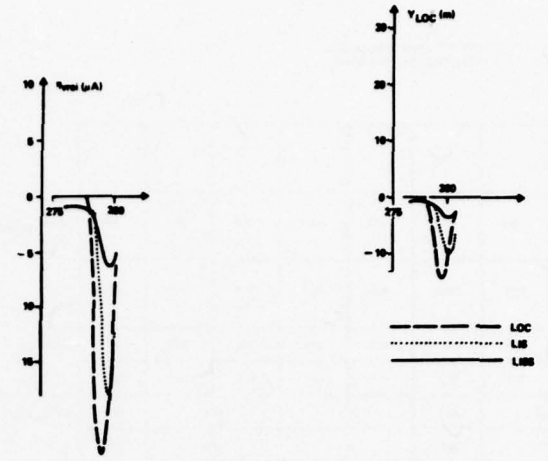

AIRBUS A300 B P.A. MAINTIEN DE LOC
CRENEAUX SUR LE SIGNAL LOC DE 20 µA PENDANT 3 SEC.
H = 100 FT GUIDAGE LISS

Figure 5.10d

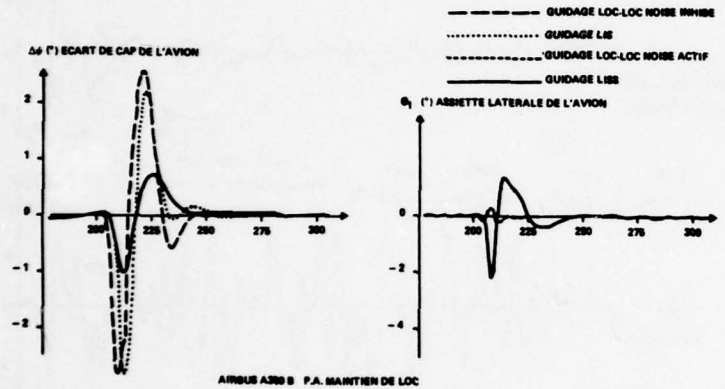

AIRBUS A300 B P.A. MAINTIEN DE LOC
CRENEAUX SUR LE SIGNAL LOC DE 20 µA
H = 1 000 FT GUIDAGE LISS

Figure 5.10b

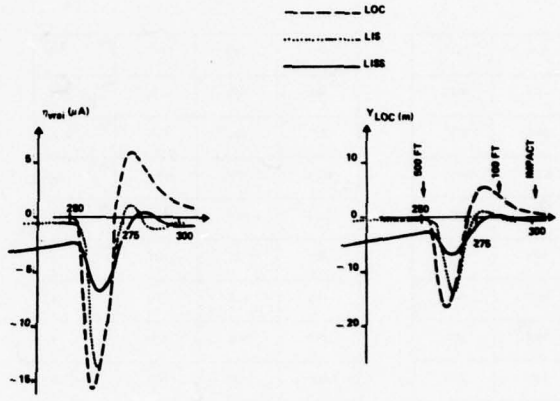

AIRBUS A300B P.A. MAINTIEN DE LOC
CRENEAUX SUR LE SIGNAL LOC DE 20 µA PENDANT 3 SEC
H = 500 FT GUIDAGE LISS

Figure 5.10c

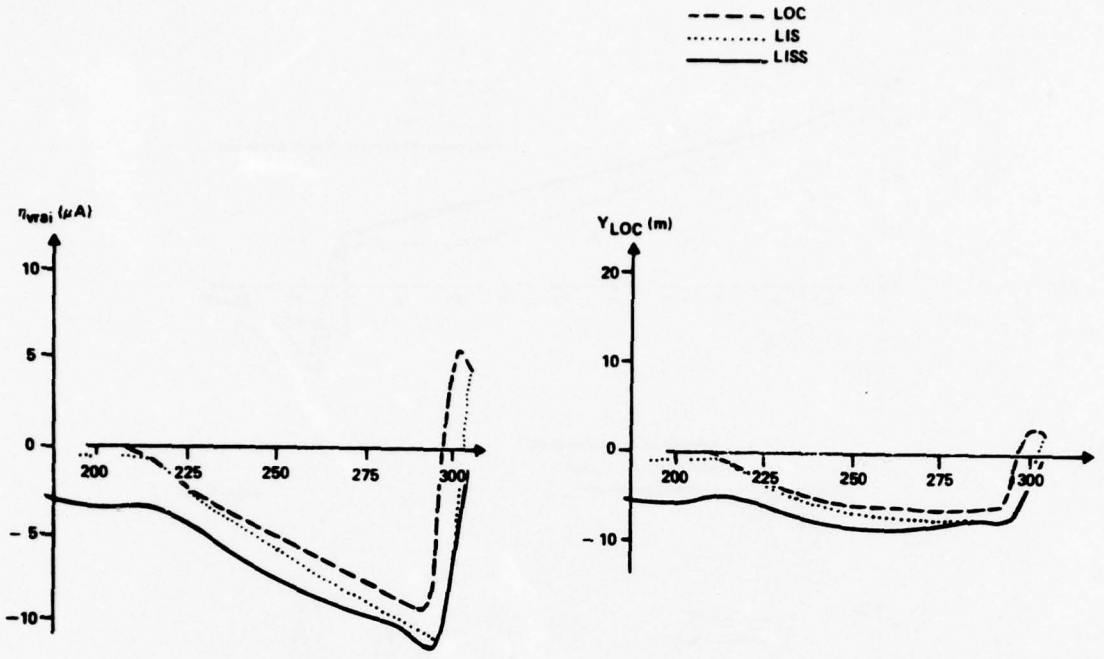

AIRBUS A300 B P.A. MAINTIEN DE LOC

RAMPES D'ERREUR LOC

H = 1 000 FT 0.1 μA/SEC GUIDAGE LISS

Figure 5.11a

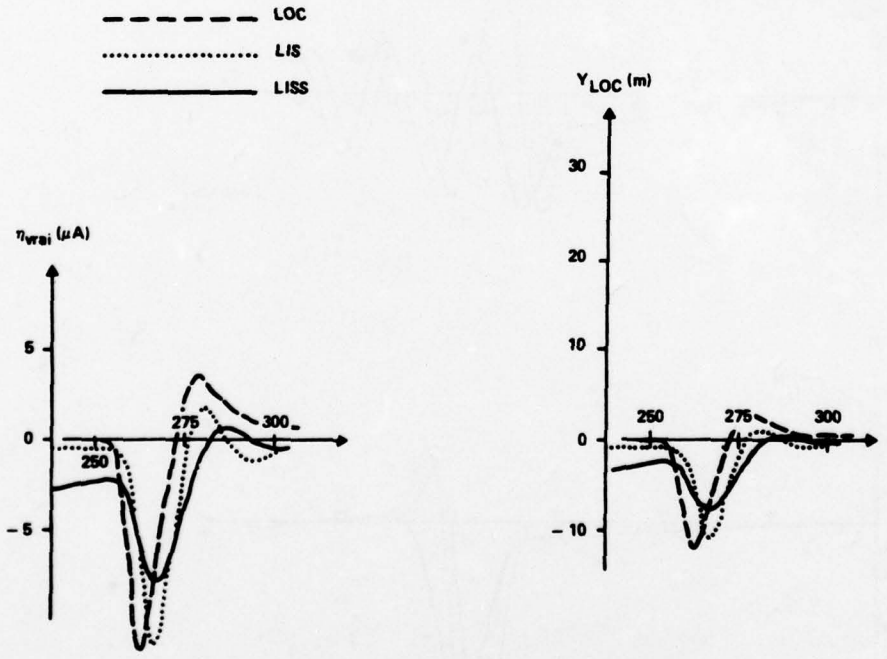

AIRBUS A300 B P.A. MAINTIEN DE LOC

RAMPES D'ERREUR LOC

H = 500 FT 2. μA/SEC GUIDAGE LISS

Figure 5.11b

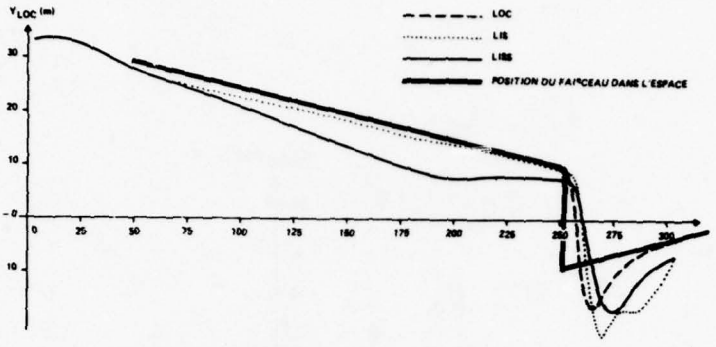

AIRBUS A300 B P.A. MAINTIEN DE LOC
PASSAGE AXE LOC - A = 8,5 μA
H = 500 FT – GUIDAGE LISE

Figure 5.12a

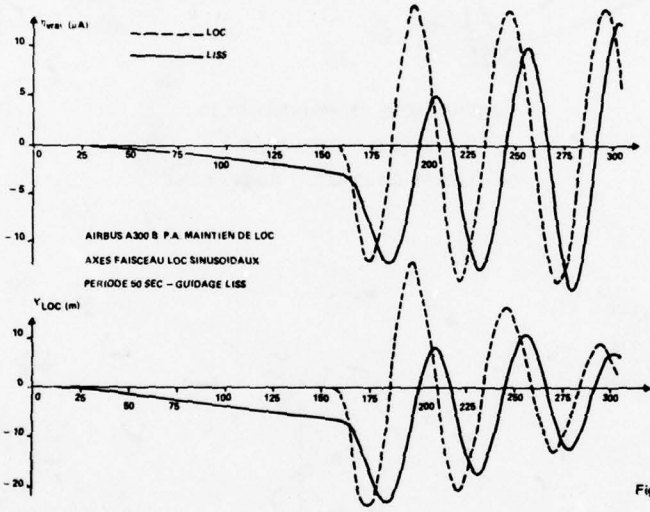

Figure 5.12b

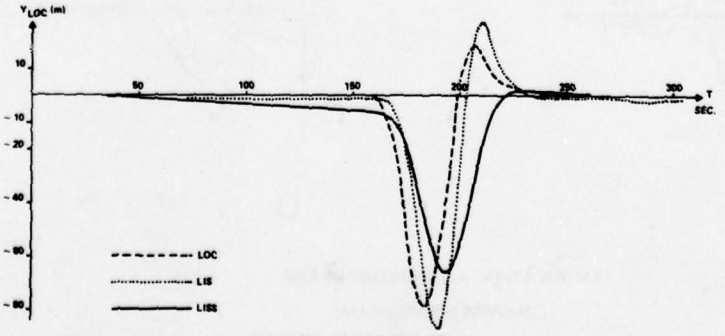

AIRBUS A300 B P.A. MAINTIEN DE LOC
AXES FAISCEAU LOC COURBES (1 – COS)
H = 1 500 – 1 000 FT – GUIDAGE LISS

Figure 5.12c

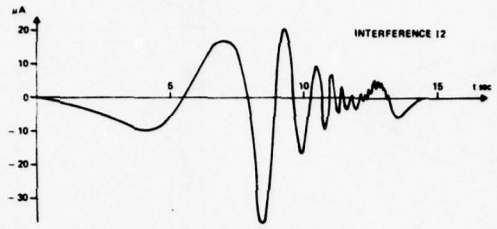

BRUITS PROVOQUES PAR UN AVION SURVOLANT L'EMETTEUR LOC
(ISSUS DU RAPPORT RAE No. TR68156 DE JUIN 1968)

Figure 5.13a

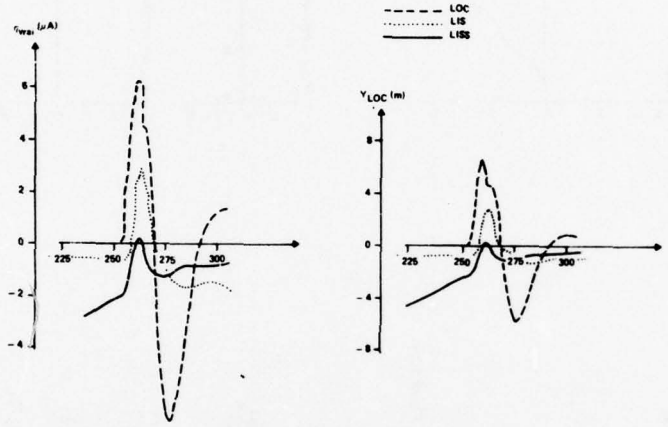

AIRBUS A300 B P.A. MAINTIEN DE LOC
INTERFERENCES
I2 H = 500 FT GUIDAGE LISS

Figure 5.13b

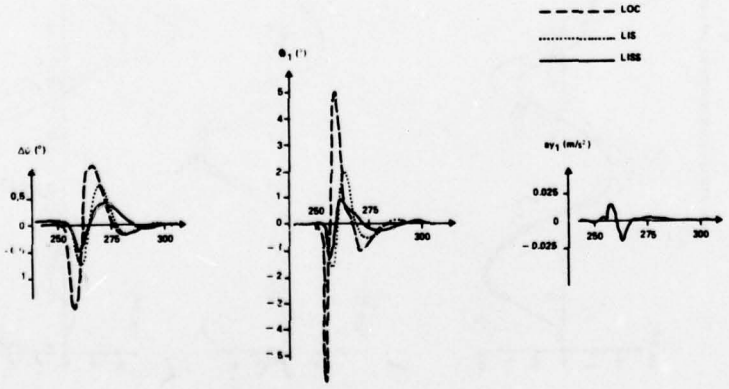

AIRBUS A300 B P.A. MAINTIEN DE LOC
INTERFERENCES
I4 – H = 500 FT – GUIDAGE LISS

Figure 5.13c

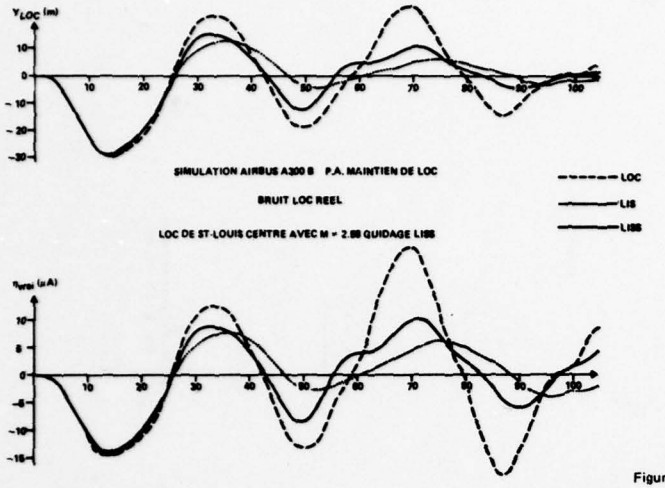

Figure 5.14a

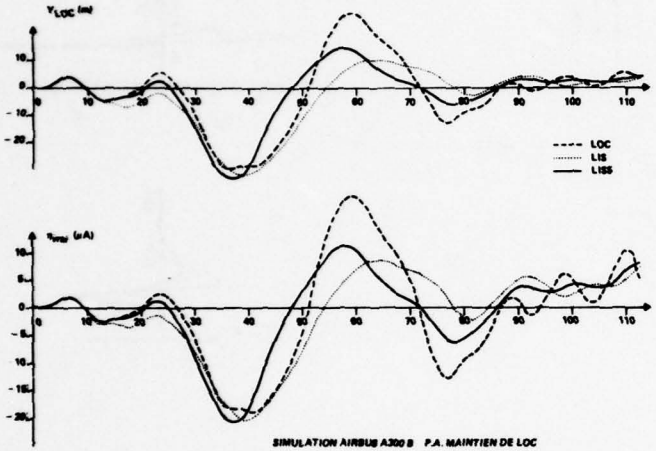

Figure 5.14b

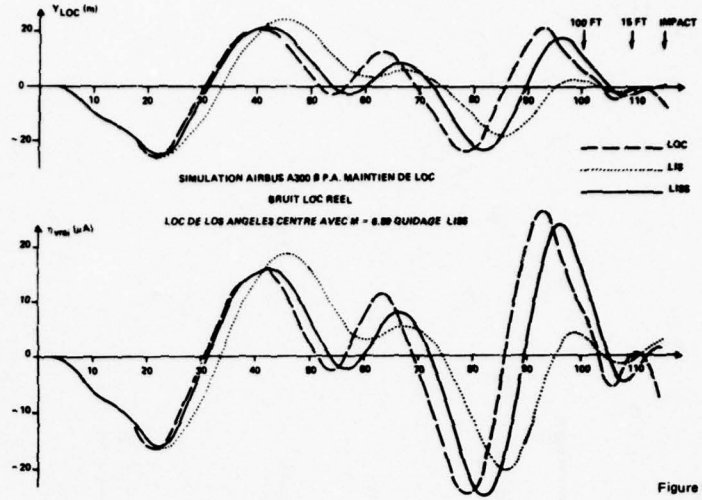

Figure 5.14c

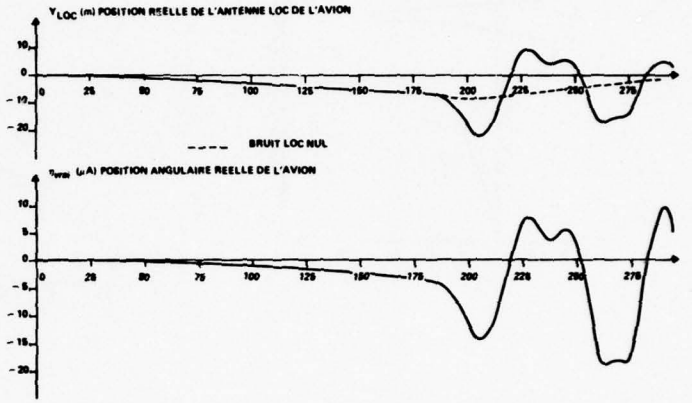

Figure 5.14d

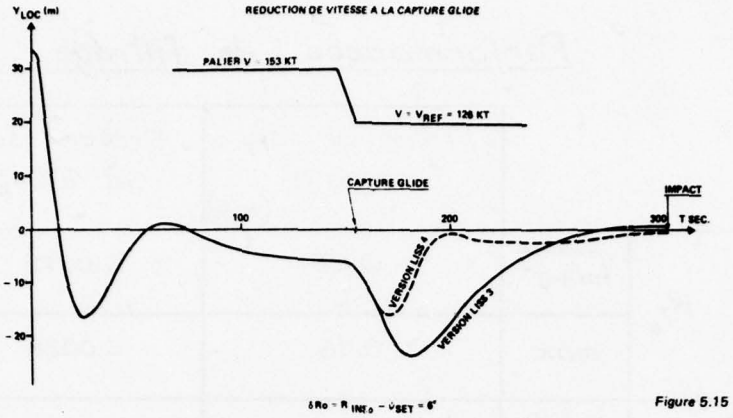

Figure 5.15

Figure 6.1

Caractéristiques calculateur UTD SAGEM

Format opérandes	16 ou 32 bits, virgule fixe
Format d'instruction	16 bits
Registres	8 par niveau
Codes d'ordres	32 instructions microprogram^{ées}
Interruptions	1 niveau ; 10 entrées
Capacité mémoire	≤ 65 K mots
Durée du cycle mémoire	0.2 à 2 µs
Durée addition	9 cycles
Durée store	4 cycles
Durée multiplication	73 cycles
Durée addition double longueur	19 cycles

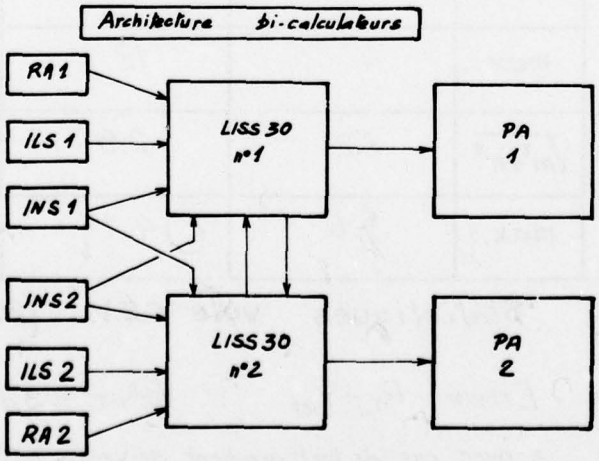

Figure 6.2

Figure 7.1

Performances de filtrage

Référence de projection		Erreur sur $\widehat{\Delta V_T}$ à 100 ft (m/s)	Erreur sur $\widehat{\gamma_T}$ à 100 ft (m/s^2)
R_{I_o}	$\sqrt{m^2+\sigma^2}$	0.08	0.0015
	max.	0.16	0.0028 *
Ψ_{set}	$\sqrt{m^2+\sigma^2}$	0.08	0.0018
	max.	0.16	0.0037

Statistiques vols C.E.V. (20 approches)

Erreur $R_{I_o} - \Psi_{set}$: $\sqrt{m^2+\sigma^2} = 3$ deg max = 6.15 deg.

* avec cas à fort gradient de vent ($\Delta V_{sol} = 50$ kt)

$\Delta\gamma_T$ max = 0.0222 m/s^2

Figure 7.2

Performances de guidage inertiel pur (panne loc 100ft)

Référence de projection		Ecart à l'impact (m)	Ecart à $t_{impact} + 10$ sec (m)	Ecart à $t_{impact} + 15$ sec (7 approches) (m)
R_{I_o}	$\sqrt{m^2+\sigma^2}$	2.5	4.7	9.5
	max.	4. *	12.	21.
Ψ_{set}	$\sqrt{m^2+\sigma^2}$	2.2	2.5	3.2
	max.	5.6	4.1	5.4

Statistiques vols C.E.V. (20 approches)

Erreur $R_{I_o} - \Psi_{set}$: $\sqrt{m^2+\sigma^2} = 3$ deg. max = 6.15 deg.

* avec cas à fort gradient de vent ($\Delta V_{sol} = 50$ kt)

Y_{cg} max = 8. m

INERTIAL SMOOTHING AND EXTRAPOLATION OF ILS BEAMS

Application to the Airbus A 300 B

by

J.Irvoas and D.Buisson
S.N.I. Aérospatiale
316, route de Bayonne, Toulouse, France

and

P.Lloret and X.Lagarde
S.A.G.E.M.
6, Avenue d'Iéna, Paris, France

SUMMARY

One of the problems of automatic approach and landing is the accuracy of aircraft guidance as the aircraft flies along the ILS Beams. If the beam is noisy, or disturbed by undesirable reflections of the emitted signal on natural obstacles or on an aircraft which is flying over the localizer transmitter during its take-off, the lateral displacement and the roll movements of the aircraft could be very large. As far as ILS transmitter or receiver failures are concerned, they increase go-around probability, which is undesirable as far as the airlines are concerned. The system studied here can smooth the Loc data and ensure continuation of aircraft guidance in the event of a Localizer failure. This system only needs complementary speed information from an inertial sensor system in order to provide the auto-pilot with a filtered Loc signal instead of the raw signal. The final system, based on Kalman filtering, was implemented by means of a digital computer, then flight tested on the AIRBUS A.300.B. Certification of this system with reduced operational visibility minima is expected in the Spring of 1978.

NOTATION

y	lateral deviation in metres of the aircraft from the runway centre line
η	angular deviation between the straight line from the LOC transmitter to the aircraft and the runway centre line, converted into microamps
D	distance between the aircraft and the localizer transmitter
h	altitude of the aircraft (ft) along the landing runway centre lines
V	aircraft speed
ΔV_N, ΔV_E ΔV_T, ΔV_L	constant speed errors of the INS along the respective North, East, transverse and longitudinal axes of the aircraft
γ_N, γ_E	variation with time of the INS errors
$\hat{x}$	estimated value of the variable x by the LIS filter
S_l, S_{l_F}	LOC beam deviation sensitivity (μA/deg), actual value and value set in the computer respectively
R, R_I	track; track indicated by the INS
ψ_{set}	true runway heading
$\delta R_o = R_{I_o} - \psi_{set}$	track erro at $t = 0$ (initialisation of filtering)
LIS	LOC-Inertial system
LISS	LOC-Inertial statistical system

1. INTRODUCTION

The use of inertial terms to improve methods of guiding aircraft on ILS beams has already been under consideration, particularly in the United States[1]. It can therefore be hoped to operate aircraft in Category II landing conditions, although the ILS system is only Category I.

In France, under a Government contract from the Service Technique de l'Aéronautique (STAé) and following a request from the AIR INTER French domestic airlines, SNIAS and SAGEM undertook research on a system for reducing the rate of go-arounds, considered to be too frequent on certain runways where the localizer (LOC) beams were too noisy or were subject to interference.

The system had the following three objectives:

(1) to smooth Category II or III ILS information in order to reduce the rate of failed approaches due to imperfections in the ILS system;

(2) to ensure the survival of the system following failure of the LOC transmitter at low altitudes during a Category II or III approach and, in the longer term, during a Category III approach without a decision height;

(3) to smooth Category I ILS information in order to improve the quality of the guidance both during manual approach using the flight director, and during automatic approach.

The problems encountered by AIR INTER were concerned mainly with the lateral guidance axis of the aircraft, involving principally the localizer beam. The research was conducted on the Airbus A 300 B and its SFENA lateral auto-pilot which it was proposed not to modify. The system was in fact for general application and could be used for the approach guidance of any aircraft.

The filtering system was defined by means of the digital computer simulation of the aircraft guidance loop and then programmed in the SAGEM UTD computer before being tested in the laboratory Airbus flight simulator, and then flight tested in the Airbus No.3 equipped with a suitable flight test installation.

2. BRIEF DESCRIPTION OF THE COMPUTER SIMULATION STUDY

A general diagram of the digital simulation study is shown in Figure 2.1, and consists of a number of sub-assemblies:

- aircraft flight mechanics – lateral movements only;
- lateral auto-pilot, which generates the commands to be given to the ailerons and the rudder (in particular the LOC HOLD and the ALIGNMENT modes);
- the various sensors in the aircraft:
  - ILS receiver (localizer and glide path) providing a current propotional to the angular deviation between the aircraft and the beam: $\eta_{meas.}$ (μA) for the LOC beam and ϵ_{glide} (μA) for the glide path;
  - radio-altimeter giving the altitude of the aircraft h_{RA}, which is different from the actual altitude in the reference of axes for the runway because of the profile of the ground flown over;
  - inertial platform, which provides the aircraft speed in the local geographical reference: V_{NI}, V_{EI} are its components along the North and East axes;
- the LIS (LOC-Inertial System) filter which plots the position of the aircraft $\hat{\eta}$ from the ILS data ($\eta_{meas.}$, ϵ_{glide}), the altitude h_{RA} and the inertial speeds V_{NI} and V_{EI}, this position then being transmitted to the A/P (position (2)) instead of the raw output from the LOC receiver position (1)).

The various disturbances acting as simulation inputs are as follows:

- lateral wind and associated atmospheric turbulence as specified in the FAA regulations quoted in the Circular AC 20-57. Two types of wind are used:
  - V_Y = 10 kt (zero head wind)
  - V_Y = 15 kt head wind V_X = 20 kt (total 25 kt)

  The spectrum of the associated turbulence is the same as that of white noise which is filtered by a low bandpass filter of the first order.
- localizer beam noise.

  Annex 10 of the ICAO Regulations gives the requirements in regard to the course bends of the localizer beams. Figure 2.2 shows the maximum value not to be exceeded with a 95% probability. Annex 10 does not, however, specify the noise spectrum. After a study of certain French LOC beams which had been checked in flight by the STNA, as well as of some American beams[2], the random noise model shown in Figure 2.3 was chosen. This corresponds to white noise which is filtered through a low bandpass filter with a time constant which varies with the distance of the aircraft from the runway threshold. The noise level can also vary with the distance. It is possible to superimpose on this random noise a spatial distortion of the beam so that the maximum permissible ICAO level can, in fact, be achieved.

- ground profile. The altitude measured by a radiosonde is used to plot the distance to the LOC transmitter. The ground profile therefore affects the calculation. It is thus possible to simulate either ground which is mostly flat, or ground which rises or descends. Random disturbances representing unevennesses in the ground being sounded, or measurement noises are added to the average profile.
- glide path noise. It is assumed that, in the vertical plane, the aircraft is fully stabilised on the theoretical glide path as defined by the glide beam. In the simulation study glide beam noise is therefore present only for the purpose of disturbing the calculation of the distance between the aircraft and the LOC transmitter. Again, this is random noise generated filtering white noise.
- speed errors in the inertial platform. The SAGEM MGC 30 unit selected for installation (optionally) in the Airbus is of the gimbal type, the mechanisation being of the 'free azimuth' type. It can therefore be considered that the errors along each of the North and East axes are independent. Since the time during which the speeds are used by the hybrid system is short compared with the Schüler period (84 mn), the speed errors can be approximated by a constant error and drift during the time:

$$V_{N_{INS}} = V_{N_{true}} + \Delta V_N + \gamma_N \cdot t$$

$$V_{E_{INS}} = V_{E_{true}} + \Delta V_E + \gamma_E \cdot t$$

in which ΔV_N, ΔV_T, γ_N, γ_E are constants during a given approach.

3. DESCRIPTION OF THE CONVENTIONAL VERSION OF THE LIS 1 FILTER (VERSION 1)

SAGEM's initial proposal was a conventional filtering arrangement between localizer data and inertial speeds.

With this selective filter, which provided the basis for the preliminary studies and later on for the very first flight tests at CEV, Brétigny, it was possible to verify the basic design principles of the system.

3.1 Basic Design Principle

This filter uses the method of inserting an additional filter.

The estimated position of the aircraft is evaluated from the localizer radio data and from the ground speed data supplied by the inertial unit.

The data from the LOC receiver are available in the form of angular deviation between the straight line from the aircraft to the LOC transmitter, and the runway centre line.

The metric error with respect to the runway centre line is obtained from a knowledge of the distance between the aircraft and the transmitter and the sensitivity of the LOC beam.

$$y_{meas.} = \eta_{meas.} \cdot \frac{\hat{D}}{S_{I_F}} .$$

The North and East speeds provided by the inertial system, and the runway heading, are used to obtain the transverse speed of the aircraft $\dot{y}_I$ (Fig.3.1).

These two items of data are subject to errors of different types:

(a) $y_{meas.} = y_{true} + y_{LOC\ noise}$

in which $y_{LOC\ noise}$ includes radio noise and beam distortion.

(b) $\dot{y}_I = \dot{y}_{true} + \Delta V_T$

in which ΔV_T is the constant (or slowly varying) drift of the inertial system.

ΔV_T comprises the actual drift of the inertial system and the error due to the projection of the North and East speeds over a reference direction which is slightly different from the true runway heading.

This latter error is constant as long as the longitudinal speed of the aircraft does not vary.

We then have the additional filter:

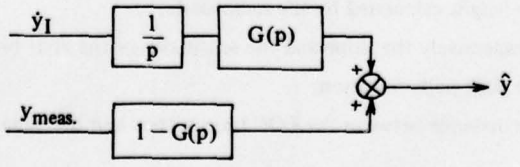

with $G(p) \frac{p^2}{p^2 + ap + bp}$.

We thus obtain:

$$y = y_{true} + \frac{p}{p^2 + ap + b} \Delta V_T + \frac{ap + b}{p^2 + ap + b} y_{LOC\ noise}$$

The LOC noise is therefore filtered by the filter $\frac{ap + b}{p^2 + ap + b}$, while the inertial errors are resorbed by the drift filter, namely: $\frac{p}{p^2 + ap + b}$.

The general arrangement for such a filter is given in Figure 3.2.

3.2 General Arrangement

Figure 3.4 shows the block diagram for the complete filter. In addition to calculation of lateral deviation, this diagram includes the inertial filtering of the distance between the aircraft and the LOC transmitter which is necessary for converting angular errors into metric errors.

3.2.1 Calculation of Filtered Lateral Deviation

The system provides two estimates of the filtered lateral deviation, which are generated by two loops of similar structure forming two additional filters but with different cut-off frequencies.

The transverse inertial speed is corrected by the sum of the outputs of a low pass filter and a feedback integrator. This corrected speed is integrated to give the calculated deviation from the runway centre line.

(a) Slow loop

The cut-off pulse of this loop decreases with time and reaches 0.1 rd/s at the end of the approach phase.

The position error is filtered to give an estimated drift variation of the inertial system.

(b) Fast loop

This has a higher cut-off frequency: 0.55 rd/s.

The position error is corrected and then filtered, to give an estimate of the noise associated with the LOC signal.

(c) Weighting

The final lateral deviation is the result of double weighting:

- weighting of the deviation calculated in the slow loop and in the fast loop. Generally speaking, the greater the ILS noise, the greater the importance attached to the slow loop in the matter of weighting and vice versa, the greater the inertial drift variation, the greater the significance of the fast loop;
- weighting for the gradual transfer of the lateral deviation data in the raw LOC signal $\eta_{meas.}$ to the filtered LOC signal $\hat{\eta}$, to avoid discontinuity in the data fed into the auto-pilot.

(d) Switching to a pure inertial system

When there is a loss of the LOC beam, lateral deviation is calculated by integrating the corrected inertial speed from the estimated drift given by the slow loop.

3.2.2 Calculation of the Distance between the LOC Transmitter and the Aircraft

The basic principle is the same as for filtering the lateral deviation of the aircraft from the runway centre line.

The distance in metres to the LOC transmitter is calculated from glide path and radiosonde measurements (Fig.3.3):

$$D_{meas.} = \frac{h_{RA}}{\gamma_g + S_g \cdot \epsilon_{glide}} + d_{gl}$$

in which h_{RA} is the height calculated by the radiosonde,

γ_g, S_g are respectively the slope and the sensitivity of the glide beam,

ϵ_{glide} is the glide path deviation,

d_{gl} is the distance between the LOC transmitters and the glide path.

This distance is filtered by the longitudinal inertial speed. In the event of loss of radiosone or glide path information, the distance is calculated by integrating the inertial speed.

3.2.3 Initialisation

Filtering of the lateral deviation data is initialised at the end of capture of the LOC beam if the aircraft has remained for at least 10 seconds in the area defined by a LOC deviation of less than 15 μA.

Filtering of the distance data is initialised on capture of the glide path. Before this initialisation, which generally occurs after initialisation of lateral deviation filtering, the raw distance will be used in the equations for calculating the filtered lateral deviation, a distance which will be falsified if the glide receiver is giving a signal which is not proportional to the actual angular error.

3.3 Lessons Drawn from Optimisation of the Conventional LIS 1 Filter

The conventional filter was subjected to the simulated conditions described in Section 2 and flight tested at CEV. The advantage of these tests was that they provided a means of making a precise plot of the aircraft's flight path, using the STRADA laser system which produces a fine analysis of the performance achieved during actual flights. In addition, CEV Brétigny was subsequently able to play back the approaches made, using recordings of the LIS computer input data.

The simulation studies proved to be a very effective analysis tool because of the possibility of varying the filtering parameters.

The main lessons learnt, both from the simulation studies and the flight tests, were as follows:

(a) With regard to its smoothing function, the LIS 1 filter reduces quite significantly (in a ratio of more than 1 to 3) LOC beam distortions in a frequency band of more than 0.03 Hz (periods of less than 30 s). This reduction is particularly evident during roll and yaw movements of the aircraft, which are reduced in a ratio of 1 to 3, even in the presence of ILS beams which are considered to be not very noisy.

(b) In the case of survival of the system following an ILS failure at low altitudes ($h \leqslant 100$ ft), the LIS 1 filter provides correct emergency guidance: the accuracy at touch-down is of the order of 3 m (on a 1 sigma basis) in unfavourable cases, a result which is consistent with the accuracy of estimation of inertial errors at the end of the approach.

Section 7 reports the main results obtained. It was considered desirable, however, to continue the work in order to eliminate certain inherent limitations in the conventional LIS 1 filter. The following main limitations were found:

(a) If an attempt is made to reduce LOC beam distortions at frequencies of less than 0.03 Hz, a static error (drag) of the filter occurs which quickly becomes prohibitive and impairs the touch-down accuracy obtained without this new system. The final adjustment shows only a 3% reduction in touch-down accuracy (it goes from 2.94 m on a 1 sigma basis during LOC guidance to 0.03 m with LIS 1 guidance), but there is very little smoothing of the flight path data.

(b) Ground which rises or descends upstream of the runway involves errors when assessing the metric deviation $y_{meas.}$ from the angular deviation $\eta_{meas.}$. A similar effect arises from the fact that a mean beam sensitivity value (75 μA) is used, whereas the actual value may vary from 55 to 110 μA/deg, depending on the runway length and the respective positions of the transmitters. For these various reasons, the period of survival of the system following a LOC failure is shorter, and there may even be some divergence of the guidance loop in an extreme case.

(c) Finally, with the conventional design it was not possible to estimate the error between the reference direction for projection of the speed vectors and the true runway heading. This term, which is unimportant if we are concerned only with guidance of the aircraft at a constant speed, comes into play at each change of speed and particularly during deceleration on the runway. To overcome this problem with the LIS 1 design, the only solution is to feed into the computer the heading of the runway on which the aircraft is to land. In a statistical design this term can be evaluated provided the aircraft decelerates sufficiently during the approach.

The statistical design filter (Kalman filter) was therefore adopted for the versions described below. It also provides greater flexibility since it takes into account the various initialisation possibilities which depend on the approach procedure used, whereas the conventional type of filter is optimised for a 'standard' approach.

4. DESCRIPTION OF THE LOC-INERTIAL STATISTICAL SYSTEM (LISS)

4.1 Basic Design of Version 2 (LISS 2)

To achieve optimum filtering between LOC data and inertial speeds, it seemed an advantage to use the Kalman-Bucy filter equations. For this, it was necessary to write the state equations for the system, taking into account, in addition,

the variation with time of the inertial speed error. We thus have:

$$\dot{y} = \dot{y}_I + \Delta V_T + \gamma_T \cdot t \tag{4.1}$$

in which ΔV_T and γ_T are constants.

The LOC receiver provides the angular position of the aircraft, except for the sensitivity (observations of the system):

$$y_{meas.} = \frac{\hat{D}}{S_{I_F}} \eta_{meas.} = y + y_{LOC\ noise} \tag{4.2}$$

It is now assumed that $y_{LOC\ noise}$ is white noise. The recursive Kalman-Bucy filter method, in which the observations are continuous, evaluates the three variables y, ΔV_T and γ_T from the $\dot{y}_I$ and $\eta_{meas.}$ measurements. Compared with the conventional version of the LOC-Inertial filter, an additional loop was added to provide the drift with time of the speed error of the inertial system. This term was, however, evaluated in the LIS 1 version by filtereing the static error $\hat{y} - y_{meas.}$.

4.2 Basic Design of the Version 3 (LISS 3)

The difficulties encountered with the first version of the statistical filter arose from the fact that the errors in the ratio $\frac{\hat{D}}{S_{I_F}}$ behave differently according to whether this ratio is over or underestimated as compared with the actual conversion ratio $\frac{D}{S_I}$. Any readjustment of the estimates, taking account of the LOC receiver data, is therefore falsified.

In order to relate the errors due to an incorrect estimate of the distance, not to the observation Equation (2), but to the state Equation (1), a further design was tried out. This consisted in using, as a state variable, the angular deviation η instead of the metric deviation y. The new equations for the system can therefore be written as follows:

$$\dot{\eta} = \frac{S_I}{D}(\dot{y}_I - \Delta V_T - \gamma_T \cdot t) + \frac{V}{D} \cdot \eta \tag{4.3}$$

$$\eta_{meas.} = \eta + \eta_{LOC\ noise}. \tag{4.4}$$

Still assuming that $\eta_{LOC\ noise}$ is white noise, the Kalman-Bucy filter equations can be written to evaluate the three variables $(\eta, \Delta V_T, \gamma_T)$.

In order to reduce the effect of the errors on S_{I_F} and $\hat{D}$, the epsilon technique[3] was used. This made it possible to weight the calculation of the three advantages of re-establishing the confidence placed in the calculations arrived at by the Kalman mehod.

4.3 Basic Design of Version 4 (LISS 4)

The equations written so far have assumed that the longitudinal speed of the aircraft remained appreciably constant throughout the approach, from initialisation to touch-down. Extension of the undercarriage or the high lift flaps means that the aircraft must reduce its speed. Such speed changes lead to immediate flight path deviations which are caused by the difference between the aircraft's track, as indicated by the inertial system at the time of initialisation of filtering, and the actual true runway heading. With a more complicated model for the transverse speed errors it is possible to anticipate being able to evaluate this track error, provided however that the aircraft changes speed during the filtering time.

The new inertial speed error model will therefore be:

$$\dot{y}_I = \dot{y} + \Delta V_T + \gamma_T \cdot t + \delta R_o (V_{L_o} - V_{L_n}) \tag{4.5}$$

in which ΔV_T, γ_T and δR_o are constants.

The four state variables calculated by the filter will be: $\hat{X}^T = [\hat{\eta}, \Delta\hat{V}_T, \hat{\gamma}_T, \delta\hat{R}_o]^T$.

- The presence of the term $(V_{L_o} - V_{L_n})$ in Equation (4.5) makes the system non linear and the change in the covariance of the various estimation errors therefore depends on the change in the longitudinal speed of the aircraft.

4.4 Integration of the Basic Loop in the Complete System

The analogue equations described above are not directly programmable in a digital computer. Furthermore, the inputs from the radio receivers are analogue inputs which must therefore be converted to digital form before they can be used. In addition, the inertial platform transmits the aircraft's ground speed components by means of an ARINC 571

type bus line at the booster frequency of 5 Hz. The calculation interval selected was therefore 0.2 s. The various gains have to be calculated from the various covariances of the estimation errors according to the discrete programming of the Kalman-Bucy filter[3].

The general overall diagram for the complete filtering calculations was the same as for the conventional version (LIS 1); it included a loop for evaluating the distance between the aircraft and the localizer transmitter, which comes into operation only on the occurrence of the logic signal indicating that the glide path has been captured. The loop for estimating the lateral deviation value to be transmitted to the auto-pilot, as described above in its various versions, is used instead of the slow and fast loops and dispenses with calculation of the weighting between these two computation loops. Filtering of the lateral deviation of the aircraft from the runway centre line is initialised as soon as the ILS localizer beam has been captured, on switching to the LOC-TRACK mode.

5. RESULTS OBTAINED WITH THE STATISTICAL FILTER DURING SIMULATION TESTS

5.1 Lateral Deviation Statistics at 100 ft, 15 ft and at Touch-Down

To check the advantages of Version 3 of the LISS filter over Version 1 or 2, 200 simulated approaches were made in each case:

- 100 approaches using long runways ($\overline{S_l} = 100\ \mu A/deg$) over descending ground so that the measured altitude is 2000 ft, while the altitude recorded in axes related to the landing runway is only 1500 ft;
- 100 approaches using short runways ($\overline{S_l} = 60\ \mu A/deg$) over rising ground ($h_{true} = 1500$ ft; $h_{measured} = 1000$ ft).

With the mean crosswind in the same direction, the mean values of the lateral shift of the centre of gravity of the aircraft were not zero. To obtain the mean quadratic deviation for a wind which on the whole is zero, the number of simulated approaches has to be combined with an identical number of approaches with a crosswind in the opposite direction. The standard deviation will then be $\sqrt{m^2 + \sigma^2}$. The Table in Figure 5.1 contains the statistical data for the various cases of guidance:

LOC: from the raw LOC signal

LIS 1: from the hybrid signal from the conventional filter (No.1)

LISS 2: from the hybrid signal provided by the statistical filter, Version 2, of state variables (y, ΔV_T, γ_T)

LISS 3: from the signal from the statistical filter, Version 3, of variables (η, ΔV_T, γ_T)

The advantage of the two versions of the statistical filter over the conventional filter can easily be seen. It will be noticed, however, that in the case of guidance using the LISS 2 and a short runway the advantage is very slight compared with LOC guidance. Version 3 of the statistical filter resolved this problem, although the dispersion was slightly greater when the aircraft landed on a long runway. This version was, however, the one adopted for the final programming of the LOC-Inertial filtering system, since it eliminated the differences encountered with the other versions for the various types of landing runways.

400 approaches were simulated with the LISS 3 filter so as to combine the various wind (strong – mild) and runway (average length, long and short) possibilities. Including the 600 approaches with a head wind, a total of 1200 approaches were made, the statistical details of which are given in the Table in Figure 5.2. The help afforded by the statistical filter in smoothing the flight path is quite clear, since the standard deviation for lateral displacement when coming down to 100 ft, 15 ft and at touch-down decreased by 5 to 8% as compared with LOC guidance, while it was 3 to 7% less in the case of the hybrid system using the conventional filter. The flight path parameter λ between 700 ft and touch-down was also much reduced (– 30%).

Finally, 200 simulated approaches were made by assuming that the speed errors of the inertial platform were halved. The results are shown in the Table in Figure 5.3 for comparison with the results of the hybrid guidance system, but with nominal performance of the inertial platform. No appreciable differences are noticeable, except for the maximum values, that is, the quality of the inertial unit has practically no effect on the final result.

5.2 Typical Flight Paths

With beam noise and atmospheric turbulence as defined for example in Section 2, the flight paths with LIS 1 guidance and then with the LISS 2 or 3 systems were compared with those obtained with the pure LOC guidance system (Figure 5.4 and Figure 5.5). The flight path was also disturbed when using the conventional LIS 1 filter, but improved with the statistical filter. The sensitivity to beam noise is greater during the first few moments of filtering with the LISS 3 version than with the LISS 2. After capture of the glide path the flight path is exactly the same, irrespective of the statistical filter version used.

For the same approach the corrections made by the filter to the transverse speed calculated from the inertial speed data are shown. It will be seen that the beam noise exerts a much greater influence when the conventional filter is used (Fig.5.6) than in the case of the statistical filter (Fig.5.5).

5.3 Movements Around the Aircraft's Centre of Gravity. Deflection of the Control Surfaces

The movements around the centre of gravity of the aircraft, as reflected in the sideslip (β), angle of bank (ϕ_1), heading ($\Delta\psi$), track (ΔR_V) or lateral acceleration (ay_1) parameters, as also in the angle of bank controlled by the auto-pilot ($-\phi_c$) and the deflections of the ailerons (δp_V) and the rudder (δr_g), are caused by LOC beam noise and atmospheric turbulence. With regard to the atmospheric disturbances, these did not affect the behaviour of the aircraft, since a requirement was made that the auto-pilot should not be touched in the 'LOC HOLD' mode. With respect to beam noise, its high frequency affected the above parameters so that the existence of LOC-Inertial filtering should be very beneficial. The standard deviation values for these variables are shown in the Table in Figure 5.8. They were calculated during a single approach, the approach already used for the typical flight paths referred to in paragraph 5.2. The conventional filter had already provided appreciable advantages, but the statistical filter gave even better results.

5.4 LOC Beam Failures: Disappearance of Beam with Failure Flag at h = 100 ft

The hybrid radio-inertial guidance system must be capable of guiding an aircraft in the event of failure of the localizer transmitter involving the disappearance of the beam and the occurrence of an alarm signal in the aircraft receiver. It will be assumed here that there is a system for confirming the position of the aircraft while the latter is following the glide path and reaching an altitude of 100 ft. This system, designed by the STNA, makes it possible, by providing the aircraft's lateral position, to ascertain whether the last few moments of the approach have been satisfactory or otherwise and, consequently, whether the LOC beam was correct or not. The transmitter is assumed to have failed immediately after such a test. To make a true assessment of the ability of the system to survive such a failure, 200 approaches were simulated for this case, including 100 with an average length runway, during which distance and sensitivity were evaluated fully, and 100 for the opposite case (short runway). The Table in Figure 6.9 contains lateral displacement details.

The observations can be made:

- *average length runways*: the two filters, LIS 1 and LISS 3 give comparable performances; the statistical filter reduces the standard deviation value, although with a slight increase in the maximum value;
- *short runways*: the statistical filter provides much better guidance for the aircraft, based on inertial data only. The corrections to be made to the transverse speed of the aircraft ($\dot{y}_I$) are thus much more exact.

The survival time of the statistical filter is not therefore dependent on the type of runway on which the aircraft is to land. The shortest time is 16 to 20 seconds, that is, if failure occurs at 100 ft the aircraft is correctly guided to touchdown, even if the latter is delayed because of a longer flare-out than usual. With the LISS 4 version, provided the approach procedure indicates a change in the aircraft's speed during filtering, guidance is correct down to very low speeds, and Category IIIB landing can be envisaged, even in the event of a permanent LOC failure.

5.5 Detected LOC Beam Faults (Square Waves and Slopes)

The assumption is made here that the centre line of the LOC beam is suddenly offset by 20 μA (square waves) or offset slowly at a constant rate (slopes). The monitor located at the runway threshold monitors the course of the centre line of the beam: as soon as the latter exceeds a distance corresponding to 8.5 μA (the Category III value) for more than 2 seconds, the incorrect course is detected and it is assumed that the first transmitter ceases operating and that the second transmitter comes into action in less than 1 second. Correct transmission is then resumed after a maximum of 3 seconds.

The flight path deviation varies with the altitude of the aircraft at the time of the LOC failure. Figures 5.10 and 5.11 show how the aircraft behaves in three cases of square waves (h = 1000 ft, 500 ft and 100 ft) and in two cases which were characterised by slopes (h = 1000 ft, beam drift of 0.1 μA/s and h = 500 ft, beam drift of 2 μA/s). With regard to sudden failures of the beam, the statistical filter provides very definite assistance, while for slow beam divergences, there is no improvement, whatever the type of filter used for aircraft guidance.

5.6 Undetected LOC Beam Faults

This paragraph concerns space or time faults in the LOC beam which cannot be detected by the runway threshold monitor, since they do not result in any exceeding of the detection threshold values. These faults are: a sudden jump of the beam centre line from one side of the threshold to the other ($\pm$ 8.5 μA) when the aircraft is at 500 ft; a sine wave curve with a period of 50 s ($V \simeq 70$ m/s) which begins while the aircraft is completing its level flight at 1500 ft and is starting to descend the glide path, and finally, a single sine wave period which is offset from the runway centre line (Fig.5.12).

For all these disturbances the hybrid guidance system provides a very slight improvement, but the periods of these phenomena are long, which makes it difficult to filter the signals; if the periods are less than 50 seconds, filtering achieves definite results.

5.7 Interference due to an Aircraft Flying Over the LOC Transmitter

The British Royal Aircraft Establishment has investigated this phenomenon[4] caused by an aircraft flying over the

the LOC transmitter during its take-off while the aircraft under investigation is beginning its approach. A noise is heard, for example, at the LOC receiver output, such as that shown in Figure 5.13a. Figures 5.13b and c show the behaviour of the aircraft without LOC guidance or with the conventional filter (LIS 1) or the statistical filter (LISS 3). There is a distinct smoothing of the flight path at the same time as the roll and heading movements are reduced in a ratio of 3 to 4, depending on the parameter involved.

5.8 Behaviour of the Filter in the Presence of Real LOC Beam Noise (Recorded in Flight)

The LOC beams recorded in flight, which had already been used to find a representative model of beam noise with a view to its assessment, were also used during the simulation studies. They have the disadvantage, however, of being limited in total time and the filtering time is not long enough to have any smoothing effect. Figure 5.14 shows the flight paths obtained on three American LOC beams. In the case of the Los Angeles beam (Fig.5.14c) the noise was considered to be zero before the actual recording, so that the filtering time could be increased. A greater degree of smoothing was then achieved than in cases where initialisation was delayed (Fig.5.14b).

5.9 Effect of the Longitudinal Movement of the Aircraft

Because of a change in speed on glide path capture for example (when the undercarriage is extended and the V_{REF} is set in the auto-throttle), the LISS 3 version of the statistical filter involves deviations of the flight path which are then resorbed and have no effect on lateral displacement at touch-down. To reduce these lateral displacements, the LISS 4 was implemented, and provided the very clear reduction which can be seen in Figure 5.15. This version thus lessens the effect of ground speed changes caused by wind gradients or by voluntarily decelerated approaches, and has the advantage of permitting automatic guidance of the aircraft during braking on the runway in the event of a LOC failure at the end of the approach. Furthermore, the results obtained with a constant aircraft speed are not affected.

6. DESCRIPTION OF THE SAGEM LOC-INERTIAL SYSTEM, LIS 30

6.1 Integration in the Aircraft

The digital LOC-Inertial system was designed to be transparent to the auto-pilot, that is, it can be inserted in the aircraft wiring between the ILS receivers and the auto-pilot computers without requiring any modification of the latter.

It receives deviation data from the ILS receiver, North and East speed vector information from the inertial platform and height data from the radiosonde.

It provides the auto-pilot with deviation data which are electrically analogous to those from the ILS receiver, but which have been smoothed by the inertial system.

It enables guidance to be continued in the event of loss of the LOC beam; in addition, it becomes functionally short-circuited when such a fault occurs, and the auto-pilot is then coupled direct to the ILS receiver.

6.2 Description of the System

Physical characteristics: The system is ½ ATR long and meets the requirements of the ARINC 404A Standard. It weighs a maximum of 12 kg and its power consumption never exceeds 150 W.

Layout: It is arranged around a digital processor (French initials: UTD). All the data processing, as well as the majority of the monitoring tests, are carried out in the UTD by program.

Input/output sections: These provide the input quantities for the UTD and convert the output quantities to a format which is suitable for use.

UTD processor: This is a general purpose computer, with a 16 bit parallel organisation; its control unit is micro-programmed.

For a list of its main characteristics see Figure 6.1.

The implanted memory in the LIS 30 computer will be 4K program words and 1K working memory words.

Reprogramming memory: The program memory is erasable and rewritable direct on to the memory cards, which gives the computer wide flexibility when a program has to be modified.

Encoder: This permits acquisition of the analogue quantities (LOC, glide path and radiosonde signals) and converts the output data (filtered LOC signals) fed into the auto-pilot.

resolution: 12 bits
accuracy: 1/2 LSB

Digital inputs/outputs: These make it possible to acquire and to transmit the discrete signals and the digital data from the inertial platforms by means of a bus line, and also permit inter-system dialogue in the case of dual lines.

6.3 Single and Twin Computer Operation

The basic installation of the Airbus auto-pilots has a particularly high level of redundancy for achieving Category III landing and uses the following:

- 2 sets of self-monitoring sensors (ILS and radiosonde),
- 4 computing channels in the auto-pilots.

The level of redundancy is lower for Category II landing (2 computing channels for 1 set of self-monitoring sensors).

For integration in the present Airbus layout, the LISS 30 system can have the following configurations:

Single computer configuration: a single computer used in conjunction with one side only of the auto-pilot.

Twin computer configuration: two computers, one associated with side 1 and the other with side 2 (Fig.6.2).

A digital bus line allows dialogue between the two computers for the prupose of probability tests between the two channels.

6.4 Failure Detection

Short-circuiting: Because the LISS 30 system is inserted between the ILS receiver and the auto-pilot, the system is required to short-circuit if a failure is detected, that is, a set of relays enables the raw localizer signal to be transmitted direct to the auto-pilot input (transparent system).

System self-tests: a negative result from one of the following tests will cause the system to short-circuit:

- computer test (microprogram),
- test of software performance (hardware),
- static memory test (software),
- dynamic memory test (software),
- operations test (software),
- encoder test (software).

Inter-computer probability tests: These are performed in the case of a twin computer configuration. If the two lines show any differences, the two LISS 30 systems are short-circuited.

Automatic detection of inertial sensor failure: The system becomes transparent.

Localizer failure: In the event of a localizer failure, the inertial system continues to provide guidance for a period which depends on the convergence of the filter. On expiry of this period the system is short-circuited.

Below 100 ft the inertial system will continue to operate until touch-down.

Glide path or radiosonde failure: Glide path and radiosonde data are used to assess the distance to the localizer transmitter. This distance is filtered by means of the inertial speed and, in the event of failure or one of the two radio sensors, the inertial system will continue to function for a period which depends on the filtering time. At the end of this period, the system is short-circuited.

Below 250 ft the distance is calculated solely on the basis of inertial speeds, since the glide path signal ceases to be of use as soon as flare-out has begun.

6.5 Recorded Data Output

The prototype computers have a digital output for recorded data, which takes the form of a two-wire bus line.

This output transmits 17 24-bit words every calculation cycle (input, output, internal logic parameters, and internal filtering parameters). It provides rapid analysis of any in-flight phenomena.

7. FLIGHT TESTS AT CEV

7.1 Background

All the preliminary evaluation tests of the LOC-Inertial system took place at the Flight Test Centre at Brétigny (CEV).

The tests were made during 1975. The filtering calculations were performed in real time by a commercial designed computer installed in a NORD 262.

The filter put forward by SAGEM was very simple in its structural design and consisted of an elementary loop in the conventional version (LIS 1).

The results obtained, however, were very encouraging and confirmed the feasibility of the system.

In early 1976 evaluation of the LOC-Inertial system was continued by ground simulation studies using in-flight recorded data.

This method provided a preliminary study of the conventional version of the filter (LIS 1).

As these were made outside the aircraft control loop, however, they could not indicate the performance of the system when coupled to an auto-pilot.

7.2 Flight Tests of the SAGEM LIS 30

A programmed LIS 30 computer in the conventional filter was flight tested at CEV, Brétigny in December 1976 in a NORD 262, and again from March 1977 in a Mystère 20.

In both cases the LIS 30 was coupled to the aircraft auto-pilot.

The flight test programme consisted of a statistical study at Brétigny (50 to 60 approaches) and a series of investigations of airfields with ILS systems which were felt to be poor.

At Brétigny the performance of the system was evaluated by means of the STRADA trajectory plotting system (laser telemetry).

On outside airfields the flight path was plotted using airborne facilities (inertial system with camera).

These tests are to be continued with a programmed computer in Version 4 of the statistical filter. The inertial platform used for all these tests will be a SAGEM MGC 30 unit.

7.3 Preliminary Results with the Conventional Filter LIS 1

Tests on the LIS 30 system are proceeding at CEV. To date, some 50 approaches carried out at Brétigny with the conventional version in the NORD 262 have been used for purposes of analysis. The STRADA trajectory plotting system was used to assess system performance, both in regard to plotting the position of the aircaft and evaluating inertial errors.

Using recordings of the data input to the LIS 30 system, about 20 approaches were simulated by feeding in the true runway heading as a reference direction. The Table in Figure 7.1 shows the filtering performance in the normal case (use of the inertial track at the time of initialisation), compared with the use of the actual runway heading. Similarly, Figure 7.2 shows aircraft guidance performance when using the pure inertial system at 100 ft. The very distinct improvement afforded by the use of the actual runway heading for guiding the aircraft after touch-down will be noted. One approach was made with a steep wind gradient involving a speed change of 50 kt, which had resulted in a large error at touch-down in normal conditions (8 m). Feeding in the runway heading eliminated this extreme case.

Summarising, the flight tests point to the conclusion that with the conventional filter inertial guidance can be continued to touch-down, provided the approach is made at a constant ground speed.

If the actual runway heading is fed in, guidance is maintained during ground taxying and the approach can be made with changes in speed.

8. SNIAS TESTS

8.1 Flight Simulator Tests

Following the CEV flight tests of the conventional version of the LOC-Inertial system, the new filtering equations (LISS 3) were programmed in a second SAGEM digital computer. Before it was fitted in the aircraft, this computer was placed in the Aérospatiale flight simulation laboratory in Toulouse-Blagnac, coupled to actual Airbus equipment. The tests brought to light some minor programming and aircraft wiring faults. These were quickly rectified, for example by using reprogrammable memory stores. Further tests in the same conditions as for the computer simulation tests yielded exactly the same results as those obtained previously.

8.2 Tests in the Airbus A 300 B No.3

The LISS 30 computer was then made available for flight testing by AIRBUS-INDUSTRIE. The first flight (25/3/77) proved that the system functioned correctly both in the normal filtering mode and during a simulated localizer signal failure. Modification of the filtering program used in the LISS 3 version (in which only 3 variables were estimated) to make it suitable for the LISS 4 version (with 4 variables) was completed within a week. A short run in the flight simulator checked the functioning of the system, after which flight tests were resumed. The system for in-flight recording of the aircraft parameters and the system internal parameters made it possible to compare the estimated performance of the real system with the estimates obtained by the simulation program. The lower degree of accuracy with the real computer (32 bits for the critical parameters) did not result in errors of more than 1%, even after a long filtering time.

The Airbus No.3 was then used for investigating some noisy localizer beams. The increased comfort for the crew was very marked: 3 approaches were made over each airfield: the first without the LISS system (open loop), the second with the system in the guidance loop (closed loop), and the third still with the closed loop, but with a failure of the LOC signal at 100 ft. The system functioned satisfactorily, even when braking on the runway, until the aircraft came to a halt, whereas with the previous version (LISS 3) the pilot was obliged to disconnect the auto-pilot as soon as the aircraft speed began to decrease appreciably ($V \leqslant 100$ kt).

9. CONCLUDING REMARKS

The hybrid radio-inertial guidance system described above performs the following functions:

- smoothing of the aircraft's flight path during an ILS automatic approach, particularly in the final phase ($h \leqslant 700$ ft);
- a very marked reduction in the lateral movements of the aircraft around its centre of gravity and in the deflection of the control surface due to LOC beam noise;
- the continuance of guidance in the event of failure of the LOC receiver. If failure occurs while the aircraft is coming down to 100 ft, the period of survival of the system is 20 to 25 seconds, which means that the aircraft will touch-down correctly, even in the case of a long landing. Provided there has been a change of speed during the filtering time, the aircraft will also continue to be guided during its reduction of pseed along the runway;
- in the event of serious or sudden failures (period less than 50 seconds) which interfere with guidance of the aircraft, the LISS system dispenses with the need for LOC signals and reduces any deviation movements of the aircraft;
- The system requires only a relatively low performance inertial unit (CEP $\leqslant$ 2.5 NM/h), although one with a higher performance would slightly improve the overall system.

The system should thus allow operation on a landing running in meteorological conditions of a higher category than that of the airfield, while improving passenger comfort. As far as the rate of go-arounds due to LOC failures or faults is concerned, this should be reduced by the inclusion of this system in the aircraft guidance loop.

REFERENCES

1. Bleeg, R.J.; Tisdale, H.F.; Vircks, R.M. — *Inertially Augmented Automatic Landing System (A/P Performances with Imperfect ILS Beams).* Boeing Company. FAA Contract RD-72-22, April 1972.

2. – — *Analytical Study of ILS Beam Characteristics.* Bendix Corproation, Eclipse, Pioneer Division. F.A.A. Contract ARDS-451, August 31, 1962.

3. Faurre, P. — *Navigation inertiele optimale et filtrage statistique.* Collection "Méthodes mathématiques de l'Informatique, Ed. Dunod, Paris, 1971.

4. Hughes, N.H. — *The Effects on Automatic Landing Lateral Performance of Interference to the ILS Localizer by Reflection from an Aircraft Taking Off.* RAE Technical Report 68156, June 1968.

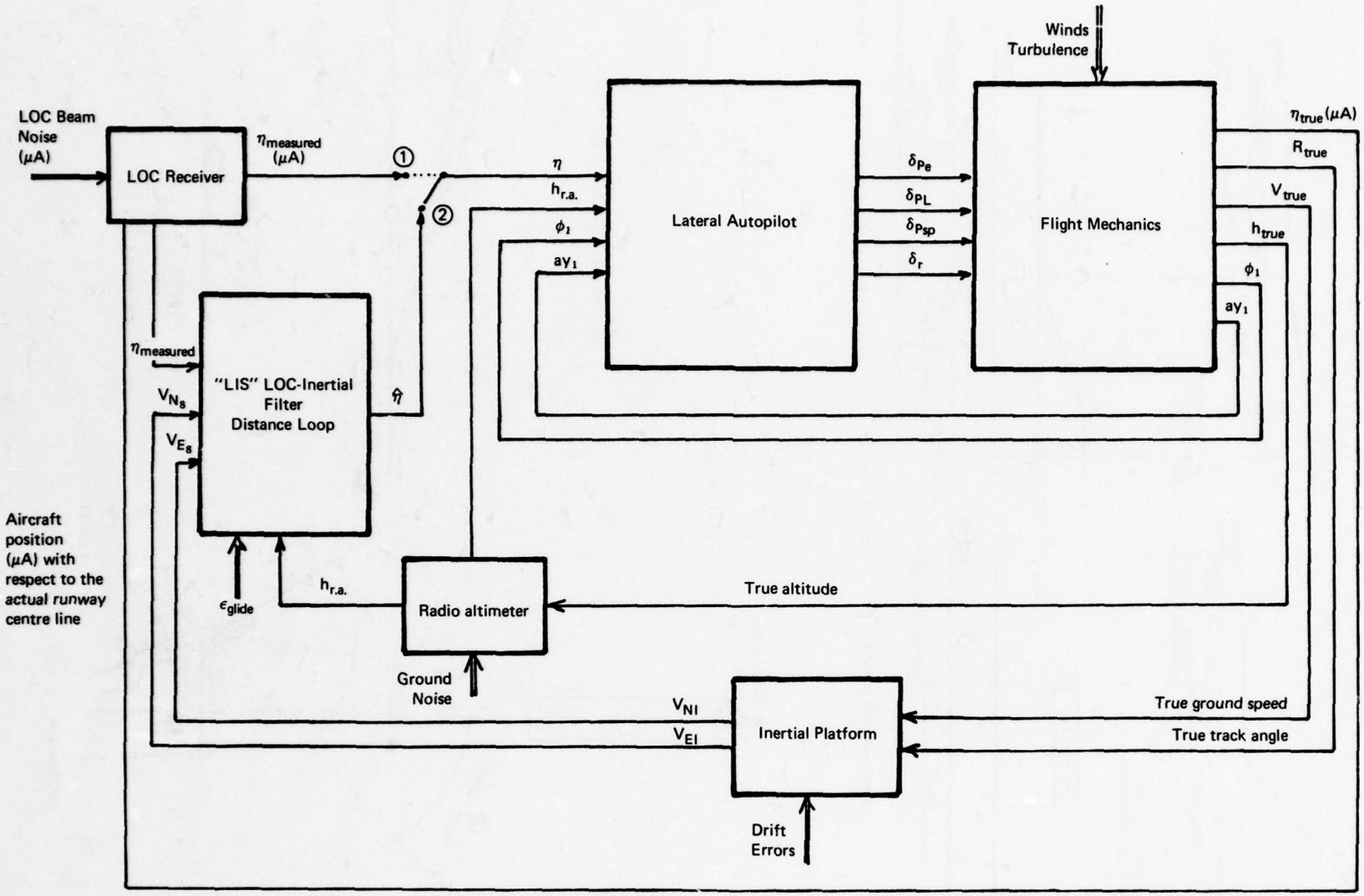

General Diagram of Simulation Study

Figure 2.1

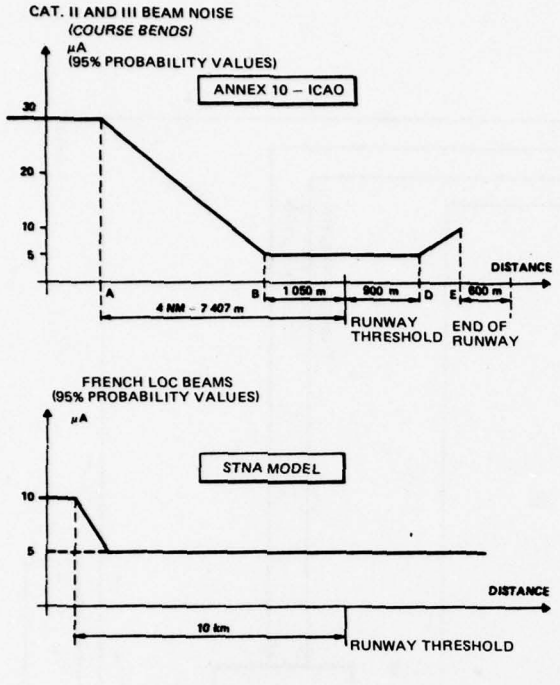

LOC BEAM NOISE MODELS Figure 2.2

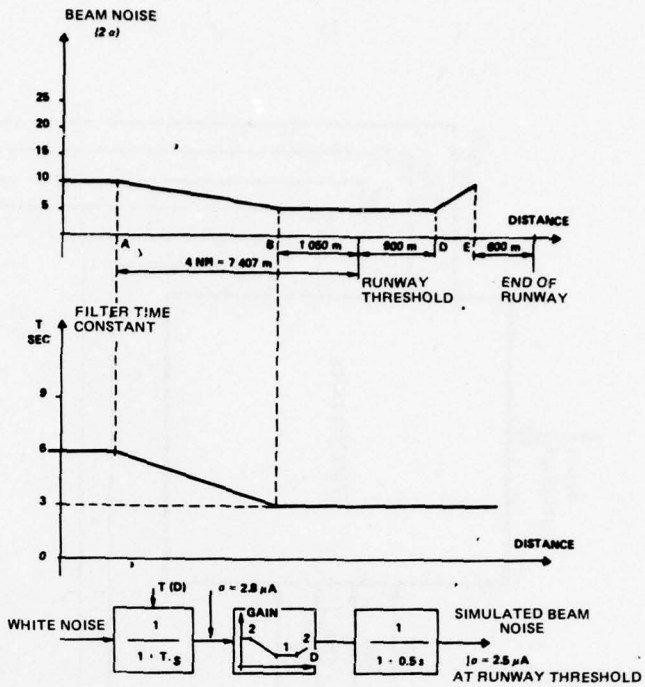

PROPOSED BEAM NOISE MODEL Figure 2.3

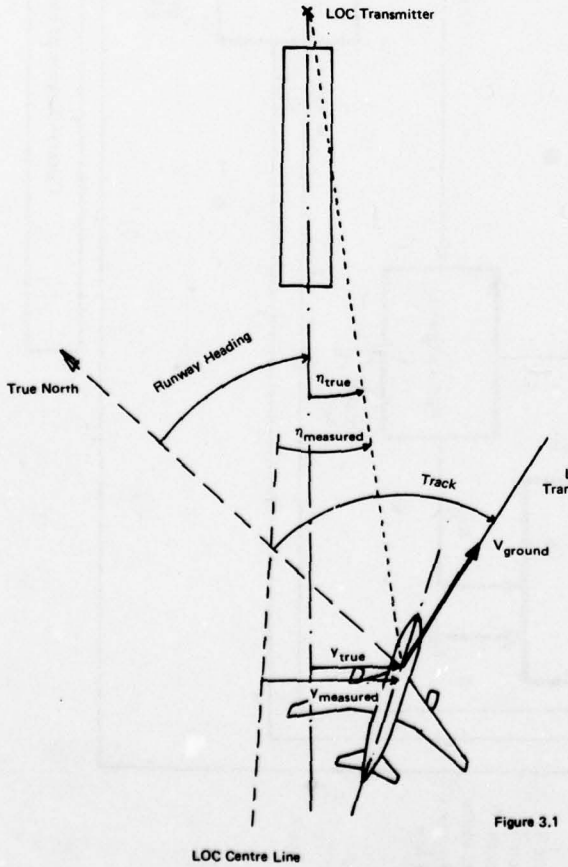

Figure 3.1

Evaluated Distance From Aircraft to LOC Transmitter

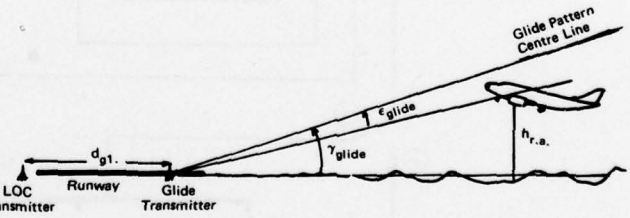

$$D = \frac{h_{r.a.}}{\gamma_{glide} + \delta_g . \epsilon_{glide}} + d_{gl.}$$

$d_{gl.}$: distance between LOC and glide transmitters

γ_{glide} : glide slope

δ_g : glide beam sensitivity

ϵ_{glide} : glide receiver output

Figure 3.2

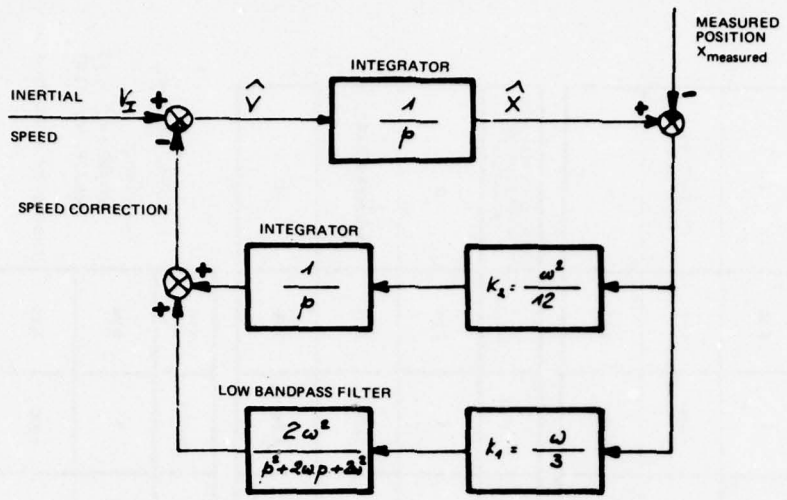

Figure 3.3 BASIC FILTERING UNIT – CONVENTIONAL VERSION (LIS1)

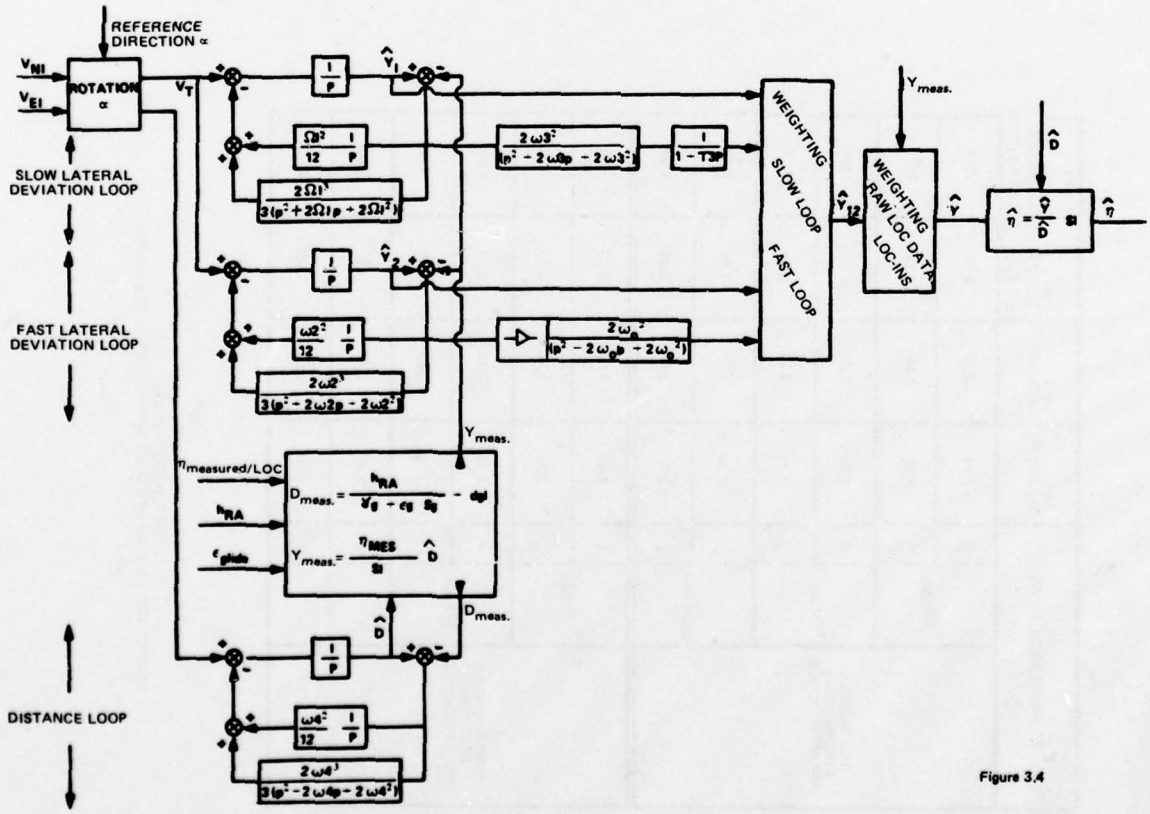

Figure 3.4

STANDARD DEVIATION			LOC GUIDANCE	LIS 1 GUIDANCE	LISS 2 GUIDANCE $(\gamma, \Delta V_T, \dot{\gamma}_T)$	LISS 3 GUIDANCE $(\eta, \Delta V_T, \dot{\gamma}_T)\epsilon \neq 0$
LONG RUNWAY STRONG WIND (100 APPROACHES)	$Y_{CG_{100ft}}$	σ	2,54	2,70	2,04	2,17
		$\sqrt{m^2+\sigma^2}$	3,36	3,55	3,13	3,17
	$Y_{CG_{15ft}}$	σ	2,06	2,23	1,66	1,84
		$\sqrt{m^2+\sigma^2}$	3,39	3,30	2,99	3,12
	$Y_{CG_{touch-down}}$	σ	2,34	1,87	1,48	1,56
		$\sqrt{m^2+\sigma^2}$	3,07	3,04	2,80	2,88
SHORT RUNWAY MILD WIND (100 APPROACHES)	$Y_{CG_{100ft}}$	σ	2,60	2,59	2,47	2,01
		$\sqrt{m^2+\sigma^2}$	3,37	3,38	3,03	2,78
	$Y_{CG_{15ft}}$	σ	2,25	2,40	2,12	1,90
		$\sqrt{m^2+\sigma^2}$	2,70	3,02	2,70	2,60
	$Y_{CG_{touch-down}}$	σ	1,95	2,14	1,81	1,63
		$\sqrt{m^2+\sigma^2}$	2,34	2,56	2,32	2,22

STATISTICAL RESULTS
COMPARISON OF BOTH VERSIONS OF THE STATISTICAL FILTER

Figure 5.1

$Y_{CG_{100\ ft}}$ (m)		σ	RATIO	MAX. VALUE	Failed Approaches (Performance Confirmed)*
GUIDANCE	LOC	3,18	1	8,54	0
	LIS	3,36	1,056	9,74	6 (INCLUDING 1 DIVERGENCE)
	LISS	2,97	0,934	9,12	1

$Y_{CG_{15\ ft}}$ (m)		σ	RATIO	MAX. VALUE	FAILED APPROACHES (EXCESSIVE LOC DEVIATION)*
GUIDANCE	LOC	2,95	1	8,61	0
	LIS	3,15	1,068	9,11	1 (DIVERGENCE)
	LISS	2,80	0,949	7,09	0

$Y_{TP_{touch-down}}$ (m)		σ	RATIO	MAX. VALUE
GUIDANCE	LOC	2,94	1	9,24
	LIS	3,03	1,030	8,41
	LISS	2,71	0,922	7,23

LOC NOISE: AS MODEL

TURBULENCE

600 APP. : V_y = 10 KT

600 APP. : V_y = 15 KT

* OUT OF 600 APPROACHES ONLY

STATISTICS FOR 1200 APPROACHES

Figure 5.2

Y_{CG} 100 FT	σ	MAX.
LOC	2.63	7.61
LISS INS Nominal	2.67	7.76
LISS Error INS/2	2.53	6.85

15 FT	σ	MAX.
LOC	2.61	7.53
LISS INS NOMINALES	2.36	6.89
LISS INS/2	2.31	6.71

Y_{CG} Touch-down	σ	MAX.	λ vrai
LOC	2.76	8.76	5.61
LISS	2.34	6.07	4.49
LISS INS/2	2.21	5.26	4.27

$$\lambda_{true} = \sqrt{\frac{\sum_{i=1}^{\eta} \max\,(\eta_{meas.})^2}{2n}}$$

400 APPROACHES

Figure 5.3

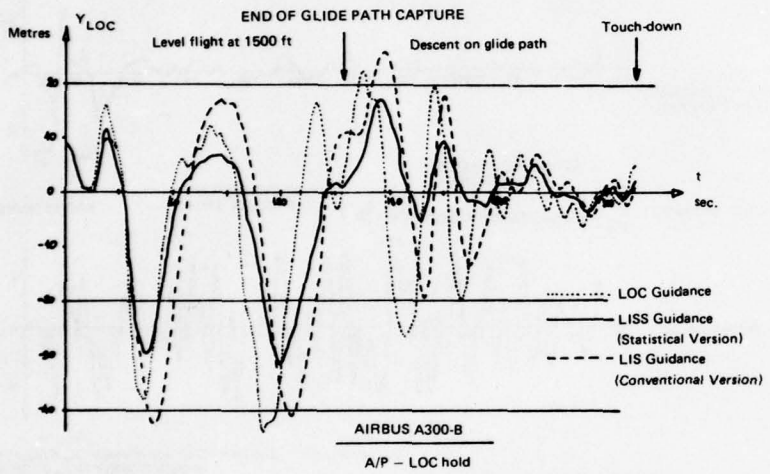

Figure 5.4 COMPARISON OF FLIGHT PATHS OBTAINED WITH THE VARIOUS VERSIONS

SIMULATION OF AIRBUS A 300 B AND A/P LOC HOLD STRONG WIND –
STATISTICAL FILTER $(\eta IV_T, \gamma_T)$ $\epsilon_o = 0.03$
APPROACH 102 – AVERAGE LENGTH RUNWAY –
LISS GUIDANCE – FULL STRESSING

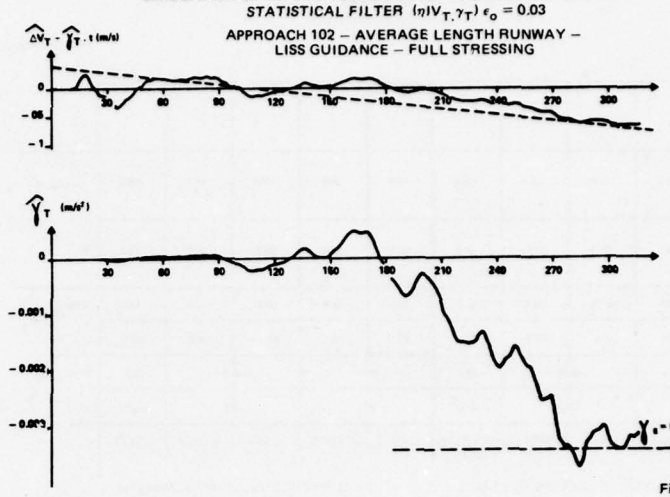

Figure 5.5

SIMULATION OF AIRBUS A 300 B AND A/P LOC HOLD
BEAM NOISE (AS MODEL) AND WINDS + TURBULENCE (25 INCLUDING 15 kt)
AVERAGE RUNWAY ----- MODIFIED SAGEM FILTER. LIS GUIDANCE ISI 102

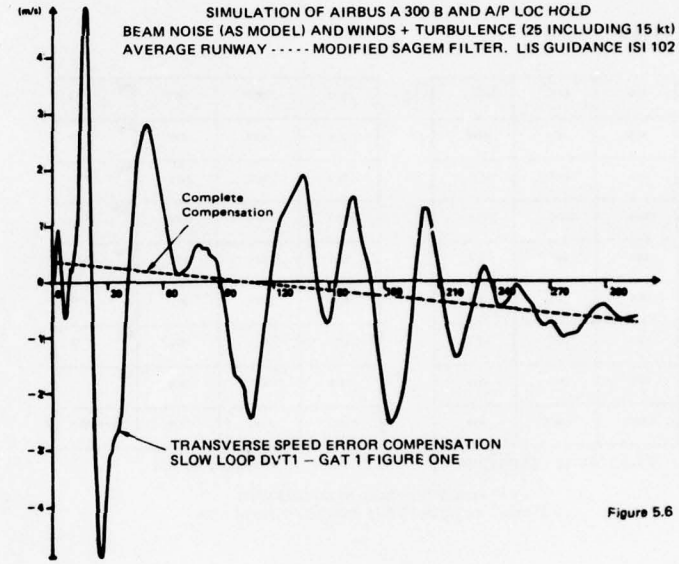

Figure 5.6

STRESSES: LOC BEAM NOISE ONLY

SIMULATION AIRBUS A300 B
AUTOMATIC APPROACH AND LANDING – LATERAL A/P

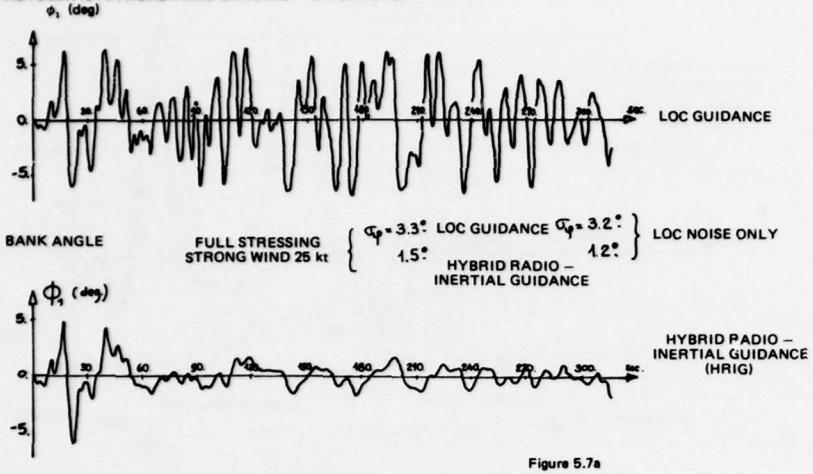

Figure 5.7a

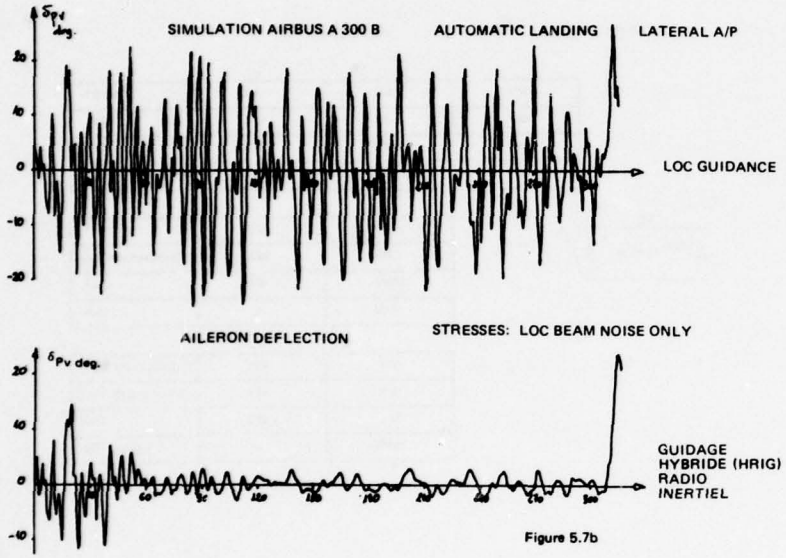

Figure 5.7b

MOVEMENTS AROUND THE CENTRE OF GRAVITY
DEFLECTION OF CONTROL SURFACES

GUIDAGE	LOC NOISE ONLY			LOC NOISE + TURBULENCE		
	LOC	LIS 1	LISS 3	LOC	LIS 1	LISS 3
β deg	0.79	0.49	0.47	1.13	0.91	0.91
Θ deg	3.34	1.73	1.21	3.34	2.04	1.47
$\Delta\psi$ deg	1.85	1.51	1.09	2.11	1.87	1.41
ΔR_V deg	2.04	1.61	1.12	2.83	1.88	1.88
$\sigma_{\dot{y}_1}$ m/s²	0.071	0.045	0.039	0.110	0.085	0.082
Θ_c deg	3.73	1.88	1.38	3.73	2.03	1.47
δ_{P_V} deg	10.07	4.05	3.60	10.04	6.47	10.09
δ_{r_0} deg	1.90	0.88	0.61	1.86	0.83	0.79

Figure 5.8

	MEDIUM RUNWAYS. STRONG WIND					SHORT RUNWAYS. STRONG WIND				
	LOC*	LIS1*	LIS 1	LISS 3*	LISS 3	LOC No Failure	LIS 1 No Failure	LIS 1	LISS 3 No Failure	LISS 3
V_{eq} 100 FT σ	2.31	2.61		1.88		2.46	2.04		2.39	
V_{eq} 100 FT MAX.	7.70	8.69		7.39		7.87	9.09		9.12	
V_{eq} 15 FT σ	2.35	2.49	2.47	1.84	1.45	2.39	2.37	3.11	1.85	2.53
V_{eq} 15 FT MAX.	8.61	9.11	8.49	6.70	9.35	7.39	8.71	10.39	6.17	7.69
σ	2.77	2.11	2.89	1.72	2.35	2.65	2.39	4.02	1.61	2.63
V_{eq} Touch-down	6.89	7.49	6.32	6.85	9.69	6.33	6.97	10.07	6.65	9.45

* No Failure

LOC TRANSMITTER FAILURES
LOSS OF BEAM AT 100 ft

Figure 5.9

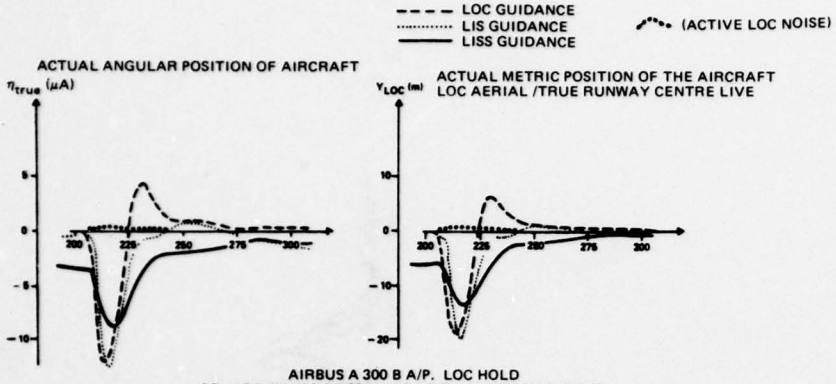

AIRBUS A 300 B A/P. LOC HOLD
SQUARE WAVES OF 20 μA LOC SIGNAL FOR 3 SECONDS
H = 1000 ft; LISS GUIDANCE

Figure 5.10a

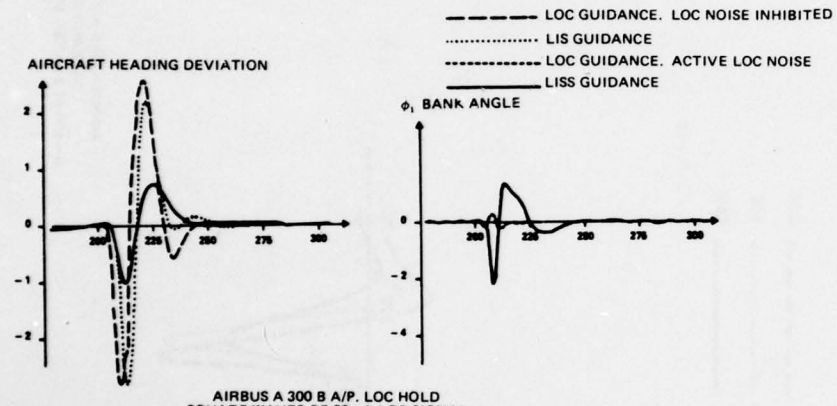

AIRBUS A 300 B A/P. LOC HOLD
SQUARE WAVES OF 20 μA LOC SIGNAL
H = 1000 ft; LISS GUIDANCE

Figure 5.10b

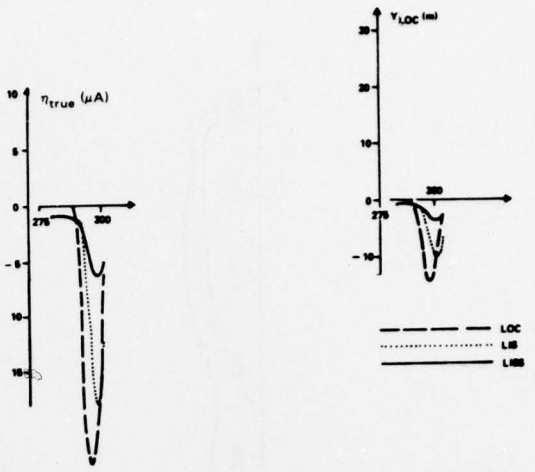

AIRBUS A 300 B A/P. LOC HOLD
SQUARE WAVES OF 20 μA LOC SIGNAL FOR 3 SECONDS
H = 100 ft; LISS GUIDANCE

Figure 5.10d

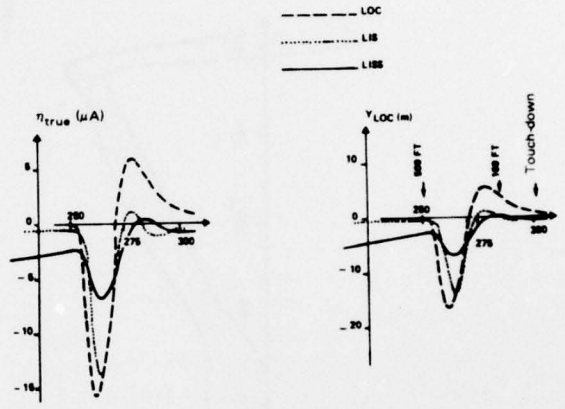

AIRBUS A 300 B A/P. LOC HOLD
SQUARE WAVES OF 20 μA LOC SIGNAL FOR 3 SECONDS
H = 500 ft LISS GUIDANCE

Figure 5.10c

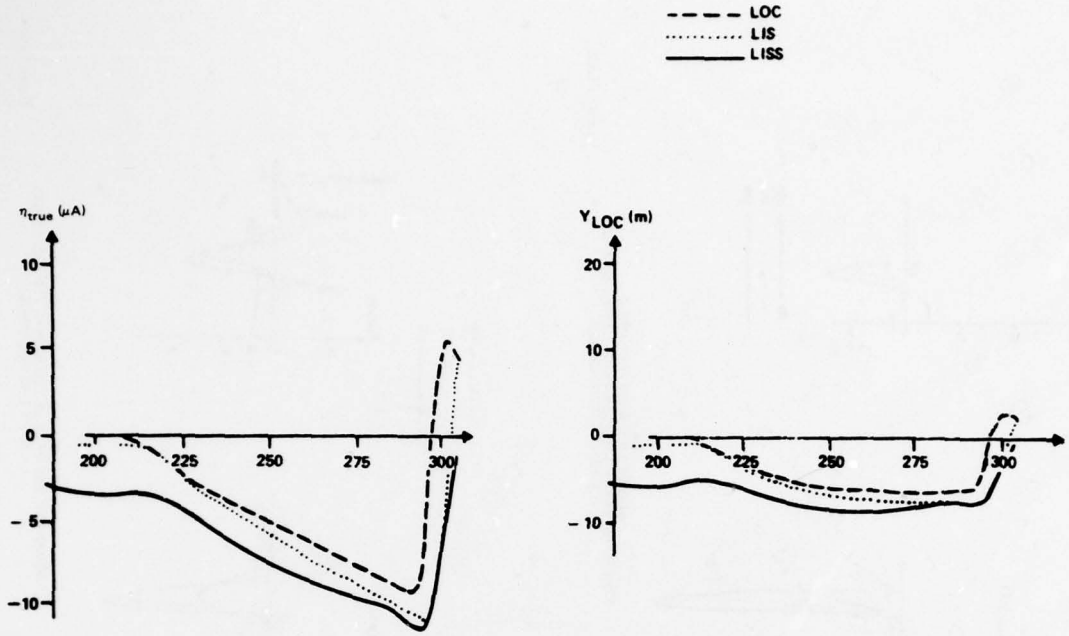

AIRBUS A300 B A/P. LOC HOLD
LOC ERROR SLOPES
H = 1000 FT 0.1μA/SEC LISS GUIDANCE

Figure 5.11a

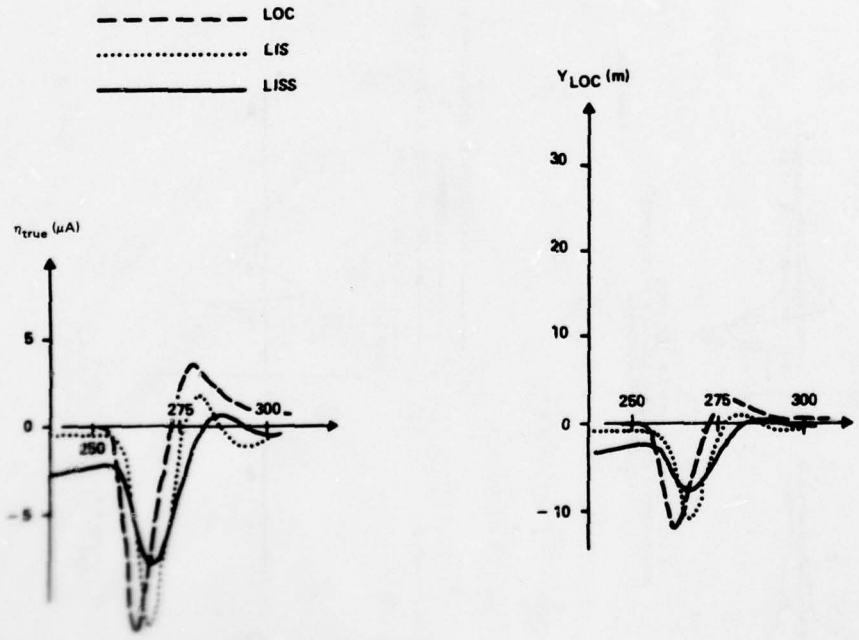

AIRBUS A300 B A/P. LOC HOLD
LOC ERROR SLOPES
H = 500 FT 2 μA/SEC LISS GUIDANCE

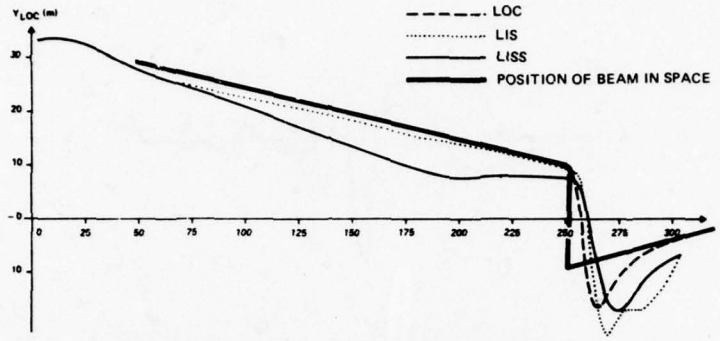

AIRBUS A300 B A/P. LOC HOLD
LOC CENTRE LINE, A – 8. 5μA
H = 500 ft. LISS GUIDANCE

Figure 5.12a

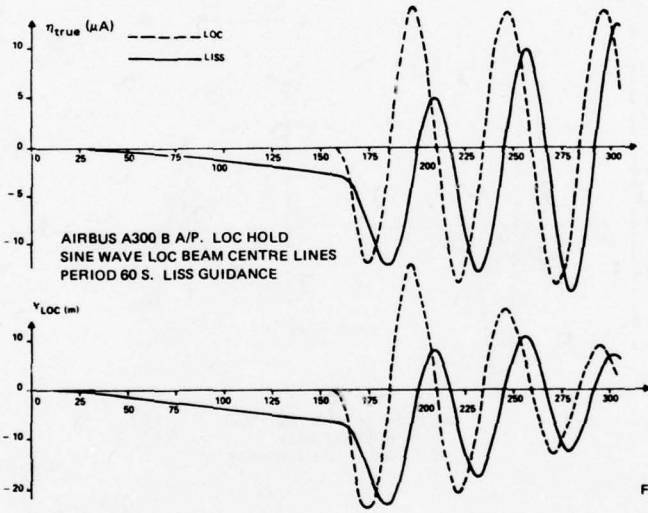

AIRBUS A300 B A/P. LOC HOLD
SINE WAVE LOC BEAM CENTRE LINES
PERIOD 60 S. LISS GUIDANCE

Figure 5.12b

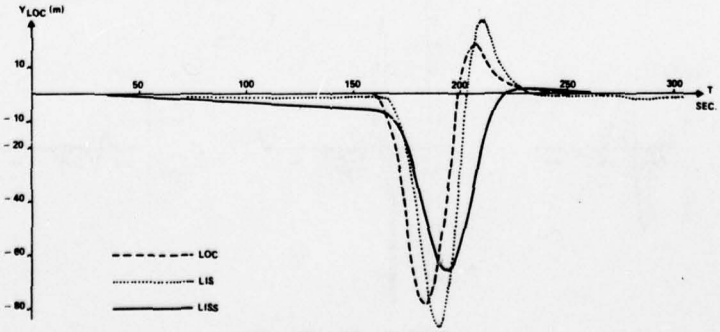

AIRBUS A300 B A/P. LOC HOLD
LOC BEAM CENTRE LINES CURVES (1–COS)
H = 1500–1000 ft; LISS GUIDANCE

Figure 5.12c

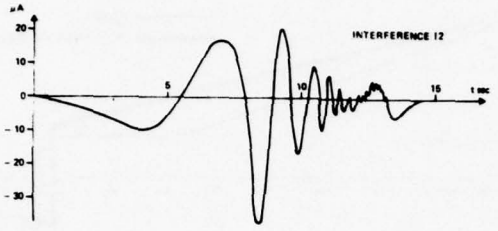

NOISE CAUSED BY AIRCRAFT PASSING OVER LOC TRANSMITTER
(FROM RAE REPORT No TR68156, JUNE 1968)

Figure 5.13a

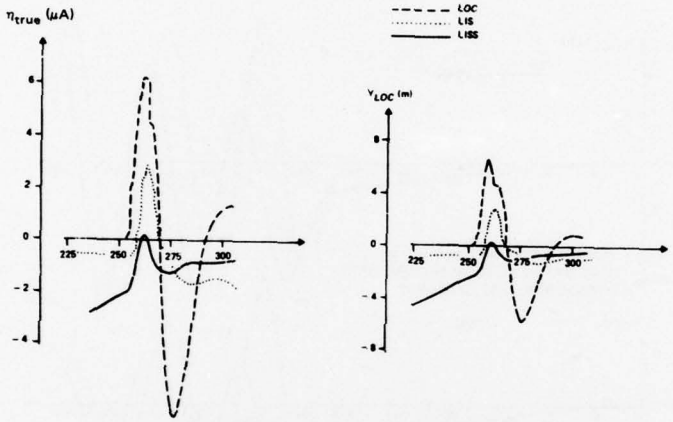

AIRBUS A300 B A/P. LOC HOLD
INTERFERENCE
12 H = 500 FT LISS GUIDANCE

Figure 5.13b

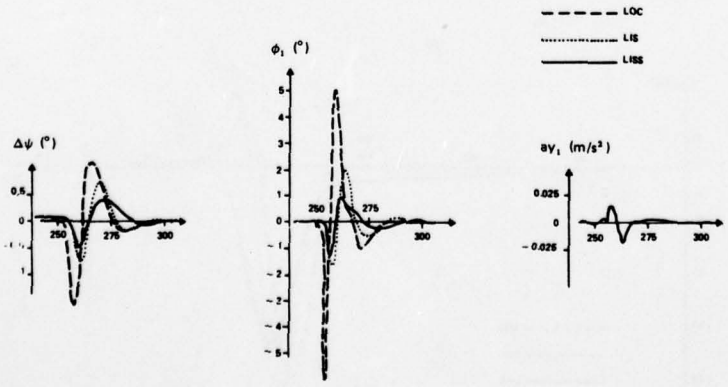

AIRBUS A300 B A/P. LOC HOLD
INTERFERENCE
14 – H = 500 FT – LISS GUIDANCE

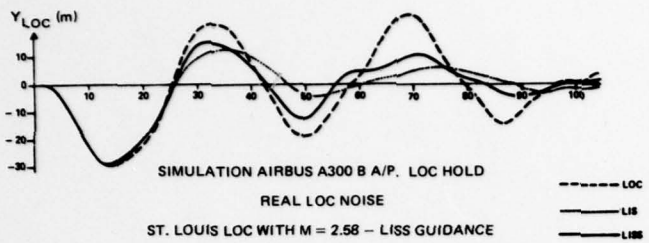

SIMULATION AIRBUS A300 B A/P. LOC HOLD

REAL LOC NOISE

ST. LOUIS LOC WITH M = 2.58 – LISS GUIDANCE

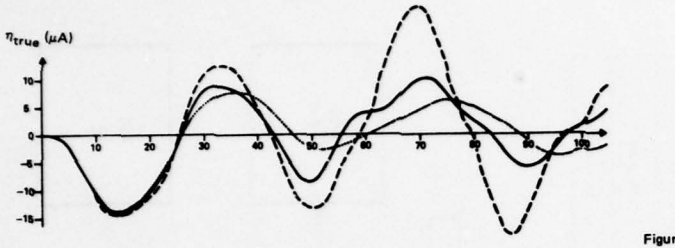

Figure 5.14a

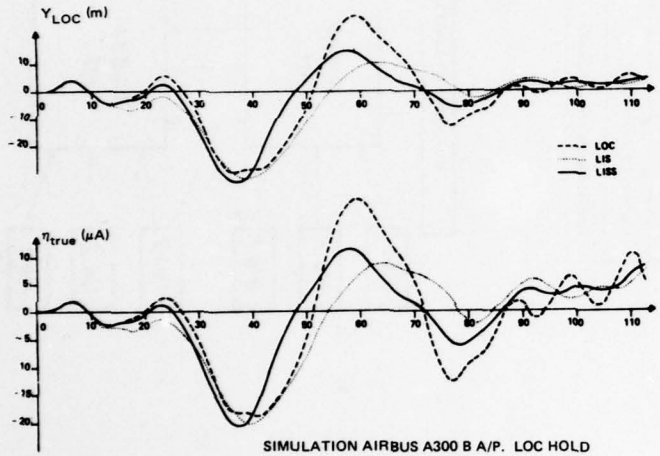

SIMULATION AIRBUS A300 B A/P. LOC HOLD

REAL LOC NOISE

SAN FRANCISCO LOC WITH M = 3.85 – LISS GUIDANCE

Figure 5.14b

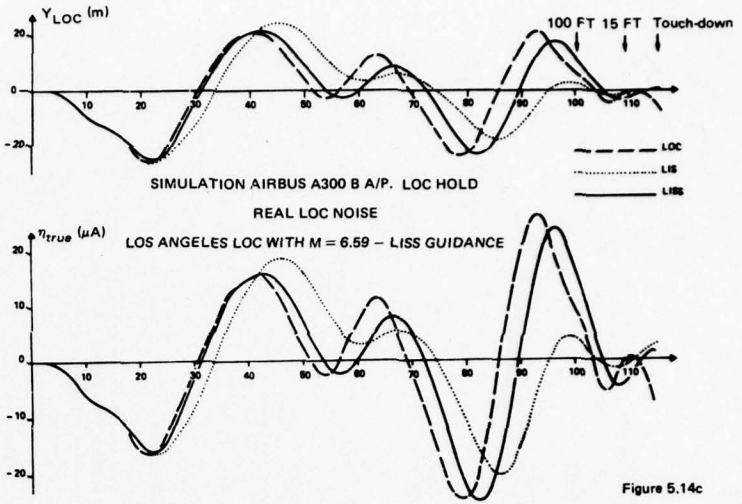

SIMULATION AIRBUS A300 B A/P. LOC HOLD

REAL LOC NOISE

LOS ANGELES LOC WITH M = 6.59 – LISS GUIDANCE

Figure 5.14c

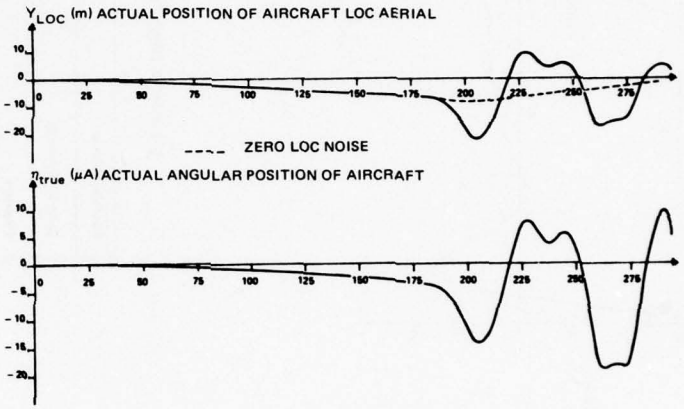

SIMULATION AIRBUS A300 B A/P. LOC HOLD

REAL LOC NOISE

LOS ANGELES LOC WITH M = 6.59 – LISS GUIDANCE

Figure 5.14d

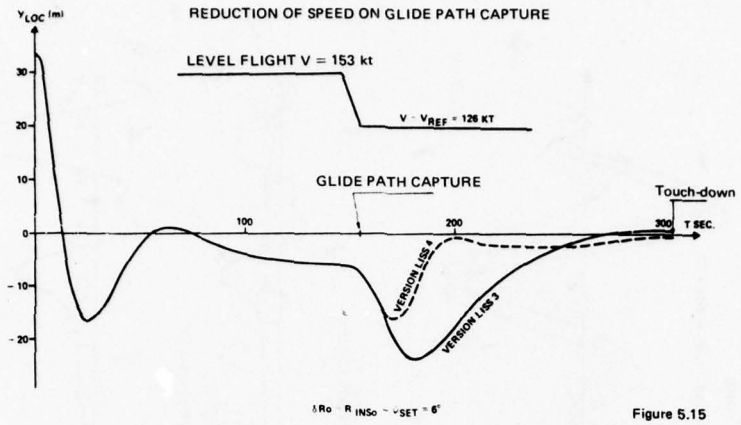

Figure 5.15

Figure 6.1 SAGEM UTD COMPUTER CHARACTERISTICS

Operand Format	16 or 32 bits, fixed comma
Command Format	16 bits
Registers	8 per level
Command Codes	Microprogrammed Commands
Interrupts	1 level; 10 inputs
Memory Capacity	≤ 65 K words
Duration of Memory Cycle	0.2 to 2 μs
Duration of Addition	9 cycles
Duration of Store	4 cycles
Duration of Multiplication	73 cycles
Duration Double Length Addition	19 cycles

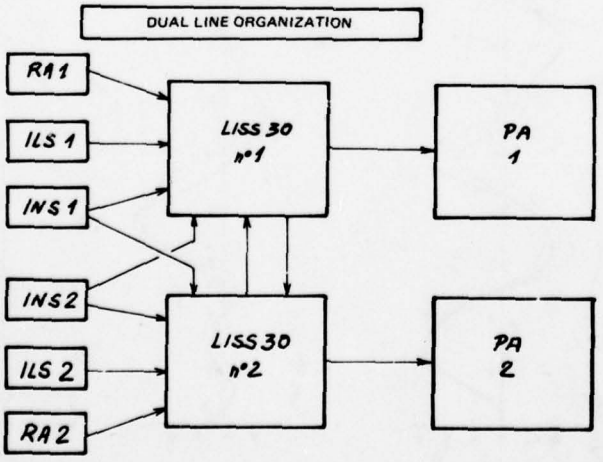

Figure 6.2

FILTERING PERFORMANCE

			$\Delta\hat{V}_T$ ERROR AT 100 FT (m/s)	$\hat{\gamma}_T$ ERROR AT 100 FT (m/s^2)
PROJECTION REFERENCE	R_{I_0}	$\sqrt{m^2 + \sigma^2}$	0.08	0.0015
		max.	0.16	0.0028 *
	ψ_{set}	$\sqrt{m^2 + \sigma^2}$	0.08	0.0018
		max.	0.16	0.0037

RESULTS OF CEV FLIGHTS (20 APPROACHES)

Error $R_{I_0} - \psi_{set}$ $\sqrt{m^2 + \sigma^2} = 3$ deg max = 6.15 deg

* With steep wind gradient ($\Delta V_{ground} = 50$ kt)

$\Delta\gamma_T$ max = 0.0222 m/s^2

Figure 7.1

PERFORMANCE OF PURE INERTIAL GUIDANCE SYSTEM (LOC FAILURE AT 100 FT)

			DEVIATION AT TOUCH-DOWN (m)	DEVIATION AT TOUCH-DOWN + 10 sec. (m)	DEVIATION AT TOUCH-DOWN + 15 sec. (7 approaches) (m)
PROJECTION REFERENCE	R_{I_0}	$\sqrt{m^2 + \sigma^2}$	2.5	4.7	9.5
		max.	4. *	12.	21.
	ψ_{set}	$\sqrt{m^2 + \sigma^2}$	2.2	2.5	3.2
		max.	5.6	4.1	5.4

RESULTS OF CEV FLIGHTS (20 APPROACHES)

Error $R_{I_0} - \psi_{set}$ $\sqrt{m^2 + \sigma^2} = 3$ deg max = 6.15 deg

* With steep wind gradient ($\Delta V_{ground} = 50$ kt)

Y_{CG} max = 8. m

Figure 7.2

RECENT ADVANCES IN HIGH RESOLUTION INERTIAL NAVIGATION

BY: K R BROWN AND R A R TAIT,
FERRANTI LIMITED,
SILVERKNOWES,
EDINBURGH,
SCOTLAND,
UK

SUMMARY

An inertial navigator can survey to great accuracy and resolution if its self-generated velocity errors are determined by stopping and comparing the indicated velocity with the zero velocity at standstill. Three examples of the uses of this technology in the exploration of the North Sea oil fields are described to demonstrate the performance that is possible. The relationship between survey and accuracy is examined and an estimate of the inertial instrument performance is made. It is found that the instruments are capable of far higher resolution than previously considered and to realise the benefit requires higher resolution interface units and a flexible computing system.

1. INTRODUCTION

Inertial Navigation was originally developed and has been used to navigate vehicles over great distances, on sea, in the air, and in space. The adoption of the technique of velocity updating in the late 'sixties has increased the accuracy of Inertial Navigation Systems to a level where survey became possible to better than 10 metres over 20 kilometres with Inertial Platforms in production at the moment. The first outcome of this work was a survey equipment for the Army. The vehicle carrying the equipment stops at intervals not greater than 10 minutes: while stopped a velocity update is completed. Position and heading are accurate to 10 metres and 1 minute of arc respectively.

However, it became evident during the development programme that the inertial platform then in production was capable of far higher accuracy over short distances and much finer resolution. The system is now developed to a stage where it is possible to survey to an accuracy of a few centimetres and a resolution of tens of microns, and there is no indication that this is a practical limit.

2. VELOCITY UPDATE

The key to high resolution inertial navigation is in the velocity update technique, that is, by stopping the vehi le carrying the system, over a DWELL period, and determining the velocity error which has accrued since entering the navigation phase. Only while stopped can the error velocity be measured to the desired accuracy. The velocity error can be determined to an unlimited accuracy by stopping for sufficient time, practical limits being imposed by vehicle random motion and the resolution of encoding the velocity detected by the system.

3. VELOCITY ERROR MODEL

The Inertial Navigation system is Schuler-tuned and oscillates with an 84-minute period in a smooth and systematic manner. Fitting the velocity measured at standstill to this smooth curve leads to a very accurate estimate of the velocity errors between the DWELL periods and the drift in position arising from these errors. It is possible to determine position during the movement of the vehicle between DWELL periods by interpolation. The movement is referred to as the TRANSIT.

The update technique may be classified generally depending upon whether or not the Schuler loop is interrupted when the actual update is made. The velocity errors in either case may be approximated piece-wise; the process which models closely the velocity error profiles over the DWELL intervals is considered optimum. This process of dynamic curve fitting may be accomplished by a number of schemes of which polynomial models are preferable because of their simplicity and are adequate over the short Transit times considered. Very high resolution is required both to give a sufficiently good fit during the modelling in the Dwell period, and adequate resolution during Transit, velocity is quantised to 3×10^{-4} ft/sec (9×10^{-3} cm/sec). In general, performance improves dramatically as the Transit intervals are reduced, and improves as Dwell time is increased to 20 seconds at which a plateau is reached.

4. OPERATIONAL EXPERIENCE

Three practical examples are presented to illustrate the performance of the equipment. In each case the operation is related to activities associated with the North Sea oil fields.

4.1 Pipeline Survey

This refers to a survey of the two intersecting sections of pipeline by an Inertial Navigation equipment carried in a manned submersible.[1] This operation was carried out at a considerable depth with a visibility of about 5 feet through the water. The actual survey was very rapid and as this was the first use of the Inertial Navigator in this context, the remaining endurance of the submersible (8 hours) was used to complete twenty-five circuits as shown in Figure 1. The operators carrying out the survey concluded that an accuracy of 5 cm was possible.

Two major problems had to be resolved to achieve this performance:

(a) The inertial system had to be aligned at sea before use and a simple technique was developed to overcome the effects of the motion of the mother ship. The method was to roughly align the system on the mother ship before launch. An estimate of the North direction, derived from the ship's compass, was inserted through the equipment control unit keyboard and the inertial platform levelled on its own accelerometers whilst the mother ship was hove to. The submersible was then launched and taken down to sit on the sea bed where a full gyro compass alignment could be carried out. A datum point on the pipeline was established and the survey started.

(b) The process of coming to rest for the 'dwell' to update the velocity error gave problems. To stop the submersible for the Dwell period, it was required that the bouyancy be reduced so that it sat on the sea bed, preferably astride the pipe. It was originally intended to use a Transit time of a minute to get the highest accuracy, but it proved too lengthy a process to change the bouyancy at such frequent intervals and a transit of two to three minutes had to be used.

The range of the bouyancy change limited the amount of 'sink' available to hold the submersible on the sea bed and, hence, it was prone to movement during the Dwell time. This complicated the velocity updating process, but a compromise was found by extending the Dwell. There was a limit to the precision with which the submersible could be positioned over the survey point and, inevitably, errors arose in the estimation of the offset from the actual point being surveyed. The navigation and steering features in the Inertial System proved invaluable in getting from point to point in such a limited visibility.

4.2 Movement of Production Platform

A second example is the measurement of the movement of a production oil platform situated in 250 feet of water, measurements being taken at a point approximately 100 feet above sea level. Records were taken continuously over a period of about 9 days. To limit the growth of the velocity errors over such a lengthy period, a system was modified to be velocity-damped (5.6 Schuler) on the assumption that the net movement of the production platform is zero over the time involved. Figure 2 shows a sample of the data obtained, both in calm and extremely rough weather. These are presented as histograms showing the percentage of time spent in each displacement. In this case, the position data is recorded to 0.01 inches (0.25 mn) with an inherent resolution in the displacement of 0.001 inches (25 micron).

Although very severe weather was encountered with wave heights of up to 42 feet, the platform deflections were generally under $\pm$1.5 inches, although one isolated peak of 2.9 inches was recorded.

4.3 Oil Well Survey

The Inertial System has been re-packaged into a form in which it can survey oil wells. A production platform in the North Sea can have more than 40 wells. These are vertical for the first few thousand feet and are arranged as a regular array with a nominal separation between well centres of about seven feet. It is imperative that the wells do not touch as a well can be drilled whilst an adjacent one is delivering oil. This has obvious hazards.

The equipment provides a very rapid method of precisely determining the position of each well, and this particular configuration has an inertial height channel the survey is in three dimensions.

An example of a typical survey is shown in Figure 3, and to give an indication of the accuracy and resolution, Figure 4 shows a single channel in section with the clearance between the pressure vessel, containing the equipment and oil well. The equipment is lowered on the drill string, a very stiff 5-inch tube. Initially, the well is vertical and the vessel can vibrate from wall to wall within the clearance. As the well deviates the pressure vessel is forced onto one side of the well and the excursion is greatly reduced.

The inertial system is packaged into a long cylindrical configuration and is equipped with batteries and data recording for self-contained operation over four hours. It is inserted into a torpedo-shaped water-tight pressure vessel which gives it the capability to operate to the depth of the North Sea wells.

5. INVESTIGATION OF ERROR SOURCES

The two variables under the control of the surveyor are the length of 'Dwell' period over which the velocity update is made, and the time in 'Transit' between updates. The minimum time in the 'Dwell' is that required to filter out the velocity arising from vehicle motion when stopped. It was established very early that a 'Dwell' of 5 seconds was sufficient to remove the motion caused by an engine running in the survey vehicle. This leaves only the randomness arising from the inherent noise in the measurement of velocity. The question was, could the performance be improved by lengthening the 'Dwell'?. It was also obvious that a great improvement would arise from shortening the Transit time between velocity fixes, and could this be quantified?

To analyse the problem an Inertial system with comprehensive data recording was run for a continuous period in the navigate mode after a typical self-gyro compass alignment. A complete program was devised using this detailed data which, offline, divided the navigate time into 'Dwell' and 'Transit' periods of various lengths so that an assessment could be made of the performance which would have been obtained for a range of the two variables. The important point is that identical data is used to arrive at the various results.

The analysis was considered valid as it was established that the performance was unaffected by travelling at low speed in a Land Rover survey vehicle and that for the particular applications considered, the distance travelled was such that scale factor and heading-induced errors within the distance travelled in a typical application could be neglected.

A typical build-up of radial error within time is shown in Figure 5. The radial position error at one hour against 'Transit' time for a range of 'Dwell' periods is shown in Figure 6 together with a similar plot of the variance of the various samples from the mean of each of the chosen Dwell times. This data appears to indicate a reasonably consistent pattern to the error growth with 'Transit' time and it can be used to check the validity of and establish the coefficients of a simple error model.

The single channel position errors in an inertial navigation system can be expressed in general terms as:

The North/South channel velocity error time function is

$$V_N = a_1 \cos \omega_o t + a_2 \frac{\sin \omega_o t}{\omega_o} + a_3 (1 - \cos \omega_o t)$$

$$+ a_4 \left(e^{\frac{-t}{T_o}} + \frac{\sin \omega_o t}{\omega_o t} - \cos \omega_o t\right) + a_5 \left(t - \frac{\sin \omega_o t}{\omega_o}\right)$$

$$+ a_6 \left(t^2 + \frac{2(\cos \omega_o t - 1)}{\omega_o T_o}\right) + a_7 + a_8 t + a_9 t\, e^{\frac{-t}{T_o}}$$

where t is time in navigate and the coefficients are defined in the Appendix. Coefficients a_5 and a_6 are absent for the East/West channel error function which, otherwise, has similar form.

However, if the velocity update is accurate, each 'Transit' can be considered as a separate navigate operation: the sum of these separate operations growing as a random walk. In the high resolutions considered, the 'Transit' times are kept short, say, a maximum of 5 minutes, and terms higher than third order can be neglected. The total position error equation can be reduced to the vector sum of three quantities. In any survey period there will be a number (N) Transits, and it appears that there is little or no correlation between the position errors generated in the successive Transits. The error equation can be reduced to

$$\sqrt{N}\left(\overline{V_I T} + \overline{\frac{\theta_I g T^2}{2}} + \overline{\frac{\omega_T g T^3}{6}}\right)$$

where N is Number of Transits

T is Transit Time

g is Acceleration due to gravity

V_I is Equivalent initial velocity error

θ_I is Equivalent platform tilt

ω_T is Equivalent vertical gyro drift

That is, a model with three terms listed in Table 1, which can be considered as arising from

(a) An initial velocity error existing at the start of each 'Transit' period.
(b) An acceleration error which can be considered as an equivalent tilt of the inertial platform.
(c) An equivalent Vertical gyro drift expressed as the mean drift averaged over the 'Transit' time.

The result of fitting this simple model is listed in Table 1, as shown below, which indicates the performance required of instruments to obtain the performance being discussed.

TRANSIT TIME	INITIAL VELOCITY	PLATFORM TILT	VERTICAL GYRO DRIFT
(Minutes)	Ft/sec	Milligals 'g' x 10^{-6}	Degrees/hour
1	$< 10^{-4}$	0.22	0.0011
2	$< 10^{-4}$	0.29	0.0008
3	$< 10^{-4}$	0.29	0.0005
4	$< 10^{-4}$	0.37	0.0005
5	$< 10^{-4}$	0.37	0.0003

PLATFORM ERRORS/TRANSIT TIME (DWELL 20-60 SECS)

TABLE 1

(1) The initial velocity error represents a fraction of a bit of the velocity encoder and so the system performance is not limited by a velocity resolution.

(2) The tilt error calculated is approximately the smallest change in tilt which can be detected in testing the accelerometer. It is about 0.05 of the bias uncertainty quoted for the accelerometer type used (Ferranti FA2F) over similar integration periods. This is typical of the problems of relating Inertial instrument performance to that of the system. In this case, the instrument test data may be dominated by the tilt of the test plinth due to ground movement.

(3) The equivalent vertical gyro drift for a 5-minute Transit is similar to the test data for the gyro for drift values extracted from 1-hour test runs with 5-minute averaging in each sample. The higher value for shorter Transit times almost certainly arises from the inherent noise in the gyro giving an apparent increase in drift for shorter averaging times. This is being further investigated.

There is a large increase in performance by increasing 'Dwell' times to 20 seconds with no significant increase in performance for longer times. It is concluded that there is nothing to be gained by increasing 'Dwell' beyond 20 seconds unless the vehicle motion at rest is such as to require a longer correlation time.

This leads to the conclusion that a model based on a third order polynomial will closely follow the errors arising with 'Transit' times compatible with the high resolution short range applications described in this paper and that the length of 'Dwell' required to establish an adequate Velocity update does not unacceptably increase the length of time required to complete a survey task. An error of the order of 3 centimetres after 1 hour from leaving the datum point of the survey with the possibility of improving this if a closure is made completing a circuit.

6. POSSIBLE APPLICATIONS RELATED TO AVIATION

The resolution of the survey equipment is too fine for normal aviation purposes. It could, however, be of use in certain specialised applications.

(1) During the evaluation of the landing and take-off performance of an aircraft, a velocity fix could be taken before and after each circuit. An exact profile during the take-off and approach (within, say, 2 ft) could be measured and if two equipments were positioned in different stations, the deflection of the airframe between them could be recorded.

(2) A rapid survey could be made of the proposed site for a runway and the calculations made to indicate the optimum earth moving required to generate a level runway.

(3) It may be possible to modify existing aircraft Inertial Navigation systems to give steering signals during taxying and take-off within acceptable limits in dense fog.

7. CONCLUSION

The technique of velocity update by holding an Inertial Navigator stationary at intervals during navigation can give an accuracy only limited by heading and scale factor if stops are made sufficiently often. The experimental results obtained on practical working equipments agree closely with the gyro test data and indicates that accelerometer bias stability is very much better than expected from instrument tests.

REFERENCE 1 "Underwater Survey using an Inertial Navigation System",
A Stankoff and R A R Tait, Paper 2815 Proceedings of Offshore Technology Conference, Houston, Texas, May 1977.

APPENDIX

The coefficients used in velocity error function are of the form:

$a_1 = (K_A + K_I + K_L)\, V_A + V_{IA}$

$a_2 = b_A + 2K_C \omega \sin \Phi_o\, V_X + g\theta_o + g\, \omega_{VM}\, V$

$a_3 = K_T\, V_A + \frac{g\,\omega_V}{\omega_o^2} + \frac{g\,\omega_{VC}}{\omega_o^2}$

$a_4 = \left(\omega_o^2 + \frac{1}{T_o^2}\right) \frac{g\,\omega_{VT}}{}$

$a_5 = \chi_o\, \omega_e \sin \Phi_o\, V_A + a\, \omega_{ZD}\, \omega_e \cos \Phi_o$

$a_6 = \omega_{ZD}\, \omega_e \sin \Phi_o\, V_A$

$a_7 = \chi_o\, V_X$

$a_8 = \omega_{ZD}\, V_X$

$a_9 = \omega_{ZDT}\, V_X$

where

K_A = accelerometer scale factor error

K_I = velocity encoder scaling factor

K_L = accelerometer non-linearity error

K_C = coriolis acceleration correction error

K_T = effective error in gyro torquing

b_A = accelerometer bias stability

θ_o = initial tilt error for the channel

χ_o = initial azimuth error

Φ_o = latitude of the place

ω_{ZD} = azimuth gyro drift

ω_{ZDT} = azimuth gyro thermal drift

ω_V = effective vertical gyro drift

ω_{VC} = combined gyro drift effect due to vertical gyro random drift, anisoelastic drift, rectified drift effects and coupled rotation from other two axes

ω_{VT} = vertical gyro thermal drift

ω_{VM} = mass unbalance drift

ω = earth's rate

ω_o = Schuler frequency

T_o = a time constant

a = earth's radius

g = acceleration due to gravity

V_{IA} = initial velocity error

V_A = "along-channel" velocity

V_X = "across-channel" velocity

V = total system velocity

Coefficients a_5 and a_6 are absent for the East/West channel

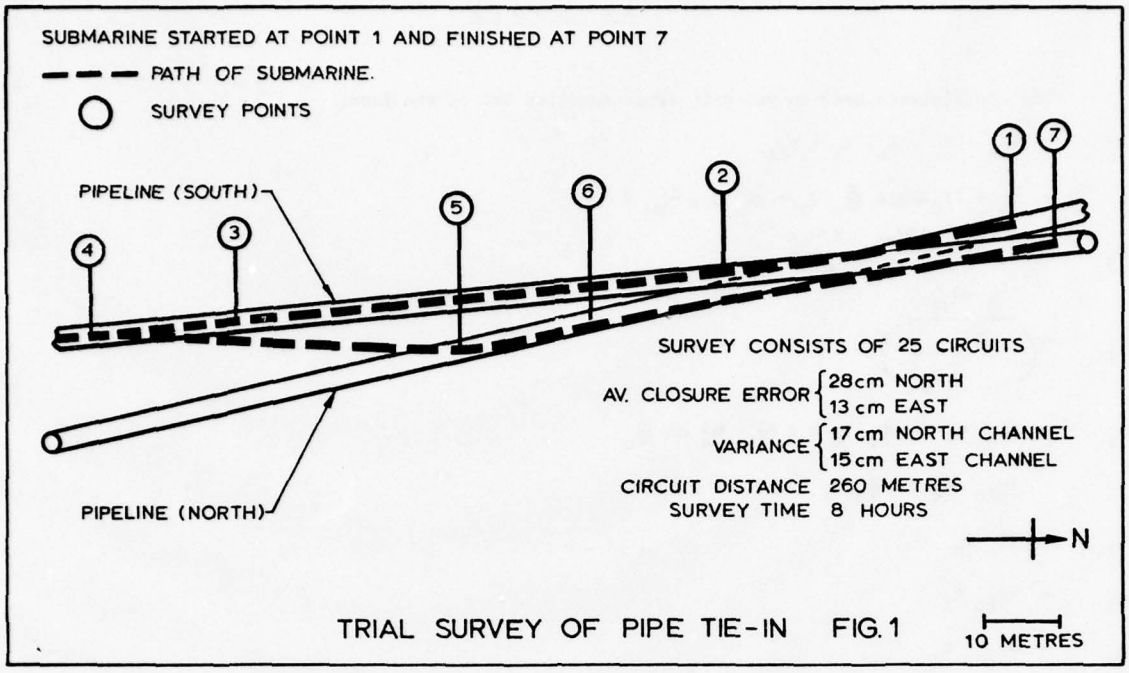

TRIAL SURVEY OF PIPE TIE-IN FIG. 1

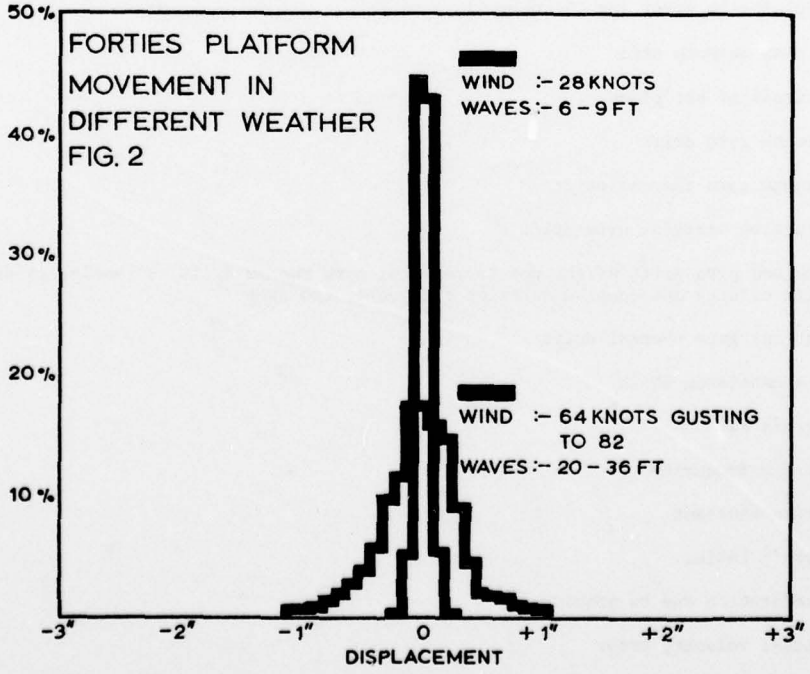

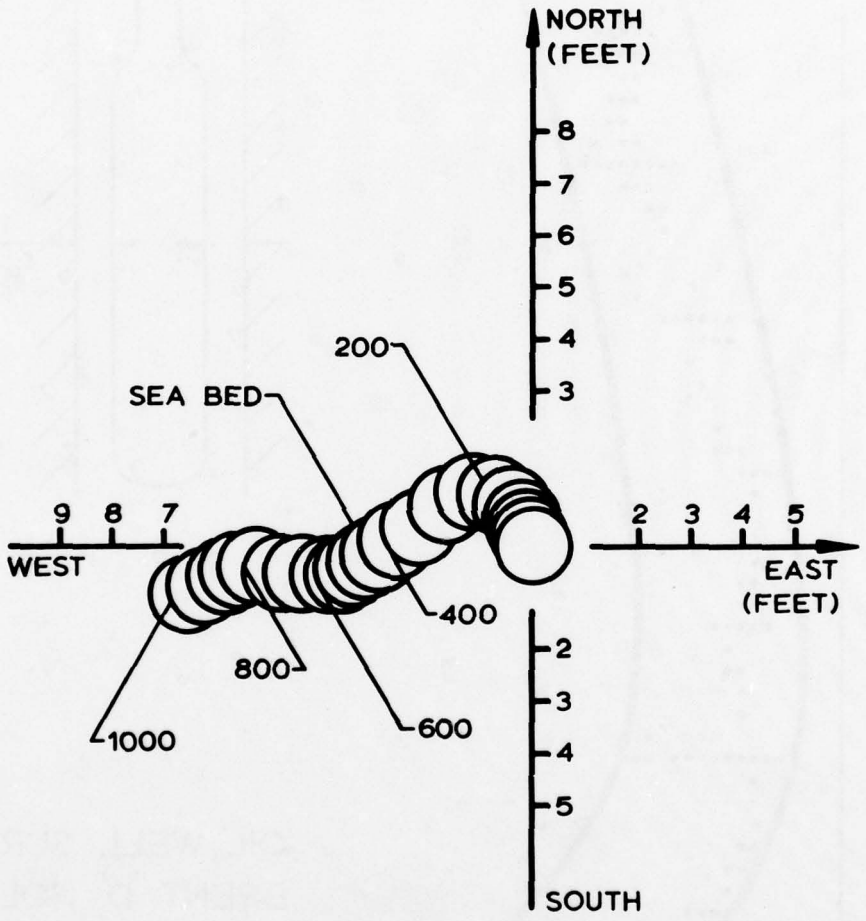

OIL WELL SURVEY
PIPER FIELD FIG. 3

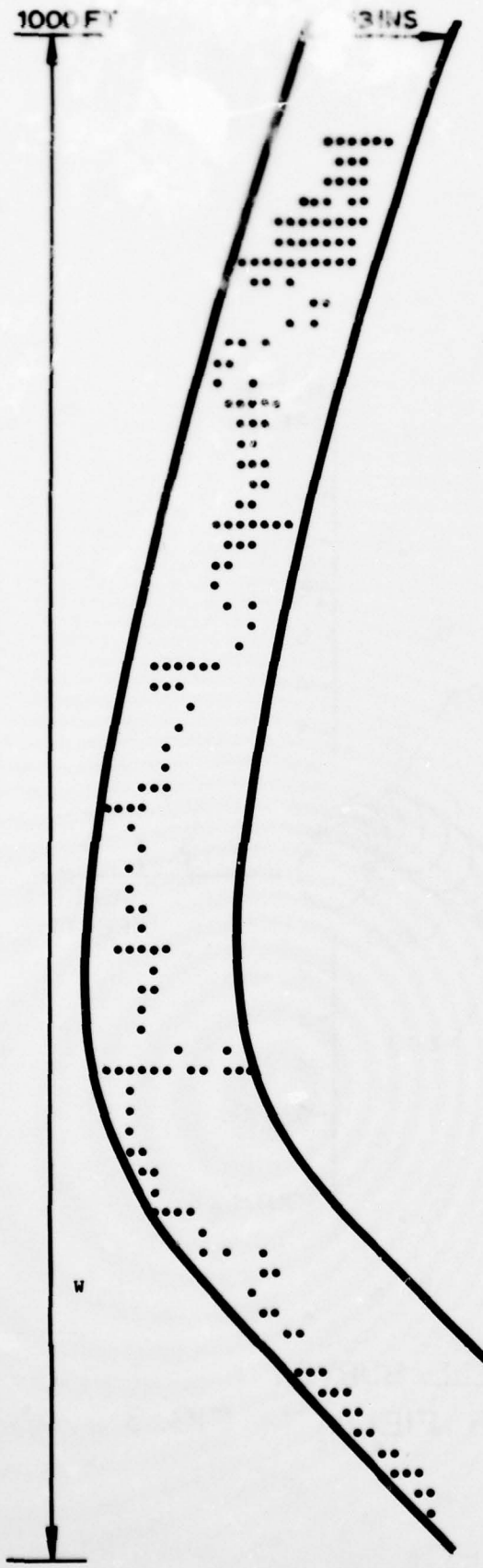

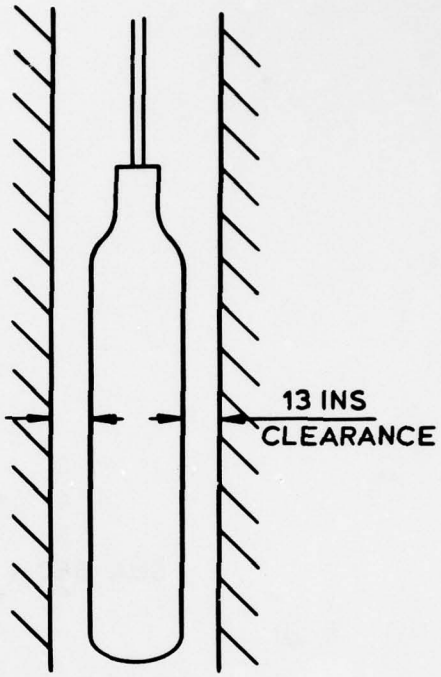

OIL WELL SURVEY
BRENT 'D' HOLE 28
FIG. 4

AD-A052 862 ADVISORY GROUP FOR AEROSPACE RESEARCH AND DEVELOPMENT--ETC F/G 17/7
APPLICATIONS OF ADVANCES IN NAVIGATION TO GUIDANCE AND CONTROL.(U)
FEB 78

UNCLASSIFIED AGARD-CP-220 NL

2 OF 3
AD
AD052862

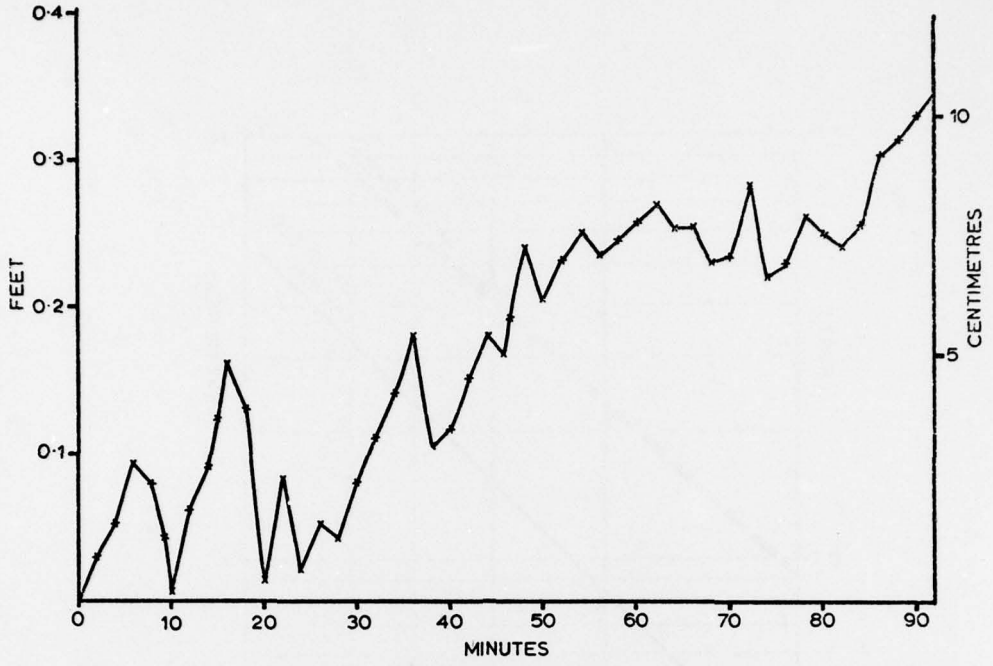

RADIAL ERROR
40 SEC DWELL 2 MIN TRANSIT

FIG. 5

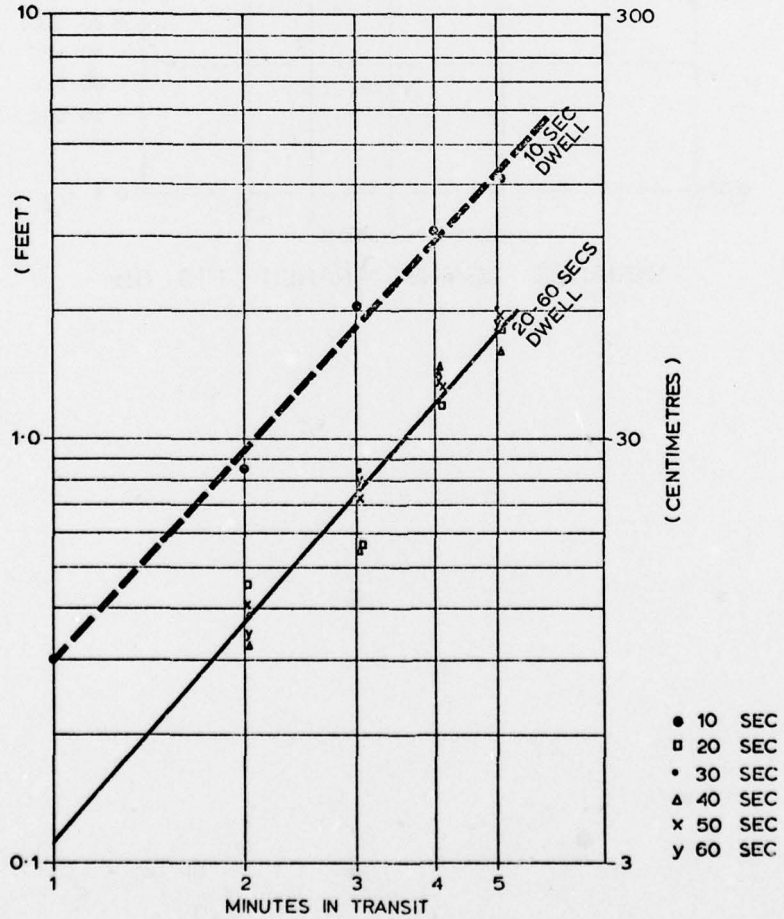

ERROR AT 1 HOUR FIG. 6a

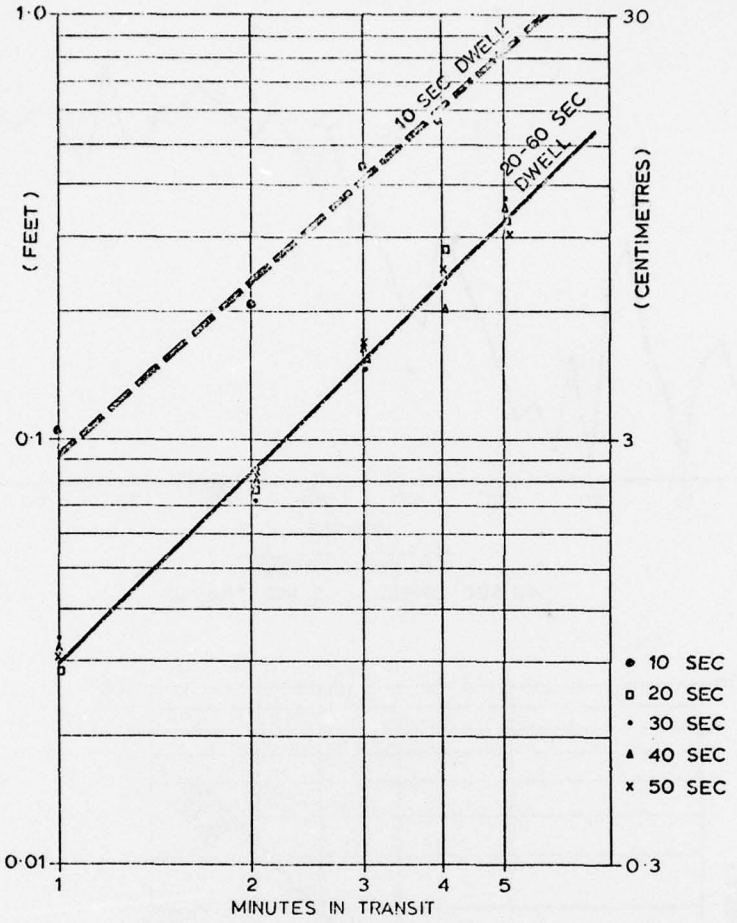

VARIANCE AGAINST TRANSIT FIG. 6b

CALIBRATION OF AN INS BASED ON FLIGHT DATA

B. Stieler, W. Lechner

Deutsche Forschungs- und Versuchsanstalt
für Luft- und Raumfahrt e.V. (DFVLR)
Institut für Flugführung

3300 Braunschweig-Flughafen

West Germany

SUMMARY

The paper deals with the calibration of an INS based on flight data from the INS and external measurements such as radar and cinetheodolites.

The results presented are based on an off-line evaluation of the data using optimal smoothing algorithms. This is an effective way to be followed for flight-testing an INS and getting an insight into the sensor and system errors under flight conditions.

The user of an INS, especially in the military field, is in general more interested in the in-flight alignment and calibration of an INS, i. e. in the on-line evaluation of the data on board the aircraft for which optimal filtering algorithms are at hand. This opens the way for the fast take-off of an aircraft with a coarse-aligned platform. Corresponding simulation results are discussed.

1. INTRODUCTION

Optimal estimation algorithms are successfully applied for the on-line aiding of an INS on board the aircraft |1, 2, 3| or the off-line "aiding" for flight path measurements |4|. For both applications the accuracy improvement on the position and the velocity levels is of primary interest.

In this paper the INS itself is in the center of attention. It is shown that optimal smoothing algorithms applied to the off-line combination of position measurements from an INS and external tracking devices (radar, cinetheodolites) recorded during the flight allow to fit the actual INS errors including the misalignment and sensor errors to a given model in an optimal way. This allows to see how well the real world and theory are matching.

It is shown in a second topic that the optimal filtering algorithms applied to the on-line combination of position measurements from the INS and a microwave landing system opens a new way for INS operation - the alignment of the platform in the take-off phase.

The results presented for both topics do not yet reflect the final state of the research. Topics for the continuation of the efforts are the improvement of the INS- and its sensor error models based on more flight test experience.

It should be mentioned that the flight tests described in this paper had been carried out with an uncalibrated LN-3A system in which essential parts of the computer had been exchanged.

Beginning with a review of the dominant INS error sources, comparison is made between the alignment and calibration of a platform stationary on the ground and on a manoeuvering vehicle.

2. REVIEW OF THE DOMINANT ERROR SOURCES IN AN INS

The accuracy of an INS is affected by the sensor errors and the platform misalignment angles with respect to the navigational reference coordinate frame. Fig. 1 shows the 1σ position errors due to these different error sources for an easterly flying vehicle. We may conclude from it |5|:

- the dominant long-time errors are caused by the gyro drift and the misalignment angles, especially the azimuth misalignment angle;
- the accelerometer errors as well as the horizontal misalignment errors cause major position errors only for short times; their long-time effect is bounded.

While the misalignment angles are determined and nulled during each preflight alignment process, the sensor errors are in general determined and nulled only when the INS passes a check-up process. Compensation is possible under the assumption that they are constant.

3. REVIEW OF THE ALIGNMENT AND CALIBRATION OF A STATIONARY PLATFORM

The preflight alignment and especially the calibration of the sensor errors is time-consuming. Based on the analog gyrocompassing procedure |6|, the former lasts up to 10 minutes and more. As to the calibration of the sensor errors practically only the north-south gyro drift can be determined on the stationary plat-

form in the preflight alignment mode |6|.

Fig. 2 shows the simplified error block diagram for the stationary platform in the gyrocompassing alignment mode. One may deduce from it |6, 7, 8, 9|:

- the east accelerometer output allows to control the north misalignment angle and to observe the north gyro drift;
- the gyrocompassing loop starting from the north accelerometer output allows to control the east and the azimuth misalignment angles;
- the vertical gyro drift is practically non-observable if no additional measurements are taken from the vertical synchro;
- the horizontal accelerometer errors and the east gyro drift are non-observable; they contaminate the horizontal and vertical alignment accuracy through the following relationships:

Horizontal misalignment = corresponding accelerometer bias / gravity

$$\bar{\varepsilon}_{N,E} = \pm B_{E,N}/g \qquad (1.1)$$

Azimuth misalignment = East-West gyro drift / horizontal component of Earth rate

$$\bar{\varepsilon}_{D} = -D_{E}/(\Omega\cos\varphi). \qquad (1.2)$$

Through the application of Kalman filtering the process of aligning the platform and calibrating the north-south gyro can be shortened up to 1 to 2 minutes under the benign laboratory environment. The physical limitations due to non-observability or alignment accuracy cannot be surpassed with a stationary platform |6, 7, 8, 9|.

4. REVIEW OF THE INS ERROR MODEL AND STATE VECTOR OBSERVABILITY

Fig. 3 shows the simplified block diagram of the INS error model on a moving vehicle. For the purpose of discussion the following neglections have been made:

- the error sources for the 24-hour oscillation have been curtailed to the effect of the azimuthal misalignment on the horizontal axes;
- the Coriolis compensation has been assumed to be perfect;
- the torquing error of the vertical axis due to an error of the geographic latitude has been neglected.

As compared to the block diagram of the stationary platform in Fig. 2, the measurement signals (accelerometer outputs) contain additional information on the azimuthal misalignment via the signal lines $\dot{V}_{N,E}$, $\dot{\varphi}$ and $\dot{\Lambda}\cos\varphi$. They are the sources for the so-called "cross-track" error. Provided external position measurements are at hand, these additional error sources have the benefit that

- the azimuth misalignment error and the constant east-west gyro drift become distinguishable on a maneouvering vehicle, i. e. the east-west gyro drift becomes an observable state and the above-mentioned physical limitation on azimuthal alignment accuracy does no longer exist.

Since with respect to Fig. 2 the measurement signals contain no further information on the accelerometer bias and horizontal misalignment errors, both remain practically indistinguishable on a maneouvering vehicle as it is the case on a stationary vehicle. But one can live with this limitation, since it may be seen from Fig. 1 and | 5 | that their long-time effect on the INS error is bounded.

5. SET-UP FOR FLIGHT-TESTING THE LITTON LN-3A INERTIAL NAVIGATIOR

The flight tests were carried out in the middle of 1976 on a HFB 320. The aircraft shown in Fig. 4 is an Executive Jet, used by DFVLR as a test aircraft. The following installations were used for the test: the INS to be tested, the altimeter (Conrac), the CAMAC interface crate for connecting the instruments to the Honeywell DDP 516 computer, the on-board clock (Patek Philipe) and the digital magnetic tape recorder (Ampex ATM 13591 II) for recording all essential on-board data.

Tests were carried out from Braunschweig towards west and north.

On the westerly flight to Bedford, UK, the following tracking facilities were used, as shown in Fig. 5:

Braunschweig (DFVLR)
1 tracking radar (1σ-accuracy in angle 0.05°, in range 8 m)

Meppen (Erprobungsstelle 61 der Bundeswehr)
1 tracking radar (1σ-accuracy in angle 0.025° in range 2.7 m)

Amsterdam (National Lucht- en Ruimtevaartlaboratorium)
1 terminal approach radar (1σ-accuracy in horizontal position 200 m)

Bedford, UK (Royal Aircraft Establishment)
2 cinetheodolites (1σ-accuracy in angle 0.025°).

On the northerly flight to Oslo, Norway, the tracking facilities were those of Braunschweig and of

Oslo (Directorate of Civil Aviation)
1 terminal approach radar (1σ-accuracy 1 NM).

Valuable position and velocity measurements were yielded also when the aircraft was stationary on a reference point before take-off and after landing.

The second aircraft shown on Fig. 5 served as a relais plane, for the long-distance transmission of the measurement data in the HFB 320 to Braunschweig were they could be recorded on-line for the purpose of quick-look.

In the following we will concentrate on the test results of the flight from Bedford back to Braunschweig only because the constellation of the tracking facilities plus the measurements of the stationary run allow us:

a. to draw conclusions on the off-line calibration of an INS treating its data and the position measurements by smoothing algorithms;

b. to simulate the alignment of an INS during take-off by treating its data and the position measurements from a microwave landing system (MLS) with filter algorithms.

For the simulation in case b. the measurements of the 2 cinetheodolites were assumed to come from an MLS. The covariance of the position fixes were contaminated so that they corresponded approximately to the 1σ-values of an MLS, e. g. the DLS |1, 4, 10|.

Reference |1| covers the aiding of an INS with an MLS for approach and landing. Though the techniques for aligning a platform in the take-off phase and the aiding in the approach phase are related, the operational use is different and worth to be treated separately. Not covered in this paper but in |1| is the problem of required on-board computer capacity for aiding the INS on-line.

6. DATA EVALUATION

All data on-board (INS, altimeter) and on ground (radar, cinetheodolites) were recorded synchroneously. From the ground measurements the position of the aircraft in geographic longitude, latitude and altitude had to be calculated as well as the covariance matrix based on the above mentioned sensor specifications |4|.

Optimal filtering and smoothing algorithms are well treated in the literature |8, 11, 12|. Let us briefly remember the major differences between both methods for optimally combining data from different sources (e. g. INS and radar). Fig. 6 shows schematically the estimation accuracy i. e. the 1σ-band over time for the forward Kalman filter, the backward Kalman filter and the forward/backward filter or smoother. The forward filter gives for a time t_o the optimal estimate based on all data before t_o, the backward filter gives the optimal estimate based on all data after t_o, and the forward/backward filter gives the optimal estimate based on all data before and after t_o. In Fig. 6 also the simple relationship for the accuracy gain of the smoothed estimate as compared to that of a forward and a backward filter estimate is mentioned.

Between t_1 and t_2 in Fig. 6 it is assumed that the INS navigates unaided with the 1σ-band growing according to the unaided error model (s. Fig. 1) for the forward and the backward filters. The smoothed estimate bridges the time with much smaller loss in accuracy. This proves that for the off-line calibration of an INS the smoothing algorithms are suited best. Not only is the 1σ-band smoother than that of the Kalman filter, but also the estimate itself because the forward filter estimate is much more sensitive to stray points in the measurements |4|.

In practice one applies the Kalman filter algorithms forward in time, and when the end time is reached, the Rauch-Tung-Striebel or Fraser algorithms backward in time |11, 12|.

Suffice to say that for the on-line alignment and calibration of an INS the Kalman filter algorithms are the only optimal means to combine data from different sources.

7. RESULTS FOR THE OFF-LINE INS CALIBRATION

Fig. 7 shows the plot of the flightpath with the crosses indicating the city of Bedford (UK), Amsterdam, Meppen (Ger) and Braunschweig. The aircraft carried out manoeuvers in the range of each radar/cinetheodolite station in order to improve the observability of the INS errors.

The following discussion shall be based on the test results for the north-south and the azimuth channels only.

If all available position fixes and stationary measurements are combined with the INS data by means of smoothing algorithms, the accuracy of the reference flightpath is better than 45 m according to the self-diagnosis of the forward/backward filter, s. Fig. 8. The highest value is at 1/2 h elapsed time when the aircraft is above the North Sea. The position differences (reference flightpath minus position fix) are well distributed about the center line of the plot, indicating that the results are reasonable.

In Fig. 9 the results for the INS geographic latitude error estimation are plotted. The 1σ-band corresponding to the 45 m maximum mentioned above is indistinguishable on the plot. The smoother estimates a linearly increasing error due to azimuth misalignment and vertical gyro drift (cross track error).

Fig. 10 shows the corresponding results for the north velocity error estimation. The 1σ-band is < 0,1 m/s. The estimation shows a Schuler oscillation with spikes superposed. Due to the cross track error, the spikes are correlated with turns of the aircraft.

In Fig. 11 the results for the east-west misalignment are plotted. The smoother's self diagnosis is at ± 1,1 sec. The estimation of the misalignment error shows Schuler oscillations.

Fig. 12 shows us that the east-west gyro drift can very well be calibrated on a manoeuvering vehicle. The 1σ-band is at $\pm\ 5 \cdot 10^{-3}$ °/h, the mean estimate is approximately at $3 \cdot 10^{-2}$ °/h with a change of approximately $-5 \cdot 10^{-3}$ °/h.

In Fig. 13 the results for the azimuth alignment error are plotted. According to the 1σ-band the error estimate is better than 2 min. The initial misalignment error in Bedford, UK was according to this plot -0.5°, changing linearly with time according to the azimuth gyro drift of -0.27 °/h. The final alignment error is approximately -1° when the aircraft lands in Braunschweig. These results prove that for this uncalibrated INS

- the initial misalignment error and
- the azimuth gyro drift

by far exceed the requirements for an operational system.

8. SIMULATION RESULTS OF AN IN-FLIGHT INS ALIGNMENT

Having calibrated the platform, we will concentrate in the following on the possible use of an MLS for the alignment of a platform during take-off. We will assume that the platform is just prior to take-off misaligned by 2 mrad (1σ) in the horizontal axes and 6° (1σ) in the vertical axis. For simulating the physically misaligned platform we assume an initial misalignment estimate of the same amount. The gyro drift rates are compensated and assumed to be known within 10^{-2} °/h (1σ). The simulation results for the north-south and the vertical misalignment angles are plotted in Figs. 14 and 15. Within 4 minutes of the take-off time the horizontal misalignment can be brought down to 0.5 min (1σ) and the vertical misalignment to 12 min (1σ). The results for the unaided INS position, i.e. the 1σ-band and its difference with respect to the external measurements in Amsterdam, Meppen and Braunschweig are shown in Figs. 16 and 17. The INS error corresponds to a shifted cosine function with Schuler period and 3 NM peak amplitude approximately. Except for the latitude error in Amsterdam the INS position difference is within the margin to be expected.

In order to prove the validity of this alignment method more flight tests have to be carried out. Furthermore, one should extend the in-flight alignment time above the 4 minutes or better to say the in-flight alignment range above the 7 km used in this simulation so that possible measurement errors may weigh less.

It should not be kept secret that in this simulation some stray points in the measurements have been taken out (to be seen in Figs. 14 to 17 at 2 minutes elapsed time) and corrections due to the synchronization of the INS and the "MLS"-measurements in the order of 0.05 s have been undertaken. From both off-line corrections one may obtain a feeling for the tight requirements which are put on the MLS in order to utilize it for the alignment of an INS. This applies especially to the azimuth channel because "holes" in the MLS-azimuth measurements or errors in the mean value or the synchronization do affect the INS in-flight alignment accuracy.

If one extrapolates from the German microwave landing system, the DLS, to the performance of the other systems which are competing in the ICAO contest, the present technology meets the requirements (s. |10|, Fig. 14).

REFERENCES

|1| Hurraß, K. "A Hybrid Guidance System for All-Weather Approach and Landing", Paper No. 52 on the 24th Meeting of the AGARD Guidance and Control Panel, Stuttgart, Germany, 10 - 13 May 1977.

|2| Schwegler, H. F. "Development of the Integrated Allweather Navigation System for Tornado (MRCA)", Paper No. 53 on the 24th Meeting of the AGARD Guidance and Control Panel, Stuttgart, Germany, 10 - 13 May 1977.

|3| Pickel, F. E. "A Multi-Sensor Implementation for Navigation, Position Location, Position Update, Reconnaissance, and Weapon Delivery - AN/ARN - 101 (V)", Paper No. 31 on the 24th Meeting of the AGARD Guidance and Control Panel, Stuttgart, Germany, 10 - 13 May 1977.

|4| Hurraß, K. Stieler, B. "Zum Einsatz des Hybriden Flugmeßsystems bei der Vermessung eines Mikrowellen-Landesystems", Paper presented at the Symposium Kreiseltechnik, Braunschweig, 1976; published in Bücherei der Ortung und Navigation, Düsseldorf, Am Wehrhahn 94, Bestell-Nr.: 112.

|5| Stieler, B. "Einführung in die Trägheitsnavigation", DFVLR Interner Bericht IB 153 - 76/28, 1976.

|6| Stieler, B. "Ausrichten einer Trägheitsplattform nach dem Kreiselkompaßverfahren", DFVLR Interner Bericht IB 153 - 76/25, 1976.

|7| Kortüm, W. "Design and Analysis of Low-Order Filters Applied to the Alignment of Inertial Platforms", AGARD-LS-82 Practical Aspects of Kalman Filtering Implementation, 1976.

|8| Schrick, K. (Editor) "Anwendung der Kalman-Filter-Technik, Anleitung und Beispiele", to be published in Oldenbourg Verlag, 1977.

|9| Stieler, B. "Ausrichten einer Trägheitsplattform nach dem Kalman-Filter-Verfahren", DFVLR Interner Bericht IB 153 - 76/26, 1976.

|10| Becker, A. "Accuracy Considarations on New Microwave Landing Systems (MLS) from an Operational Point of View", Paper No. 25 on the 24th Meeting of the AGARD Guidance and Control Panel, Stuttgart, Germany, 10 - 13 May 1977.

|11| Gelb, A. (Editor) "Applied Optimal Estimation", The MIT Press, Cambridge, Mass., USA, 1974.

|12| Fraser, D. "A new Technique for the Optimal Smoothing of Data", MIT Doctoral Thesis, T 474, 1967.

ACKNOWLEDGEMENT

The authors are very grateful to Mr. Symmons and Mr. Whitehouse from RAE, to Mr. Hagenberg from NLR and to Mr. Jenschek from Erprobungsstelle 91 der Bundeswehr for their excellent support of the tests.

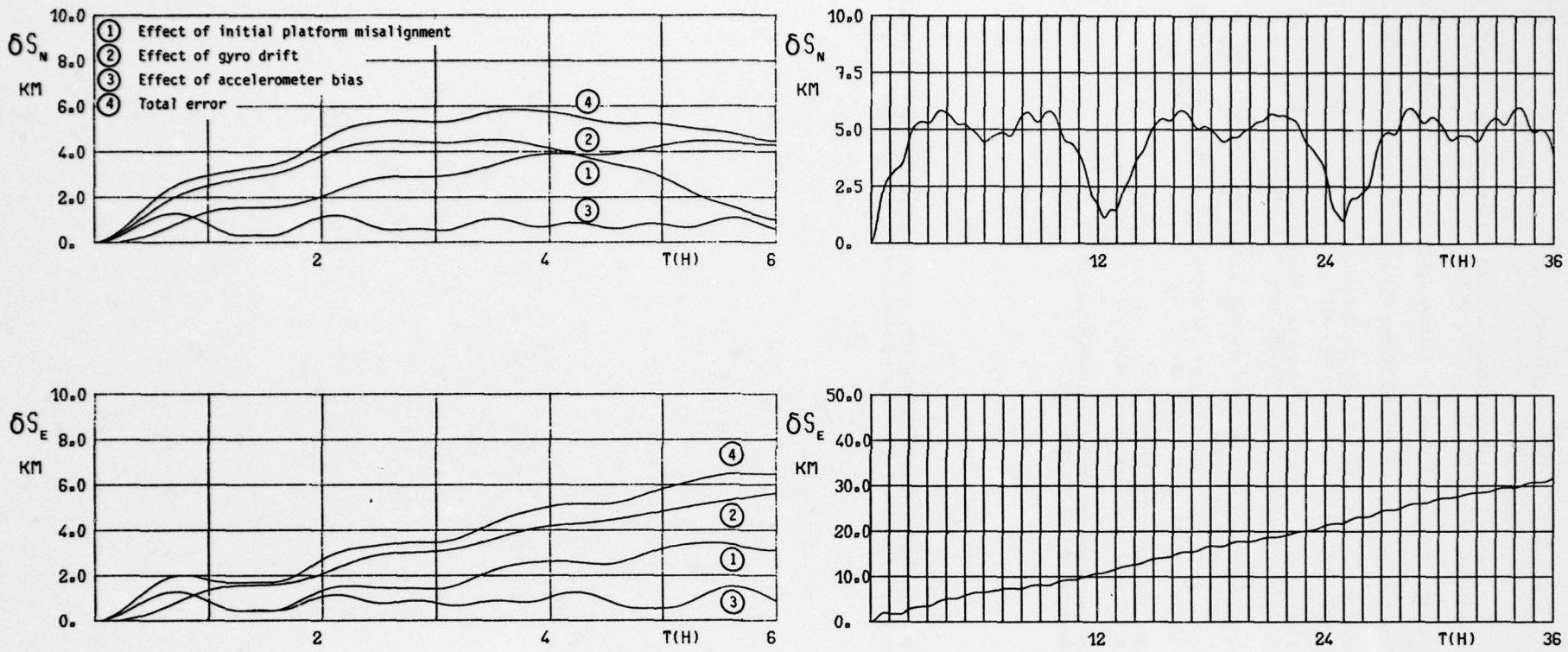

Velocity: 1080 km/h towards east

Initial misalignment angles: $\varepsilon_N = \varepsilon_E = 0.1$ mrad = 0.34 $\widehat{\text{min}}$; $\varepsilon_D = 1$ mrad = 3.4 $\widehat{\text{min}}$

Gyro drift: $D_N = D_E = D_D = 0.01\ ^{\circ}/h$

Accelerometer bias: $B_N = B_E = 0.0001$ g

Fig. 1 1σ-Position Error of an Inertial Navigation System

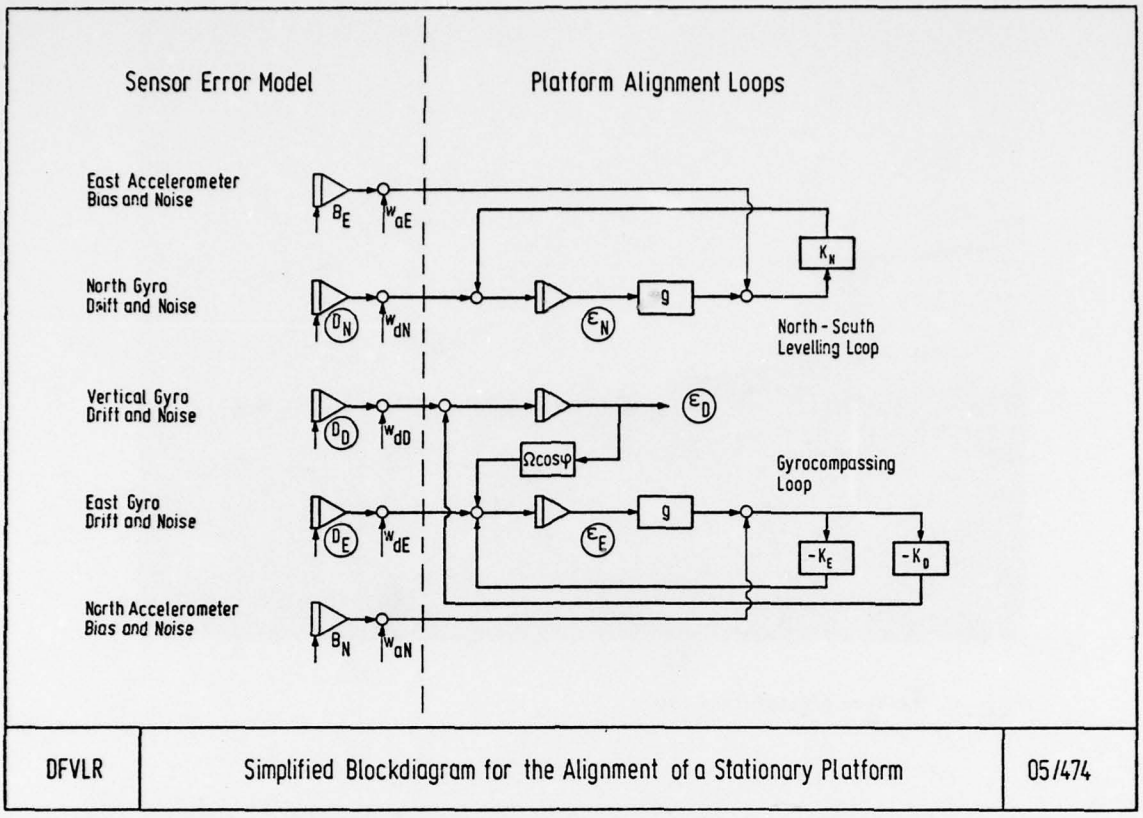
Sensor Error Model
Platform Alignment Loops
East Accelerometer Bias and Noise
North Gyro Drift and Noise
Vertical Gyro Drift and Noise
East Gyro Drift and Noise
North Accelerometer Bias and Noise
North - South Levelling Loop
Gyrocompassing Loop
DFVLR
Simplified Blockdiagram for the Alignment of a Stationary Platform
05/474

Fig. 2

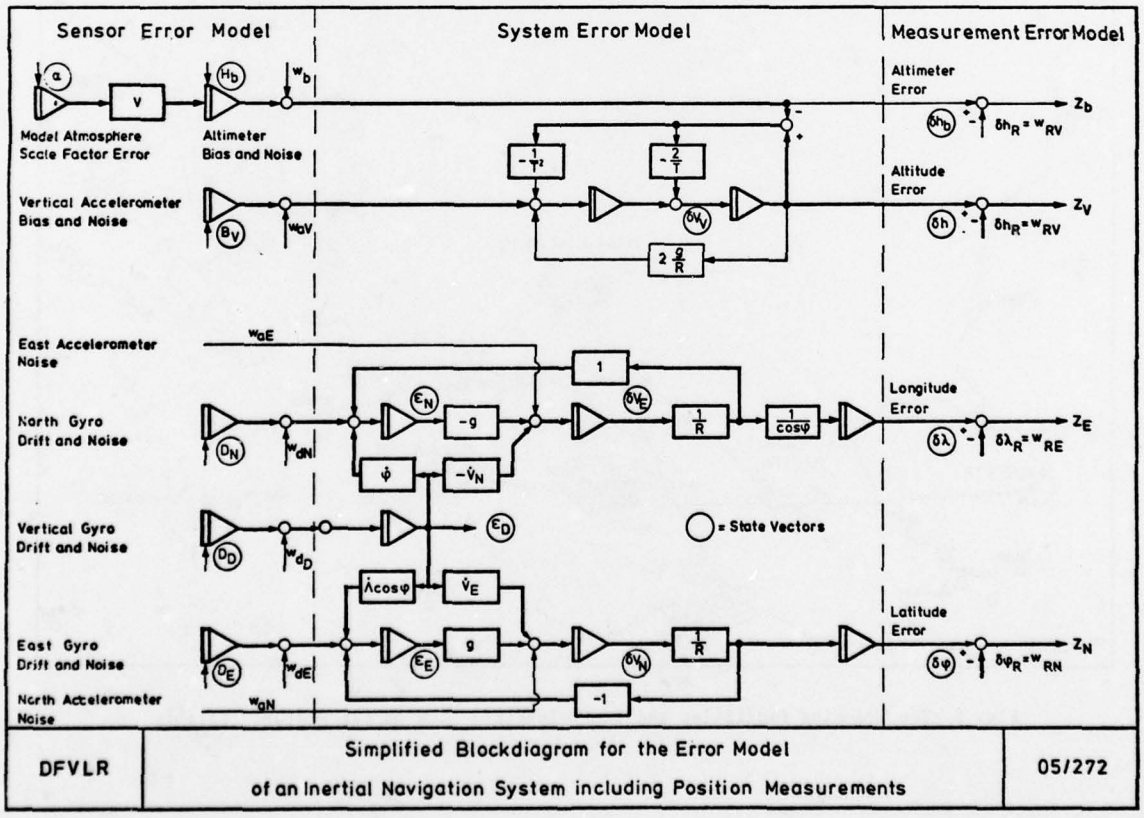
Sensor Error Model
System Error Model
Measurement Error Model
Model Atmosphere Scale Factor Error
Altimeter Bias and Noise
Altimeter Error
Vertical Accelerometer Bias and Noise
Altitude Error
East Accelerometer Noise
North Gyro Drift and Noise
Longitude Error
Vertical Gyro Drift and Noise
= State Vectors
East Gyro Drift and Noise
Latitude Error
North Accelerometer Noise
DFVLR
Simplified Blockdiagram for the Error Model
of an Inertial Navigation System including Position Measurements
05/272

Fig. 3

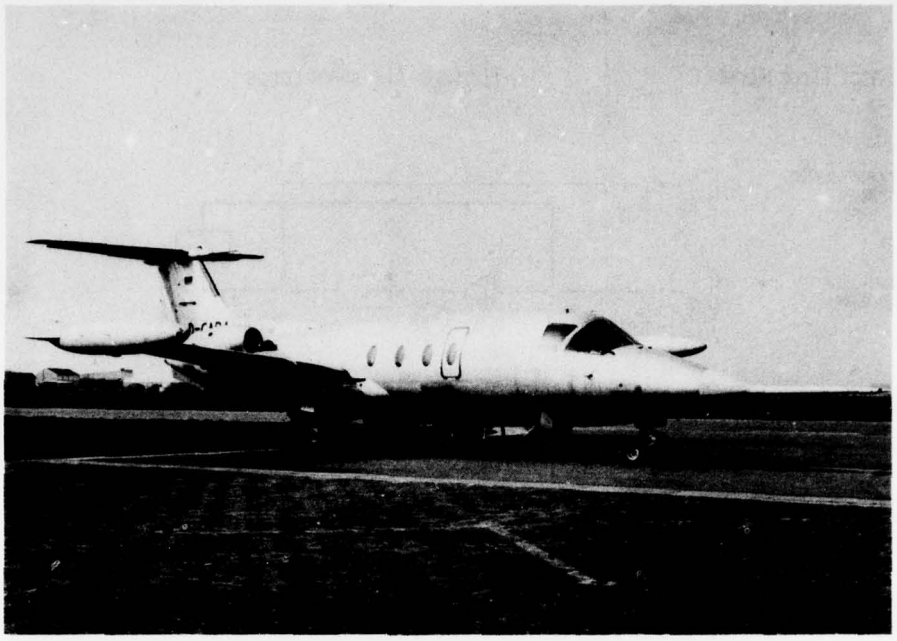

Fig. 4 The Test Aircraft HFB 320

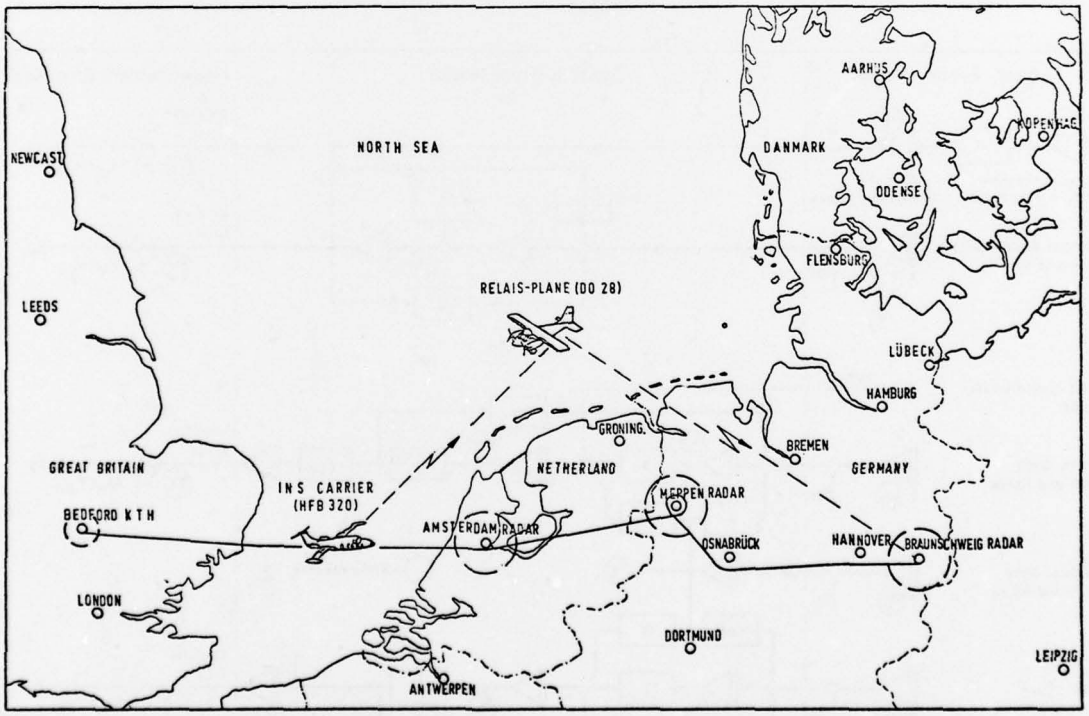

Fig. 5 The Tracking Facilities and the Telemetrie Link on the Westerly Flights

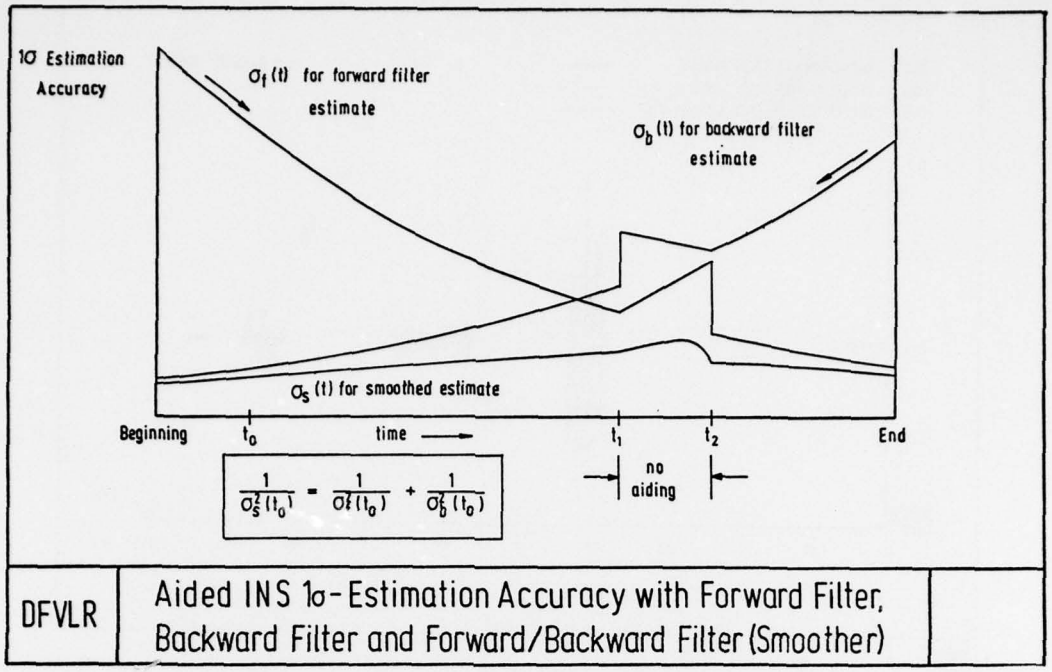

Fig. 6

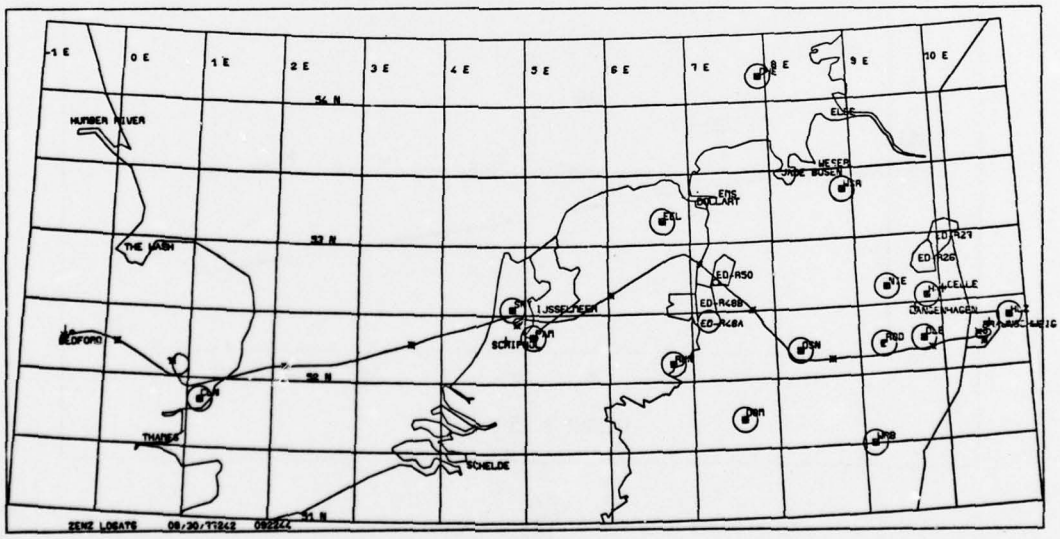

Fig. 7 The Flightpath from Bedford to Braunschweig

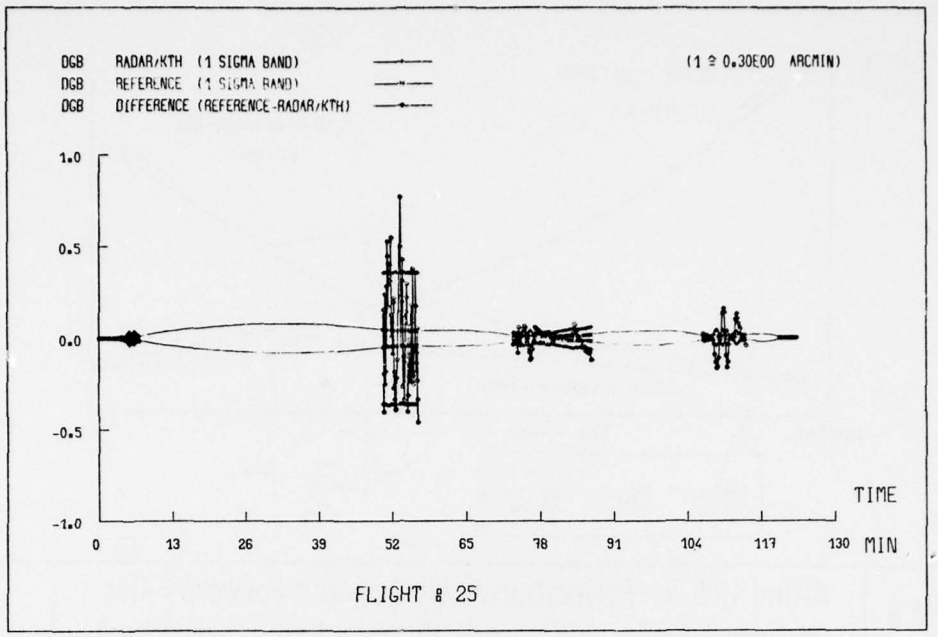

Fig. 8 The 1σ-Band of the Reference Flightpath and the External Measurements

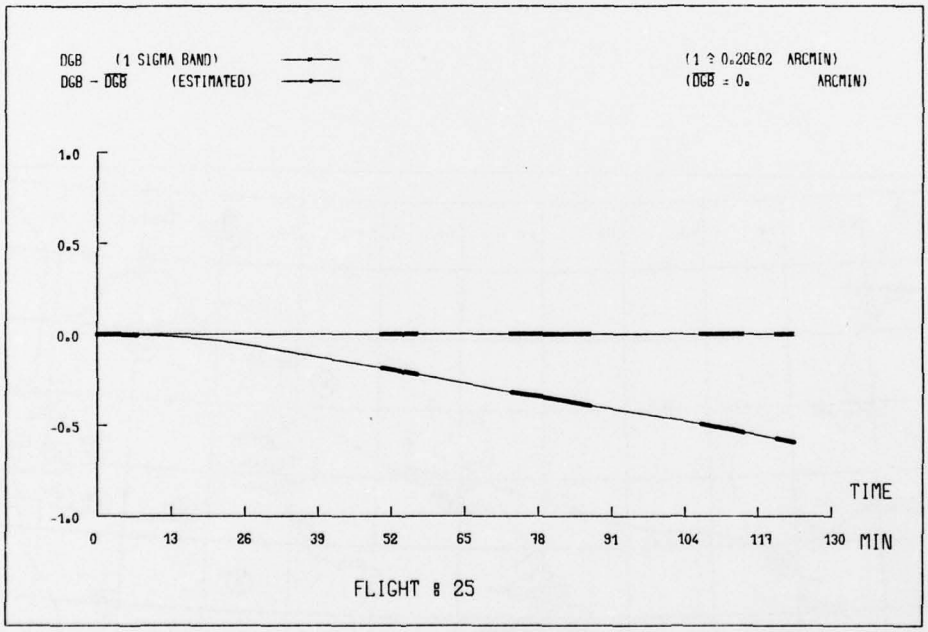

Fig. 9 Optimal Estimate of the INS Latitude Error

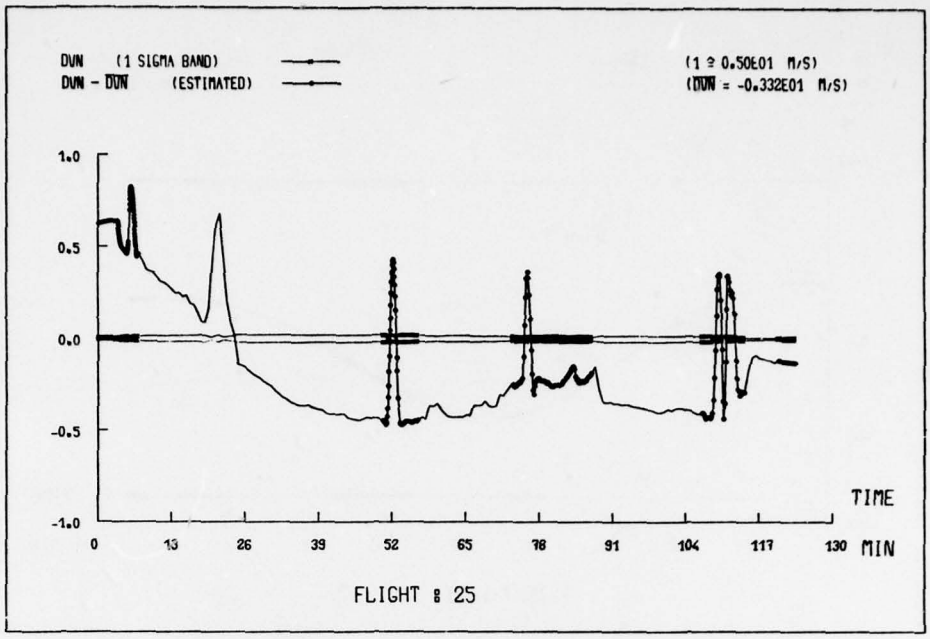

Fig. 10 Optimal Estimate of the INS North Velocity Error

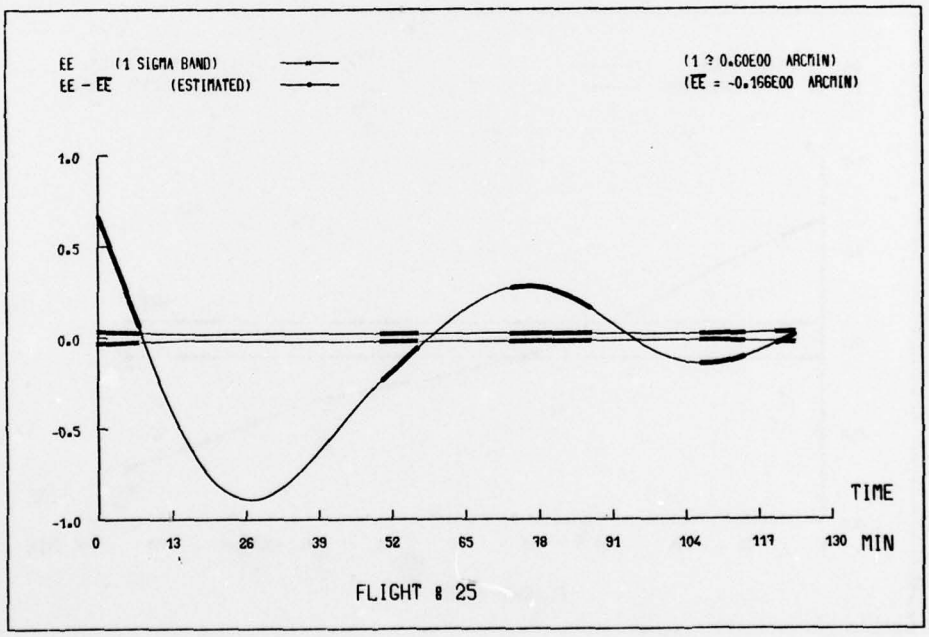

Fig. 11 Optimal Estimate of the INS East-West Misalignment Error

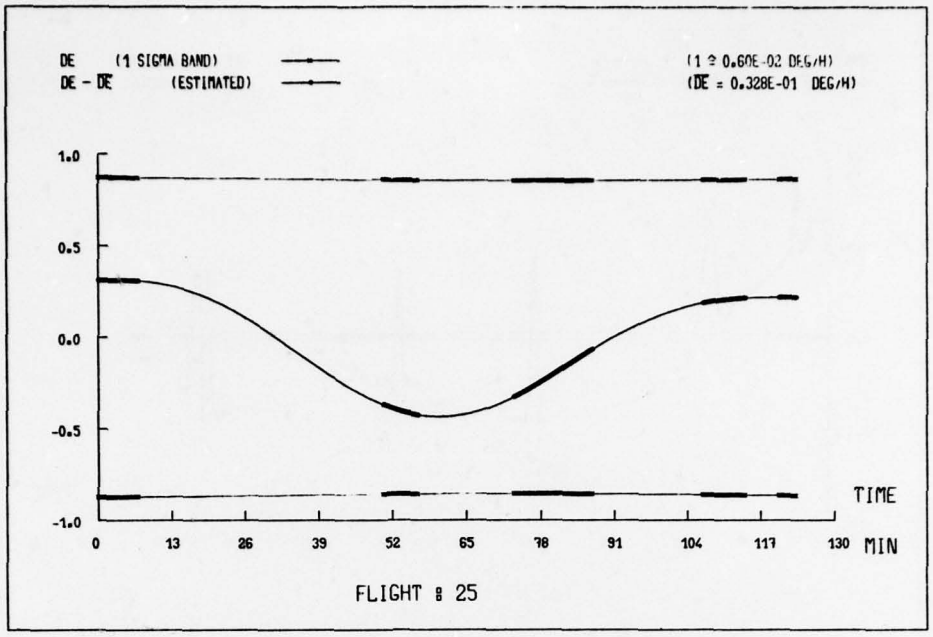

Fig. 12 Optimal Estimate for the East-West Gyro Drift

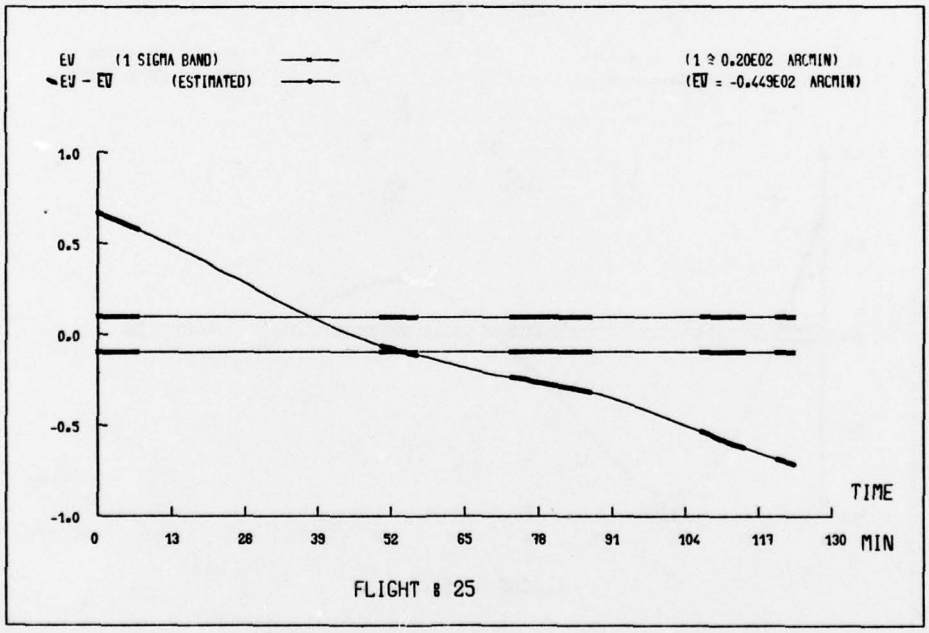

Fig. 13 Optimal Estimate for the Azimuth Alignment Error

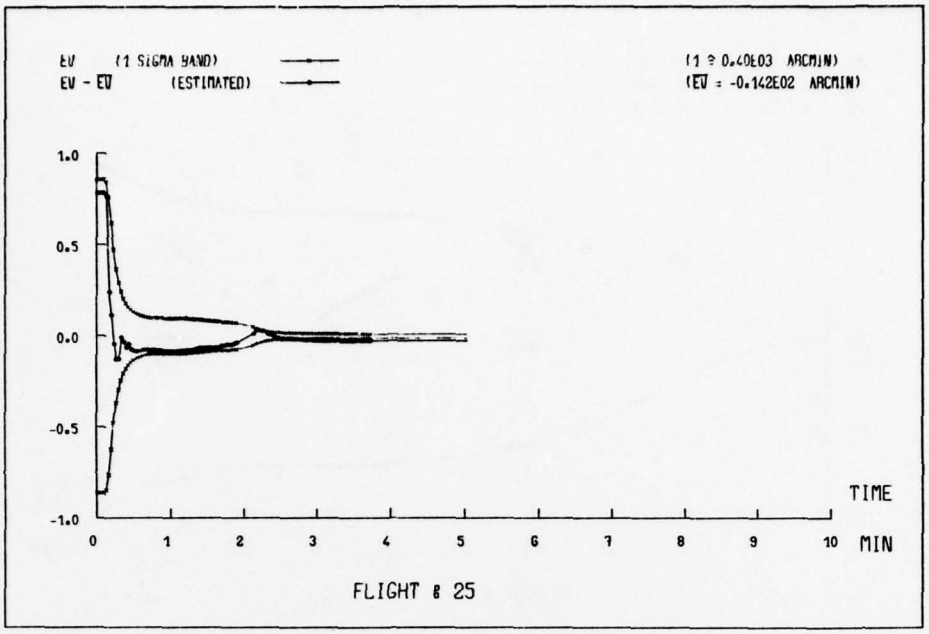

Fig. 14 In-Flight Alignment; Results for the Misalignment about the North-South Axis

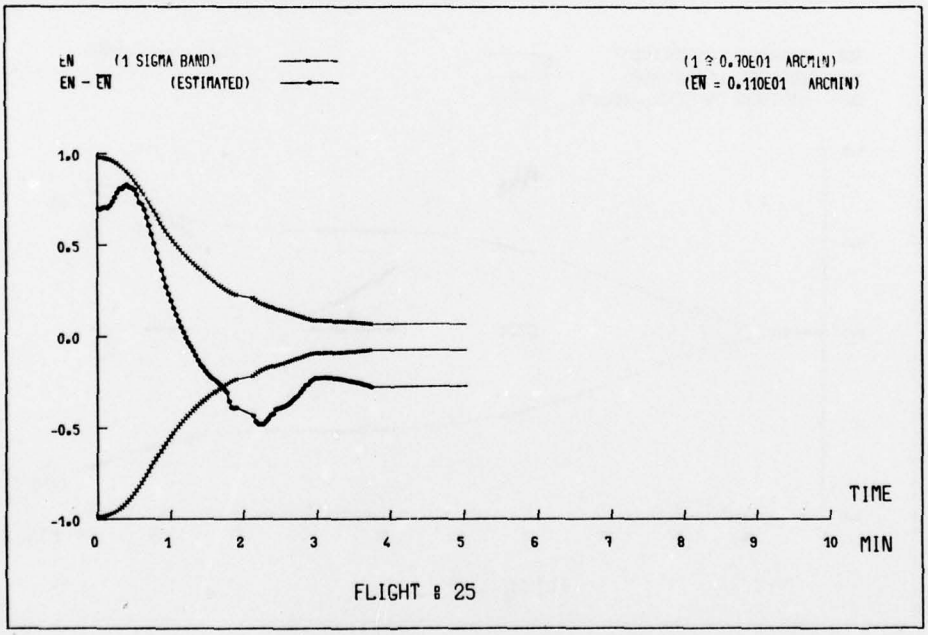

Fig. 15 In-Flight Alignment; Results for the Azimuth Misalignment

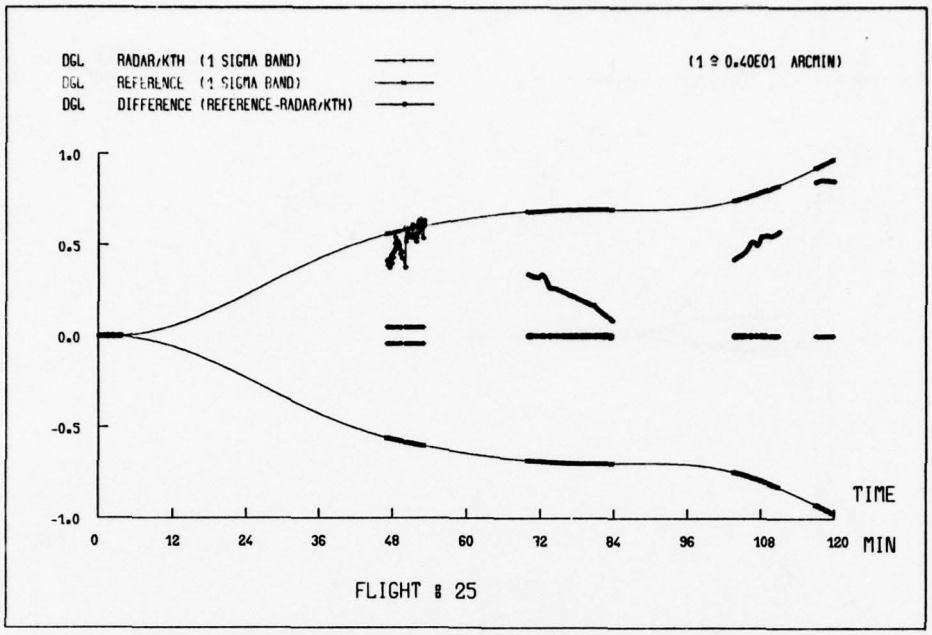

Fig. 16 In-Flight Alignment; Results for the INS Longitude Error

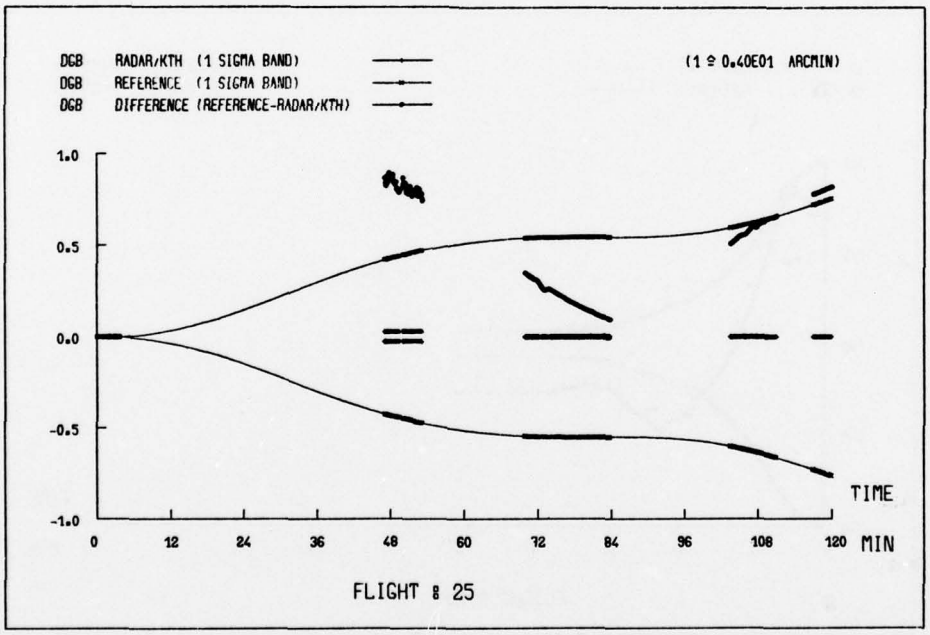

Fig. 17 In-Flight Alignment; Results for the INS Latitude Error

UHF DF Triangulation System for Control and Guidance of Military Aircraft

by
Dipl. Ing. Bernhard F. Ernst
ROHDE & SCHWARZ
Entwicklung Ortung und Satellitentechnik
Mühldorfstr. 15
8000 München 80
Germany

Summary

This paper deals with a system for the guidance of aircraft from ground stations. The system consists essentially of a network of direction finders, and is intended to complement, rather then replace, conventional radars and other landing aids normally installed at airports.

As a guidance technique, a network of direction finders offers the advantage of surface coverage, or, in other words, it permits a form of surface navigation. The system has a further advantage of particular significance in emergency situations such as may follow an error in navigation or a loss of fuel: nothing more than an operational radio set need be available on board the aircraft before use can be made of the DF guidance network. This feature can also be useful in the guidance of military aircraft since, as practice has shown, maneuvers at low level can often take the aircraft outside the airspace covered by ground-based radars.

1. System configuration

The system presented here (see Fig. 1) is so arranged that all practical flight altitudes within the airspace of interest can be monitored from a single station. An extension of the system offers determination of the best possible radio link with the aircraft, by way of the communications equipment, on the basis of the established position of the aircraft.

The complete system is made up of a series of direction finders located within the area to be monitored and distributed in such a way that, bearing in mind the local topography, a coverage as free from gaps as possible is achieved. The direction finders are connected by means of conventional communications links (telephone lines or directional radio where necessary) to the central station. The main functional units of the central station are the peripheral data input-output system, the data processing system, one or more operators' positions and, according to the particular requirements of each installation, the centralized and local display units.

The operating frequencies are partly or fully specified by the central station and communicated to the direction finders over the data links. While radio communication is taking place with the aircraft on this frequency each DF station which picks up the signal establishes the bearing of the aircraft. These bearing values are sent back to the central station over the data lines and, in the normal course of events, processed to give the instantaneous position of the aircraft. In special cases, such as emergencies, it can also be useful to offer the operator a display on which the bearing values can be examined individually. The result of the triangulation computation, together with other data such as the frequency, is presented on a central display or on local displays at the operators' positions. As previously indicated, the system

can be expanded to include a transmitter at each DF station. This permits the operator to make use of the transmitter which provides the best communication with the aircraft at any instant. Choice of the best transmitter may be made automatically by the computer on the basis of the established position of the aircraft, or manually by the operator. The receiver incorporated in the DF unit of the transmitting station is used to receive signals from the aircraft.

2. Description of subsystems

As the description of the system configuration has shown, the equipment is made up of a number of independent subsystems or functional units which must be accurately matched to one another to ensure perfect operation of the overall system.

Direction finder

This system uses Doppler direction finders such as are used in civil airtraffic control. The Doppler method has already proved itself in practice, particularly with regard to accuracy and immunity to interference. The bearing value is established by comparing the phase of the Doppler-frequency-modulated incoming signal (produced by simulated rotation of the receiving antenna dipole) with the phase of a reference signal. This phase-sensitive DF technique is particularly insensitive to distortions of the electromagnetic field, since the antenna system can be made large in comparison to the wavelength. Through the use of a special sampling-filter technique, the DF system achieves very high sensitivity and thereby a large coverage. Fig. 2 shows the antenna system for a typical Doppler DF system and Fig. 3 shows the equipment which goes to make up a single-channel UHF direction finder for the frequency range 225 to 400 MHz. The block diagram of this system is given in Fig. 4. The signal from the "rotating" antenna is taken to the input of the DF receiver. A second channel of the receiver is fed with the signal from an omnidirectional antenna mounted at the centre of the circular DF antenna. This second channel is used for compensation of static and dynamic changes in the frequency of the DF signal, and permits the Doppler technique to be used even with frequency- or phase-modulated signals. The IF outputs of the receiver channels are both taken to the bearing demodulator. The output of the demodulator provides the demodulated Doppler signal which will be used in the bearing indicator for extracting the bearing. The bearing is measured by determining the phase difference between the demodulated Doppler signal and a reference signal which is synchronous with the simulated rotation of the DF antenna. Since the bearing can be measured in this way with simple digital circuitry, a fully automatic process involving no personnel is possible. A control-frequency generator produces all the frequencies, especially the antenna-rotation frequency, required by the system.

Data transmission system

A wide choice of data transmission systems is possible according to the geographical and operational conditions to be taken into account. A data multiplexer controlled by a microcomputer represents a suitable method of connecting a number of direction finders to one triangulation station. Fig. 5 shows a typical unit for this function. The principal content of the data flow from the central station to the direction finders is information on operating frequency and functional commands such as test-transmission signalling, request for repeat of bearing and so on. The data flow from direction finder to central station consists mainly of the bearing information and a signal confirming the frequency of operation. It is also possible to transmit data on the status of the DF station. This data link can further be used to switch on the optimum transmitter in

the optional expansion described earlier. The data channels will normally use telephone lines, although directional radio links may be used in some cases. Use of a microcomputer as controlling element permits flexible organization of the data flow and protected transmission of information.

Data processing system

Within the central triangulation station of the DF network, data flow to and from the direction finders take place via the peripheral data input-output system. Information from the direction finders, in particular the bearing values, is routed to the data processing section of the station. The principal function of this subsystem is to determine the position of the target aircraft within the DF-network area. In the course of this processing, the incoming bearing signals are monitored and classified according to quality. Fig. 6 shows a possible bearing-value processing sequence. The first step is to establish whether an actual DF determination is being carried out, or a test or simulation. Each bearing is then evaluated to determine its suitability for use in the triangulation calculation. Unusable bearing values are extracted on the basis of an "expected accuracy" criterion. The determined intersect points are then correlated to establish the most probable location of the target. A second computation is carried out to check on the existence of a second discrete target point, that is, to check if a second aircraft is present. The operator is also provided with a recommendation as to which tranceiver station should be used. The definitive location, with a statement of its accuracy, is then provided for display at the various operators' positions.

Operators' positions and displays

The provision of operating positions may vary widely, according to the particular requirements of each installation. The triangulation result may be represented on large-area displays such as a projection screen or a data terminal with synthesized landmarks for orientation. The individual operating positions are equipped with the control units necessary for operation of the DF network such as frequency selectors, communications sets an emergency facilities. It is also possible to superimpose single DF beams or the triangulation result on a radar display of the monitored airspace. This is useful as an aid to identification and is already popular in civil ATC systems.

3. Prospects

Triangulation networks such as have been described here represent a useful complement to the existing, principally radar-based, systems of aircraft guidance. The exact configuration of such a network is dependent on a great number of parameters. Of particular importance here is the accuracy of the direction finders used, since this fixes the mesh size of the network. Clearly the geography of the area to be controlled and the range of the direction finders are also significant parameters. In principle, however, it may be said that networks using direction finders of conventional 0.5-degree accuracy or markedly more accurate types (0.1°) are both possible. From the arguments of redundancy and of maintaining the highest possible coverage it would appear that a network made up of a large number of direction finders of moderate accuracy is to be preferred to one using few higher-accuracy DF stations.

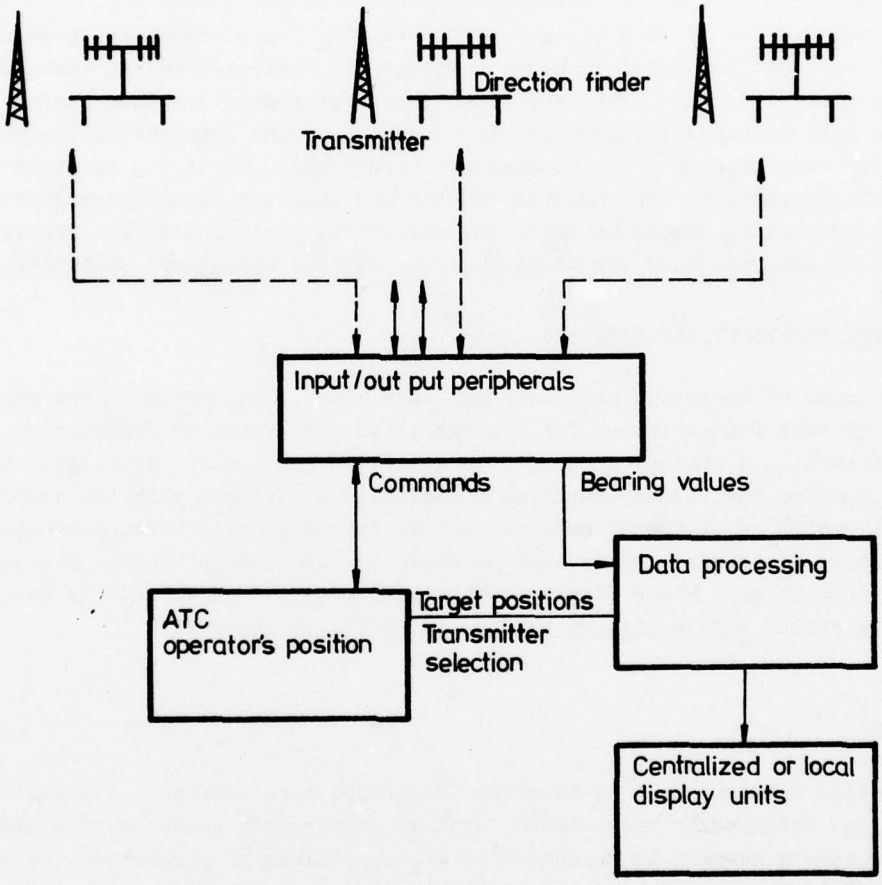

Fig. 1 System configuration

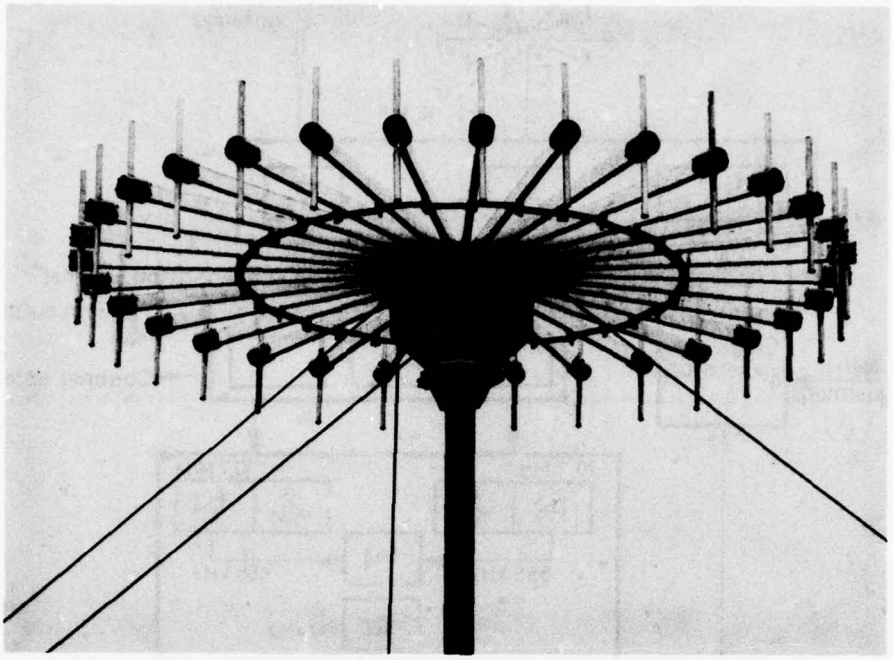

Fig. 2 UHF-DF antenna

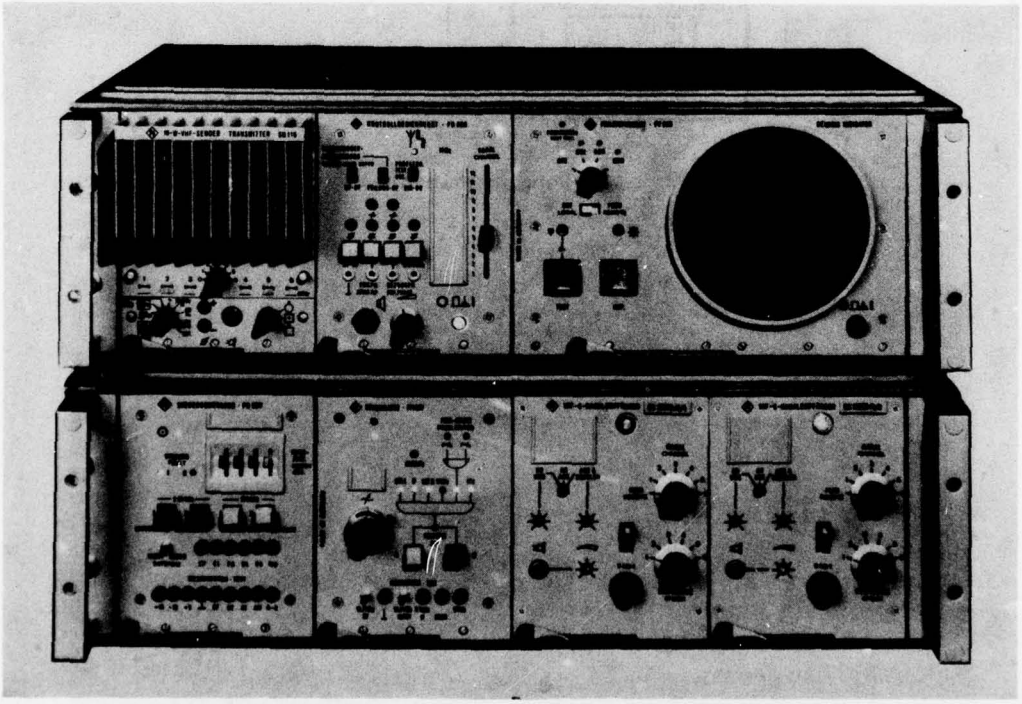

Fig. 3 VHF-DF equipment

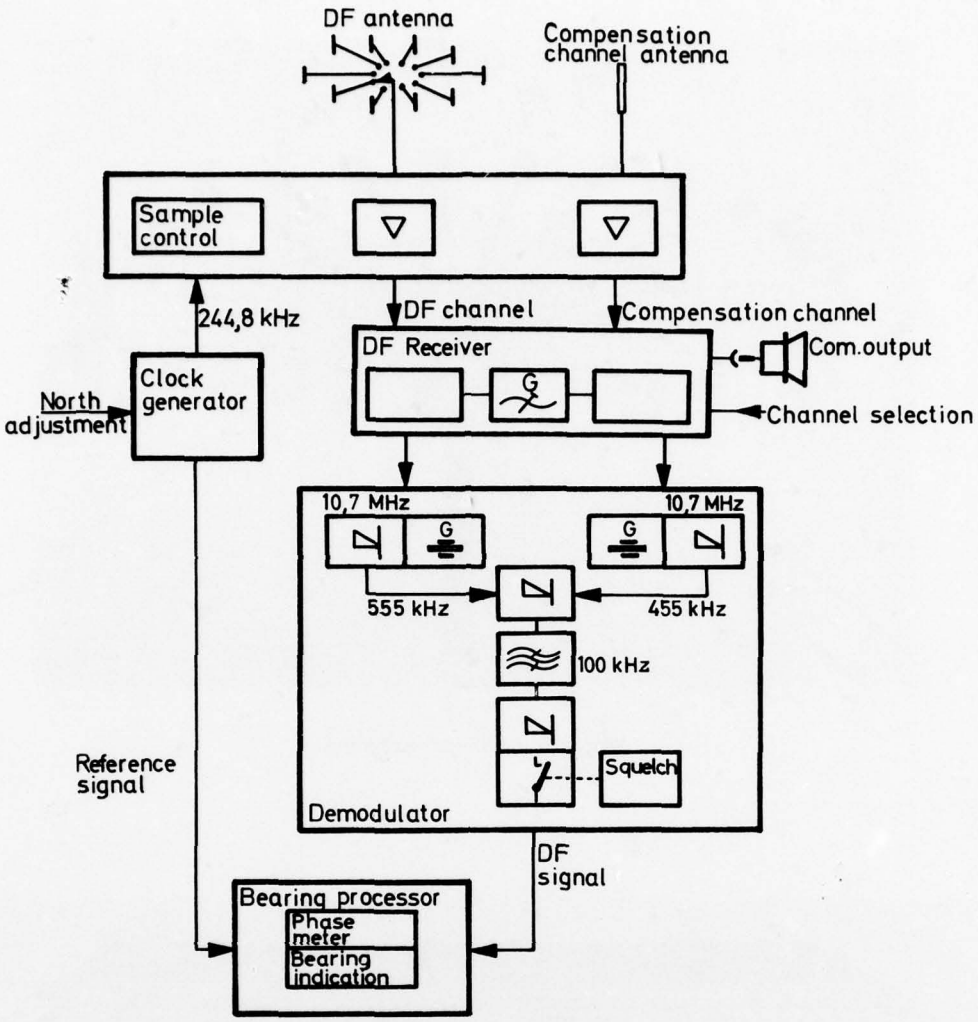

Fig. 4 UHF-Doppler direction finder

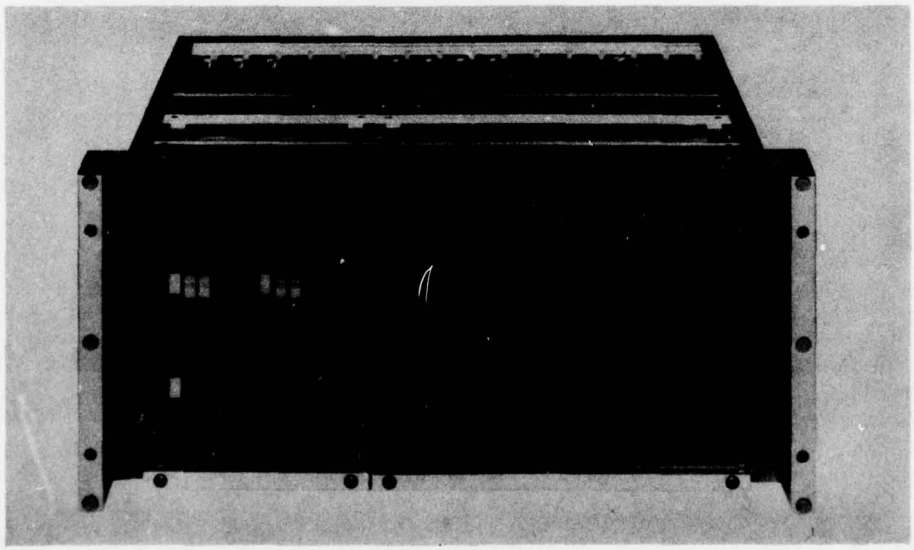

Fig. 5 Data multiplexer

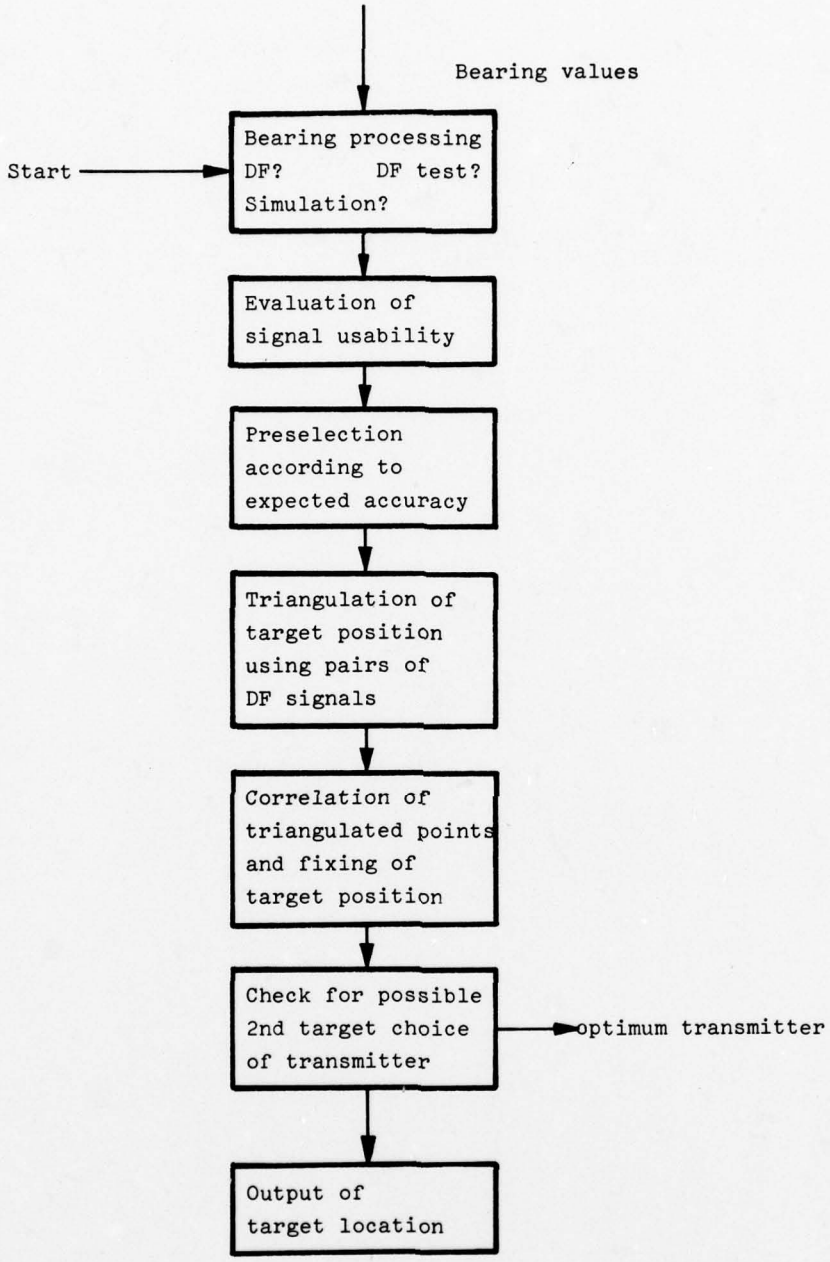

Fig. 6 Bearing-value processing

PRECISE ENROUTE NAVIGATION BASED ON GROUND-DERIVED TECHNIQUES

G. Blaschke, G. Peuker
Standard Elektrik Lorenz AG (ITT)
Stuttgart, Germany

Summary

Rho/Theta radio location techniques today used for Enroute Navigation suffer from errors due to multipath propagation especially at several difficult sites. The development of Doppler-VOR was one answer to reduce this problem for the angle measurement (azimuth theta). As signal processing is still done in the airborne set (air-derived system), an accuracy of better than 1° is not easily achievable. Together with improved standard L-band DME (distance rho) and with the development and use of RNAV equipment, a more accurate angle measurement is highly desirable. This should be achievable without strong effort in airborne equipment, in order to allow economic world-wide introduction.

A solution is offered by a ground-derived concept for azimuth measurement. It is based on the standard L-band DME, using also the existing airborne DME set. The DME interrogation pulses of the aircraft are received at the ground via a special antenna array by DF equipment that allows immediate determination of angle of incidence. This angle is sent back to the aircraft by a third pulse synchronized with the according DME reply. In the aircraft a search and track system extracts the "angle reply", the time delay of which relative to the DME reply represents angle information (azimuth).

The signal format is the key element of the system, allowing for simplicity of airborne equipment and flexibility of ground stations. Basic error considerations show that errors due to airborne signal processing can be neglected and that the ground system can be adapted to a large extend to the special multipath environment, if necessary. This allows the deployment of ground stations tailored to a special site leading to very economic solutions also on the ground.

The ground antenna array can be circular or linear according to special conditions. At each antenna amplitude and phase of the received interrogation pulse are measured and from these the angle is calculated in a digital computer. This principle is unique in one respect: no matter what is installed or processed in the ground station, the airborne set receives always the same "angle reply" coding.

Implementation of airborne equipment is described followed by a more detailed presentation of ground station design (DME transponder, antenna array, receiver multiple, processing method, transmitter and data encoder, calibration and monitoring).

Field test results from the experimental model of the landing system DLS and from the military system ORTAC-M are given to show, that a 0.2 degree angle accuracy is readily achievable.

A possible way of operational introduction of such an approach as a future Standard Enroute Navigation Aid is then considered.

Special aspects of the proposal, such as capacity, co-channel operation, use of directional ground transmitter antennas and future growth potential are briefly discussed.

Finally some possible military applications will be described.

1. Introduction

Since many years medium range navigation is based on the standardized radio location systems VOR and TACAN for civil and military aircraft resp. The coordinates used are the azimuth theta and the distance rho. For direct guidance of the aircraft up today the azimth information only is used by selection of a fixed course and display of course deviation to the pilot or processing by an automatic flight control system. Distance measurement is so far used only for the definition of fixed points to derive a new course for a determined procedure. In general this enroute navigation concept is satisfying all needs, it is especially low in cost, reliable and safe.

One property of radio systems as VOR and TACAN, that creates sometimes a problem, is their susceptibility to multipath propagation. This causes errors on coordinate measurements or even does not allow the selection of a ground station location, that would be desirable from a navigation point of view.

The navigation based on fixed courses has some disadvantages, e.g. no free selection of ground station locations and restrictions for air traffic control in case of high traffic density in terminal areas (separation criteria). This was one of the reasons, that full use of angle and distance information was introduced, allowing flights on nearly arbitrary paths by selection of a number of way points and display to the pilot of the deviations from the path given by straight connections between the waypoints. This is basicly achieved by transformation of the measured values for distance and azimuth to to the next waypoint. In such a concept also the errors of the primary coordinates are transformed and can be amplified to an unacceptable amount depending on the crossing angles. From this point of view, a higher accuracy in coordinate measurement would be required. The enroute navigation system proposed in this publication is based on the standard DME with improved accuracy (error $\leq$ 100 m). An azimuth measurement concept is added, that is matched with this DME to optimize the overall system.

For VOR + DME or for TACAN the time/frequency area is fully occupied by the combination of a DME having large bandwidth and short time duration with an angle measurement that is just the contrary. Consequently a great percentage of the time/frequency domain is unused. The optimum matching is achieved, if the angle measurement has the same characteristics concerning time/frequency needs. This leads to the use of the DME pulses also for angle determination. It is implemented by receiving the DME interrogations at the ground with special antenna arrays that allow measurement of azimuth at the ground. The result is then transmitted to the specific aircraft. The outstanding advantages of this concept are:

- improvement of angle accuracy due to use of pulses (first pulse timing, known from DME)
- flexibility of antenna array and processing of information in the ground station
- very low cost airborne equipment
- multiplication of number of channels by pulse coding (co-channel operation).

2. DME Based Ground Derived Concept

As already stated the existing L-band DME system can be expanded to a rho/theta enroute navigation system in a very economic way, especially with respect to cost of the airborne equipment.

The following proposal illustrates an attempt for an overall optimisation of the existing airborne equipment, needed for ground based navigation purposes. Of course, this optimisation cannot be accomplished by adding only some more sophisticated electronic hardware to the aircraft. The main reason, leading to the optimisation is the introduction of a ground derived angle measurement concept, adapted to the present in use DME system.

2.1 General Description

The principle of this concept is quite simple (see Fig. 1). The DME interrogations from the aircraft are measured on the ground with respect to their angle of incidence by means of a special receiving antenna array. The results are transmitted back to the aircraft using a data format compatible with the DME time frame and with minimal influence on system capacity.

Airborne reception of angle information is accomplished by the same receiver as used for DME. Some slight modifications for angle decoding have to be introduced. One approach is to add a supplement to the existing standard DME, the other solution is to integrate DME and angle decoding in an advanced DME transmitter/receiver configuration.

2.2 Signal Format

The key to the system design is the signal format. Some basic conditions shall be fulfilled by adding the angle component to DME:

- no interference between DME reply and angle information for the same aircraft
- a simple method of identification for the angle information
- a coding principle allowing use of existing DME receivers, requiring a minimum technical effort for decoding
- immunity against multipath distortions.

The coding principle chosen for angle data transfer is a time difference between two certain pulses. An additional reply pulse pair - equal in shape and pulse spacing to the DME reply - is needed for angle information transmission.

Proper identification and acquisition is realised by exactly the same principle as used for DME today. Whilst for the distance the information is coded by the spacing of DME interrogation and reply , the angle is coded by the spacing of the DME reply and angle reply. The measured time interval, subtracted by a fixed bias time, is directly proportional to the angle of incidence measured at the ground station (Fig. 2). A schematic diagram of angle data transmission is shown in Fig. 3. An angle pulse, received 5 msec after the DME reply corresponds to 0^{o} azimuth, an angle pulse received 11.55 msec after the DME reply corresponds to 360^{o} azimuth. The 5 msec bias time is chosen to provide sufficient time for angle processing on the ground and simultaneously to prevent an erroneous identification of this pulse as a DME reply - it lies outside the search region for DME. The coding sensitivity is chosen for easy and reliable encoding and decoding of the angle information, it is about $1^{o}/18/us$. With this sensitivity a resolution of 0.005^{o} is achieved, assuming a triggering accuracy of better than $0.1/us$ of the TACAN DME pulse pair, which corresponds to modern first pulse timing techniques.

This angle coding principle has also an inherent immunity against multipath distortions. The time interval between DME reply and angle reply is short enough, so that the reflection geometry will be practically unchanged. This leads to an equal distortion (if any) of the pulses. As measurements of time are performed on the 50 % point of the positive slope of the (first) pulse, no erroneous time spacing will result compared to measurements with undistorted pulses. Thus errors due to airborne equipment can be neglected.

In a similar manner auxiliary data (as TMA informations, QNH, wind direction, velocity etc.) can be transmitted from ground to air. These data are transmitted simultaneously to all aircraft word by word, each consisting of an address and the corresponding information. Address and information are coded by the positions of pulse triplets with respect to a reference pulse triplet. The positions of the address and information triplets are varied in steps of $4/us$. Using a scheme as shown in Fig. 4, 96 different addresses and 96 informations per address are possible. Word repetition rate is proposed to be 100 per second. This scheme has the advantage, that priority can be given to any information, since no discrete time order is prescribed.

Due to the data format chosen, the airborne equipment for decoding of angle information is rather simple. An angle supplement to the standard DME airborne set basically is a duplication of a DME search and track video system. Future DME sets would already contain the necessary decoding circuitry for angle information.

With the introduction of modern microprocessors, the signal processing - i.e. acquisition, validation and tracking - of DME and angle information only differs in software, additional hardware for angle function basically then consists of some additional ROM's for program storage. This means an optimisation of the airborne equipment with respect to cost, reliability and weight.

3. Equipment Design

3.1 Airborne Design

An advanced solution for a DME airborne equipment is shown in Fig. 5. The RF part is of the same type as for a known precision DME transceiver, including receiver, frequency generation, modulator, transmitter, T/R switch, and a pilot pulse module for PDME function.

The video part is splitted up into a signal processing part (real time measurement) and a data processing part (microprocessor). The signal processing circuitry basically delivers time labels to the microprocessor which is responsible for DME and angle reply processing and for auxiliary data. Other functions as monitoring controls and further data processing for area navigation also can be handled by the microprocessor. Compared with the technical solutions in use today for DME, this proposed DME/angle equipment has additional capabilities without adding weight or cost, it may even be less expensive.

To demonstrate the simplicity of the signal processing unit and its interface to the microprocessor the data sampling is shown in Fig. 6. The decodes from pilot pulse, ground replies, and data triplets are fed directly to the microprocessor, requesting an interrupt operation if the decodes are accepted. Simultaneously these decodes cause a register to sample the content of a real time sampling counter. To define the beginning and end of the DME and angle time slots a magnitude comparator compares computed reference data with the sampling counter.

The search and track functions entirely are based on processor software. As an advantage over present in use systems the over all search time is reduced considerably, as all replies within the DME or angle time interval can be handled simultaneously. A reliable acquisition normally will be accomplished already after three correct replies. Therefore no higher interrogation rate during search mode - compared to tracking mode - is necessary any longer.

A computer block diagram down to IC level demonstrates the simplicity of the microprocessor hardware (Fig. 7). It consists of 24 IC's, 9 of them being interface units. More progress in large scale integration can be expected in the future.

3.2 Ground Station Design

Fig. 8 gives a basic block diagram of the ground station. The DME transponder operates as usual, except that for precision DME measurements a pilot pulse loop is incorporated to ensure an exact transponder delay time varying less than ± 100 ns with respect to the nominal value. In addition to the DME transponder a special receiving antenna array is used for angle determination. Each single antenna is coupled to its own receiver, allowing for amplitude A and phase Ø measurement of the received signals on each antenna. The measured phases and amplitudes are then processed within a digital processor to obtain the angle of incidence. This angle is coded into a time interval by a set of angle encoders. These encoders determine the exact time point of angle reply transmission. Depending upon the maximum requested traffic handling capacity it might be necessary to have a greater number of processors. The block diagram in Fig. 9 shows a processor multiple. Each station thus may be adapted to the capacity required. One important feature of the receiver multiple shall be described in some more detail. The receivers must be capable, to amplify signals varying in field strength from pulse to pulse up to 80 db. Amplitude and phase measurements must be linear over the whole range. Therefore a special calibration system is incorporated. At fixed time intervals calibration pulses with well defined amplitude and phase are fed into the receiving antennas.

For a circular antenna array, this is done simply by transmitting the calibration signal by the centre of the array. For a linear antenna array a special distribution network with calibrated cables is used to feed the calibration signal direct into the antenna elements. In each case the exact actual amplification and phase shift is measured for each receiver channel. The results are stored in the prcessor memory for different field strengths of the input signal. By this, the measured values from received interrogations can be corrected according to the characteristics of the individual receiver.

At the same time this calibration system provides an excellent monitoring for the station. Each receiver channel from the antenna up to the processor input can be checked simply by a simulated interrogation signal from the calibration system. The processor itself and all the following circuitry can be checked completely by internal test signals, i.e. simulating digital test input signals corresponding to predetermined angles. Thus the whole system can be monitored internally without the need of an external monitor. An external monitor can also be provided merely consisting of a transmitting antenna, fed by the calibration transmitter. The additional information it provides, is the check of the physical alignment of the station. With some more sophisticated software an automatic self-calibration can be realised with two external monitor antennas, eliminating bias errors nearly totally.

An essential part of the angle measurement in the ground station is the processing of the measured amplitudes and phases in order to calculate the angle of incidence of the received interrogation. The main objective is, to find a mechanism, by which multipath effects are reduced as much as possible. First approaches for mathematical methods are given by simulation of all known conventional principles by which

angle measurement is performed with a given antenna array. Those principles are phase evaluation (rotating interferometer for a circular array), doppler type processing (for linear and circular arrays), rotating or scanning pencil beam diagrams, cross-section of two amplitude diagrams. The very low equipment error, resulting from digital processing as far as possible, leads to smaller total azimuth errors also for such more conventional methods.

The low equipment error is, on the other hand, a necessary condition for the application of more unconventional processing methods. Fig. 10 illustrates, what is meant. The real world appears as consisting of several transmitters distributed in space. One of those transmitters (T1 ... T/u) is the wanted one, the others are generated by multipath effects. The basic idea to develop a mathematical formalism is, to establish a model of the real world in the computer and to analyse the received signal against this model. The problem ist, that the real world is generally not known and is very complex. A simplified first approach is therefore, to define a model and to use mathematics without considering differences to real world. In many cases this leads to reduced errors in angle determination. Another, more complex way is to establish a model with free parameters concerning number of reflectors and their properties and to correlate this model with the received set of amplitudes and phases. This method needs much more calculations and is not yet possible in a system with high update rate requirements. Further increase of computer speed with more advanced technology may lead to the use of such processing, which should reduce errors further and allow the employment of smaller antenna arrays. Here a wide field is open for mathematicians to establish useful procedures. This again shows, that the concept proposed is open for the future and flexible enough to introduce newest results of research without modification of airborne equipment.

It may finally be mentioned, that also the combination of results from different processing methods of the conventional or unconventional type is possible and leads to reduced errors, if the errors are not correlated between the methods.

4. Field Test Results

The field test results being presented are from two systems based on the described concept and proving its usability: DLS, the German MLS contribution and ORTAC, a military system that was designed for a special application of rho/theta navigation. The field test results are given in Figs. 11 and 12, without more comments, because its only intended to give an impression, that the errors well below one degree can be achieved with a circular array of 5 to 10 wavelengths diameter and a special phase processing. The distances during the field tests were rather small (max. 32 NM), because in both cases a landing aid was to be evaluated. Similar results can, however, be expected also for greater distances, because power budget would be adjusted accordingly.

5. Special System Characteristics

5.1 Co-Channel Operation

For a single azimuth measurement only one DME interrogation and one angle reply is necessary. The number of pulses that must be transmitted is therefore considerably reduced as compared to TACAN azimuth. A small number of pulses transmitted and complete measurements performed with single pulse groups are the conditions that allow the capacity of one rf channel to be shared in a time multiplex manner. In addition to one pulse pair spacing as it is now for standard DME further pulse codings will be introduced for each interrogation and reply. The number of those codes per frequency channel depends on operational needs; from an equipment point of view it is a matter of complexity for coding and decoding.

If only pulse pair spacing is the coding means, the possible number of extra channels could be as follows (taking into account other standardized spacings and properties of decoding):

X - Mode	
	airborne interrogation/ ground reply
X - 0 (standard)	12/us
X - 1	17/us
X - 2	21/us
X - 3	27/us
3 additional codes	
4 x 126 = 504 total number of channels	

Y - Mode		
	airborne interrogat.	ground reply
Y - 0 (standard)	36/us	30/us
Y - 1	23/us	15/us
Y - 2	33/us	19/us
2 additional codes		
3 x 126 = 378 total number of channels		

This number should be good enough for standard enroute navigation, while for special military application a greater number is desirable. It is achieved by additional codings using phase modulation of the carrier during single pulses. Figure 13 shows one way of this modulation that has been studied in detail so far. The phase deviation during the pulse must be limited in order not to exceed the specified frequency spectrum for one standard DME rf channel. It must also be considered, that there is enough protection of codings against multipath propagation. Calculations have shown, that the proposed scheme of Fig. 13 is sufficiently protected in this respect.

It must be mentioned, that special consideration is necessary for the layout of airborne receiver AGC to live with very different rf levels received from ground stations transmitting with the same rf but with different codes. Some kind of a "search" mode starting with low sensitivity at the receiver input, must be implemented. This is, however, possible in a very elegant manner with a microprocessor as the central element of airborne control and processing.

5.2 Capacity

For the standard DME system the capacity, which is meant to be the number of aircraft that can be served simultaneously, is greater than 100 aircraft. By some means this number can be increased to 300 or even 600 aircraft (reduced interrogation rate, lower reply efficiency in the airborne set, range dependent interrogation rate). So far, no real limitation in practical use of the DME system, was reported. If this would happen in a special area, a second station on a seperate rf channel could be installed. It is important to note, that the random access principle of the DME prevents a sudden degradation of coordinate measurement due to overload.

Adding the described angle measurement system reduces the capacity of a DME ground station, due to the required transmission of angle replies at certain points in time. If an interrogation arrives at such a time or a DME reply should be transmitted at such a time it will be lost. The reduction is in the order of about 30% as calculations have shown. A somewhat more complex situation shows up for a time multiplexing in rf channels. Additional distortions due to pulse overlapping at the airborne receivers of pulses transmitted from different ground stations reduce capacity. It depends, however, very much on the geometric distribution of ground stations operating on the same rf channel and of aircraft using these stations. A very rough result of simulations is, that the total number of aircraft using the same rf channel in a time multiplex mode is slightly more than if there would be no multiplexing of the channel. In other words, the capacity of one rf channel is distributed over as many ground stations as co-channels are existing. The advantage of co-channel operation is therefore not an increased capacity, but the possibility to distribute it over ground stations at different locations, which not in each case need to have maximum capacity.

5.3 Directional Transmitter Antennas

It is a unique feature of the proposed system, that the transmission of all replies can be made over directional antennas into the direction from which the interrogation was received. The directivity will preferably be in the horizontal plan. The basic advantages of such a concept are:

- available antenna gain reduces necessary rf power generation
- multipath effects are reduced
- locating of station by direction finders is more difficult.

For ORTAC-M system (see Fig. 14) eight directional antennas are used, each having a horizontal 3 db-beamwidth of 45^{0}. In order to transmit also the DME reply over one of the directional antennas, a fast processing and determination of azimuth is necessary (time < 50 µs). As the accuracy for this coarse azimuth can be very low (some degrees), a simple analog method of processing the received singal can be chosen.

6. Operational Considerations

6.1 Enroute Navigation

As the DME is the key element in the proposed system, and DME is used today by military and civil aircraft, the future enroute navigation system should be a common civil/military standard. In this publication it is named ORTAC-M, also if civil applications are meant.

The introduction of this system would mean to have the new generation airborne DME or a supplement to the existing DME installed in the aircraft. Such a new DME would have the same mechanical dimensions as a standard DME has today, thus it would be a replacement. The VOR receiver, that delivers azimuth from a VOR ground station could still remain in the a/c. In a mixed ground stations situation, which would be the case in the early phase of introduction, both azimuth equipments are available. For military aircraft in most cases the modification of their airborne TACAN would be necessary, this being also possible without increase of the equipment, so that a pure replacement in this case is possible with automatic selection by the airborne receiver of the azimuth whether it is conventional TACAN or, if available, from an ORTAC-M installed at the ground.

As already mentioned, improved distance measurement is optimally supplemented by an accurate azimuth measurement in the ORTAC-M system. For a distance of 100 km the errors caused from distance and angle measurement are nearly the same (between 100 m and 200 m), so that a circular error area results. Accurate determination of any position in the coverage volume of a ground station is thus possible, a feature essential to the future of effective area navigation. Exact position determination of a point in space is also important for updating of autonomous airborne navigation systems, such as Doppler navigation and inertial systems.

6.2 Military Applications

For military application the combination of autonomous airborne systems and an ORTAC-M ground network could be an optimum solution. The short time needed to determine a position with ORTAC-M is very important in this respect. The ability of co-channel operation offers the possibility of installing an ORTAC-M ground network e.g. for the Federal Republic of Germany using only one TACAN rf channel. This is made possible, as the capacity per station is very low, if it is used preferably for updating purposes.

On the other hand, a smaller area could be covered with radio location information down to very low heights. This is achieved by locating as many ground stations as necessary in this small area, all working on one rf channel, each with enough time multiplexed channels. Again capacity per station is small and, as the stations are relatively near together, azimuth accuracy could be lower, that means low cost stations would solve the cost problem that exists, if many stations in a small area are to be installed. It must be mentioned, that no protection areas between these stations are required, so that a free selection of locations is possible. In a short study for such a case, assuming an area of 80 km x 80 km near Ulm (Germany) it was shown, that for a radio coverage down to 100 m above surface requires 6 stations, a coverage down to 50 m requires 63 stations and a coverage down to 20 m requires 190 stations. From these results it is obvious, that there are certain limitations, so that again the combination with some airborne aid would be more economic.

Finally it should be noted, that a mobile version of ORTAC-M is well suited for tactical applications, again because of co-channel operation, transmission on request only, directional transmission. Those applications may be to control observation missions with conventional aircrafts or helicopters or the guidance of remotely piloted vehicles.

6.3 Growth Potential

One of the outstanding features of the proposed concept for future rho/theta radio systems is its flexibility. After the airborne equipment is installed in all aircrafts, nearly every special ground station necessary for any reason, can be developped and the airborne reception is possible. Those cases could be:

- highest accuracy systems (well below 0.10 degrees) for special applications
- lowest accuracy systems for highest mobility applications
- linear antenna arrays to cover a sector with high accuracy angle information (e.g. landing aid).

Another growth potential inherent in the system is given, because the angle coordinates are measured at the ground. A limited air traffic control for tactical situations is possible. This could be supplemented by data transmission in both directions in the same channel. Growth potential is also provided with respect to processing methods for evaluating the amplitudes and phases measured at each antenna. Up to now more conventional processing was implemented. There are, however, theoretical approaches, that could lead to a reduction in antenna aperture but still maintaining high accuracy. The use of such methods depends on theoretical work to be done and on todays computer speed limitations, which may not exist tomorrow. To introduce such methods, no change in signal format and thus in airborne equipment would be required.

Conclusions

A system concept is proposed for accurate rho/theta radio navigation as a future standard, that would meet all foreseeable needs for civil and military purposes. It is based in the standard DME and therefore uses a frequency band with many advantages. As economic use of available frequency bands is one of the greatest demands, it seems worthwhile to consider the introduction of such a flexible ground derived system.

The authors would like to thank the German civil and military authorities, which supported the studies of the system described.

Bibliography

- ICAO-publications DLS
- ORTAC-M: A successor to TACAN; G. Peuker, Electrical Communication Vol. 50, No. 4, 1975

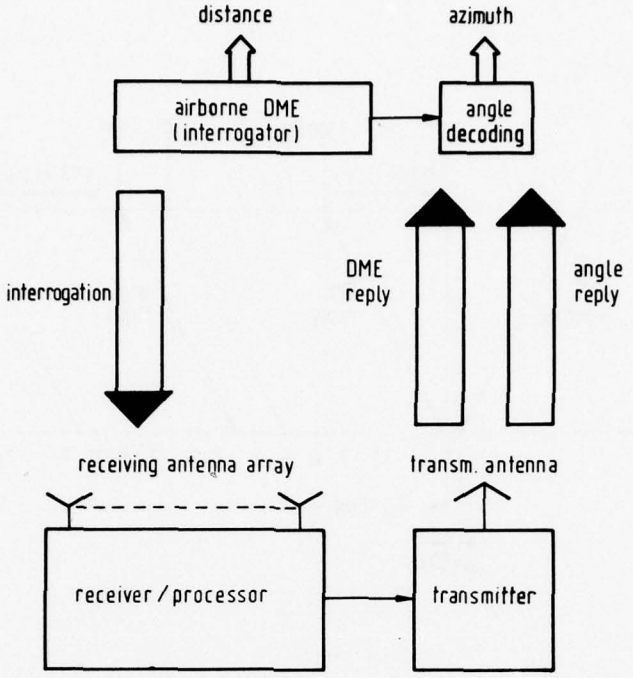

Fig. 1 Basic Concept

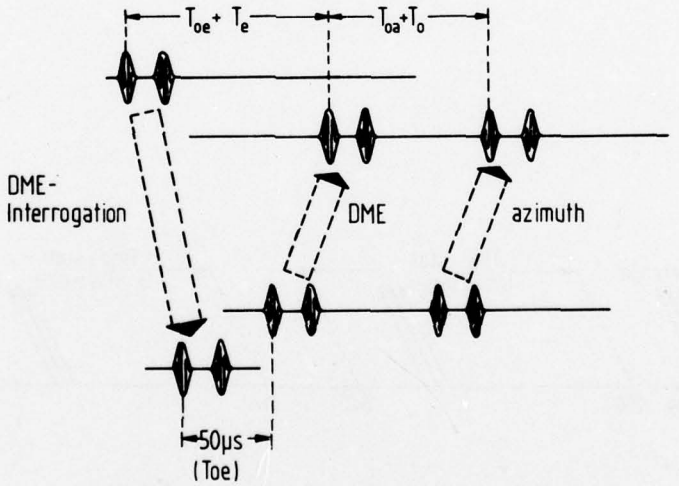

Ta - time equivalent to azimuth
Te - time equivalent to distance
Toa, Toe - bias time interval

Fig. 2 Signal Format

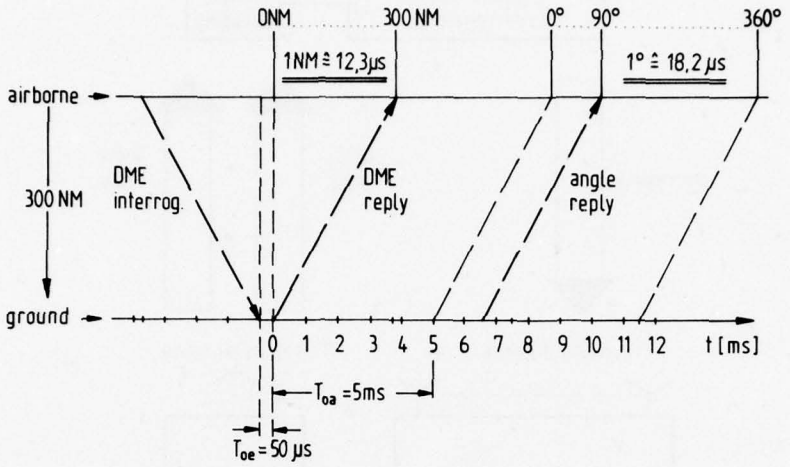

Fig. 3 Time coding for dme and angle replies

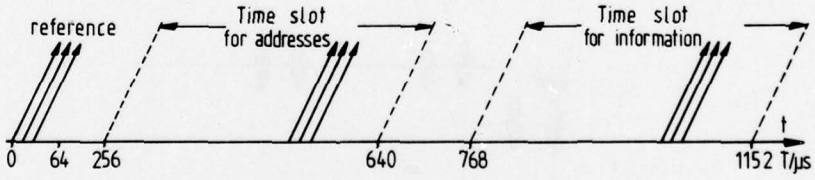

Fig. 4 Schematic Diagram of Auxiliary Data Transmission

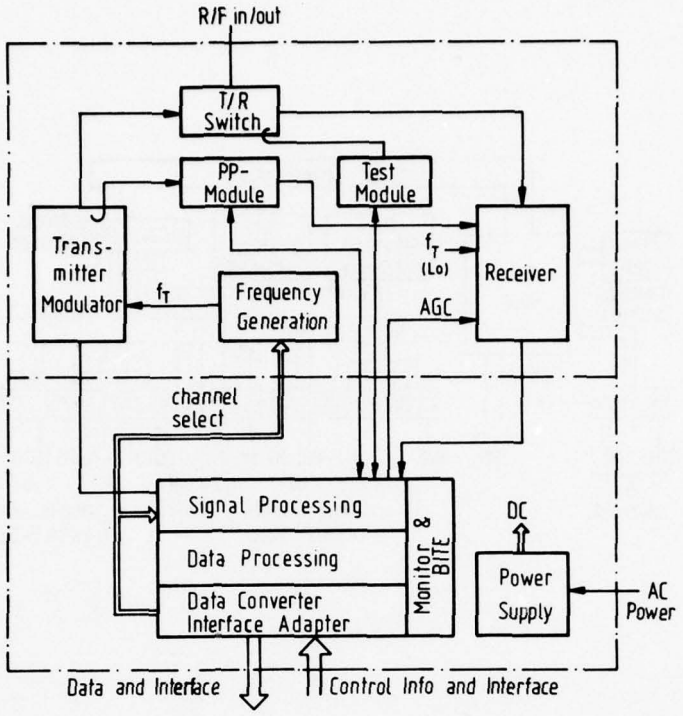

Fig. 5 **Airborne Equipment**

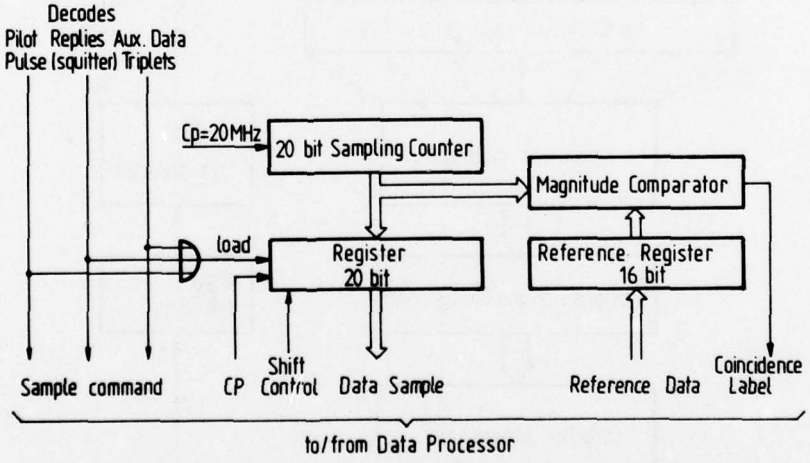

Fig. 6 **Data Sampling**

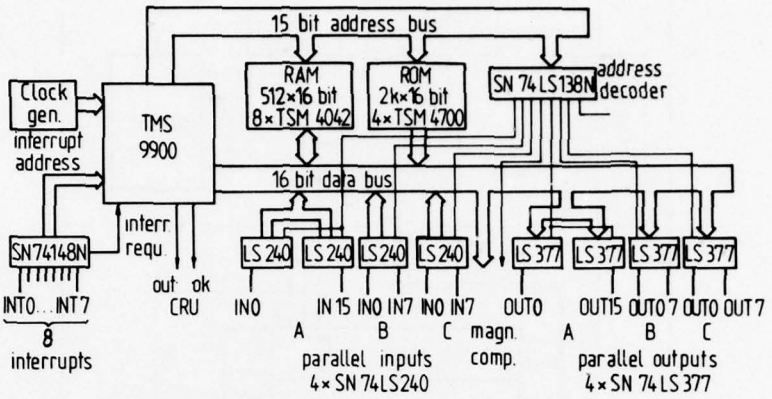

Fig. 7 Computer Block Diagram

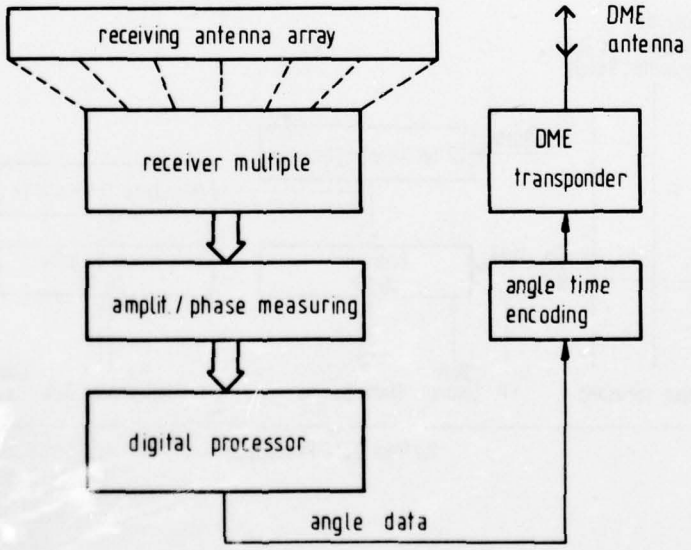

Fig. 8 Basic Block Diagram of Ground Station

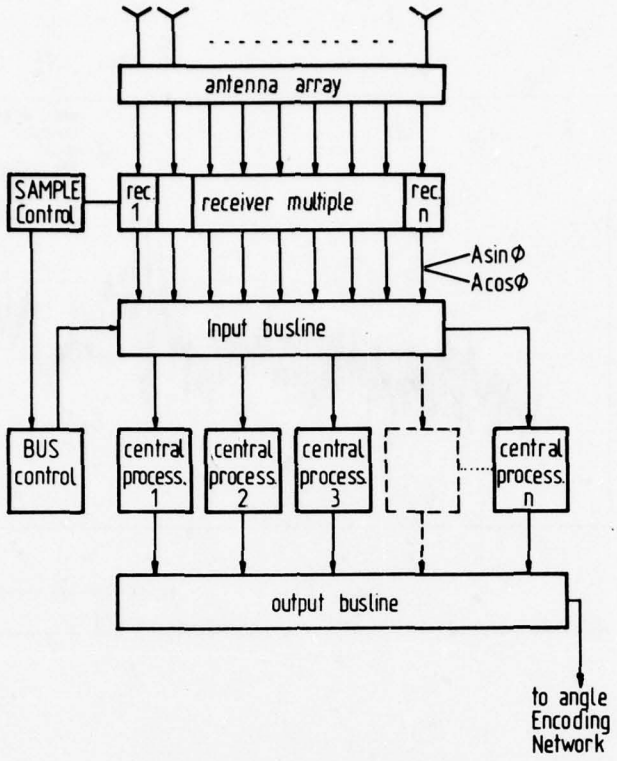

Fig. 9 Block Diagram for angle Determination

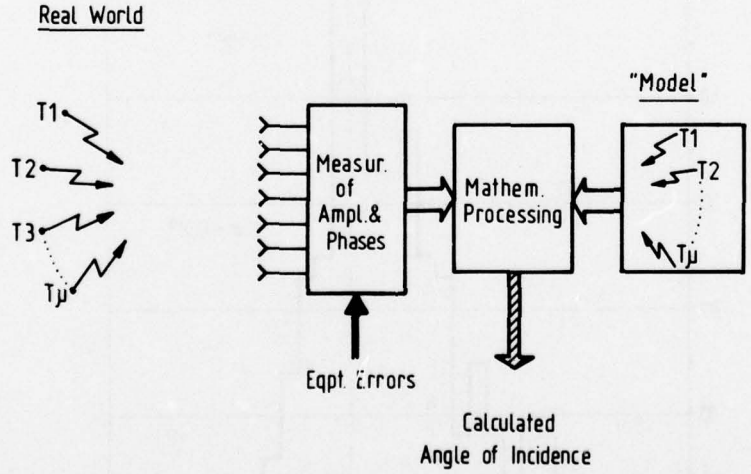

Fig. 10 "Unconventional" Angle Measurement

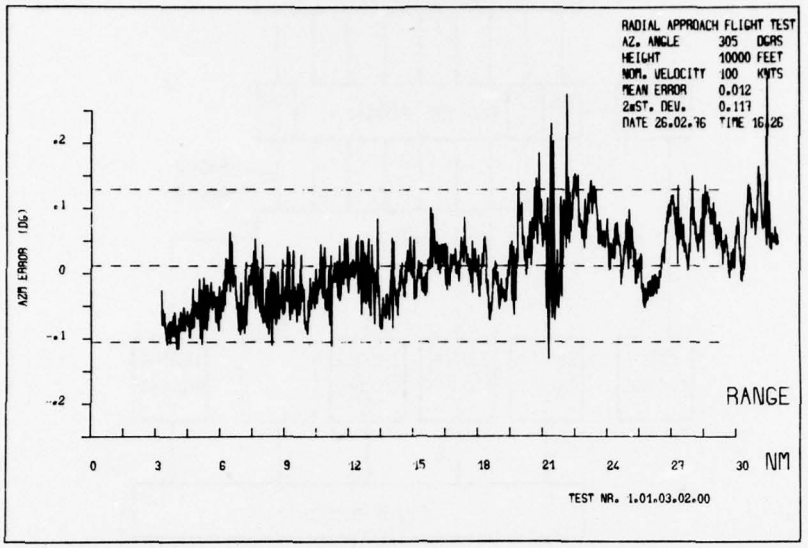

Fig. 11 Radial approach flight test for DLS at Braunschweig
(10 λ circular array, 32 elements)

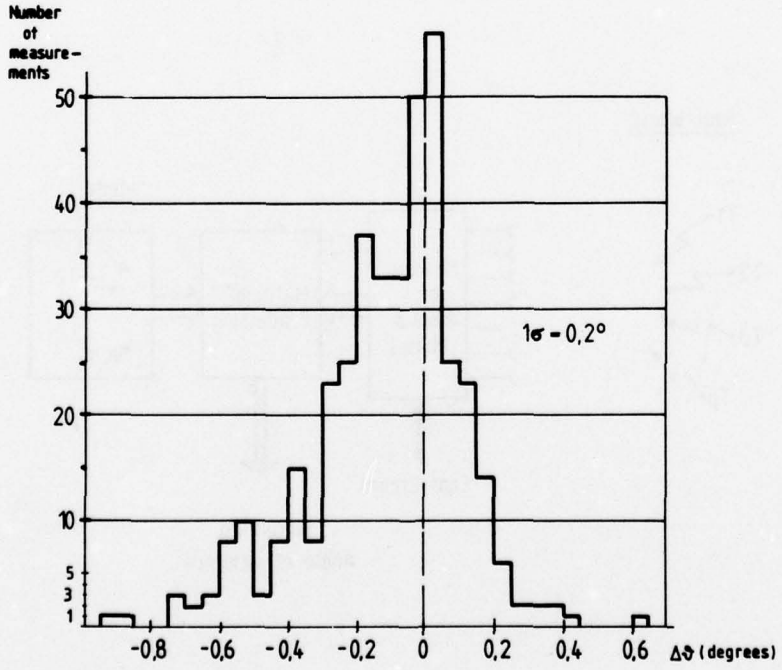

Fig. 12 Summary of all measurements with the ORTAC-System
(5 λ circular array, 39 elements)

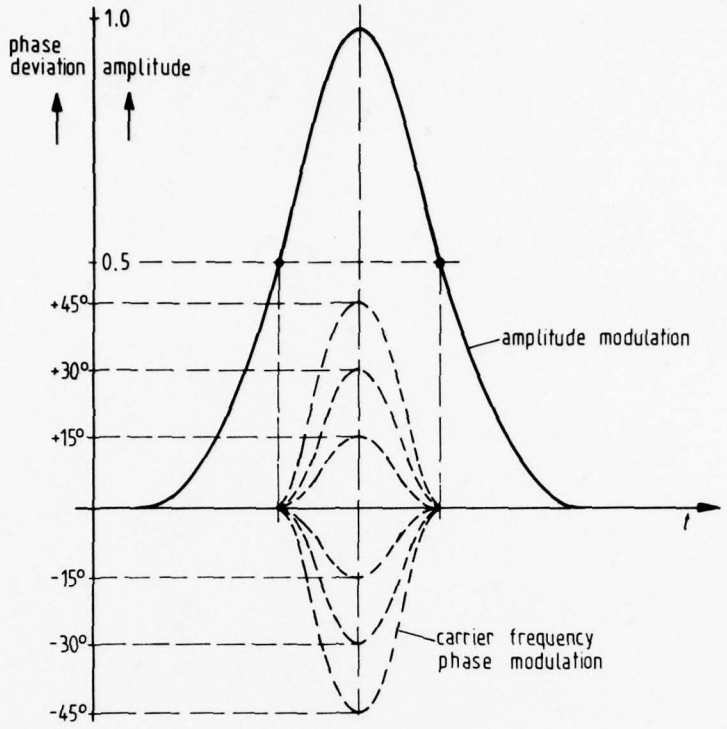

Fig. 13 DME pulse coding by carrier phase modulation

Fig. 14 ORTAC-M Ground Station

One-Way Ranging with TACAN

M. Böhm
Standard Elektrik Lorenz AG (ITT)
Stuttgart, Germany

SUMMARY

TACAN has been a proven standard Nato en route radio navigation system for about 20 years. Developed in the USA by ITT, airborne and ground equipment is now being used also outside Nato. The DME-part of TACAN is fully compatible with the standard ICAO DME.

The distance measuring principle of TACAN-DME is two-way ranging. An aircraft interrogates the desired ground station and receives replies delayed in the ground station by 50 µs. Pulse round trip time minus 50 µs equals twice the travelled distance divided by the propagation velocity of light.

Due to this round-trip principle a ground station normally cannot serve more than about 120 interrogating aircraft. It is therefore desirable to have one-way ranging as the superior alternative. In addition, "silent" aircraft, which do not interrogate, are frequently required.

The technology for one-way ranging has matured considerably over the past five years, and it seems appropriate now to consider extremely stable time sources for being introduced also to the TACAN system.

The paper discusses principles of TACAN, one-way and pseudo one-way ranging, and describes their possible application to TACAN, ground and airborne. Particular emphasis is put on synchronisation techniques.

The paper concludes with an outlook on some new operational applications which would be made possible by one-way ranging with TACAN.

1. Introduction

TACAN is a proven standard Nato radio navigation system which has been successfully in service for more than two decades. More than a thousand ground stations are in operation, and more than 50 000 airborne sets have been built [1]. An additional lifetime of about another two decades is expected, resulting in further demand for modern ground and airborne equipment.

Since the beginning of the current decade various types of new improved airborne equipment have been introduced to different services. And at the beginning of the next decade introduction of a new generation of ground stations is expected, which will provide all the benefits of the solid state technology available today.

Surprisingly enough, however, very few system improvements appear to be planned for the new generation of TACAN equipment though there are several opportunities to do this for both the azimuth and the distance part of the system.

This paper deals with a significant improvement possibility of the DME part of TACAN. This system, as is well known, employs a two-way ranging system requiring aircraft to interrogate a selected ground station which replies to any appropriately coded interrogation it receives provided the number of interrogating aircraft is less than 120. If more than 120 aircraft are interrogating, those beyond this number are denied service which are the most distant ones.

Limited capacity is one constraint of the present TACAN system, the other one being the requirement for airborne transmissions in the DME mode. "Silent" aircraft are much more desirable, and even required in many cases.

The solution to this problem is one-way ranging which has been discussed since the mid fifties [2]. But little has been achieved as far as implementation is concerned. Clock technologies, synchronization techniques and cost problems apparently advised to stay with the conventional but proven two-way ranging. For example, when SC-117 of RTCA discussed this in 1969, they concluded that one-way or pseudo one-way DME was needlessly expensive, and settled for two-way DME.

This paper describes solutions which indicate, however, that earlier constraints appear not to exist any more.

2. Objectives

A one-way ranging capability is to be proposed for TACAN which maintains full compatibility. It is desirable to provide this capability not only in new equipment but also for equipment already in service by using retrofit kits.

Cost increase for airborne equipment by this new feature should not be more than 5 %, while maintaining or improving reliability. Employment of atomic clocks is to be kept at a minimum in favour of crystal clocks.

Employment of one-way ranging must not increase related pilot work load. In contrast, a reduction of it is desirable.

3. Principle and Problems of One-Way Ranging

The principle of one-way ranging is explained in fig. 1. A transmitter at a known position transmits a signal at a point of time t_0 which is also known at the receiver. The transmitted signal travels a time corresponding to the distance between transmitter and receiver and arrives at the receiver at the time t_1. If the difference of time $t_1 - t_0$ is now measured in the receiver, the distance ϱ can be determined by using the speed of light as the appropriate factor [3].

This extremely simple principle has its problems, of course, in providing the standard time generators on ground and in the air, and having synchronized them before each measurement is made.

In order to provide system measurement errors of less than 100 ns - corresponding to a metrical error of 30 m - the synchronization error should be less than 20 ns or 6 m.

Time generator technology has developed rapidly over the past five years, though, and appears to provide the tools to solve the task. Fig. 2 shows a table of properties of various standard time generators. It is surprising to see, how close crystal frequency standards have come to atomic clocks with regard to accuracy [4, 5, 6].

After having the accurate clocks, it is another task to synchronize them. The various space programs of recent years, however, provided the know-how to also solve this task efficiently. Fig. 3 summarizes several synchronization schemes developed for space applications.

Where two-way ranging is used as a means for synchronizing the airborne clock, it depends on the clock stability whether real one-way ranging can be achieved during a mission, or only pseudo one-way ranging is available. Employing an airborne crystal oscillator with an accuracy of say 10^{-5} and remembering the desired synchronization error of less than 20 ns, there would be required a refresh synchronization every 2 ms at the TACAN rf frequencies of 1 GHz, which the TACAN system would not provide with a prf of 30 pulses per second, and which would be anyway no one-way ranging at all. Even with an oscillator accuracy of 10^{-7} a one-way scheme would not be better than two-way ranging because there would be required a new synchronization every 200 ms. Only with a clock accuracy of 10^{-10} a new synchronization would be required after every 200 s or 3.33 minutes. This is still no real one-way ranging, but pseudo one-way ranging as illustrated in fig. 4. It would be helpful, however, to increase ground system capacity in that each interrogator would use a drastically reduced number of interrogation pulses in a given time period, and hence much more than a hundred aircraft could be served. The well acknowledged Alexander Report to the FAA in the 1960s suggested capacity improvement from 100 to 800 aircraft by just reducing the PRF of each interrogator, i.e. a one order of magnitude increase. However, the requirement for improved accuracy of the DME is contradictory in that it asks for an increased prf. In addition, the difference between a 10^{-10} clock and a 10^{-12} - which would provide real one-way ranging during a five-hour mission - is small compared to that between these two types of clocks and the conventional 10^{-5} crystal clock employed in average TACAN airborne equipment. And despite all the progress of precise time standard equipment it will still be a while before such equipment can be used as a synthesizer clock for airborne TACAN equipment economically. Therefore another solution is to be looked for.

4. Ground Synchronization and Equipment

TACAN has already a receive-only mode. Azimuth can be measured by any number of aircraft, without saturation, because in this mode no aircraft transmissions are involved. Fig. 5 summarizes the signal format of TACAN. The basic signal element is the pulse pair sketched in fig. 5a, the transmission of which requires about 400 kHz bandwidth. About 3600 pulse pairs per second are transmitted and amplitude modulated as indicated in fig. 5c by a rotating antenna. The phase of the detected 15/135 Hz pulse envelope compared to the reference pulses - north and auxiliary - comprises azimuth and shall be discussed no further.

The reference pulses are sketched in fig. 5b. They provide a most suitable means for transmitting also the reference time signals for one-way ranging. The refresh frequency - 135 Hz - is high enough to also meet requirements for high accuracy landing DME applications, and low enough to provide unambiguity within any coverage for en route navigation.

These pulses are generated in the ground station with an accuracy which allows for transmitting the reference time points for distance measuring as well as frequency controlling the airborne oscillator, thus eliminating the need for an ultra stable clock there. This will be described later.

At first, however, synchronization of a ground station shall be discussed. Fig. 6 indicates how synchronization can be achieved using a time transmitting station. If the position of this station is known as well as the positions of the TACAN stations to be synchronized, then also the distances d1 to d6 are known and with these distances the time delays by which the time signals arrive later at the TACAN stations. By these travel times the signals of the TACAN station clocks are delayed internally and compared to the received signals. The received time signal and the TACAN station clock signal are made equal in time by setting the delay circuit accordingly.

In order to compensate for drifts of the TACAN clock, another variable delay is provided which is controlled by the output of the comparator circuit for the two time signals.

In fig. 6b the synchronization is shown for the case of a time transmitter but also for the case with no time transmitter. In this application synchronization has to be achieved by two-way ranging between the TACAN stations. This requires line of sight between two neighboured stations, directly or via fixed relay stations. This method is requiring more equipment effort and therefore will not be discussed any further. It would be, however, the same as described for synchronizing the airborne equipment a little later.

The block diagram of a ground station is shown in fig. 7. The basic design looks rather conventional. And it is, except the special clock and the time receiver.

The clock has to be stable enough to control the reference over an unlimited period of time with an error of less than 20 ns, compared to the desired standard time of the TACAN net under consideration. In addition to providing clock stability, synchronization to this standard time has to be made possible. For this purpose the time receiver is used.

The clock can be either of the atomic or crystal type, the difference being essentially in the necessary refresh synchronization intervals. Fig. 7b shows the basic block diagrams of both circuits, which are the same. The oscillator frequency is divided to provide 135 sharp pulses per second. These pulses are delayed by the travel time of the time signal received from a distant time transmitter with known position. At the input of the fixed delay circuit the same timing pulses are available as at the time transmitter. This is done for all TACAN stations of the net under consideration to provide the required standard or reference time of the net.

In addition to synchronizing the timing pulses, the frequency of the oscillator can be stabilized to the accuracy of the oscillator of the time transmitter. Therefore, in principle, this oscillator has to be the only one of utmost accuracy and stability, for instance a cesium standard, uninterrupted time transmitter service provided. The oscillators at the TACAN stations can be crystal oscillators, of top quality though.

Fig. 7c indicates how a frequency control signal could be generated. Instead of any phase-locked loop technique - which is also possible - a conventional gating method and a special fast clock of about 135 MHz prf are advised. Frequency adjustment or compensation of oscillator drift are achieved by means of two counters and a microprocessor. Accuracy of the fast clock does not matter due to this nulling principle.

5. Antenna Control

Antenna control is not very critical in both cases, that of the mechanical rotated antenna and that of the electronically rotated antenna - which at present still plays a minor or neglectable role for TACAN. The required accuracy is comparatively low, two to three orders of magnitude less than for one-way ranging. Fig. 8a shows how control of a mechanically rotated antenna is achieved. The signal from the antenna north pick-up device is no more used to trigger the reference pulses, but only to generate the drive control signal by comparison with the station clock. For the airborne azimuth circuits, however, this does not involve any perceivable difference nor any perceivable accuracy degradation.

For an electronically rotated antenna control is very simple, as is shown in fig. 8b. The reference pulses from the station clock are used to trigger the antenna control circuit, which immediately responds because of no antenna inertia involved.

6. Airborne Synchronization and Equipment

Synchronization of airborne equipment can be achieved with highest possible accuracy only before a mission when the reference distance is exactly known. Synchronization during a mission leads to less accuracy due to the limitations of two-way ranging.

A straightforward method of synchronization is sketched in fig. 9. An aircraft due for a mission is rolled to specific parking areas or to a marked area on the runway. These areas have known distances to a nearby TACAN station. All the pilot has to do at these areas to achieve synchronization is to select this distance at his control box and push a synchronization button. (Instead of selecting a distance, pushing a code button might be the more comfortable approach and the one less exposed to pilot errors.) Synchronization

is then achieved automatically within seconds. A synchronization light is indicating to the pilot that synchronization is achieved. It is maintained as long as TACAN stations are received.

After interruption of TACAN service during a mission, new synchronization can be achieved only by applying two-way ranging. The workload for the pilot in this case is, however, as low as for synchronization before a mission. He only has to switch his TACAN set to the T/R mode, and then to push the synchronization button. Within seconds the synchronization light is coming again, and the pilot can switch back to the receive-only mode, the aircraft becoming "silent" again. The related signals are sketched in fig. 9b.

In fig. 10 the block diagram of the airborne TACAN equipment is shown together with some circuit details, which are essentially the same as for the ground station. The block diagram of the airborne equipment does not disclose a significant difference to a conventional TACAN set. The difference is in the clock, as fig. 10b and 10c indicate. Of course, this TACAN set allows conventional two-way ranging as well as one-way ranging.

The velocity of an aircraft is the basic problem with using the reference pulses transmitted by the ground station also as a reference to control the airborne clock. At high subsonic speed, the change of a plane's position between the first and second pulse of a 1/135 s gate represents a distortion of the gate time by around ± 7 ns, dependant on the flight direction. This distortion results in a periodic change of the number of clock pulses falling into each gate. The frequency of this change is proportional to the speed of the aircraft. Additionally, any oscillator drift may lead to a variation of the number of clock pulses falling into each gate. However, the frequency of this drift is small and can be determined by the comparator shown in fig. 10c. Therefore, separating the distortion due to aircraft speed and the distortion due to oscillator drift can easily be achieved by first determining the change frequency, then deriving from this the number of clock pulses which make the balance between the number of clock pulses within a chosen number of gates, e.g. 135, in the undistorted case, and the number of total clock pulses within this chosen number of gates in the case of distortion by aircraft movement only. Finally the number of clock pulses representing the oscillator drift can be derived by getting the balance between the total number of clock pulses within the 100 gates and the number of clock pulses in the undistorted case increased by the number of clock pulses contributed by aircraft movement only. This compensation method may advise not to control the clock, but to correct erreaneous divider results using a microprocessor circuit with appropriate peripheral circuits.

The clock therefore comprises both a synchronization and reference correction capability. Instead of introducing an expensive, voluminous atomic frequency standard, a conventional crystal oscillator is recommended, as is already used in current airborne equipment. Fig. 10c shows an example of how frequency control might be realized without VCO techniques. A special 135 MHz clock feeds two counters which are gated by signals from the decoder and the airborne crystal clock respectively. Thus a comparison of the length of the two gates, i.e. the oscillator frequencies, is possible with a resolution of about 7 ns, and the change frequency can be determined as well as the crystal oscillator drift. Controlled by the microprocessor the divider is corrected and the crystal oscillator stabilized.

Synchronization is achieved as shown in fig. 10 b. If the synchronization button is pushed, a digital delay is switched into the control loop. The delay corresponds to the distance between ground station and aircraft and is selected either via the control box or automatically in the two-way ranging mode during flight.

7. Operational Considerations

One-way ranging with TACAN opens some new operational advantages for en route radio navigation. Fig. 11 gives a summary.

The most obvious application is Rho-Theta navigation (fig. 11a), with Rho derived by one-way ranging. The aircraft has no need for transmission, and no saturation of a ground station is possible. A certain disadvantage of this kind of navigation is the difference in accuracies of distance and azimuth measurement. DME errors are much smaller than metrical azimuth errors for distances of more than 10 km.

If a second ground station transmitting on another frequency can be received, trilateration would be the more accurate approach. However, the need for this second station may sometimes prevent this application from being usable. On the other hand, in this application no azimuth parts of the ground station would be required, simple DME stations would suffice.

If three stations can be received at any time, the well-known hyperbolic navigation would be possible. For this application no accurate airborne clock would be needed, and a simplified airborne receiver for special missions and applications might be used. Again, only DME ground stations would be needed, and no azimuth signals would be involved. A disadvantage of the approach sketched in fig. 11c is, however, the need for hopping continuously between various frequency channels.

Therefore the scheme sketched in fig. 11d is preferable. All ground stations would operate on the same frequency channel. The reference pulses of the various ground stations would be transmitted not at the same time but delayed against each other to

an extent which guarantees separate reception of these pulses in any aircraft at any distance within the coverage.

Overall system accuracy is determined mainly - as is the case with conventional TACAN - by equipment and multipath errors. The best systems today like SETAC provide operational system errors down to 20 to 30 m. A one-way DME as described would provide errors of no more than twice that figures with airborne equipment like MITAC, while the much larger errors of conventional TACAN airborne equipment would not be perceivably increased by the one-way DME bias and noise errors.

8. Conclusions

One-way ranging with TACAN offers "silent" radio navigation to aircraft which at present have continuously to transmit signals in order to measure their radio position with TACAN.

In contrast to frequently heard opinions one-way ranging can be achieved without an atomic clock in a TACAN-airborne equipment. Synchronization and frequency control can be provided to stabilize a conventional crystal oscillator sufficiently with the necessary accuracy.

Synchronization and frequency control in the ground stations can also be achieved without top performance atomic clocks there, if time transmitter signals are used appropriately.

Thus a very economic way to improve performance of TACAN and also SETAC [7] becomes available and can be used without penetrating compatibility of new and existing equipment to any extent.

One-way DME may find advantageous applications - besides extending conventional TACAN service - for RPV and drone missions over the battlefield, where radio silence is a requirement. These applications appear particularly attractive, as cost of the one-way ranging circuits are supposed to add to the overall airborne TACAN equipment cost not more than 5 %.

References

[1] S.H. Dodington
Neue Entwicklungen des Navigationssystems TACAN
Elektrisches Nachrichtenwesen, Band 44, Nr. 4, 1969

[2] W. Stanner
TACAN-AT, ein Vorschlag zur Erweiterung der Einsatzmöglichkeiten von TACAN-Anlagen
Interne SEL-Notiz, Oktober 1970

[3] M. Böhm
Distance Measuring Methods
AGARD-AG-209, Vol. II, July 1975, pp 437-446

[4] Durchführbarkeitsstudie Zeitsynchronisation und Einwegentfernungsmessung
SEL Stuttgart, CNS/EWN, März 1976
BMFT-Auftrag 01 QV 165 A - V22 - WRT 1075-2.19

[5] P. Kartaschoff; J.A. Barnes
Standard Time and Frequency Generation
Proc. of the IEEE, Vol. 60, No. 5, May 1972, pp 493-501

[6] D.W. Hanson; W.F. Hamilton
One-Way Time Synchronisation via Geostationary Satellites at UHF
IEEE Trans. on Instr. and Meas., August 1971, pp 147-153

[7] K.D. Eckert
SETAC - eine Anflug- und Landehilfe
Elektrisches Nachrichtenwesen, Band 50, Nr. 4, 1975

[8] L.E. Gatterer; P.W. Bottone, A.H. Morgan
Worldwide Clock Synchronisation Using a Synchronous Satellite
IEEE Trans. on Instr. and Meas., Vol. IM-17, No. 4,
Dec. 1968, pp 372-378

[9] D.W. Hanson; W.F. Hamilton
Clock Synchronisation from Satellite Tracking
IEEE Trans. on Aerospace and Electronic System, Vol. AES-7,
No. 5, September 1975, pp 895-899

[10] J. Ramasastry; B. Rosenbaum; R.D. Micheliné; G.K. Kuegler
Clock Synchronisation Experiments Performed via the ATS-1 and ATS-3 Satellites
IEEE Vol. IM, March 1973, pp 9-12

[11] D. Rother
Ein Spacelab-Experiment zur Zeitsynchronisation und Einweg-Entfernungsmessung
NTZ 29 (1976), Heft 9, Seite 673-677

[12] Dan Boyle
Omega-Navigation: Kommt der große Durchbruch?
Interavia 3/1977

[13] D. Holmes
Navstar Technology
Countermeasures, Dec. 1976, pp 27-30 and 54-56

[14] E.D. Micozzi
TACAN yesterday, today, and tomorrow
Countermeasures, Dec./Jan. 1975/1976

[15] G. Peuker
ORTAC-M, ein neues TACAN-System
Elektrisches Nachrichtenwesen, Band 50, Nr. 4, 1975

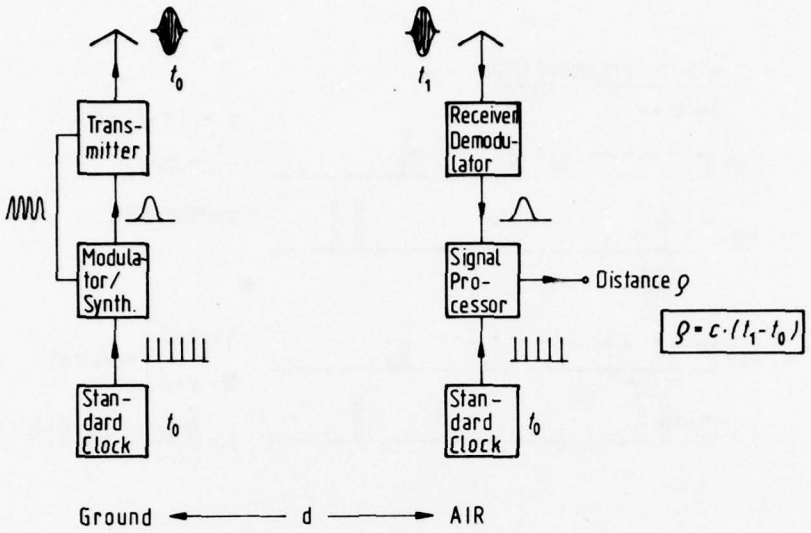

Fig. 1 Principle of One-Way Ranging

	CRYSTAL	RUBIDIUM	CESIUM	H-MASER
TYPICAL ACCURACY	10^{-10}	10^{-12}	$5 \cdot 10^{-13}$	$2 \cdot 10^{-12}$
DRIFT				
f(temperature)	$10^{-11}/^{o}C$	$2 \cdot 10^{-12}/^{o}C$	$10^{-13}/^{o}C$	$10^{-13}/^{o}C$
f(voltage)	$5 \cdot 10^{-11}/10$ %	$2 \cdot 10^{-12}/10$ %	$2 \cdot 10^{-12}/10$ %	-
f(acceleration)	$10^{-9}/g$	$\approx 0{,}4 \cdot 10^{-11}/g$	$10^{-13}/g$	$10^{-12}/g$
WEIGHT	< 1 kg	< 5 kg	< 50 kg	-
VOLUME	< 1 ℓ	< 5 ℓ	< 50 ℓ	-
POWER	< 5 W	< 20 W	< 50 W	-

Fig. 2 Typical Crystal and Atomic Clock Properties

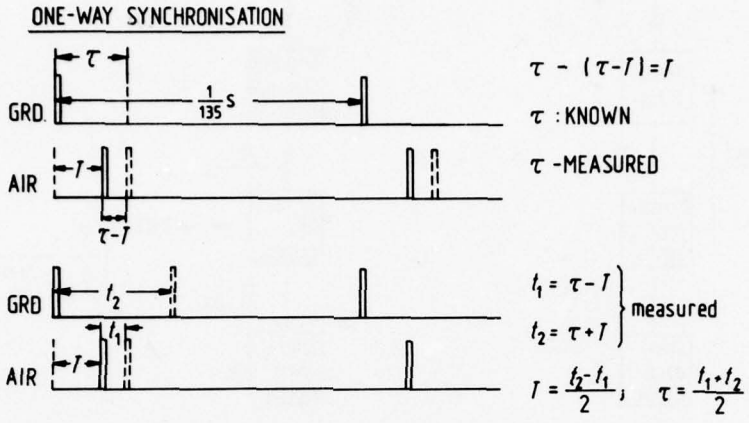

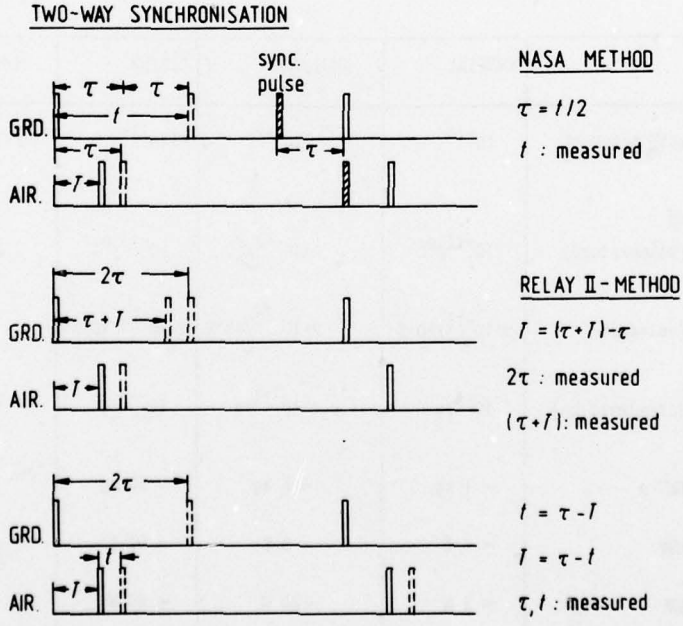

Fig. 3 Different Synchronisation Methods

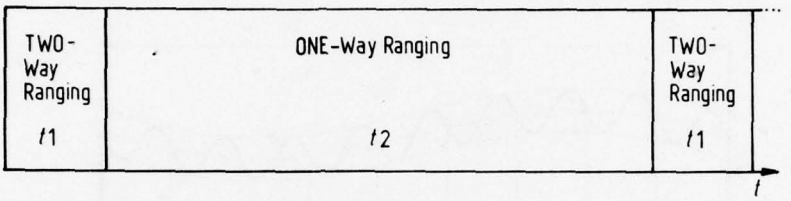

$$\frac{t1}{t2} > 0{,}01$$

Note: Main purpose is
to increase station
capacity by reducing its
oading by each single interogator

Fig. 4 Pseudo-One-Way Ranging

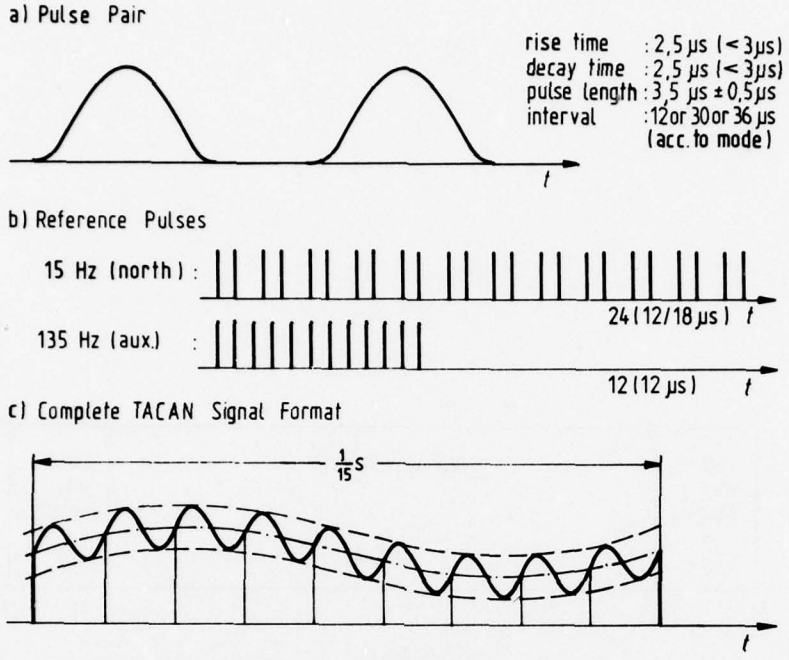

Fig. 5 TACAN Signal Format

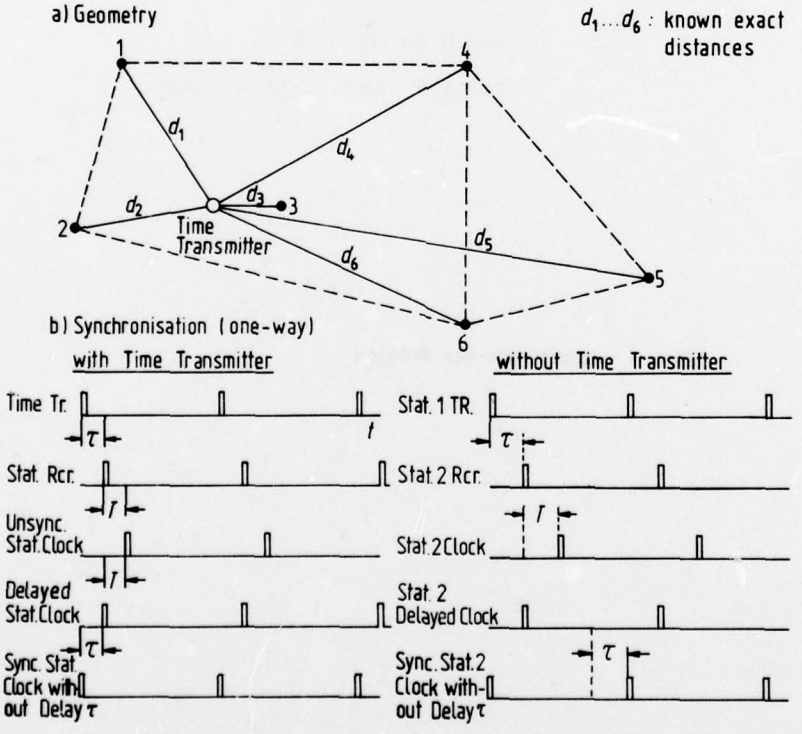

Fig. 6 Ground Stations Synchronisation

a) Overall Block Diagram (Example)

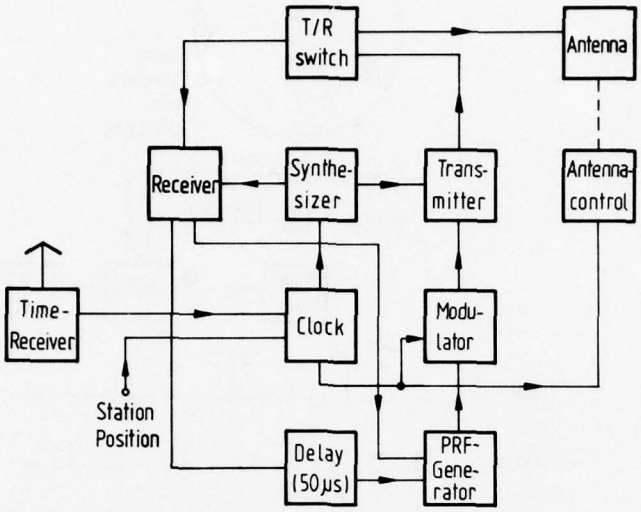

b) Clock Alternatives

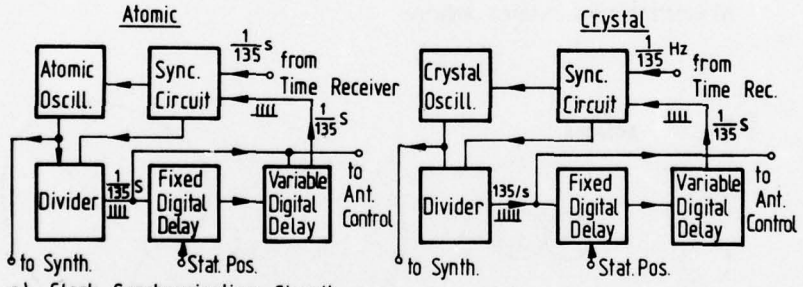

c) Clock Synchronisation Circuit

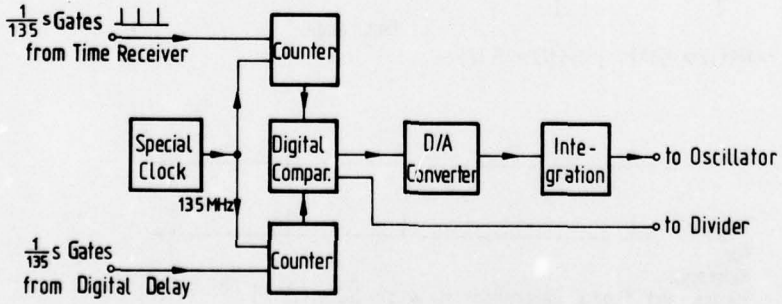

Fig. 7 Block Diagram of Ground Equipment

a) Mechanically rotated Antenna

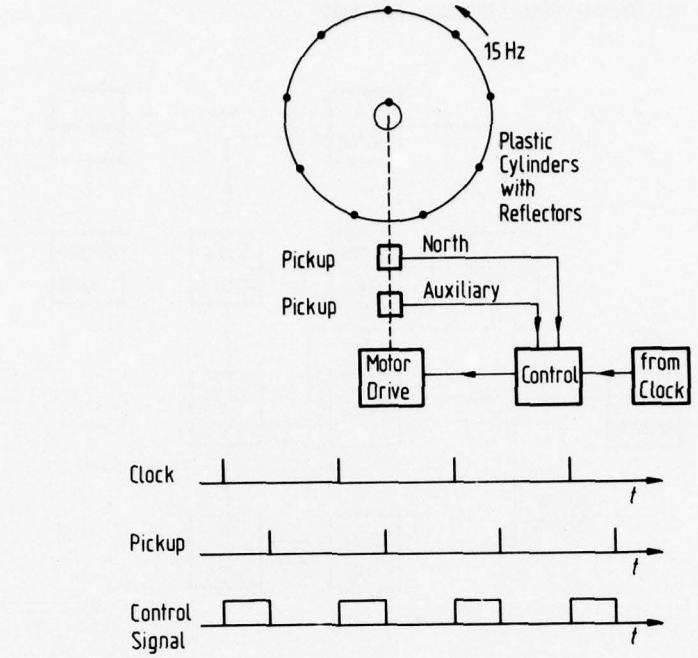

b) Electronically rotated Antenna

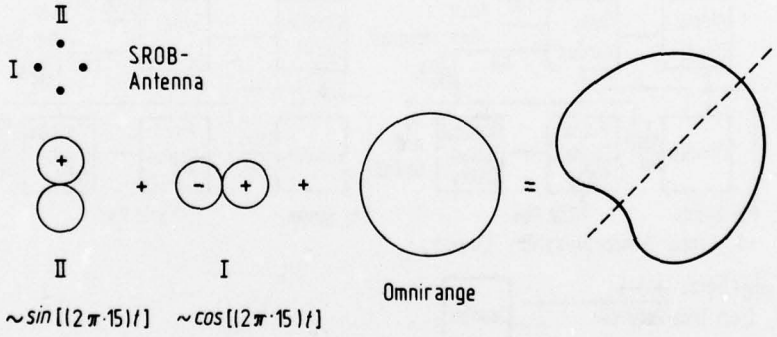

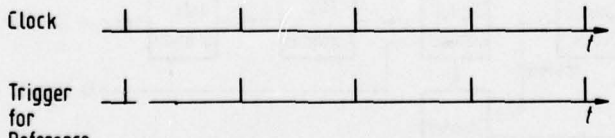

Pulses and Digital Generation of $A \cdot \sin[(2\pi \cdot 15)t]$

Fig. 8 Antenna Control

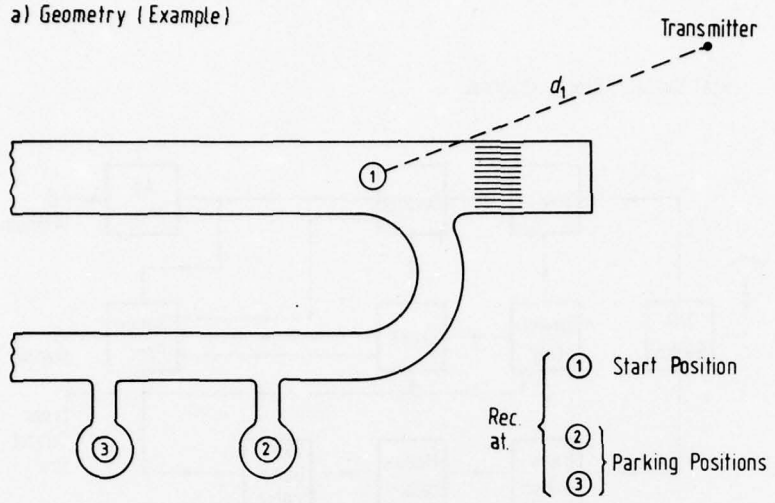

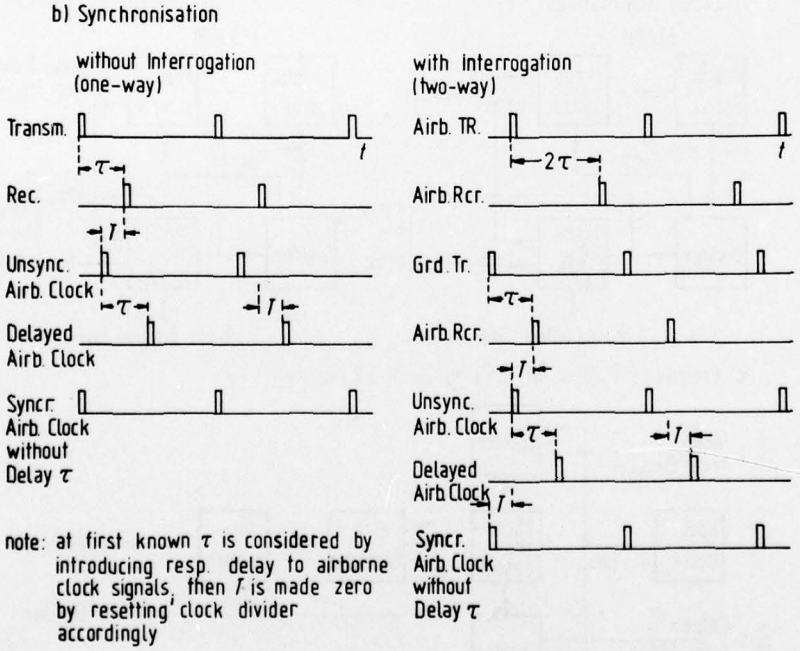

Fig. 9 Principles of Airborne Synchronisation

a) Overall Block Diagram

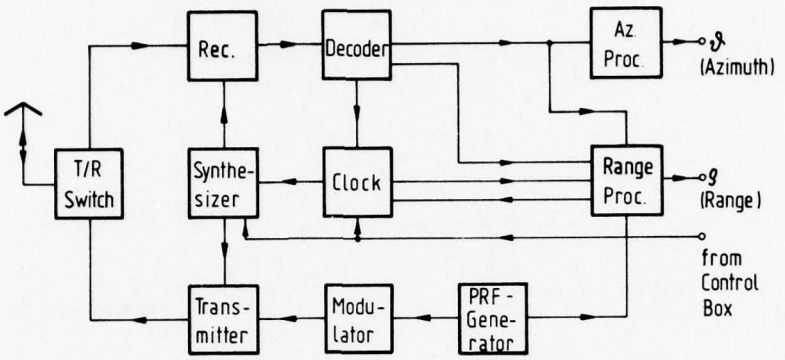

b) Clock Alternatives

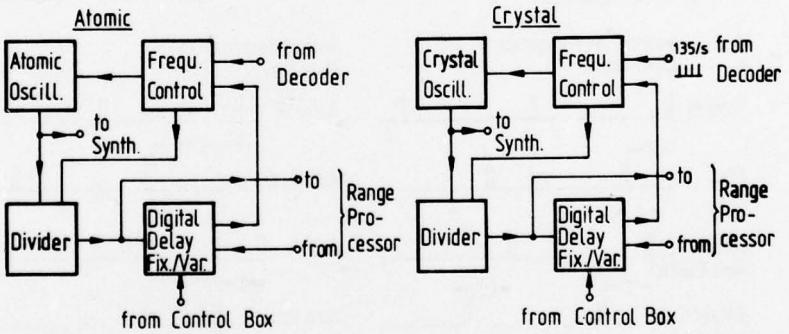

c) Frequency Control of Crystal Clock (Example)

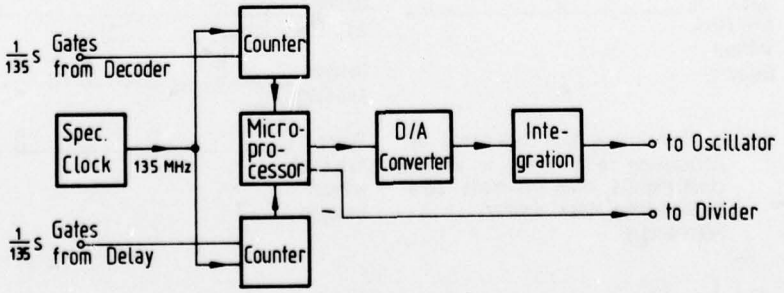

Fig. 10 Block Diagram of Airborne Eyipment
(Two-Way and One-Way range capability)

a) RHO (ONE-WAY) - THETA

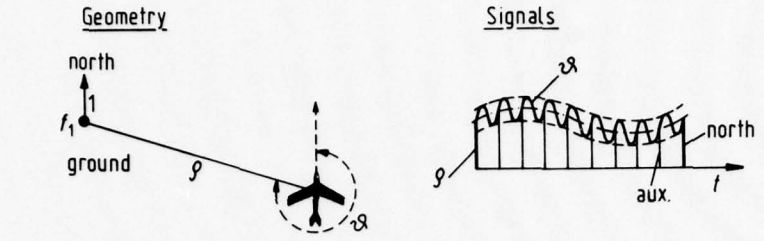

b) RHO-RHO

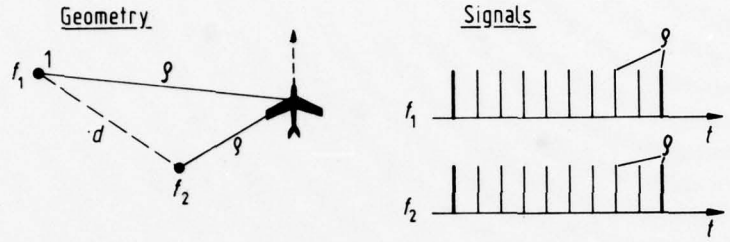

c) Hyperbolic

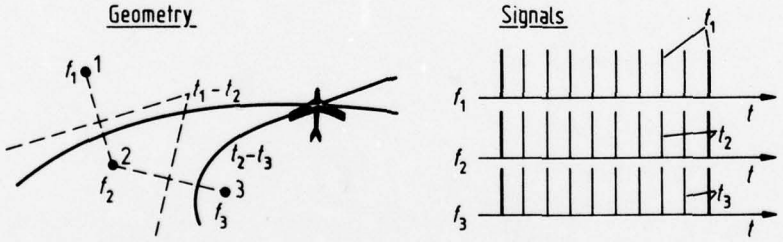

d) RHO-RHO (CO-CHANNEL)

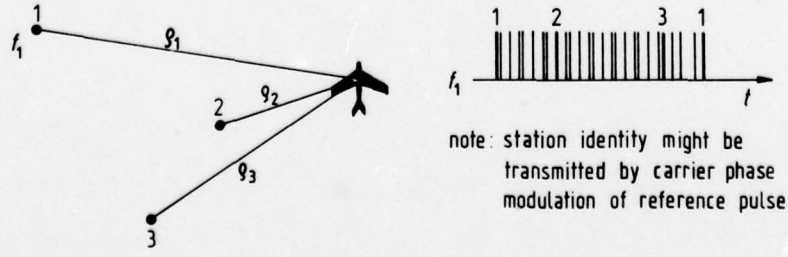

note: station identity might be transmitted by carrier phase modulation of reference pulse

Fig. 11 Operational Capabilities of System (All Modes with Passive Airborne Equipment)

AN ECM-RESISTANT COMMUNICATION AND RANGING SYSTEM FOR REMOTELY PILOTED VEHICLES

by
Hermann Sepp
Associate of Central Telecomunication Laboratories
Siemens Aktiengesellschaft
8 München 70, Hofmannstr. 51

Summary

Accurate ECM-resistant navigation and two-way ECM-resistant data transmission are significant requirements in RPV systems. Both problems can be solved simultaneously by the SIECON system which achieves its high ECM-resistance with the aid of pseudo noise phase shift keying modulation (PN PSK). To assure high resistance against all kinds of jammers including sophisticated types, a number of different PN-codes with high clock frequency and various acquisition modes can be chosen. A combined up- and down-link configuration optimizes system performance and minimizes cost and weight. Moreover the combination of the two links allows accurate jam-resistant range measurement if the RPV receiver and RPV transmitter use the same timebase for their PN-codes. The requirements for low primary input power, long range and high ECM-resistance necessitate the use of high gain antennas associated with an antenna tracking system. SIECON employs spread spectrum conical scan.

1. Introduction

This paper describes a jam-resistant communication and ranging system designated SIECON (Siemens ECM-Resistant Communication and Navigation). SIECON can be used in any application where anti-jam two-way data links together with jam-resistant, accurate ranging are required. One important application for SIECON is therefore in RPV's (Remotely Piloted Vehicles). Normally one data link is necessary to transmit command and control information from a control station to the RPV, but often an additional link is required to relay real-time RPV data and video signals. Accurate positioning is important in order to navigate the RPV. During all RPV-missions hostile electronic countermeasures (ECM) must be anticipated and therefore the data links and the navigation system must be sufficiently ECM-resistant.

2. The Problem

Fig. 1 illustrates a typical case of RPV operation. The double lines represent two-way data links for simultaneous distance measurement and data transmission. In the example shown positioning of the RPV is based on the well-known trilateration, however SIECON can also work in the rho-theta mode. At higher radio frequencies airborne control stations are needed to meet line-of-sight requirements.

It is necessary to know the requirements on the electronic equipment and the expected threat environment in order to permit selection of suitable concepts for data transmission and ranging. Table 1 shows the most important RPV requirements.

These requirements drastically reduce the number of suitable methods. Today and even more in the near future several jamming strategies will form an essential part of electronic warefare. Therefore sophisticated jammers such as repeaters and jammers designed specifically against the considered system must be taken into account.

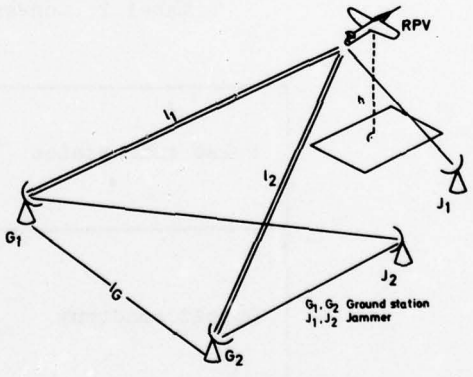

Fig. 1: RPV Operation.

High ECM-resistance
Two-way data transmission
Jam-resistant, accurate ranging
Long range
High transmission quality, small error rate
Low primary power consumption
High relative velocity between the RPV and the control stations
Suitable for high and low altitude operation
Simultaneous operation of several RPV's
Difficult to detect by the enemy
Safety from interception
Small volume, light weight, low cost

Table 1: Important RPV requirements.

3. Principles to Achieve High ECM-Resistance

In addition to tactical countermeasures such as short transmission time, rare use and versatility of equipment a number of technical countermeasures are known to achieve ECM-resistance. Table 2 enumerates some of the more conventional techniques. Table 3 shows the two most important modern ECCM techniques (ECCM Electronic Counter Counter-measures).

Cable connection
High transmitter power
Various operating frequencies
Directional antennas, Adaptive antennas
Redundancy

Tabel 2: Conventional ECCM techniques.

Pulse compression	chirping
	phase shift keying, PSK
Spread spectrum	pseudo noise phase shift keying, PN PSK
	frequency hopping, FH

Table 3: Modern ECCM techniques.

The use of cable connection and high transmitter power usually create problems for RPV operation. The other techniques listed in this table are not adequate on a stand-alone basis but they work very well in combination with one of the modern ECCM techniques. This "hybrid" solutions in the form of spread spectrum modulation combined with conventional measures, or the combination of two types of spread spectrum modulation offer certain advantages over single methods. See [1, 2, 3] for more detailed information.

4. Principle of PN PSK with SIECON

For every spread spectrum system in addition to a conventional modulator a spread spectrum modulator is necessary to distribute the desired signal over a wide frequency range. The selection of the conventional modulator depends on the kind of data to be transmitted. Fig. 2 shows the analog and digital version of the transmitter with simplified power density spectra.

The message from the analog signal source having a bandwidth B_b is applied to the frequency modulator. The modulation index ß is chosen as described in /2/. The signal at the output of the message modulator with the bandwidth B_1 is fed to the spread spectrum modulator. In our case it is a 0^o to 180^o bi-phase modulator which shifts the phase of the signal in rhythm with a binary pseudo random sequence (PRS) of high clock frequency. A phase shifted FM-signal is shown in fig. 3. The PN modulation causes an extreme spreading of the bandwidth to

$$B_2 \approx 2 \cdot f_c,\ f_c \gg B_b.$$

Fig. 4 illustrates the spectrum of a pseudo random sequence and a section of this pseudo random sequence in the time domaine. The spectrum is a line spectrum with the envelope

$$S_{PRS}(f) \sim \left[\frac{\sin(\pi f/f_c)}{\pi f/f_c}\right]^2$$

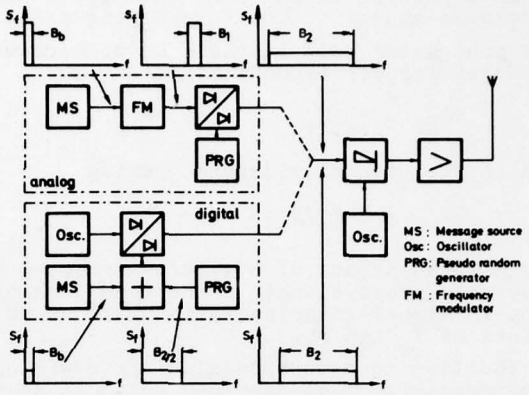

Fig. 2: Block diagram of the transmitter (digital and analog version).

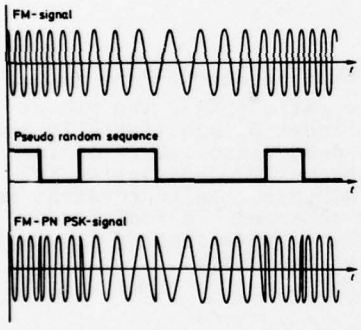

Fig. 3: Phase shifted FM-signal.

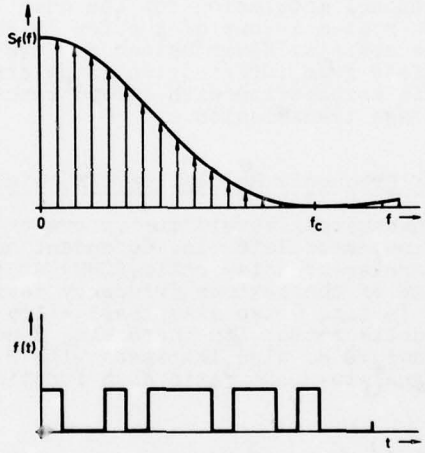

Fig.4: Pseudo random sequence.

The spread spectrum signal at the output of the bi-phase modulator is converted into the RF-band in an upconverter, amplified in a traveling-wave tube (TWT) and radiated.

The message from a binary digital source can be added modulo-2 to the pseudo random sequence as shown in fig. 2. The pseudo random sequence "falsified by the message" is then fed to the spread spectrum modulator similar to the analog system.

In addition to the desired signal, spurious signals will also be present at the front end of the receiver. Fig. 5 shows a block diagramm of the receiver. As an example in the power density spectra a strong CW-Jammer in the centre of the band of the desired signal is introduced. The band spread can be cancelled by reshifting the phase of the input signal by means of the pseudo random sequence of the receiver, provided that the synchronisation circuit in the receiver is able to control the pseudo random generator. As a consequence a pseudo random sequence is produced which is identical and synchronous with the pseudo random sequence in the desired input signal. Thereafter the signal only contains the modulation produced by the message because

$$m(t) \cdot m(t) = 1,\ m(t) = PRS,$$

and the signal bandwidth is reduced to its previous value.

While the phase shifts of the desired signal in the receiver are cancelled, the interference signals are phase shifted with respect to the pseudo random sequence of the receiver and therefore the jammer and all the other spurious signals are spread similar to the spreading of the desired signal in the transmitter. A bandpassfilter following the phase shifter in the receiver with a bandwidth equal to the bandwidth of the compressed desired signal can eliminate a considerable amount of the interfering power.

The processing gain in the case of narrow band jamming corresponds to [2]

$$PG_{NB} = f_c/B_1$$

and in the case of wideband jamming

$$PG_{WB} = 2\ f_c/B_1.$$

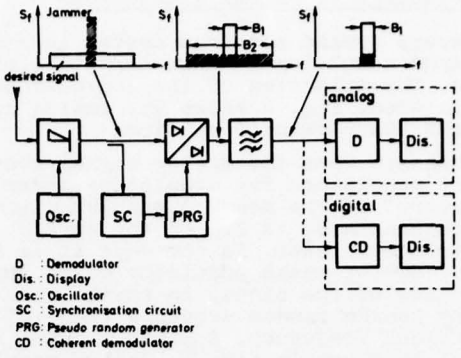

Fig. 5: Block diagram of the receiver (digital and analog version).

The ECM-resistance of a system increases proportional to the clock frequency f_c and inversely proportional to the bandwidth of the message to be transmitted. An improvement in signal-to-noise ratio up to 50 dB can be achieved today, depending on the values of f_c and B_1.

In addition to band spreading the advantage of PN PSK is to screen the message from eavesdroppers. The enemy can only decode the message if he knows the code. Especially long pseudo random sequences have a large multiplicity of different codes and therefore it is extremely difficult and takes considerable time to decode a message. SIECON works with a number of different codes which can be controlled by external signals.

Different codes additionally permit code mutliplexing for simultaneous operation of several RPV's.

The conventional modulation for the down link with SIECON is FM. It can be proved that a FM PN PSK system is one of the few PN PSK systems from which it is fairly easy to extract the message. Nevertheless two reasons have influenced our decision to select FM: firstly safety from interception is no stringent requirement for the down link and secondly, FM in combination with spread spectrum is a highly efficient ECCM technique for analog message transmission.

Comparison: Frequency Modulation (FM) with Spread Spectrum Modulation (SSM)

FM is a conventional method to improve the signal-to-noise ratio (SNR). The SNR at the output of the demodulator is, dependent on the modulation index ß, substantially larger than the carrier-to-noise ratio (CNR) at the input of the demodulator. ß is defined as the quotient of the maximum frequency deviation f_Δ to the maximum modulation frequency f_m. In fig. 6 two examples ß = 1.5 and ß = 50 are stressed. An improvement in signal-to-noise ratio with increasing ß can be distinctly observed. In fact the required bandwidth B_1 also increases with ß. It is relatively easy to specify the improvement in signal-to-noise ratio as a function of the required bandwidth.

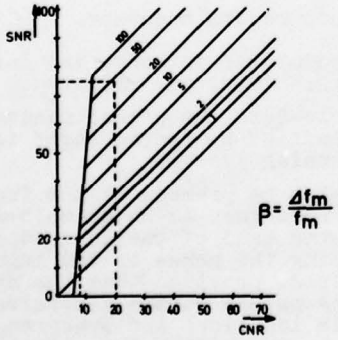

Fig. 6: Signal-to-noise characteristics of a conventional FM system

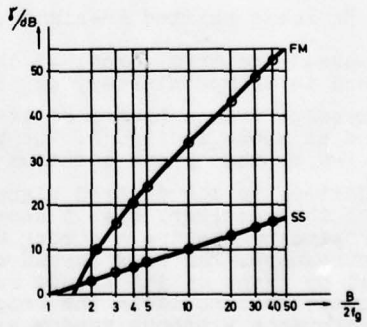

Fig. 7: Comparison of the attainable SNR improvement of FM against SSM.

Fig. 7 shows the comparison of the attainable SNR improvement of FM against SSM, if the same bandwidth is considered. At a glance SSM compares poorly with FM and the question arises: Why spread spectrum modulation, if frequency modulation is much better?

A more detailed consideration of fig. 6 shows that with FM the improvement in SNR only becomes effective above a minimum CNR_{min}.

CNR_{min} is known as the FM-threshold. Because of this effect two important requirements on an ECM-resistant system can be deduced:

- large improvement in SNR
- low minimum CNR_{min}:

It is worth noting that every process which achieves ECM-resistance by "waste of bandwidth" shows more or less a pronounced threshold effect.

There are a few techniques such as spread spectrum where this effect occurs at a very low CNR_{min}. A sound system concept is based on the principle of using two different processes. The first with a low threshold and probably lower efficiency to increase the SNR up to the minimum allowable SNR of the second process. At this point, the latter takes over with high efficiency but a high threshold. In this context efficiency means high improvement in SNR.

Synchronisation

The aforegoing assumes synchronism between the pseudo random code of the receiver and the pseudo random code in the input signal. Synchronisation of the codes is a key problem in every spread spectrum system. Two separate cases have to be considered:

- Acquisition
- Tracking.

Acquisition means the initial synchronisation at the beginning of a transmission or any resynchronisation after loss of synchronisation. Tracking is the maintenance of synchronism after successful acquisition. Both problems are solved by utilizing the properties of the autocorrelation function of pseudo random sequences. Fig. 8 illustrates a typical autocorrelation function for a m-sequence, i.e. a maximum length pseudo random sequence.

Acquisition is realized by detection of the correlation peak which is generated periodically if the pseudo random code of the receiver is shifted with respect to the code of the input signal. This can be achieved by choosing a clock frequency in the receiver different from the clock frequency in the input signal. The acquisition time depends on the frequency difference, The length of the codes and the probability of detection.

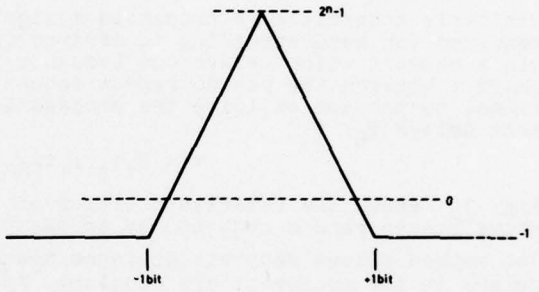

Fig. 8: Autocorrelation function for a m-sequence.

We shall see later that the distance measurement is based on the measurement of the phase shift between the pseudo random codes of the transmitter for the up link and of the receiver for the down link. This phase shift is stored permanently and can be used in case of resynchronisation to start the pseudo random generator in the receiver at a definite instant with a definite position. This procedure reduces the time for resynchronisation significantly because only a small part of the code must be shifted with respect to the code in the input signal until a synchronisation peak appears.

Tracking can be achieved with a Delay-Locked-Loop (DDL) [4]. An important parameter affecting the jam-resistance of the synchronisation section is the loop filter bandwidth of the DDL. SIECON works with different loop filter bandwidths depending on actual requirements. The bandwidth can be controlled by an internal logic network.

5. ECM-Resistant Ranging with PN PSK Systems

Navigation requires accurate determination of position. The radiolocation methods employed today use conventional receivers which fail to operate in the presence of interference. Moreover they do not range point targets with sufficient accuracy. SIECON on the other hand assures accurate radiolocation with high ECM-resistance.

Principle

SIECON normally utilizes trilateration for positioning but a rho-theta mode is also possible. Trilateration is based on the measurement of distance to known points whereas the principle of rho-theta is to determine the position of a missile by measuring angle and distance. J. Spilker and D. Magill introduced a delay lock discriminator for distance measurement in 1961 [5]. The principle is to determine the propagation time and to derive the distance by measuring the phase shift between two pseudo random sequences (e.g. the pseudo random sequence of a transmitted signal and the pseudo random sequence of the received signal reflected on a target). Modern systems utilize the pseudo random sequences which are primarily necessary for high ECM-resistance to determine the distance.

Technological advances now permit generation of very fast pseudo random sequences. The achievable accuracy depends amongst other things on the "velocitiy" of the pseudo random sequence or in other words on the clock frequency of the pseudo random generator.

Fig. 9 shows the simplified block diagram of an ECM-resistant distance measuring system. A signal coded with a pseudo random sequence is transmitted from transmitter A to receiver B. In receiver B a pseudo random sequence is generated which can be synchronized to the pseudo random sequence contained in the input signal by the synchronisation circuit. The delay time of the pseudo random sequence generated in receiver B to

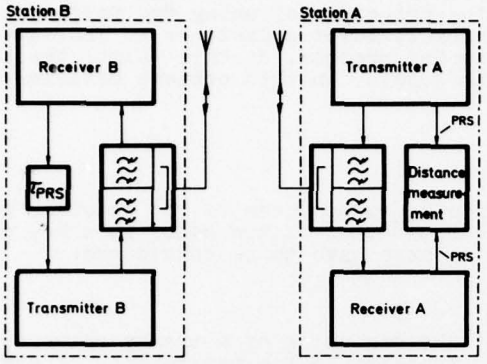

Fig. 9: Block diagram of an ECM-resistant distance measuring system.

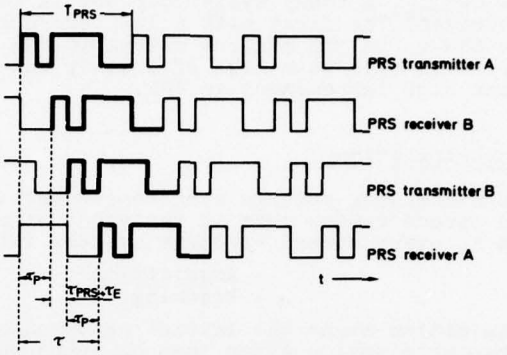

Fig. 10: Relative position of the pseudo random sequences.

the sequence in transmitter A is equal to the propagation time τ_p of the signal.

Similarly transmitter B transmits a signal to receiver A. The pseudo random sequence required for band spreading is derived from the pseudo random generator of reciever B via a network which delays the sequence for a defined time duration τ_{PRS}. The phase shift τ between the pseudo random sequences of transmitter A and receiver A is proportional to the sum of twice the propagation time τ_p, the delay τ_{PRS} and various equipment delays τ_E.

$$\tau = 2\,\tau_p + \tau_{PRS} + \tau_E.$$

Fig. 10 shows the relative position of the sequence of the four units using a very short pseudo random sequence as an example.

The method allows accurate distance measurements if τ can be determined exactly and the delays in the equipment are constant. Apart from this the described method is ECM resistant because the communication equipment itself is ECM resistant.

Ambiguity of the Distance Measurement

Because of the finite length of the pseudo random sequences the distance measurement is generally ambiguous due to the fact that the maximum measurable phase shift is equal to the length of the sequence. The maximum distance s_{max} for unambiguity dependent on the length of the sequence is enumerated in table 4. The clock frequency is 100 MHz. If s_{max} is exceeded, additional measures are necessary to secure unambiguous distance measurement. A simple method is to add a separate low-cost measuring unit of limited accuracy. In many applications it is not practical to use very long sequences because the acquisition time for the inital synchronisation or a resynchronisation then increases appreciably.

r	2^r-1	s_{max}/km	T_{PRS}/µs
10	1 023	1.53	10.2
11	2 047	3.07	20.5
12	4 095	6.14	40.9
13	8 198	12.3	81.9
14	16 383	24.6	164
15	32 767	49.2	328
16	65 535	98.3	655
17	131 071	197	1 311

Table 4: Unambiguity of the distance determination dependent on the code length ($f_c = 10^8\ s^{-1}$).

Error Sources and Measuring Accuracy

The most important error sources are shown in table 5.

The error resulting from inaccurate measurement of the phase shift can be kept small provided that the clock frequency is high enough, e.g. $f_c \geq 100$ MHz. Laboratory experiments have shown that in the worst case the distance error produced by the instability of the equipment delay is in the centimeter range.

Error of the circuit for measuring the phase shift between the sequences
Instability of the equipment delay
Synchronisation error
Atmospheric influences

Table 5: Error sources.

Every synchronisation error produces a distance error. Synchronisation errors are caused by strong interference, offset errors in the synchronisation circuit and multipath effects. In principle the synchronisation circuit guarantees synchronism within a fraction of the chip width of the pseudo random sequence [4]. Typically the distance error is ± 30 cm if an usual synchronisation error of $\varepsilon = 0{,}1 \cdot 1/f_c$ is assumed (f_c = 100 MHz). This error is independent of the absolute distance.

Additional synchronisation errors [6] can be caused by multipath propagation if the difference of the line-of-sight path and an indirect path is smaller than c/f_c (c = light velocity) in our example with f_c = 100 MHz smaller than 3 m. This kind of multipath propagation causes distortion of the synchronisation circuit control signal when the reflected signal is strong enough. Due to this effect the synchronisation error can increase up to $\pm\, c/4 \cdot f_c$ (for Central European landscape) and therefore a distance error of ± 75 cm can occur. In fig. 11 the area with critical multipath reception of an arbitrarily chosen example is shown shaded.

Atmosperic influences to the measuring accuracy depend amongst other things on the transmission frequency. These atmospheric effects will be investigated in the near future.

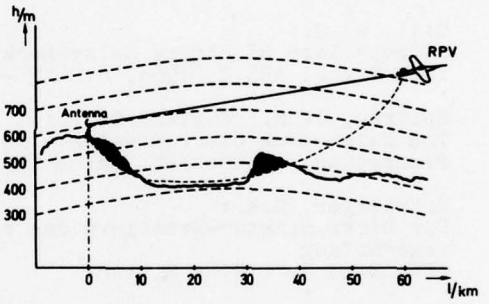

Fig. 11: Area with critical multipath reception. (arbitrary example l = 60 km, $f_c = 10^8 s^{-1}$)

6. ECM-Resistant Antenna Tracking

The requirements for low primary input power, long ranges and high ECM-resistance have led to the use of high gain antennas in the control station. Therefore an antenna-tracking system is required to follow accurately the course of the RPV. However, the use of an antenna-tracking system can only be effective if its ECM-resistance is as high as that of the communication systems. This is achieved in the SIECON system by employing a spread spectrum conical scan technique. Moreover an accurate antenna tracking is especially attractive for a rho-theta navigation system. The principle of this antenna-tracking system will be explained in the following with the help of fig. 12.

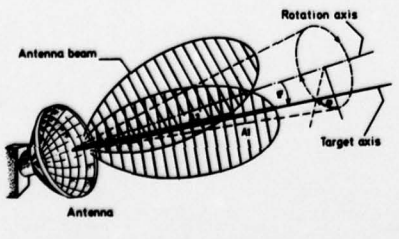

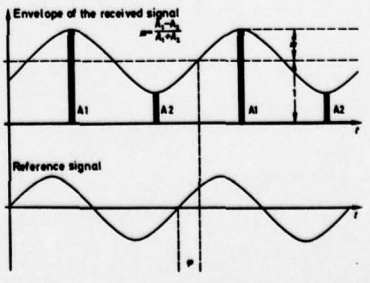

Fig. 12: Antenna-tracking system.

The beam axis of the antenna rotates round a rotation axis of a constant [7] or a pseudo statistical variated angular velocity corresponding to the conical scan frequency. The received signal will be modulated at a frequency equal to the rotation frequency of the beam. The modulation index of the received signal is proportional to the squint angle, which is the angle between beam axis and rotation axis. The phase difference of the modulation and the reference signal from the antenna determines the direction of the deviation. The conical-scan modulation is extracted from the compressed signal so that interference is reduced due to the processing gain of the system. The antenna is piloted via the tracking circuit in such a manner that both modulation index and phase difference tend to zero.

7. Conclusion

Siemens has been engaged in the development of ECM-resistant communication systems on behalf of the Bundesministerium für Verteidigung (Ministry of Defense) since 1970. These efforts resulted in the design, fabrication and testing of various prototypes. The tests included flight tests with ECM-resistant TV transmission equipment in order to demonstrate the negligible influence of multipath propagation on the communication system.

References

[1] AGARD Lecture Series No. 58
On Spread Spectrum Communications
Neuilly sur Seine: Advisory Group for Aerospace
Research a. Development 1973

[2] Baier, W.P.:
Überlegungen zu störsicheren drahtlosen Nachrichtenübertragungssystemen
Siemens Forschungs- und Entwicklungsbericht Bd. 4 (1975) Nr. 2, Springer Verlag

[3] Dixon, R. C.:
Spread Spectrum System
John Wiley u. Sons, New York-London, 1975

[4] Gill, W. J.:
A Comparison of Binary Delay-Lock Tracking-Loop Implementations
IEEE Trans. AES 2 (1966) S. 415 - 423

[5] Spilker, J. H.; Magill, D. T.:
The Delay-Lock Discriminator - An Optimum Tracking Device
Proceedings of the IRE, March 1961

[6] Grünberger, G.K.:
Die Diskriminator-Kennlinie des bandpaßkorrelierten Delay-Locked Loop bei Mehrwegeempfang
AEÜ, Band 30 (1976) S. 1-8

[7] Skolnik, M. I.:
Introduction to Radar Systems
Mc Graw-Hill Kogakusha, LTD
Tokjo

ACCURACY CONSIDERATIONS ON NEW MICROWAVE LANDING SYSTEMS (MLS) FROM AN OPERATIONAL POINT OF VIEW

by

Alfred Becker

Deutsche Forschungs- und Versuchsanstalt für Luft- und Raumfahrt e.V. (DFVLR)
Institut für Flugführung
3300 Braunschweig, Flughafen
Germany

1. INTRODUCTION

Some years ago the International Civil Aviation Organisation (ICAO) startet a competition aiming at the replacement of the presently used Instrument Landing System (ILS) by a more powerful new Microwave Landing System (MLS). This paper deals with some selected problems related to the accuracy of the different systems from an operational point of view. The complexity of the matter does not allow a complete and well balanced consideration of all the related aspects in the time available and I ask for your understanding.

In my paper, I first will make some general remarks to the ICAO MLS competition. Than I briefly will introduce the ICAO Accuracy Requirements on the new MLS. This is followed by a short description of the competing systems. The performance of the systems, i.e. the accuracy and the coverage, is discussed in the next chapter, followed by a short discussion of the flare guidance problem. Finally, some prospective considerations on growth potential will give an indication of possible future performance improvements.

In 1971 at the 4th Meeting of the ICAO All Weather Operations Panel (AWOP) the need for a replacement of the presently used ILS was stated and the Operational Requirements (O.R.)for the new MLS were established. In 1972 the ICAO invited the member states for participating in a competition. Five states responded to this invitation: Australia, France, the Federal Republik of Germany, the United Kingdom and the United States of America. At the 5th meeting of AWOP with some reservations it was found, that all proposed systems have the potential for meeting the O.R. In order to facilitate the assessment of the proposals the AWOP Working Group A (WGA) was constituted. At seven meetings of this WGA the assessment methodology was defined, the test programms for the required field tests were harmonized, and standardized methods for the evaluation of the test results were established. Finally in a very difficult and time consuming process, the systems and the results of the tests were compared to the requirements and to each other. This comparison became extremely difficult because of the continuous system improvements during the competition period. Though some important points could not be clarified within the available time AWOP tried at it's 6th full meeting in March of this year to finalize the assessment and to come to a recommendation of a preferable system to ICAO (see Ref. [1]). The final selection of a system will be made by a World Wide Conference of all member states which will take place not before the end of this year.

Before we come to the main points of my subject I would like to recall shortly some drawbacks of the presently used ILS (see Fig. 1). It provides only one linear guidance path in space. A distance information is only available in a very inaccurate form, when the aircraft overflies the outer and the inner marker beacons. Moreover, the ILS is very sensible to reflections from buildings and to uneven ground near the antenna.

Fig. 2 shows the advantages of MLS. The azimuth angle as well as the elevation angle of the approach path can be selected on board the aircraft. When using an airborne computer segmented or curved approach paths can be flown, thus allowing noise abatement procedures. A distance measuring equipment (DME) is an integrated part of the MLS. Further advantages with respect to multipath suppression, to the influence of the ground profile, and to the size of the antennas on the ground are given by the use of microwaves (L-Band and/or C-Band). Moreover, the MLS provides a flare guidance signal, which is not shown in this figure.

The next two figures illustrate the potential of MLS for curved approaches in the vertical plane (Fig. 3) as well as in the horizontal plane (Fig. 4). Thus, overflying of villages can be avoided or can be done in a greater height, which results in a considerable reduction of noise.

2. SOME CONSIDERATIONS ON THE ICAO ACCURACY REQUIREMENTS

The ICAO accuracy requirements for the new MLS are given in Table 1. The guidance error g is devided into two parts: the bias error b and the noise error n. Both figures are $2\cdot\sigma$ values from a statistical point of view. The guidance error g is composed of b and n in a quadratic manner

$$g = \sqrt{b^2 + n^2}$$

In most cases the guidance error is equally distributed on b and n. Thus $b = n = g/\sqrt{2}$.

The most stringent accuracy requirements exist on the extension of the centerline and near the conventional glide path angle of 3°. Towards the limits of the required

coverage volume a certain degradation is tolerated.

The operational significance of the MLS error can be judged by comparing the effect of these errors with other not MLS related effects such as air turbulence. MLS errors as well as air turbulence result in a deviation of the flight path of an aircraft from the desired flight path. Reducing the influence of MLS errors far below the flight path errors caused by air turbulence is operationally insignificant and ineffective from the viewpoint of system cost.

Simulations of automatic conventional centerline approaches with an HFB 320 aircraft were performed by the DFVLR at Braunschweig (Ref. |2|). For simulating the influence of turbulence a MIL-specified standard turbulence model was used. In order to meet the operational conditions with low visibility a weighting factor of 0.25 was applied (slight turbulence). As the time period of the simulated approach is short compared with the period of the turbulence waveform, a number of runs were performed using different sections of the turbulence waveform.

The MLS error signals were taken from CCL approach flight tests with the DLS trials system. It must be taken into account that the elevation errors of this test system are slightly out of the ICAO error limits while the azimuth errors are well within the limits.

The results of this simulation are shown in the next two figures. In Fig. 5 the azimuth path following error is plotted. The heavy line indicates the errors caused by the MLS errors without air turbulence. The set of thin lines describes the error behaviour when, in addition, the standard turbulence is applied with a weighting factor of 0.25. In Fig. 6 the corresponding elevation path following error is plotted. Again, the heavy line shows the error behavior without added turbulence.

From both figures the following conclusions can be drawn:

- The azimuth path following error due to simultaneous application of gusts and MLS errors is predominated by the influence of gusts.
- The elevation path following error shows a significant influence of the MLS errors. This is due to
  - the comparatively high elevation error of the DLS trials system, which exceeds the ICAO error limits
  - the control characteristics of the vertical channel of the simulated aircraft, which is optimized for the suppression of turbulence.

Under "real world conditions" (i.e. standard flight control systems; MLS errors within the ICAO error limits) the situation is about the same as in the azimuth case. Therefore, it can be concluded that:

- The path following errors for automatic landings in the presence of slight or heavy air turbulence are predominated by the influence of the air turbulence. MLS errors well below the ICAO error limits are of insignificant influence on the total path following error. Systems which perform well within the ICAO error limits can be regarded to be equivalent from an accuracy point of view.

3. SHORT SURVEY ON THE COMPETING SYSTEMS

Five proposals have been given to ICAO from the following States: Australia, France, Federal Republik of Germany, United Kingdom and United States of America (see Table 2). In the meantime, the proposals of the USA and Australia were matched to a high degree (especially a common signal format is used) and the proposal of France was withdrawn. Thus, only three proposals have to be regarded further (see Table 2). In the last column of Table 2 it is indicated, that two of the remaining systems, i.e. TRSB and DMLS, are "air derived", while the german DLS is "ground derived" with respect to the angle measurements and air derived with respect to the distance measurement (use of standardized ICAO-DME). This two principles are illustrated by Fig. 7. The air derived system generates the required position information on board the aircraft, while the ground derived system does the same on the ground. In the latter case this information has to be transmitted to the aircraft via a data link. It is obvious, that only the ground derived system makes the position information available on the ground.

It should be mentioned, that for different reasons the air derived principle had been a requirement in a former national MLS competition of the USA. Later on, ICAO did not follow this line and did not demand for an air derived system. In the meantime the very rapid development of computer capabilities makes the ground derived principle more and more attractive. DLS participated on this development and demonstrated considerable flexibility and growth potential. It can be expected that in the future the former arguments against the ground derived systems will get unsubstantial whilst the arguments in favour of this principle will get stronger. However, a detailled discussion of the pros and cons is not possible within the limited time available.

In Fig. 8 the principle of the Time Reference Scanning Beam System is illustrated. For azimuth as well as for elevation it makes use of antenna fan beams which are scanning the appropriate sectors within the coverage volume. Fig. 8 is drawn for the azimuth case. The beam starts at the + 40° position (i.e. at one limit of the required coverage sector) and moves with a constant speed to the - 40° position, which is the opposite coverage

limit. This phase is named "To Scan". Then, the beam moves back until the starting position is reached again ("Fro Scan"). When the fan beam passes the position of the aircraft, a pulse is generated on board. It is obvious, that the time difference ΔT is directly related to the azimuth angle ϑ. The same principle is used by the approach elevation subsystem (E_1), the flare elevation subsystem (E_2) and the missed approach azimuth subsystem. These different measurements are received and detected on board the aircraft in a time division multiplex frame, along with a set of auxiliary ground data (airport data, meteorological data, status of the MLS).

Fig. 9 demonstrates the principle of the DMLS. It makes use of the Doppler shift of a received frequency due to a relative movement between the receiver and the radiating source. This movement is artificially generated by sequential switching of a transmitter to a number of antennas in a linear array. It can easily be seen that the velocity vector of the radiating source has a component in the direction to the aircraft which varies with $\sin \vartheta$. In order to eliminate the influence of the aircraft movement on the Doppler shift a reference frequency with an offset F_o is continuously transmitted from a reference antenna element. In the on-board receiver the beat frequency of the commutated signal and the reference signal which is $F_o + (v \sin \vartheta)/\lambda$, is generated. F_o allows an unambiguous detection of the Doppler frequency $(v \sin \vartheta)/\lambda$ for positive as well as for negative angles of ϑ.

The third system, the DLS, is based on the commonly used DME, which generates the distance information on board the aircraft. This air derived part of the system is supplemented by an interferometer on the ground, which detects the angle of incidence of the DME interrogation wave front with respect to the boresight of the antenna system, i.e. the extended centerline in the case of the azimuth subsystem. In Fig. 10 this principle is illustrated. It can be applied in a similar way to the elevation subsystem.

From Fig. 10 follows the relation

$$\Delta s = d \cdot \sin \vartheta$$

with d = distance between the outer subarrays of the interferometer and Δs = distance between the two wave fronts which run into these subarrays at the same moment.

For accuracy reasons, d has to be in the order of 50 times the wavelenght λ. Thus, Δs can be a high multiple of λ. This, in consequence, causes an inherent ambiguity of the interferometric angle measurement as Δs is measured via the phase difference between the outer subarrays. The ambiguity resolution can be solved by using additional pairs of antennas which are positioned with a smaller distance d. Starting with $d < \lambda$, a stepwise increase of d is accompanied by a proportional increase of accuracy without ambiguity problems. In the last step the maximum baselength and the corresponding maximum accuracy is obtained. The different antenna elements can be identified from Fig. 10.

The azimuth angle ϑ and the elevation angle φ are measured on the ground and have to be transmitted to the aircraft via a data link. With DLS, the DME uplink is utilized for this purpose, too. Thus, there is no need for a separate data link.

Some more explanation of DLS can be obtained from the signal flow diagram of Fig. 11. The consecutive steps are the following ones:

1. The DME interrogation is transmitted from the aircraft.
2. The DME interrogation is received by the elevation antenna array; the processing of the measured signals creates the elevation angle φ.
3. Approximately at the same time the interrogation arrives at the azimuth antenna array and is processed to the azimuth angle ϑ.
4. The elevation angle is transmitted to the azimuth station.
5. The DME replies as well as the angle replies along with a set of auxiliary ground data are transmitted back to the aircraft.
6. The received replies are detected and processed in the airborne equipment.

4. PERFORMANCE OF THE SYSTEMS WITH RESPECT TO THE OPERATIONAL REQUIREMENTS

The MLS coverage requirement which already has been touched in Fig. 2 is given in some more detail in Fig. 12 (i.e. for approach azimuth sector, missed approach azimuth sector and approach elevation sector). The systems TRSB and DMLS, at the minimum, meet these requirements. In the data format some space is left for the extension of the coverage limits and for additional informations (i.e. for a missed approach elevation).

In the case of DLS, the presently proposed system already exceeds these requirements considerably (see Fig. 13). The azimuth subsystem provides high precision information in the required approach azimuth sector. Because of the symmetrical layout of the antennas the same coverage and the same high precision is given in the missed approach sector. In addition, a hemispherical coverage is given by some subarrays of the azimuth antenna system. Though the accuracy in this part of the coverage volume is lower than in the approach sector (typical $0{,}2^{\circ}$) it is by far sufficient for terminal area navigation. Because of the hemispherical coverage a separate back azimuth system, as it is needed for TRSB and DMLS, can be avoided for DLS.

The elevation subsystem provides high precision information in an extended approach sector of $\pm 60^{\circ}$, thus covering the threshold region of the runway. This must be required due to the different flare concept of DLS (see below). In addition, a hemispherical conical elevation information is obtained from the DLS-A station. The accuracy of this information is best right above the station, i.e. with $\varphi = 90^{\circ}$; the standard deviation is typically $\sigma = \bar{\sigma} = 0{,}1^{\circ}$. At lower elevation angles the standard deviation increases with

$$\sigma = \frac{\bar{\sigma}}{\sin \varphi}$$

This elevation information is used within the DLS ground system for coordinate transversion purposes. Besides, it is of operational value for 3 D-take off guidance and 3 D-missed approach guidance (see Ref. [3]).

Fig. 14 gives an indication of the accuracies which can be expected from the new MLS. In the case of TRSB and DMLS the plotted values are directly taken from the available test results (see Ref. [4]); in the case of DLS the test results, obtained with the trials system are extrapolated to those which can be expected from the proposed system. This has to be done because of the great difference between the tested DLS and the proposed DLS. The results of the extrapolation are based on theoretical investigations, computer simulations and field tests (see Ref. [5]).

The comparative error data for azimuth, elevation and DME, used in Fig. 14, are taken from conventional centerline approaches. For DME, only DLS data were available. As already mentioned above, the guidance error is composed of the bias error and the noise error in a quadratic manner. Thus, the guidance error can be plotted as a vector with the components b and n. The ICAO error limits are indicated in the figure by the hatched areas. It is obvious that all systems exceed the requirements with respect to bias and noise considerably. Having in mind other disturbing influencies on the flight path, i.e. gusts, as discussed before, it can be concluded that there is no significant difference between the three systems with respect to accuracy at the conventional centerline approaches. About the same is true for the rest of the ICAO required coverage volume (compare Ref. [4] and Ref. [5]).

5. SOME CONSIDERATIONS ON THE FLARE GUIDANCE PROBLEM

THE ICAO operational requirements ask for a flare guidance signal which allows a precise height computation until touch down. Thus, the well known problems related to radio altimeters and uneven ground in front of the runway threshold are solved.

The flare system concepts of TRSB and DMLS on the one side and of DLS on the other side differ considerably as can be seen in Fig. 15. In the case of TRSB and DMLS, a second elevation station (E_2) is provided which predominantly illuminates the flare region. In addition, a special wide band DME, operating at C-band (5 GHz) is provided for measuring the slant range D. In order to get the required height accuracy, an excellent accuracy of the E_2 and DME measurement is mandatory. This accuracy can hardly be obtained by an ICAO compatible L-band DME. Therefore, in the DLS flare subsystem, the slant range measurement is replaced by a second azimuth measurement at the location of the elevation station. The accuracy requirement on this second azimuth measurement is comparatively low. Most of the antenna elements which are needed for this measurement are already part of the DLS lateral diversity elevation antenna. So, the additional hardware cost for the DLS flare subsystem is very low. The height is computated on the ground from the angles ϑ_1, ϑ_2 and φ and then it is transmitted to the aircraft in an allocated space within the data format.

Thus, no further height computation on board the aircraft is needed. It is a part of the DLS flare concept that for final flare the radio altivmeter is used again, where the aircraft already has passed the threshold and the radio altimeter has a valid ground reference, namely the surface of the runway.

In the course of the AWOP assessment it was found that the accuracy requirements are difficult to be met by the TRSB and DMLS flare subsystems. Regarding the problems of reliability and system redundancy in this very critical final phase of flare, in addition to the accuracy problems, the DLS concept with the incorporated well proved radio altimeter becomes a very attractive and cost effective solution.

6. UTILIZATION OF THE GROWTH POTENTIAL FOR PERFORMANCE IMPROVEMENT

Conclusively, some problems related to the area of growth potential of systems should be discussed briefly.

In the AWOP Assessment Report (see Ref. [1]) it is mentioned that none of the competing systems meets the requirements with respect to shadowing of the guidance information by a large aircraft in the roll out phase or by buildings. This is true to all systems, as proposed. In the case of DLS, however, a solution can be offered, if both approach directions of the runway are equipped with a separate azimuth station (see Fig. 16). Because of the ground derived angle measuring principle, both stations can be operated simultaneously at the same channel. Regarding the symmetry of the DLS-A coverage it can be seen that two redundant azimuth measurements ϑ_1 and ϑ_1' can be taken. As, in addition, the second azimuth angle ϑ_2 is available (see DLS flare concept), the angle ϑ_1' can be converted to ϑ_1. If shadowing occurs at A_1 the disturbed signal can be detected by proper

methodes (i.g. ground tracking or processing the amplitude distribution of the antenna element signals). Thus, the disturbed measurement ϑ_1 can be eliminated and replaced by the converted measurement ϑ_1'.

Another possibility for solving the shadowing problems to a certain extent, which, moreover, allows a simplification of the DLS concept is illustrated in Fig. 17. In this proposal the DLS-A station is moved to the middle of the runway with an appropriate offset from the centerline. Because of the symmetry of the DLS-A station and the availability of the second azimuth angle ϑ_2 the measured angle ϑ can be converted to the angle ϑ_1'. This obviously also can be done for the second approach direction. Thus, one azimuth station can provide all the azimuth information for both approach directions. The possibility of azimuth signal blocking in the most important centerline direction is excluded. A further advantage exists, as the problem of colocation of the presently used ILS with the future MLS in the transition period is facilitated considerably.

It should be mentioned that the growth potential of DLS covers some more aspects, i.e. roll guidance, en route navigation and ATC-problems which are beyond the scope of my topic.

7. SUMMARY

It has been shown, that the new Microwave Landing Systems as proposed to ICAO make use of three different concepts. All concepts have the potential to fulfil the ICAO requirements to a high degree. Especially, the demonstrated accuracy is excellent. Thus, other not MLS related effects such as air turbulence are of predominating influence on the flight path accuracy. In the case of flare guidance, however, the TRSB and DMLS concept using a second elevation station and a special wide band DME, raises some questions with respect to accuracy, reliability and cost efficiency. The continuing use of the well approved radio altimeter, integrated in the MLS system concept, seems to be a preferable solution. The inherent flexibility of the ground derived principle as used for DLS offers some advantages which should deserve further consideration.

8. REFERENCES

[1] AWOP, "All Weather Operations Panel, Report of the Sixth Meeting" Montreal, 28. Febr. - 18. March 1977

[2] DIERKE, R., "Untersuchung der Fehler von DLS vor dem Hintergrund von Böenstörungen", Deutsche Forschungs- und Versuchsanstalt für Luft- und Raumfahrt (DFVLR), Interner Bericht IB 153-77/15

[3] BECKER, A., "Modellbetrachtungen zum Fehlerverhalten der Führungssignale des neuen Landesystems DLS im 'Missed Approach'-Bereich und Schlußfolgerungen für die 'Missed Approach'-Navigation mit DLS", Deutsche Forschungs- und Versuchsanstalt für Luft- und Raumfahrt (DFVLR), Interner Bericht IB 153-76/21

[4] AWOP WGA, "All Weather Operations Panel, Working Group A, Report of the Sixth Meeting (amended version)", Den Haag, 5. - 16. July 1976

[5] BIP 80 (presented by T. BOHR), "Performance Improvement of Proposed DLS with Respect to the DLS Trials System", Background Information Paper 80 (BIP 80) of the Sixth Meeting of the All Weather Operations Panel, Montreal, 28. Febr. - 18. March 1977

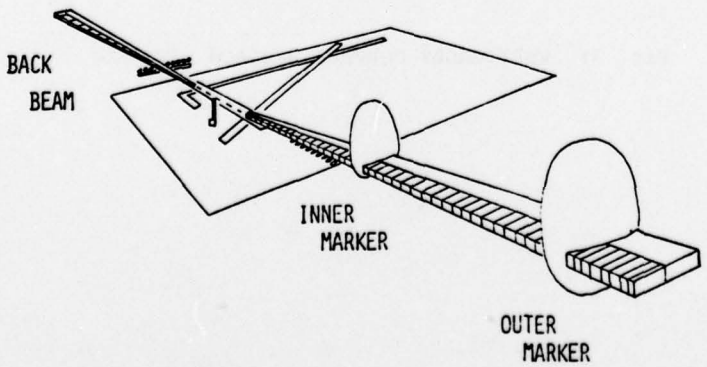

Fig. 1: ILS GUIDANCE INFORMATION

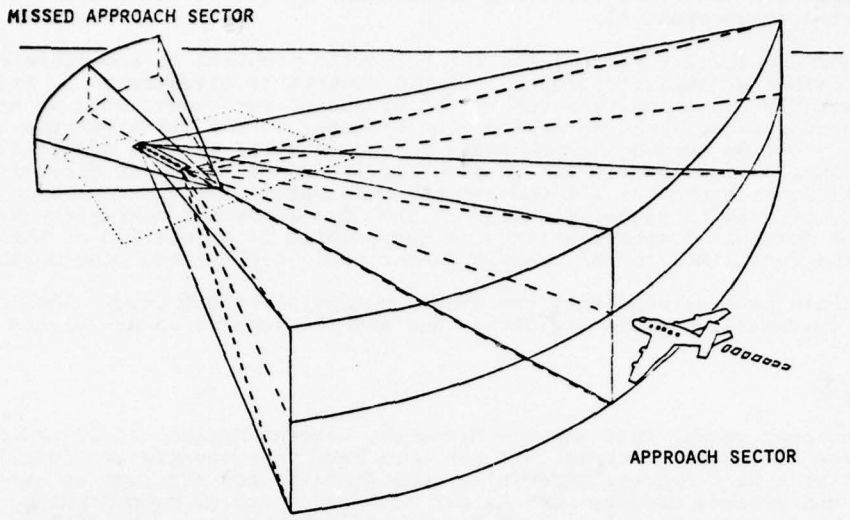

Fig. 2: MLS GUIDANCE INFORMATION

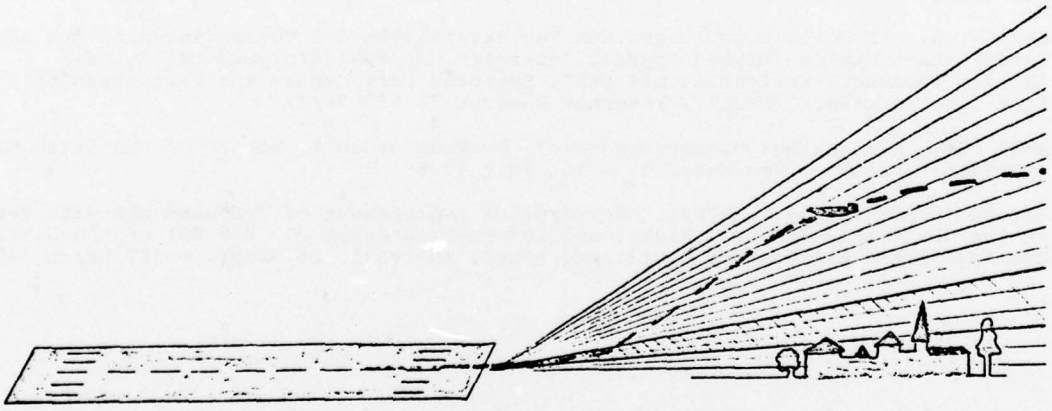

Fig. 3: VERTICALLY CURVED APPROACH WITH MLS

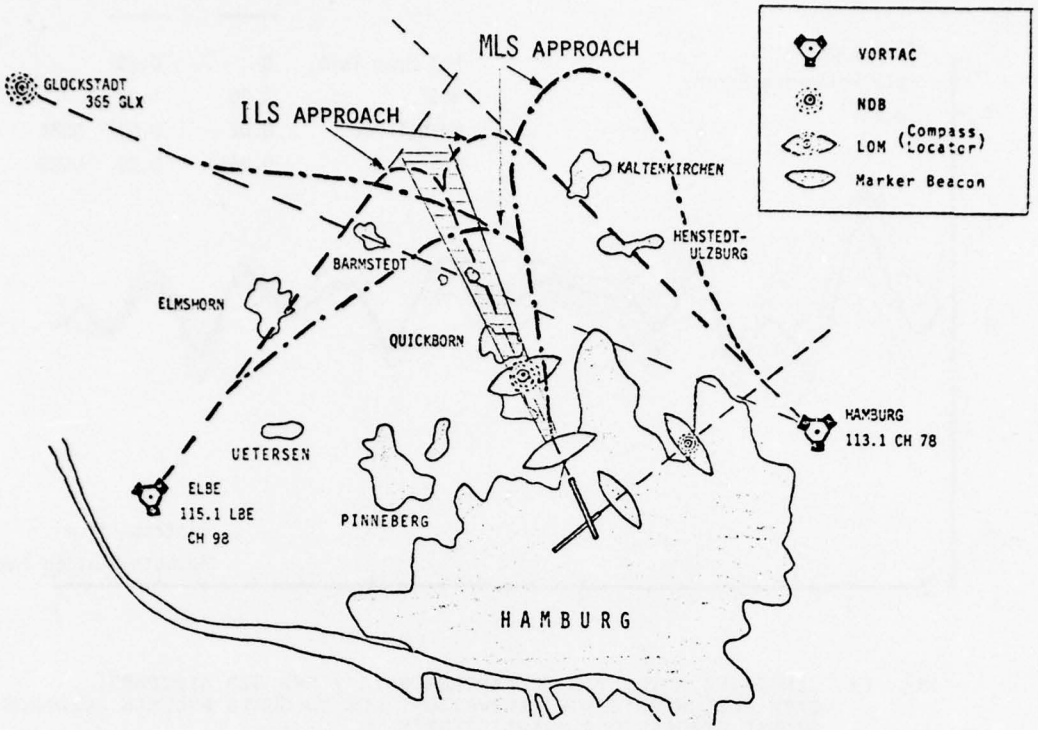

Fig. 4: HORIZONTALLY CURVED APPROACH WITH MLS

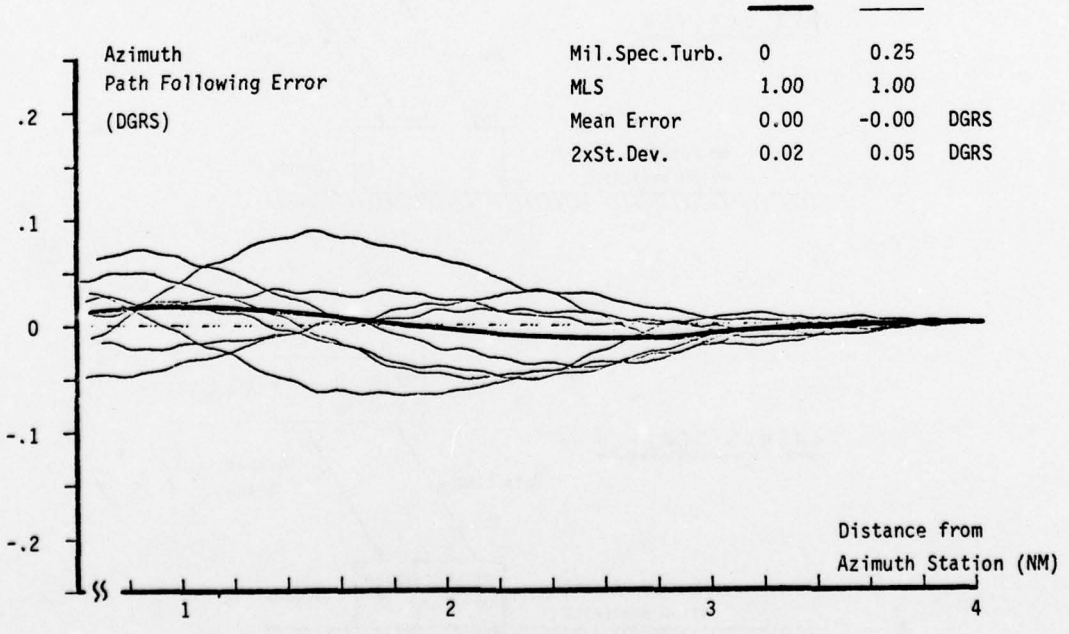

Fig. 5: SIMULATED AUTOMATIC CCL APPROACH (3°; HFB 320 AIRCRAFT)
PATH FOLLOWING ERROR (AZIMUTH) DUE TO GUSTS AND MLS GUIDANCE
SIGNAL ERRORS (DLS TRIALS SYSTEM)

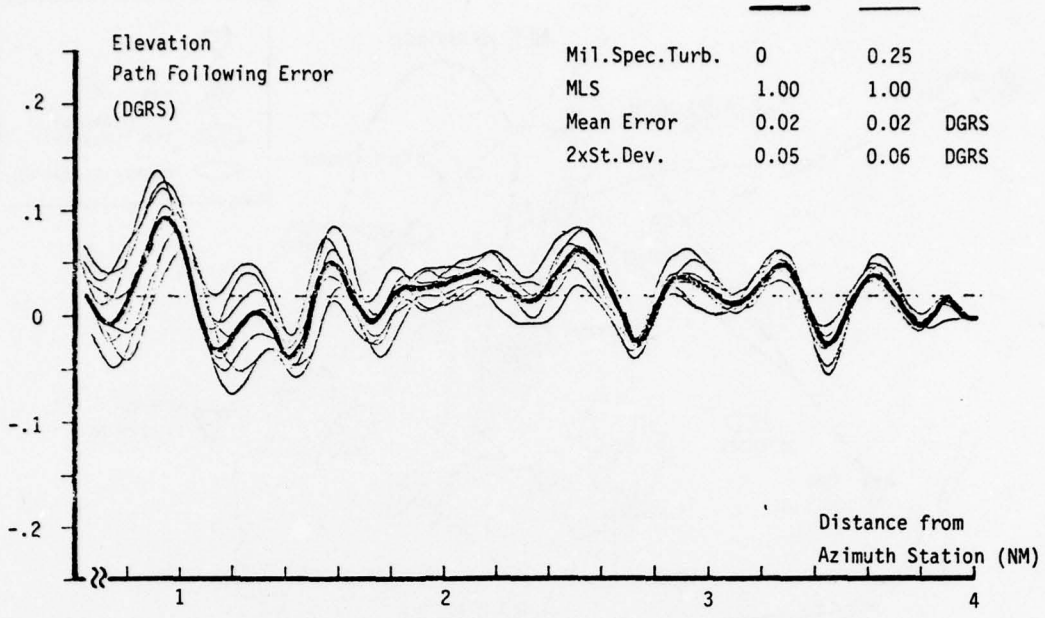

Fig. 6: SIMULATED AUTOMATIC CCL APPROACH (3°; HFB 320 AIRCRAFT) PATH FOLLOWING ERROR (ELEVATION) DUE TO GUSTS AND MLS GUIDANCE SIGNAL ERRORS (DLS TRIALS SYSTEM)

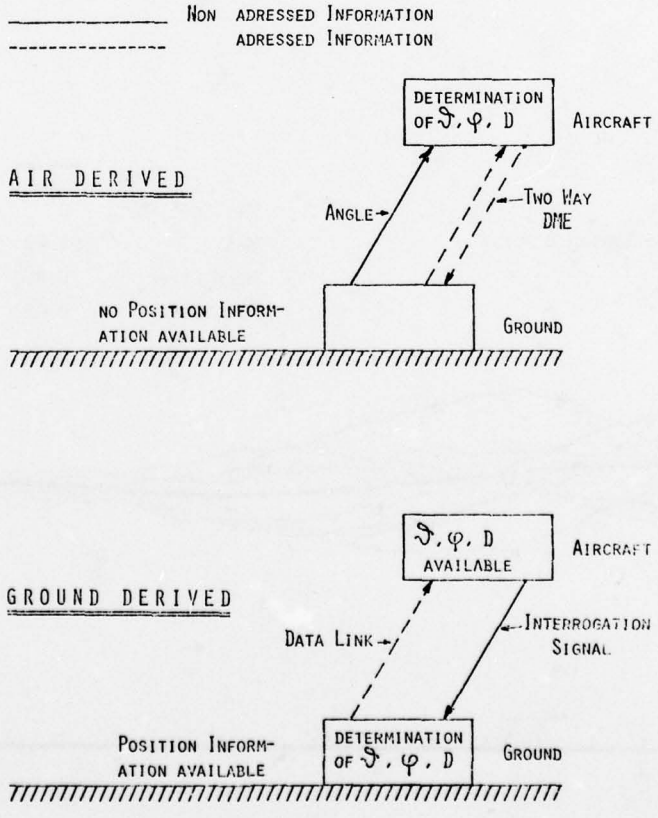

Fig. 7: PRINCIPLES "AIR DERIVED" AND "GROUND DERIVED"

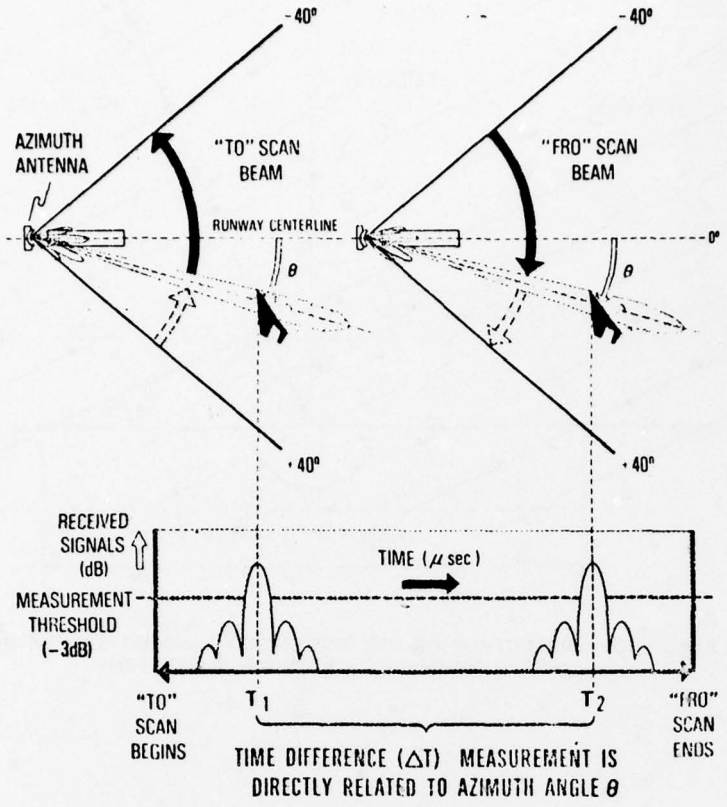

Fig. 8: PRINCIPLE OF THE TIME REFERENCE SCANNING BEAM (TRSB) SYSTEM (US-AND AUSTRALIAN PROPOSALS)

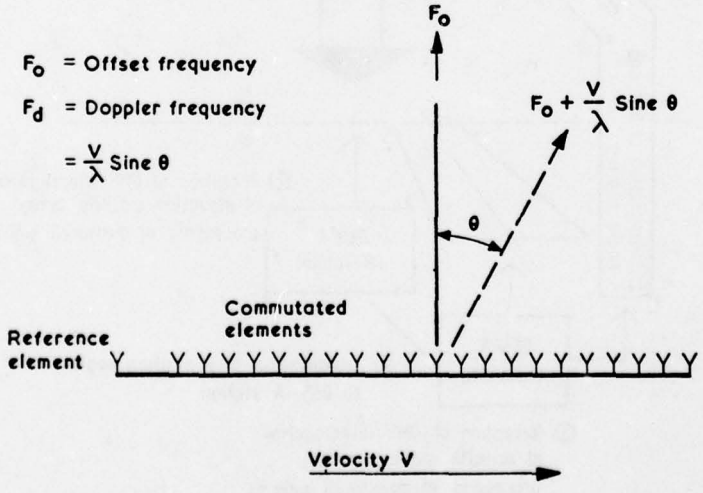

Fig. 9: PRINCIPLE OF THE DOPPLER MICROWAVE LANDING SYSTEM DMLS (UK-PROPOSAL)

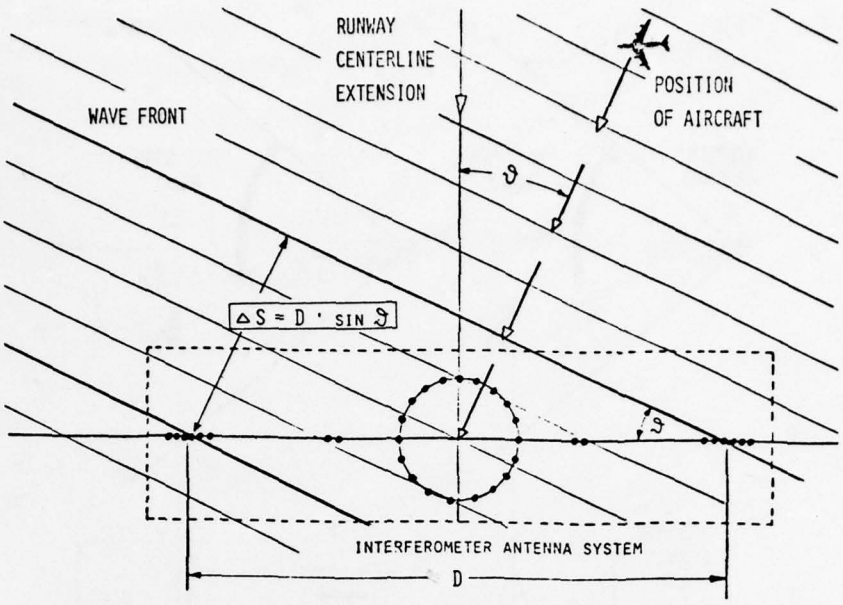

Fig. 10: PRINCIPLE OF THE DME-BASED LANDING SYSTEM DLS (FRG - PROPOSAL ; AZIMUTH SUBSYSTEM)

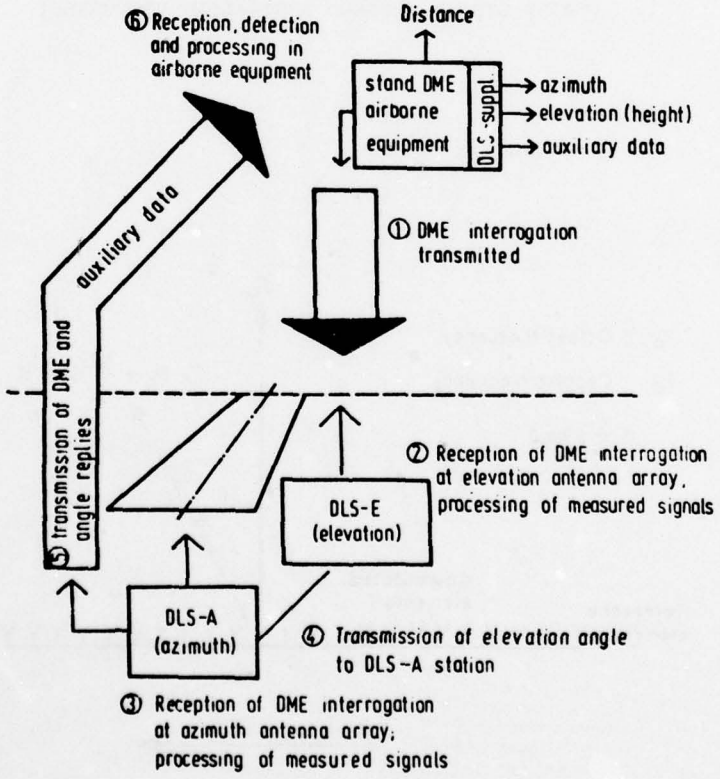

Fig. 11: DLS SIGNAL FLOW

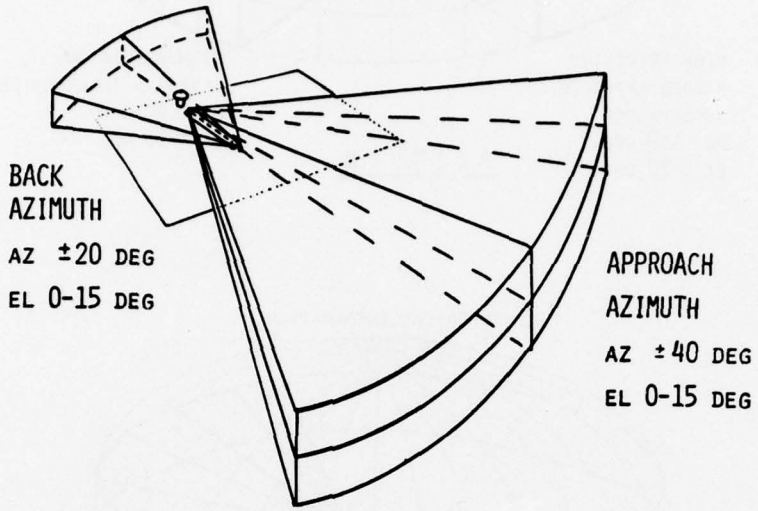

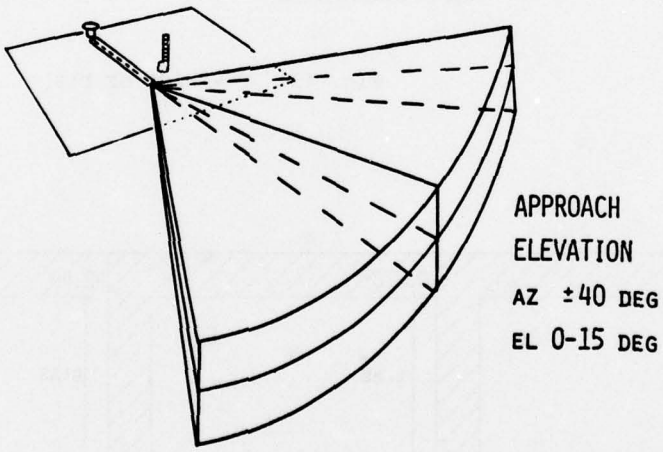

Fig. 12: MLS COVERAGE REQUIREMENTS

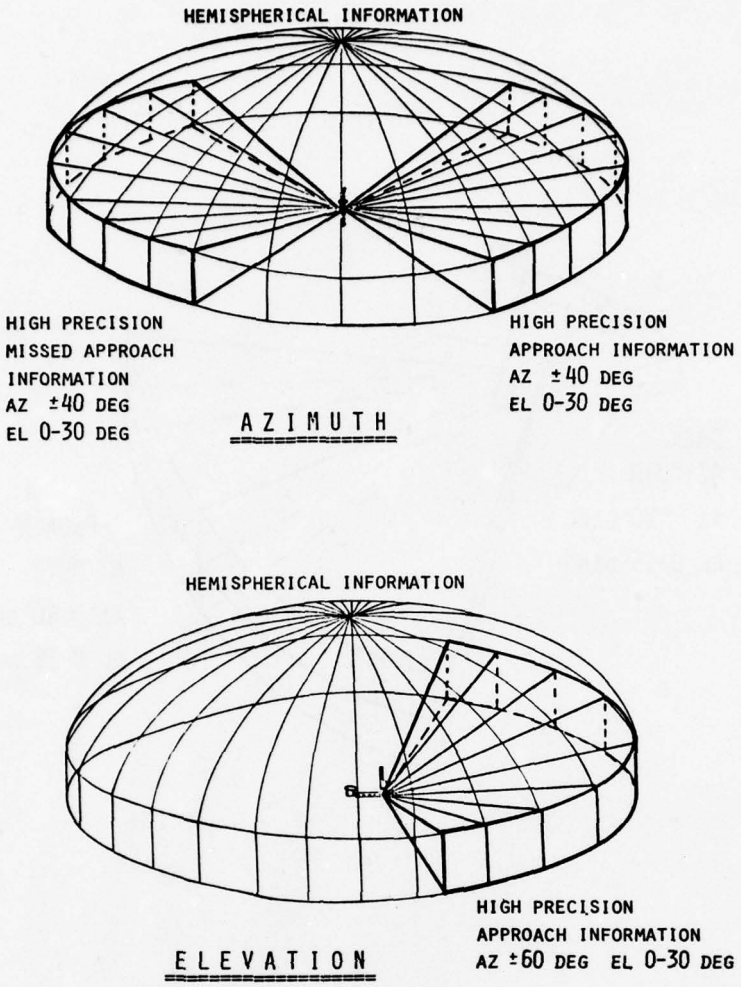

Fig. 13: COVERAGE OF DLS

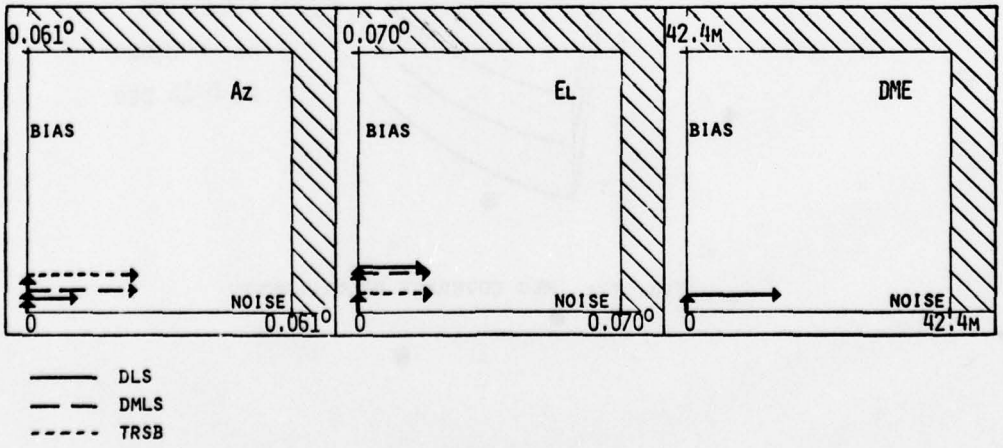

Fig. 14: MLS ACCURACY TEST RESULTS RELATIVE TO THE ICAO ERROR LIMITS (CCL APPROACHES)

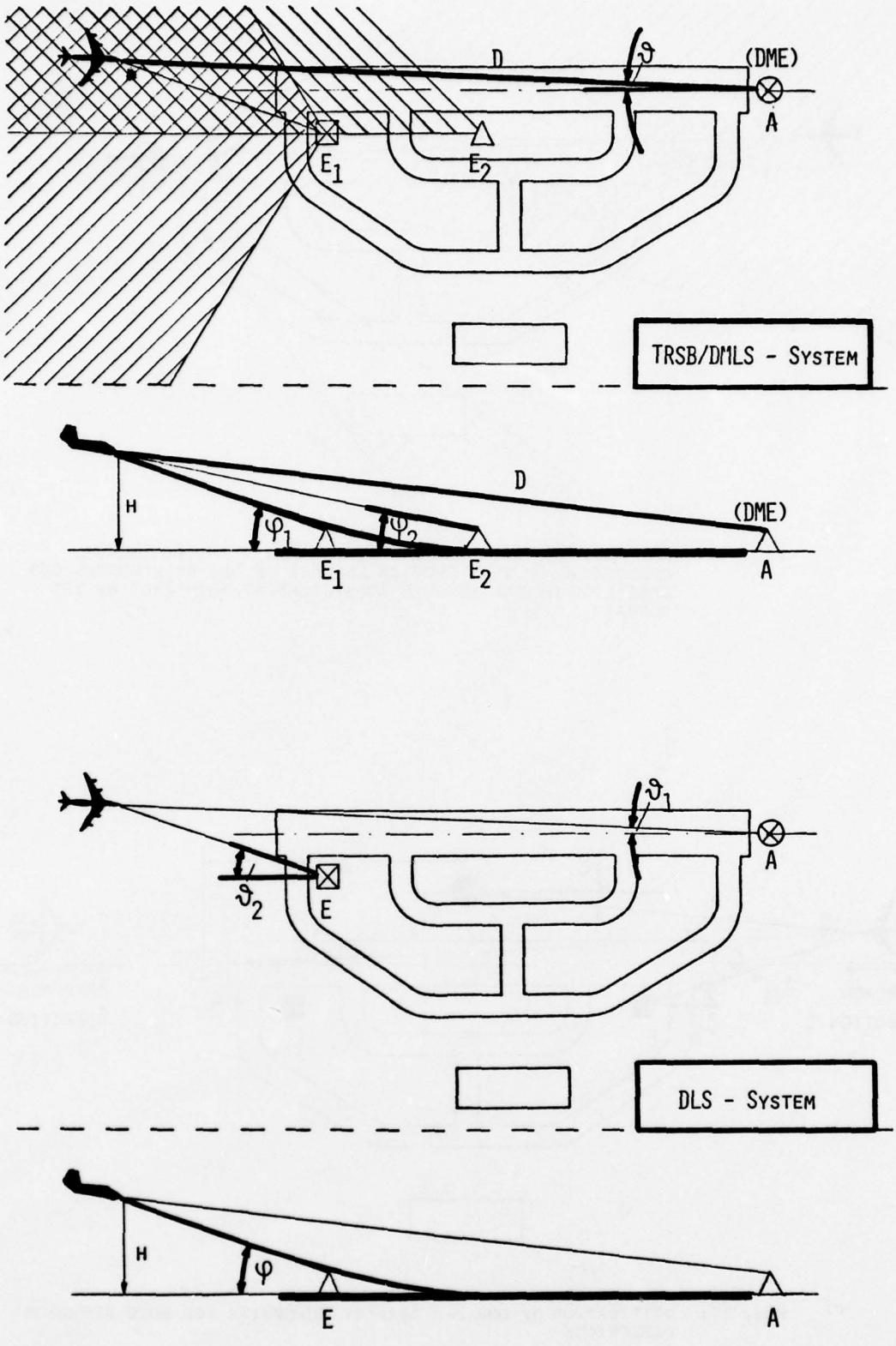

Fig. 15: PRINCIPLES OF FLARE PROPOSALS OF TRSB/DMLS AND DLS, RESPECTIVELY

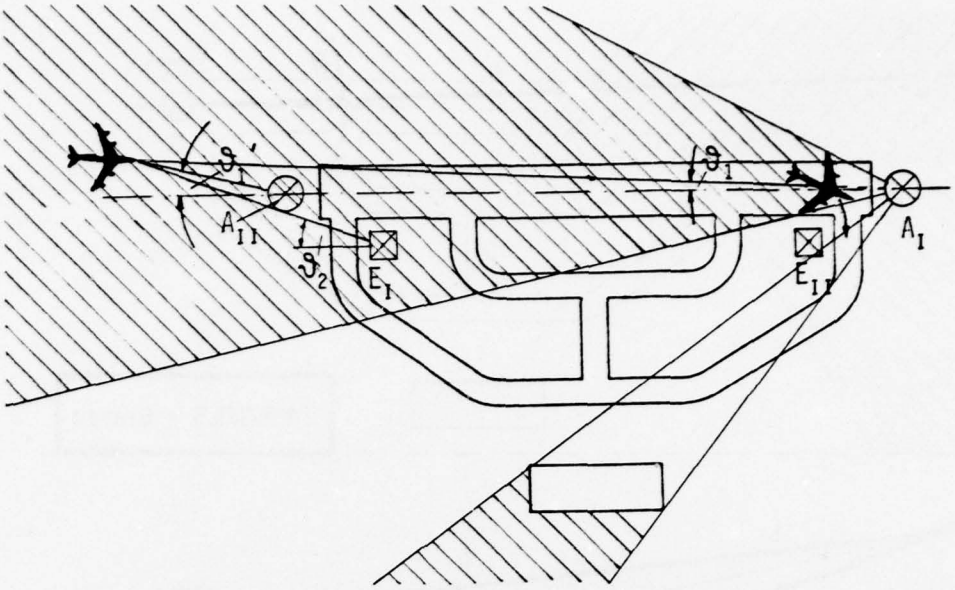

Fig. 16: MLS AZIMUTH SHADOWING BY LARG AIRCRAFT AND BUILDINGS; OVERCOMING OF THIS PROBLEM IN CASE OF DLS BY SIMULTANIOUS OPERATION OF THE AZIMUTH SUBSYSTEMS AT BOTH ENDS OF THE RUNWAY

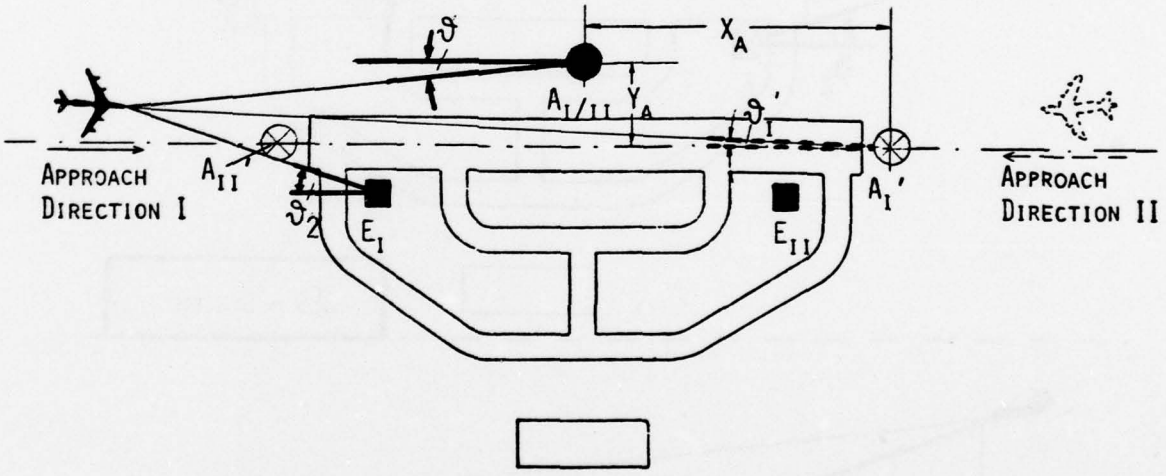

Fig. 17: UTILISATION OF ONE DLS AZIMUTH SUBSYSTEM FOR BOTH APPROACH DIRECTIONS

	DISTANCE D (NM)	EL-ANGLE φ (DGRS)	AZ-ANGLE ϑ (DGRS)	MEAN ERROR	2 x ST. DEV.	GUIDANCE ERROR
APPROACH AZIMUTH	2.5 (D_T)	0...9 (φ_A)	0 $\pm$ 40 ($\pm \vartheta_M$)	0.054° 0.081°	0.054° 0.081°	0.076° 0.114°
		15 (φ_{AM})	0 $\pm$ 40 ($\pm \vartheta_M$)	0.108° 0.162°	0.108° 0.162°	0.152° 0.228°
	22 (D_M)	0...9 (φ_A)	0 $\pm$ 40 ($\pm \vartheta_M$)	0.108° 0.162°	0.108° 0.162°	0.152° 0.228°
		15 (φ_{AM})	0 $\pm$ 40 ($\pm \vartheta_M$)	0.216° 0.324°	0.216° 0.324°	0.304° 0.456°
MISSED APPR. AZIMUTH	0...-10	-	-	0.106°	0.106°	0.150°
ELEVATION	R $\geq$ 0.19	0...4 (φ_B) 15 (φ_M)	- -	0.070° 0.380°	0.070° 0.070°	0.100° 0.386°
DME (FLARE)	2.5 (D_T) 22 (D_M)	- -	- -	- -	- -	12.2 M 122 M
DME	2.5 (D_T) 22 (D_M)	- -	- -	- -	- -	60 M 122 M

Tab. 1: ICAO ACCURACY REQUIREMENTS FOR NEW MLS

NAME OF SYSTEM	PROPOSING STATE	CLASS
• TIME REFERENCE SCANNING BEAM (TRSB)	USA	AIR DERIVED
• INTERSCAN	AUSTRALIA	"
• DOPPLER MICROWAVE LANDING SYSTEM (DMLS)	UNITED KINGDOM	"
AGDLS	FRANCE	GROUND DERIVED
• DME DERIVED LANDING SYSTEM (DLS)	FEDERAL REPUBLIK OF GERMANY	ANGLE: GROUND DERIVED RANGE: AIR DERIVED

Tab. 2: CLASSIFICATION OF ICAO PROPOSED SYSTEMS

A MULTI-SENSOR IMPLEMENTATION FOR NAVIGATION, POSITION LOCATION, POSITION UPDATE, RECONNAISSANCE, AND WEAPON DELIVERY - AN/ARN-101(V)

F. E. Pickel
Lear Siegler, Inc./Instrument Division
4141 Eastern Avenue, S.E.
Grand Rapids, Michigan, USA 49508

SUMMARY

The AN/ARN-101(V)* is a digital system developed to replace and/or functionally improve the present avionics in the USAF F-4E and RF-4C aircraft. It upgrades the operational capability of the total weapon system through a multi-sensor implementation for navigation, offset aim point and target location, weapon delivery, and reconnaissance. The navigation, position locating, and position updating capabilities utilize a digital Inertial Measurement Unit (IMU), Loran, fire control or mapping radar, Pave Tack, TISEO (Electro-Optical Target Identification System), and Lead Computing Optical Sight System (LCOSS) interfaces. Performance features include long-range and tactical navigation, all-weather blind bombing, adverse weather landing approach, uncanned weapon delivery profiles, and automatic reconnaissance steering.

PURPOSE

The development of the AN/ARN-101 grew out of programs in the 1960's such as the AN/ARN-92 Loran Navigation System, and the Pave Phantom F-4 navigation/blind bombing system. After successes for both programs in Southeast Asia, a second-generation competitive procurement was initiated by the USAF Systems Command, Aeronautical Systems Division, for the AN/ARN-101 system. Management of the effort was later transferred to the Electronic Systems Division (ESD). The technical specification, ESD Specification ENVG 70-44, specified both blind and visual weapon delivery modes with an accuracy equal to or greater than Pave Phantom without deleting any F-4D capability. The primary requirements were:

- Replace the old F-4D analog Weapon Release Computer System (WRCS) and the Navigation System, while adding the Pave Phantom-type Loran capability.
- Improve the reliability of the F-4 avionic system in the operational environment.
- Meet or exceed the weapon delivery accuracy for F-4 blind and visual modes while avoiding the shortcomings of "canned" air-to-ground modes, limited dynamic maneuvers, and frequent "break-lock" incidents of Pave Phantom missions.
- Add a modern high-accuracy low-cost inertial reference capability for better navigation and velocity determination.
- Provide a system maintainable by USAF Skill Level 3 and 5 personnel through the use of on-aircraft automatic fault isolation to the line replaceable unit (LRU), and automatic fault isolation to the repairable subassembly at the Intermediate Level.
- Develop a system concept which provides a maximum of growth flexibility when considering future requirements such as JTIDS (Joint Tactical Information Distribution System) and GPS (NAVSTAR Global Positioning System).

Lear Siegler and ITT Avionics were in direct competition from February 1972 through July 1975. This activity resulted in prototype and preproduction hardware development, extensive Loran receiver testing on the ESD AN/GRM-99 Loran Signal Simulator, MIL-STD-785 reliability testing, MIL-STD-810 qualification testing, and extensive head-to-head F-4D DT&E flight testing at Eglin Air Force Base. In April, 1972, Headquarters Tactical Air Command issued TAC ROC 12-72 to update the avionics in the F/RF-4 aircraft. This document described the required operational capability for an integrated digital central navigation and weapon delivery for the F-4D/E, and for a reconnaissance sensor data processing system for the RF-4C. Lear Siegler won the production contract competition in August 1975 to retrofit USAF RF-4C reconnaissance aircraft and F-4E strike aircraft with 1st option deliveries starting in the Fall of 1977.

FUNCTIONAL DESCRIPTION

The AN/ARN-101(V) is composed of eleven boxes (seven Line Replaceable Units and four control-display panels) and a Loran antenna subsystem. It replaces the AN/ASN-46A Navigational Computer Set, the AN/ASN-63 Inertial Navigation Set, and the AN/ASQ-91 Weapon Release Computer Set Systems in the F-4E, and the AN/ASN-46A and the AN/ASN-56 Inertial Navigation Set Systems in the RF-4C. The old analog inertial navigation and weapon delivery equipments have been replaced with new digital equipment with much greater operational capability. A block diagram of the F-4E configuration is shown in Figure 1.

* Developed under competitive procurement through Electronic Systems Division, USAF Systems Command, L. G. Hanscom Air Force Base, Bedford, Mass., USA.

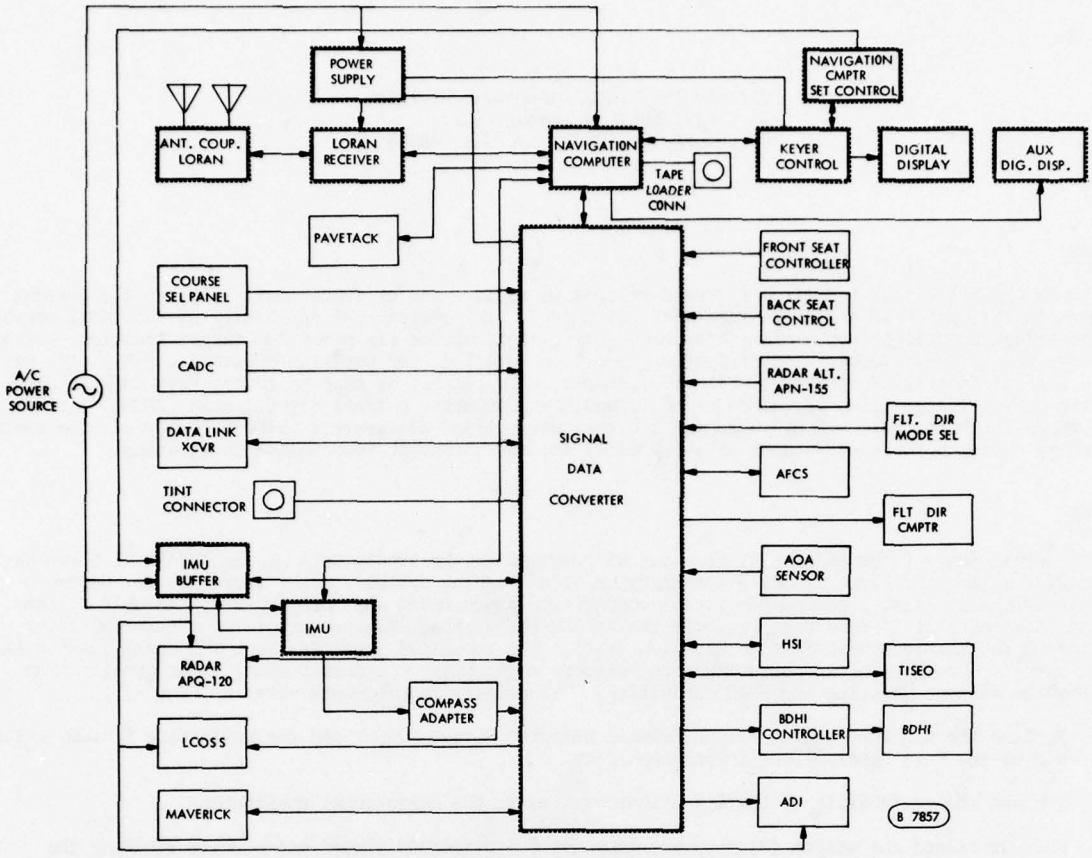

F-4E SYSTEM BLOCK DIAGRAM
FIGURE 1

The system utilizes a central digital computer to process both inertial platform and Loran data (in a Kalman filter) to provide precise position and velocity information in three coordinate frames -- Latitude-Longitude, Universal Transverse Mercator, and Loran time differences. Interfaces with the central air data computer and Attitude Heading and Reference System provide several backup modes of operation.

Interfaces are provided in the F-4E with the existing aircraft displays, and with the following special sensors: AVQ-26 Pave Tack Infrared/Laser target designator, ASX-1 TISEO (Target Identification System, Electro Optical), APQ-120 fire control radar, ASG-26 LCOSS (Lead Computing Optical Sight System), and AGM-65C/D Laser/IR Maverick missiles. In the RF-4C, the integration includes the AVQ-26 Pave Tack designator, ASQ-154 data display set for film annotation, ALQ-125 TEREC (Tactical Electronic Reconnaissance), AAD-5 infrared mapper, APQ-99 radar cursors, and APQ-102 side-looking radar. This total system integration provides the basis for the following mission-related functional capability.

Navigation/Position Location - The RF-4C and F-4E navigation modes are identical and consist of on primary mode and six back-up modes. Back-up modes are selected either manually or automatically in the case of loss of valid Loran or inertial data. In order of priority, the modes are:

- Integrated Loran-Inertial (primary)
- Loran with inertial velocity aiding
- Loran with true airspeed and heading aiding
- Inertial only
- Loran only
- Dead-reckoning (true airspeed and heading)
- Attitude (back-up INS attitude for displays)

A system feature is the automatic selection of position and velocity parameters from the best available sensor combination. From system turn-on, the best available position and velocity source is continually chosen. As inertial and Loran data become available, progressively more precise velocity and position data are chosen for use by all other system functions. Performance criteria are continually monitored to provide immediate graceful degradation to an alternate position and velocity source in the event of data sensor failure. Manual override to a lower priority mode is also available.

Position Update - The ARN-101 is configured to allow position update in flight using any one of the available sensors (radar, cursors, LCOSS, TISEO, or Pave Tack), or manually through an over-fly technique. If the coordinates of an update point are known and inserted in the computer, and the sensor is tracking the point, angular data on the geometry of the sensor head and the aircraft position is used to update the position solution. The update is not automatic. The Weapons System Officer (WSO) initiates the update procedure, evaluates the errors between the system and update positions, and determines if the update should be completed. In a similar manner, data stored manually when directly over a known point is used to identify errors in a navigation solution, and to update that solution.

Offset Target Position Computation - Offset targeting capability is provided to compute the geographical coordinates of a target of interest. For example, Pave Tack pointing angles, laser ranging data, and aircraft position data are used to compute and store the coordinates of any target being designated by Pave Tack. If the laser is not being used, the altitude of the target is determined from the baro-inertial altitude computation. These coordinates may be either new targets-of-opportunity or updates to the target coordinates that were used to cue the sensor initially. Similar operation is provided with the radar cursors and the LCOSS.

Altitude Update - An important part of the position update process, and especially for weapon delivery computations, involves the use of sensor ranging data to update system altitude, and hence height-above-target. The ARN-101 is configured to use valid radar range or laser range data, or, in the event neither is available a barometric-inertial implementation. Laser range is the most accurate and has top priority.

Sensor Cueing - Target designator cueing capability is provided to cue aircraft sensors to targets of interest which have coordinates stored in the system's memory. For the F-4E, these sensors include the AVQ-26 Pave Tack infrared/laser target designator, ASX-1 TISEO, APQ-120 radar and radar cursors, ASG-26 optical sight, and AGM-65 Laser/IR Maverick. For the RF-4C, Pave Tack and the APQ-99 radar cursors are cued to the target.

A coordinated philosophy was established for both manual sensor search and automatic sensor cueing. Initial cue operation causes all the sensors to point to the same location (determined by mode and by the coordinates inserted in the computer). If one sensor is selected for display by the WSO and trim adjustments are made to exactly center the target in the field-of-view, the other sensors, or weapon seeker heads, may then be also positioned to the new point. This provides much faster target acquisition with very narrow field-of-view sensors than is possible with manual search.

Weapon Delivery - The ARN-101 provides the F-4E with the following modes of operation:

- All-weather blind bombing (Loran or radar)
- Dive-toss
- Visual continuously-computed impact point (CCIP)
- Air-to-ground missile
- Integrated AJB-7
- Improved nuclear delivery
- Air-to-ground guns and rockets

The present F-4E ASQ-91 weapon delivery system requires the Aircraft Commander to fly a preplanned or "canned" delivery profile for all but dive-toss, allowing effective delivery only at a specific dive angle, altitude, and airspeed. Any deviation between this profile and dynamic aircraft conditions during the actual weapon delivery approach adversely affects the weapon delivery system's accuracy. The "canned" system forces the pilot to fly fixed delivery patterns which can be recognized easily by air defenses.

The AN/ARN-101(V) provides all the modes of the ASQ-91. More important, it is an "uncanned" system which allows effective delivery of ordnance at any dive angle, altitude, or airspeed within a large delivery envelope. The dynamic aircraft conditions may be varied during the weapon delivery approach without adversely affecting the system's accuracy. The Aircraft Commander (AC) is not restricted to flying through a predetermined altitude at a particular airspeed or dive angle. For all modes, the weapon delivery solution compensates for weapon ejection velocity and rack delay. Multiple releases are generated to give weapon spacing on the ground in feet, accounting for speed and flight profile.

Reconnaissance - Reconnaissance operations with the ARN-101 involve the selection of either the racetrack or adjacent-parallel coverage patterns, definition of the desired rectangular coverage area, and path width defining variables. Steering commands to the attitude director indicator and the automatic

flight control system (AFCS) result in a succession of straight paths covering the desired area with turns accomplished under optimized steering commands. In addition, circular avoidance area locations may be identified and the ARN-101 will automatically interrupt the path coverage, or turn at an optimum time, and steer the aircraft around the avoidance area periphery. A camera control discrete for area coverage and a pilot anticipatory cue are furnished under computer control.

Adverse Weather Approach-to-Landing - The AN/ARN-101(V) computes approach-to-landing information for display on the aircraft instruments and for automatic control via the AFCS based on deviations from a mathematical glide path generated in the central computer. Lateral position and velocity deviations from this path are obtained from the integrated Loran/inertial information. Vertical deviations are obtained from a blend of vertical axis inertial and barometric altimeter data. The approach path is based on the inserted Loran coordinates of the touchdown point, the approach heading, the barometric altitude of the touchdown point, and the desired glide slope angle (2° to 5°). Steering is provided in both the vertical and horizontal axes. Accuracy of this mode is sufficient to provide approach guidance for conditions down to about 300 feet ceiling and one mile visibility.

Automatic Flight Control System Commands - The system provides lateral command signals to the AFCS for the navigation modes, for the weapon delivery modes, and for the reconnaissance steering mode. The signals are generated from the same control equations and logic used for the flight director steering commands. Pitch axis commands are provided to the AFCS only in the approach-to-landing mode.

Steering Commands - The system computes steering to operator-inserted destinations based on inserted or computed course data. Steering information is presented on the ARN-101 display, aircraft instruments, attitude director indicator (ADI), LCOSS, and to the AFCS. The AN/ARN-101(V) features the capability of automatic sequencing steer commands to up to 60 inserted waypoints or destinations, with the option of fixed course or direct-track steering modes. When AFCS steering is selected, performance is monitored on the ADI/LCOSS and temporarily overridden with stick force in the normal F-4 operating manner. Navigation parameters presented to the Aircraft Commander on the horizontal situation indicator (HSI) include aircraft magnetic heading, required magnetic heading to destinations, keyboard selected course, deviation from selected course, selected course to-from destination, and distance to destination.

Interactive Control-Display - A unique feature of the system is the keyer control (KC) and digital display indicator (DDI) in an interactive mode. The keyer control is a full alphanumeric keyboard which is used to direct, interrogate, and program the navigational computer (NC). The digital display indicator is the computer readout device and has a three-line 24 alphanumeric character capability. Several data lists and checklists are provided under software control to cue and guide the WSO through data input, data checking, and normal system operation. It is manipulated and followed easily and, more importantly, can be changed simply, through software, to reflect revised requirements.

Command and Control Data Link - The ARN-101 incorporates provisions to interface with a command and control system via an airborne up-link and down-link. The down-link interface will be used by the ARN-101 to report its present position and altitude. The up-link interface will supply the ARN-101 with target data.

Data Freeze - Data storage capability is provided for either navigation or weapon release information. The "Freeze" button on the keyer control is used by the WSO to hold parameters relating to the existing present position. In addition, position and velocity data describing each weapon release point is automatically stored in memory. All such data may be read out at any time through the keyer control and digital display indicator.

Built-In Test (BIT) - The system contains built-in test hardware and software to isolate hardware failures to the particular failed unit. Tests of various functions in each unit are initiated under computer program control and the results monitored in the navigation computer. When the malfunction light on the DDI goes on, it indicates a failure of any of the continuous BIT tests. Pushing the BIT button displays the name of the failed line replaceable unit (LRU) and the failure mode on the digital display indicator. Organizational and Intermediate Level testing of the BIT and fault isolation capability has demonstrated a 95% confidence of identification to a faulty LRU.

DESIGN HIGHLIGHTS

IMU Management - The system provides the RF-4C and F-4E aircraft with a digital inertial navigation system (INS) that is more accurate, reliable, and maintainable than the older LN-12 INS which it is replacing. The ARN-101 INS function is accomplished in two units -- the inertial measurement unit (IMU) and the navigation computer (NC). The IMU provides an all-attitude capability of maintaining a stable reference frame and measuring attitude, platform azimuth, and acceleration components. The NC manages the IMU by processing the accelerations, solving the navigation equations, and supplying digital torquing commands to the IMU's gyros. In case of NC failure, the IMU has a stand-alone attitude mode where the IMU keeps the stable reference erect without input from the NC.

For the inertial mechanization, the central computer accepts aircraft incremental velocities measured by the IMU and computes vehicle velocity, position and heading, and the IMU gyro torquing commands. The IMU platform coordinate frame is a locally level, wander azimuth system and has a precession rate about

the vertical axis nominally equal to the vertical component of the earth's angular velocity. This coordinate frame reference for the IMU is chosen to allow world-wide navigation -- including both polar regions -- and to minimize platform drift.

Ground alignment of the IMU and inertial navigation equations can be performed by the ARN-101 without aid from Loran or any other external sensors. The ground alignment technique uses an eight-state Kalman filter, functionally different from the Loran/inertial integration filter described later, to perform wide angle gyro compassing. The mechanization accepts best available true heading (BATH) when it is supplied to reduce alignment time. Ground alignment can be performed, however, when BATH is not available.

Integrated Loran/Inertial Mode - The prime navigation mode -- Integrated Loran-Inertial -- provides the best information available from the Loran and inertial measurements for the navigation, reconnaissance, and weapon delivery functions of the ARN-101.

An eight-state Kalman filter combines the long term stability of the Loran positional measurements with the short term accuracy of the inertial position and velocity data to provide a navigation accuracy that is superior to that provided by either sensor by itself, or by conventional filtering techniques.

The Kalman filter differences the INS position solution and the Loran position solution (Loran TD's) and estimates eight inertial navigation error sources. Three of these errors are associated with the direction cosines that establish aircraft position in the unipolar inertial navigation coordinate system. Two are the error components of the ground-referenced inertial velocity vector in the horizontal plane. Two others are associated with the roll and pitch alignment errors of the inertial measurement unit, and the last is associated with the error in the azimuth wander angle of the INS.

The basic iteration period of the INS equation is 50 milliseconds. Error estimates are added to the INS navigation solutions to obtain the corrected solutions for position, velocity, and heading every 400 milliseconds. If the Loran data being processed by the Kalman filter is valid, the INS is periodically updated by the Kalman filter to correct the INS navigation solutions and to re-level the platform stable element by physically torquing the platform inner axis. Updating the INS with the integrated Loran-inertial navigation solutions damps out the long-term growth of the errors in the Schuler-tuned INS. If the Loran information is lost for any reason, the mission can be completed with an INS whose errors start growing from the time the Loran system was lost. The INS update period is dependent on Loran signal-to-noise ratio but typically ranges between 5 and 10 minutes. The Loran receiver uses the INS velocity solutions to obtain better dynamic performance in its time difference measurements and computations.

Another feature that enhances operational performance is designed into the Loran/inertial mechanization; the Loran/inertial Kalman filter performs an in-flight alignment of the INS after the IMU stable element has been rotated so that it is approximately level. The in-flight alignment feature provides a rapid reaction capability to the aircraft with only an initial platform verticality established on the ground prior to departure, and allows the IMU to be restarted in the air with platform verticality established during a brief period of wings level.

The ARN-101 system's altitude and vertical velocity are obtained by combining the inertial vertical acceleration measurements with barometric altitude measurements. A second-order filtering technique continuously integrates this information together in the vertical channel mechanization. The vertical accelerometer's bias is estimated during ground alignment to minimize its effect on vertical channel performance.

The majority of the Loran receiver (signal processor) functions are performed in the central computer in the ARN-101 mechanization. The Loran subsystem is a linear receiver mechanization and consists of four pieces of hardware:

a. A three axis H-field antenna system that provides nearly constant signal levels under all aircraft attitudes,

b. An antenna coupler,

c. The Loran receiver which contains gain control circuits and four notch filters under control of the central computer and performs the time-consuming tasks of data sampling and simple manipulations of the sampled data,

d. The central computer which performs the more sophisticated data processing necessary to acquire Loran signals, track a reference point in each signal, and suppress interfering signals through digital detection and placement of notch filters.

Loran Subsystem - The Loran receiver has been designed to provide trouble-free operation in all of the known problem areas of previous Loran receivers. These include cycle selection, atmospheric noise, long and short delayed skywaves, break-lock during dynamics, and break-lock during refueling. In the past, Loran receivers have experienced severe break-lock problems when the aircraft hooked up to a tanker for refueling. Several steps were taken in the ARN-101 Loran receiver to prevent this problem. First, the H-field antenna used in the ARN-101 prevents the signal inversion that occurs due to the electrical center shifting when the tanker hook-up occurs. Second, a properly discharged aircraft and properly grounded antenna minimize the noise burst that the receiver sees during hook-up. Third, the ability of the receiver to operate in a burst-noise environment (whether atmospheric burst noise or due to tanker hook-up) further improves the ability of the receiver to operate correctly during tanker hook-up.

The three-axis H-field antenna system provides the receiver with nearly constant signal level under all aircraft attitudes. The axis that provides the maximum signal reception is continually selected for each station. This results in nearly constant signal reception even in aircraft maneuvers with up to 6-g turns, inverted flight, steep pull-ups, and steep dives. By placing the Z-axis on top of the F-4 aircraft tail, the receiver obtains Z-axis benefits even with low level (20 μV or less) noise conditions.

The Loran Receiver signal processor communicates with the central digital computer through a direct memory access (DMA) channel. This mechanization was selected so that replacement of the Loran preprocessor with other radio positioning aids such as GPS, JTIDS and DME could be accomplished with minimum impact on system architecture.

Weapon Delivery Management - The basic philosophy adopted in the system design was that of continuously anticipating and preparing for the earliest possible weapon delivery solution. To do this the most likely release condition is projected ahead of the aircraft and used in the ballistic range computation. (For the immediate release flight situation of the CCIP mode, the predicted release condition is at essentially zero range projection.) Three important operational advantages are derived from this design approach. An accurate pull-up cue(In Range) allows the pilot the option of a maximum stand-off range pull-up initiation. Secondly, the proper up-wind track offset for a pull-up delivery is provided -- thereby resulting in a nominal wings level pull-up. Finally, the weapon release time, which must be computed by up to 150 milliseconds early because of rack delay and computer cycle time, is based upon accurate extrapolation along the curved aircraft path predicted from the measured normal acceleration.

The pilot is allowed freedom in his vertical maneuvering for weapon delivery after the In Range situation cue is computed. Initially, a normal 4-g pull is assumed for the Blind and Dive-Toss modes since this would result in the earliest release. Following the In Range time, the predicted release condition is re-estimated continuously, in a smoothly changing manner, based on the currently measured normal acceleration. This anticipation of the probable release condition permits steering corrections -- for any cross-track error that develops -- to be made as early as possible. Prior to target designation in Dive-Toss, this adjustment will affect the aimpoint position slightly and after designation will affect the roll steering command. Besides allowing for any pull-up profile maneuver, a dive angle cue is provided for use in the Blind mode to show the allowable fixed dive angle to release. This ADI cue shows the dive (or glide) angle which, if followed, will result in a release just before obtaining the Break-Altitude cue pull-up warning.

Ballistic range estimation computations are performed by numerical integration every 200 milliseconds and adjusted through sensitivity coefficients every 50 milliseconds. Release time is quantized to 1 millisecond. A fixed number of integration steps (10) provide an essentially constant execution time for all weapons and all release conditions, including dual drag weapons. Particular features are that (1) there are only two basic drag vs Mach functions stored (low and high drag), and (2) each weapon is characterized by at least a drag scale factor, Mach bias shift, and drag bias shift coefficients. A standard Runge-Kutta numerical integration technique of second order is used to solve the ballistic differential equations in a three-dimensional, ground-referenced coordinate system. The size of the time integration intervals is individually controlled for best overall accuracy, and dual drag (e.g., cannister) weapons are accounted for by changing coefficients at the trajectory transition point. The weapon total drag at each step is a function of the total weapon speed relative to the local air mass, thus permitting wind variations with altitude. This approach is in contrast to the more usual approach of integrating in an assumed homogeneous air mass, and then compensating for an estimated, constant average wind vector.

The interactive control-display is configured to provide three complete, and separate, weapon release scenarios. Data for particular attack conditions may be inserted in three different software lists well in advance of the release time. This is a big factor in relieving crew workload in a high-stress situation.

Sensor Interface - The sensor interface philosophy adopted was to present an operating procedure to the aircraft crew that would be essentially common for any of the sensors being used. The prime purpose of providing the number of different sensors was to give the crew flexibility in the choice of device that would assist in target recognition, acquisition, and attack or reconnaissance. Considering the speed with which things happen in a 500-knot vehicle during a reconnaissance or attack scenario, simplicity and commonality in operating procedures is mandatory.

Manual slew and trim signals are provided from a single hand control in each cockpit. Sensor video or the radar image is displayed on the digital scan converter in each cockpit. The optical sight system is only in the F-4E forward cockpit. The function and operation of each sensor is described in the following paragraphs.

F-4E LCOSS - The Lead Computing Optical Sight System (LCOSS) provides an electronically controlled reticle which is optically displayed in the Aircraft Commander's line-of-sight. The Aircraft Commander uses this image as a visual sight for air-to-air guns, missile attack, and delivery of conventional weapons against a ground target. The LCOSS ARN-101-aided mode enables the Aircraft Commander to select targets or identification points visually and cue all other sensors to the selected ground point. The roll steering signals from the ARN-101 provide lateral steering information to the LCOSS when operating in the visual bombing or aided AJB-7 modes from the time the target has been designated until the weapon is released, provided the steering enable discrete is present. Steering signals are available for all navigation or blind bombing modes. The roll index is controlled to provide steering signals to the destination or to the identification point.

The aiming reticle is controlled in azimuth and elevation according to the delivery mode selected. Signals are obtained from the ARN-101 when in the LCOSS-aided mode. The reticle points to the current steer destination when in the navigation mode or to the cue point when in the Blind or LABS mode (LABS/WPN SEL switch in the OFF and navigation mode selected or the BLIND/LABS position, respectively) if it is within

the LCOSS field-of-view. The aiming reticle will be cued to the impact point when in the Continuously Computed Impact Point (CCIP), Guns, Rockets, or AGM-45 modes and to the aircraft velocity vector with crosswind drift correction when in the Dive-Toss mode.

The ARN-101 accepts trim signals from the forward hand controller to adjust the computed position of the LCOSS reticle when operating in the navigation or blind modes and the infrared Maverick video has not been selected for viewing in the forward cockpit. When the in-flight refueling (IFR) switch (located on the forward stick assembly) is depressed, the sight reticle will slew in response to the forward hand control inputs and the reticle will be ground stabilized by the ARN-101 to the position at which the inputs cease. The accumulated best estimate of offset position is available for cueing the other sensors. Release of the IFR switch causes the reticle to revert to the current steer destination.

F-4E TISEO - The Target Identification System, Electro-Optical (TISEO) provides a visual identification of targets beyond the visual identification range of the naked eye. The TISEO sensor is a narrow field-of-view television camera with the ability to lock-on to an image via a contrast tracker. Two high resolution axial-aligned vidicon cameras provide a wide angle and an optically magnified narrow angle field-of-view, thus providing a television display of an area in front of the aircraft for visual identification of selected targets. The television camera video outputs are applied to the radar set indicator which displays the selected field-of-view.

The Weapon System Officer (WSO) points the TISEO telescope, via the azimuth and elevation rate commands, to a ground point or an airborne target. The ground point selection is by manual or a combined manual and computer-aided operation. When a target has been identified and centered in the field-of-view by the WSO, he can have the TISEO lock-on to this image. When TISEO has acquired lock-on, it will no longer accept hand control or computer rate command inputs but continues to provide azimuth and elevation line-of-sight pointing angles to the radar set and the ARN-101. The ARN-101 will use the pointing angles to update a target position or update navigation coordinates. The forward and aft digital scan converters present a television display of either the spotting (side angle) or precision (narrow angle) video developed by TISEO.

The ARN-101 provides the means of quickly cueing the TISEO telescope to the cue point or target coordinates regardless of previous aircraft maneuvers (ground stabilized). The TISEO will be pointed by the ARN-101 to a ground point described by the stored coordinates. The aircraft position, altitude, ground track, roll and pitch angles are used to establish the pointing angles for ground stabilizing the telescope to the initial coordinates. The WSO in the aft cockpit can trim the ground point coordinates via the Pave Tack thumb control.

F-4E APQ-120 Radar - The radar (APQ-120) obtains signals from the air data computer, the Attitude Reference Bombing Computer Set (ARBCS), the ARN-101, and the TISEO. The ARN-101 signal data converter (SDC) -- in conjunction with the thumb trim control -- provides the signals to position the offset cursor and the range cursor (bombing range strobe) during the map and beacon modes, and the SDC provides the radar antenna pointing angles when the radar is in the air-to-ground mode. The radar video is displayed on the forward and aft digital scan converters. The Map-PPI sweep mode displays a range cursor (bombing range strobe) and an offset cursor that are automatically positioned over the target or identification point by the ARN-101. Cursors cannot be positioned or trimmed from the forward cockpit. If TISEO and Pave Tack power are off, the display automatically reverts to the radar display.

Maverick Missile - There are four types of Maverick missiles. Maverick AGM-65A/B are television-guided air-to-ground missiles with the ability to lock-on and track a target (light or dark) in contrast to the opposite (dark or light) background. The ARN-101 does not interface with either the A or the B missile.

The AGM-65C Maverick Missile is a laser-guided air-to-ground missile with the ability to lock onto and track an appropriately coded laser illuminated target. The target-reflected laser beam can be generated by the attack aircraft or by any available means. A synthetic scan is presented on the digital scan converter in either cockpit when laser weapon video is selected for display. The ARN-101 cues the laser receiver to a reference point, a cue/update point or a target as previously described, until laser lock-on has been achieved provided the Maverick is in the aided mode. ARN-101 cue signals will be ignored after laser lock-on.

The AGM-65D Maverick Missile is an infrared-guided air-to-ground missile with the ability to lock onto and track a target (hot or cold) in contrast to the opposite (cold or hot) background. The Maverick video display is an infrared (IR) image which is provided by a receiver located in the selected weapon. The display of weapon infrared is presented on the scan converter in either cockpit. In the Maverick-aided mode, the ARN-101 cues the missile IR receiver to a reference point, cue/update point or the target according to the rules described in a previous section. The missile cue point may be trimmed from either cockpit provided the IR image is displayed on the appropriate indicator.

Pave Tack - The Pave Tack target designator provides precision laser range and designation of ground targets under adverse weather conditions. It consists of a narrow beam laser transmitter, laser range receiver, and an infrared detector for target search and acquisition. The infrared detector has a wide field-of-view for target search and a narrow field-of-view for target identification and tracking. The laser and IR line of sight are controllable over the lower hemisphere of the aircraft.

The Cue mode points the sight line at a ground aimpoint designated by the ARN-101 to allow target acquisition. The sight line is stabilized to the aircraft velocity vector, cue/update coordinates, or target, depending upon the status of the IP insert and target insert switches. Offset coordinate calculations and navigation solution position updates can be performed via Pave Tack when in the Cue/Track modes. The ARN-101 will calculate offset coordinates via Pave Tack when Pave Tack is in a mode other than Cue and is

actively tracking, but the ARN-101 will not position update the navigation solution. The offset coordinates can be erased, stored, used as a Fly-To, or both stored and used as a Fly-To at the operator's option.

RF-4C Sensors - The RF-4C aircraft contains APQ-99 radar cursors and a Pave Tack sensor which can be individually selected for ARN-101-aided cueing to an operator-selected position. The offset and range cursors are in the aided mode whenever the radar video is displayed. The radar cursors are cued through the ARN-101 regardless of the mode selected for display; however, the cursors are not displayed in all radar modes. Initially, the ARN-101 cues the radar cursors to zero range and Pave Tack to the aircraft velocity vector. The displayed sensor may be trimmed from its reset or reference position by normal trimming procedures. The ARN-101 will stabilize the sensor trimmed to the position, with respect to the aircraft velocity vector, at which the manual trim input signal ceases.

The modified hand control contains a thumb trim control which, in conjunction with the action switch, allows the aft operator to trim the position of the aided sensor selected for viewing on the aft indicator. The thumb trim control is activated by pressing the action switch to half action and it remains active until a second sensor is selected for display or the reset switch is depressed. The full action position is used to initiate Pave Tack track. The operator selects the desired aided sensor for display on the aft digital scan converter, presses the action switch to half action, and applies pressure to the trim control to trim or reposition the sensor cue point. The ARN-101 will ground stabilize the sensor to the point at which trim inputs cease if the IP insert and/or target insert is set. In general, the manual update of a sensor's cue position from the aft cockpit is accomplished by pressure on the thumb trim control when the sensor is in the aided mode and displayed on the scan converter. There is no sensor updating from the forward cockpit. The forward cockpit left indicator displays radar video and radar cursors, while the right indicator displays Pave Tack video. The aft indicator displays both radar video and cursors or Pave Tack video.

Pilot-System Interaction - Considerable effort was devoted in the design of the ARN-101 to providing both crewmen with a fully integrated set of tactical navigation controls and displays. The system performs all the computations of a standard navigation system, and considerably more. With the addition of a narrowly bounded position error furnished by the Loran capability and an integrated general-purpose computer with good aircrew controllability, the design of a much more capable and useful navigation system has been accomplished.

The flexibility of the system in the tactical situation is the result of the interactive input/output control-display concept. Two units in the aft cockpit -- one a digital display indicator with a three-line 24 alphanumeric character readout, and the other a keyer control with a 36-push-button, full alphabet, 10-digit keyboard -- are software controlled to operate as interactive terminals to guide the Weapons System Officer through a number of data lists. The control-display design is highly flexible. With no change to hardware components, display capabilities are easily expandable to include parameters of special interest to specific applications. The modularity and structured design of the software controlling the display promote simple alteration of display sequences for new parameters of interest. The overall system design is thus an efficient solution to the complex display problem and also can support system growth with only simple software changes.

The major data entry and management tasks that the WSO must perform will normally be done during preflight. At this time the WSO will use the interactive list control features to either enter or accept previously entered data for the flight plan variables. Simple sequencing with the skip key provides a succession of flight plan variable names and variable values to be accepted or changed. In this manner the "checklist" is built into the computer program and the WSO can be sure that no variable has been neglected. Data lists requiring preflight management are the ground update list for system initiation, destination data for later selection by destination number, Loran chain data, and weapon delivery definition parameters. Occasionally the data in these lists will be checked or modified while in flight, but generally there will be no requirement for any extensive data insertion while airborne.

While flying, the WSO will be using the ARN-101 to perform tactical navigation. For the great majority of time this flight-following assistance will be done using the display-only flight data list as selected on the keyer control. Eleven keys allow instand selection for display of 11 pairs of variables such as computed wind, TAS, time-of-day, glide path error, as well as more common position, velocity, and flight path to destination data. Thus, while flying, the WSO will be using the ARN-101 for convenient display of flight variables in monitoring progress of tactical navigation. In addition, simple means of commanding new flight destinations and weapon delivery parameters are provided.

An auxiliary digital display indicator is provided for the Aircraft Commander in the forward cockpit to advise him on specific parameters pertinent to mission progress. This added display significantly decreases intercom chatter between cockpits.

The major navigation position and computed flight director information displays are furnished to the Aircraft Commander on his ADI and HSI in exactly the same manner as he has been used to. Thus, the ARN-101-computed bearing and range as well as cross-track error and course to the selected destination are displayed on the HSI with flight director commands on the ADI.

The WSO has a similar, but more limited, navigation display on his bearing-distance-heading indicator (BDHI). Although the ARN-101 adds several panels and displays to control the total capability of the system, all other aircraft instrument interfaces have been maintained with their normal displays.

DEPLOYMENT STATUS

The production installation activity has been initiated by Ogden Air Logistics Center, Hill Air Force Base, Ogden, Utah. The Class V modification contractor was selected in March 1977 with the proof-kit installations scheduled in the September to December 1977 time period. Production retrofit installations are scheduled for RF-4C and F-4E aircraft in the European, Pacific, and Continental U.S.A. theatres starting in September 1978.

A second effort has been proceeding to provide Intermediate and Depot Level support equipment and spares on a schedule that supports USAF organic capability in the September, 1978 time frame. Organizational Level operations are performed entirely with an on-aircraft software built-in-test program that isolates to the line replaceable unit. The Intermediate Maintenance Electronic System Test Set contains diagnostic software to isolate the problem to the replaceable printed-circuit card. The Depot Test Station then examines each of the cards for the failed component.

The present production contract provides for the delivery of Intermediate and Depot Level support equipment and spares, while the Class V Modification contract supplies updated Technical Order documentation.

RESULTS

The objectives of the original development were met. The AN/ARN-101(V) is a system with a high degree of accuracy, flexibility, and expansion capability which, in turn, is the basis for accurate reconnaissance and weapon delivery operation in the RF-4C and F-4E aircraft.

- The system has demonstrated a weapon delivery accuracy less than 7 mils circular error probability (CEP) for the visual delivery modes.
- Target acquisition, identification, and tracking performance has been greatly improved by the sensor management capability.
- A free-inertial navigation capability with errors less than 1.0 nmi/hr CEP and velocity errors less than ± 4 ft/sec have been achieved with either ground or Kalman filter airborne alignment.
- The F-4 capability is improved by adding a Continuously-Computed Impact Point (CCIP) mode and allowing as nearly an unrestricted envelope of weapon delivery flight profiles as possible.
- All F-4E air-to-ground visual modes are uncanned. The CCIP accuracy provided is 2-to-1 better than the requirement, and both delayed and immediate release submodes are supplied.
- Improvement in the Loran antenna/receiver to maintain lock-on through high dynamics in poor signal conditions, and to function in a sophisticated electromagnetic environment has been achieved.

Coupled with the reliability and maintainability improvement of the ARN-101 over the present F-4E avionics, the operational capabilities and service life of the RF-4C and F-4E are extended, making them versatile and cost effective strike and reconnaissance aircraft for many years to come.

4D APPROACH CONTROL USING VOR/DME/ILS GUIDANCE

by
Dr. Juergen M. H. Bruckner and Thomas G. Sharpe
Advanced Technology and Engineering
Collins Avionics Division
Rockwell International
Cedar Rapids, Iowa 52406 U.S.A.

SUMMARY

This paper presents the results of a study to design, develop, and implement a 4D approach control system using conventional aircraft sensors and displays augmented with area navigation capability. The goal was to arrive at a system capable of retrofit with most air transport aircraft. Multifunction CRT (MAP) displays and inertial complementation were to be avoided. The only additional equipment item required in the final design is a Mark II type RNAV system capability used specifically to automatically define the nominal multiple-ordered-leg 4D RNAV approach path. The capability for close-in ILS captures (including those from above) was also included to allow for diverse aircraft separation and noise abatement requirements.

INTRODUCTION AND CONCLUSION

With the expected increase in air traffic, more precise control of aircraft in the terminal airport area is required if intolerable delays are to be avoided. The situation is compounded with increased utilization of heavy aircraft requiring increased separation from other aircraft to avoid wake turbulence; the increased average separation results in decreased air traffic capacity. Computer aided time control is expected to be the major source of increasing airside capacity under IFR conditions.[1] Two approaches to time control which the FAA is studying are automated metering and spacing using ground based computers and area navigation using airborne computers.

As part of this activity, the FAA in February of 1973, awarded a contract to Rockwell International, Collins Avionics Division, to investigate the application of three- and four-dimensional (3D/4D) airborne navigation concepts in the airspace with particular emphasis on the terminal area. Reference 2 documents the results of the initial study and simulation effort. Significant conclusions reported were: 1) metering and spacing with area navigation results in the most precise control of aircraft, 2) delivery errors less than 10 seconds (1σ) were feasible over a wide range of aircraft/equipment complements, and 3) precise time control to the outer marker and beyond requires simultaneous use of final approach guidance (ILS or MLS) and of VOR/DME based RNAV guidance.

The initial system design was modified to eliminate certain deficiencies observed during the Phase I simulation effort. The time control algorithms were desensitized resulting in much smoother speed commands and better control throughout the approach. An automatic base offset procedure was also incorporated to allow for simple, less blunder prone base leg extensions. Finally, the capability to capture and track ILS beams while under RNAV (time control) guidance was included. With this system, terminal area time control procedures can be conducted anywhere from initial approach fix to touchdown.

The simulation effort verified that significant improvements in final delivery accuracy can be achieved under suitable RNAV aided time control. Under autopilot control, tight 4D tracking is possible throughout the approach. The major contribution to delivery errors is the non-stationary nature of the prevailing wind. The 4D flight control errors are as low as 3-5 seconds (1σ). These numbers do not include wind shear effects which were not modeled. The ability to predict and compensate for wind shear effects has not been determined.

The study verified that ILS captures through the RNAV system can significantly improve capture performance and reduce pilot work load provided proper operational techniques are utilized. The RNAV defined path must be made to intercept the ILS defined path in the presence of navaid error. If the paths do intercept, close-in ILS captures are ensured. Improvements in ILS tracking result from the ability to linearize the beam data.

TIME CONTROL SYSTEM DESIGN

Many definitions can be offered on what constitutes a 4D Air Traffic Control System. Certainly the manual systems in use today control aircraft position, velocity, and time. However, for this discussion a 4D control system assumes that computer assisted time-of-arrival computations are performed - hopefully to better manual system performance.

The exact form of these computations is quite flexible. It would appear that the computer-aided time control system would monitor the airport acceptance rate, sequence aircraft on a (nearly) first-come-first-served basis, calculate the estimated time of arrival (including delays) of all aircraft in the system, and possibly aid in metering and spacing the aircraft. The latter task would include determining a departure time from the holding fix and assigning an arrival route to adjust for the remaining required delay. Since this task would require various sophisticated decision making capabilities in a computer, tasks most successfully performed in the past by the controller, the best man machine allocation of tasks is difficult to predict: a completely manual system would not take advantage of the rapid computational capabilities of the computer while a completely automatic system would still require the controller (and, of course, the aircraft pilot) to understand the computer decisions.

On the other hand, it would appear that the level of metering and spacing automation is not a dominant factor in the design of airborne time control procedures and equipment complement. Automation will affect the precision of the time control commands and thus affects total timing accuracy. However, the level of ground based metering and spacing automation has no affect on how well the pilot can control his aircraft to meet the controller requests. What is of concern in airborne system design is the controller and pilot/aircraft command and response loop. Since the controller must understand the control strategy to be followed and communicate the pertinent information to the pilot, similar commands should be used in both manual and semiautomated metering and spacing environments. Efficiency, capacity,

and safety may be improved with computer aiding, but airborne equipment design is essentially independent of the overall metering and spacing technique.

The basic airborne system must provide for easy insertion and execution of an ATC-assigned, delay free, nominal arrival profile and for impromptu modifications to that profile to compensate for system delays. Using area navigation (RNAV) equipment, the nominal profile can be specified by means of standard 4D RNAV STAR consisting of 3D waypoints with assigned speeds. The delay is allocated between the time to be spent at a holding fix and the delay to be absorbed during the approach. The latter delay is used to specify the 3D RNAV flight path modifications as delay fans, base leg, extensions, and speed assignments. Nominal speed assignments could be taken care of by including them in the RNAV STAR. Speed modifications would then be handled in the same manner as flight path modifications.

In general, both speed and path modifications would be required since speed control alone is insufficient for providing adequate spacing particularly when tracker velocity is only good to 20 knots, 1σ (ref. 3). In contrast, the on-board RNAV system can maintain less flight technical error and better velocity control (down to 5 knots 1σ) provided the on-board avionics can easily handle impromptu RNAV route and airspeed changes. With on-board time control, ground speed can be controlled so that the ground based and airborne systems have equivalent speed data.

The authority over path and speed changes from nominal is the subject of much concern. In general all systems have assumed that when the deviation from nominal is small, slight speed deviations from nominal are commanded to return to schedule. When it is not possible to meet the schedule by slight speed changes, then extensive path or speed modifications from nominal are required. Here one sees two schools of thought. The first allows the airborne system to independently choose a new speed/path profile to return to the nominal while the second assumes that all extensive path and speed modifications must be performed by ATC. The latter position is taken because flight profile assignment must be based on the position of all aircraft in the area and cannot be based on solely arrival time at a given fix. In addition, since monitoring of system performance is the responsibility of ATC, ATC must maintain knowledge of all flight paths. Aircraft/ground flight profile verification is therefore required regardless of where the flight profile is chosen. Since ATC is responsible for time assignment (which requires knowledge of all aircraft and their potential path assignments) it is reasonable to assume that path modifications should also be made by ATC to obtain non-conflicting flight profiles. If these were then communicated to the pilot, it would eliminate the need for a multiplicity of airborne equipments performing the same function with no apparent increase in system performance.

Because of these reservations about on-board flight profile selection, the analysis and simulation done in this program assumed that the entire flight profile, including expected time at the time-fix, is assigned by ATC. The airborne system would attempt to fly this profile in a closed loop fashion.

The aircraft's estimated time of arrival at a designated approach fix (initial, final, or intermediate) would be communicated to the pilot. The pilot could use this time to make minor airspeed modifications to assist in obtaining the expected time of arrival. Controller/pilot communication would be kept to a minimum. Except for ad hoc variations to reflect changing conditions or "fine tuning", the entire a priori arrival route would be known by both pilot and controller. The use of a nominal 4D RNAV STAR (3D fixed path plus nominal speed assignments) would limit communication to the STAR name; adjustments would then be by exception instead of by rule. In addition, these exceptions need not be communicated at the precise moment of path adjustment, but at any time prior to the required modification, thereby reducing the possibility of improperly timed path modifications.

The preceding paragraphs described the airborne/ATC interaction. The ATC system was given a great deal of flexibility in assigning flight profiles. Manual (controller) intervention and a minimum of pilot/controller communication were assumed although a data link capability could also be used. The same degree of flexibility is required in the airborne system design to allow for a near term implementation in most aircraft with a minimum of retrofit.

The following guidelines were therefore established for the airborne time control system design:

- Rely, as much as possible, on existing RNAV procedures and equipment so that a minimum of new control/display functions are required.
- Permit a simple definition and communication of 4D clearances by the controller and easy understanding and execution of these clearances by the pilot.
- Not produce operational penalties for different classes of RNAV equipment users provided their equipments meet the minimum operational requirements.
- Increase pilot's awareness of position/time error and allow anticipation of speed/path changes.
- Be compatible with existing RNAV charting formats.
- Reduce communication so that speed/path reclearances are only given for conflict resolution, safe operation, or time reassignment that would result in significant traffic flow advantages.

Several different flight path and speed control procedures were studied to determine a suitable minimum complement for 4D control. The following procedures were chosen from this study. The 4D procedures developed require cockpit controls/displays that allow the following.

Presetting the WAYPOINTS of an RNAV STAR

For a minimum system, this would probably involve manual entry of the STAR waypoints in terms of bearing/distance from the terminal area navaid to be used, navaid tuning (and station elevation entry for slant range correction), and entry/selection of course to each waypoint as it was selected for use. For a transport type system, waypoint entry is accomplished by selection of a STAR from a list of available STAR's for the particular airport. The STAR selection would produce a list of identifiers of waypoints in the STAR, altitudes, and nominal leg speeds. With the minimum RNAV equipment, leg speeds and waypoint altitudes would only be available on the RNAV approach chart and entered manually into the RNAV control unit.

Establishing a Course From Present Position DIRECT TO Any Waypoint

This capability is available in most RNAV equipment. For the systems with a manually driven course arrow, the specified waypoint is selected and the course knob is turned until cross track deviation is zero. In the systems with a servoed course arrow, an AUTO COURSE or DIRECT TO switch is provided to slew the course arrow to the zero crosstrack deviation position. The DIRECT TO function in the RNAV environment is used to establish an impromptu track through a waypoint for purposes of shortening the nominal RNAV route. The procedure is shown in Figure 1. If a delay fan is required from path A to C, the aircraft proceeds to B until cleared to proceed DIRECT-TO C a specified distance prior to B; if no delay is required, waypoint B is merely deleted from the flight plan.

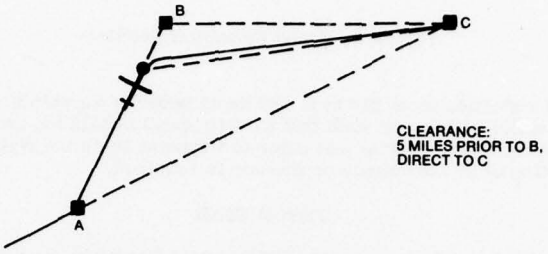

Figure 1. Delay Fan Using Delay Waypoints and DIRECT-TO Procedures

Defining A Base Leg Extension

Figure 2 illustrates a base leg extension typically used for final sequencing and spacing. Depending on the RNAV equipment not all turnpoints need be waypoints inserted into the RNAV equipment. In general, the base leg does not

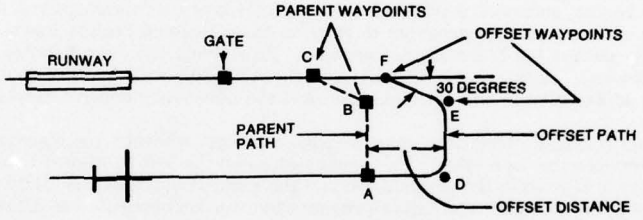

Figure 2. Base-Leg Parallel Offset

intercept the final approach course, but transitions into a more shallow intercept leg to avoid overshoots. Note that on an extension the intercept leg offset is different from the base leg offset. For transport systems with leg-at-a-time offset capability this poses no technical problems. For minimum systems with only a single parallel offset capability, the best procedure utilized was to fly the base leg under RNAV parallel offset guidance and intercept the localizer using heading. It was also found that for the transport system, a base offset procedure which automatically offset the legs in the proper direction upon insertion of the base leg extension yielded the best performance at a minimum of complexity.

Entry of GMT and Time Assignment

The time control systems require a real-time clock on-board the aircraft. Time is input either by the pilot prior to entry into the area or by interface to a ground station clock.

The capability to enter the desired time of arrival (DTA) at any waypoint is required. For minimum capability systems capable of only defining legs, the speed commands derived from a DTA input will be applicable only to the leg to the time fix. For a transport system with route definition capability, the speed commands can be defined for all legs to the time fix.

Control of Leg Speed

In order to minimize communication requirements and to maintain aircraft separation, speed assignment on each leg of a STAR should be part of the STAR definition and speed reclearances would be given to aircraft only on an as required basis. For a minimum capability system, leg speeds would only be available from the RNAV approach chart, while for more sophisticated equipment leg speeds should be stored as part of the STAR definition just as waypoints and altitudes are stored. The pilot would have the capability to edit these leg speeds in the case of speed reclearance. In the speed command algorithm for systems that compute time error over several legs, leg speed is an integral part of the calculations and thus must be available in the computer for each leg on which time error is based. Thus, when waypoints are added to the 4D flight plan, leg speed should be provided either by pilot entry or by interpolation of prior and subsequent leg speeds.

The interpolation procedure chosen assumed that all speed changes are accomplished at the rate of 40 kts/minute just prior to the arrival of a speed control waypoint unless a higher rate is required in which case it is chosen. The two situations are depicted in Figure 3.

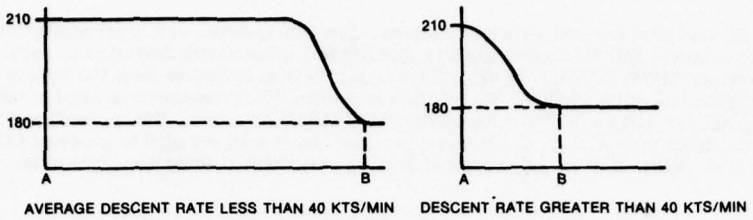

Figure 3. Speed Reduction Profiles

The figure depicts a speed reduction from 210 kt to 180 knots between waypoints A and B. In the situation depicted on the left, the leg distance is sufficiently great such that the 210 speed is held for most of the distance and then the aircraft shows to 180 at the rate of 40 kts/minute just prior to waypoint B; on the right, the leg distance is so short that an immediate speed reduction of 40 kts/minute or greater is required.

Typical STAR

The procedures were investigated using a proposed 1983 Denver Terminal Area RNAV route design. Figure 4 illustrates the southwest RNAV STAR called BRAND. A delay fan and path shortening area are provided early in the approach for initial path adjustments. Base leg extensions are used for fine tuning prior to final approach. Nominal airspeeds consist of entry at 250 knots and a slowdown to 210 knots somewhere in the delay fan prior to DOWN. The 210 knot clean aircraft configuration airspeed is maintained until the turn to base leg. The slowdown to final approach speed is provided just prior to the localizer capture leg. Speed changes are assumed to occur at the rate of 40 kts/minute and effected prior to crossing the waypoint.

Time Control Equipment Complement

The Collins ANS-70A Automatic Navigation System was used as the basis for the time control system design. An operator's guide for this system is listed as reference 4. The system utilizes a general purpose computer and CRT control/display unit. As a result, software modifications were relatively straightforward. A limited production version of the 8564B computer was utilized for this program to provide the additional sensor inputs required for the analog display of the speed commands and for the ILS capture/tracking. Effectively the only difference is in the Aircraft System Coupler (the input/output device). Software modifications to the ANS-70A software for emulating an air carrier level 4D system were limited to adding a time control algorithm and the necessary control display capability.

The 70A system utilizes an interactive time shared "page concept" whereby the appropriate CRT page presentations are called into view by operator selection. The presentation on the left in Figure 5 depicts the Flight Plan Page upon actuation of the FLT PLN key while the presentation on the right illustrates the additional data called into view by actuating the upper right lever switch. The latter presentation was incorporated to allow for entry/display/modification of the speeds at waypoints.

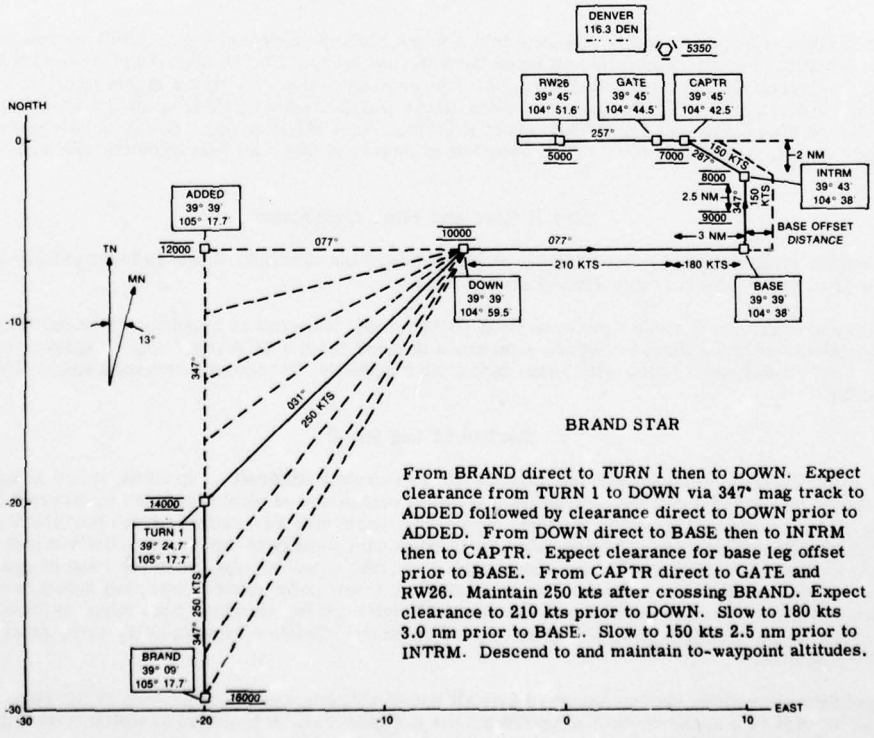

BRAND STAR

From BRAND direct to TURN 1 then to DOWN. Expect clearance from TURN 1 to DOWN via 347° mag track to ADDED followed by clearance direct to DOWN prior to ADDED. From DOWN direct to BASE then to INTRM then to CAPTR. Expect clearance for base leg offset prior to BASE. From CAPTR direct to GATE and RW26. Maintain 250 kts after crossing BRAND. Expect clearance to 210 kts prior to DOWN. Slow to 180 kts 3.0 nm prior to BASE. Slow to 150 kts 2.5 nm prior to INTRM. Descend to and maintain to-waypoint altitudes.

Figure 4. BRAND STAR

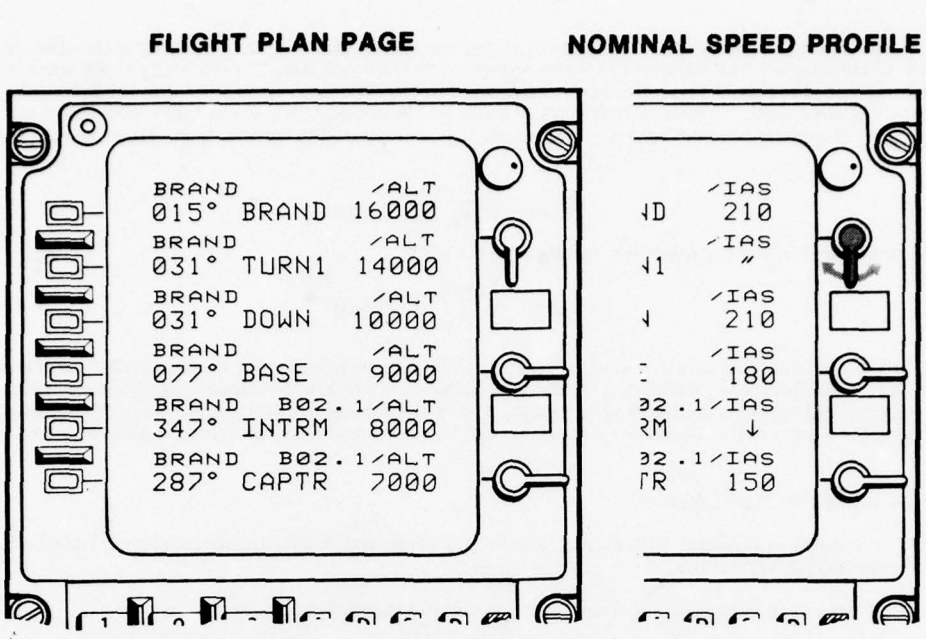

Figure 5. Alternate Flight Plan Page Presentations

Ditto marks (") below the IAS for TURN 1 indicate that no speed has been entered for TURN 1 but that the internally computed speed for TURN 1 is the same as for BRAND. The downward pointing arrow (↓) below the IAS for INTRM indicates that no speed has been entered and that the internally computed speed profile requires a speed reduction from 180 to 150 knots through this waypoint. Similarly if an acceleration were required, an upward pointing arrow (↑) would be shown.

Any base offset data is inserted and presented on the flight plan page. In Figure 5, BØ2.1 indicates that a 2.1 nmi base leg extension is to be flown. The offset legs are to waypoints INTRM and CAPTR. The offset was entered at INTRM. It can be deleted at INTRM or CAPTR by entering BØ or by means of a DIRECT TO procedure to any waypoint beyond BASE.

The progress page (PROG) of the -70A system was modified to allow for insertion of the time fix and desired time of arrival data and display both the commanded IAS and the EARLY/LATE data. Data/label lines 5 (which normally display HDG CMD and REQ. V<) now display the following format (Figure 6).

Under IAS on the left, 180 represents the nominal airspeed over the leg as given in the flight plan. The commanded airspeed is equal to the nominal until entry of a valid DTA/waypoint-in-the-flight plan in the TIME/WPT data lines. Following valid data entry, the display could look like that depicted on the right. The display indicates that the IAS required to meet the DTA at the time fix GATE is 165 knots and that the present airspeed is such that the expected time of arrival is 1.2 minutes late. The error (given as EARLY or LATE) is given in minutes and tenths of minutes.

The speed commands are also displayed on the IAS indicator and the ADI. The servoed bug on the IAS indicator is driven to the commanded IAS. The SLOW/FAST needle on the ADI is driven by the difference between the commanded IAS and the actual IAS. A 15 knot full scale deflection provided acceptable range and resolution.

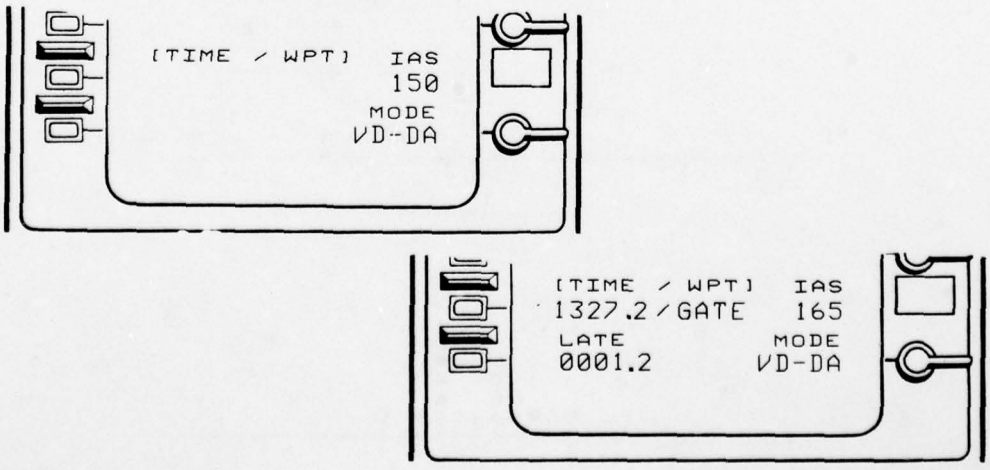

Figure 6. Time Fix and Commanded Airspeed Presentations

The RNAV computer generates the commanded IAS and early/late data by first computing the time to reach the fix at the nominal airspeeds. The assigned IAS are converted to TAS and added to the along track wind component resulting in a ground speed for each leg. After compensating for the difference in leg lengths for turns, the nominal time-to-go (TTG) is computed. If the nominal TTG is equal to the actual TTG, the actual commanded IAS is set equal to the nominal IAS. If not the percent overspeed for each leg is computed to arrive at the fix on time. Hence:

$$V_{COM} = \frac{TTG_{NOM}}{TTG_{COM}} V_{NOM} \qquad \text{Eq. 1}$$

Similarly to compute early/late the following relationship is used

$$TTG_{ACT} = \frac{V_{NOM}}{V_{ACT}} TTG_{NOM} \qquad \text{Eq. 2}$$

This relationship resulted in much smoother performance than trying to meet each waypoint on schedule internally computed from nominal TAS, estimated winds and position. With this technique navigation and wind estimation errors are not amplified early in the flight plan as they are in the former strategy. The resultant timing errors at intermediate waypoints turn out to be far less also because the commands are not cyclic. This will be seen in the following section.

TIME CONTROL COCKPIT SIMULATION

The real time cockpit simulation utilized the Denver Southeast and Southwest approaches. A total of eight different types of approaches were flown.

On the BRAND approach with base leg extension, the phraseology used upon entry was:

> "ATC clears Gulfstream N71CR to Stapleton Airport via BRAND RNAV arrival. Reduce airspeed to 210 knots 5 nmi prior to DOWN. Expect crossing GATE at (present GMT + 14.3 min) Zulu."

After passing DOWN the base leg extension was given as follows:

> "ATC reclears N71CR on 1.1 nmi base leg offset. Expect crossing GATE at (prior time + .7 min) Zulu."

Note that a minimum of additional communication is required over the RNAV route description and far less is required compared to a typical vectored localizer intercept.

Histograms of the timing errors are shown in Figure 7. Timing errors at LOCAL (for the SIMOL approach) and at INTRM (for the BRAND approach) represent timing errors at an intermediate fix just prior to final approach spacing. The errors are significantly less than the errors experienced in the earlier 3D/4D study.[2] The 4D system errors at the intermediate fix were reduced from $[\mu = -0.5, \sigma = 9.7]$ to $[\mu = 4.4, \sigma = 4.6]$ where the tupplet $[\mu,\sigma]$ represents the mean and standard deviation in seconds. It was felt that the new time control algorithm was smoother throughout the approach so that the pilot actually tracked the command instead of filtering the command via a built in lag. Basically the commanded airspeed in the phase 1 experiments indicated a large cyclic error while in this phase a cyclic error pattern was unnoticeable and the airspeed commands appeared to be monotomically decreasing (as they should). In addition, the present simulation did not include any wind shear experiments and hence wind estimation errors were not biased.

The timing errors at GATE for the 4D system were reduced from $[\mu = 4.7, \sigma = 5.4]$ to $[\mu = 0, \sigma = 2.8]$. This is again attributed to the smoothness of the time control algorithm. In the phase 1 experiments, erratic commands appeared while passing waypoints. A smooth command on the BRAND approaches was received only after passing waypoint CAPTR and following a 10-second update cycle; thus only 26 to 36 seconds of smooth command data was available. The present algorithm does not concern itself with non-time control waypoints, and hence its performance is not limited by a short leg to the time fix.

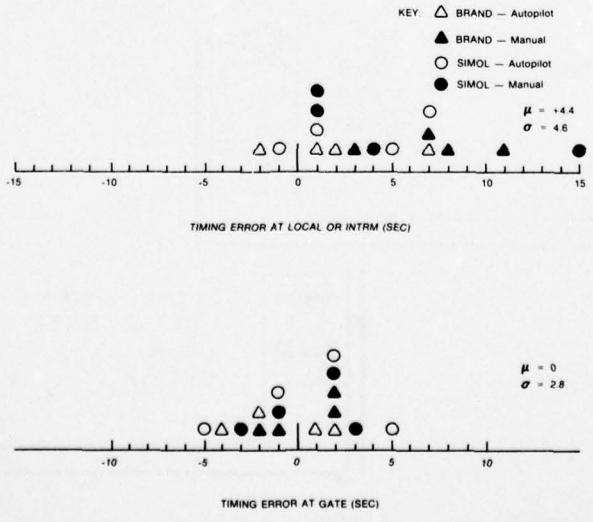

Figure 7. 4D System Delivery Errors

The experiments did not reveal any significant time control difference between runs with FAST/SLOW analog data on the ADI and without the data. While this is true in simulated performance, in practice a large difference is predicted. The pilots almost never looked down on the CDU with FAST/SLOW on the ADI, resulting in a significant decrease in workload. Nominal speed changes over a leg were easily monitored without the need for an alert light. FAST/SLOW was the basic display used both far out in the approach (less sensitive to small velocity changes than EARLY/LATE) and near the GATE provided approach speeds were not violated. While EARLY/LATE was helpful in the latter region as a performance measure, FAST/SLOW was still the more adequate command display. Both pilots recommended this display as the primary time control display.

There was no appreciable difference in delivery errors at the GATE under autopilot or manual (flight director) control. The workload was low enough for an experienced pilot to manage closed loop control of path and speed given the present information. However, it is possible to stay closer to the nominal 4D path over the entire approach while under autopilot control as workload goes down appreciably. The pilot can then temporarily override the speed control commands when off nominal to return to the nominal speed profile. For example, assume that the nominal leg speed is 210 knots, the commanded and actual airspeeds are 205 knots (and hence early/late is 0). This implies that the aircraft is slightly ahead of schedule (205 commanded vs. 210 nominal) but by maintaining the present speed reduction the aircraft will cross the time fix on schedule. If the indication is steady (implying wind shear or navigation errors are not disruptive), the pilot can return to nominal schedule by further reducing his speed (EARLY/LATE will temporarily indicate LATE) until the commanded airspeed is 210 knots at which time actual airspeed is increased to 210 knots and LATE returns to zero. The aircraft is now predicted to be back on schedule both at the time fix and also at its present position. The additional workload associated with this activity was possible only during autopilot controlled experiments.

Two procedural items which were deemed highly desirable during this phase were the limited required speed data insertions and the procedural RNAV base leg extensions. The speed entries were limited in number to the actual number of different speeds used during the approach. The speeds were entered at existing 2D or 3D waypoints - additional waypoints at the start of the speed reduction need not be created. Hence navigation was maintained to the normal 2D or 3D waypoints, thereby reducing both pilot workload and blunders during data insertion and navigation.

Base leg extensions were previously flown by means of leg-at-a-time offsets for the 4D system and by parallel offsets for the 2D system. When shallow course intercepts were flown with the 4D system, offsets on two legs were required. This was cumbersome and blunderprone. The use of a single base offset entry without the need to specify right or left resulted in an acceptable base offset procedure.

3D/4D ILS COMPUTATIONS

Area navigation aided ILS localizer and glideslope capture and track laws were also developed to provide final approach capability for the 3D/4D system. Lateral and vertical steering commands are provided by the RNAV system prior to ILS capture. The control laws provide an automatic, smooth transientless capture of the ILS beams with automatic adaptation for varying airspeed, wind, and beam angles. In addition, the system accommodates beam intercepts from above or below. The technique developed assumed an integrated RNAV/ILS flight computer, but could be readily adapted to separate RNAV and flight computers with minimal interface requirements.

Lateral Control Laws

There has been interest for some time in using RNAV derived data to aid in localizer captures. Localizer capture algorithms in general suffer from two important disadvantages. Without an area navigation system range information is not generally available, hence the capture law is usually optimized for a given range and performance degradation occurs on either side of the optimum range. The second difficulty is that the localizer beam provides angular deviation from a reference centerline. Hence as one moves closer to the localizer antenna, the "beamwidth" of the localizer beam in distance units (e.g., ft.) grows smaller. Thus the available space to execute a turn onto final course once the beam is intercepted shrinks rapidly. As an example, the turn radius associated with 30° of bank at an airspeed of 200 ft/sec implies that for a 90 degree beam intercept, centerline overshoot will occur at ranges shorter than 7.6 nmi from the localizer antenna, assuming capture starts (with instantaneous 30° bank) at 200 μA deviation. At higher airspeeds the minimum range without overshoot will increase. An RNAV system offers potential alleviation of this situation by permitting the initiation of capture prior to beam intercept thus avoiding the geometry limits described above.

The RNAV position and velocity errors, however, are such that if care is not exercised, a capture initiated on RNAV data may turn short missing the beam entirely or such a capture may turn late resulting in gross overshoots. One potential solution would be to never turn to a lesser course cut than 45° before intercepting the beam. This works well in terms of localizer overshoot but results in two distinct "up-down" bank commands or a "double bank" characteristic which is considered by some to be objectionable. An alternate approach is to always initiate the RNAV aided capture with maximum available bank command (e.g., 30 degrees), but to start fading the bank command almost immediately so that hopefully a smooth blend with beam based bank commands at localizer intercept results. The latter approach has a more desirable bank characteristic but appears to pose formidable difficulties in properly programming the bank command fade in general.

The approach discussed here avoids the double bank characteristic, uses an adaptable initial bank command (i.e., not always 30 degrees), and provides a solution to the bank command fade problem in the case where the system is tending to turn short of the beam.

Figure 8 illustrates three potential situations that may occur when performing an RNAV aided capture. For convenience they will be referred to as the "turn short", "good data," and "turn long" cases. For captures with trip point within the beam, as shown in the fourth case of Figure 8, no RNAV aiding is needed. Also shown in Figure 8 are the required bank traces for each case if a successful capture is to occur. The following argument serves to validate the selection of these three RNAV aided cases as basic.

If one is to start the capture based on RNAV data, one has no choice but to establish a trip point algorithm based on RNAV data and consequently must design a system to be tolerant of trip point shifts due to RNAV errors. Not only cross track distance errors but also velocity errors will affect the trip point computation. Assuming a constant bank capture algorithm, the three possible situations that may exist once an RNAV aided capture has begun are shown in Figure 8. The "turn long" case is critical in terms of amount of bank command to use. If the system is turning long

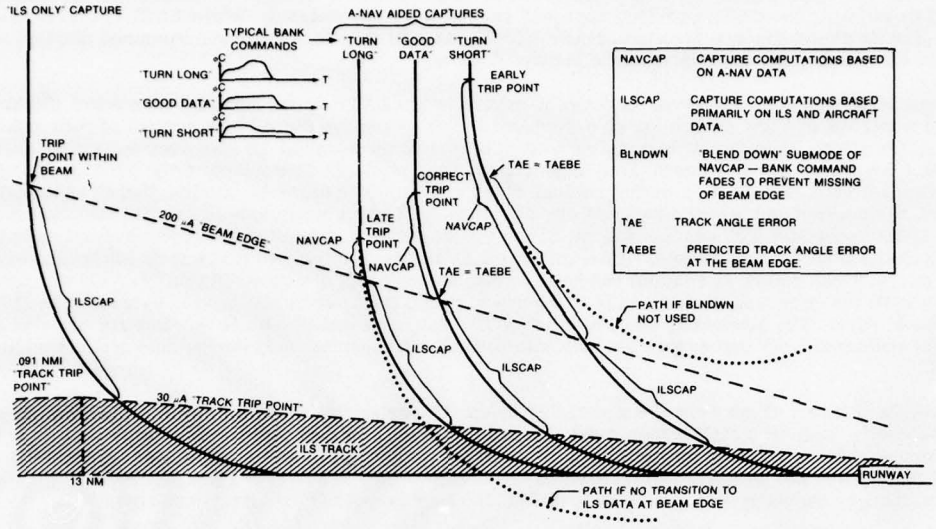

Figure 8. Area Nav Aided Localizer Capture

then a "reserve" of bank command must be available (once beam data is present) to increase the bank command to the required amount. Hence the nominal bank in a RNAV aided capture should not be as great as the bank command limit (normally about 30° in transport aircraft). Note, however, that this is not an absolute constraint but rather a consequence of the strategy being considered here. One could always force the system to "turn short" (see below) and thus avoid the "turn long" case entirely, but the strategy adapted here seems more natural to the author. In summary, the approach adopted is to leave some room for bank to increase in case the "turn long" case occurs.

The other situation that can occur is the "turn short" case. Here the beam could be missed entirely (i.e., beam intercept might not occur). To guard against this situation, some means must be present to detect when the system has turned far enough. The approach here restricts minimum course cut relative to the beam, but conditions the permissible minimum course cut based on the state of the system and provides a precise bank command fade algorithm which is a function of the computed minimum course cut. This will be discussed in more detail below but in the "turn short" case a "blend down" algorithm must be provided to prevent turning parallel to the beam and to smoothly transition computations to beam based data.

The need for a blend-down algorithm arises in the "turn-short" case. There are two aspects of the blend-down problem; when should the blend-down be initiated, and how should the blend-down be programmed?

The first of these questions requires addressing the problem of "when has the system turned far enough?" The system will execute an approximately circular turn onto final course if the bank command (BNK.CMD) obeys the relationship

$$BNK.CMD = \tan^{-1}\left[\frac{V_g^2 * (1 - COS(TAE))}{g * CTD}\right] \qquad \text{Eq. 3}$$

where V_g is ground speed, TAE is track angle error or angle of ground velocity vector relative to the runway centerline, CTD is cross track distance to localizer centerline, g is gravitational constant (32.17 ft/sec^2), and consistent units are assumed. Equation 3 holds through the entire capture maneuver; and if all assumptions are satisfied, TAE and CTD change in such a way that BNK.CMD remains constant, assuming no wind. If there is a wind, the bank must change during the capture in order to maintain a circular track over the ground.

In particular, for a capture initiated outside the beam on RNAV data and neglecting wind for the moment, Equation 3 should hold at the instant of beam intercept. Now at beam intercept, knowledge of range and localizer deviation (LOC.DEV) permits computation of cross track distance at the beam edge (CTDBE). Further, since V_g and BNK.CMD are known, track angle error at the beam edge (TAEBE) can be computed by solving Equation 3 for TAE as

$$TAEBE = COS^{-1}\left[1. - \frac{g * \tan(-BNK.CMD) * CTDBE}{V_g^2}\right] \qquad \text{Eq. 4}$$

where CTDBE = Range * Sin (LOC.DEV) with appropriate units used. If wind is present Equation 4 will still hold at any particular instant in the turn.

Simulation results indicated it was best to compute TAEBE once only at capture initiation and accept any resulting anomalies due to wind. Equation 4 is basically only used to define the trip point for transition to the blend-down submode. That is, one computes TAEBE at the initiation of capture and as the capture proceeds, he continually tests TAE against TAEBE. If the condition TAE = TAEBE occurs prior to encounter of the beam edge, the system is presumably turning too fast and fading of the bank command should begin. If beam encounter occurs prior to TAE = TAEBE, then the system should fade immediately to bank command based on beam data.

The second aspect of the blend-down problem is the question of how to fade the bank. Assuming an exponential fade on bank command, it can be shown that the time constant of the fade can be computed such that for a fade beginning at the point TAE = TAEBE, the system will never turn further than to TAE = k*TAEBE where $0<k<1$. In particular, under no conditions will the system turn parallel to the beam. The bank command is faded exponentially from its initial value with a time constant (τ) computed as shown in Equation 5.

$$\tau = \frac{Uo\ (k * TAEBE)}{g\phi(to)} \qquad \text{Eq. 5}$$

where $\phi(to)$ is the bank angle at the initiation of the fade and Uo is airspeed.

The basic requirement for capture trip point is that it be such that reasonable banks are used in capture and reasonable overshoots occur under all conditions. Generally bank command is restricted to less than 30° in magnitude in transport aircraft and it is highly desirable to keep overshoots less than 30 μA ($\simeq$.4°) of localizer deviation. Other factors also enter. For example, if no RNAV system is available, clearly the trip point must be within the beam resulting in geometry limits for certain close-in captures. Pilots often have very definite opinions about how the bank should behave under given conditions. The conditions above imply that the desired form of the capture bank command might be a feasible basis for computing the capture trip point. If one assumes a circular capture (i.e., constant bank), it is interesting to solve Equation 3 for CTD to illustrate the CTD required to execute a circular capture as a function of Vg, TAE, and BNK.CMD

$$CTD = \frac{Vg^2\ (1 - COS\ (TAE)\ )}{g\ tan\ (BNK.CMD)} \qquad \text{Eq. 6}$$

Equation 6 illustrates the generally applicable point that capture trip point expressed in CTD terms is a function of ground speed, TAE, and bank command to be used in the capture. Since it appeared feasible to specify a desired constant bank during capture, the approach decided on in this study was to specify the capture bank (CAP.BNK) and then use Equation 6 to determine the trip point. However, the bank rate command limit is a significant factor and the trip point should be adjusted to account for its effect. Further, it was felt that CAP.BNK should be a function of TAE, that is at high angle course cuts more bank should be used than for lower angle course cuts. Further, to prevent very small bank captures, the restriction was added that $|CAP.BNK| \geq 5°$ in all cases.

Tolerance to RNAV position and velocity errors must be considered in determining MAX.CAP.BNK, the maximum bank to be used in capture. In the event of a "turn long" case, the required "room to increase" on bank once the beam is encountered is a function of range. To see this, consider captures beginning at the same CTD and course cut but at varying range (RNAV data is used until beam intercept). Intuitively, at longer ranges more beam width in feet is available after beam intercept to correct the problem or conversely less time is spent using an erroneous command.

Making MAX.BNK.CAP sufficiently large at longer ranges will force the capture to be within the beam in those cases (see Equation 6). This is desirable since RNAV aiding should be used only when necessary. It was decided to make MAX.CAP.BNK = 25° at longer ranges and to decrease the value at shorter ranges. Further, it can be shown that for a 90° intercept at 200 fps, MAX.CAP.BNK = 25° implies RNAV aided captures at ranges shorter than 13 nmi range; hence this seems a reasonable point to start programming MAX.CAP.BNK down. Numerical examples and simulation results indicated that provision for about 15° possible increase in bank during capture at 5 nmi seemed advisable.

Collecting the above discussion, the trip point computer is performed as follows:

$$CTD\ Trip\ Point = \frac{Vg^2\ (1 - COS\ (TAE))}{g\ tan\ (CAP.BNK)} + CTD.ADJ \qquad \text{Eq. 7}$$

where

$$CTD.ADJ = \frac{CAP.BNK}{RCL} * Vg\ sin\ (TAE)$$

$$CAP.BNK = \begin{cases} -MAX.CAP.BNK * \frac{TAE}{90} \ldots \text{ if magnitude of result is} \geq 5° \\ -5 * SIGN(TAE) \ldots \text{ otherwise} \end{cases}$$

$$MAX.CAP.BNK = (8. + \frac{17}{13} * RNGLOC) \leq 25°$$

RCL is the bank command limit, and RNGLOC is range to localizer in nmi and the units on MAX.CAP.BNK are degrees.

The transition from capture to track normally occurs when

$$LOCDEV < 30\ \mu A \text{ for } RNGLOC \leq 13 \text{ nm}$$

and for

$$LOCDEV * RNGLOC < .091 \text{ nm for } RNGLOC > 13 \text{ nm}$$

The transition from angular to linear CTD criterion for transition to track prevent going to track at high values of TAE at long ranges where 30 μA represents significant linear deviation. The advantage here lies in maintaining capture mode and hence the circular nature of the capture as long as possible. However, in the event of severe crosswinds or unusually bad initialization the possibility of turning parallel to the beam during ILSCAP exists. To provide a final safeguard against turning parallel an override trip to track feature is also provided based on predicted TAE at the Track Trip point.

The system implementation will now be described. A block diagram of the total RNAV aided ILS localizer capture and track system is shown in Figure 9. It should be noted that there are basically two potential capture modes. Capture computations are based on RNAV data (NAVCAP) or based on ILS data (ILSCAP). Further there is a blend-down submode (BLNDWN) of NAVCAP which is provided to fade the bank command down in the "turn short" case. If RNAV aiding is needed, the NAVCAP mode will occur first, transitioning to ILSCAP when localizer deviation becomes less than 200 μA. If during NAVCAP the system turns too far (determined by continually comparing TAE with predicted TAE at the beam edge (TAEBE) during NAVCAP), the BLNDWN submode is automatically selected and fades the bank command according to the fade algorithm discussed earlier.

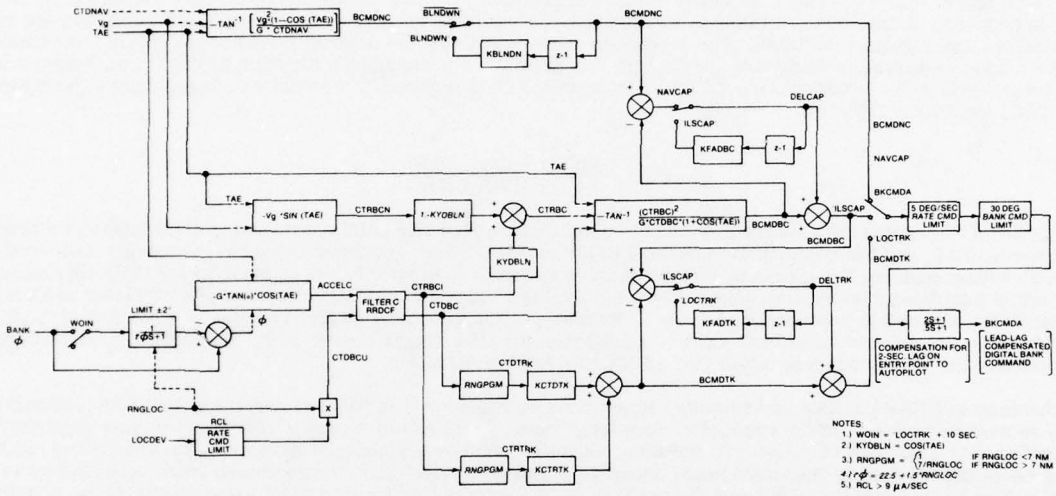

Figure 9. 3D/4D Lateral Axis Control Laws

ILSCAP can occur in two days. First, if NAVCAP is in progress and localizer deviation decreases below 200 μA, then ILSCAP is selected immediately. The other case occurs when the capture trip point is such that localizer deviation at that point will be less than 200 μA. In this case no RNAV aiding is needed and the ILSCAP mode is selected immediately.

Notice that during NAVCAP a fader circuit is provided to fade from NAVCAP to ILSCAP. Similarly during ILSCAP a companion fader is provided to blend to the track mode. The bank command in either NAVCAP or ILSCAP is the proper one to generate a circular capture and both are essentially the same as Equation 3 although the form used in ILSCAP is modified to more appropriately use beam data and to lessen its dependence on TAE and ground speed estimates from the RNAV system.

The track mode is a conventional proportional combination of position and rate relative to the beam center to form bank command.

Notice that the output of the data processing filter is position and position rate to provide the requisite data to the capture computation. This is also the appropriate form for the track mode at close ranges. However, at longer ranges the effects of beam noise, particularly excessive bank activity, require that gains be softened, usually such that the track law becomes angularly based rather than position based. The RNGPGM block of Figure 9 provides this feature since at ranges beyond 7 nmi (neglecting the filter for the moment since its parameters are not range dependent), CTDTRK is really in angular units. Alternately, the combination of RNGPRGM programming downstream of the filter and RNGLOC programming of LOCDEV upstream of the filter provides linearization of LOCDEV out to 7 nmi and a constant gain beyond that range.

The final aspect of the system block diagram is the output command processing shown at the right side of Figure 9. Basically a 5 degree per second rate command limit and a 30 degree command limit are imposed. The lead-lag compensation is necessary for the specific autopilot interface used in this application and would not in general be included in the design.

Glideslope Control Laws

The vertical portion of the ILS approach control laws does not rely on area navigation data as heavily as do the lateral control laws. However, the range to glideslope intercept is used for radio programming or beam linearization in place of the more conventional radio altitude, and the vertical navigation function can be used to initiate a capture from above the glideslope beam.

The 3D/4D system glideslope operation is similar to conventional flight guidance computations (see Figure 10). Basically glideslope capture is initiated from a flight path which has been set up to intercept the glideslope beam. Usually the glideslope is intercepted from a zero flight path angle or altitude hold maneuver; however, the control laws will also allow the user to capture from above. This capability permits initiation of an intercept from a vertical navigation maneuver above the beam. Once an intercept has been established, capture is completely automatic. The system senses beam rate and vertical rate and compares this mixture with beam deviation and beam polarity to establish a capture trip point. Capture logic is shown in Figure 10. When pitch command goes through zero in the correct direction (determined by comparing its polarity with that of beam deviation) capture is initiated.

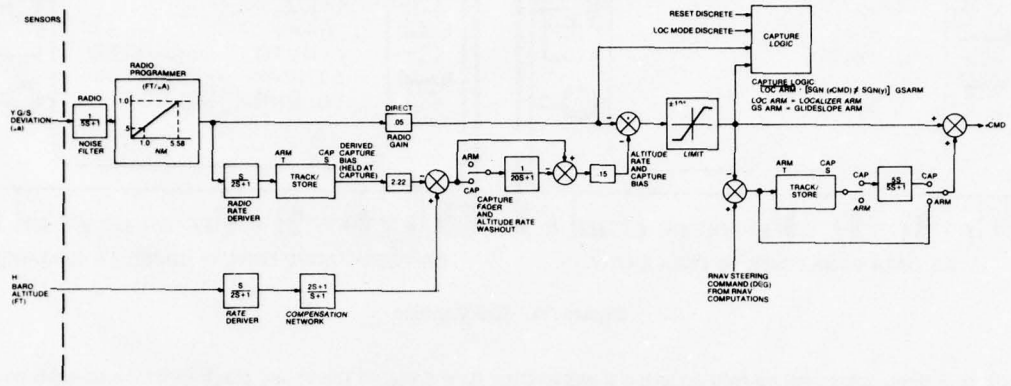

Figure 10. 3D/4D Glideslope Capture and Track Control Laws

Since the capture is a function of both beam closure rate and vertical rate, the trip point is a function of ground speed and flight path angle. Ground speed in turn makes the capture a function of aircraft speed and wind. Similarly, if the aircraft has a vertical rate established, capture will adjust to compensate for the vertical rate. Of course, beam rate is also sensing this higher closure rate, but the addition of vertical rate has proved to be more accurate in adjusting the trip point especially in above the beam capture.

The capture trip point will vary as a function of how fast the glideslope beam is approach, moving further from the glideslope beam center as the closure rate increases regardless of the reason. At capture initiation the beam rate is memorized and held. Also, a fader or washout is initiated on both stored beam rate and vertical rate. The action is such that at the instant of capture, pitch command is zero, and the aircraft continues toward the glideslope beam.

Deviation decreases faster than the slowly fading rate signals to provide appropriately a nose up or nose down pitch command to transition the aircraft onto the glideslope. The fader washes out all of the beam rate and initial vertical rate as the aircraft acquires the beam centerline. After capture, tracking is provided by the deviation and washed out vertical rate paths. Vertical rate is washed out to prevent the vertical rate or descent rate from causing a deviation standoff in the control laws. It should also be pointed out that for autopilot operation, vertical rate is required to damp the deviation path, since the autopilot pitch attitude (which also provides path damping) is washed out (by the 5 second forward integration) faster than normally permissible to maintain adequate stability.

Although it is possible to initiate a capture outside the linear range of the gain programmer, the effect of the nonlinearity on the capture detector is marginal and the following discussion will assume linear programmer range. Referring to Figure 11, an internal pitch command is formed when the glideslope computation is in the arm condition (GSARM). The value of that signal will be

$$\theta_c = K_h \left[\frac{K_{\dot{h}}}{K_h} \left(K_{\Delta\dot{h}} \dot{\Delta h} + \dot{h} \right) + \Delta h \right] \qquad \text{Eq. 8}$$

where θ_c equals degrees of pitch command (+ directs a pitch down attitude), $\dot{\Delta h}$ equals approach rate of the glideslope beam (ft/sec), $\dot{h}$ equals ascent rate (ft/sec) and Δh equals cross track distance (ft), positive above the glideslope.

Any flight path intersecting or roughly paralleling the glideslope will result in rate terms having a polarity opposite to that of Δh. When the rate term equals or exceeds the position term, the glideslope capture mode will be enabled (GSCAP).

The glideslope capture window may be more clearly defined by expressing the rate terms as functions of flight path angle:

$$\dot{h} = V_g \sin(\alpha)$$
$$\dot{\Delta h} = V_g \sin(\alpha - \alpha_g) \qquad \text{Eq. 9}$$

where V_g equals groundspeed, α equals flight path angle measured as positive counterclockwise from horizontal, and α_g equals glideslope angle (nominally -2.5 deg.).

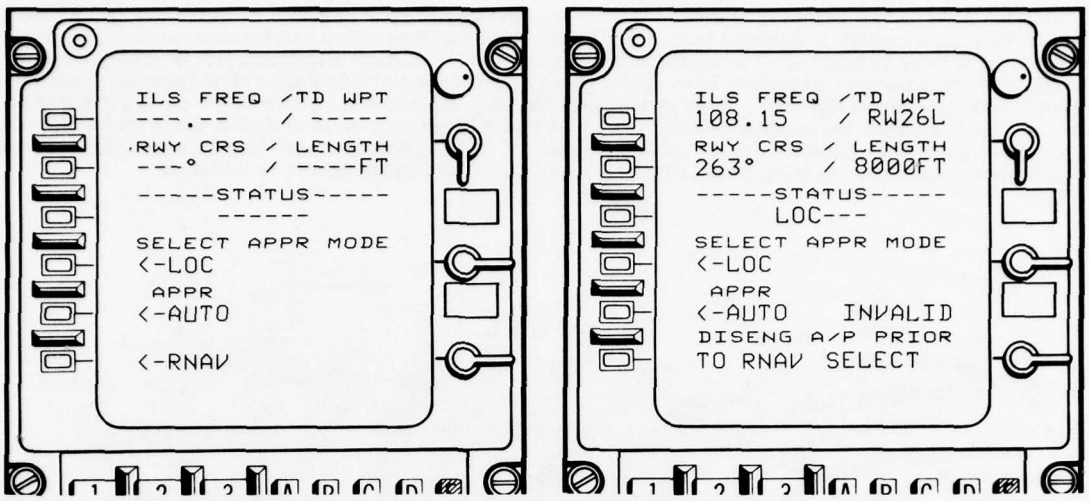

ILS DATA PAGE PRIOR TO DATA ENTRY

REPRESENTATIVE DISPLAY UNDER ILS GUIDANCE

Figure 11. ILS Capture

Substituting those expressions into equation 8 and setting $\theta_c = 0$ yields the cross track distance at capture as a function of flight path angle:

$$\Delta h_c = -\frac{K_h^{\cdot}}{K_h} V_g \left[K_{\Delta h}^{\cdot} \sin(\alpha - \alpha_g) + \sin \alpha \right] \qquad \text{Eq. 10}$$

Since the capture window is actually determined by measured position and rate information, the capture point will be moved to compensate for along track and cross track wind conditions as well as variations in glideslope angle. Simulation data demonstrated the use of capture point movement to maintain a relatively smooth performance during the capture maneuvers in varying environmental conditions.

ILS Capture Definition

The ANS-70A CDU was also used to set up the ILS captures. A separate page was created to allow the pilot to specify the capture modes and ILS definition. Figure 11a illustrates the display prior to data entry while Figure 11b illustrates the display under localizer guidance.

In an operational system, the ILS definition would be resident in the data base along with the other navaid data (this was accomplished for a selected number of airports in a Collins two-segment approach operational evaluation). In this program the ILS frequency had to be identified. The distance from touchdown waypoint was used for gain programming the glideslope signal while it in combination with runway length was used for gain programming the localizer signal. The course data was used to compute track angle error.

Three approach modes were defined. LOC consisting of a localizer capture mode, APPR AUTO consisting of a localizer capture followed by a glideslope capture mode and RNAV consisting of an RNAV approach or a return to RNAV. The modes were inhibited if the data was not valid. If a valid ILS mode was selected, one of the VOR receivers was tuned to the localizer frequency, the HSI course was slewed to runway heading and raw localizer deviation was displayed on the HSI lateral deviation bar. After ILS mode selection, the RNAV guidance was retained until localizer capture/track.

The RNAV mode could always be selected prior to localizer capture. Once localizer capture occurred (in LOC or APPR AUTO), the autopilot must be disengaged before a return to RNAV mode was possible. This is the status displayed in Figure 11b. A return to RNAV was inhibited since the system was not designed for RNAV go-around.

ILS COCKPIT SIMULATIONS

A limited real time cockpit simulation was also undertaken to checkout and evaluate the performance of the ILS capture tracking algorithms under manual and autopilot control. A total of 6 different intercept conditions were established, namely 90° captures at 3, 5, and 7 nm from runway touchdown point, and 10°, 20°, and 30° shallow intercepts to a simulated outer marker 5.4 nm from runway touchdown point. All approaches utilized a 3° descent to localizer capture, an altitude hold to glideslope followed by 2-1/2° descent to touchdown. All approaches were flown at a nominal approach speed of 120 knots.

Table 1 lists the ILS approach conditions along with a yes/no summary of system performance. Strip chart recording of two approaches are shown in Figures 12 and 13. The data under Turn Initiation indicates whether the RNAV based steering module or the ILS based steering module was used to initiate the turn. The method for accomplishing this will be described later. The last column indicates if Category II type performance of 35 μA RMS outside of 200 feet and 12 feet RMS within 200 feet of altitude was maintained. For autopilot approaches, no sustained oscillations were allowed or observed. Manual approaches experienced a somewhat cyclic deviation. For these approaches an RMS value of 35 μA was replaced by a requirement to limit peak excursions within 50 μA beyond .75 nm (200 ft/tan 2.5°) from runway touchdown point. At 120 knots .75 nm correspondes to a little over 20 seconds or 2 major time divisions on the charts. Runway touchdown point coincides roughly with the glideslope deviation saturation on the charts.

Table 1. RNAV Aided ILS Approach Conditions

APPROACH	RUN NUMBER	CONTROL	TURN INITIATION	CATEGORY II TYPE PERFORMANCE
7nm-90°	1	Autopilot	RNAV	No
	2	Autopilot	ILS	Yes
	3	Manual	RNAV	No*
	4	Manual	ILS	Yes
5nm-90°	5	Autopilot	RNAV	No
	6	Autopilot	ILS	Yes
	7	Manual	RNAV	No*
	8	Manual	ILS	Yes
3nm-90°	9	Autopilot	RNAV	Yes
	10	Autopilot	ILS	Yes
	11	Manual	RNAV	No
	12	Manual	ILS	Yes
10°	13	Autopilot	RNAV	No
	14	Autopilot	ILS	Yes
	15	Manual	RNAV	No
	16	Manual	ILS	Yes
20°	17	Autopilot	RNAV	No
	18	Autopilot	ILS	Yes
	19	Manual	RNAV	No
	20	Manual	ILS	Yes
30°	21	Autopilot	RNAV	No
	22	Autopilot	ILS	Yes
	23	Manual	RNAV	No*
	24	Manual	ILS	Yes

*Yes for last 2 nmi.

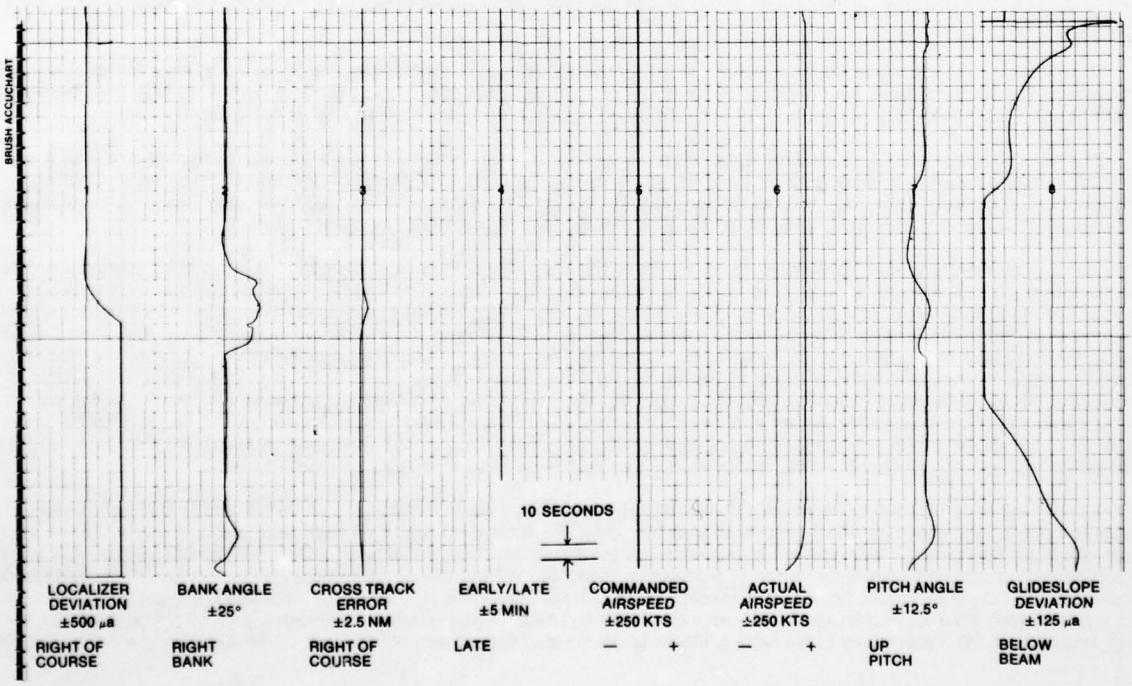

Figure 12. ILS Test 1
7 nm 90° Capture, RNAV Initiated Turns, Autopilot

AD-A052 862 ADVISORY GROUP FOR AEROSPACE RESEARCH AND DEVELOPMENT--ETC F/G 17/7
APPLICATIONS OF ADVANCES IN NAVIGATION TO GUIDANCE AND CONTROL.(U)
FEB 78

UNCLASSIFIED AGARD-CP-220 NL

3 OF 3
AD
AD52862

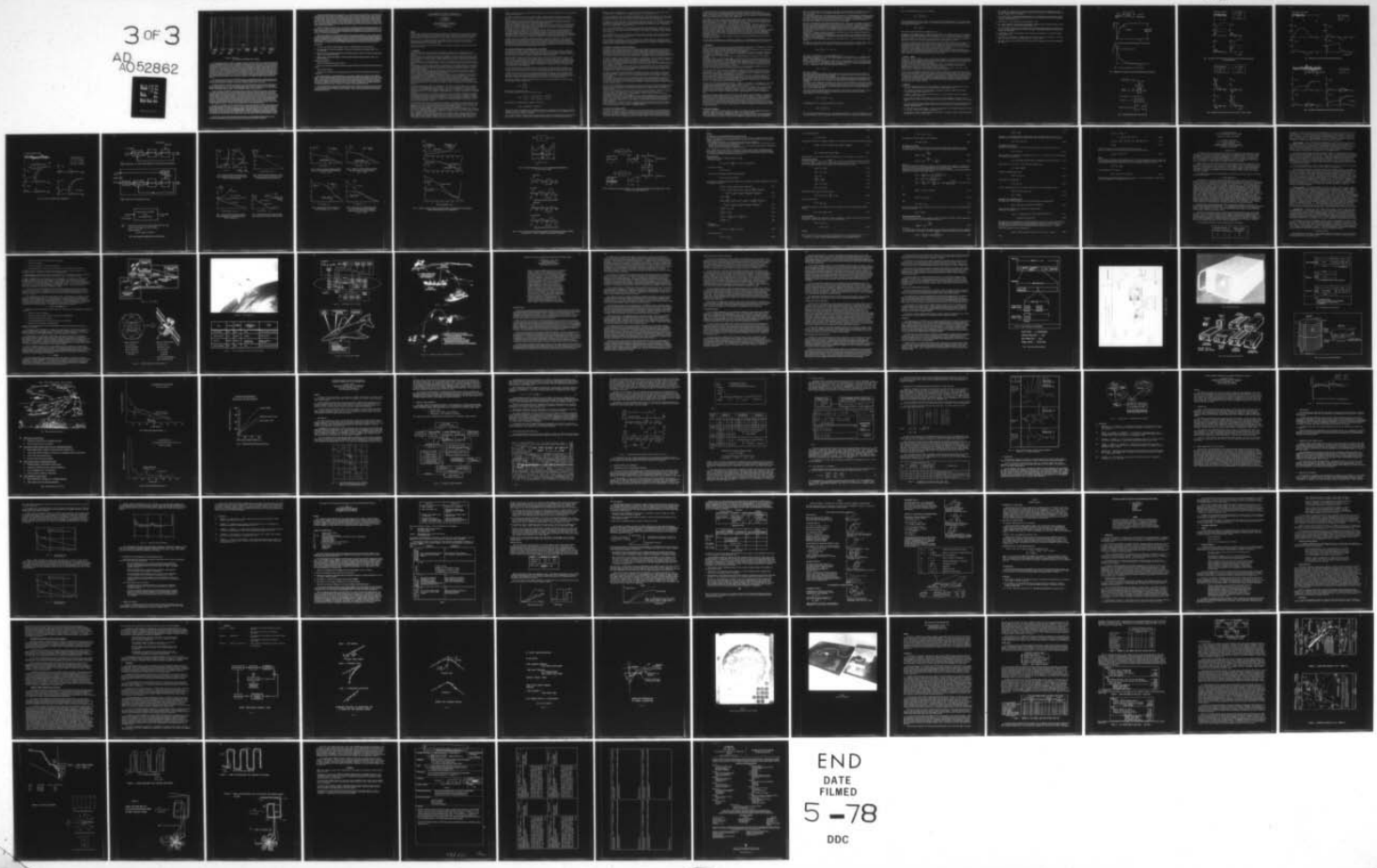

END
DATE
FILMED
5-78
DDC

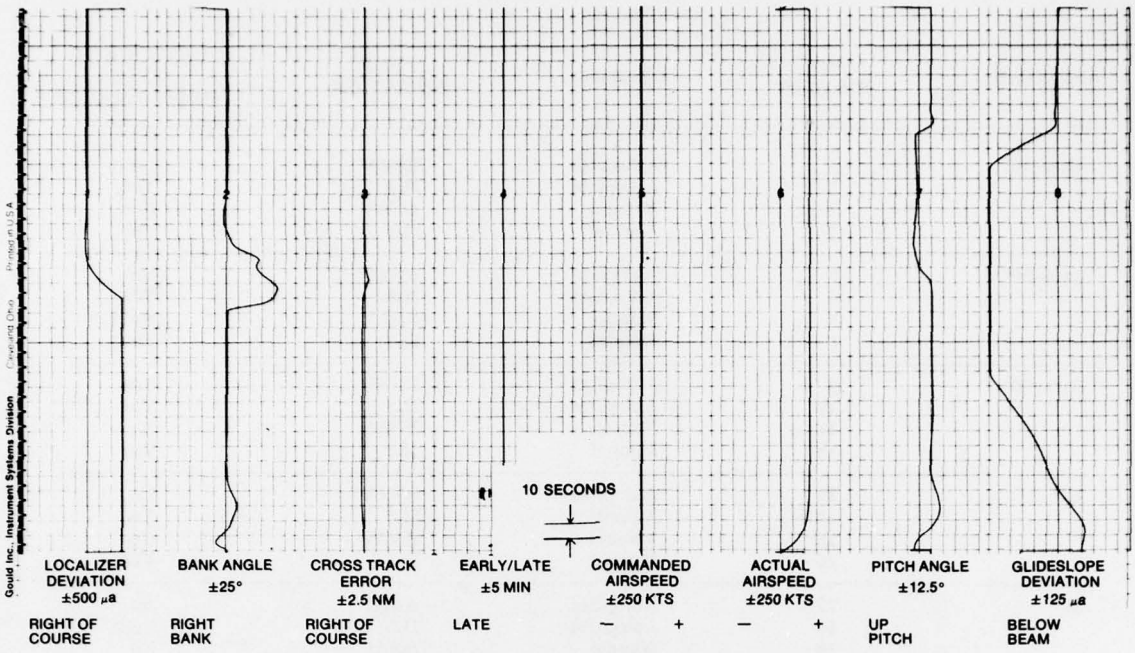

Figure 13. ILS Test 2
7nm 90° Capture, ILS Initiated Turns, Autopilot

The turn initiation procedure will now be explained. Assume for the moment that the RNAV approach overlays the localizer and glideslope during the localizer and glideslope tracking segments. Assume also that the RNAV system has no knowledge that the ILS is the next leg to be captured. Since the RNAV (cruise) steering laws are not as stiff as the ILS (final approach) steering laws, turn to the localizer (and later glideslope) will initially be commanded by the RNAV steering laws. When the aircraft flies within the localizer (and later glideslope) window, steering is taken over by the ILS control laws. Until this window is reached, RNAV steering is provided. Under ideal conditions the scenario would consist of a lateral RNAV turn initiation to localizer leg followed by transition to ILS steering when localizer data is valid and the aircraft is on an apparent localizer intercept (within the window). Vertical steering would remain under VOR/DME/baro altitude referenced RNAV control. The pitchover to capture the glideslope leg would be initiated by the RNAV system as again its control laws are less stiff. Transition to final capture and tracking under glideslope based data is initiated when the glideslope data is valid and the aircraft is on an apparent glideslope intercept (within the window).

If an RNAV route has been set up which parallels the localizer or glideslope, localizer or glideslope capture will not occur. Similarly if the RNAV system errors are of sufficient magnitude that the ILS data assumes that the RNAV route is parallel (vertically or laterally) to it, localizer or glideslope capture will also not occur.

The lateral axis can accommodate RNAV errors up to .5 nm provided that the localizer intercept angle is greater than 10° (which it should be). However, the glideslope intercept angle is typically less than 3° from an (equivalent) altitude hold glideslope intercept. Hence it is essential that the RNAV errors do not effectively create a parallel path outside of the glideslope capture window. If they do glideslope capture will not be achieved.

To ensure localizer and glideslope capture (given the data is valid) it is sufficient that the RNAV route intersects the localizer and glideslope paths. This was accomplished in the simulation by placing an additional waypoint 5 nm beyond the localizer intercept waypoint in line with the localizer intercept leg, with an altitude equal to the localizer intercept altitude. (In an actual implementation, the final RNAV turns to the ILS would be delayed.) The RNAV system would then attempt to fly through the localizer. Assuming the system was armed for localizer capture, the ILS steering modules would command localizer capture based upon RNAV desired track angle error and cross track deviation from localizer, RNAV linearized localizer deviation data (if valid), and roll gyro data. Localizer capture/tracking would then occur. Vertical navigation would command an altitude hold as the vertical path assumed is the level path to the waypoint beyond the localizer; glideslope capture/tracking would then occur based upon derived altitude rate, and RNAV linearized glideslope deviation. This then was the procedure used to ensure ILS initiated turns.

The effect of RNAV initiated versus ILS initiated turns is dramatically displayed in the strip chart recording of the autopilot controlled experiments Figures 12 and 13. Observe first the strip chart for test 2 and in particular the localizer and bank angle data. The system commands the localizer capture based upon RNAV track angle error and cross track deviation and roll gyro data in the ILS steering module. This phase is called NAV CAP. When the localizer deviation is 200 μA, RNAV data is not used (except for localizer deviation linearization) and the bank angle is reduced as the system goes through ILS based localizer capture (ILS CAP). When localizer deviation passes through 25 μA, localizer tracking (LOC TCK) takes place with a slight increase and then decrease in bank angle indicating stiffer tracking.

Note that during localizer capture the pitch angle returns to zero. When glideslope deviation reduces to 25 μA, pitch down is commanded by the ILS module and the system enters glideslope capture and tracking.

The situation is significantly more complex in test 1. Localizer capture occurred as follows. The initial bank is commanded by the RNAV system and is beginning to be faded out as localizer deviation leaves the 300 μA saturation. At this point the aircraft has arrived in the localizer capture window and the ILS lateral steering module takes over. The initial control laws are RNAV based but complemented with roll data which allows for greater stiffness without incurring potential stability problems. A greater bank is therefore commanded at roughly 300 μA (NAVCAP in this example). At 200 μA (ILSCAP) the bank command changes slightly and is being bled off until 25 μA of localizer deviation. At this point localizer tracking takes over and the maneuver is completed. Note that while the smoother RNAV cruise steering laws initiated the turn the resultant reduced track angle error did not prevent the aircraft from reaching the localizer capture window.

This is not the case in the vertical axis. The pitch down command after localizer tracking is commanded by the RNAV system. The along track error is almost so great that the flight path parallels the 2.5° glideslope beam. The flight path angle settles to 2°, and the resultant flight path enters the glideslope capture window within 1 nm of touchdown. At this point an increase in pitch angle is commanded by the ILS glideslope steering module but the system is too close-in to stabilize on the glideslope.

These same conditions were observed during all RNAV initiated autopilot approaches. Under manually steering with flight director guidance, it was possible to trip earlier by observing the standoff in glideslope path and pitch the aircraft up slightly to enter the capture window. However, it was then necessary to pitch down and this oscillatory behavior was difficult to arrest while maintaining control over both axes. In contrast when the glideslope initiated the final pitchdown, all autopilot and manual approaches exhibited Category II type tracking performance under the simulated conditions. As a result some means of inhibiting or delaying the RNAV turns to the ILS must be provided.

REFERENCES

1. DOT-FAA, "FAA Report on Airport Capacity", Volume I - National Summary, 1974, FAA-EM-74-5.

2. N. B. Hemesath, et al, Rockwell International, "Three and Four Dimensional Area Navigation Study", 1974, FAA-RD-74-150.

3. DOT-FAA, "ATC Performance Requirements for Developing Prototype Versions of the Discrete Address Beacon System", 1973, FAA-EM-73-6, pp 2-9.

4. Collins Avionics, Rockwell International, "ANS-70A Automatic Navigation System Operators' Guide", 1974, 523-0765197-00117.

SUBSEQUENT DISCUSSION

Question by Donald Richardson, Systems Control:

Were there any quantitative differences in RNAV/ILS capture performance between autopilot coupled and manual modes?

Reply by Juergen Bruckner:

I will restrict the comments to the ILS initiated turns, since any operational system would require this type of control law.

The greatest difference is in glideslope captures. For the shallow captures and 90° captures where glideslope capture is initiated following localizer tracking, autopilot performance exhibited good damping (0.707 or better) and capture occurred within 25 seconds with about 5 μA of overshoot; the manual captures had poorer damping (0.5 or less with a response period of 15 to 20 seconds) and capture occurred within 30 seconds with about 25 μA of overshoot. For 90° close in captures overshooting increased to 25 μA with autopilot coupling and to 50 μA under manual control. Overshoot is a misnomer for the 3-nmi case as capture is from above. Here the system is designed to prevent the aircraft from going under the beam so overshoot is, in reality, an initial standoff from above.

Under autopilot control, localizer capture occurred within 20 to 25 s with, at most, 20-μA overshoot, except for the 3-nmi case which had 40-μA overshoot. Manual captures occurred within 25 to 50 seconds with overshoots of 10 μA for the shallow and 7-nmi 90° captures with good damping. Closer in, poorer damping resulted with overshoots increasing to 20 and 40 μA.

THE CALCULATION OF RMS VALUES OF DEVIATIONS OF AIRCRAFT CONTROLLED TO FLY ALONG A DESIRED FLIGHT PATH

by
J.C. van der Vaart
H.L. Jonkers
F.K. Kappetijn

Delft University of Technology
Department of Aerospace Engineering
Kluyverweg 1
Delft, The Netherlands

SUMMARY

This Paper gives a description of a method to calculate the covariance matrix, as a function of time, of a linear system perturbed by a number of random noise signals. Using basic principles of modern system theory it allows the computation of variances or r.m.s. values of aircraft variables in the case where system dynamics and statistical properties of the disturbing noise signals are a function of time.

Results are shown of a numerical example of the symmetric motions of a present day jet transport in a coupled approach followed by an automatic landing, the random disturbing signals being gaussian atmospheric turbulence and ILS electronic noise.

The problem of wind shear is briefly touched upon and an analytical approach to "worst case" wind time histories is presented.

1. INTRODUCTION

One of the aims of the control of flight, be it manual or automatic, can be considered to be the reduction of the effects of external and internal disturbances acting on the controlled system i.e. the aeroplane.
These disturbances can be divided into two distinct categories, one being caused by malfunctions of any part of the controlled system, the other category being caused by signals of a random nature, resulting in errors relative to a desired state or trajectory while all parts of the system are functioning within specifications.
The first category of obvious malfunctions is left out of consideration here. The present Paper is only concerned with the class of random disturbances such as atmospheric turbulence, electronic and mechanical noise.
When designing or evaluating control systems it is important to be able to make estimates of the effects of these random signals on the performance of systems. Considering the disturbing signals as so-called random processes and making a number of assumptions on these processes make them accessible to practical statistical calculations.
Assuming that the random processes under consideration are normal or gaussian and that the dynamic behaviour of the systems can be described by linear differential equations (system linearity) opens the road to a number of straightforward mathematical methods.
It should be mentioned that atmospheric turbulence, for example, can only approximately be described as a normal (gaussian) process. Attempts have been made by others to tackle the phenomenon of non-gaussian turbulence which is especially important in the field of flight simulation (Refs. 1 and 2).
When designing control systems for the purpose of reducing system sensitivity to disturbing signals it can often be assumed that noise processes are gaussian. The calculation method described in this Paper is based on such an assumption and on the one of system linearity. For the sake of completeness, it should be mentioned that it is, in principle, possible to treat non-linearities in a quasi-linear manner, see Ref. 3.

Statistical ensemble properties such as variances or r.m.s. levels of output signals of a system driven by a number of random noise signals can be divided in two classes. Steady state properties are namely clearly to be distinguished from transient properties. This is illustrated by Fig. 1, showing a system, initially at rest, perturbed by a random noise input signal from t = 0 onwards. The variance of the output signal, being zero at t = 0, grows through a transient response to its final or steady state if the system is stable.
Suppose for instance that one is interested to know r.m.s. levels or exceedance probabilities of normal accelerations, load factors, altitude or course deviations of an aircraft due to atmospheric turbulence in cruising flight. Here the statistical characteristics of turbulence as well as the dynamic properties of the aircraft can assumed to be constant and the r.m.s. levels and exceedance probabilities of interest can be considered steady state properties. A number of well-established methods are available for such steady state problems (Refs. 4 and 5).

A quite different problem is best illustrated by the example of an aircraft in a coupled approach to land. Due to the decreasing altitude during the approach and the altitude dependent statistical properties of atmospheric turbulence, the aircraft experiences time-varying random turbulence. Moreover ILS glide path beam geometry may cause changes in effective gains of the glide slope coupler.
Finally, if an automatic landing is carried out, the autopilot mode changes drastically while in this phase also the aerodynamic characteristics change due to ground effects. Still one would like to calculate r.m.s. values of motion variables during the approach and landing, especially at certain instants in time such as at decision height and touch down.
Such a calculation could be carried out by a Monte Carlo simulation. Another method is the one using impulse responses in an analogue computation (Ref. 6). A much more accurate, straightforward and faster method using transient statistical properties is the one reviewed in the present Paper. Basically it is an application of known elements of modern system theory and the concept as such can of course not be

claimed to be entirely novel. A similar method, described in less detail, was apparently used in a publication by Holley and Bryson (Ref. 7).

The purpose of this Paper is to give a practical example of some capabilities of modern system theory and it is to be hoped that it gives some guidance to control engineers faced with problems of a stochastic nature.
The main advantage of the method presented is perhaps that it permits statistical calculations on any linear system perturbed by gaussian random noise signals when either the statistical properties of the noise signals or the dynamics of the system, or both, are changing with time.
In the example mentioned earlier of an aircraft in the approach to land, the influence of altitude dependent properties of atmospheric turbulence can then be determined. Changes in electronic noise in the ILS signal during such an approach, gradual changes in autopilot gains and also the effect of a sudden decoupling of the autopilot are also easily studied in this way.
The present Paper gives an overview of the underlying theory and some results. A detailed description of the pertaining computer program is to be published shortly (Ref. 8). The second Chapter illustrates, by some simple examples, the principle of using transient responses to obtain statistical properties of a time-varying system. Chapter 3 deals with the particular manner in which noise processes are to be modelled, followed by a survey in Chapter 4 of the numerical simulation of the aircraft, the autopilot, the atmospheric turbulence and the ILS noise process. Results of a number of calculations are given in Chapter 5.

Although the nature of the phenomenon usually denoted by the term "wind shear" is such that a statistical treatment appears hardly possible, this subject is briefly touched upon in Chapter 6. It is shown that deviations from a desired trajectory caused by certain, analytically derived, deterministic "worst case" wind time histories are proportional to statistical properties in a special case of stochastic wind signals. Some insight into the effects of worst case wind time histories (or windshears) might thus be gained using the calculation method that forms the main subject of this Paper.

2. THE TRANSIENT RESPONSE OF THE COVARIANCE MATRIX. SOME EXAMPLES

This Chapter gives a number of simple examples of the calculation of the transient response of statistical characteristics of output signals of a system driven by a white noise input signal. It will be shown how this calculation can be done in the case of time-varying properties of either the driving noise signal, the driven system itself or both. The Appendix contains a more detailed description.

Consider a dynamic system, initially at rest and driven by a random noise input signal v(t) from t = 0 onwards, see Fig. 1. The variance σ_x^2 of the output signal x (or the r.m.s. value σ_x of x), being zero at t = 0, will reach a steady state level in a finite time if the system is stable, Fig. 1a. The steady state value can be calculated by a number of methods, for instance by a frequency domain technique. The transient response can only be calculated by time domain techniques such as the one described in this Paper or by a time consuming Monte Carlo simulation in which a large number of replications is taken, the system being at rest initially for each replication.

If the random input signal is switched off after the steady state has been reached, the variance of x returns to zero after another transient, Fig. 1b. This transient is identical with the one that would be obtained if v(t) were zero for all t, the initial condition being equal to the steady state value of σ_x^2.

In modern system theory the more important statistical quantities are expressed by the covariance matrix $C_{xx}(t)$ of the state vector $\underline{x}(t)$ of the system under consideration. In the case of an aircraft the state vector $\underline{x}(t)$ is the vector of the motion variables, and the covariance matrix then contains the variances of the motion variables as the diagonal elements and the covariances as the off-diagonal elements.

Next, by way of example, a simple second order system such as the mass-spring-dashpot combination of Fig. 2 is considered. The state vector $\underline{x}(t)$ is

$$\underline{x}(t) = \begin{bmatrix} x_1(t) \\ x_2(t) \end{bmatrix}$$

where $x_1(t) = d(t)$ and $x_2(t) = \dot{d}(t)$.
The covariance matrix of the state vector $\underline{x}(t)$ is then:

$$C_{xx}(t) = \begin{bmatrix} c_{11}(t) & c_{12}(t) \\ c_{21}(t) & c_{22}(t) \end{bmatrix} = \begin{bmatrix} \sigma_{x_1}^2(t) & \sigma_{x_1x_2}(t) \\ \sigma_{x_2x_1}(t) & \sigma_{x_2}^2(t) \end{bmatrix} \tag{1}$$

Now according to the Appendix $C_{xx}(t)$ consists of two terms:

$$C_{xx}(t) = D_{xx}\{C_{xx}(0),t\} + E_{xx}\{w(t),t\} \tag{2}$$

The two terms in Eq. (2) represent the two different responses just mentioned. The first term D_{xx} gives the response to the initial conditions $C_{xx}(0)$, the second term E_{xx} is an expression for the response to a white noise input signal w(t) acting on the system.

Fig. 3 shows the response of each element of $C_{xx}(t)$ caused by a white noise signal acting on the second order system of Fig. 2 from t = 0 onwards, initial conditions $C_{xx}(0)$ being zero. The responses are shown for

different values of the damping ratio ζ. It can be seen that the covariances of x_1 and x_2 become zero in the steady state, a peculiarity of this example, where x_2 is the time-derivative of x_1.

In Fig. 4 the response to unit initial conditions is given (first right hand term of Eq. (2)). Fig. 5 shows the response caused by a white noise signal of limited duration (5 secs). The responses from t = 5 onwards are given by the term D in Eq. (2) by setting the initial conditions of C_{xx} at the values at t = 5.

Calculating the transient response to a noise signal of limited duration opens the possibility of determining the response to an input noise signal with time-varying statistical properties. If it is known how these properties are changing with time, the response can be determined as illustrated in Fig. 6, where the intensity of the input signal is increased at t = 5.

Fig. 7 shows an example where one of the systems' characteristics, the damping ratio ζ, changes from 0.7 to 0.2 at t = 8 sec. As in Fig. 6, the total response after the change is obtained as the sum of the terms D and E of Eq. (2), the initial conditions in D being set at the values of the elements of $C_{xx}(t)$ reached up to that moment.

In the examples of Figs. 5, 6 and 7 the instants in time at which the changes in input signal and damping ratio occur were, for the benefit of simplifying the figures chosen such that steady states had been reached. This is of course not necessary.

From the examples of this Chapter it will be evident that the covariance matrix, as a function of time in the case of gradually changing system or input characteristics, can be calculated by approximating these changes by small, stepwise variations. Details of the modelling and the calculation of responses to coloured noise signals will be dealt with in the next Chapters.

3. MODELLING THE AIRCRAFT AND THE NOISE PROCESSES

The examples in the foregoing Chapter were of systems perturbed by white noise processes. The theory on which the calculation of the covariance matrix is based indeed assumes a system driven by one or more white noise signals. These idealized processes do not occur in reality. The coloured noise processes such as atmospheric turbulence and electronic noise are therefore usually modelled such that they can be thought to be obtained by the filtering of white noise. The technique to mathematically derive the differential equations and the transfer functions of these shaping filters is well established. Details can be found in Ref. 5.

The numerical example, of which details will be given in the next Chapter, is of the symmetric motions of an aircraft in a coupled approach, followed by an automatic landing manoeuvre. The noise processes considered are horizontal and vertical turbulence and ILS glide slope electronic noise (Fig. 8a).
The box in Fig. 8a denoted by "observation process" would represent a pure summation in classic control theory if there is no observation noise. Apart from ILS noise, no observation noise was assumed to be present in the example of this Paper.
If the shaping filters are next joined to the aircraft, as visualized in Fig. 8b, one system perturbed by a number of white noise signals is obtained, see Fig. 8c. Mathematically this operation is achieved by combining the differential equations of the shaping filters with the aircraft's state equations to obtain the augmented state equations, see the Appendix.

One remark should be made on the modelling of the atmospheric turbulence. Generating the coloured noise representing atmospheric turbulence velocities by filtering white noise is only possible if the power spectral densities have a rational form. The well known Dryden spectra used in the example, indeed fulfil this condition.
The Von Karman spectra in contrast, have no rational form and can only be approximated by linear filters. An alternative, exact method to calculate the covariance matrix for a given correlation function of a coloured noise input signal is briefly treated in the Appendix. This enables carrying out calculations as the ones described in this Paper, using atmospheric turbulence as characterized by the Von Karman correlation functions or power spectra.

Now that in the second Chapter the principle of statistical calculations for a time-varying system have been dealt with and the equations have been arranged in the proper form it seems worthwhile to summarize the changes in statistical properties of input signals and changes in the dynamics of the system itself that can now be studied.
First the level of atmospheric turbulence or the ILS noise can be altered either by changing the intensity of the white noise input signals or by changing the gain in the filter transfer functions.
Further the shape of the power spectrum of the atmospheric turbulence may be altered by changing the appropriate parameters (integral scale lengths).
Next changes in the autopilot can be modelled, such as the gradually changing gain due to glide path beam geometry. When performing an automatic landing, the effect of the changing operating mode of the autopilot on the statistics of deviations from an ideal trajectory can be evaluated. Also in the landing phase changes in aerodynamic properties due to ground effects can be modelled by changing the appropriate aerodynamic coefficients.
Another possibility is to study the effect of a sudden decoupling of autopilot or autothrottle. Finally, it will in principle be possible to evaluate programmed changes in aircraft configuration for instance flap settings as required for decelerated or two-segment approaches.

4. DETAILS OF THE NUMERICAL EXAMPLE

To illustrate the capabilities of the calculation method it has been applied to a numerical example of a present day, four engined, subsonic jet transport in a coupled approach followed by an automatic landing. Details of the aircraft, the autopilot and autothrottle gain settings for the coupled approach and for the automatic landing can be found in Refs. 5 and 9. No efforts have been made to optimize the autopilot according to some criterion. Although the layout and the gain settings of the autopilot do not represent

any existing installation, they can be considered to represent the present state of the art.
In order to calculate, in the landing phase, the variances and covariances of deviations relative to an average landing flare, small perturbation equations of motions relative to an ideal, unperturbed automatic landing flare have been used. The ground effect during the flare was also modelled as a small perturbation effect due to deviations from the (known) ideal landing flare.

The atmospheric turbulence, acting during the approach down to flare initiation, was characterized by the Dryden spectra (Ref. 10). The integral scale lengths and turbulence intensity were chosen according to the model of Pritchard (see Ref. 10) for a neutral atmosphere, see Fig. 9. The wind speed at reference height (9.15 m) was chosen at 1 m/sec (approx. 2 knots) in most of the examples.
The terrain factor R_T was chosen at 1,1 (flat agricultural land) resulting in turbulence that could be considered "light" (standard deviation 0,5 m/sec approx. at 200 m altitude). Under the assumption of system linearity, the results computed can be readily extrapolated for more severe turbulence intensities.
The ILS noise intensity, see Fig. 10, and scale length were those specified for CAT I (Ref. 10).
Two cases of changes in gain due to glide slope beam geometry were considered. In one case the gain, expressed by elevator angle per degree angular deviation from the glide path, was taken to decrease exponentially in two distinct phases as shown in Fig. 11, representing a realistic example of a practically implemented compensation. The result is a nearly constant effective gain (elevator angle per foot deviation from the glide path), see Fig. 11.
In another case, no compensation was assumed, resulting in an increasing effective gain as the aircraft approaches the threshold.

All these gradually changing gains, coefficients, intensities etc. were approximated by stepwise variations in time, the entire white noise driven system remaining constant during relatively short time intervals.

5. SOME RESULTS

In Figs. 13, 14 and 15 some results are given of the calculation of variances, due to atmospheric turbulence only, of deviations from the glide path and from an ideal flare, see Fig. 12.
Variances of flight speed, altitude deviations and sink rate can be seen to decrease due to the decreasing intensity of the turbulence and the decreasing integral scale length.
A decreasing scale length is to be seen as a shift in the maximum level of the power to higher frequencies. If the aircraft is considered as a low pass filter, a decreasing scale length has a tendency to decrease the variance of aircraft output signals.
Also shown in Figs. 13, 14 and 15 is the effect of a sudden decoupling of the autopilot at 40 seconds to touchdown.
The subsequent growth in variances shown supposes no corrective action by a pilot. The periodic nature of the responses of the variances of flight speed and sink rate is due to the fact that the natural motions of the unstabilized aircraft are of course much more lightly damped than those of the tightly controlled aircraft in the coupled approach. Still the variance of the flight speed and sink rate can be seen to decrease in the long run as the unstabilized, free aircraft is stable with respect to flight speed and sink rate, which is not the case with respect to altitude.
It can be seen from Fig. 14 that the variance of altitude is increasing after decoupling due to the indifferent or neutral stability of the free aircraft with respect to altitude.

An interesting result can be observed if atmospheric turbulence is made to occur during the last 30 secs. only, see Figs. 13, 14 and 15. It can be concluded that deviations at a certain instant in time (say at decision height, flare height or touchdown) can, for a well damped aircraft, be considered to be mainly caused by the turbulence during the preceding 20 to 30 seconds.
In Fig. 16 the variance of the altitude deviations caused by ILS noise only is given. The effect of this at decision height or touchdown can be seen to be roughly equal to the effect of moderate turbulence. It will be evident that the variance of altitude deviations caused by ILS noise will never be less than the variance of the noise of the ILS reference signal itself if expressed in altitude deviations, (see also Fig. 10), as no prefiltering of the ILS signal was presumed.

The effect of the (non-ideal) compensation of Fig. 11 turned out to be small. To more dramatically illustrate the ability of the computation method to cope with the effect of changing gains, or more generally with changing dynamic system properties, another example is given in Fig. 17.
A change in effective gain, if not compensated at all, is shown in the top figure of Fig. 17. For a modern transport aircraft this change is perhaps less realistic but it can be considered to be representative of general aviation autopilots where the gain with respect to angular deviation from the glide path, is constant. Obviously the aircraft is becoming less stable from approximately 20 seconds to touchdown onwards.

Apart from deviations in flight speed, altitude and sink rate, another important parameter is of course the deviation Δx in distance along the runway, at a certain fixed altitude, relative to an ideal, undisturbed approach path and flare trajectory. The along the runway deviations are related to the deviation relative to the glide path by the simple relation depicted in Fig. 12. For along the runway scatter of touchdown point the influence of the changing value of the flight path angle γ should be taken into account.
Finally it will be evident that the present method has possible applications in the field of 4-D navigation. The variance of the deviation along the flight path can be computed by including this deviation as an element in the aircraft's state vector. In this way the variance of the time of arrival at a certain point in space is easily established.

6. WORST CASE WINDSHEARS

Statistical calculations of aircraft motions in moving air are based on the usual mathematical models of atmospheric turbulence such as the Von Karman or Dryden spectra mentioned before.
There are a number of atmospheric phenomena that are not, or not properly accounted for in these statistical models. For example more or less stationary mean wind gradients or shears may occur, causing a descending or climbing aeroplane to experience relatively slowly changing wind speeds and directions. Deterministic

models of mean wind speed as a function of altitude under certain meteorological conditions are available (Ref. 10), but there are still more atmospheric phenomena that are not properly represented in the statistical models.
It is well known, especially at low altitudes, where the intensity of random atmospheric turbulence according to the usual models should be low, strongly changing winds due to special terrain features or buildings may be met with. Thermals in, apart from that, quiet conditions or more obviously downdraughts in thunderstorms may induce hard landings or even worse. Some or all of these low frequency turbulence phenomena at low altitudes are also sometimes less correctly referred to as "wind shears".

Apart from the deterministic mean wind gradients mentioned above, there is as yet no means of realistically modelling the statistical characteristics of the entire class of low altitude, low frequency turbulence.
One way to gather some understanding of aircraft motions due to low frequency turbulence is to theoretically study aircraft motions caused by actually recorded wind time-histories of a notoriously unfavourable character. Another way is trying to find, according to some criterion, the particular deterministic wind (or turbulence) time-history that causes the greatest deviation of one of the motion variables relative to an ideal course.
Corbin (Ref. 11) derived such worst case turbulence time histories by a search procedure yielding "worst" combinations of a number of sines and cosines.
It appears, however, that worst case time histories can also be found by a more analytical approach. The following is a brief description of attempts made by the authors of this Paper to describe the worst cases in terms of linear system theory.
This concept, of which a more formal derivation is to be given in Ref. 12, can be illustrated by a simple example.

The response of one particular state or motion variable x_i of the state $\underline{x}(t)$ of a constant linear system on one single input signal v(t) if the system is at rest initially can be written as (see Ref. 13):

$$x_i(t) = \int_0^t h_i(t - \tau) \cdot v(\tau) \cdot d\tau \tag{3}$$

where $h_i(t)$ is the response of x_i to a unit impulse $\delta(o)$ at $t = 0$.
The integral according to Eq. (3) has been visualized in Fig. 18. The function $h_i(t - \tau)$, being the time reversed impulse response of x_i from t to τ, can be considered as a measure of the contribution of v at instant τ, to the value of x_i at t.
Without a formal derivation it can easily be seen from Eq. (3) and from Fig. 18 that it is plausible that, for a given fixed value of t, the absolute value of $x_i(t)$ will be maximal if $v(\tau)$ is exactly proportional to $h_i(t - \tau)$ for all τ. In other words the worst case time-history of v(t), to obtain a maximum deviation of $x_i(t)$ is proportional to the time reversed impulse response of x_i:

$$v(\tau) = C \cdot h_i(t - \tau) \tag{4}$$

where C is a constant.
Now consider a system with a number of output signals such as an aircraft, then all output signals (or motion variables) have different impulse responses. As a consequence there will be one particular worst case input signal for each of the output variables.
Fig. 19 gives two such worst case time histories of the horizontal wind velocity and the resulting largest deviations of altitude and sink rate. The deviations were calculated by generating the response of the (unstabilized) example aircraft by solving the governing differential equations for the given input time-histories.
It can be seen that maximum wind excursions of only 1 m/sec (2 knots approximately) in both cases, induced an altitude loss of 25 m (80 ft) in one case and an excess sink rate of 2.3 m/sec (450 ft/min) in the other. As already mentioned the aircraft was not stabilized in this case and no pilot action was supposed to be involved. As a vigilant pilot would of course take immediate corrective action, the example represents a worst case in more than one sense.

Apart from solving the governing differential equations for the given worst input time histories there is still another way to obtain the values of the maximum deviations, which can be shown as follows.
Substituting Eq. (4) into Eq. (3) yields:

$$x_i(t) = C \int_0^t h_i^2(t - \tau)\, d\tau \tag{5}$$

By considering Fig. 18 it is easily seen that this is equal to:

$$x_i(t) = C \int_0^t h_i^2(t)\, dt \tag{6}$$

Now it has been shown elsewhere, see Ref. 5, that the integral in Eq. (6) is equal to the variance at t of the output signal $x_i(t)$ if the system under consideration is perturbed by a white noise random input signal

w(t), with intensity equal to C, from t = 0 onwards:

$$\sigma_{x_i}^2 = C \int_0^t h_i^2(t)\, dt$$

Thus the maximum deviation of x_i at time t, caused by its particular deterministic, worst case input signal is seen to be equal to the variance $\sigma_{x_i}^2(t)$ in the stochastic case where the system is perturbed by a white noise signal with intensity C:

$$x_i(t) = \sigma_{x_i}^2(t)$$

This result has been visualized in the diagram of Fig. 20.

As regards the non-maximum deviation of some other motion variable for instance $x_j(t)$, due to the particular deterministic input signal causing the largest deviation of x_i at t, it can be shown that $x_j(t)$ is equal to the covariance $\sigma_{x_i x_j}(t)$ of $x_i(t)$ and $x_j(t)$ in the stochastic case just mentioned. The problem of finding all deviations caused by any particular worst case time history is thus reduced to calculating the covariance matrix of the state vector of a linear system perturbed by one white noise input signal.

The tentative concept of worst case wind time histories as briefly summarized above, could be used as a tool to evaluate the sensitivity of given aircraft control systems to the class of low frequency atmospheric turbulence broadly described as wind shears. It will be evident that also the response to other worst case input signals, such as "bends" in ILS patterns could be evaluated in a similar way. In the case of terrain following, as another example, a worst case terrain profile could be defined.
In the case of an automatic landing, the analytic concept of worst case wind time histories should be extended to account for changing system characteristics. It appears that this could be achieved by defining worst case initial conditions for the deterministic case and establishing a relation with the response to initial conditions of the covariance matrix in the stochastic case.

7. CONCLUDING REMARKS

For the calculation of variances or r.m.s. levels of output variables of a time-varying noise driven system advantage can be taken of concepts of modern system theory by formulating the problem as one of a white noise driven system. Using a computation method as described in this Paper it is possible to avoid relatively inaccurate and time consuming Monte Carlo simulations.
The method described can also be adapted such that input signals, characterized by given correlation functions, can be used. This enables an exact representation of the Von Karman turbulence spectra. Approximating these spectra by linear filtering can thus be avoided.
Finally it may be obvious that the formulation in terms of system theory concepts is such that it opens possibilities for the design of control systems by optimization techniques.

As to the worst case windshears discussed in Chapter 5 only some tentative conclusions appear to be appropriate at the present moment. Of course any so-called "worst case" wind time history is only worst according to the criterion chosen. The concept of interpreting the time-reversed impulse response as a measure for the contribution at a certain altitude to deviations at decision height or touchdown seems attractive. Moreover, the computation of maximum deviations obtained is straightforward as the problem can again be formulated as one of a white noise driven linear system. For automatic approaches, followed by an automatic landing, in which case the system's dynamic properties change with time, the method should be extended in the way of defining "worst case" initial conditions.

8. REFERENCES

1. G.A.J. van de Moesdijk, Simulation of patchy atmospheric turbulence, based on measurements of actual turbulence, AGARD-CP-198 on Flight simulation/Guidance systems simulation, 1975.

2. B.N. Tomlinson, Developments in the simulation of atmospheric turbulence, AGARD-CP-198 on Flight simulation/Guidance systems simulation, 1975.

3. K. Sidwell, A method for the analysis of non-linearities in aircraft dynamic response to atmospheric turbulence, NASA TN D-8265, 1976.

4. O.H. Gerlach, Calculation of the response of an aircraft to random atmospheric turbulence. Part I-Symmetric motions, Report VTH-138, Technological University Delft, Department of Aeronautical Engineering, 1966.

5. J.C. van der Vaart, The impulse response method for the calculation of statistical properties of aircraft flying in random atmospheric turbulence, Report VTH-197, Delft University of Technology, Department of Aerospace Engineering, 1975.

6. O.H. Gerlach, G.A.J. van de Moesdijk, J.C. van der Vaart, Progress in the mathematical modelling of flight in turbulence, AGARD-CP-140 on Flight in turbulence, 1973.

7. W.E. Holley, A.E. Bryson, Wind modelling and lateral control for automatic landing, Journal of Spacecraft and Rockets, Vol. 14, no. 2, Febr. 1977.

8. H.L. Jonkers, F.K. Kappetijn, J.C. van der Vaart, Digital calculation of the propagation in time of the aircraft gust response covariance matrix, Report LR, Delft University of Technology, Department of Aerospace Engineering (to be published).

9. J.C. van der Vaart, De automatische afvangmanoeuvre van een verkeersvliegtuig (the automatic landing flare of a transport aircraft, in Dutch), Report VTH-182, Delft University of Technology, Department of Aeronautical Engineering, 1974.

10. AGARD Report No. 632 on Approach and Landing Simulation, 1975.

11. M.J. Corbin, Turbulence time-histories causing greatest touchdown errors following an automatic flare. Tech. Memo Avionics 152, Royal Aircraft Establishment, 1973.

12. J.C. van der Vaart, Worst case wind time-histories causing largest deviations from a desired flight path. An analytical approach, Report LR, Delft University of Technology, Department of Aerospace Engineering (to be published).

13. H. Kwakernaak, R. Sivan, Linear optimal control systems, Wiley-Interscience, Inc. New York, London, Sydney, Toronto, 1972.

14. H.L. Dryden, S.K. Friedlander, L. Topper, Review of the statistical theory of turbulence, in: Classic papers on statistical theory, Interscience Publ. Inc., New York, 1961.

15. A.P. Sage, J.L. Melsa, Estimation theory with applications to communications and control, McGraw-Hill, New York, 1971.

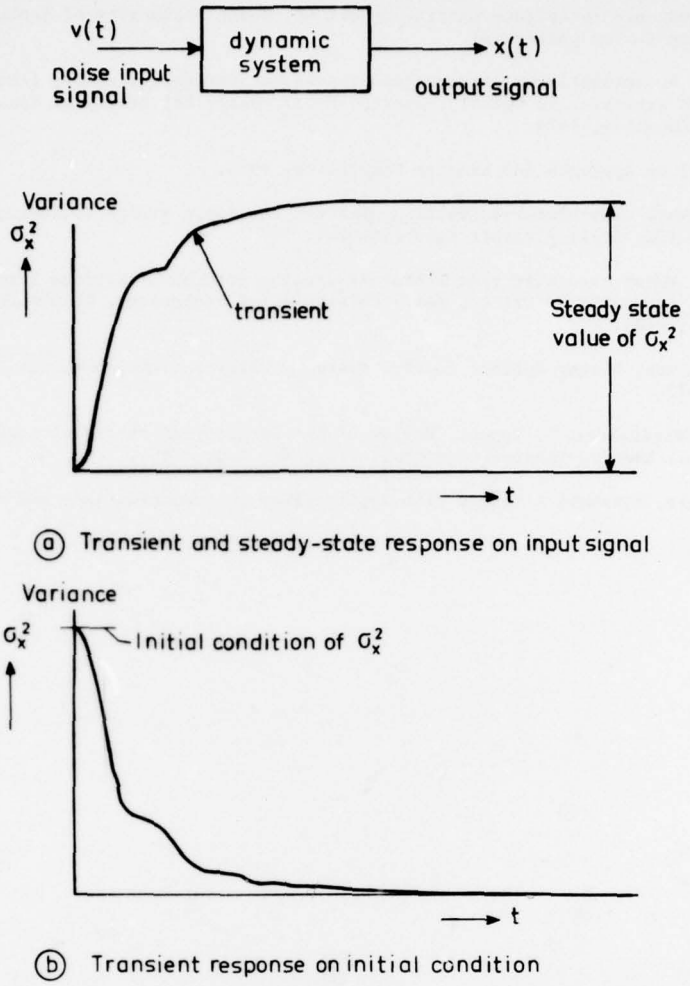

Fig. 1 Responses of the variance on a noise input signal and on initial conditions

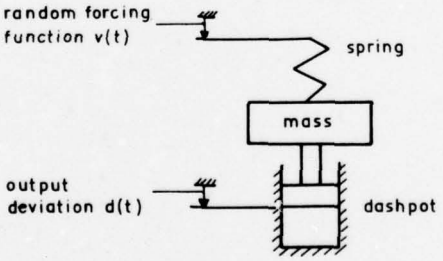

State equation : $\dot{\underline{x}}(t) = A\,\underline{x}(t) + \underline{b}\,.\,v(t)$

State vector : $\underline{x}(t) = \begin{bmatrix} x_1(t) \\ x_2(t) \end{bmatrix} = \begin{bmatrix} d(t) \\ \dot{d}(t) \end{bmatrix}$

Covariance matrix: $C_{xx}(t) = \begin{bmatrix} \sigma^2_{x_1}(t) & \sigma_{x_1x_2}(t) \\ \sigma_{x_2x_1}(t) & \sigma^2_{x_2}(t) \end{bmatrix}$

Fig. 2 Mass-spring-dashpot system of second order

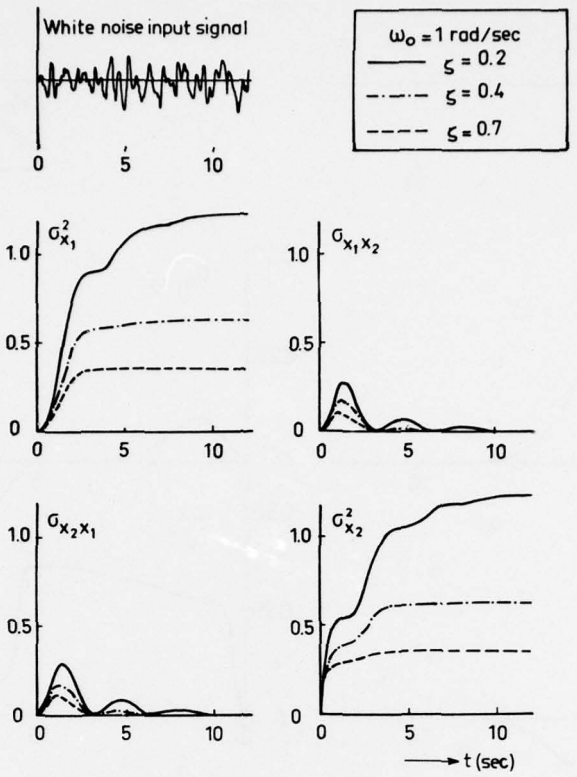

Fig.3 Responses of the elements of the covariance matrix on a white noise input signal, initial conditions zero

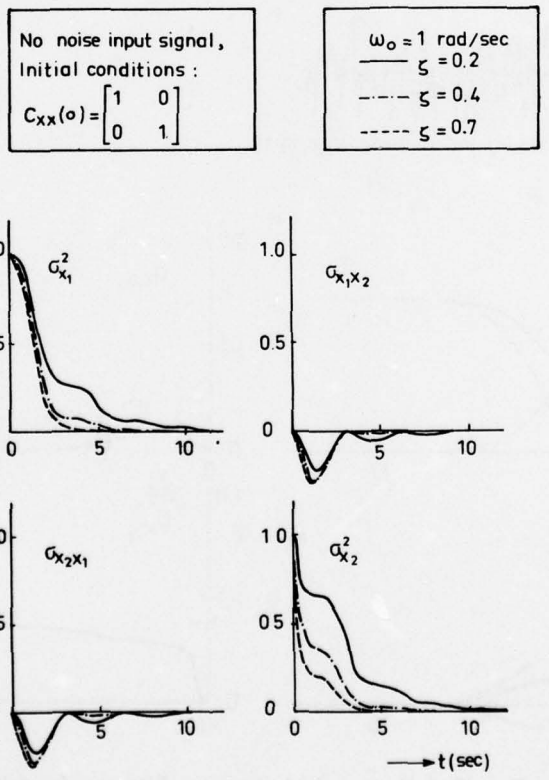

Fig.4 Responses of the elements of the covariance matrix on initial conditions

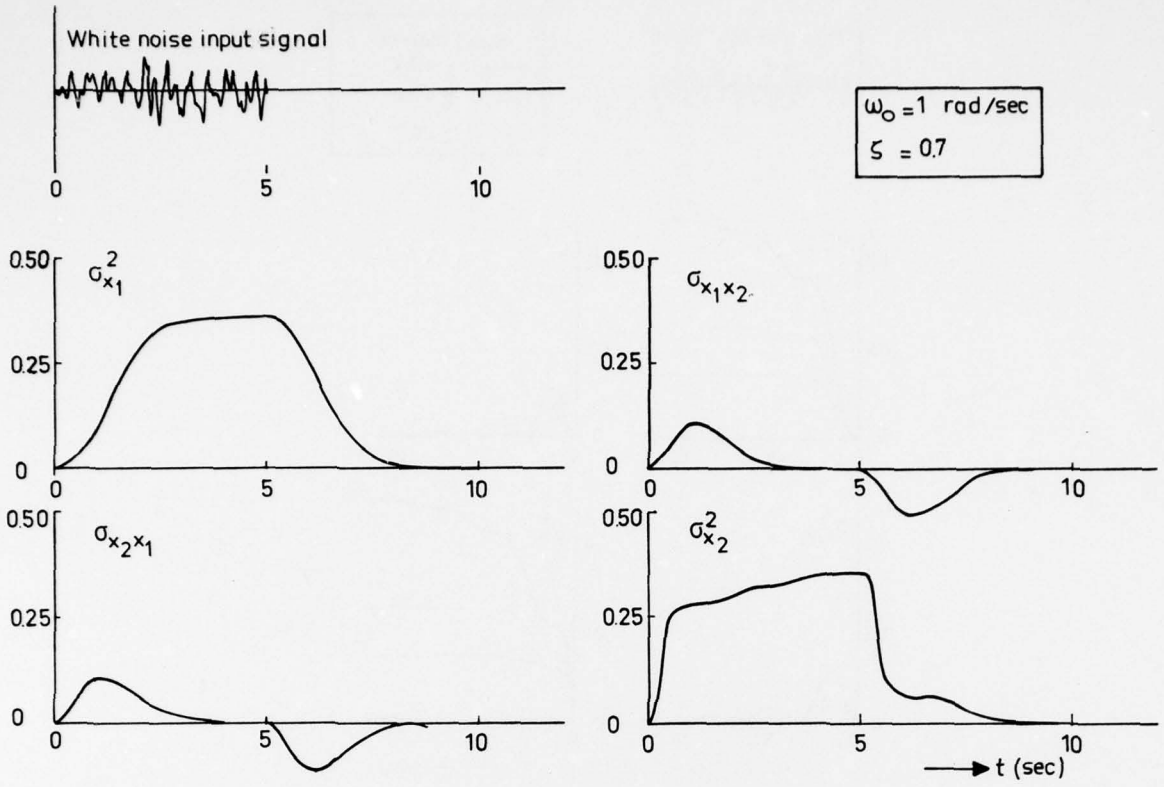

Fig.5 Response on a white noise input signal of limited duration.

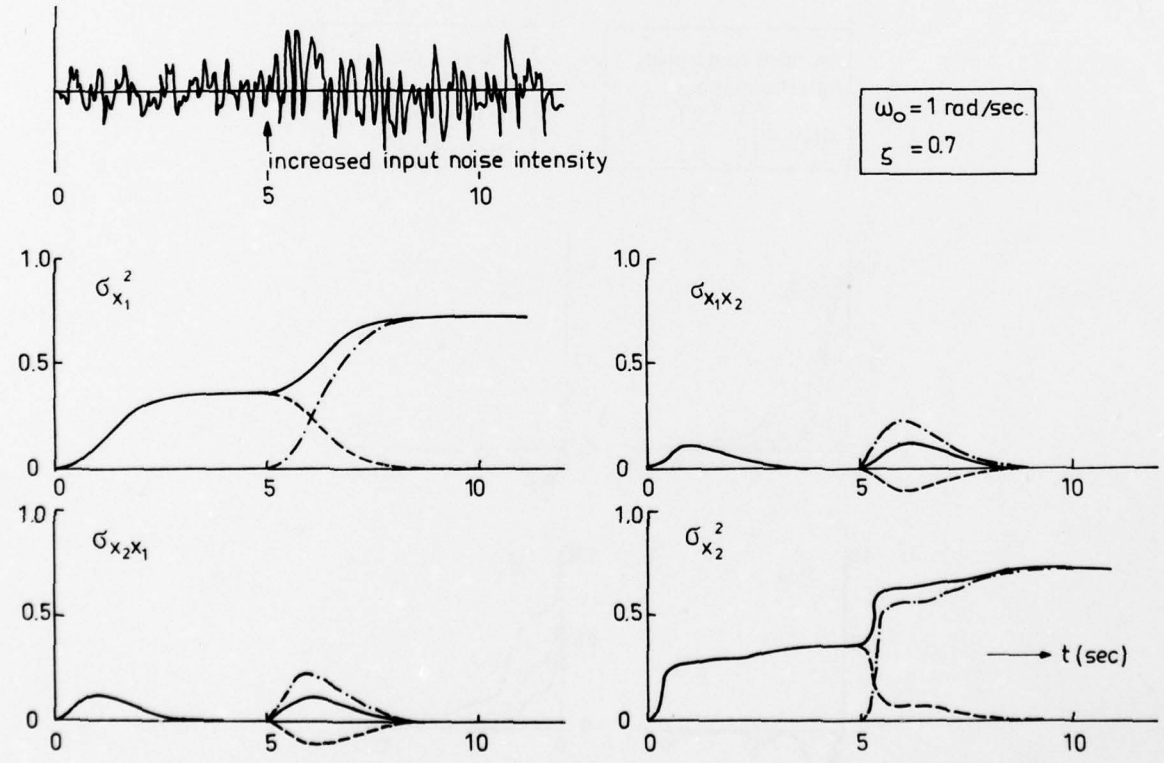

Fig.6 The effect of a stepwise increase in white noise input intensity

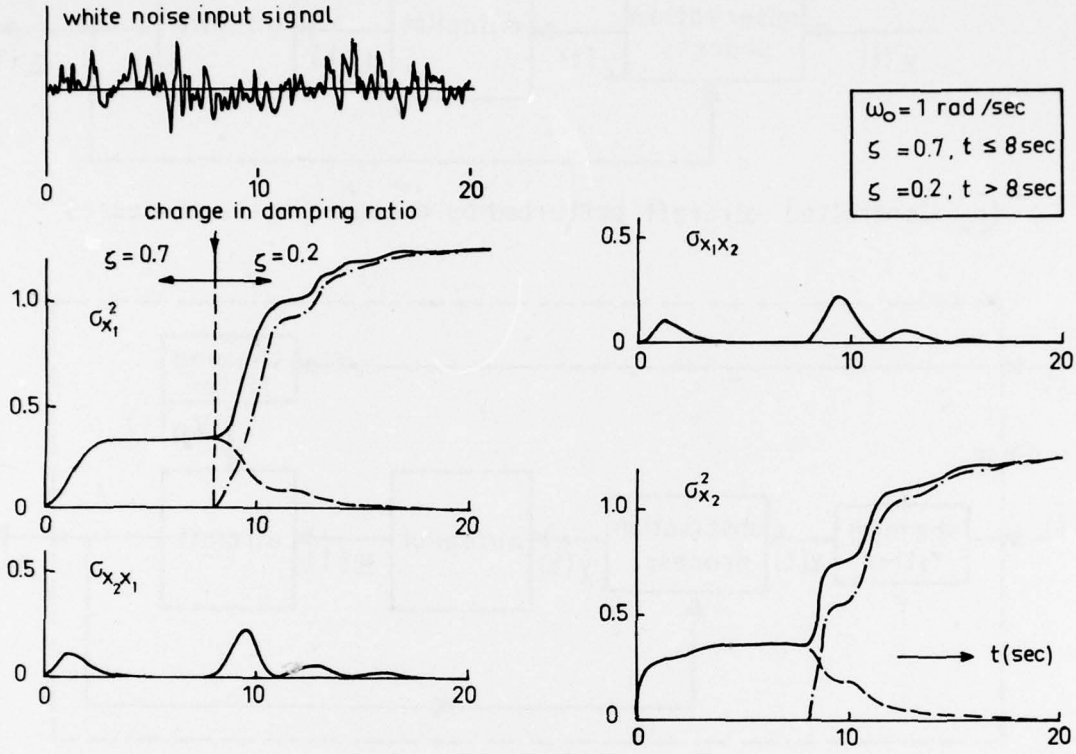

Fig.7 The effect of a stepwise change in damping ratio

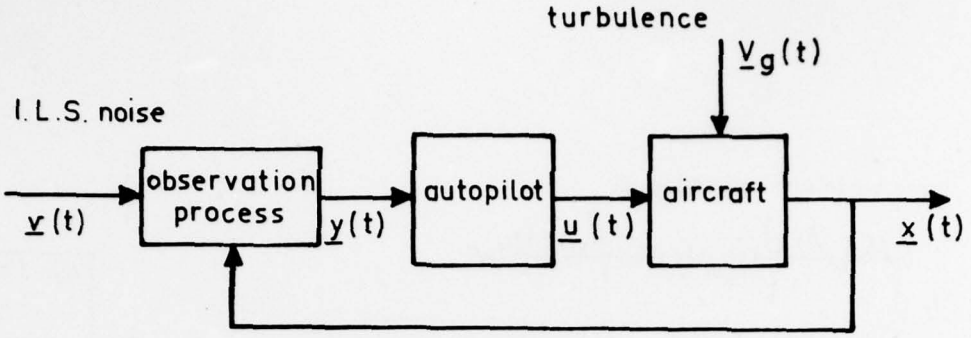

(a) Controlled aircraft perturbed by coloured noise processes

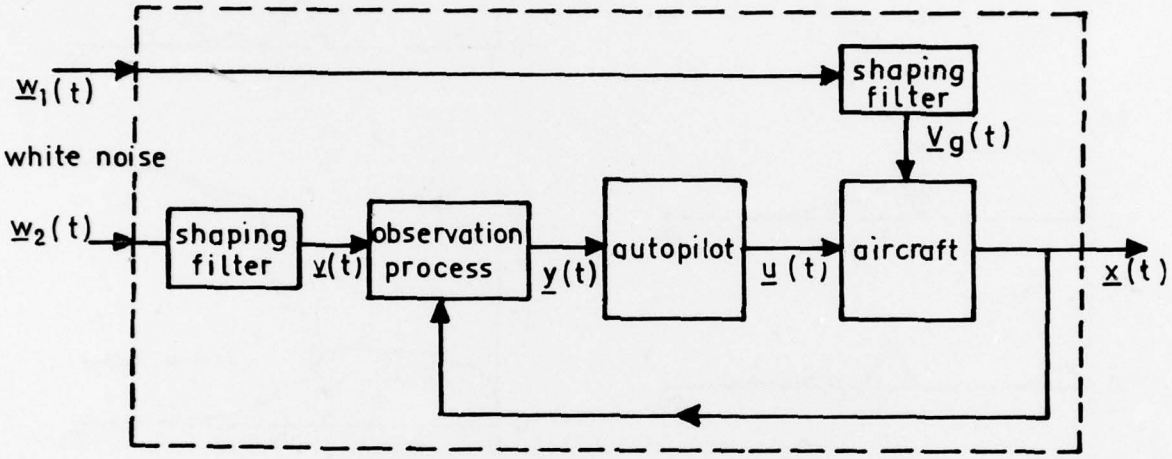

(b) Addition of shaping filters

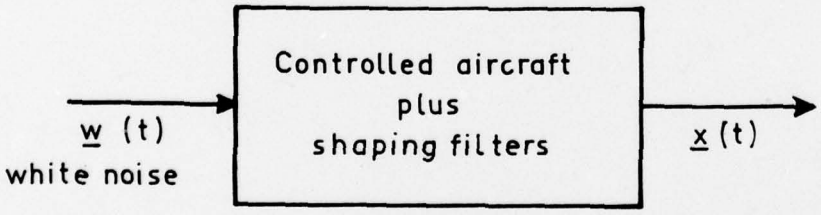

(c) Controlled aircraft and shapingfilters as one system perturbed by white noise
State equation:

$$\dot{\underline{x}}(t) = A\underline{x}(t) + B\underline{w}(t)$$

Fig.8 Block diagrams of shaping filters and controlled aircraft

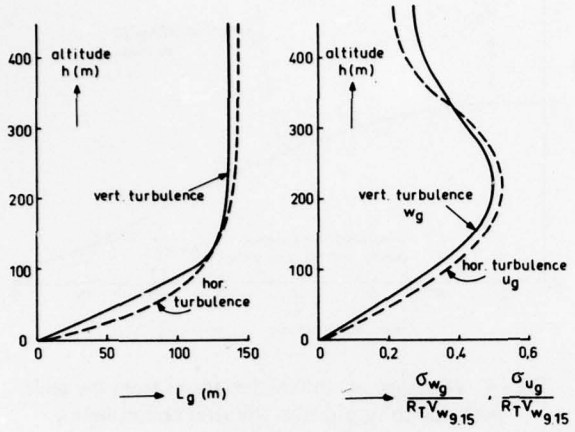

Fig.9 Integral scale lengths and intensities of low altitude atmospheric turbulence according to Pritchard (see Ref.10). Neutral atmosphere

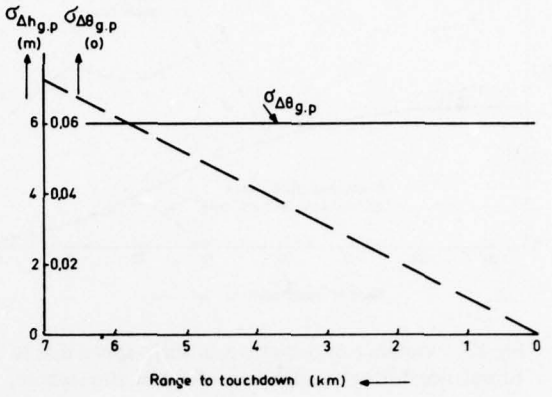

Fig.10 Maximum standard deviation of I.L.S. glide slope noise expressed in angular deviation ($\Delta\theta_{g.p}$) and altitude deviation ($\Delta h_{g.p}$) (Ref.10)

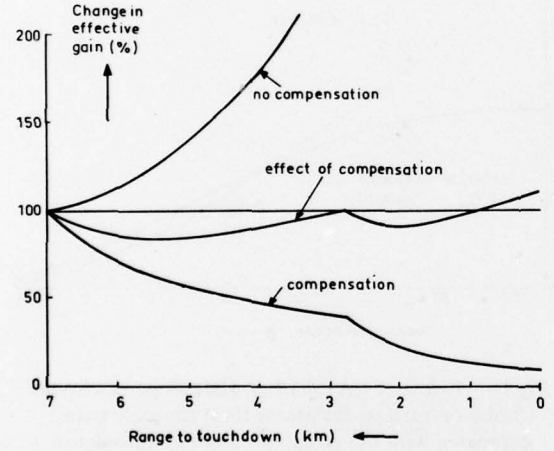

Fig.11 Change in effective gain (elevator angle per unit altitude deviation) due to glide path geometry. Effect of compensation

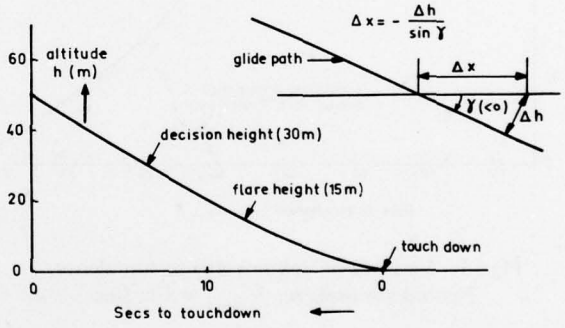

Fig.12 Effect of deviations Δh relative to the glide path on deviations Δx in distance along the runway

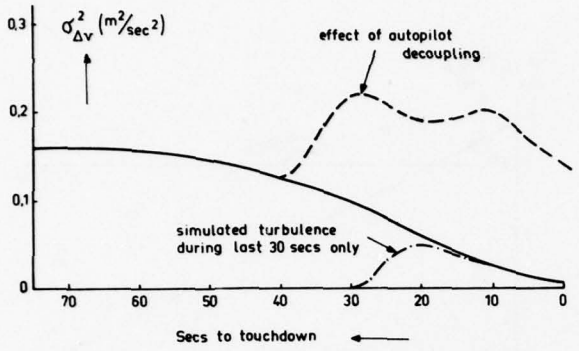

Fig.13 Variance of deviations in flight speed due to turbulence during an approach. Neutral atmosphere, $V_{w_{9.15}} = 1$ m/sec

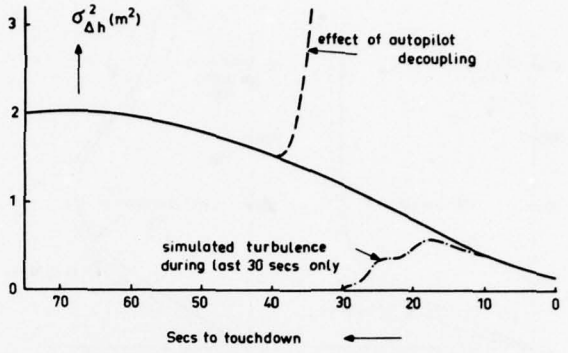

Fig.14 Variance of vertical deviations from the glide path due to turbulence. Neutral atmosphere, $V_{w_{9.15}} = 1$ m /sec

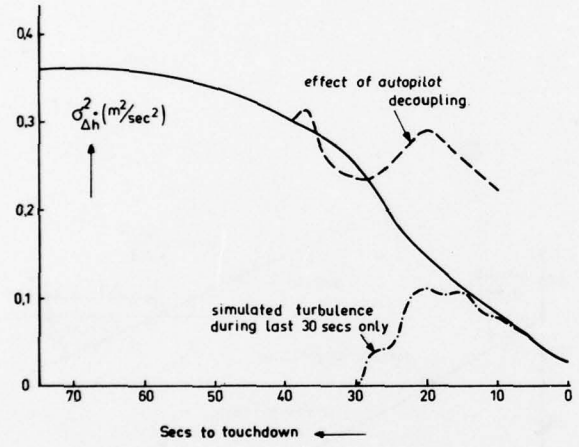

Fig.15 Variance of sink rate due to turbulence. Neutral atmosphere, $V_{w_{9.15}} = 1$ m /sec

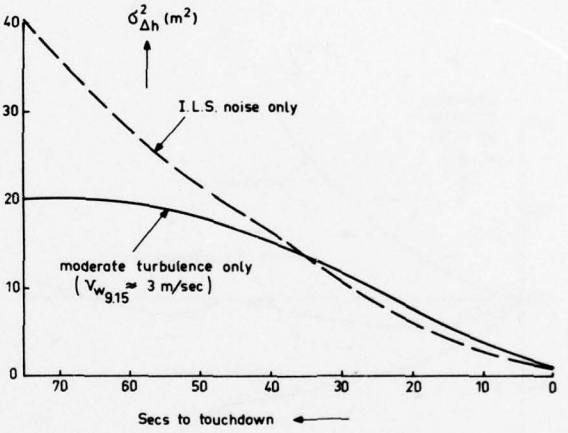

Fig.16 Effect of CAT. I I.L.S. glide slope electronic noise on vertical deviations from the glide path compared with the effect of moderate turbulence ($V_{w_{9.15}} = 3$ m/sec)

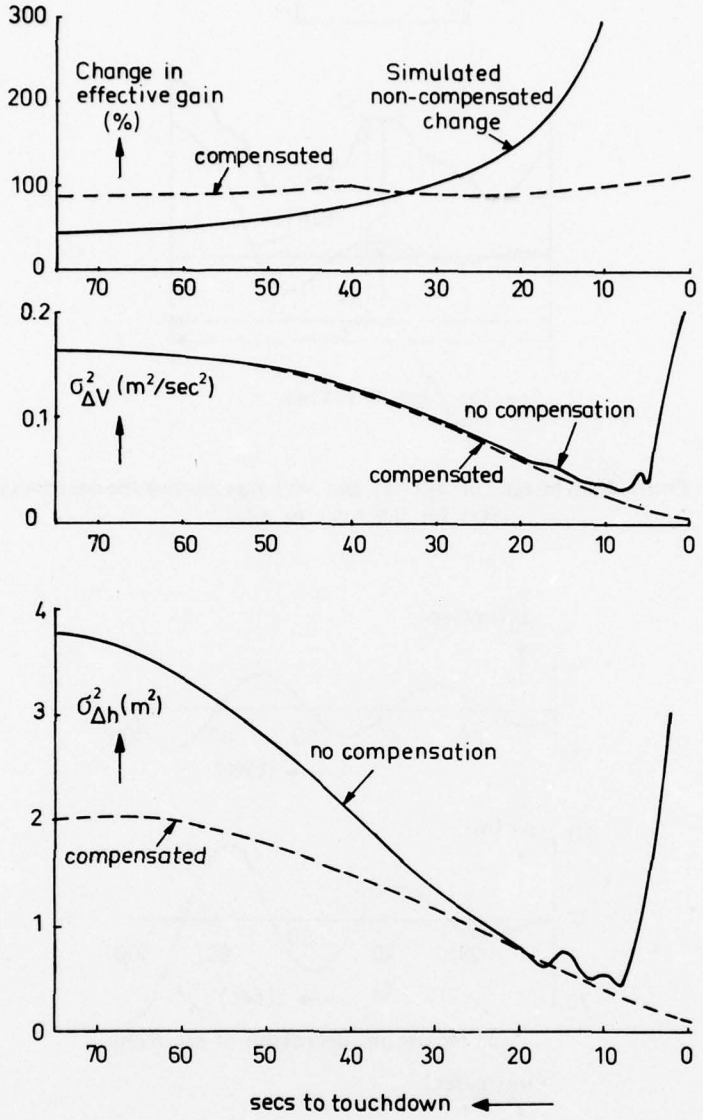

Fig.17 Variance of deviations in flight speed and deviations from the glide path for non-compensated changes in effective gain due to I.L.S. beam geometry

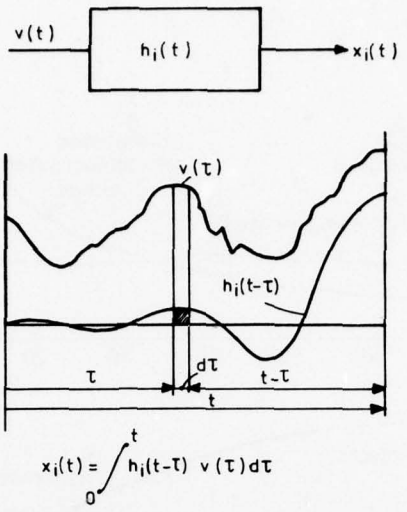

Fig.18 Convolution integral of $h_i(t-\tau)$ and $v(\tau)$ representing the contribution of $v(\tau)$ for $0 \leq \tau \leq t$ to $x_i(t)$

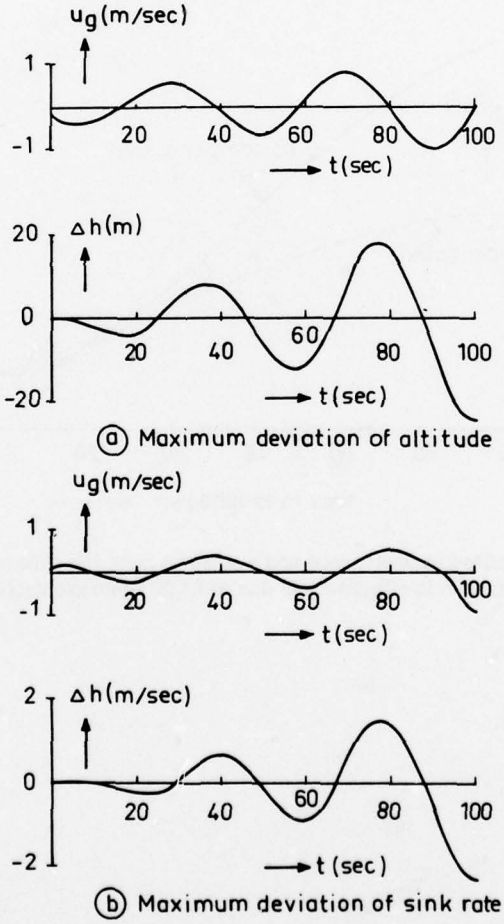

Fig.19 Worst case time-histories of horizontal wind speed and resulting maximum deviations of altitude and sink rate at t = 100 sec. Unstabilized aircraft, approach configuration

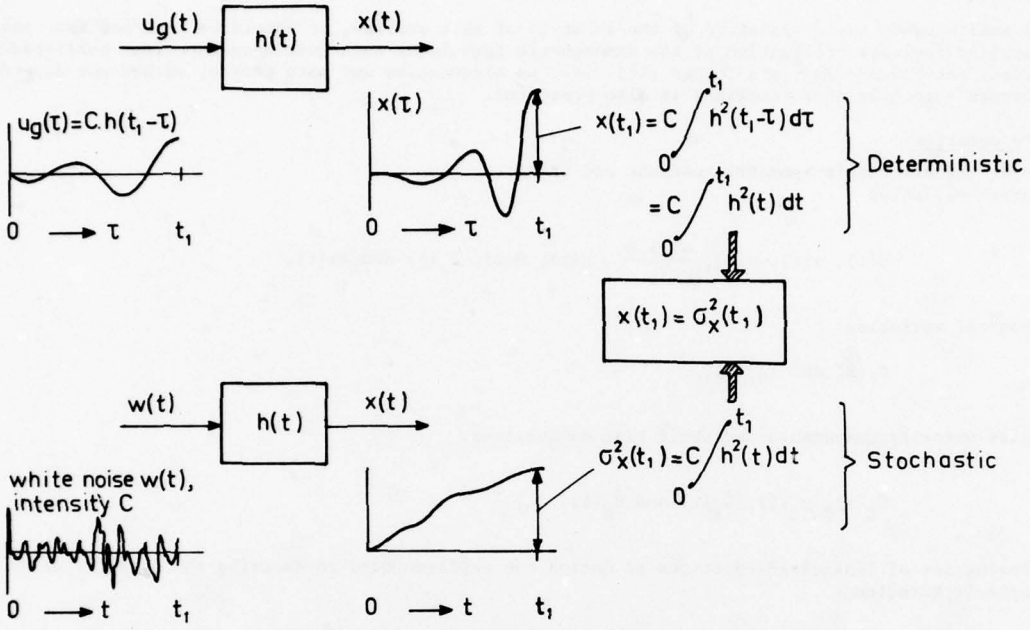

Fig.20 Relation between maximum deviation x at t_1 (worst case, deterministic) and the variance $\sigma_x^2(t_1)$ of x(t) in the white noise driven stochastic case

APPENDIX

THE COMPUTATION OF THE COVARIANCE MATRIX AS A FUNCTION OF TIME

The problem of computing variances and covariances of aircraft response to atmospheric turbulence can be reduced to computation of the corresponding response statistics of a linear system driven by zero mean, gaussian, white noise, if:

1. the atmospheric perturbations are assumed zero mean and normally distributed;
2. the atmospheric perturbations are assumed small enough to justify linearization of the aircraft's aerodynamics and the aircraft's equations of motion;
3. Taylor's frozen field hypothesis is assumed valid, i.e. if the aircraft's mean airspeed is assumed large as compared to the rate of changes in atmospheric motions.

Prior to embarking on the explanation of the solution of this problem, it should be remarked that the method applied includes utilization of the atmospheric turbulence autocovariance functions published by H.L. Dryden, see Friedlander and Topper (Ref. 14). An alternative and more general method not depending on the Dryden autocovariance functions is also presented.

The state equation

Considering the aircraft's symmetric motions and using:

1. the state variables

$$\hat{u}(t),\ \alpha(t),\ \theta(t),\ \frac{q(t)\,\bar{c}}{V_o},\ h(t),\ H(t),\ T_c(t) \text{ and } \Delta x(t),$$

2. the control variables:

$$\delta_e(t) \text{ and } T_{c_i}(t),$$

3. the gust velocity components and their time derivatives:

$$\hat{u}_g(t),\ \alpha_g(t),\ \dot{\hat{u}}_g(t) \text{ and } \dot{\alpha}_g(t),$$

the following set of linearized equations of motion can be formulated to describe the dynamics of an aircraft in atmospheric turbulence

$$2\mu_c D_c \hat{u}(t) = C_{X_u}\hat{u}(t) + C_{X_\alpha}\alpha(t) + C_{Z_o}\theta(t) + \Delta C_{X_h}(t)h(t) \tag{A.1}$$

$$2\mu_c D_c \alpha(t) = C_{Z_u}\hat{u}(t) + C_{Z_\alpha}\alpha(t) - C_{X_o}\theta(t) + (C_{Z_q} + 2\mu_c)\frac{q(t)\,\bar{c}}{V_o} + \Delta C_{Z_h}(t)h(t) +$$
$$+ C_{Z_\delta}\delta_e(t) + C_{Z_{u_g}}\hat{u}_g(t) + C_{Z_{\alpha_g}}\alpha_g(t) + C_{Z_{\dot{u}_g}}D_c\hat{u}_g(t) + C_{Z_{\dot{\alpha}_g}}D_c\alpha_g(t) \tag{A.2}$$

$$D_c\theta(t) = \frac{q(t)\,\bar{c}}{V_o} \tag{A.3}$$

$$2\mu_c K_y^2 D_c \frac{q(t)\,\bar{c}}{V_o} = C_{m_u}\hat{u}(t) + C_{m_\alpha}\alpha(t) + C_{m_{\dot{\alpha}}}D_c\alpha(t) + C_{m_q}\frac{q(t)\,\bar{c}}{V_o} + \Delta C_{m_h}(t)h(t) +$$
$$+ C_{m_\delta}\delta_e(t) + C_{m_{u_g}}\hat{u}_g(t) + C_{m_{\alpha_g}}\alpha_g(t) + C_{m_{\dot{u}_g}}D_c\hat{u}_g(t) + C_{m_{\dot{\alpha}_g}}D_c\alpha_g(t) \tag{A.4}$$

$$D_c\frac{h(t)}{\bar{c}} = -\alpha(t) + \theta(t) \tag{A.5}$$

$$D_c\frac{V_o}{\bar{c}^2}H(t) = \frac{1}{\bar{c}}h(t) \tag{A.6}$$

$$D_c T_c(t) = -\frac{\bar{c}}{V_o\,\tau_{eng}}T_c(t) + \frac{\bar{c}}{V_o\,\tau_{eng}}T_{c_i}(t) \tag{A.7}$$

$$D_c\frac{\Delta x(t)}{\bar{c}} = \hat{u}(t) \tag{A.8}$$

Introducing:

1. the state vector:

$$\underline{x} \triangleq \text{col}\left(\hat{u},\ \alpha,\ \theta,\ \frac{q\bar{c}}{V_o},\ h,\ H,\ T_c,\ \Delta x\right), \tag{A.9}$$

2. the control vector:

$$\underline{u} \triangleq \text{col}\ (\delta_e,\ T_{c_i}), \tag{A.10}$$

3. the perturbation vector:

$$\underline{V}_g = \text{col } (\hat{u}_g,\ \alpha_g), \tag{A.11}$$

the equations of motion can be combined to formulate a first order linear vector matrix differential equation:

$$M_o D_c \underline{x}(t) = M_1 D_c \underline{x}(t) + M_2(t)\underline{x}(t) + M_3 \underline{u}(t) + M_4 \underline{V}_g(t) + M_5 D_c \underline{V}_g(t) \tag{A.12}$$

or:

$$\dot{\underline{x}}(t) = A(t)\underline{x}(t) + B\underline{u}(t) + C\underline{V}_g(t) + D\dot{\underline{V}}_g(t) \tag{A.13}$$

The matrices M_o, $M_1,\ldots,M_5$ can be specified by comparison of Eqs. (A.1) through (A.11) with Eq. (A.12).

The observation equation

The quantities $\hat{u}_{a_m}(t)^{(*)}$, $\alpha_{a_m}(t)$, $\theta_m(t)$, $\frac{q_m(t)\ \bar{c}}{V_o}$, $h_m(t)$ and $H_m(t)$ can be considered as system output signal perturbations. Taking account of noisy ILS observations, these quantities are related to the state vector $\underline{x}(t)$, the atmospheric perturbation vector $\underline{V}_g(t)$ and ILS observation noise, writing:

$$\hat{u}_{a_m}(t) = \hat{u}(t) + \hat{u}_g(t) \tag{A.14}$$

$$\alpha_{a_m}(t) = \alpha(t) + \alpha_g(t) \tag{A.15}$$

$$\theta_m(t) = \theta(t) \tag{A.16}$$

$$\frac{q_m(t)\ \bar{c}}{V_o} = \frac{q(t)\ \bar{c}}{V_o} \tag{A.17}$$

$$h_m(t) = h(t) + h_{gp}(t) \tag{A.18}$$

$$H_m(t) = H(t) + H_{gp}(t) \tag{A.19}$$

Introducing the output signal perturbation vector:

$$\underline{y} \overset{\Delta}{=} \text{col } (\hat{u}_{a_m},\ \alpha_{a_m},\ \theta_m,\ \frac{q_m\ \bar{c}}{V_o},\ h_m,\ H_m) \tag{A.20}$$

and the ILS noise vector:

$$\underline{y} \overset{\Delta}{=} \text{col } (h_{gp},\ H_{gp}) \tag{A.21}$$

the observation equations (A.14) through (A.19) can be combined to yield the vector matrix observation equation:

$$\underline{y}(t) = E\underline{x}(t) + F\underline{V}_g(t) + G\underline{y}(t) \tag{A.22}$$

The output equation

The variables of interest when analyzing the effects of atmospheric turbulence and ILS noise on an aircraft following the ILS glide slope are $\hat{u}(t)$, $h(t)$, $\Delta x(t)$ and $\Delta\dot{h}(t)$, where

$$\begin{aligned}\Delta\dot{h}(t) &= V_o \sin \gamma(t) \\ &\simeq V_o\{\theta(t) - \alpha(t)\}\end{aligned} \tag{A.23}$$

Defining:

(*) the suffix "a" is used to denote quantities, defined relative to the surrounding air-mass.
the suffix "m" is used to indicate measured magnitudes of the corresponding variables.

$$\underline{z} \triangleq \text{col } (\hat{u},\ \hat{u}_a,\ h,\ \Delta x,\ \Delta\dot{h}) \tag{A.24}$$

the following vector matrix equation can be formulated:

$$\underline{z}(t) = R\underline{x}(t) + S\underline{V}_g(t) \tag{A.25}$$

The atmospheric turbulence

The random atmospheric perturbations acting upon the aircraft during flight in turbulence are often considered normally distributed, zero mean, and sequentially correlated with autocovariance functions:

$$C_{\hat{u}_g\hat{u}_g}(\tau) = \sigma_{\hat{u}_g}{}^2\, e^{-\frac{V_o}{L_{u_g}}|\tau|} \tag{A.26}$$

$$C_{\alpha_g\alpha_g}(\tau) = \sigma_{\alpha_g}{}^2\, e^{-\frac{V_o}{L_{w_g}}|\tau|}\left(1 - 2\,\frac{V_o}{L_{w_g}}|\tau|\right) \tag{A.26}$$

see Ref. 14.
Under these assumptions the atmospheric turbulence velocity components may be modelled as stochastic outputs of linear, low pass filters driven by gaussian, zero mean, white noise. Mathematical expressions for these filters can be derived using conventional Fourier transform techniques.
Specifying two white noise input processes $w_{11}(t)$ en $w_{12}(t)$ with unit intensity, the following mathematical expressions are obtained for the filters required:

$$\dot{\hat{u}}_g(t) = -\frac{V_o}{L_{u_g(t)}}\,\hat{u}_g(t) + \sigma_{\hat{u}_g}(t)\sqrt{\frac{2}{V_o L_{u_g}(t)}}\,w_{11}(t) \tag{A.28}$$

$$\dot{\alpha}_g(t) = \alpha_g{}^*(t) + \sigma_{\alpha_g}(t)\sqrt{\frac{3}{V_o L_{w_g}(t)}}\,w_{12}(t) \tag{A.29}$$

$$\dot{\alpha}_g{}^*(t) = -\frac{2V_o}{L_{w_g}(t)}\,\alpha_g{}^*(t) - \frac{V_o{}^2}{L_{w_g}{}^2(t)}\,\alpha_g(t) + \sigma_{\alpha_g}(t)\,\frac{1}{L_{w_g}(t)}\sqrt{\frac{V_o}{L_{w_g}(t)}}\,(1 - 2\sqrt{3})\,w_{12}(t) \tag{A.30}$$

or:

$$\dot{\underline{V}}_g{}^*(t) = P(t)\,\underline{V}_g{}^*(t) + Q(t)\underline{w}_1(t) \tag{A.31}$$

where

$$\underline{V}_g{}^* \triangleq \text{col } (\hat{u}_g,\ \alpha_g,\ \alpha_g{}^*) \tag{A.32}$$

and:

$$\underline{w}_1 \triangleq \text{col } (w_{11},\ w_{12}) \tag{A.33}$$

The vector-valued quantity $\underline{V}_g(t)$ occurring in Eqs. (A.13) and (A.22) can be related to the quantity $\underline{V}_g{}^*(t)$, see Eq. (A.31) writing:

$$\underline{V}_g(t) = T\,\underline{V}_g{}^*(t) \tag{A.34}$$

Glide path observation noise

Glide path observation errors may be described in terms of a normally distributed, zero mean, sequentially correlated random process with given autocovariance function:

$$C_{h_{gp}h_{gp}}(\tau) = \sigma_{gp}{}^2\, e^{-\frac{V_o}{L_{gp}}|\tau|} \tag{A.35}$$

see Ref. 10.
In a similar manner as shown for the atmospheric turbulence glide path observation noise can be considered as an output signal of a low pass filter, driven by gaussian, zero mean, white noise with unit intensity.

$$\dot{h}_{gp}(t) = -\frac{V_o}{L_{gp}}\,h_{gp}(t) + \sigma_{h_{gp}}(t)\sqrt{\frac{2V_o}{L_{gp}}}\,w_2(t) \tag{A.36}$$

$$\dot{H}_{gp}(t) = h_{gp}(t) \tag{A.37}$$

where $H_{gp}(t)$ is the integrated glide path observation noise, specified in Eqs. (A.36) and (A.37). Using the vector-valued quantity $\underline{v}(t)$, defined by Eq. (A.21) this filter expression can be written:

$$\dot{\underline{v}}(t) = M\underline{v}(t) + N(t)\ w_2(t) \tag{A.38}$$

The augmented state equation

Relating the control signal $\underline{u}(t)$ to the system output signal $\underline{y}(t)$, according to the control law

$$\underline{u}(t) = -K(t)\ \underline{y}(t) \tag{A.39}$$

where the gain $K(t)$ is prespecified and combining the Eqs. (A.13), (A.22) and (A.34) the following system state equation can be obtained:

$$\dot{\underline{x}}(t) = [A - BK(t)E]\ \underline{x}(t) + [CT + DTP(t) - BK(t)F]\ \underline{V}_g^*(t) - BK(t)G\underline{v}(t) + DTQ(t)\ \underline{w}(t) \tag{A.40}$$

Substitution of Eq. (A.34) in Eq. (A.25) yields the following result:

$$\underline{z}(t) = R\underline{x}(t) + ST\underline{V}_g^*(t) \tag{A.41}$$

Defining the augmented system state:

$$\underline{x}^* \triangleq \text{col}\ (\underline{x},\ \underline{V}_g^*,\ \underline{v}) \tag{A.42}$$

and the white noise system input:

$$\underline{w} \triangleq \text{col}\ (\underline{w}_1,\ w_2) \tag{A.43}$$

with unit intensity, the Eqs. (A.31), (A.38), (A.40) and (A.41) can be re-arranged to yield:

$$\dot{\underline{x}}^*(t) = A^*(t)\ \underline{x}^*(t) + B^*(t)\ \underline{w}(t) \tag{A.44}$$

$$\underline{z}(t) = D^*\underline{x}^*(t) \tag{A.45}$$

Computation of the covariance matrix

The system state covariance matrix $C_{xx}(t)$ can be found solving the following equation:

$$\dot{C}_{xx}(t) = A^*(t)C_{xx}(t) + C_{xx}(t)A^*(t)^T + B^*(t)VB^*(t)^T \tag{A.46}$$

with the initial condition $C_{xx}(t_o)$ and where V is the unit matrix.
Solving Eq. (A.46) yields:

$$C_{xx}(t) = \Phi(t,t_o)C_{xx}(t_o)\Phi(t,t_o)^T + \int_{t_o}^{t} \Phi(t,\tau)B^*(\tau)VB^*(\tau)^T\Phi(t,\tau)^T d\tau \tag{A.47}$$

$$= D_{xx}\{C_{xx}(t_o),t\} + E_{xx}\{w(t),t)\} \tag{A.48}$$

where $D_{xx}(t)$ is the covariance matrix of the system response at time t on the initial condition $C_{xx}(t_o)$ and $E_{xx}(t)$ denotes the covariance of the system response on the white noise input $w(\tau)$ for $t_o \leq \tau \leq t$.
For computation of the solution of this equation the problem is discretized in time. This implies that the system matrices $A^*(t)$ and $B^*(t)$ are assumed piecewise constant for $t_{k-1} \leq t \leq t_k$, for $k = 1, 2, \ldots$
The solution obtained can then be formulated as:

$$C_{xx}(t_k) = \Phi(t_k,t_{k-1})\ C_{xx}(t_{k-1})\ \Phi(t_k,t_{k-1})^T + \Gamma(t_k,t_{k-1})\ V_k\ \Gamma\ (t_k,t_{k-1}) \tag{A.49}$$

where:

$$\Phi(t_k, t_{k-1}) = \exp(A^*_{k-1}\,\Delta t)$$

$$= I + A^*_{k-1}\,\Delta t + (A^*_{k-1}\,\Delta t)^2/2! + \ldots \tag{A.50}$$

$$\Gamma(t_k, t_{k-1}) = B^*_{k-1}\,\Delta t + B^*_{k-1}\,A^*_{k-1}\,\Delta t^2/2! + B^*_{k-1}\,A^{*2}_{k-1}\,\Delta t^3/3! + \ldots \tag{A.51}$$

$$V_k = \frac{V}{\Delta t} \tag{A.52}$$

see Ref. (15). Here Δt is the discretization time interval $t_k - t_{k-1}$.
Finally the covariance of the system output $\underline{z}(t_k)$ can be computed according to:

$$C_{zz}(t_k) = D^*\,C_{xx}(t_k)\,D^{*T} \tag{A.53}$$

Remark

If the atmospheric turbulence velocity components cannot be modelled as stochastic outputs of linear, low pass filters driven by gaussian, zero mean, white noise (i.e. the power spectra have a non-rational form), then an alternative method for computation of $C_{xx}(t_k)$ can be applied. Defining the variable:

$$\underline{\xi}(t) \overset{\Delta}{=} \underline{x}(t) - D\underline{V}_g(t) \tag{A.54}$$

and rearranging Eq. (A.13) yields:

$$\dot{\underline{\xi}}(t) = A(t)\underline{\xi}(t) + \left[\bar{C} + A(t)\,D\right]\,\underline{V}_g(t) \tag{A.55}$$

provided that the perturbation covariance function $C_{\underline{V}_g\underline{V}_g}(t,\tau)$ is given. The computation of $C_{\underline{\xi}\underline{\xi}}(t)$ under the latter assumption will be explained in Ref. 8.

APPLICATIONS OF THE NAVSTAR GLOBAL POSITIONING SYSTEM TO MILITARY GUIDANCE AND CONTROL

Bradford W. Parkinson
Colonel, United States Air Force
Program Director
NAVSTAR Global Positioning System
Space And Missile Systems Organization
El Segundo, California

1. INTRODUCTION

The NAVSTAR Global Positioning System (GPS) is a satellite-based navigation system that will provide extremely accurate timing and three-dimensional position and velocity information to properly equipped users anywhere on or near the earth. The system will be available continuously, worldwide, regardless of weather conditions, and will find extensive utilization in improved weapons delivery accuracies, range instrumentation, etc. Furthermore, it will provide an ultimate savings in the number and cost of navigation and position-fixing systems currently employed or projected.

NAVSTAR GPS is a Joint Service Program with the Air Force as the executive service. The system concept evolved from Air Force and Navy programs which were initiated in the mid-1960s. The program is now in Phase I of three phases. Phase I (concept validation) calls for the deployment of six satellites in 1977-1978 which will permit demonstration and evaluation tests. The system will then be expanded in Phases II and III through deployment of additional satellites until the full-up operational 24-satellite configuration is achieved.

This paper presents several applications of GPS and its potential impact on military guidance and control.

2. SYSTEM DESCRIPTION

The NAVSTAR/GPS consists of three major segments: Space, Control, and User, as shown in Figure 1. The concept requires accurate knowledge of the position of a satellite versus time and the transmit times of signals from these positions. Each satellite carries an atomic clock with stabilities of the order of 1 part in 10^{13}. This clock is used to synchronize the timing of the dual-frequency, pseudo-random noise (PRN), spread-spectrum, L-band navigation signals which each satellite radiates continuously. These navigation signals also transmit information regarding the satellite ephemerides and clock behavior. Geographically dispersed monitor sets receive these signals and thereby collect precise satellite tracking information. This information is then transmitted to a master control station (MCS) which predicts future satellite position, as well as the behavior of each clock. The MCS ensures that the satellite clocks are synchronized within a few nanoseconds. The control segment periodically (usually daily) uploads this information into each satellite's memory. Each satellite then continuously transmits its position and system time. If a user had an accurate clock, synchronized to system time, he could measure the precise time a signal from a satellite was received and thus determine the time difference between transmission and reception. By multiplying this time difference by the speed of light, the user could determine his distance or range from the satellite. By listening in this manner to three satellites, his position would be uniquely determined.

Unfortunately, equipping each user with a sufficiently accurate clock would be prohibitively expensive and cumbersome. To circumvent this difficulty, the user is equipped with a fairly inexpensive crystal clock. The simultaneous reception of four navigation signals allows algebretic solution of three satellite-to-user ranges plus the time bias in the users relatively inaccurate clock.

To utilize the satellite clocks properly in determining range to user, and thereby his position, the refraction effects on path length of the radio transmission must also be known. Hence, for high accuracy users two radio frequencies with different propagation properties are used to measure the ionospheric delay and other medium effects (less accurate users can employ a modeling technique to account for the delay). In addition, user velocity information is extracted from the system by noting the doppler frequency shift of the signals from each of the "tuned-in" satellites.

The expected performance of the full-up system is as follows:

Accuracy (meters)		Percent of time that accurate or better
Horizontal	Vertical	
5	7	50
8	10	90

Position and velocity "fixes" in three dimensions plus time will be derived by the user equipments, to the accuracies shown, and displayed on a continuous basis. Also, all users operate in the same common grid and can communicate their positions in the same reference frame. (Also, atomic standard timing information is available worldwide from GPS.) Being passive, the system requires no active transmission from the users, and therefore can support an unlimited number of users. It will be available at any point on earth or in near-space and can be used in all weather conditions.

Space Segment. In its operational configuration, the GPS satellite constellation will consist of 24 satellites in circular, 10,900 nmi orbits with an inclination of 63 degrees (See Fig. 2). They will be approximately deployed in three planes ± 500 nmi, each plane containing eight satellites. This satellite constellation ensures that at least 6 satellites are always in view from any point on the earth and that on the average, nine satellites are in view, thus ensuring redundant satellite coverage for three-dimensional positioning and navigation on a worldwide basis.

An artist concept of the satellite is shown in Figure 3. The design life is five years with enough expendables to last seven years. The on-orbit weight is 950 pounds and the end of life power available is 400 Watts. The power is supplied by five square meter solar arrays that continually track the sun. Three nickel-cadmium batteries are available for eclipse operations. The satellite is three-axis stabilized by means of four skewed reaction wheels. A hydrazine propulsion system is used for station keeping maneuvers and to accomodate a momentum dump capability for the attitude control system. A 12-element shaped beam helix array provides an earth coverage antenna pattern for the L-band navigation signals.

Time is maintained with a bank of triply redundant rubidium oscillators; transitioning to a Cesium Beam oscillator in the later stages of the program.

Each satellite transmits two spread-spectrum PRN navigation signals, one signal at 1575 MHz and a second signal at 1227 MHz. The signals are coherently generated and can be used to determine the ionospheric signal delay. Both navigation signals consist of a sequence of binary digits (PRN sequences) bi-phase modulated onto the carriers at a rate of 10.23 Mbps. The ephemeris and satellite clock data are modulo two added to the PRN sequence at a rate of 50 bps. The basic navigation signal is "spread" over a bandwidth of approximately 20 MHz by the PRN sequence. The PRN sequences are unique to each satellite and mutually orthogonal permitting the use of a common carrier frequency for all satellites in the constellation. A coarse/acquisition (C/A) code is quadraphase modulated with the precise (P) navigation code onto the same carrier to provide a rapid acquisition capability. The C/A code can also be used as a navigation signal for many utility applications which do not require high accuracy and desire a lower cost version of the user equipment.

Control Segment. The control segment consists of a master control station (MCS), widely separated monitor stations (MS), and an upload station (ULS). Redundant master control, monitor, and upload stations are planned for the operational system. The widely spaced MS, located on U.S. controlled territory, will passively track the satellites accumulating ranging data from the navigation signals. This data will be transmitted, along with meterological and status information, to the MCS in the CONUS. At the MCS the ranging data will be corrected for transmission delays (e.g., ionospheric and tropospheric delays, relativistic effects) and processed by a filter algorithm to provide best estimates of Space Vehicle (SV) position, velocity, acceleration (e.g., due to solar pressure variations), and SV clock drift relative to system time. Additionally, MS clock drifts relative to system time, polar wander parameters and tropospheric correction residuals are estimated. Subsequent post-event data processing will be done to generate progressively refined information defining: a) the gravitational field influencing the satellite motion, b) MS locations, and c) other observable system influences. The data thus derived will be used to generate more accurate future navigation messages to be loaded into the satellite memories via the ULS, also located in the CONUS, at least once a day.

User Segment. A typical user set consists of an antenna, receiver, data processor with software, and control/display unit. Some configurations will be integrated with auxiliary sensors such as inertial measuring units. The receiver measures pseudo-range and pseudo-range-rate using the navigation signal from each of four satellites. The processor converts these data to three-dimensional position, velocity, and system time. The position solution is developed in earth-centered coordinates, which are subsequently converted and presented on the display unit as either geographic coordinates, Universal Transverse Mercator grid coordinates, or any other coordinate system desired by the user.

Projections of total user equipment needs for the U.S. Department of Defense exceed 25,000. Although the system is designed to meet military requirements, it will be made available to civilian users, when it is fully deployed. In order to minimize user equipment costs, the space and control segments are designed to emphasize low user costs. The four classes of user equipment to be prototyped during Phase II (full scale development) of the program are summarized in Table 1. The user requirements identified and defined by the military services are satisfied by these four equipment classes.

3. WEAPON DELIVERY

The capability of the GPS to locate military vehicles worldwide within approximately 10 meters spherically will make it possible to improve the accuracy of weapon delivery. The following are typical applications:

a. Target location using reconnaissance vehicles.

b. Coordinate bombing.

c. Mid course guidance for tactical missiles.

d. Land navigation and launch point determination for mobile missile systems.

The applications of the GPS to tactical missiles is discussed in another paper to be presented at this symposium and will not be presented here.

Blind Bombing. Studies have shown the utilization of the operational GPS for position fixing will considerably increase the probability of kill with unguided weapons.

In order to demonstrate this capability in a high dynamic environment, the GPS test pod has been developed. The test pod includes the following: two antennas for orbital coverage and one antenna for IR coverage, a four channel receiver (called the X-Set), a data processor, a Control/Display unit, a power supply unit, a LP36 inertial measurement unit (IMU), a pilot steering display, an environmental control unit and suitable instrumentation for recording and time tagging GPS navigation data. The test pod and its associated equipment are depicted in Figures 4 and 5.

The GPS Test Pod will be mounted on a Navy F4 aircraft on the center-line station. It is expected that a full dynamics profile of the F4 with attached pod will be flown during the test program. We anticipate that 5g turns, supersonic dashes and rapid rolls of 90^{0} per sec will be accomplished to test various performance characteristics of the X-Set and the IMU.

The software within the X-Set data processor will be mechanized to optimally process both GPS pseudo range and IMU data. This will allow us, during periods of signal loss caused by antenna blanking due to wing shadowing, to propagate the navigation state and reacquire the GPS signals when they become available. Also mechanized in the software is a bombing algorithm that will allow the test pod to provide steering signals to the pilot via the Pilot Steering Display. This capability will provide us the opportunity to demonstrate GPS's unique feature of accurate all-weather blind bombing.

4. RANGE INSTRUMENTATION

Potential range instrumentation applications for GPS include the following, as presented in Figure 6.

a. Geodetic siting of stations

b. Range ship and aircraft position fixing and stationkeeping

c. Aircraft recovery operations aid

d. Time Synchronization and timing reference for instruments

e. Vehicle track and dynamics determination

All of the above applications can be accomplished worldwide permitting more realistic operational testing.

An example of GPS utilization for range instrumentation is the SATRACK system being employed during Phase I testing. The purpose of this tracking system is to provide accurate missile trajectory measurements, estimates of initial condition and in-flight error contributors. The SATRACK system overview is presented in Figure 7.

Basically the GPS L_1 satellite transmission reaching the missile are translated to S-band and relayed to range support ships, where the missile position is determined. This position is then compared with the ship's position, determined from directly received dual frequency GPS signals. The dual frequency signals provide data for propagation corrections to the single frequency satellite-to-missile paths as well as the ship tracking data. In addition to collection of the missile tracking data, the range support ships also recover missile telemetry data from the S-band stream.

All the collected data are sent to the SATRACK processing facility for postflight processing. Missile trajectory and estimates of initial condition and in-flight errors are determined by a Kalman filter smoother in the SATRACK processing facility. The filter compares guidance derived quantities (from missile telemetry data) with corresponding SATRACK measured quantities (from missile tracking data), and systematic differences are attributed to various system error sources.

5. SUMMARY

The GPS applications briefly presented herein only begin to address the possible effects this precise navigation system will have upon guidance and control in the military environment. During the next 5 to 10 years we fully expect that the GPS accuracy will improve over that shown here. As the cost of the receivers decreases due to inovative design and more extensive large scale integration the revolution created by NAVSTAR in the guidance and control area will most certainly continue.

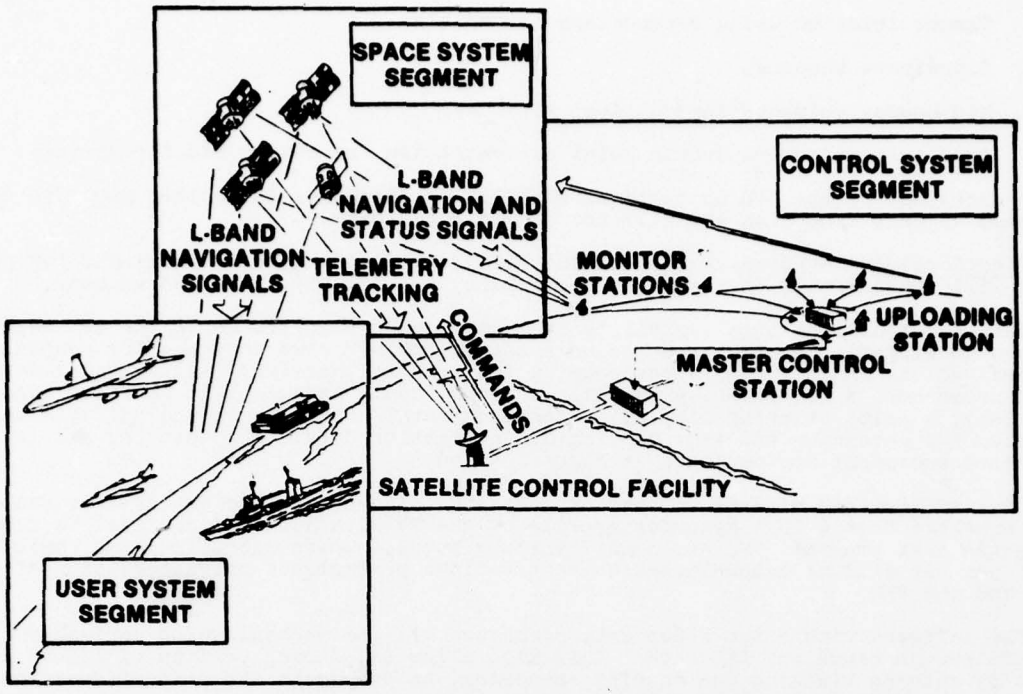

Figure 1. GPS SYSTEM

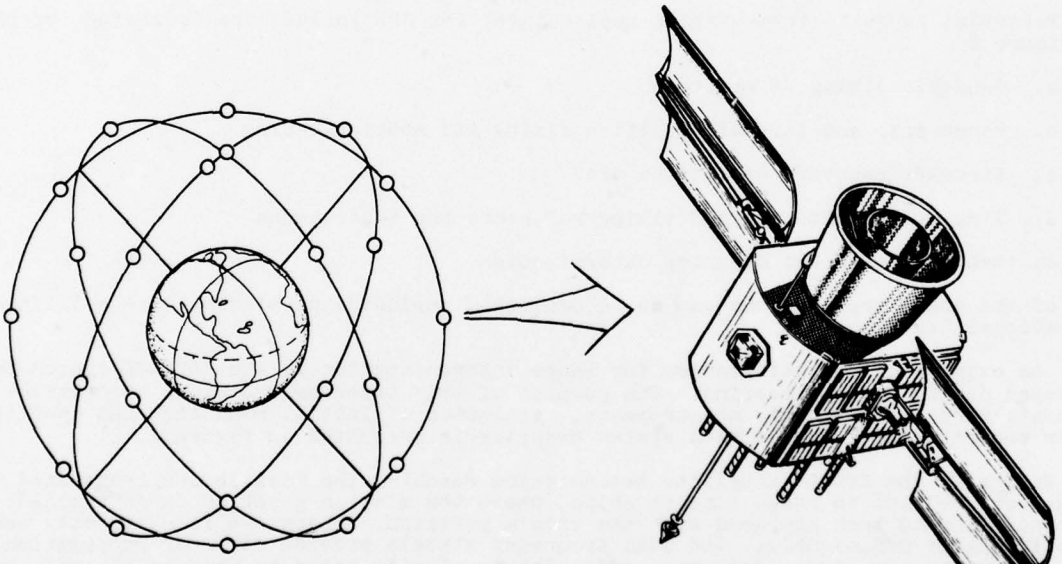

ORBITAL CONFIGURATION

- 12-hr PERIOD
- CIRCULAR ORBITS
- 63° INCLINATION
- EIGHT SATELLITES PER PLANE

SPACECRAFT CONFIGURATION

- 950 lb (typical)
- 450 Watts (typical)
- NAV SIGNALS
  - 1200 MHz
  - 1600 MHz
- 10^{-13} CLOCK STABILITY
- 5-YEAR DESIGN LIFE

Figure 2. ORBITAL/SPACECRAFT CONFIGURATION

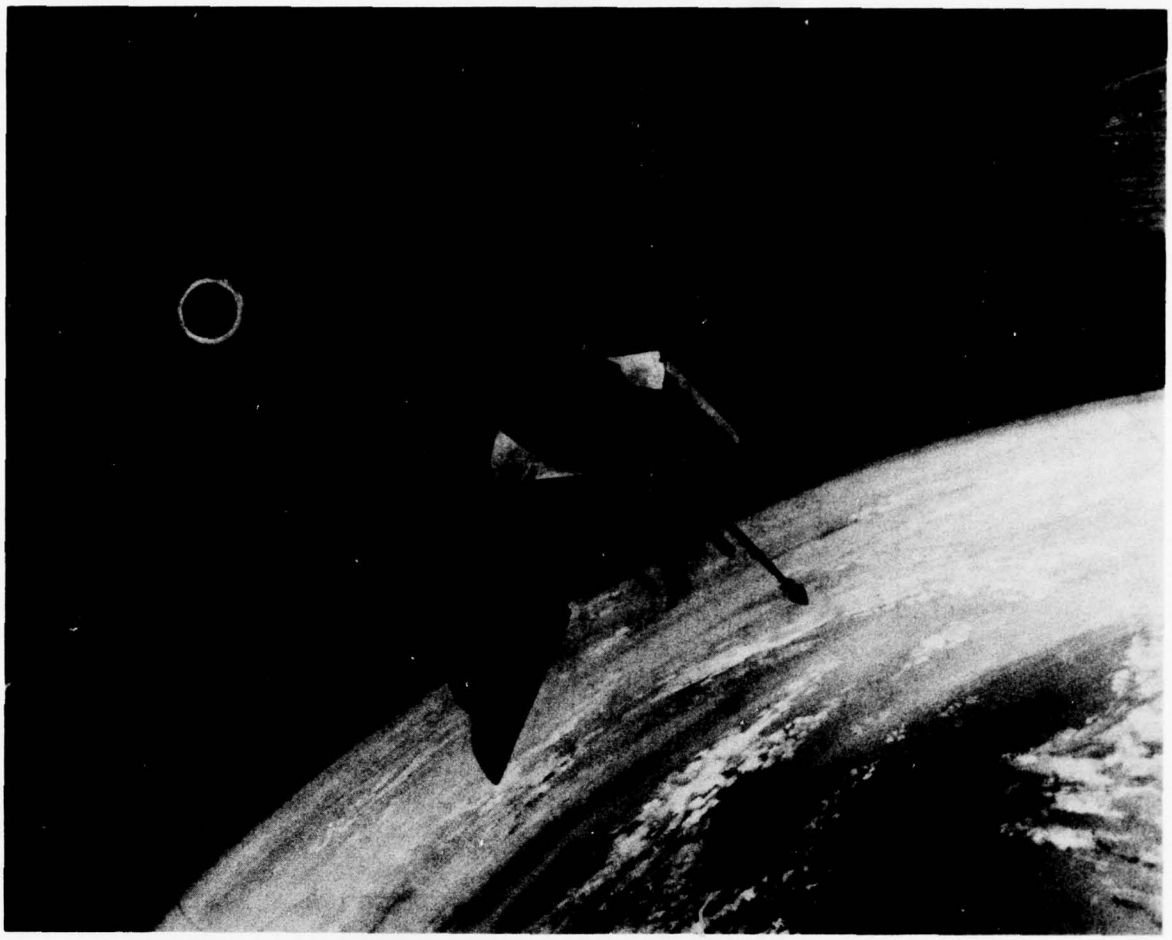

Figure 3. GPS SATELLITE

CLASS	ACCURACY	USER DYNAMICS	IMMUNITY TO ELECTROMAGNETIC JAMMING	TYPICAL USER
HIGH DYNAMIC	HIGH	HIGH	HIGH	HIGH PERFORMANCE AIRCRAFT
MEDIUM DYNAMIC	HIGH	MEDIUM	MEDIUM	SHIP/HELICOPTER
LOW COST	MEDIUM	MEDIUM	NATURAL EMI IMMUNITY ONLY	GENERAL ENROUTE NAVIGATION
VEHICLE/MANPACK	HIGH	LOW	HIGH	LAND VEHICLE/MAN BACKPACK

Figure 4. USER REQUIREMENT CLASSES AND APPLICATIONS

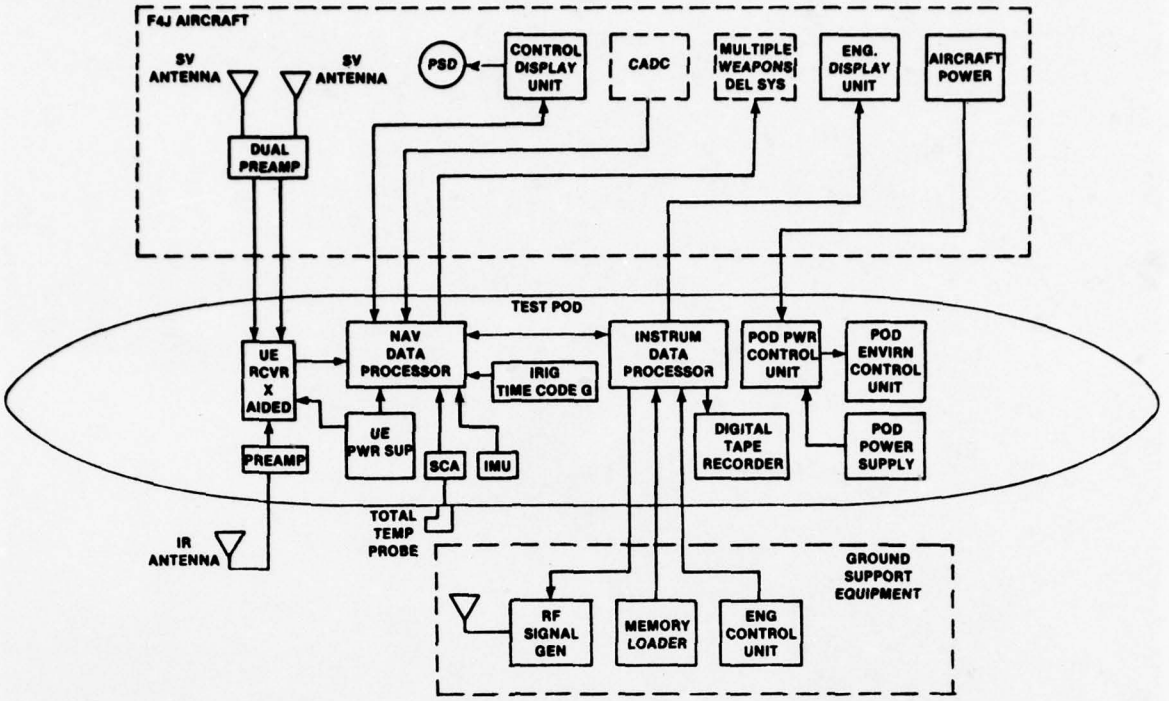

Figure 5. FUNCTIONAL BLOCK DIAGRAM

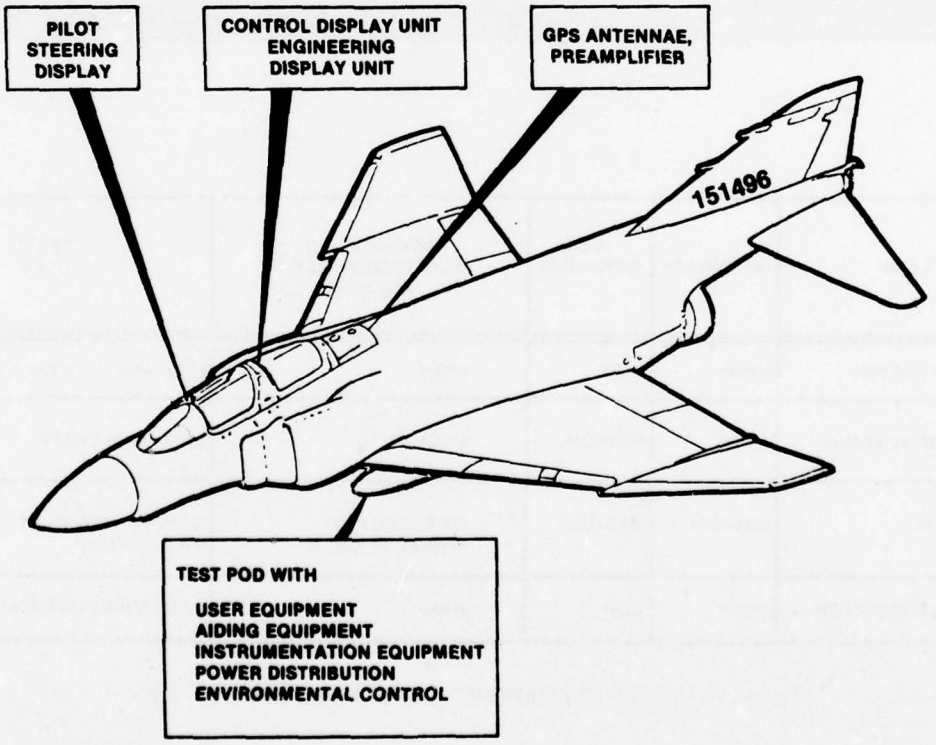

Figure 6. F4J TEST BED SYSTEMS

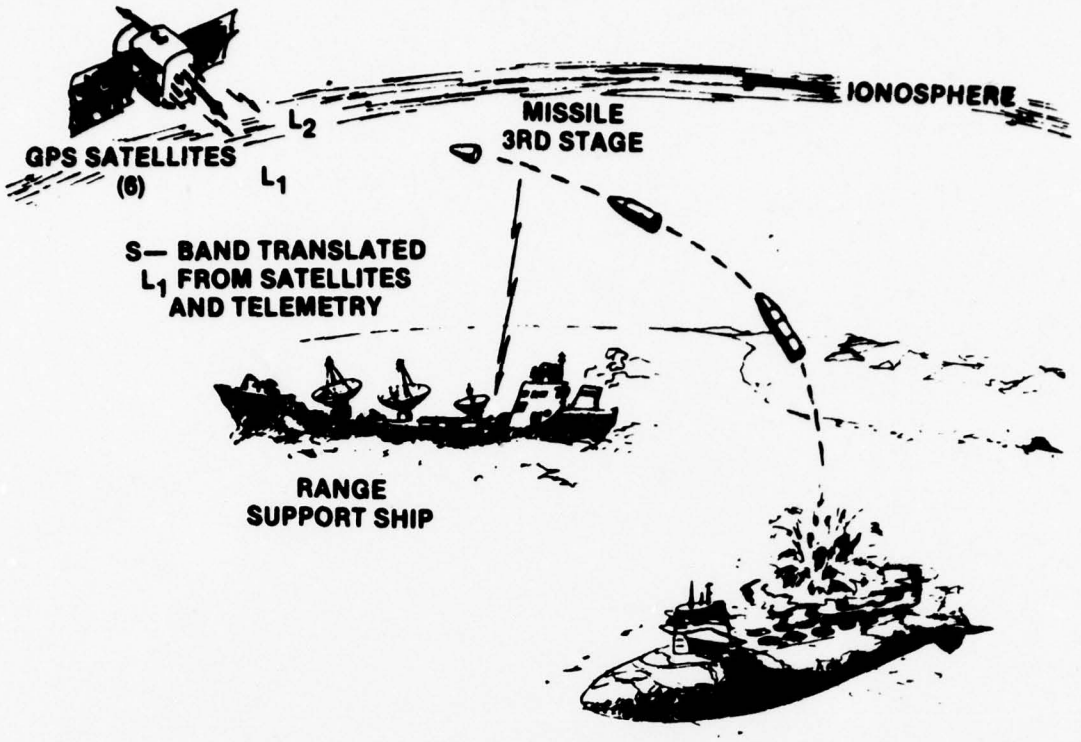

Figure 7. SATRACK

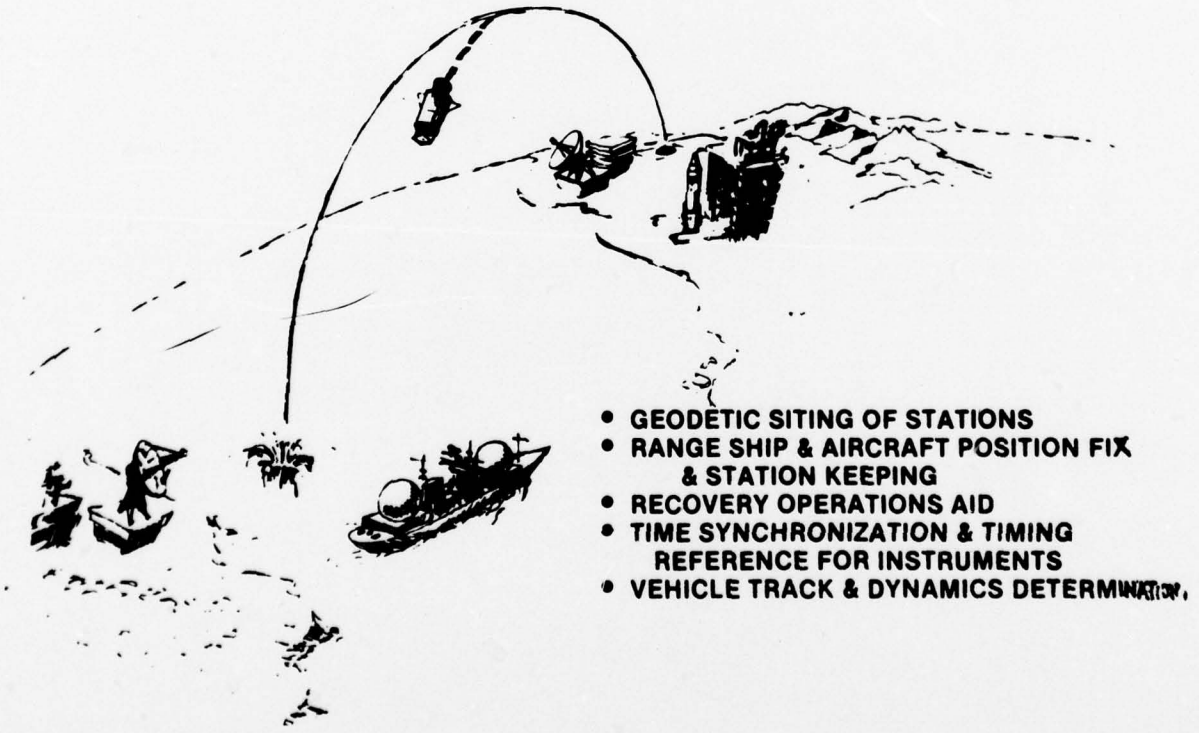

Figure 8. POTENTIAL RANGE INSTRUMENTATION APPLICATIONS

THE JOINT TACTICAL INFORMATION DISTRIBUTION SYSTEM (JTIDS)

B. BRENTNALL, COL, USAF
PROGRAM MANAGER
JTIDS JOINT PROGRAM OFFICE
HANSCOM AFB, MA 01731

JTIDS is a joint development program by the U.S. military services. JTIDS is a radio Communication Navigation Identification (CNI) system providing tactical elements for a broad range of services. Receiver-transmitter terminals are being developed for a range of applications including airborne, ground-based, and seaborne communications, command and control; CNI for tactical vehicles; data links for unmanned systems; and C^3 relay through unmanned stations and platforms. The system provides jam-resistant digital data exchange, precision relative ranging between units, and positive identification and position correlation of users. Design of the system is based on a pseudo-noise modulated, frequency hopped signal characteristic which provides for jam-resistant, secure, data communications on a rigidly structured time division access basis. The relative ranging data is used in several ways, including precision relative grid community navigation, multi-lateration survey of beacons, weapons control, TACAN functions, and community distribution of geographic fix data. The various relative navigation techniques are described, and the relation to other navigation devices is discussed.

INTRODUCTION

The Joint Tactical Information Distribution System (JTIDS) is a defense development which will be a principal element of tactical command and control systems, and weapon systems, of the next decade. JTIDS will provide the integrated functions of secure communication, relative navigation, and unambiguous identification to broad classes of users, including surface command and control units on land and at sea, airborne units of various classes, airborne command and control units, missile systems, and manpacks as the program is currently structured.

JTIDS is a joint services program, with the participation of all U.S. military services under the executive leadership of the Air Force. The program merges technologies which were under development by separate services in the SEEKBUS and ITNS/ITACS programs. The U.S. Air Force SEEKBUS program emphasized a secure digital information distribution system while the U.S. Navy ITNS/ITACS programs emphasized relative navigation and integrated communications, navigation and identification functions. Since both programs were driving toward the same basic goals with different emphasis, the merger of the programs was directed by the Department of Defense in 1975.

The merger of the two programs has produced handsome dividends. A major accomplishment was the program office definition of a development and test plan which would permit development of a low risk approach for early system implementation, while more advanced concepts were further refined in the laboratory. As a second step, the program office defined a JTIDS signal standard which assured compatibility between different types of terminals now being constructed, by various contractors under overall direction of the Joint Program Office (JPO). This signal structure standard also allows considerable flexibility in growth of JTIDS to accomodate advanced concepts now under development.

The JPO has also established standards for subscribers to the relative grid navigation function of JTIDS and has begun integrating various additional functions in the JTIDS terminals. Because the JTIDS system operates at radio frequencies in the same band used for the TACAN and Identification-Friend or Foe (IFF) functions, the earliest steps toward hardware integration address these two functions.

The JTIDS program is addressing two phases of development. The first phase provides for a structured time division multiple access (TDMA) architecture with emphasis on connectivity for all users and a limited number of nets and message structures. It includes TACAN and relative navigation capabilities. The second phase of JTIDS development involves additional integration of Navigation and Identification functions in the equipment, plus increased system capacity. One approach being pursued is a distributed time division multiple access (DTDMA) architecture, which is expected to allow more flexibility in the operational use of JTIDS equipment with other communications links. Where the TDMA architecture uses code orthogonality and frequency orthogonality to achieve separation between nets, the DTDMA process adds statistical orthogonality in time to provide additional net separation. Alternatively, studies are underway to determine practicability of enhancements to the TDMA architecture to satisfy the Phase II objectives.

The two phases are being developed to permit controlled evolutionary introduction of the second phase in the presence of the first. For DTDMA, this is assured by treating the structured TDMA as a special case of the DTDMA architecture. This is accomplished by eliminating the stochastic time distribution feature of the DTDMA signal, observing the message constructs required of the Phase I architecture, and using the same basic rules of pulse and symbol infrastructure. This infrastructure includes the characteristics given in Figure I. Observation of these standards in Phase I and Phase II of JTIDS development insure interoperability and connectivity between users equipped with either type of hardware. The TDMA growth alternative is based on compatibility with the Phase I TDMA terminals.

Two types of terminals are currently under development in the Phase I architecture. One terminal type built by Hughes Corporation, is primarily for command and control platforms, such as AWACS, 407L CRC/CRPs, and NADGE sites. This terminal includes all the JTIDS features of secure, anti-jam digital communications, and is shown in Figure 1. Additionally, contractual efforts are underway to put the relative navigation function in these terminals.

The second type of Phase I terminal, being built by the Singer Corporation is for tactical aircraft. It contains digital communications features of JTIDS and incorporates the relative navigation function required by the U.S. Navy. The terminal is shown in Figure 3. It also incorporates TACAN as an integrated CNI feature utilizing common hardware for JTIDS and TACAN pulse reception and processing. Users of this terminal will not require a separate TACAN transceiver.

The JTIDS program office is also pursuing Phase II. The DTDMA terminal is being developed by ITT (Figure 4) which incorporates the advanced flexibility and increased system capacity of the Phase II objectives, and is designed to be fully compatible in operations with Phase I terminals. This terminal will also incorporate the relative navigation and TACAN functions, and will further the integrated CNI concept by adding full Mark XII IFF functions to its capabilities. Similarly, the TDMA growth studies by Singer Corporation and Hughes Corporation address the same Phase II objectives.

JTIDS communication is accomplished in the Lx band, 960-1215 MHz, with narrow guard bands around the IFF frequencies, 1020 MHz and 1090 MHz. The Phase I system can be operated in a frequency hopping antijam mode across this entire spectrum, or at a single center frequency with a 25db bandwidth of +5 MHz. Additional modes include operation with or without secure data encryption. The typical message structure for the Phase I architecture is shown in Figure 5. Some of the communications characteristics for a Phase I net are shown in Figure 6.

The capability is extended to multi-netted operation through the use of code division multiplex techniques superimposed on the basic TDMA structure. Each participating subscriber is assigned to operate on one or more nets and is allocated speciric time intervals (time slots) during which it may transmit information on a specific net. Transmitted information may be in the form of formatted or free text digital messages. Each subscriber may receive information during all time slots not used to transmit. Since each subscriber has access to information transmitted on its assigned nets, selective filtering is employed to extract only information of interest. Each subscriber enters the net and maintains synchronization with system time independently. Intial entry is executed by the reception of any message transmitted by any other unit that has achieved fine synchronization.

Initial entry allows a unit to achieve coarse synchronization with system time and thereafter, to receive information transmitted during all subsequent time slots. Fine synchronization is achieved thereafter, either passively through the receipt of position and status reports (Category P messages), or actively through the use of "round-trip" transmissions (RTT). Passively, the receipt of a position and status report in conjunction with a knowledge of "own" position allows a unit to account for message propagation time in refining its estimate of system time. Actively, the RTT method allows a unit to synchronize without any knowedge of position.

JTIDS RELATIVE NAVIGATION CONCEPT

Now let us turn to the navigation feature of JTIDS. The Navigation feature derives not only from information external to JTIDS, but from important features which are inherent within JTIDS. The most important of these is the precision mutual synchronization of the clocks in all of the JTIDS terminals. This synchronization is achieved initially by the use of RTT messages exchanged between members and refined by observing the time of arrival of the synchronization preamble of all succeeding messages. This then allows the interpretation of the time of arrival of subsequent message transmissions to be interpreted as pseudo-range measurements between pairs of JTIDS users.

It is clear that if two or more fixed, surveyed JTIDS community members periodically report their position, other users could use range measurements from such members to locate themselves in the coordinate system used for the survey of the fixed members positions. This mode of navigation is used in JTIDS in such cases where fixed, surveyed stations are available, or accurate knowledge of position is known from a precise navigation system, such as GPS. This is an almost trivial case of the relative navigation mode of JTIDS. However, tactical situations arise in which accurate knowledge of true position is not available, particularly in open ocean tactical areas. The JTIDS relative grid navigation, which is derived from the Integrated Tactical Navigation System (ITNS) concept, was developed to be useful in a wide variety of combinations of types of JTIDS users, their missions, spatial distribution, modes of communication, and quality of users equipment. Figure 7 shows some of the varied environments in which JTIDS relative navigation is designed to operate.

The most important result of a tactical community using the relative navigation mode of JTIDS is that consistency of position location among all elements is obtained. This consistency applies not only to positions of JTIDS community members, but to all data in the tactical community derived from other sensors, such as radar or acoustics, so long as such measurements are made in the JTIDS relative grid. This also applies to velocity data and directional information if derived in the common relative grid. This in turn, insures that accurate fire control solutions may be made from sensor data from several different platforms or stations, even if the fire control solution is incomplete from individual station data alone.

Fundamental to the JTIDS concept is that no single station or platform shall be necessary to the operation of JTIDS. In JTIDS relative navigation, this means that each JTIDS user of the relative grid must share in the maintenance of the grid's orientation and his location in the grid, at least to the degree required by his mission or his contribution to an integrated mission or operation.

GRID MAINTENANCE

As a part of grid maintenance, all active JTIDS users maintain a common time for the JTIDS net referenced to a JTIDS user who is designated as a part of the JTIDS protocol as the NTR (Net Time Reference), or indirectly to the NTR through other users when the NTR is not within direct line of sight. The NTR need not have the most accurate absolute time reference in the JTIDS community, but should have one of the most stable. In order to assure nodeless JTIDS operation, any JTIDS community member may be designated NTR, with order of succession determined by JTIDS net protocol. All JTIDS users calibrate their own clocks to that of the NTR, including clock drift rate.

In a similar manner, each JTIDS relative navigation grid user participates in maintaining the grid origin and prime direction of the grid, as well as his own position and velocity in the grid. For JTIDS users which are in motion, this is achieved by calibrating their dead reckoning system, i.e., directional and velocity reference, to produce position data consistent with the range measurements made to other members of the JTIDS relative grid. Having located himself in the grid by combining the range measurements to other users with the dead reckoning data derived from his own platform, the user can then continue the process to help maintain the JTIDS grid, and serve as a reference to other potential users.

It is not necessary for a JTIDS grid user entering the system to have a multiplicity of range measurements available from many other users in order to determine his position in the grid. Repeated, single range measurements to another JTIDS user over a period of minutes during which the grid azimuth between the two JTIDS elements changes by 20 degrees or more is sufficient for one user to acquire another user's grid. The availability of more range measurements to a multiplicity of JTIDS grid users in different directions merely helps reduce the time required for a new user to acquire the JTIDS grid.

The grid acquisition process in a sparse community has been demonstrated in several ITNS experiments listed in Figure 8, as well as in the simpler cases of multiple grid members, both fixed and moving. To date, the experiments have used moving user platforms equipped with a moderate quality inertial system (1-2 n mi/hr) or a doppler velocity system with a good quality heading reference, and sometimes with fixed stations for which no precision survey data was used except the self-surveyed relative range between them.

In the relative navigation architecture currently defined in JTIDS standards, the reference grid which is acquired by all JTIDS relative grid users is that defined by one community member, designated the NC (Navigation Controller), which may or may not be the same as the NTR. In the JTIDS protocol, the order of NC succession is determined by the stability of each user's dead reckoner, which is an information item distributed throughout the community by each grid member when he transmits. The function of the NC is merely administrative, since grid users use ranges to all appropriate JTIDS grid members (those with a grid accuracy and stability equal or superior to their own), and need not even be in direct line-of-sight communication with the NC. The effect of this convention is that all users will maintain a grid which has the absolute error characteristics of the dead reckoning system of the NC, although the relative characteristics among the various grid users will be much more stable and repeatable.

It is not necessary that a single NC be used, although it is the more probable situation. For example, the ideal NC is a dual NC formed by two fixed JTIDS terminals within line-of-sight so that accurate range between them can be measured by their JTIDS equipments. In such a case, a perfectly stable grid origin and directional orientation is maintained, with the baseline between them providing the latter. Similarly, two ships with precision navigators such as SINS can provide such a stable dual-NC reference in the open ocean. A single, slowly moving user does not serve as a good reference for the grid azimuth. Alternatively, a single faster-moving aircraft serves better, where his constantly reported movement provides the reference baseline.

The JTIDS relative grid architecture has been structured to provide growth to modes involving multiple, moving NC's, although such action increases computational complexity somewhat.

PASSIVE RELATIVE NAVIGATION

Thus far, we have discussed the use of the relative grid by actively transmitting JTIDS community members. Just as it is possible for non-radiating passive JTIDS users to synchronize and receive transmissions from active users, passive users can acquire the common JTIDS relative grid and navigate in it. If there are two or more active JTIDS users within line-of-sight of the passive users, the time differences between receipt of their transmissions, together with their position reports, is interpreted as a pseudo-range difference. Such information represents a hyperbolic locus of the passive user's own position in the grid. The solution for grid position by the passive user then proceeds much as if the active users formed a LORAN net, with each station moving, but reporting its coordinates periodically. Should the passive user then be required to report target data which he has obtained, such data would be reported in common JTIDS grid coordinates, without waiting for further grid convergence. The passive mode of the JTIDS relative grid has been demonstrated to provide full grid convergence, but with a lesser accuracy as might be expected from the geometric problems of hyperbolic solutions. In addition, grid convergence to the community reference is slower, particularly in a spare community. However, clock bias and clock error rate are obtained to a high degree of accuracy in the passive mode, which further enhances the anti-jam capabilities of JTIDS communications functions.

The accuracies obtained in navigation in the JTIDS relative grid is a function of a number of parameters. First, the ranging accuracy of the JTIDS terminal tends to be the limiting parameter. Additional factors include the community geometry, the quality of each users dead reckoner, and the rate at which range measurements are used to update the grid navigation.

IMPLEMENTATION AND ACCURACY

Terminals are currently being built by the Singer Corporation, in a form suitable for tactical aircraft including all software for grid maintenance and acquisition in all modes, including NC, active grid user, and passive grid user. In this version of the relative grid software, the interpolated navigation in the relative grid is performed using outputs from an aircraft inertial navigator. The inertial grid navigation is performed in a cartesian coordinate grid, in parallel with the normal inertial computations performed in earth-centered spherical coordinates, in order to maintain the integrity of the inertial absolute navigation solution.

Convergence of the user's grid to the community reference is accomplished by processing pseudo-range pairs (or pairs of pseudo-range differences in the passive mode) every 16 seconds in a Kalman filter designed to calibrate the user's notion of grid origin, velocity of the grid origin in inertial space, and the grid azimuth orientation. This is accomplished by an algorithm that selects range pairs from those available and correlates the range with the reported grid position of the user whose message transmission is used for ranging and the reported quality of the user's time and grid data.

Linearity requirements of the Kalman filter requires that care be taken in the selection of algorithm to use ranges which are large with respect to the users uncertainty in grid position in quadrature to the range direction, or that the Kalman filter be adjusted accordingly.

Convergence of a user's grid occurs rapidly for elements of the Kalman filter which are directly observable, and at a rate which depends partly on platform maneuvers for parameters which are indirectly observed, such as grid azimuth, which is the slowest parameter to converge. Figures 9 and 10 show such convergence in flight experiments which have been conducted in a similar configuration.

Experiments have also been conducted using doppler velocity references in aircraft, which validate the theoretical accuracy predictions of Figure 11. Because of the near-universal application of inertial navigation in U.S. military aircraft, it is not intended to implement a doppler system relative grid algorithm in JTIDS equipment initially, although the algorithm exists for use in another computer, if a user should so require.

An important feature of the JTIDS relative grid is that it is completely self-contained and self-sustained by the JTIDS users. It does not depend on any resources or references outside the JTIDS community. As such, it can be established when and where the tactical situation requires, and then discontinued when the tactical requirements is ended. This, combined with the secure access features of JTIDS communications, effectively denies the enemy the use of the JTIDS relative grid for his own navigation needs.

RELATION TO GEOGRAPHIC NAVIGATION

Although the relative grid coordinates have an arbitrary origin, the origin is relatively stable with respect to the earth, and the prime grid axis is nominally north. The relative grid can be stabilized to and correlated with any external geographic position reference which may be available.

If any single grid user obtains a geographic fix from the Global Positioning System, for example, this fact is automatically transmitted throughout the community by the JTIDS message structure. Since the geographic position and the relative grid position of the user obtaining the fix is transmitted, other JTIDS community members can use the fix data to obtain an equivalent geographic position fix to apply to their own inertial navigator, degraded only by the inaccuracies of the relative grid operation.

This automatic feature insures that all JTIDS community members share in a navigation position reference available to any single member, without having each member bear the cost and weight of a multiplicity of fix devices. For example, a single JTIDS relative grid net may share in LORAN fix data from a surface ship member, the satellite fix data from a GPS equipped aircraft member, and a radar fix from yet another community member.

We intend to use these complementary features to provide a spectrum of capabilities to our various combat elements, each appropriate in cost and function to their respective missions

SUMMARY

The navigation features of JTIDS come at a relatively small additional cost over the communications functions of the JTIDS terminal. The relative navigation capability requires no additional radio hardware. Additional software is required, however. The entire grid acquisition and management function in high speed tactical platforms requires less than 8000 words of 16 bit memory, and imposes a timing load of less than 20% in currently available aircraft computers. In the tactical terminals currently being built in the JTIDS program, these requirements are easily accomodated in the small computer used for terminal communications data formatting and management. An additional minimal amount of processing is added when JTIDS performs conventional TACAN.

The flexibility of the JTIDS concept for navigation, communications, command and control functions, identification, and weapon systems provides opportunities for real time battlefield integration of the tactical commanders resources, and the more rapid response of interconnected combat forces in a survivable tactical grid system. The broad applicability of the JTIDS system is assured by the various classes of terminals which are being developed.

JTIDS terminals are presently in fabrication and test. System tests of the first models of JTIDS equipment in the laboratory and aboard aircraft and other platforms starts this summer and continues in 1978, leading to engineering development models of the Class 2 (fighter terminal) in 1979, and deployment in the 1980's. Class 1 terminals for use with large platforms or surface elements will be available in 1980.

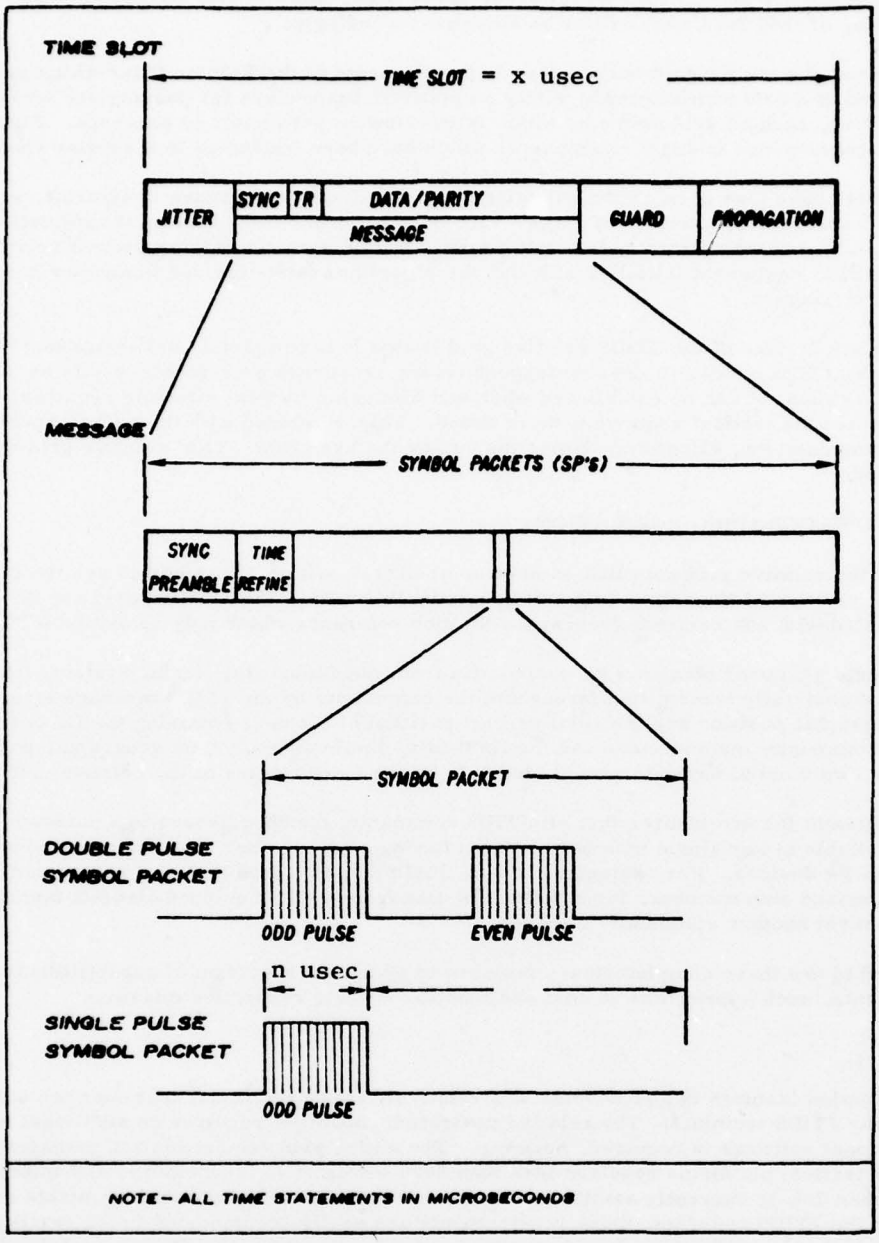

PULSE WIDTH - N MICROSECONDS

CARRIER MODULATION - CPSM

DATA MODULATION - CCSK

SYMBOL CODING - 31/15 RSED

Fig.1 Pulse and symbol characteristics

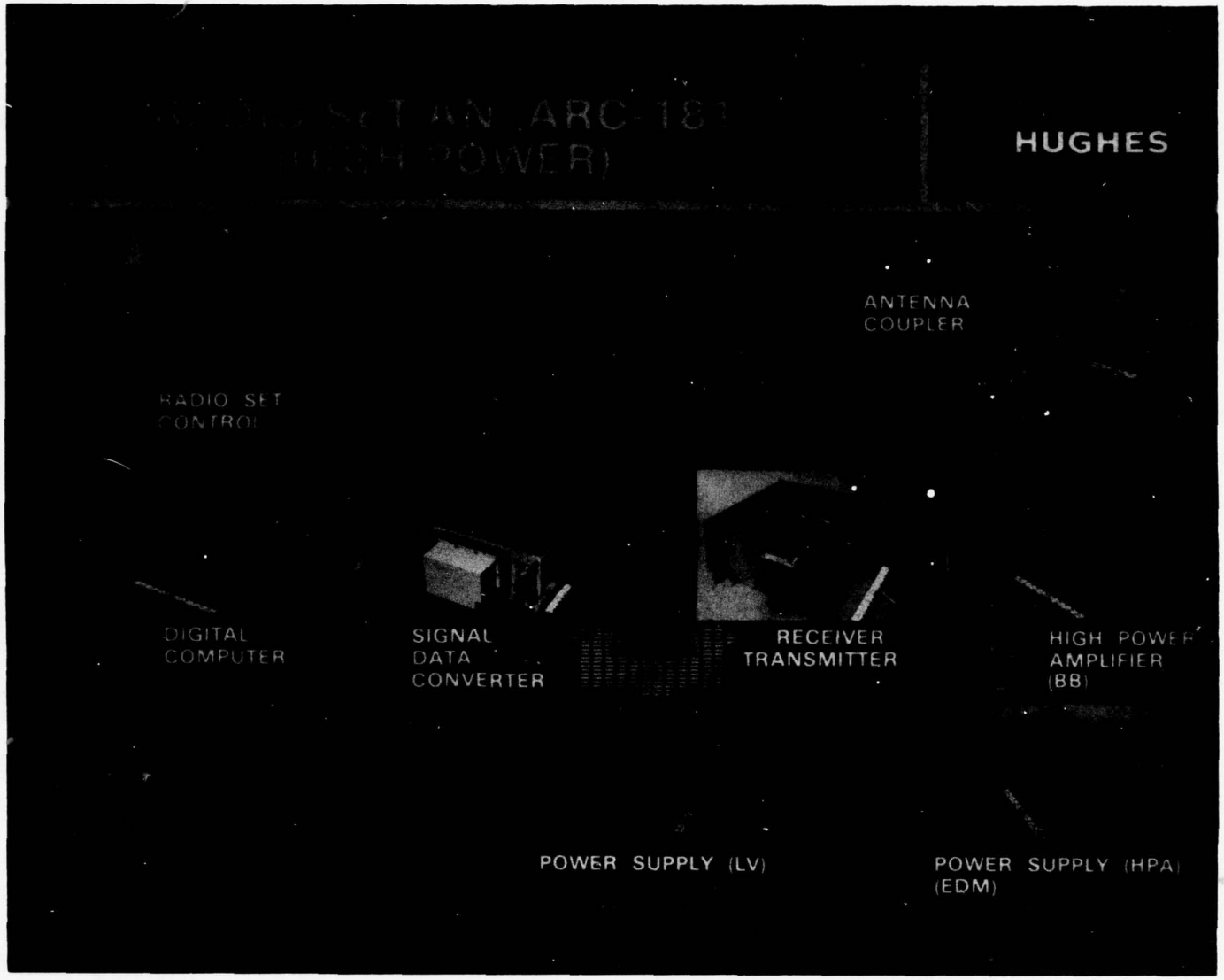

Fig.2 Hughes class 1 terminal

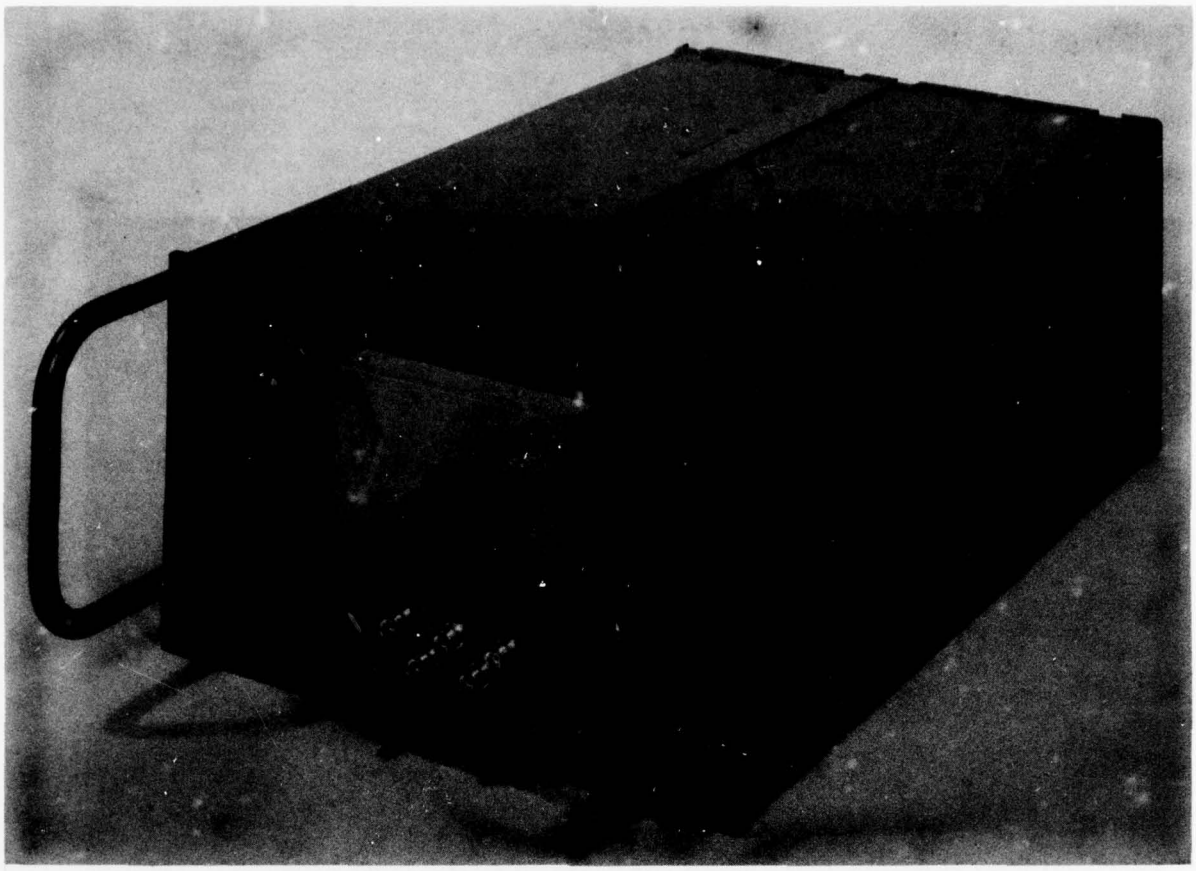

Fig.3 Singer aircraft terminal

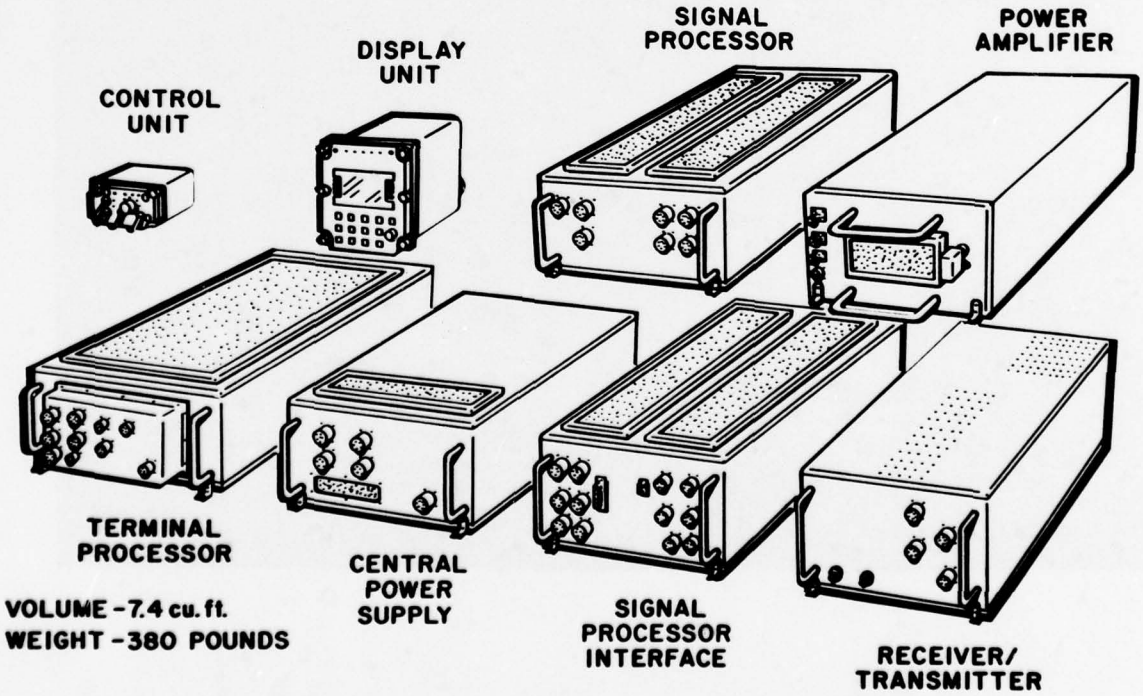

Fig.4 ITT command and control terminal

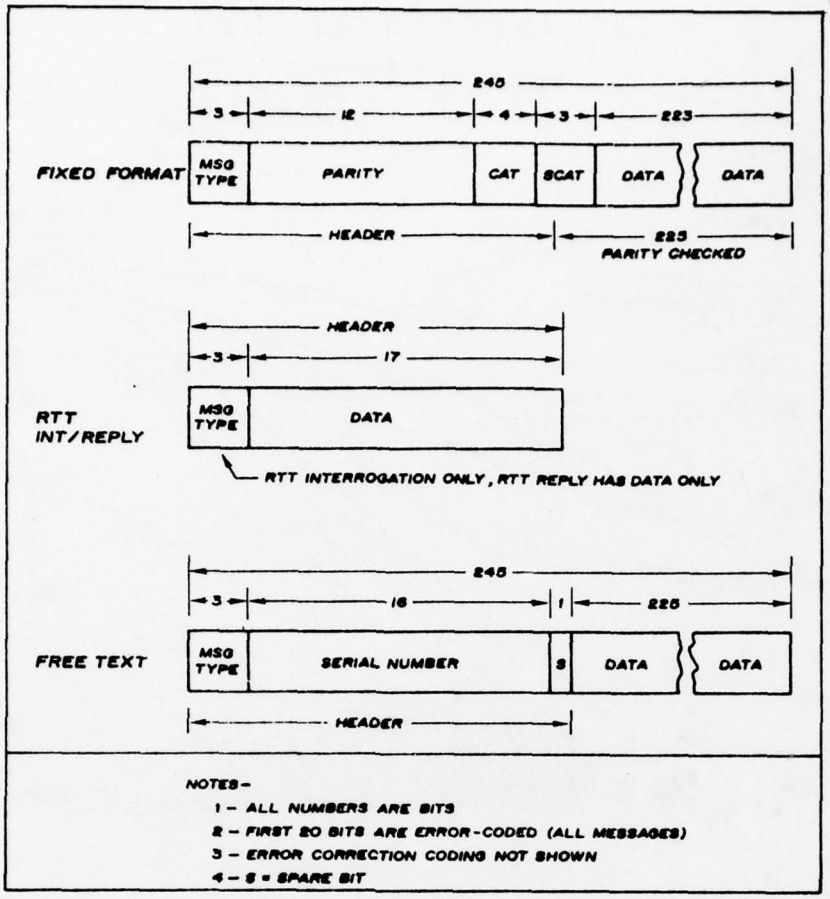

Fig.5 Typical phase I message structure

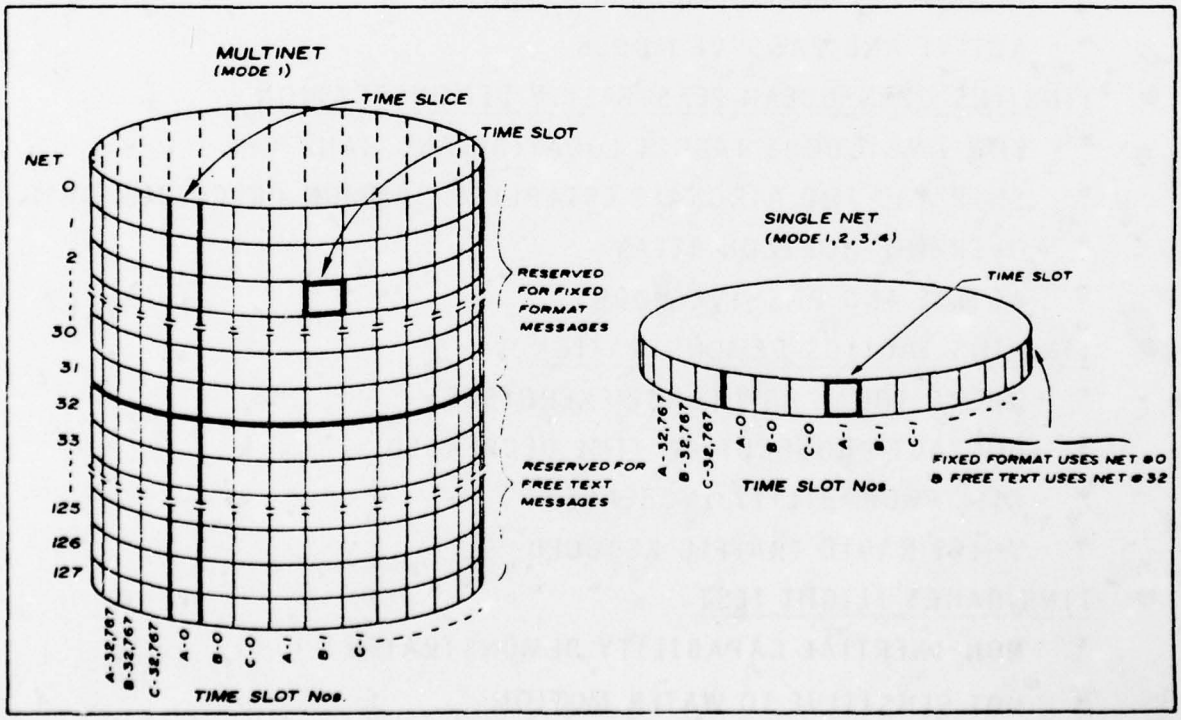

Fig.6 Phase I communications characteristics

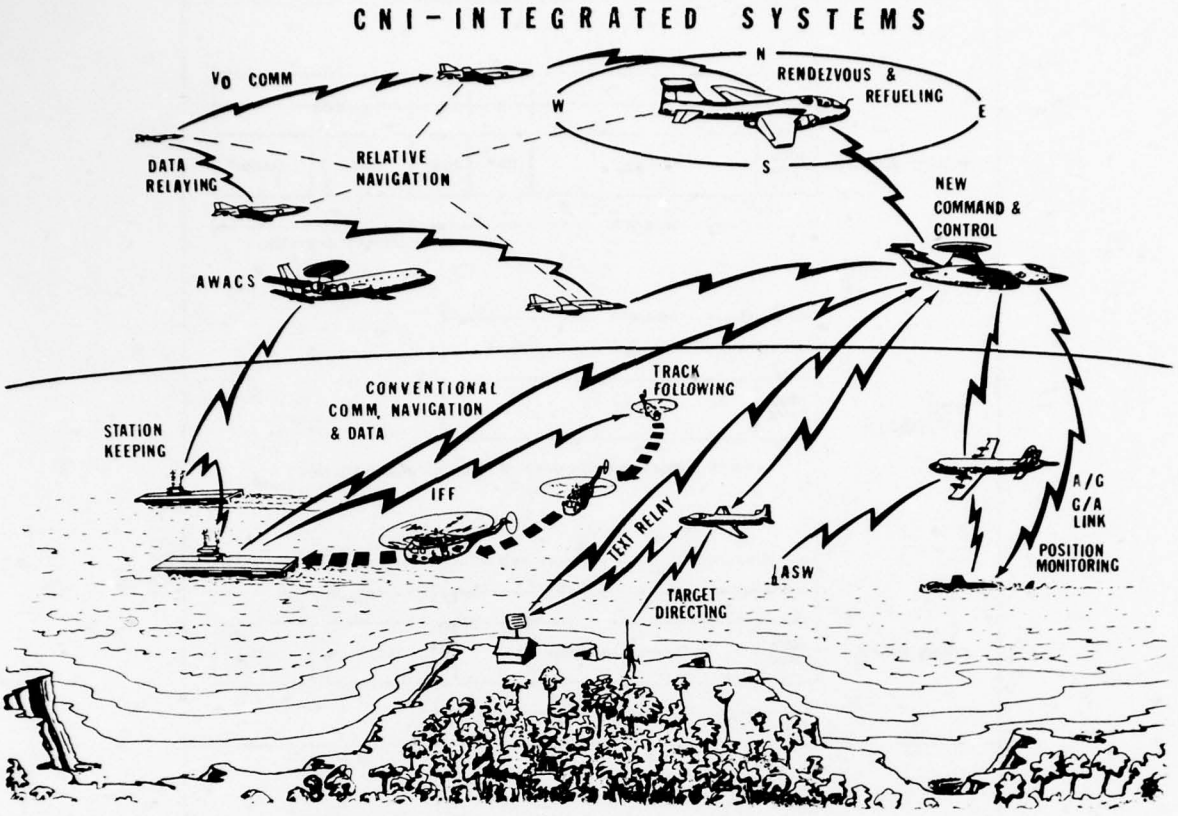

Fig.7 Relative navigation environment

- ITNS/INS FLIGHT TEST
  - CONCEPT FEASIBILITY DEMONSTRATED
  - ACTIVE AND PASSIVE MODES
- ITNS/INS OPEN-OCEAN FEASIBILITY DEMONSTRATION
  - NON-AMBIGUOUS TARGET LOCATION AND HAND-OFF
  - SHIP AND TWO AIRCRAFT ESTABLISH COMMON PRECISION GRID
  - OVER-THE-HORIZON RELAY
  - ACTIVE AND PASSIVE MODES
- ITNS/INS TACTICS DEMONSTRATION
  - OPERATIONAL ASW FORCE EXERCISES
  - CONTACT PROSECUTION TIME DECREASED
  - KILL PROBABILITY INCREASED
  - VOICE RADIO TRAFFIC REDUCED
- ITNS/DAHRS FLIGHT TEST
  - NON-INERTIAL CAPABILITY DEMONSTRATED
  - NOT SENSITIVE TO WATER MOTION

Fig.8 ITNS experiments (1972–1975)

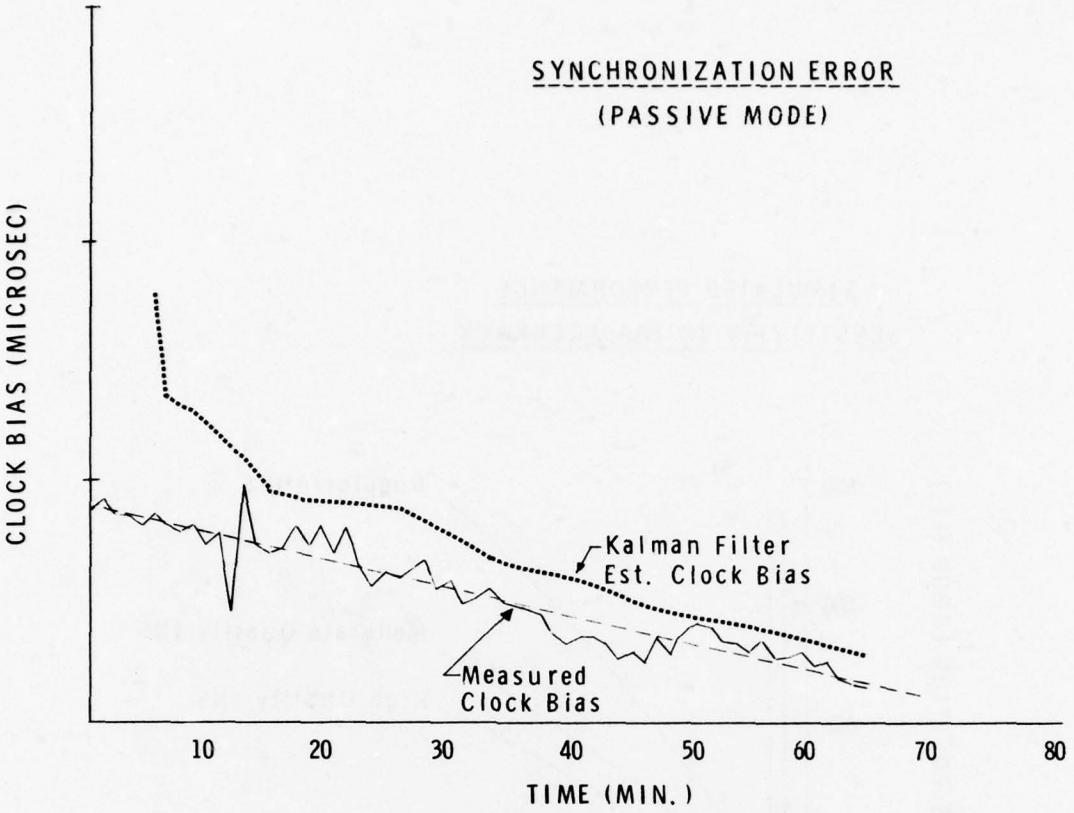

Fig.9 Relative grid experimental results: A

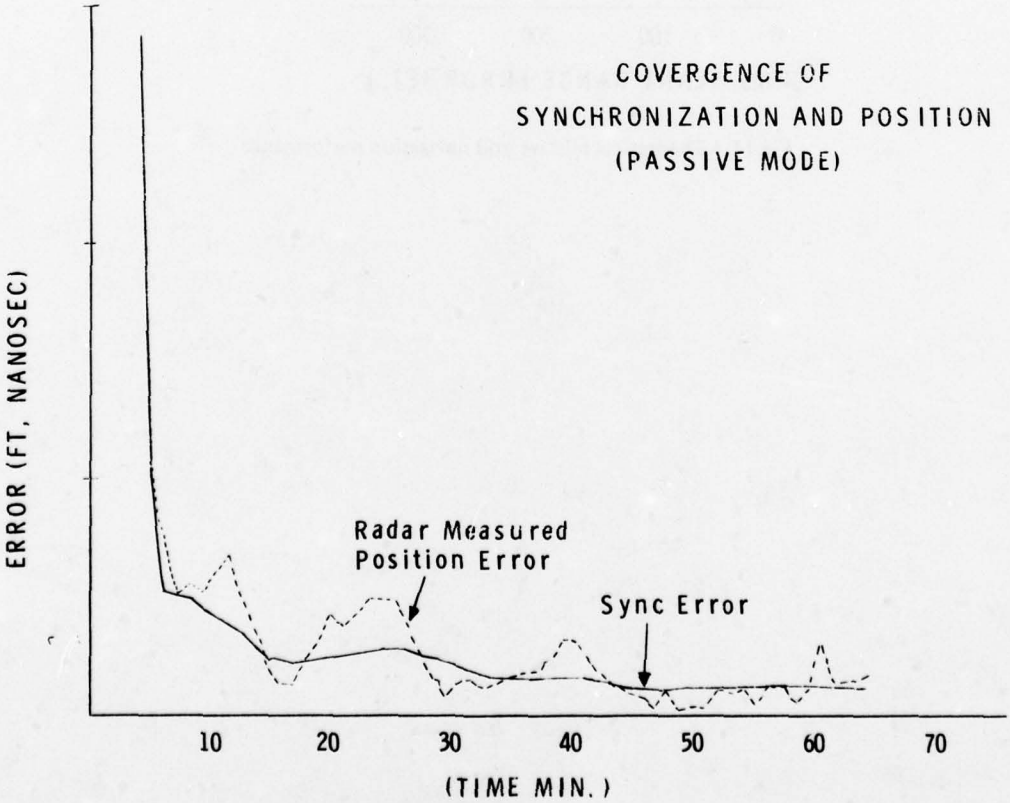

Fig.10 Relative grid experimental results: B

SIMULATED PERFORMANCE
SENSITIVITY TO TOA ACCURACY

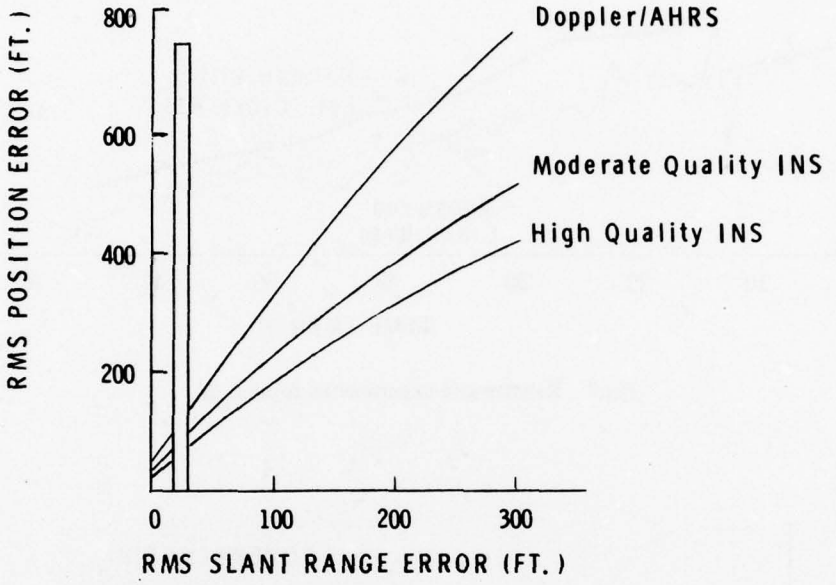

Fig.11 Theoretical relative grid navigation performance

IMPROVED AIRCRAFT TRACKING USING MANEUVER STATISTICS ENROUTE AND IN THE TERMINAL AREA

Ulrich Brokof
Deutsche Forschungs- und Versuchsanstalt
für Luft- und Raumfahrt E.V. (DFVLR)
Institut für Flugführung
3300 Braunschweig, Germany

SUMMARY

By means of radar tracking it is possible to estimate continuously the dynamic state of an aircraft from discrete radar data. This is necessary for instance, when investigating collision risks.

In this paper autocorrelation functions have been computed from acceleration data. The autocorrelation function could be approximated by a model which corresponds to a periodic random variable. The model itself as well as the model parameters gives an indication of how to improve radar tracking algorithm (additional parameters).

A simple and an extended model are practically tested in view of predicting properties. The same example is used to show how it is possible to improve radar tracking by aiding lateral acceleration with the roll angle information of the aircraft via a data link between the control centre and the aircraft.

1. INTRODUCTION

In order to be able to carry out the extensive tasks of the airport traffic control centres, more and more electronic systems are being installed. With the help of these systems different input data are being automatically processed to support the work of the flight controllers. This development was enforced by the growing density of the air-traffic, and increasing collision risks.

EUROCONTROL are installing and partly operating with the automatic systems KARL DAP, MADAP and SHAN DAP. Bundesanstalt für Flugsicherung (BFS) are developing the system DERD (Display of extracted radar data). All these systems will be completed step by step. BFS are now operating with DERD I. One component in these systems is the processing of radar data, including the important task of flight tracking. In DERD I this task is not yet realized, but will be conceived in the next phase of DERD-MC.

Civil air-traffic control systems use mainly the method of α-β-Filter for smoothing the aircraft trajectories in radar systems. The method corresponds to a Kalman filter by which only position and velocity are estimated [1]. The results which can be reached by this technique are demonstrated by Fig. 1. It shows vector-differences between filtered

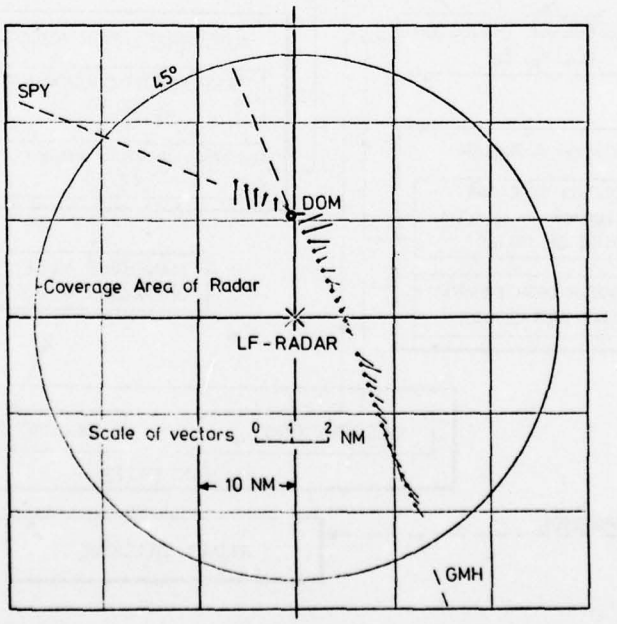

Fig. 1: Simultaneous Tracking of an Aircraft: Vector Differences between Filtered SSR-Data and Tracking Radar Data.

secondary radar (SSR) position data and accurate position data, which were measured by the tracking radar (LFR) [2] of the DFVLR, Braunschweig. Both radars were tracking an aircraft simultaneously. The standard deviation of the coordinate differences obtained from nearly 200 flights and 4000 measured points was 0.3 NM. The magnitude of this value is considerably influenced by error vector components, which occur in connection with little maneuvers, when an aircraft changes from one airway to another. Fig. 1 shows such a typical overshooting effect on the airways SPY-DOM and DOM-GMH near the Dortmund VOR. Here the deviations reach more than 0.7 NM ($\approx$ 1.3 km).

It is the aim of this paper to investigate the possibilities how to increase the accuracy of radar flight tracking. The basic quantities for this investigation are angular and acceleration data, which have been processed statistically. The results can give us an indication how an aircraft accelerates in different directions. They may show us ways how to model kinematic Kalman filter equations more realistically.

2. SURVEY OF DATA PROCESSING

The main items of this paper are given in the diagram Fig. 2. During the test phase of the german microwave landing system DLS, a lot of measured and derived data have been stored on magnetic tapes. This data source can be exploited for different tasks. Here

- accelerations,
- angular data (pitch, roll, heading),
- coordinates of the reference trajectory

of a flight are used to investigate the possibilities of improving radar tracking.

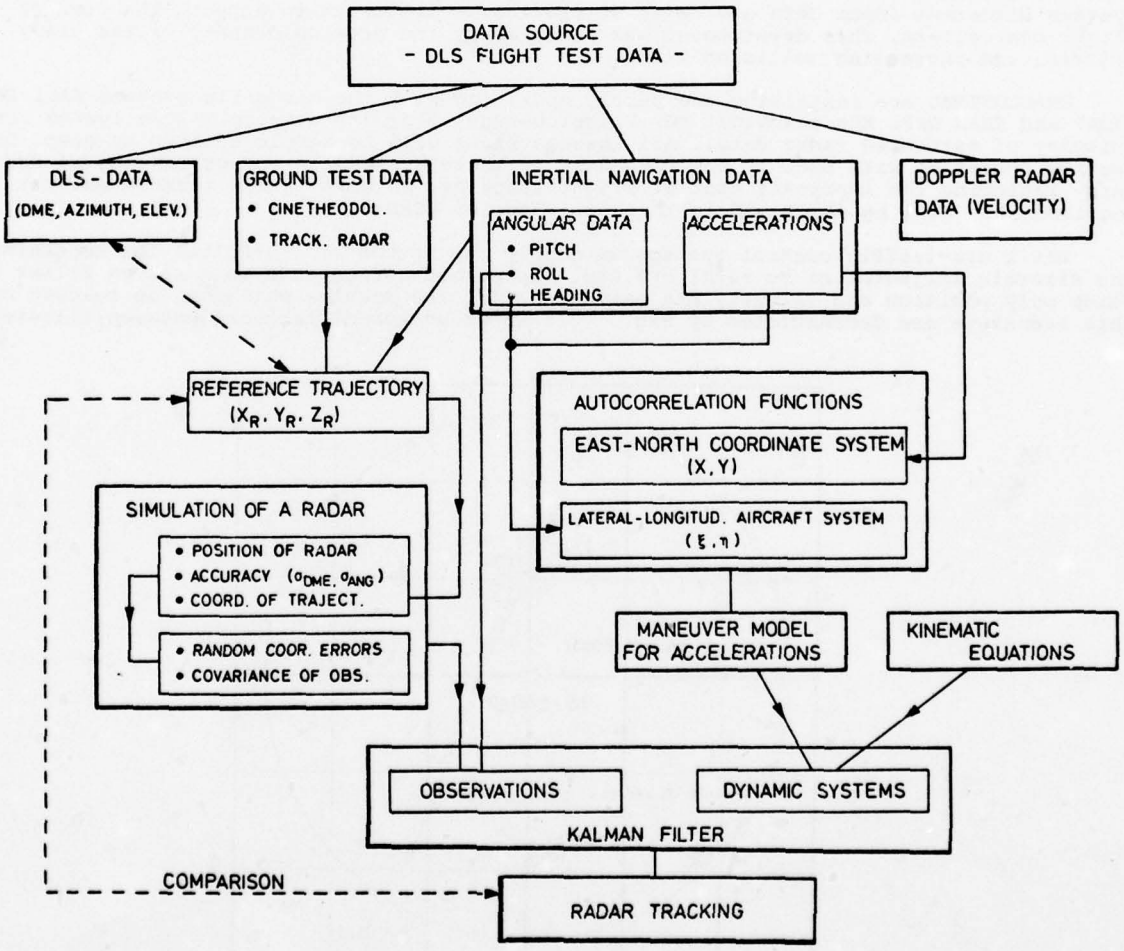

Fig. 2: Survey of Data Processing.

In comparison with other data (position, velocity), acceleration measurement data most closely describe the actual maneuvers of an aircraft. When computing the autocorrelation function of the accelerations of a flight path, these accelerations and their correlation in time is averaged. So this function contains the main maneuvering properties of the aircraft on this flight path.

The acceleration data are originally measured in an east-north coordinate system. An extentive investigation of 11 flights (5 hours flight time) had shown [4] that the autocorrelation corresponds to a periodic random variable with an exponential and a cosine function

$$A(t) = \sigma^2 \, e^{-t/\tau} \cos\left(\frac{2\pi}{T} t\right) \quad . \tag{1}$$

The parameters which we obtained for the horizontal acceleration components were nearly equal, and the σ^2-value (noise level) was rather low. This can be explained by the very different DLS flight trajectories (inbound and outbound on different radials, orbital flights), which contained only a few heavy maneuvers (turns from outbound to inbound).

Therefore the accelerations of a special flight were transformed into an airframe system with longitudinal and lateral acceleration components. The type of the functions corresponds to a periodic random variable, too.

The maneuver model which can be deduced from this type of autocorrelation function and the kinematic equations describe the dynamic of the aircraft movement.

The radar observations with time intervals of 10 s are derived from the coordinates of the reference trajectory, by simulation of measurement errors of a tracking radar (any other radar is possible). The covariance matrix of these observations was also computed. The noise level of lateral accelerations is very high in comparison with the longitudinal component, so the expected accuracy is not as high in this direction. Fortunately the roll angle, which can easily be measured, can, if it is necessary, be used as useful data to aid the lateral acceleration component.

The observations and the dynamic system are processed with the aid of the Kalman filter algorithm in order to obtain an optimal estimation of our radar trajectory. Finally this trajectory will be compared with the original reference.

3. TEST FLIGHT AND FLIGHT TEST DATA

As mentioned before one test flight was selected to make more detailed investigations of the acceleration data. The selected test flight can be seen in Fig. 3. The test part of

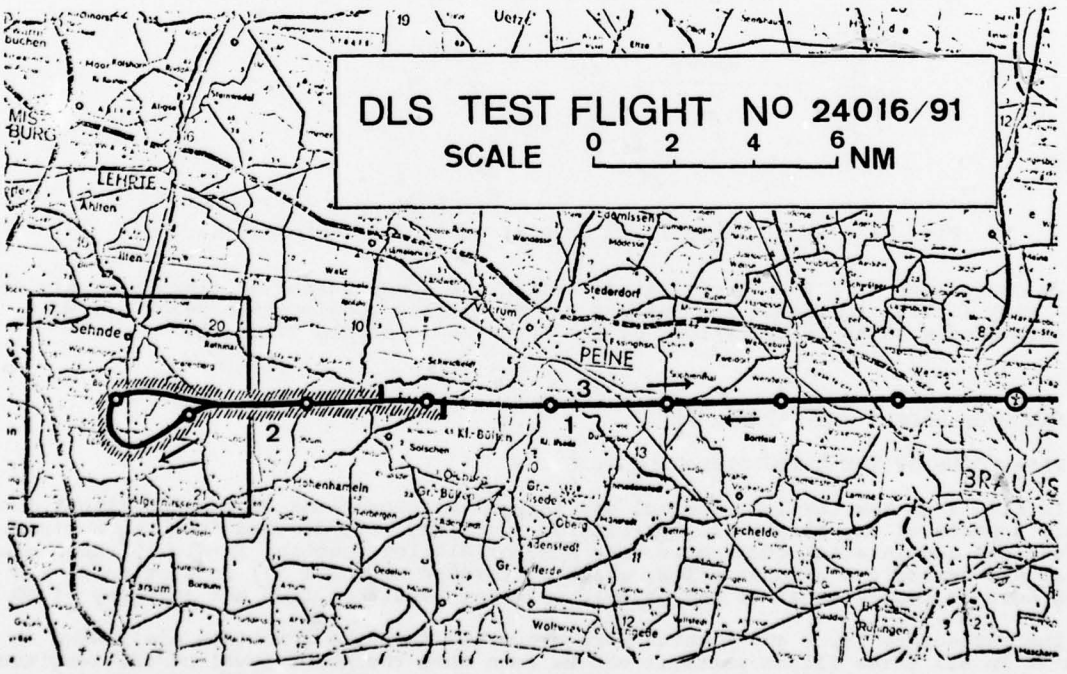

Fig. 3

the flight track begins at the DLS-Azimuth station in an altitude of 2000 ft. The heading is outbound on the 265° radial. In a distance of 23 NM the aircraft turns with bank angles reaching 17 degrees. Then the aircraft returns inbound to the DLS-A station. The first and the latter part of the flight are typical for enroute tracking, while the part with the rather heavy turn may be seen as typical for maneuvers in the terminal area, where we have to expect bank angles (roll) of 25 degrees. Such bank angles occur in the holding patterns. For detailed investigations the flight was therefore separated into these 3 parts. The window in Fig. 3 shows that part of the flight where we tested the maneuver model on overshooting properties.

By means of the heading angle, the acceleration components were transformed from a geographical into an aircraft related coordinate system, resulting into longitudinal and lateral components. In Fig. 4 acceleration data and angular data of the second part of the test flight were plotted together. They give an insight into the maneuvers of the aircraft and the relations between accelerations and the angular data. We can detect the very similar curves of the lateral acceleration and the roll angle. We can also notice the heavy changes of acceleration. The maximum values of lateral acceleration reach 3 m/s^2.

The effects of wind influence cannot be seen in this plot. The wind components sign changes when the aircraft turns from west heading to east heading. Therefore an additional acceleration during the maneuver would be caused.

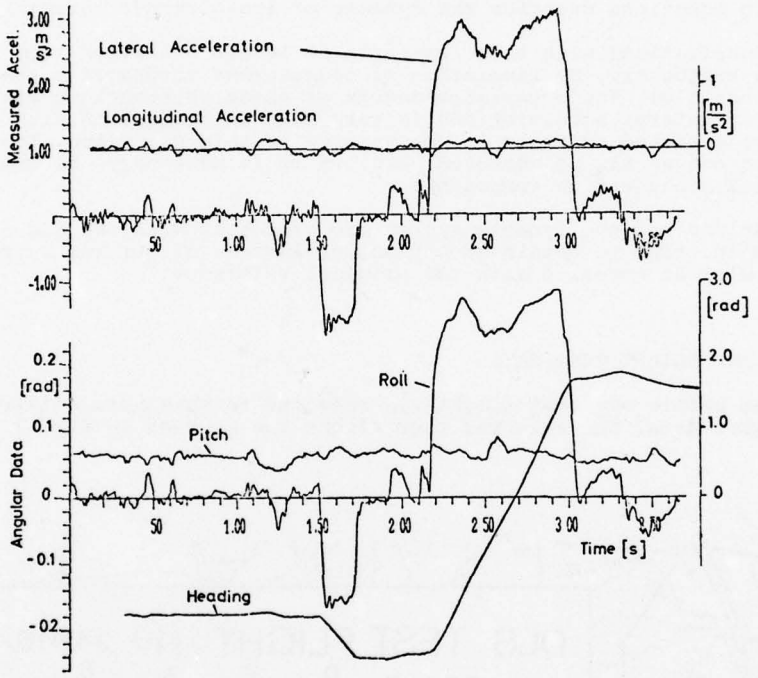

Fig. 4: Accelerations and Angular Data of Flight Part No. 2.

In comparison with the lateral acceleration the longitudinal acceleration only deviates very little from zero. The maximum values of this acceleration reach 0.5 m/s^2, they are correlated with the fluctuations of the pitch angle of the aircraft.

4. MANEUVER MODELS AND PARAMETERS

4.1 PARAMETERS OF THE AUTOCORRELATION FUNCTION

In Fig. 4 we saw the longitudinal and lateral accelerations of the 2nd flight track. For all 3 parts of the flight autocorrelation functions were derived from the horizontal and vertical acceleration components. The autocorrelation function in Fig. 5 shows exponential and periodic characteristics, which correspond to model (1) in section 2. The period here is nearly equal to the phygoid movement resulting from the velocity of 50 Knots.

The parameters σ^2, τ and T which were extracted from the functions are listed in table 1. In all three flight parts it can be seen that the noise level of the longitudinal acceleration is very low. The mean value corresponds to 0.07 m/s^2. The very different noise level of the lateral accelerations is due to the different maneuvers in the 3 flight parts. It should also be noted, that the relation of σ^2/τ is nearly equal in flight part

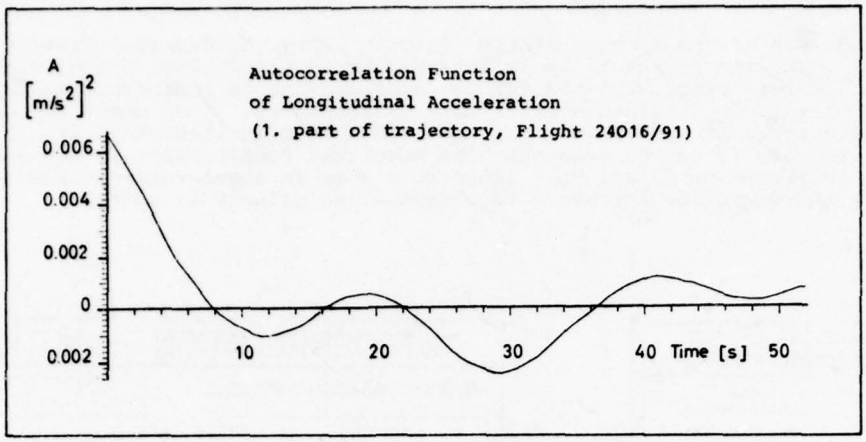

Fig. 5

Flight part No.	lateral acceleration σ_ξ^2	τ_ξ	T_ξ	longitudinal acceleration σ_η^2	τ_η	T_η	vertical acceleration σ_z^2	τ_z	T_z
1	0.23	10	40	0.0066	8	20	0.025	1	3
2	1.50	60	200	0.0038	10	30	0.020	1	4
3	0.05	12	60	0.0052	10	14	0.034	1	3
Mean	0.59	27	100	0.0052	9	21	0.025	1	3
1	0.0095	6	44	Autocorrelation of the difference $\Delta a_\xi = a_\xi - 9.81 \tan\Psi$ (Ψ = roll angle)					
2	0.003	8	50						
3	0.003	2	8						
Mean	0.0052	5	34						
1	0.075	1	3	Autocorrelation of the difference $\Delta a'_\xi = a_\xi - v_\eta \dot{\vartheta}$ (ϑ = course, v_η = velocity)					
2	0.050	5	100						
3	0.058	1	3						
Mean	0.061	2	35						

Table 1

Parameters of the Autocorrelation Model

$$A = \sigma^2 \, e^{-t/\tau} \cos\left(\frac{2\pi}{T} t\right)$$

for the accelerations of the aircraft DO 28

(Dimensions: σ [m/s^2], τ [s], T [s])

number 1 and 2. That means that the power spectral density defined by $2\sigma^2/\tau \cdot \delta$ is equal in both cases and can be interpreted by the fact that high lateral accelerations are caused by turning maneuvers, which are normally executed during a longer period of time. The vertical accelerations have a rather low noise level but a very short correlation time.

The high noise level of the lateral acceleration limits the accuracy of radar flight tracking. Improvements can be achieved by additional angular data, especially the roll angle Ψ and changes of the heading angle ϑ. The acceleration data, which were computed from the angular data were subtracted from the original accelerations. From these acceleration differences, autocorrelation functions were derived. The noise level of these functions is very low. Especially the roll angle is a good measure for lateral accelerations. The noise level can be reduced to the same order of magnitude as the noise of the longitudinal accelerations. The residual acceleration noise corresponds to a standard deviation of the roll angle of 0.3°.

4.2 Maneuver Models

The parameters of the autocorrelation function (Fig. 5) are the variance σ^2, the time constant τ and the period T. It is interesting to see in Fig. 6 that with the cosine-function a drift rate state variable for the acceleration is introduced (Model ①). Our test results have shown, that this drift rate is necessary. If we ommit the cosine function we get the model ③ $\dot{a} = -1/\tau\ a$, which is widespread in literature [1, 5, 6]. From the discrete version it can be seen that the predicted acceleration is always less than the previous acceleration value. This leads to a loss in acceleration especially in the case of heavy maneuvers and therefore to overshooting effects in curves.

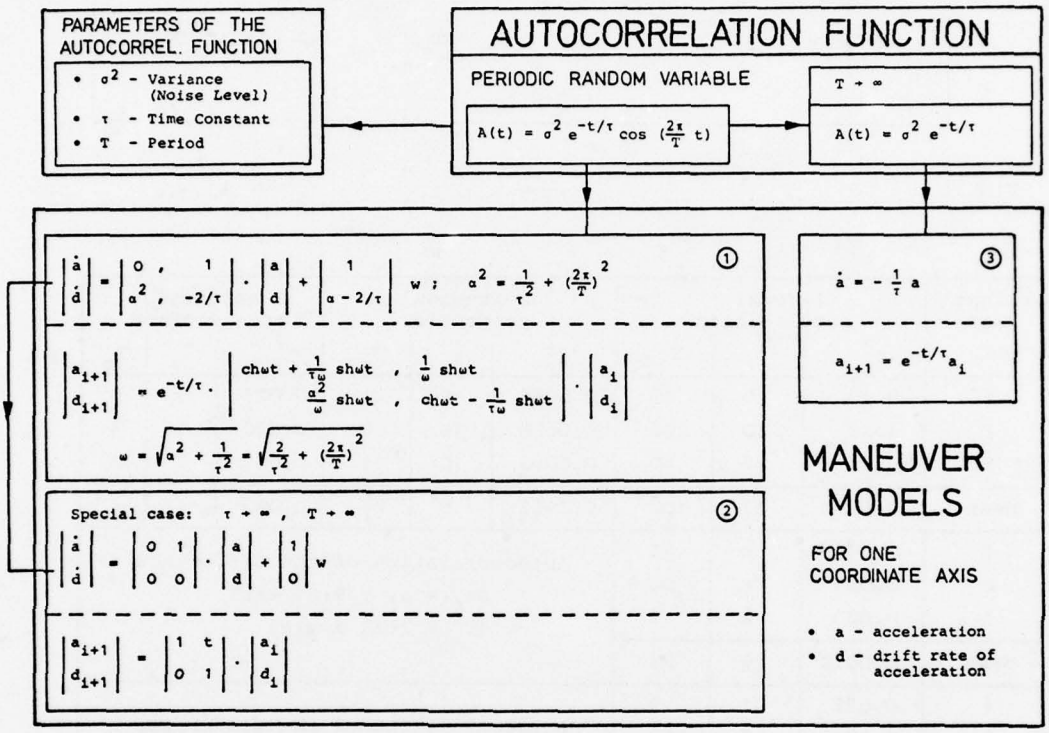

Fig. 6

From our autocorrelation functions we have got mean parameter values for σ^2, τ and T. But we have already seen from table 1, that these parameters vary with the maneuvers of the flight. In the case of heavy maneuvers we got great values for τ and T, although they are diminished by little maneuvers of nearly one half of the flight path. Because we concentrated our test computations on the turn from outbound to inbound, model ① was specialized by introducing $T \to \infty$ and $\tau \to \infty$. So we get model ② . This model is rather insensitive to the type of a maneuver. But it has the property to overcompensate errors (Fig. 7b), because the drift rate parameter d is undamped.

An optimal use of model ① is possible by adapting the parameters T and τ to the actual maneuvers.

4.3 Error Behaviour of the Model

The influence of the noise level σ of the accelerations and the correlation time τ, on velocity and position can be estimated with the covariance matrix (2) [5]

$$Q = 2\sigma^2/\tau \begin{vmatrix} T^5/20 & T^4/8 & T^3/6 \\ T^4/8 & T^3/3 & T^2/2 \\ T^3/6 & T^2/2 & T \end{vmatrix} \qquad (2)$$

The position error of an ideally calibrated system increases with time T according to $\sigma_x = \sigma\sqrt{T^5/10\tau}$. The standard deviation of the velocity error is $\sigma_v = \sigma\sqrt{2T^3/3\tau}$. That means for the longitudinal direction, that after 10 s we have only to expect position errors of 2 ~ 3 m.

The covariance matrix Q shows that the maneuver statistics model has a good short time stability. That means, that the noise of measurement data with high update rate can be filtered very well. This ability will decrease very rapidly if the time interval of updating increases.

5. APPLICATION OF THE MANEUVER STATISTICAL RESULTS TO RADAR TRACKING

Important assumptions to study the efficiency of a model are real data, extreme test situations, and objective references to control the results. In order to test several model approaches, we used that part of the flight track in Fig. 3, which includes the turn from outbound to inbound. The coordinates of this trajectory are known with high accuracy. They have been computed from radar and inertial navigation data [3]. The original data frequency of 30 Hz was reduced to 1 Hz. For every 10th point of this sequence random errors of a tracking radar have been simulated ($\sigma_{Dist.}$ = 10 m, $\sigma_{Azimuth}$ = 0.06°). The corresponding coordinate errors were added to the reference track coordinates. The covariance matrix of the simulated measurement errors was computed, too.

If we now compute the radar track with any model, we can check the main state elements with our original data. The vertical channel will not be considered in our investigations.

The test computations were executed with model (2) . The total system for both coordinate directions is given by

$$\begin{vmatrix} \dot{x} \\ \dot{y} \\ \dot{v}_x \\ \dot{v}_y \\ \dot{a}_\xi \\ \dot{a}_\eta \\ \dot{d}_\xi \\ \dot{d}_\eta \end{vmatrix} = \begin{vmatrix} 0 & 0 & 1 & 0 & 0 & 0 & 0 & 0 \\ 0 & 0 & 0 & 1 & 0 & 0 & 0 & 0 \\ 0 & 0 & 0 & 0 & \cos\vartheta & \sin\vartheta & 0 & 0 \\ 0 & 0 & 0 & 0 & -\sin\vartheta & \cos\vartheta & 0 & 0 \\ 0 & 0 & 0 & 0 & 0 & 0 & 1 & 0 \\ 0 & 0 & 0 & 0 & 0 & 0 & 0 & 1 \\ 0 & 0 & 0 & 0 & 0 & 0 & 0 & 0 \\ 0 & 0 & 0 & 0 & 0 & 0 & 0 & 0 \end{vmatrix} \cdot \begin{vmatrix} x \\ y \\ v_x \\ v_y \\ a_\xi \\ a_\eta \\ d_\xi \\ d_\eta \end{vmatrix} + \begin{vmatrix} 0 \\ 0 \\ 0 \\ 0 \\ w_\xi \\ w_\eta \\ 0 \\ 0 \end{vmatrix} \qquad (3)$$

where $\sin\vartheta = \frac{v_x}{v}$, $v = \sqrt{v_x^2 + v_y^2}$

$\cos\vartheta = \frac{v_y}{v}$.

It was not sufficient only to determine drift rates for lateral accelerations. This can be seen in Fig. 7a where we still have an overshooting effect. This effect disappears if we take into account changes of acceleration also in the longitudinal direction.

The influence of wind velocity causes longitudinal accelerations which are not in agreement with the low noise, we have found from our statistical computations. Fig. 7b and Fig. 7c show deviations between the radar trajectory, obtained with the specialized model (2) and the reference trajectory, one second before updating. Only the region around the turn from outbound to inbound is plotted, because the deviations will reach maximum values, in this part of the trajectory. Fig. 7b shows the result only with radar measurement data. The result of Fig. 7c was obtained with additional roll angle information. The deviations include the simulated radar errors. The maximum errors are less than the greatest simulated radar errors.

The improvement which could be reached by the maneuver statistics model can be read from the σ-values of table 2. The improvement is not so great if we have only radar measurements, because of the low update rate of 10 s. If we use the roll angle information the error will be decreased by ≈ 30 %.

Comp. No.	Standard Deviations [m]				Observations
	Measured Radar Data		Tracking with Maneuver Model		
	σ_x	σ_y	σ_x	σ_y	
1	8.6	34.6	8.5	31.9	Tracking Radar (10 s)
2	8.6	34.6	8.1	26.1	Tracking Radar (10 s) and Roll Angle (2 s)
3	148.1	156.3	91.6	93.6	SSR (10 s) and Roll Angle (2 s)

Table 2: Improvement of measured radar data, when tracking with the aid of a maneuver model.

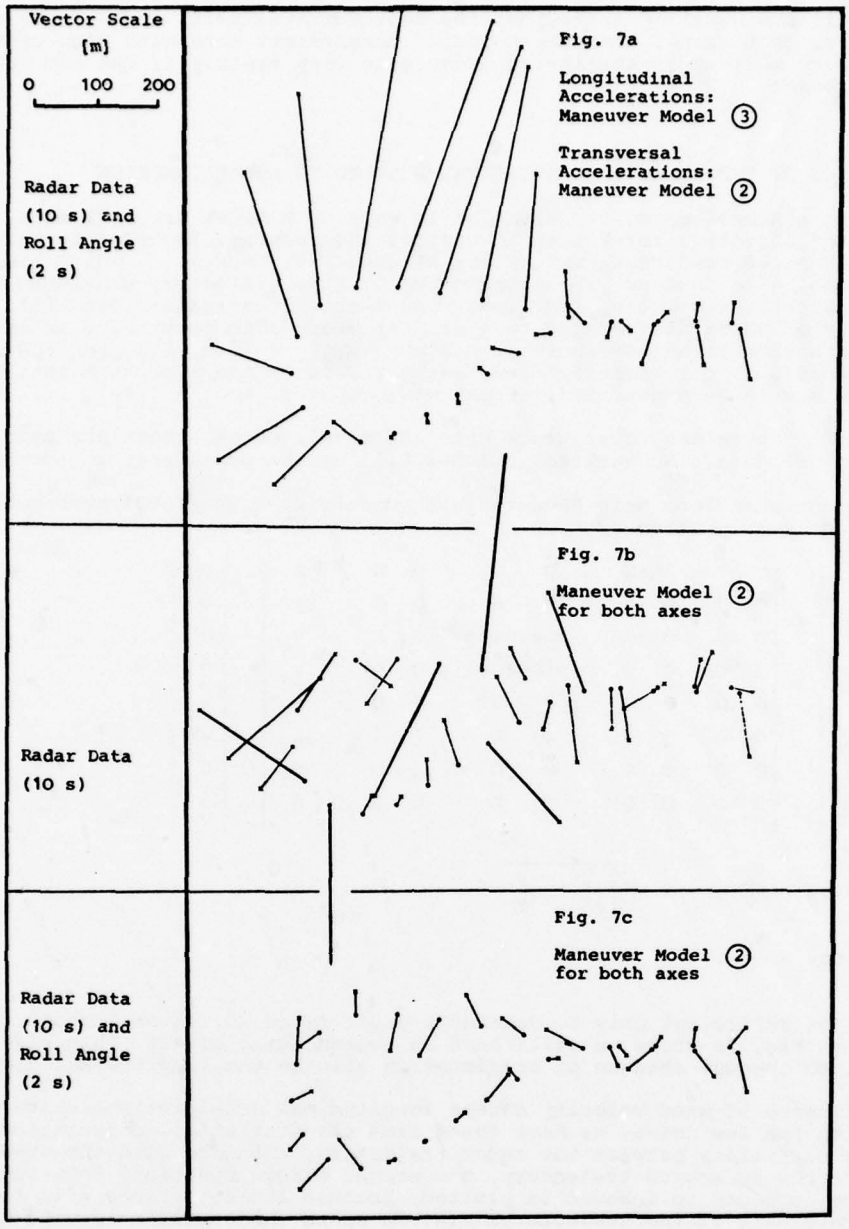

Fig. 7: Error Vectors during the turn from outbound to inbound (1.0 s before updating).

6. CONCLUSIONS

Starting from maneuver statistical investigations we have found a model which is able to eliminate overshooting effects of flight trajectories with heavy maneuvers.

If we are tracking aircrafts enroute (Fig. 8), we have to expect only little maneuvers. Moreover we do not need extreme accuracies. In this case it is sufficient, only to use radar measurements.

In the terminal area we are confronted by heavy aircraft maneuvers and the demand of accurate tracking. An example of heavy maneuvers is the holding pattern flight, where we have to expect lateral acceleration changes of 5 m/s^2 within 5 seconds. Here it would be very useful to have a data link between aircraft and the control centres to transmit the roll angle. The results in this paper are based on a data rate of 2 s. The standard deviation of the original errors could be diminished by the factor 0.75 in the case of tracking radar data and by 0.60 if we were using SSR-data.

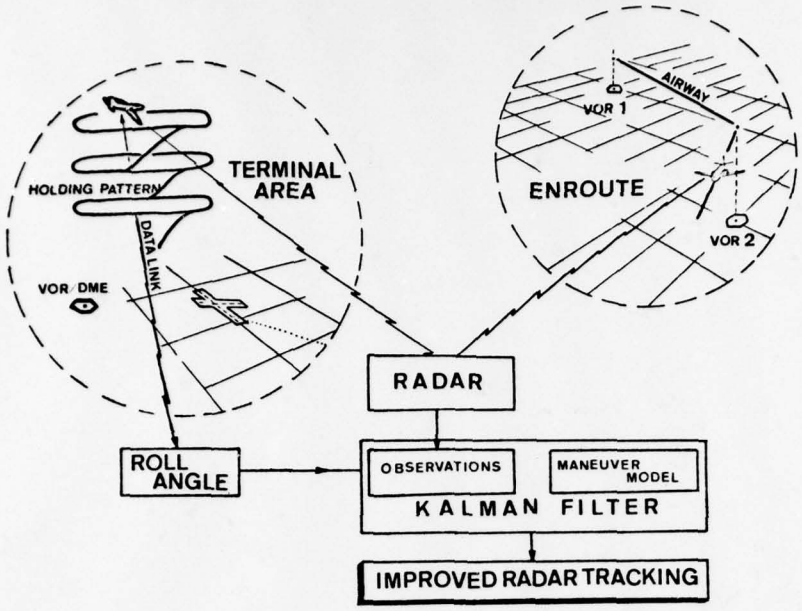

Fig. 8: Realization of Improved Radar Tracking.

7. REFERENCES

[1] HAMPTON, R.L.T., COOKE, J.R., "Unsupervised Tracking of Maneuvering Vehicles". IEEE Transactions on Aerospace and Electronic Systems, Vol. AES-9, No. 2, 1973, pp. 197-207.

[2] BROKOF, U., HAENSEL, H., HOFFMANN, H., "Evaluation of the MADAP Radar Chain - Task D: Overall Chain Evaluation -". IB 153-75/04, Deutsche Forschungs- und Versuchsanstalt für Luft- und Raumfahrt, Braunschweig, 1975.

[3] HURRASS, K., WINTER, H., "A High Precision Reference System for Aircraft Position and Velocity Measurements", DGON-Vierteljahresmitteilungen II/III, 1976.

[4] WINTER, H., BROKOF, U., HURRASS, K., "Radar Aided High Precision Navigation Systems for RPV". Symposium "Avionics, Guidance and Control for Remotely Piloted Vehicles", Florenz, 1976.

[5] SINGER, A.S., "Estimating Optimal Tracking Filter Performance for Manned Maneuvering Targets". IEEE Transactions on Aerospace and Electronic Systems, Vol. AES-6, No. 4, 1970, pp. 473-483.

[6] VAN KEUK, G., "Zielverfolgung, basierend auf Kalman-Bucy-Filter". Angewandte Informatik, 7/72, S. 302-308.

A HYBRID GUIDANCE SYSTEM FOR ALL-WEATHER APPROACH AND LANDING

Karlheinz Hurraß
Deutsche Forschungs- und Versuchsanstalt
für Luft- und Raumfahrt E.V. (DFVLR)
Institut für Flugführung
3300 Braunschweig, Germany

SUMMARY

The DFVLR has tested the micro-wave landing system DLS in Braunschweig. Apart from the DLS on-board equipment an inertial navigation system had been installed in a test aircraft for this purpose. One of the aims of these tests was to find out, to what degree the accuracy of the landing system could be improved by integrating this inertial navigation system. Both systems were combined by means of a Kalman filter. In this study, the way in which the filter operates during an approach is described. The errors of the DLS trial system set up at Braunschweig airport, could be reduced to about 20 % by using the inertial navigation system.

1. INTRODUCTION

Today, the instrument landing system, ILS, is almost exclusively used for aircraft approaches. Since this system has many disadvantages, a modern one is to replace it. Therefore, the international civil aviation organisation (ICAO) has asked its member states to submit suggestions for new systems. The Federal Republic of West Germany has suggested the micro-wave landing system called DLS, which stands for DME derived landing system.

The DFVLR in Braunschweig has tested the DLS trial system. A DO 28 was used as test aircraft. In addition to the DLS on-board equipment, an inertial navigation system of the type LN3, as well as a telemetric system, were installed in the aircraft for these tests. All data which were necessary for the tests, were transmitted to the ground, and were recorded there on magnetic tape. These data comprised among others the DLS data, the navigational results of the inertial navigation system, and the measured accelerations. The registration frequency was 32 Hz. Thus it was possible to repeat the flights with a digital computer, and with real data, in order to test various configurations of the system.

The errors of the tested DLS system mainly consist of a high-frequency noise. The error behaviour of an inertial navigation system is entirely different; i.e. the short-time accuracy is of a very high degree. The navigational errors of an INS however gradually increase. Therefore, it was interesting to find out, how the accuracy of the DLS system could be improved by integrating the DLS in the inertial navigation system.

Later on in this lecture, the combination of both systems, with the aid of a Kalman filter, will be mentioned. The results of an aircraft approach show which accuracy can be reached.

2. SHORT DESCRIPTION OF THE DLS SYSTEM

The DLS trial system consists of two ground stations, namely the azimuth and the elevation station. The azimuth station corresponds to the ILS-localizer, and is sited at the end of the runway. The elevation station replaces the glide path transmitter, and is situated likewise beside the touch-down point. The azimuth station determines the azimuth and the slant range between the station and the aircraft. The elevation station determines the elevation angle. The DLS system uses the same frequencies as the TACAN system. Figure 1 gives an impression as to the accuracy of the DLS trial system. The test results of a conventional centerline approach are shown. The aircraft was approaching at 3°. The figure shows the difference between the values derived by the DLS-azimuth station and a very accurate reference [1]. The distance from the test aircraft to the azimuth station is marked on the horizontal axis; the vertical axis shows the azimuth errors. The standard deviation is 0.017°; the mean value is 0.062° due to a small misalignment. The typical high frequent noise can be seen in this figure. A rather low frequent noise is also visible. The error behaviour of the other two measurements of the DLS trial system is similar.

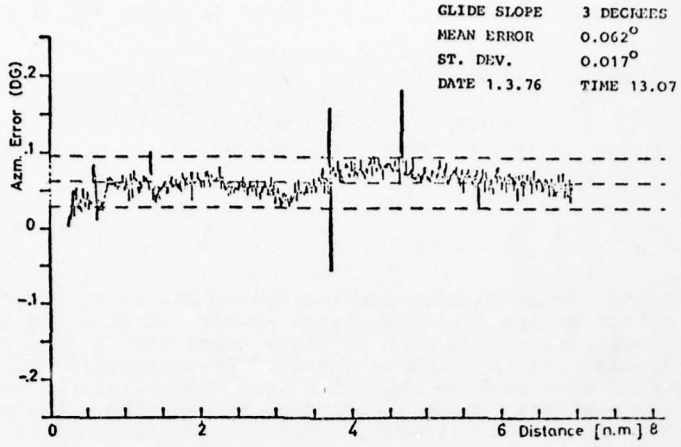

Fig. 1: Conventional Centerline Approach Azimuth Error

3. ERROR MODELS

The DLS system was combined with the inertial navigation system by means of a Kalman filter of the discrete type. For this purpose it was necessary to know the error model of both systems.

A simplified error model was used for the inertial navigation system. It contains the Schuler couplings, the earth rate couplings, as well as the couplings due to the misalignment of the platform in the azimuth. The variable, as well as the constant gyro-drifts, have been modelled by so-called random walk processes. As far as the vertical accelerometer is concerned, only a constant accelerometer error has been assumed. A more detailed description of the INS error model has already been given by Dr. Stieler.

As already mentioned, the primary measured data of the DLS system are 2 angles and a distance.

Before determining the measurements for the Kalman filter, it is necessary to convert the DLS data into the navigational co-ordinate system of the inertial navigation system. Moreover, the co-variance matrix of the errors of the DLS system has to be calculated for the same co-ordinate system.

4. OPERATION OF THE KALMAN FILTER

Before landing, the aircraft will fly into the covering range of the MLS system. When this happens, the computer program for the Kalman filter is started to operate. The first position determined by the DLS system is used as initial position for all further navigational calculations regarding the inertial navigation. The co-variance matrix of this first position is used as initial value for some elements of the co-variance matrix of the estimation accuracy.

The measurements for the Kalman filter are the differences between the positions determined by the inertial navigation system and by the MLS system, respectively. It may happen that the positions determined by the MLS system are partially invalid, for some reason or other. This is then normally notified by a flag. No measurements should be processed by the Kalman filter during such "no go times". This is achieved by setting all elements of the measurement matrix to zero.

The state vector contains, among others, the position errors Δx, Δy, and Δz of the inertial navigation system. The Kalman filter estimates these three elements. The final position of an aircraft is determined by adding the estimated position errors to the positions determined by the inertial navigation system. In the same way, the best estimates can be calculated for the three velocity components.

5. RESULTS OF AN APPROACH

The results of an approach are presented as an example for the operation of the Kalman filter. This was an approach chosen at random during the measurements taken for the DLS trial system. The approach, and thus the start of the Kalman filtering process, began at a distance of 7 nautical miles from the azimuth station. Approximately 3 minutes elapsed

until the runway threshold was reached. The heading of the approach was 85°; it was thus in eastern direction.

The cycle time of the Kalman filter was 0.5 seconds. This relatively short time was chosen, because the correlation times of the mentioned high frequency errors of the DLS system are smaller than 0.5 seconds.

Figure 2 shows the position errors in the north-south direction. The approach starts on the left hand side of Fig. 2. The flight level is here about 450 metres. After about 2 minutes and 45 seconds, the runway threshold is crossed at a height of a few metres. The thin line represents the accuracy of the DLS trial system (1σ). When the approach is started, the error is 6 metres. The thick line represents the achieved accuracy after Kalman filtering. The errors of the DLS system are reduced to approximately 20 per cent, after a comparatively short period of time. At the runway threshold the error is about 0.4 metres.

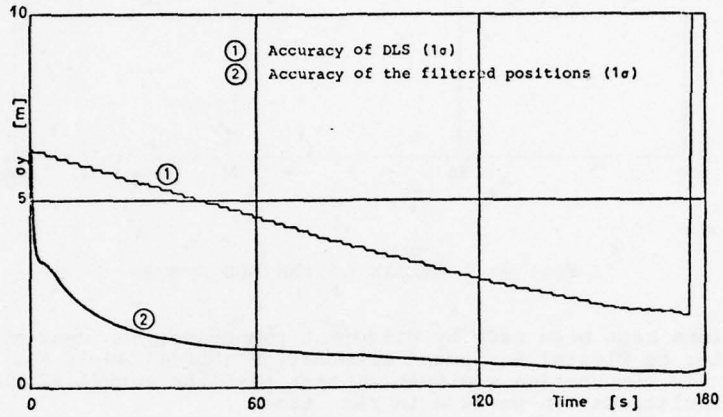

Fig. 2: DLS/INS Approach
Accuracies σ_y

Figure 3 shows the vertical errors. The error behaviour is similar to that of the last figure. At the beginning of the approach, the vertical error is 16 metres. After a short transient time, the error is once more reduced to about 20 %, by combination of the DLS system with the inertial navigation system. At touch-down the accuracy is approximately 0.3 metres. After the touch-down point there are no more measurements of the DLS system. Nevertheless, the inertial navigation system is able to continue determining the altitude very accurately.

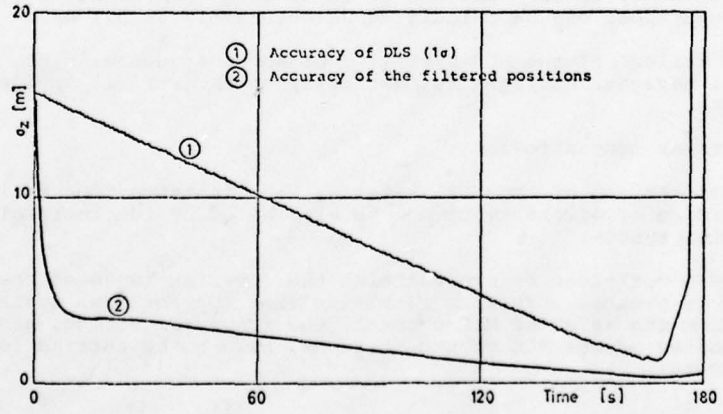

Fig. 3: DLS/INS Approach
Accuracies σ_z

Figure 4 shows the difference of two altitudes, i.e. the difference between the altitude measured by the DLS system alone, and that resulting from the combination of the DLS system and the inertial navigation system. These high-frequent errors are caused only by the DLS system, as such a noise cannot be produced by an inertial navigation system.

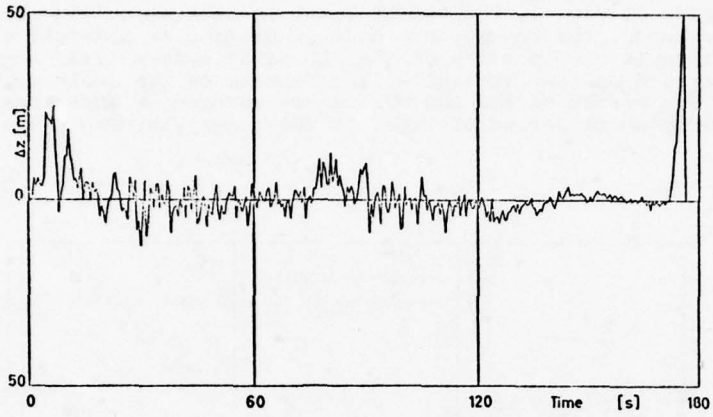

Fig. 4: Errors of the DLS System

All computations have been made by different computers, the central computer of the DFVLR and a computer by Digital Equipment Corporation (PDP 11/40-16 K). In both cases, the time required for computation was much shorter than the actual flight time; which means that the calculations can be made in real time.

6. ADVANTAGES AND DISADVANTAGES OF THE DESCRIBED SYSTEM

The combination of the micro-wave landing system DLS with an inertial navigation system has the following advantages:

the high-frequent errors of the DLS trial system are recognized by the Kalman filter, and are almost entirely eliminated. In this context, high-frequent errors are those having at least a frequency of about 0.05 Hz.

Kalman filtering means no falsification caused by high-frequent aircraft movement, for example by turbulence.

In the same way as the position of an aircraft can be determined, the ground speed can be calculated as accurately as 0.1 m/s.

A short failure of the MLS system is of no consequence, since the inertial navigation system automatically takes over all navigational functions.

The disadvantages are as follows:

Systematic errors of the MLS system as, for instance, concerning the distance of aircraft, cannot be eliminated by the inertial navigation system.

The crew's work-load before entering the covering range of the MLS system, is greater than that resulting from conventional systems. Apart from the selected MLS-channel, the runway direction, and the co-ordinates of the MLS ground stations, have to be entered into the computer.

7. SUMMARY OF RESULTS

In order to determine the position of aircraft during the approach phase, the configuration of an MLS system and an inertial navigation system has been described. Both systems have been combined with the aid of a Kalman filter.

Flight tests made by the DFVLR in Braunschweig have shown that the errors of the DLS trial system can be reduced to approximately 20 %. The following accuracy is obtained at the runway threshold: vertical direction: 0.3 metres, position error at 90° to the flight direction: 0.4 metres, position error in approach direction: 3 metres. These errors are clearly below the requirements made by the AWOP Panel, whereas the DLS trial system alone does not always meet those requirements.

8. LITERATURE

[1] WINTER, H., "Experiences in Flight Testing Hybrid Navigation Systems", AGARD Lecture Series No. 82, Mai 1976.

[2] HURRASS, K., "Anwendung von optimaler Glättungstechnik bei der Erprobung von Navigationssystemen", DFVLR-Nachrichten, Heft 17.

[3] HURRASS, K., WINTER, H., "A High Precision Reference System for Aircraft Position and Velocity Measurements", DGON-Vierteljahresmitteilungen II/III 1976.

[4] STIELER, B., "Calibration of an INS based on Flight Data", AGARD, 24th Guidance and Control Panel Symposium, Stuttgart, Mai 1977.

[5] BECKER, A., "Accuracy Considerations on New Microwave Landing Systems (MLS) from a Operational Point of View", AGARD, 24th Guidance and Control Panel Symposium, Stuttgart, Mai 1977.

DEVELOPMENT OF THE INTEGRATED ALL-WEATHER NAVIGATION SYSTEM FOR TORNADO (MRCA)

BY
Dr. H.F. Schwegler
Messerschmitt-Bölkow-Blohm GmbH
Unternehmensbereich Flugzeuge
D-8 München 80, Postfach 801160

SUMMARY.

The integrated Navigationsystem for the Tornado Weaponsystem is about to complete flight-testing. A short rundown of the various development-stages is given together with methods used and pitfalls encountered. From the experience gained in this project it seems that for the design of similar Kalmantype Navigation filters the most important tool is a data bank derived from flighttests together with welltested flexible evaluation software which allows the investigation of filter variants in a very short time on a ground based general purpose computer.

SYMBOLS AND ABBREVIATIONS.

A	System dynamic Matrix
X	State vector
IN, INS	Inertial Navigation System
P	Covariance Matrix P-P+ refer to before and after a measurement
ϕ	Transition Matrix
R	Plant Noise Matrix
M	Measurement Matrix
Y_p Y	Measurement prediction and observation
W_p W	Covariance Matrices of same
KF	Kalman Filter
Do	Doppler Radar
A/C	Aircraft

This paper deals with some aspects and problems encountered during the development of the integrated All Weather Navigation System of Tornado which is going into service in U.K., F.R.G. and Italy within the next few years.

This development has been going on at various places in the U.K. and F.R.G. during the project. Some of the envisaged roles of Tornado require careful preflight planning and a Navigation accuracy which cannot be met by single sensors. An example is Terrain following where the planned flight path may be matched to ground profiles in order to minimize detection probability and to give the crew the opportunity to check their position against Fixpoints. It was decided to use a Kalman filter (KF) to integrate various sources of navigational information. The "best" position and velocities provided by the KF are used to provide steering signals which enable the A/C to arri e at a certain position at a certain time.

During its development the KF underwent the following stages or mechanizations:

A) Review of background theory, selection of data sources

B) Definition of equations including moding and Cockpit-interface as coding instructions, for the A/C Central Computer program

C) Development of a high level language Comp. Program (FORTRAN)

D) Development of the Assembler Program for the A/C Main Computer

Boundary conditions are Computer core and time loading and handling aspects.

As to point A an Inertial Navigator and a Doppler Radar were chosen because of their different error characteristics. These data are supported by different types of position fixes which may be performed (Visual: ON TOP, Head-up display/Mapping Radar in various modes/Radio Navigation).

The next question was whether to use the Filter in a closed or open loop mechanization. In a closed loop system estimates of modelled errors e.g. velocity error or tilt angles are fed back into the platform whereas in the open loop mechanization a mathematical model is used to derive correction terms for the outputs of the otherwise self contained Inertial Navigation System. Both mechanizations have their merits and disadvantages. Open loop exhibits higher integrity and lower development risk whereas the closed loop mechanization has a somewhat greater potential with respect to INS Alignment (Ground based or in flight) but for reasons of system integrity really two independant Computers are necessary. Having just one computer and with offers of fairly well developed integral Inertial Navigation systems an open loop mechanization was selected.

Open loop	Closed loop
Higher redundancy	Needs really 2 Computers
Lower development risk	OFF Line development and optimization less straight forward
Slightly more Computer load for same task	Essential for inflight alignment using KF
Recorded flights may be "reflown" on a ground based computer with precise results	Quicker ground alignment possible and better performance when entering NAV Mode

The filter contains 11 states - 9 for the INS and 2 for the Doppler.

INS: North/East Position and velocities
Tilt angle around 3 axes
Level gyro drifts

Doppler: Along heading scale factor error and an misalignment angle

The equations governing the error behaviour of the INS follow text books, Doppler errors are modelled as very low frequency noise, a certainly wrong but workable assumption.

The development stages of the Navigation filter which was independantly programmed in a high level language and in Assembler together with the data these programs are acting upon are shown in table 1.

STEP		FORTRAN KF	ASSEMBLER KF
1	Simulated Sensor Data-Pseudorealistic behaviour	F1 Zero order optimisation Performance Prediction Confidence checks	A1 Was planned but time schedule did not permit, considered inefficient
2	TEST DATA	FA2 Software proving Debugging of the Assembler program Solving numeric difficulties using the FORTRAN KF as a test standard.	
3	Recorded Flight Data + ext. Reference	F3 Structural and numeric Optimization of the KF Assessment of sensor and system performance with and without position aiding Supporting evidence for A4	A3 Only necessary if step FA2 shows significant differences between the two programs, but a good confidence check.
4	Inflight Data + ext. Reference	F4 N.A. in this project might be possible in other applications	A4 Official proving of Navigation Subsystem performance Cross check with F3

Table 1

The next step (F1) was to construct so called real world simulation models of the INS, Doppler and Position Fixing methods which were then linked up with the Kalmanfilter containing much simpler equipment models. The aim of this exercise which was conducted in a high level language was a sensitivity analysis, zero order optimisation and confidence check. There were some errors or short comings in the initial program which were discovered during this exercise or only later on.

1) The equations governing INS behaviour may be linearized arriving at a transition Matrix A times Δt. One might try to drop Δt^2 terms also in the propagation of the Covariance Matrix which seems to have great numerical advantages but the result is rather disastrous and so this was cured without doing much harm. It seems a good idea to carry a program which monitors any anormalities of the Covariance Matrix along with the Filter as far as possible.

2) The incorporation of Doppler information in a Filter with measurement updating every 10 sec. requires presmoothing. Initially this was a low pass filter with a timeconstant of a few seconds but a straight forward summing over a fixed time interval is numerically more accurate and the separation of data collection and evaluation helps to decrease computer time load.

3) An unsuitable choice of measurement plane for some position fixes where the measurement prediction is no longer a linear Combination of state variables at short measurement ranges.

4) A serious error was an incorrect feed back of a Doppler scaling correction term. Usually such an error causes an immediate runaway of the system. In this case unfortunately the error was masked by a quite small time constant contained in the Doppler error model and the fact that the "real world" simulation provided quite small errors. Despite this performance after 1 1/2 hours became clearly inadequate. This error could have been avoided if for a check all relevant time constants would have been set to large numbers.

The main effort of the development program was concentrated on steps number 2 and 3 Software proving and off line analysis of recorded sensor data which were available before the Filter became airborne.

SOFTWARE PROVING.

Tests to confirm that the program for the on board computer really performs the required functions and with the necessary accuracy. In this case the only way to check whether the resulting program really reflects the written requirement is to have an independantly written program, preferably in another language, feed them with identical inputs and check whether the outputs are the same. Even though both programs were considered to be debugged as far as possible without cross reference results did not tie up at all initially because of program errors, wrong setting of constants and misinterpretations of the written requirement. The ratio of errors found clearly indicates the need for higher languages to be used in the development of Avionic systems.

ERRORS	ASSEMBLER	FORTRAN
Program Flow	30 %	50 %
Constants	70 %	50 %
ERRORS Found	$\frac{\text{Assembler}}{\text{Fortran}} = \frac{10}{1}$	

Further differences between the programs were due to the number representation in the on board computer (Floating point with 16 bit mantissa). Proper choice of the smoothing filter applied to the Doppler pre-smoothing filter and suitable iteration rates which at the beginning were unnecessarily high removed this problem.

As to the type of sensor inputs (realistic or "clean" data) for test purposes initially clean data were used because of their greater diagnostic power.

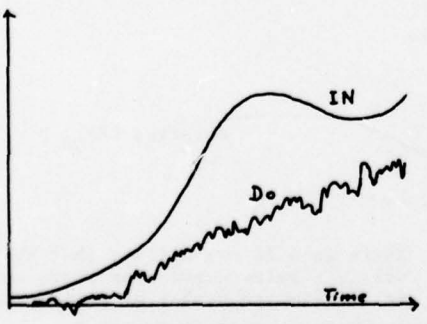

"Pseudo realistic Data"

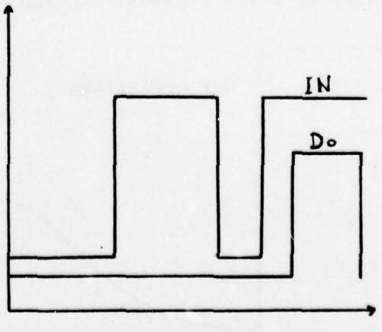

STEP Inputs

OFF LINE ANALYSIS.

Feeding suitably preprocessed flight data together with position and velocity reference data into a ground based computer it is possible to rerun a flight several times with different versions of the Navigation filter in a fraction of real time. The outputs of the high level Language Navigation Filter, corrected INS position and velocity can be checked against an external reference. It is more convenient to do this on a general purpose Computer rather than on the real Main computer because of three reasons:

1) Having done some processing of sensor data it is possible to "rerun" a flight in a couple of minutes rather than hours in realtime

2) Modifications of Program and Constants necessary to obtain the desired performance are done much quicker and safer.

3) Easy access to peripherals-Printer, plotter, tape units or disks

This approach to optimize the filter was almost exclusively concerned with adjusting the Plantnoise, the initial covariance matrix and the Measurement Monitoring. Before a measurement is processed by the Filter it is checked whether it lies within the area enclosed by an X% Ellipsoid made up by system plus measurement uncertainty in the measurement plane. If it lies outside the measurement is disregarded. It is somewhat unsatisfactory that system update versus encountered difference shows such a relation:

We have the feeling that the dotted curve is better but no evidence is available yet

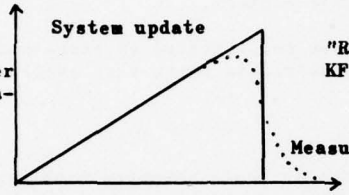

"Reasonableness checks" are strangers in KF theory but indispensable in real life.

A theoretical approach to find a better solution becomes a bit complicated and would be based on vague assumptions. So monitor thresholds were derived empirically. There are two types of measurement monitoring incorporated in the filter:

- The Doppler-IN velocity monitoring is fully computerized using a value much below the 3σ threshold one finds in many applications. If Doppler data have been continuously rejected for a certain time by the Filter a warning is given to the Navigator on a synthetic Display.

- When a Position fix is performed the Filter checks reasonableness on a more generous level. The result of this check is displayed to the Navigator. Fix data are only processed if the Filter and the Navigator agree that results are reasonable. The Navigator cannot override the Filter if it rejects the Fix. This hard limit is against the philosophy that final judgement shall rest with the man not the machine but flight test experience has shown that it is a reasonable mechanization.

The quality of a fix and thus its weight is determined by the computer based on the type of sensors used and ranges involved. Whether the performance of the Filter may be further improved if an additional input from the crew is used to define the quality of a fix will be assessed by recording the crews judgements and correlating these with the actual measurement errors encountered.

Concerning the initial Covariance Matrix and Plantnoise two different methods were tried - an analytic one to find an optimum fit of the Plantnoise and a rather empiric one which consisted basically in looking at results and trying modifications with a limited amount of analytic work. This "magic number" approach has yielded a little quicker and better results throughout. Graphical Presentation of results plays an important role in such an empirical approach. For detailed investigations we found it better to display IN errors and their estimates versus time rather than INS errors and residual errors. If a larger number of flights is evaluated it is convenient to have the net result in the form of a CEP curve for position and velocity versus time together with an indication of their statistical significance.

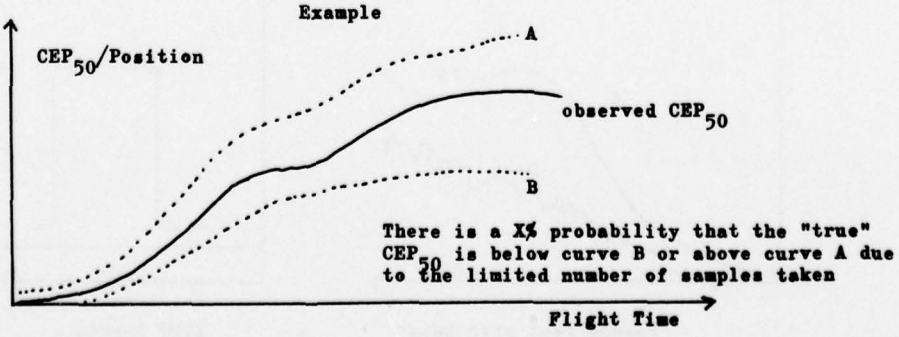

Flights stored on a data bank may be rerun under different conditions, the Doppler may be switched off and Position fixes of different accuracy may be simulated. To prove the benefits of having a Kalmantype Navigation filter and that it is working properly it has to be compared with simpler mechanizations. In our case a suitably smoothed Doppler/IN Mix was investigated with straight Resets of position after a position fix. In the course of optimization the Plantnoise was not only numerically significantly changed from the initial values provided by the suppliers but also the complexity increased.

Plantnoise

Inertial Navigator				Doppler
Level Gyro Drift	Attitude	Velocity	Position	.Scaling .Misalignment
N hour low pass Filter driven by white noise	Only compensation for the not modelled Azimuth Gyro Drift	/	/	.N minutes Low pass Filter driven by white Noise . Nil

STARTING OFF WITH

	Inertial Navigator			Doppler	
	Gyro Drift	Attitude	Velocities	Scale error	Misalignment
White Noise driving low Pass	○			○	○
A+B.Time		○ In the order of gyro drift contribution			
C.Horizontal Acceleration		Provision only			
After Completion of a turn		○	○		

ENDING UP WITH

It seems to be a good idea to make ample allowance for the structure of the plantnoise at the start of all developments involving Kalman filters.

The Maincomputer program was updated with these changes before it became air borne. Since then OFF Line Analysis of Flight data has continued and only minor changes have been incorporated in the Navigation filter in the meantime. It has provided useful information on equipment deficiencies such as a Doppler scaling error the existence of which the supplier was a little reluctant to admit, IN gyrodrifts and misalignments. Correlating the state vector estimates from flights flown with different equipments is a great help in the analysis of weakly or not observable states (such as a Doppler-misalignment and an INS heading output bias).

Three points of mayor importance emerge from the experience gained during the development of this Navigation Filter.

- Tight control of the onboard computer software is a fairly complex and time consuming task, especially with programs written in Assembler.
- The usefulness of data banks derived from flight test data in connection with flexible evaluation programs for the evaluation and optimisation of existing systems and the design of new ones.
- The need for good documentation specially in the case of designing sub-optimal Kalmanfilters which to give their best have to be tuned to the error characteristics of the sensors they are fed with. It may well take up to a decade from the first simulation program to the point where equipments have reached their production standard. Thus it is unlikely that the job is in the same hands throughout the development phase. Advances in technology may even at a much later date result in a significantly different error behaviour of equipments.

Never let yourself get buried by your problems, whether you are haunted by computers and their allied peripherals or strange Greek symbols. Free talk is the best way towards solving them and obtaining a good system.

ANNEX 1

Simplified summary of Kalmanfilters for sampled systems and geometric interpretation.

For many applications it is not necessary to dig too deep into Kalmanfilter theory. It would seem that this simplified summary is sufficient for many cases.

STATE VECTOR AND COVARIANCE PROPAGATION

STATE VECTOR X:

Quantities describing the dynamic of the system. INS position, velocity ... errors X_E denotes an estimate of same

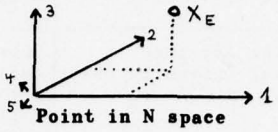

Point in N space

COVARIANCE MATRIX P:

X_E is only an estimate, the error distribution around this point is given by $P: P = \langle (X-X_E)\ (X-X_E)^T \rangle$

$\langle\ \rangle$ = statistical average.

$(X-X_E)^T \cdot P^{-1} (X-X_E) = \text{Const.}$

represents a contour of constant propability density of true value around estimate. Distributions are supposed to be normal compound probability density functions.

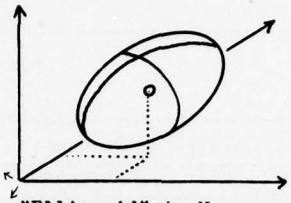
"Ellipsoid" in N space encloses area where true value lies with certain probability

SYSTEM DYNAMIC AND TRANSITION MATRICES A AND ϕ:

The dynamic of the system is basically governed by a differential equation $\dot{x} = A \cdot x$. For small Δt

$$X_{t+\Delta t} = \phi . X_t \text{ with } \phi = E + A\,\Delta t$$

P transforms accordingly

$$P_{t+\Delta t} = \phi . P_t . \phi^T$$

(Note: To drop the Δt^2 term in the expression $(E+A.\,\Delta t).P(E+A\,\Delta t)^T$ is asking for trouble.)

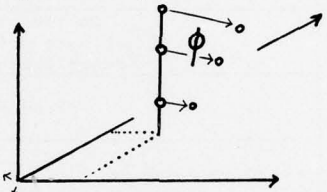

Linear Transformation in N space

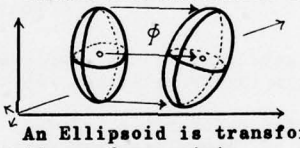

An Ellipsoid is transformed as its surface points

PLANTNOISE MATRIX R:

The dynamic of the state vector is not purely deterministic (Noise sources and simplifications). Thus P increases additionally: $P_{t+\Delta t} = \phi P_t \phi^T + R$.
For many applications R may be a diagonal Matrix.

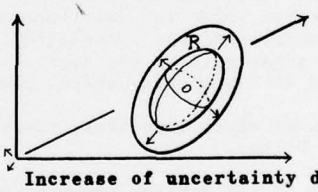

Increase of uncertainty due to noise etc.

The strict application of theory allows only "white" noise, that means no simplifications in ϕ, in other words ϕ describes precisely a linear system which is driven by white noise or for sampled systems by random input sequences. Because of the necessary modelling effort this is rarely found in applications.

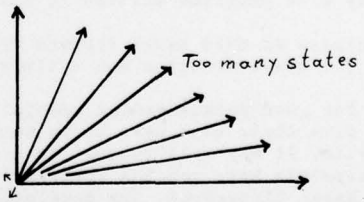

THE MEASUREMENT AND UPDATING PROCESS

MEASUREMENT MATRIX M:

A measurement is taken on the system a prediction of the outcome is a linear combination of state variables.

$$Y_P = M \cdot X$$

The uncertainty of this prediction is given by its covariance Matrix W_P

$$W_P = MPM^T$$

Again deviations from strict linearity may be compensated to some extent by an increased W_P

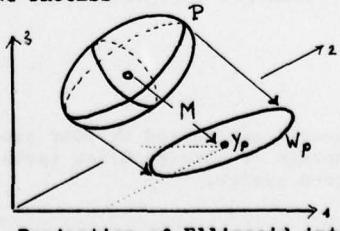

Projection of Ellipsoid into "Measurement Plane" (here 1,2 plane)

MEASUREMENT NOISE W:

The measurement result y has a measurement noise described by its covariance Matrix W

We describe the uncertainty of the measurement due to error sources not included in the state vector. In strict theory completely random disturbances.

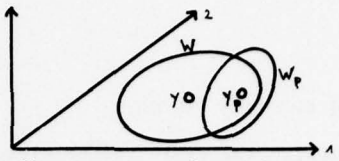

Measurement and prediction with their uncertainty Ellipsoids in Measurement plane

UPDATING OF STATE VECTOR AND COVARIANCE MATRIX:

The difference between prediction and measurement is used to update X

$$X_{E+} = (I-GM)\, X_{E-} + GY$$

for uncorrelated y and yp:

$$P_+ = (I-GM)P_- (I-GM)^T + GWG^T$$

is the corresponding P Matrix

The optimum G Matrix is given by

$$G = P_- M^T (MPM^T+W)^{-1}$$

which results in

$$P_+ = (I-GM)\, P_-$$

The optimum Gain Matrix may be simply derived by differentiating the diagonal of P_+ with respect to the elements of G or a variation principle (Geometrically one is looking for the smallest resulting Ellipsoid).
The full Kalman filter formalism for sampled systems consists of the iterative application of these equations:

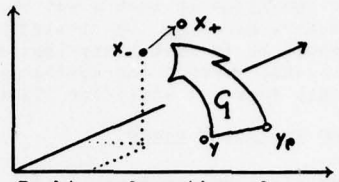

Backtransformation of encountered Discrepancy into State space

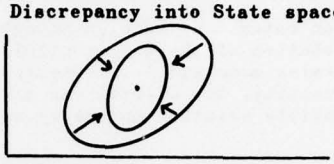

After taking measurement into acoount the new Ellipsoid is smaller. Shrinkage is independant of measurement result

X_{n+1}	=	ϕX_n	Project state estimate into future
P_{n+1}	=	$\phi P_n \phi^T + R$	Project "uncertainty" and add Plantnoise
		If a measurement is to be processed:	
Y_P	=	$M \cdot X$	Predict outcome of measurement
ϵ	=	$Y - Y_P$	Difference measurement - Prediction
S	=	MPM^T+W	Uncertainty of same
G	=	$PM^T \cdot S^{-1}$	Gainmatrix
X_+	=	$X_- + G \cdot \epsilon$	Updating of state
P_+	=	$(I-GM) \cdot P_-$	Updating of "Uncertainty"

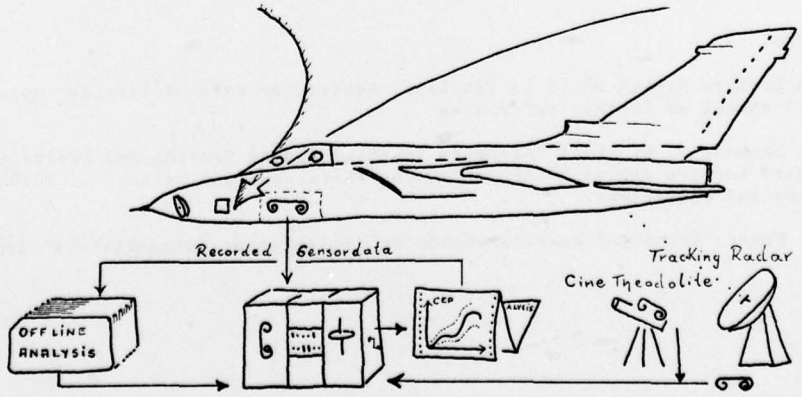

ANNEX 2

NUMERIC ACCURACY

1. ARRANGEMENT OF STATE VECTOR.

Analytically the state vector elements may be arranged in any order, however, when incorporating the equations in a computer say in the matrix formulation $X_{t+\Delta t} = (E + A \cdot \Delta t) \cdot X_t$ it does matter. Specially in an explicit formulation for the propagation of X and P (where first all rows of P are treated as a state vector and then all colums - Ref 3) it is a good idea to arrange the equations in such a way that the increments to be summed are in the "most likely" ascending order. Hence in the straight forward Matrix formulation arrangement of state vector elements should be in such a way that the contribution from the $\emptyset$ elements to X or P decreases from the diagonal towards the bottom lefthand corner when using a standard matrix multiply. Obviously this does not apply for fixpoint number representations.

2. SELECTION OF ITERATION RATES.

Two opposing requirements have to be balanced:

Iteration rates must be high enough to ensure that with the state vector propagation a sensible solution of the differential equation $\dot{x} = Ax$ is achieved, on the other hand high iteration rates mean small increments which if too small are completely lost when added to a larger quantity. The effects can easily be worked out for a given word lenght. If problems arise a possible solution may be to split the propagation into two parts with different iteration rates.

Influence of user requirements on iteration rates:

Taking todays available literature velocity correction terms for INS/Doppler systems are in the order of 1 - 4 ft/sec, iterationrates for such filters range from 10 - 60 sec's. In the standard formulation this will cause jumps in position correction terms from 10 - 240 ft. With a tight control used in automatic steering this can cause a considerable nuisance. One remedy is to use higher iteration rates for velocity to position integration within or external to the filter.

3. FORMULATION OF THE P MATRIX UPDATING EQUATION.

Purists in the field of numeric accuracy recommend the use of

$$P_+ = (I-GM)\, P_- \,(I-GM)^T + GWG^T \text{ instead of}$$

$$P_+ = (I-GM)\, P_-$$

because it is less prone to numeric difficulties. It seems to be the best approach to check numeric accuracy first with the senond simpler formulation in a simulation program performing the matrix operations with the envisaged word length. If problems arise here it is most likely that there are problems in other areas too and the more complicated formulation may not completely cure it.

ACKNOWLEDGMENTS.

Apart from many engineers and programmers involved with the design programming ground- and flight testing of the integrated Navigation system within the PANAVIA frame work valuable support was received from the Royal Aircraft-Establishment Farnborough, Hamshire, England.

REFERENCES.

1. Agard Lecture Series N^{o} 82 on Practical Aspects of Kalmanfiltering implementation containing a vast amount of further references

2. R. F. Stokes, S. G. Smith "Aircraft Inertial System Testing and Evaluation in the UK" in Agard Lecture series N^{o} 60 on Testing Philosophy and Methods of Guidance and Control Systems and Subsystems

3. J. C. Waner "Practical considerations in implementing Kalmanfilters" contained in Ref. 1

NAVIGATION, GUIDANCE AND CONTROL FOR HIGH PERFORMANCE MILITARY AIRCRAFT

BY: W.H. McKINLAY
FERRANTI LIMITED
SILVERKNOWES
EDINBURGH
EH4 4AD
SCOTLAND
UNITED KINGDOM

SUMMARY

The paper discusses some of the factors involved in applying advanced navigation to an aircraft operating at low altitude for reconnaissance or to locate and attack ground targets. It considers the distinctions between navigation accuracy and the accuracy with which a pilot can follow a given flight profile. There are references to target acquisition and the need to pre-plan the profile. Recent Ferranti developments in the display of navigation information coupled with a level of automatic pre-planning are discussed.

1. INTRODUCTION

The aim of this paper is to discuss some of the factors involved in applying advances in navigation to the guidance and control of high performance military aircraft. The aircraft concerned is considered to be operating at a relatively low altitude, either for the purposes of reconnaissance or to locate and attack ground targets.

The majority of the equipments and systems developed by Ferranti Limited are concerned with this type of mission. System complexity is to be avoided in this type of aircraft because of limitations of cost and weight and the need for maximum reliability. In addition, if the aircraft is single-seat, the question of pilot workload becomes important and it is pointless to spend money on introducing a navigation performance or navigation functions which the pilot cannot use effectively in real life conditions. At the same time, it is desirable to extract the maximum possible operational benefits from improved navigation, so the theme of the paper is system optimisation.

Clearly, an additional dimension is introduced into the problem if it is assumed that an aircraft of this type will ultimately operate in conditions of relatively low visibility or at night, or against targets which are not easily acquired visually. In these cases, the navigation system has to contribute to the acquisition process in conjunction with any vision aids provided.

The approach adopted is to review possible advances in navigation briefly, to consider their operational implications and to develop some suggestions as to the improvements required in the overall guidance and control system.

The need to optimise navigation systems has been appreciated for many years and the central prob was well expressed in a paper presented to the Institute of Navigation in 1952 by Sqn. Ldr. D. Bower. He suggested that "It is not sufficient to measure the value of a particular navigation system in purely navigational terms: the yardstick used must be the relative contribution which it makes to the overall effectiveness of the air weapon. By effectiveness, we mean not only precision but other desirable qualities such as flexibility, mobility, security, availability and ability to cooperate with other forces, air and surface. The effect of the navigation system upon the other components of the weapon must also be considered at all levels, from that of the air user down through the servicing and maintenance echelons and back to the production line." (Reference 1).

2. POSSIBLE ADVANCES IN NAVIGATION

The essentials of any navigation system can be expressed as a basic navigation control loop, shown in Figure 1. Much of the history of the development of navigation systems has been concerned with their optimisation with the availability of improved technology. The figure is in fact identical with one published in 1960 (Reference 2).

The most important improvements have taken place in the basic sensors. In the 1950's and 1960's, these were of an accuracy such that precision navigation normally had to be derived from a combination of sensors. Also because computing was then relatively primitive, many of the system concepts involved the human navigator in exercising his judgement as to the weighting to be applied to the outputs of various sensors: an extension of the earlier art of the practical navigator. In the mission forming the subject of this paper, the inertial sensor is preferable on the grounds of compactness, security and independence of ground aids. It is now customary to consider a performance of 1 nautical mile/hour CEP as being normal for an inertial system and so further developments in this field are either towards higher accuracy, lower cost or both.

Technologically, systems are no longer computer limited: the cost and weight of processors and stores have decreased so rapidly that they can be employed in any way desirable to optimise the system.

If the basic sensing of position and computing are no longer limited technologically, the emphasis must therefore shift to the two other key areas in the diagram, the method of programming the system with the flight plan, the pilot's intentions and any operational constraints and the means of coupling the resulting guidance to the aircraft controls.

There are two possibilities for increasing the accuracy obtainable from the sensors to a level at which it is no longer a dominant system problem. The first is to improve the accuracy of inertial navigation, and a paper by my colleagues, Messrs. K.R. Brown and R.A.R. Tait presented earlier in this Symposium has already pointed out the possibility of interesting developments in this field (Reference 3). From their work, it appears that it is not unreasonable to expect that inertial navigators can deliver accuracies of the order of 100 metres or better in missions of this type, in which the initial flight to a target may be between 30 minutes and 1 hour.

Secondly, the proposed Global Positioning system will, if successful, provide world-wide navigation with a potential accuracy of between 10 and 100 metres depending on the sophistication of the equipment and the means of implementing it in the system.

It therefore seems that advances in navigation should be considered in terms of accuracies ranging between 10 and 100 metres. The question is therefore how to employ such accuracies and how to modify or develop total guidance and control systems to do so.

3. OPERATIONAL IMPLICATIONS

3.1 General

It has already been pointed out that the significant areas to consider in the presence of high accuracy position data are the means of programming the system with a desired flight profile and the intentions of the pilot and the method of closing the loop through the aircraft controls. These can be considered separately for the following phases of flight:

En-route navigation.

Target acquisition.

Return to base including approach and landing.

3.2 En-Route Navigation

Although the purpose of a mission involved in attacking a target is to achieve maximum navigation accuracy as the latter is approached, there are many reasons for considering the accuracy with which a flight profile can be planned and followed in the preceding en-route phase. They include:

The need to follow a profile accurately to avoid prohibited areas and enemy defences.

The advantages of being able to do so in space, and possibly time, to facilitate the integration and control of missions carried out by large numbers of aircraft operating in the same air space.

Safety, including the need to plan the route to avoid obstructions which would be hazardous to low level flight and to enable the pilot to know precisely whether he can maintain that altitude or whether he should climb in the event of encountering low visibility. In this sense, accurate navigation is a means of terrain avoidance although ultimate protection is only achievable by direct sensing such as with a Terrain Following Radar.

It may also be desirable to plan a relatively elaborate route involving changes of track at short intervals to take advantage of the terrain or to carry out a search for suitable targets, for example, by following a road system. All these factors indicate that the system should be capable of accepting a relatively complex flight plan if desired, and methods of achieving this are discussed later.

However, it is important to establish the precision with which a pilot can follow a given flight profile, accepting the fact that the navigation sensors can provide the position data and that the necessary computing is available. To investigate these possibilities, it was assumed that the pilot would fly the aircraft visually using director signals on a Head Up Display with a relatively simple control laws similar to those in use in present systems. The following facts emerged from this investigation:

Subjective pilot opinion is that following a track within 100 metres calls for considerable concentration, and that in practice, the aircraft will tend to drift up to 400 metres off track. The precise deviations depend on a number of factors including turbulence, which increases the pilot workload needed to fly the aircraft safely at a lower altitude, and thus tends to saturate him. Time is also important: pilots are capable of high concentration over periods of approximately two minutes but are forced to relax more in a flight sector lasting 30 minutes or above.

To provide an approximate theoretical background to these assumptions, some approximate calculations were made assuming a commonly used guidance law, which is that the system develops a heading which aims the aircraft for a point on the desired track 14 miles ahead. Figure 2 shows three cases involving the use of such a control law.

Case 1, where the aircraft is virtually on track. Here, a 450 metre cross-track deviation develops a change in heading demand of 1 degree.

Case 2, in which the aircraft is regaining its track after a deliberate diversion for example, to avoid defences. This control law is particularly effective as a means of causing the aircraft to subside on to the desired track within a reasonably short time.

Case 3, in which the aircraft is approaching a destination or point of target acquisition at which maximum accuracy is desired. Once the aircraft has come within 14 nautical miles of the point, the guidance signals cause it to home, and the cross-track errors due to a 1^{o} heading error diminish steadily until the point is overflown.

It is also useful to consider the behaviour of the system when executing a sharp turn, say, 90^{o} over a waypoint. This is shown in Figure 3. At the speed postulated, a $\frac{1}{2}$g turn has a radius of 4.4 kilometres. If the turn is executed as a tangential transition from one leg to the other, the aircraft turns 1.8kms short of the waypoint, which represents a considerable deviation from the planned track unless account is taken of the turn at the planning stage. It would be possible to allow the pilot tactical freedom to delay the turn and minimise the excursion from the waypoint by an overshoot as shown, but it seems better to include the turning radius in the planning of the profile.

Figure 4 shows the effect of permitting errors of 1^{o} to persist for 1 minute. A 1^{o} heading error then produces a 231 metre cross-track error. A 1^{o} bank error held for 1 minute produces a 2.6^{o} heading error and a cross-track error approaching 600 metres. In 1 minute, the aircraft travels 13kms.

These figures given an approximate idea of the pilot workload involved in accurate path holding. If, due to other distractions involved in flying head-up, the sampling rate of navigation data is as low as 1 minute errors of up to 400 metres appear highly probable, while if additional concentration produces corrections every 15 seconds, and if it is possible to control the aircraft to relatively fine limits, a 100 metre tracking accuracy seems feasible. Anything less than this, particularly to exploit navigation aids giving positional data of the order of 10 metres accuracy, seems to indicate the need to go to automatic flight control if accurate sustained path holding is required.

3.3 Updating from Visual Features

It is sometimes suggested that the time-dependent errors of an inertial system can reasonably be removed by updating over known visual features, possibly pre-planned. The following conclusions have been reached about the validity of this approach.

Flying at about 60 metres, a pilot could be expected to cross a known point within 20 metres laterally, particularly if the drift angle is small, (it would take a 60 knot cross-wind component to give 7^{o} drift in the present case). But with the aircraft travelling at 220 metres/second, pilot judgement of the moment of crossing the feature to 1/5 of a second would still give an error of about 50 metres.

Therefore, clearly any updating must be carried out using the Head Up Display and either a range sensor or a radio altimeter, particularly where the terrain is flat. With such methods, an updating accuracy of 10 to 20 metres should be achievable.

3.4 Target Acquisition

The ability to acquire a target visually depends on a number of factors including altitude above ground, the nature of the terrain including screening and the size and nature of the target. If the target is approached after a precise local fix against a known ground feature, to the limits of 10 to 20 metres implied above and if the ensuing run to the target is minimised to 2 minutes or less, a 1 nautical mile/hour inertial system will have accumulated a total error of 60 to 100 metres by the time visual acquisition is desired and a precisely located target will be displaced by an angle of about 3^{o} from its predicted position at a range of 1.5 kms. This places it well within the field of the HUD although it has been pointed out that a compelling indication on the display as to where to find the target may be misleading if it is significantly an error. It is therefore clear that the availability of much more accurate position data of the order of 10 metres will always greatly enhance the chances of successful target acquisition. But if a system is to use precise knowledge of the coordinates of both aircraft and target location to throw up angular data on the HUD or pointer range sensor, the question of angular accuracy arises. At a range of 2 kms, an error of 10 metres corresponds to an angle of 5 milli-radians This gives an indication of the accuracy required of the combination of the heading reference and the harmonisation arrangements within the airframe to exploit this class of navigation accuracy, and indicates that a system such as GPS will always have to be associated with a heading reference of inertial quality. Figure 5 illustrates this.

Against a precisely located target, 10 metres would virtually eliminate the need for visual acquisition, and concentrated manual track holding for short periods to these levels appears possible. Assuming a run of 2 minutes or less from an extremely precise fix, an inertial system with an error growth corresponding to .25nm/hour or better would produce this order of accuracy, while GPS would produce it in absolute terms while delivering its optimum performance.

3.5 Pre-Planning

It is of course pointless to strive for accuracies which cannot be planned into the navigation system in terms of the precise definition of a feature to be used for fixing or a target. If a 1:50,000

map were used to plan precise navigation, a 1mm error deriving coordinates from the map would represent 50 metres on the ground. Opinion varies as to how precisely positional information can be derived from extremely large scale maps because a great many factors have to be considered including the surveying accuracy, varying in different regions, map stretch, operator skill etc. It is probable that some very well defined features could be known in position to within 10 or 20 metres but apart from saying that special care, techniques and precautions are clearly necessary, the precise way in which ground coordinates can be derived for planning purposes is outside the scope of this paper. It is, however, clear that whatever methods are developed are likely to introduce a time factor which will vary depending on circumstances and accuracies.

4. REQUIREMENTS FOR GUIDANCE AND CONTROL SYSTEM IMPROVEMENTS

As pointed out earlier, the main aim must be to achieve a balanced system in which the accuracy of the available positional data can be used effectively throughout the mission from the planning stage through en-route navigation to target acquisition. Navigation accuracies of between 10 and 100 metres are also compatible with relatively precise let down procedures and runway approaches in conditions of, say, 300 feet cloud base and 2 miles visibility. Therefore, there is a possible interaction between navigation, guidance and approach/landing.

The system should be optimised for the mission and the figures quoted above indicate that path holding en-route to the order of 100 metres is probably achievable although with some concentration. Over short periods, pilots concentrating and using a Head Up Display can be expected to exploit navigation accuracies down to 10 to 20 metres, particularly if the display has characteristics similar to those used for weapon delivery, in which their ability to fly to such limits has already been proved.

If more accurate path holding is required for long periods to better than 100 metres, and certainly to the limits of 10 to 20 metres achievable with future systems recourse to automatic flight control seems inevitable, with the consequent need for system redundancy if the facility is to be used at low altitudes.

Present navigation systems commonly use keyboards and similar devices to enable the crew to programme the system with the desired flight path. These have the disadvantages that their use in programming elaborate profiles is certainly time-consuming and that they are not entirely invulnerable to human error. They are relatively difficult to use in the air, particularly under conditions of high workload. Therefore, further development of the man-machine interface is essential to exploit increased navigation accuracy and computing power.

In missions in which pilots fly accurate profiles related to the terrain, their planning is likely to take account of major terrain features and some form of situation display is required for reference in the air. The moving map display, based on present or improved topographical maps, is the most attractive solution although in future, its function may well change from monitoring the accuracy achieved by the navigation system to monitoring the achievement of the desired profile and advising the pilot generally of the programmed intentions of the navigation system. It will also be useful where tactical decisions involving route changes have to be taken in flight. The main deficiency of simple moving map displays which has to be overcome is the inability to mark up the map on a flexible basis, since bulk storage media such as film cannot be used in this way. The shift to more emphasis on monitoring tactics and path holding will be reinforced if future systems have higher integrity, which would apply to dissimilar redundancy achieved by an IN/GPS hybrid or similar solution.

5. EXAMPLES OF RECENT FERRANTI WORK IN THIS FIELD

An earlier paper, Reference 3, has given the results of experimental work which indicates that the inertial instruments in service in equipment produced by Ferranti Limited have an extremely high intrinsic performance which has not yet been fully exploited. It is implied that more sophisticated alignment techniques, and particularly the use of more sustained ground running of the equipment can exploit this basic accuracy more fully. While ground running is not operationally attractive there are clearly engineering solutions which would permit it with minimum operational inconvenience.

The need to pre-plan flights to fine limits has already been referred to and subject to the positional accuracy of the available data on ground features for targets, it is clear that modern data processing techniques can develop flight plans of any required degree of sophistication and accuracy. The time taken to develop them and insert them into the aircraft computer is purely a function of the operational techniques and technologies used: many methods of reliable bulk storage are becoming available.

It is however necessary to consider how more sophisticated flight planning for missions which could benefit from it could be converted into displays easily assimilated by the pilot, who normally finds it inconvenient to refer to marked up paper maps in the cockpit except in emergencies. The Combined Display, shown in Figure 6, introduces this flexibility as well as overcoming the limitations of map marking. A projected moving map based on 35mm film is combined optically with an electronic display so that electronic symbology can be superimposed on the map. The only limitations concern the need to avoid cluttering the display unnecessarily and the availability of the information in storage acceptable to the computer. The symbol generation techniques are already available and such displays can exploit any technique of sufficient capability and resolution. Therefore, there are now flexible possibilities to display the desired flight path together with areas which should be avoided and other numerical navigation data such as mission timing, fuel availability etc. The display provides the pilot with a visual confirmation of his flight plan in the manner to which he is accustomed: relating it to a topographical map. In addition, such a display exploits two types of storage: 35mm film and digital bulk storage. This is a very powerful tool for system optimisation because fixed data is stored extremely economically on film while data which must be more flexible is more easily handled digitally. Indeed, the film storage can be used for check lists, let down charts and other information not normally associated with map displays while the electronic element can of course accept outputs from sensors producing raster information, including scan-converted radar or television. The map or the electronic component of the display can be used collectively or separately so that apart from its navigation uses the display can be integrated into an overall multi-

function display concept concerned with navigation, guidance, control and aircraft management.

Pre-planning a flight profile is an important part of the operation and represents part of the pilot workload. The normal procedure is to determine the route from a knowledge of the task, the terrain and the opposition likely to be encountered and to select turning points using a standard paper topographical map. This introduces a considerable task consisting of measuring tracks and distances, taking off the coordinates of turning points etc. The Ferranti Autoplan system is designed to streamline this process and provide the following operational facilities and advantages.

The topographical map is placed on a board and as the tracks and turning points are selected the positions of the latter are digitised automatically by the use of a simple cursor.

A mini-computer digests the information and prints out a flight plan including times, tracks, distances, fuel requirements etc.

The same computer can be used to load a digital storage medium through which the flight plan can be transferred to the airborne computer, thus programming it.

The information thus inserted into the airborne computer can be used to reconstruct the tracks and turning points as an electronic overlay on a full colour topographical map, using the Combined Display.

A total operational and system concept has thus been developed to cover all stages of flight planning, programming the guidance system and displaying the information to the pilot. Alternative flight profiles can of course be canned and retrieved in flight as necessary. The speed and convenience of the process makes it possible to programme relatively elaborate profiles with minimum pilot workload.

6. CONCLUSIONS

The present state of the art is that the accuracy of an inertial navigation system at the end of a 30 minute flight period is generally taken as about 700 metres where no discreet or continuous updating has taken place. Flying an aircraft manually at low level through a Head Up Display en-route track keeping over reasonably long periods is probably achievable within 400 metres of the computed indications, which is reasonably consistent with the navigation accuracy. The accuracy of path holding increases as a defined waypoint is approached and converges on the basic positional accuracy.

Updating these present generation systems visually is probably subject to errors of 50 metres or more when flying at 60 metres altitude and relying on pure visual observation, but updating through a Head Up Display using ground stabilisation through the INS should be able to reduce this figure to 10 to 20 metres. The paper has referred to the difficulties of locating ground features precisely in absolute coordinates.

It has been suggested that the effectiveness of this type of operation, and particularly target acquisition, would be enhanced if a basic positional accuracy of at least 100 metres were achievable over durations of about 30 minutes, which is consistent with either improved inertial navigation or GPS in its least accurate mode of operation.

The paper has also considered systems such as IN/GPS hybrids having most accurate mode of operation, giving positional data of the order of 10 metres. It is concluded that in en-route navigation, this accuracy would not be fully useable in terms of path holding unless automatic flight control was provided, but clearly turning points could be acquired extremely rapidly and because pilots can fly much more accurately for short periods of the order of minutes, problems concerned with visual target acquisition would be reduced or even eliminated.

It has been suggested that to exploit navigation accuracies of 100 metres or less, particularly if continuous path holding is desired, greater account must be taken of accurate pre-planning of the flight profile, which seems feasible using data processing subject to the accuracies of maps themselves. There is, however, a need to provide the pilot with a display against which to monitor path holding and to act as a reminder of the profile originally planned and any other relevant navigation data. It has been suggested that the Combined Display is the best solution, since it exploits the merits of both the Projected Map Display and using the full colour topographical maps and the flexibility of a full electronic display. It is relatively easily integrated into a multi-function display cockpit.

Accurate, fully automatic navigation systems will be less dominated by sensor or computer limitations than in the past, and in some applications, either similar redundancy using two inertial platforms or dissimilar redundancy provided by IN/GPS will also increase system integrity, which will change the pilot's task more towards monitoring his progress than monitoring the accuracy of the system.

In general, it has been suggested that future systems involving advances in navigation will be less limited by technology than by the ability to engineer them so that the pilot can exploit the available accuracy fully, particularly in order to gain tactical advantages, depending on the type of mission. It should also be possible to reduce the crew workload associated with navigation itself, and except in specialist applications, some of the more sophisticated features at present included in two-crew aircraft may prove unnecessary, making it easier to provide high quality navigation in single-seat aircraft. The man-machine interface is certainly the critical area for consideration in future systems which are not technology limited.

The Author acknowledges the permission of the Management of Ferranti Limited to present this paper and the assistance of his many colleagues who have assisted in its preparation. The general views expressed in it are his own.

7. REFERENCES

Reference 1	BOWER D.	The Selection of Navigation Systems for Military Aircraft. The Journal of the Institute of Navigation : April 1952.
Reference 2	McKINLAY W.H.	The Information to be Displayed by an Automatic System in the Air. The Journal of the Institute of Navigation : January 1960.
Reference 3	BROWN K.R. and TAIT R.A.R.	Recent Advances in High Resolution Inertial Navigation. This Symposium.

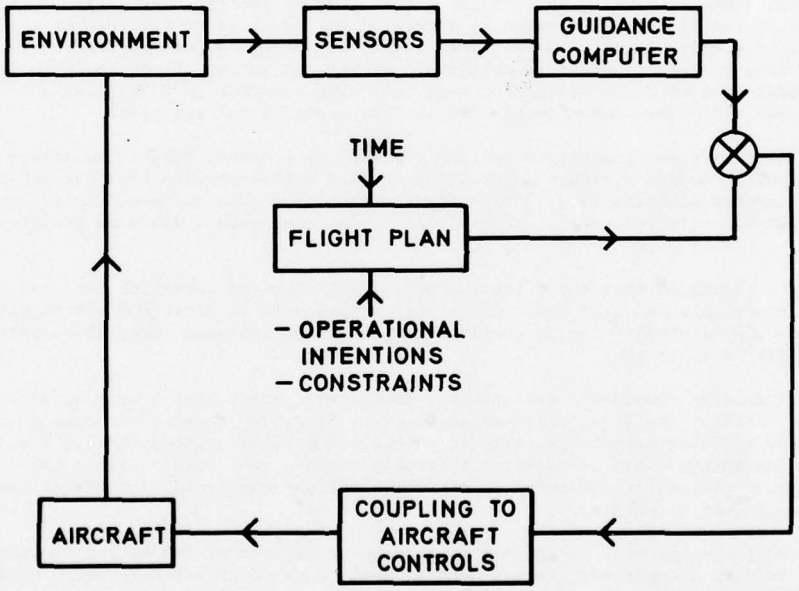

BASIC NAVIGATION CONTROL LOOP

Figure 1

CASE 1 — PATH KEEPING

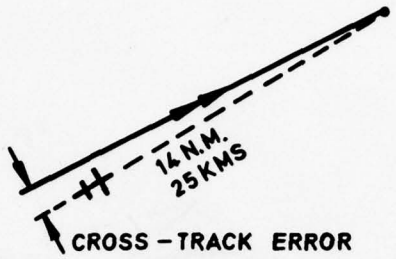

CASE 2 — REGAINING TRACK

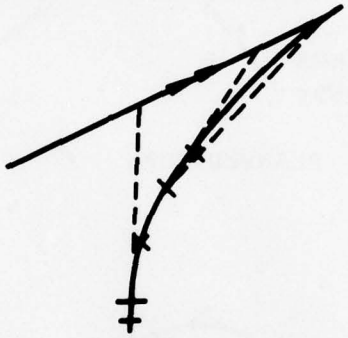

CASE 3 — APPROACHING DESTINATION

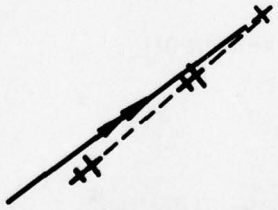

GUIDANCE RELATED TO CONVERGING ON A POINT ON THE DESIRED TRACK

Figure 2

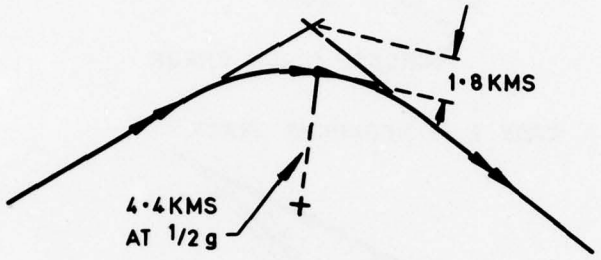

PLANNED TURN

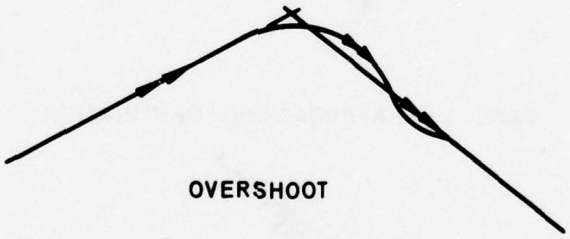

OVERSHOOT

EFFECT OF TURNING CIRCLE

Figure 3

AT 425 KTS (790 KPH/ 220 M/SEC)

IN ONE MINUTE :

1 DEG. HEADING PRODUCES:
231 M CROSS TRACK ERROR.

1 DEG. BANK PRODUCES:
2·6° HEADING ERROR
600 M CROSS TRACK ERROR

AIRCRAFT TRAVELS 13 KMS

USING 14 MILE AHEAD GUIDANCE EQUATION:

1 DEG. HEADING $\propto$:
450 M CROSS TRACK

$^1/_2$ g TURNING CIRCLE IS 4·4 KMS RADIUS

SOME GUIDANCE PARAMETERS

Figure 4

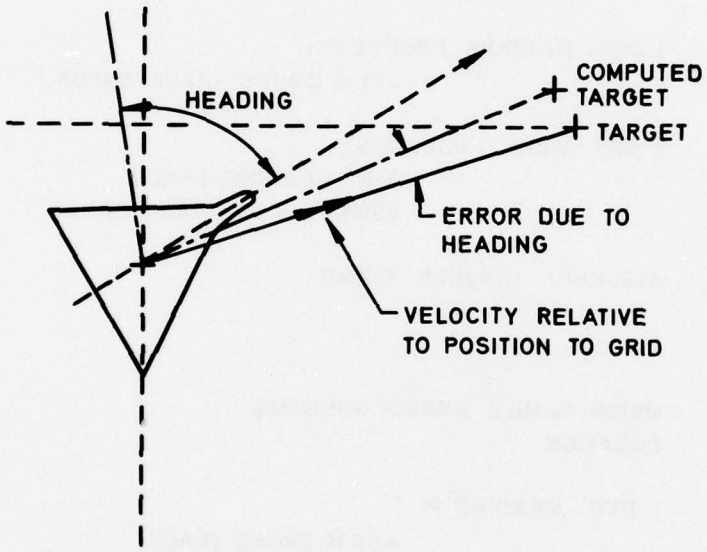

ANGULAR INFORMATION
IN TARGET ACQUISITION

Figure 5

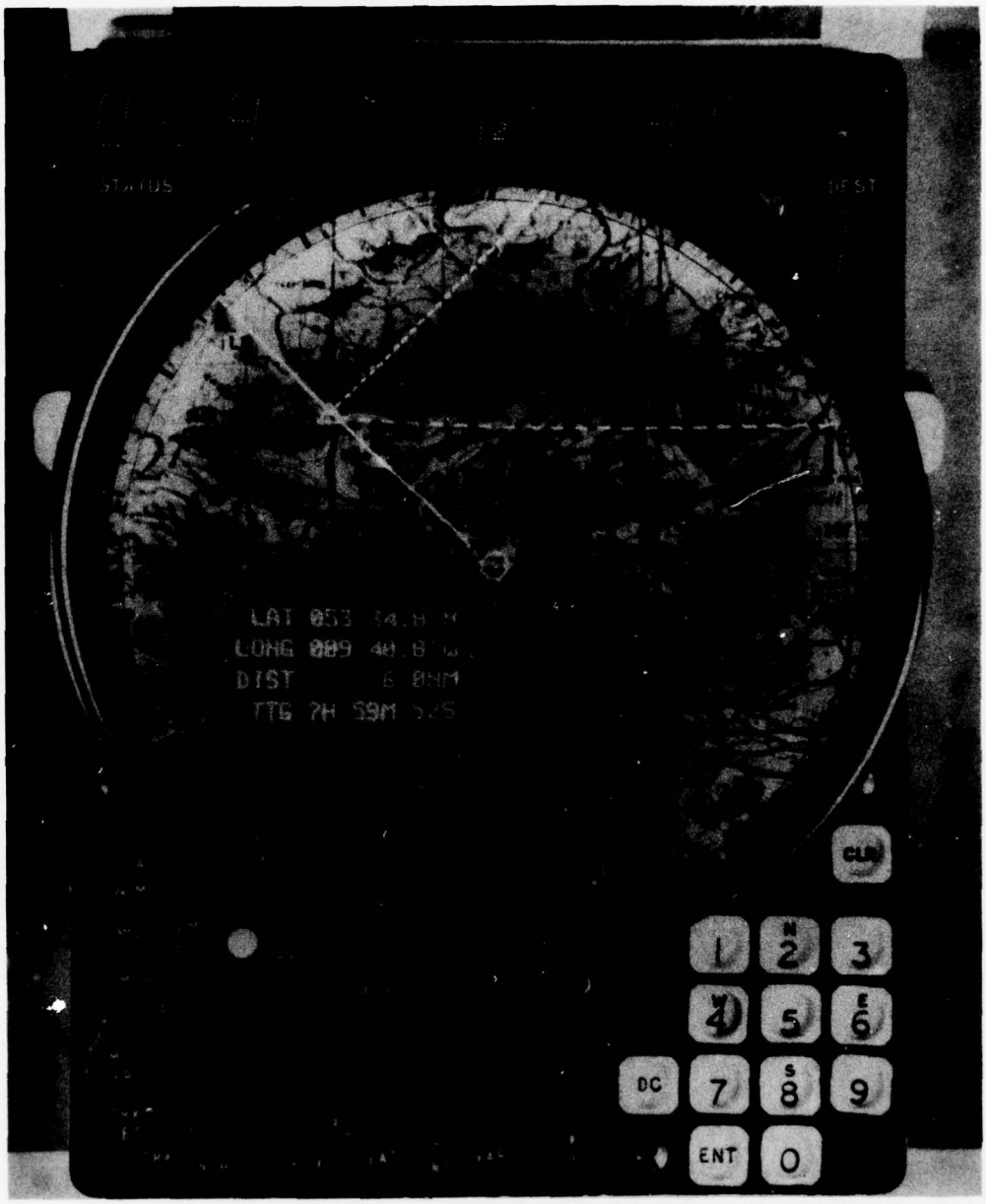

Figure 6

Combined Map and Electronic Display (COMED)

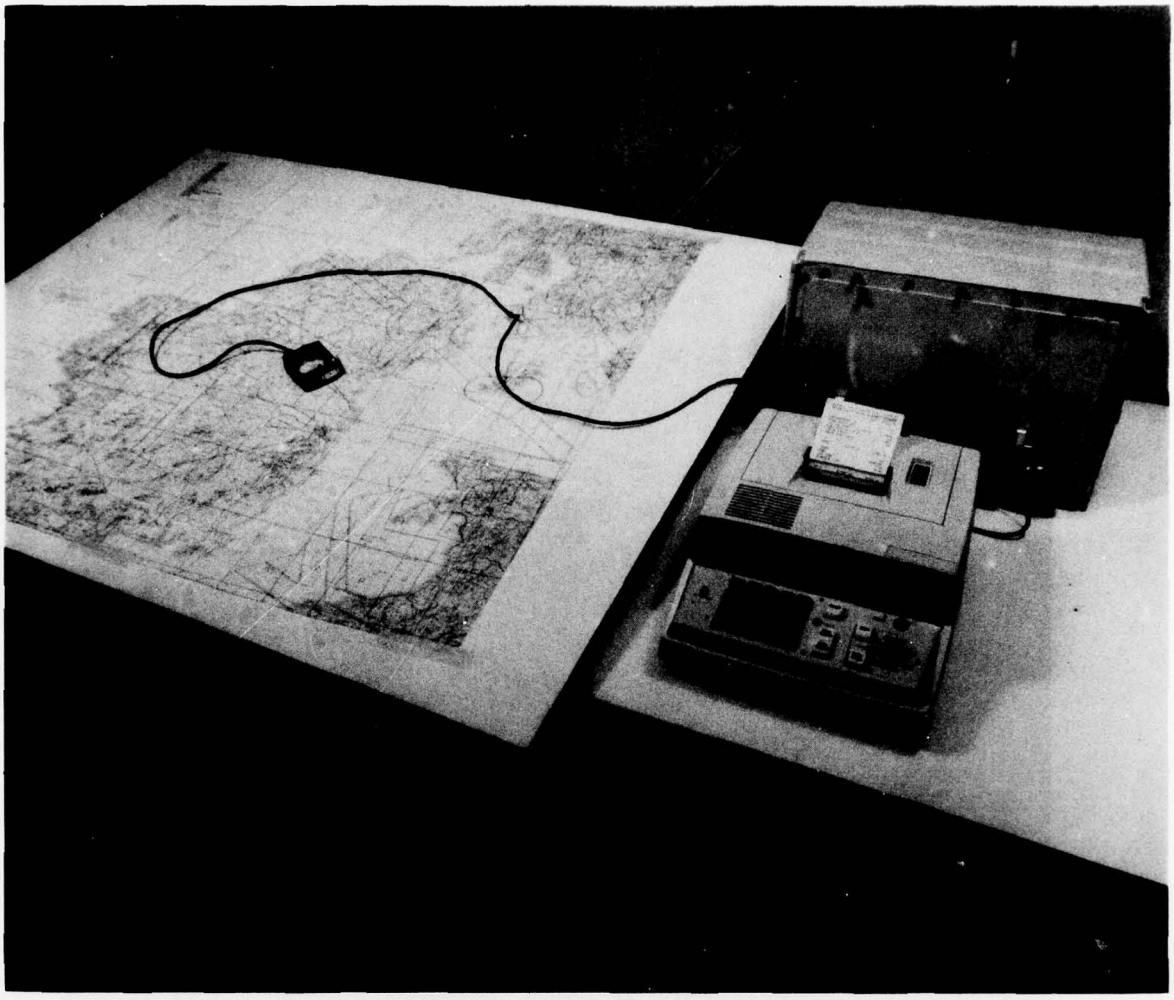

Figure 7
Autoplan Briefing Aid

AREA NAVIGATION SYSTEMS AND PROCEDURES

Donald W. Richardson and James S. Tyler
Systems Control, Inc. (Vt)
1665 Palm Beach Lakes Blvd.
West Palm Beach, Florida 33401

SUMMARY

This paper is presented as an attempt to identify, in pragmatic user-related terms, the operational significance of the overall concept of area navigation (RNAV). Its purpose is to explore, over a range of users and missions, the spectrum of functions and capabilities that this generic navigation technique offers. Starting with a summary of the correlation between current navigation systems both civilian and military and the concept of area navigation, the main content of the paper deals with two major issues, the current status of RNAV research, and future applications of RNAV. The current status is reviewed in the light of the results of extensive operational and cost benefit studies. Two illustrative examples of RNAV operational applications are discussed, namely the use of RNAV to facilitate complex noise abatement profiles, and the application of RNAV techniques to improve the efficiency of airborne search and rescue operations.

INTRODUCTION

The operational navigation concept known as area navigation (RNAV) has been sometimes described as being "all things to all people". However, this subject is frequently construed to more narrowly refer to the navigation of commercial airline aircraft with reference to VOR/DME ground facilities. In actuality RNAV encompasses a broad spectrum of applications, both civilian and military, both past and future. From a categorical point of view, the concept of area navigation, freely translated, merely means the freeing up of all of the available volume of airspace. In this regard, RNAV should be considered as a generic form of navigation, certainly not in any way limited only to the use of VOR/DME as a sensor input.

Most of us today are quite familiar with the historical applications of systems which fall into the generic category of RNAV. In the United States, as an example, the classical definition of airborne RNAV systems are those which permit flight over predetermined tracks within prescribed accuracy tolerances without the need to overfly ground based VOR/DME (VORTAC) navigation facilities (U.S. FAA Advisory Circular 90-45A, "Approval of Area Navigation Systems for Use in the U.S. National Airspace System"). Military aviation users and operators will find, within these words, many current avionics systems which equally fit this description.

Certainly the self-contained inertial navigators we have heard about during this meeting uniquely fit that category by their own specialized design criteria. Inertial navigators are designed to allow operation essentially anywhere in the world, in any direction, between any points, subject only to the specifics of the navigator design and the input of the operator, be he a missile programmer or a pilot in the cockpit. Similarly a variety of ground based electronic aids have been applied to the concept called area navigation. One recent application is that of the tactical utilization of the Loran navigation system for weapons delivery, which according to the specific techniques of system application and programming provide the capability to navigate anywhere within the coverage area, but not constrained to unique tracks, as is the case with conventional VOR navigation. A currently emerging concept is that of using VLF or Omega signals, properly input into an airborne navigator, for the purpose of providing not only continuous position determination but also precise track-keeping capability. The expanding availability of the Loran-C chain makes more and more areas in some portions of the world candidates for the application of this concept for total utilization of the available airspace. Looking to the future, the program under development in the United States called NAVSTAR or Global Positioning System possesses the potential for world-wide navigation, again by a variety of users both civilian and military.

In the military, area navigation system applications and concepts have been utilized both from a tactical and a strategic point of view. Without going into the details, I think it is worthy to mention that there have been many such applications, one example being the airborne computer/map display system installed in the Convair F-106A interceptor aircraft, where the Tacan navigation inputs were utilized to provide area navigation capability on the return-to-base missions. In this case the aircraft utilized the airborne computer and the Tacan sensor to navigate between a series of predetermined geographical waypoints, both laterally and vertically. Actually the aircraft was capable of generating and flying a totally automatic three-dimensional profile in a long range navigation mode, and indeed has performed transcontinental United States area navigation missions essentially hands-off from lift-off until landing flare.

Certainly both Loran and inertial navigators have been utilized to striking advantage from a tactical point of view in navigating military aircraft to specific ground targets. Similarly for both military transport and agressive configured aircraft, essentially area navigation concepts have been used to ferry these airplanes and perform long range redeployment missions.

It is in the civilian market place however, that area navigation as such has become perhaps a little more innovative, fine tuned, more broadly applied. It is only during the last four or five years of the preceding twenty-five to thirty years of area navigation system development that has seen the needs and the capabilities converge as far as area nav is concerned. Increasing air traffic densities in certain parts of the world and increasing shortages and costs of fuel in all parts of the world have combined to make the benefits afforded by area navigation something that is economically attractive and functionally desirable.

From a practical viewpoint, both technically and operationally we can look to the future and respon-

sibly say that our air navigation world is destined to convert over to a system centered around area navigation systems and concepts. One specific indication of that is the Policy Statement issued by Dr. John McLucas, Administrator of the U.S. Federal Aviation Administration (FAA) on January 7, 1977[1]. This document committed the United States to a combined short term and long term program of the implementation of the area navigation concept as an integral element of the U.S. National Airspace System. Within the United states, plans are currently underway to establish specific dates for various milestones such as the establishment of a master terminal and enroute RNAV route structure and the definition of RNAV avionics standards for certification. Indeed, these two issues are the key elements to the successful integration of RNAV into any ATC system, either civilian or military, as well as the realization of those operational and economic benefits postulated for this concept.

In a broader sense, it is axiomatic that similar planning must be initiated as soon as possible on an international level, in order to effectively integrate our rapidly proliferating set of navigation sensors into the common denominator of RNAV. It is the purpose of this paper to review some of the implications of RNAV implementation and to highlight some of the problems and benefits attendant to that implementation.

CURRENT STATUS

For the past five years the FAA has sponsored, through both in-house efforts and outside contractor support, a comprehensive research and development effort aimed at establishing and quantifying both the operational and economic benefits of area navigation to both the civilian operators and the ATC system[2]. Figure 1 identifies the principal technical areas of this research which included both real time and fast time simulation, technical and operational analysis, flight testing and avionics standards development.

PRINCIPAL TECHNICAL AREAS

- Enroute Route Design
- Terminal Area Route Design
- Flight Test Management & Support
- Avionics Standards Development
- Economic Payoff Analysis

FIGURE 1 RNAV TECHNICAL SUPPORT

These system and user benefits range from more direct routing in the enroute environment to decreased delays in the terminal area, plus the additional capability to perform non-precision, and precision, approaches to previously non-instrumented runways or non-instrument equipped airports. Not only is additional airspace made available, which relieves the problem, from the airspace user's point of view, of congestion delays and non-direct routings, but also RNAV makes the controller's job much easier[3]. In addition many airports themselves can be better utilized, through the ability to perform straight-in approaches to all runways, eliminating the need for circling approaches. This research effort has produced the data base necessary to allow the United States to make the decision to move forward with the RNAV implementation process, as previously mentioned.

Of particular interest at this time of continuing economic and fuel crises is a detailed study[2] that was performed of the related benefits and costs that would accrue in the domestic U.S. airspace should RNAV be implemented as called for in the FAA Policy Statement[1]. The savings summarized on Figure 2 are applicable to an all-RNAV environment in 1984. The realization of benefits, however, is not dependent upon an all-RNAV environment. Based on an assumed implementation scenario[2] it was estimated that aggregate user savings would grow almost linearly over a seven year implementation period in reaching the levels indicated in Figure 2. Of at least equal importance to the dollar savings with RNAV are the fuel savings which are contained therein. A summary of annual fuel savings at 1984 projected traffic levels is given in Figure 3 for an all-RNAV environment. The overall fuel savings due to RNAV in the domestic U.S. during the years 1982-2000 is 10.4 billion gallons, or over 1.4 times the entire U.S. domestic airline fuel demand in 1975.

	TOTAL 1984 ANNUAL SAVINGS IN MILLIONS OF 1975 DOLLARS							
	AIR CARRIER			BUSINESS			OTHER	
	AIRCRAFT	PASSENGER TIME	TOTAL	AIRCRAFT	PASSENGER TIME	TOTAL	GENERAL AVIATION	TOTAL
2D 60 MAJOR AIRPORTS	91.1	93.5	184.6	0.6	0.9	1.5	1.2	187.3
3D DESCENTS-60 MAJOR AIRPORTS	49.1	45.8	94.9	*	*	*	*	94.9
4D at 25 M&S TERMINALS	110.4	142.1	252.2	*	*	*	*	252.5
TERMINAL AREA TOTAL	250.6	281.4	532.0	0.6	0.9	1.5	1.2	534.7
CHARTED ENROUTE	98.3	95.9	194.2	1.9	2.2	4.1	3.1	201.4
DIRECT ENROUTE	119.1	116.2	235.3	2.3	2.7	5.0	5.5	245.8
TOTAL CHARTED AND TERMINAL	348.9	377.3	726.2	2.5	3.1	5.6	4.3	736.1
TOTAL DIRECT AND TERMINAL	369.7	397.6	767.3	2.9	3.6	6.5	6.7	780.5

*not estimated

FIGURE 2 SUMMARY OF 1984 ANNUAL RNAV USER SAVINGS OVER VOR

In order to properly compensate for the passage of time between the points where system implementation costs are expended and benefits are realized, overall costs and benefits must be presented in terms of their present (discounted) value. Using discounting procedures set forth by the U.S. Office of Management

and Budget, calculations were made of these benefits and costs integrated between the years 1982 and 2000, converted to 1976 present values. If the benefit/cost ratio expressed in these terms equals 1.0, the cost expenditure is technically justified. Benefit/cost ratios significantly exceeding 1.0 imply a very efficient utilization of investment funds.

	Fuel Savings in Millions of Gallons			
	Air Carrier	Business Aircraft	Other General Aviation	Total
Terminal Area-2D	156	1	1	158
3D Descents	76	*	*	76
4D in M & S Terminals	153	*	*	153
Terminal Area Total	385	1	1	387
Enroute Charted	171	2	4	177
Enroute Direct	208	3	7	218
Total with Charted	556	3	5	564
Total with Direct	593	4	8	605

*not estimated

FIGURE 3 SUMMARY OF 1984 ANNUAL RNAV FUEL SAVINGS OVER VOR

Figure 4 illustrates the results of this benefit cost ratio analysis from the point of view of the airspace user. Note that even though general aviation costs have been included but benefits have been excluded, due to problems in projecting general aviation RNAV benefits, the overall user benefit/cost ratio comes out to be a very high value, in excess of SIX. Figure 5 shows the similar computation for the impact of RNAV on the U.S. Air Traffic Control system, with a benefit/cost ratio of almost TEN. Figure 6 contains an overall summary of the benefit/cost study with a separate indication of the impact on the U.S. scheduled air carriers as well as the ATC system. Similar analysis could and should be performed for other international ATC and user entities in order to establish the particular trade-offs and benefits specific to each geography or application.

BENEFITS	
Air Carrier Fuel & Time Savings (Terminal, Enroute, VNAV, 4D)	$ 8178M
Air Carrier Passenger Time Savings*	7062M
TOTAL USER BENEFITS	$15,240M
COSTS	
Air Carrier (Avionics, Installation, Maintenance)	$ 2505M
General Aviation (Avionics, Installation, Maintenance)	345M
TOTAL USER COSTS	$ 2850M
PRESENT VALUE BENEFITS	$ 3319M
PRESENT VALUE COSTS	537M
1976 BENEFIT/COST RATIO	6.2

*$12/passenger hour

TOTAL DISCOUNTED USER DOLLAR BENEFITS ARE SIX TIMES THE TOTAL DISCOUNTED AVIONICS, INSTALLATION AND MAINTENANCE COSTS

FIGURE 4 RNAV USER BENEFITS AND COSTS - 1982-2000

BENEFITS	
Terminal VOR Maintenance Savings	$ 72.2M
Terminal Controller Productivity Savings	21.7M
Enroute Controller Productivity Savings	422.0M
TOTAL SAVINGS	$515.9M
COSTS	
Enroute VOR Capital Costs	$ 0.6M
Enroute VOR Maintenance Costs	1.8M
Engineering & Development Costs	19.8M
TOTAL COSTS	$22.2M
PRESENT VALUE BENEFITS	$144.7M
PRESENT VALUE COSTS	14.6M
1976 BENEFIT/COST RATIO	9.9

TOTAL DISCOUNTED ATC DOLLAR BENEFITS ARE TEN TIMES TOTAL DISCOUNTED RNAV IMPLEMENTATION, CAPITAL AND MAINTENANCE COSTS

FIGURE 5 ATC SYSTEM BENEFITS AND COSTS - 1982-2000

AIR CARRIER		ATC SYSTEM	
BENEFITS	$1747.3M	BENEFITS	$144.7M
COSTS	442.2M	COSTS	14.6M
RATIO	4.0	RATIO	9.9

OVERALL	
BENEFITS	$3464.0M
COSTS	552.0M
RATIO	6.3

FIGURE 6 RNAV BENEFIT/COST SUMMARY
(1976 PRESENT VALUES)

Future Applications

It is pertinent now to identify two further operational applications of area navigation technology. One of these is primarily civilian or commercially oriented. The other applies, to perhaps a larger degree, to more governmental or military functions. The problem of noise abatement procedures is one that all of us who fly must comply with. This applies not only to civilian operators, but also to military aircraft operating routinely out of fixed bases that, by necessity, are surrounded with civilian communities. From an instrument approach point of view, existing navigation technologies and procedures severely constrain the ability to avoid noise sensitive areas. In most cases where there are noise abatement procedures, both departure and arrival, either the procedure must be performed using vectors received from the ground (radar) controller, which requires, in essence, that the ground controller navigate the aircraft, or the procedures must be flown under visual conditions when those procedures are rather complex, as they must frequently of necessity be.

Illustrations of noise abatement procedures involving reasonably intricate lateral maneuvering are illustrated in these following two figures. One, Figure 7, indicates the noise abatement procedure into Washington National Airport, in which the aircraft is flown visually over the Potomac River. Note that the ceiling and visibility minimums for this approach are quite high (3500 feet and 3 miles), which means that in cases of lower visibility either an alternate noisy instrument approach must be performed or the aircraft must be diverted to some other destination. Another indication of a complex visual approach procedure because of noise abatement requirements is indicated in this next illustration, Figure 8, which represents a visual approach into La Guardia airport.

Considerable work has been done recently in utilizing airborne area navigation capabilities to perform these maneuvers within the precise accuracies required both for obstacle clearance and to constrain the aircraft's flight path as far as noise abatement is concerned[4]. Figure 9 illustrates a candidate equivalent area navigation procedure to the Washington National Airport approach utilizing the capability for programing these approach procedures into the area navigation computer using any sensors which could be certified, from an accuracy point of view, to feed the RNAV system. The ability to perform complex maneuvers of this nature under IFR (instrument) conditions to accuracies of ±0.10 nm on either side of the specified path, which satisfies both noise abatement and prohibited area avoidance requirements, allows operation at values of ceiling and visibility considerably reduced from those previously shown on Figure 7.

The second application to be discussed has many ramifications as far as system applications are concerned. There recently has been performed, under the jurisdiction of the United States Coast Guard, a series of flight tests evaluating the application of a Loran-C navigator in a Coast Guard helicopter as a device to aid and improve the performance of the Coast Guard in conducting a variety of search and rescue missions[5]. Several of these missions are illustrated on Figure 10. They can primarily be categorized as a creeping search pattern, an expanding square search pattern, and a sector search pattern. Utilizing the equipment and procedures currently available to the Coast Guard, which primarily are dead reckoning or VOR/DME-aided navigation, the flight tests that were performed off the southern New Jersey coast of the United States using precision tracking radar and airborne instrumentation and recording, indicate performance for the creeping line pattern shown in Figure 11, and combined performance for the sector search pattern and the expanding square pattern in Figure 12. For a variety of reasons both sensor, equipment, and pilot-related, the conformance of the actual tracks to the desired tracks indicate considerable divergence. Not only philosophically, but also operationally, indications are that the probability of detecting the search subject is decreased markedly due to the inability to define or to accurately follow these desired patterns.

In Figure 13 is seen the performance of the Loran-C airborne area navigation system navigator on the creeping line pattern, where both accurate and repeatable performance is obtained. The probability of detection of the search subject on a pattern of this nature is increased markedly from the performance that was achieved using the previously shown VOR/DME search patterns. Similarly, observe in the following illustrations, Figure 14, again the extremely accurate and repeatable conformance of the aircraft patterns to the desired track pattern.

Analysis of the data from the creeping line search tests indicate that a 31% reduction in the number of passes over the search patterns required to achieve stipulated Coast Guard levels of probability of detection is achievable using Loran-C area navigation equipment as compared to VOR/DME conventional navigation equipment and procedures. The results of the experiments just shown, which are reported in detail in Reference 6, should be interpreted as a demonstration of the combined performance of the Loran-C sensor and the application of an airborne area navigation processor. It should be noted that the accurate adherence to desired track is potentially achievable with a variety of navigation sensors, but is unique to the application of the area nav concept and an airborne processor operating in an area nav mode.

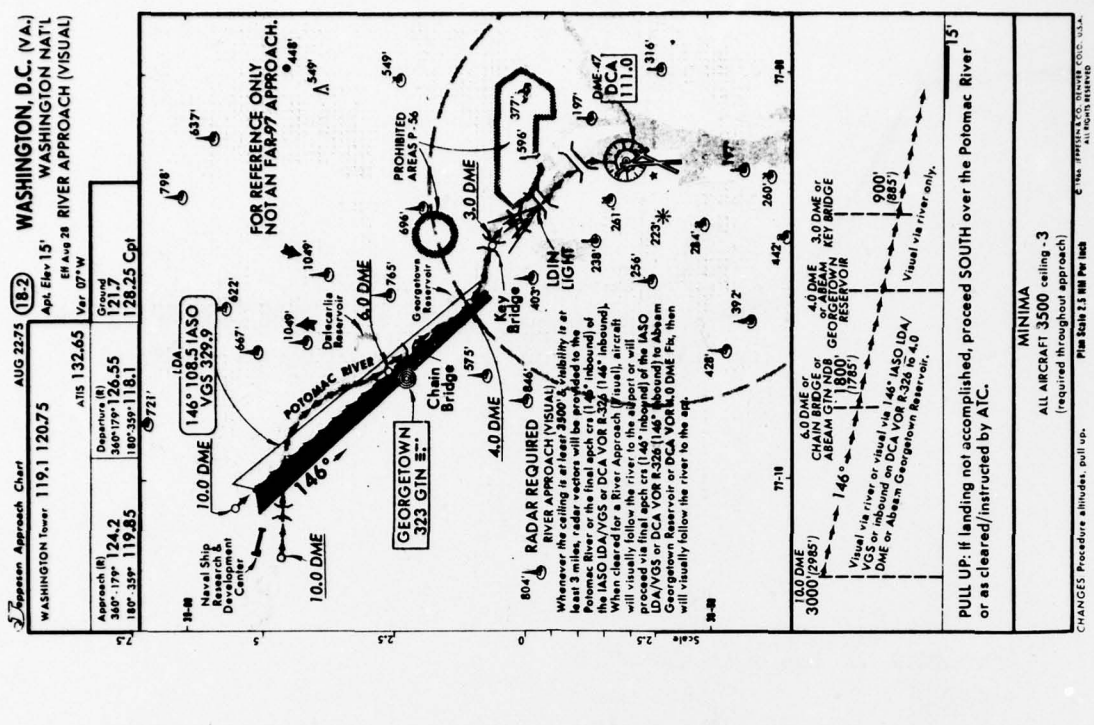

FIGURE 7 VISUAL RIVER APPROACH TO DCA - RUNWAY 18

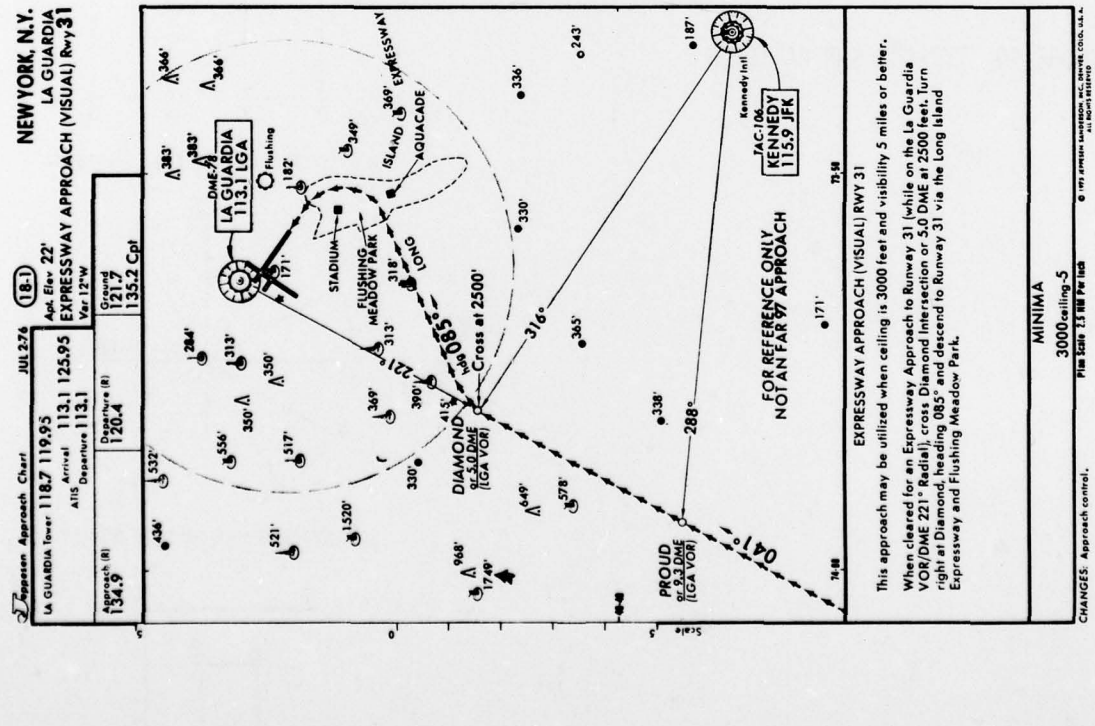

FIGURE 8 EXPRESSWAY APPROACH TO LGA - RUNWAY 31

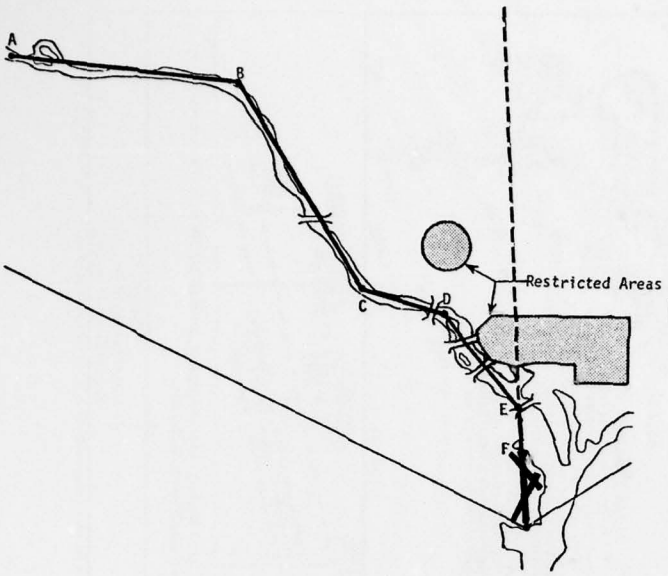

FIGURE 9 LINEAR SEGMENT APPROACH TO DCA - RUNWAY 18

Segment	Length, Km(nm)	Time, Sec., at 62 m/s (120 kt)
A-B	6.85 (3.70)	111.0
B-C	8.06 (4.35)	130.5
C-D	2.59 (1.40)	42.0
D-E	3.89 (2.10)	63.0
E-F	1.57 (0.85)	25.5

FIGURE 10 TYPICAL SAR PATTERNS

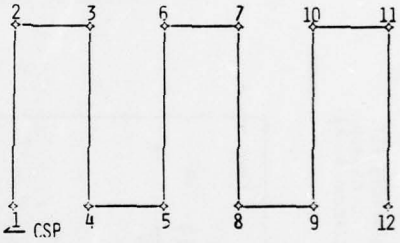

SAR CREEPING LINE PATTERN DEFINITION

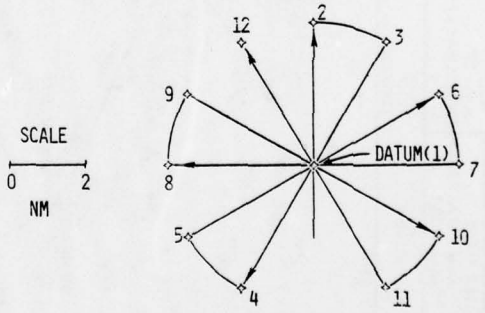

SAR SECTOR SEARCH PATTERN DEFINITION

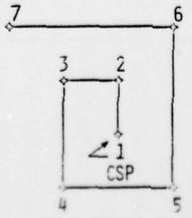

SAR EXPANDING SQUARE PATTERN DEFINITION

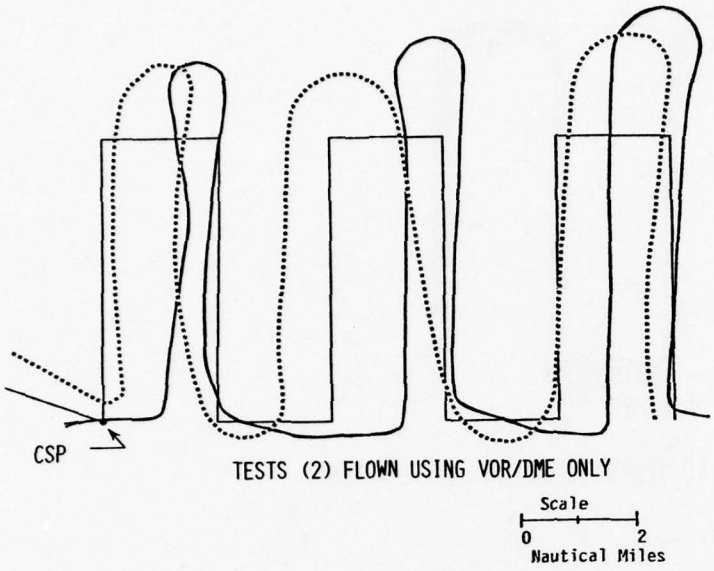

FIGURE 11 VOR/DME OPERATIONAL TESTS CREEPING LINE PATTERNS

FIGURE 12

LORAN-C SAR OPERATIONAL TEST
SECTOR SEARCH AND EXPANDING SQUARE
PATTERNS* USING ONLY VOR/DME

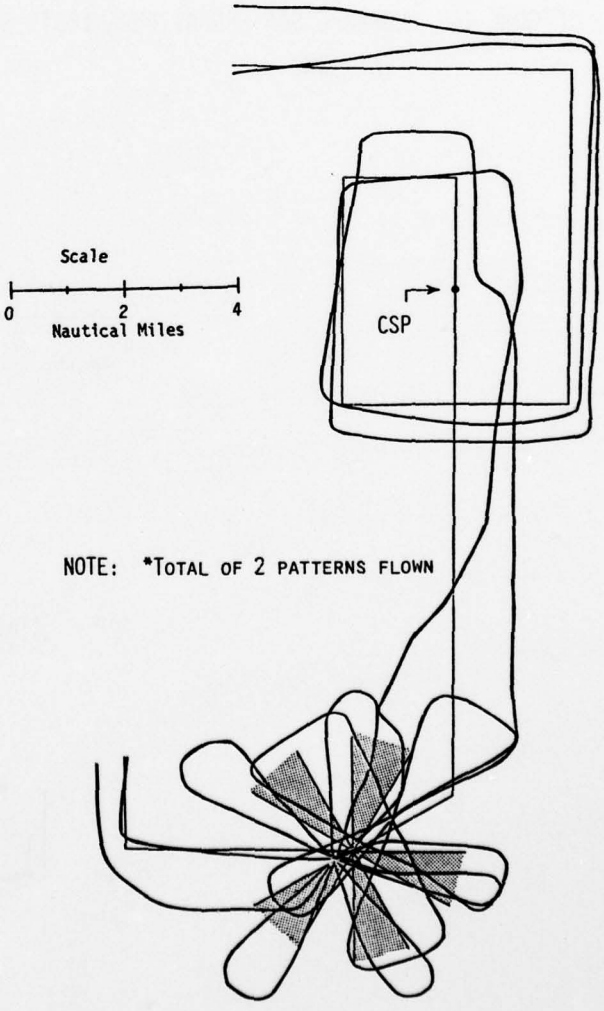

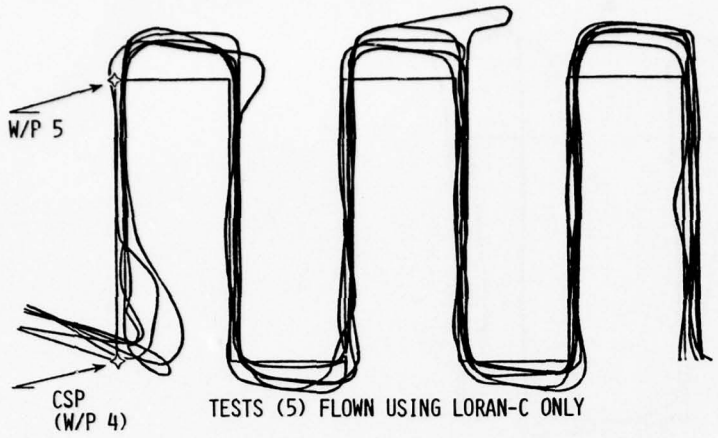

FIGURE 13 LORAN-C SAR OPERATIONAL TESTS CREEPING LINE PATTERNS

FIGURE 14 LORAN-C SAR OPERATIONAL TESTS SECTOR SEARCH* AND EXPANDING SQUARE** PATTERNS

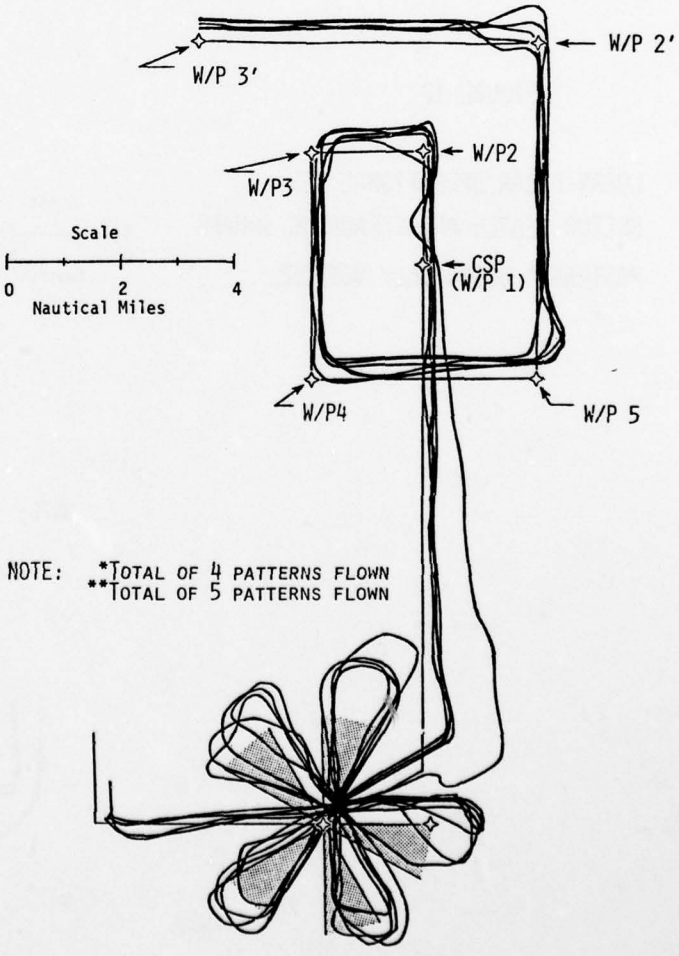

Given sensors with adequate operational range, be they VOR/DME dispersed within the geographical area of interest, or longer range sensors such as Loran, Omega, and ultimately NAVSTAR, the application of area navigation procedures and area navigation processors will markedly enhance the ability of aircraft to go precisely where they want to go accurately and repeatably, and to be able to define these paths universally and in real time in the cockpit. While the areas of noise abatement profile definition and search and rescue performance improvement are two very interesting, contemporary, and practical applications, they represent merely the forerunners of the functions and performance that we ultimately will receive from area navigation systems, both civilian and military, that will improve our total operational capability.

In the largest sense, RNAV as a concept is global in nature, and can utilize any of a variety of current or future sensors. Realization of the operational and economic advantages of RNAV is directly a function of the speed and efficiency which the concerned participants bring to bear on the critical issues of routes, procedures, and avionics standard development. Benefits will accrue in direct proportion to the timely implementation of these elements and the rate of equipage of the airborne RNAV equipment by the airspace users.

REFERENCES

[1]RNAV Policy Statement, Federal Aviation Administration, Department of Transportation, Federal Register, January 13, 1977

[2]W.H. Clark, E.H. Bolz, et al., Champlain Technology Industries Division, Systems Control, Inc. (Vt), "Implementation of Area Navigation in the National Airspace System: An Assessment of RNAV Task Force Concepts and Payoffs", December 1976, Report No. FAA-RD-76-196, Department of Transportation, Federal Aviation Administration, Final Report

[3]W. Crimbring and J. Maurer, National Aviation Facilities Experimental Center, Federal Aviation Administration, "Area Navigation/Vertical Area Navigation Terminal Simulation", April 1976, Report No. FAA-RD-76-28, Final Report

[4]R.W. Scott and E.D. McConkey, Champlain Technology Industries Division, Systems Control, Inc. (Vt), "An Avionics Sensitivity Study, Volume I, Operational Considerations", March 1977, NASA CR-145107, National Aeronautics and Space Administration, Final Report

[5]M. Hughes and R.J. Adams, Champlain Technology Industries Division, Systems Control, Inc. (Vt), "An Operational Flight Test Evaluation of a Loran-C Navigator", March 1977, Report No. CG-D-9-77, Department of Transportation, U.S. Coast Guard, Final Report

(9) Conference proceedings.

REPORT DOCUMENTATION PAGE

1. Recipient's Reference	2. Originator's Reference	3. Further Reference	4. Security Classification of Document
	(14) AGARD-CP-220	ISBN 92-835-0211-6	UNCLASSIFIED

5. Originator
Advisory Group for Aerospace Research and Development
North Atlantic Treaty Organization
7 rue Ancelle, 92200 Neuilly sur Seine, France

6. Title
(6) APPLICATIONS OF ADVANCES IN NAVIGATION TO GUIDANCE AND CONTROL.

7. Presented at
the 24th Technical Meeting of the Guidance and Control Panel, held in Stuttgart, Germany, 10–13 May 1977.

8. Author(s)
Various (12) 284p.

9. Date
(11) Feb[redacted]78

10. Author's Address
Various

11. Pages
292

12. Distribution Statement
This document is distributed in accordance with AGARD policies and regulations, which are outlined on the Outside Back Covers of all AGARD publications.

13. Keywords/Descriptors

Inertial navigation
Radio navigation
All weather navigation

14. Abstract

These Proceedings consist of twenty-two papers contained in the programme of the AGARD Guidance and Control Panel Symposium held in Stuttgart, Germany 10–13 May 1977. The papers are grouped under the following session titles: Keynote Session – I: Improvements in Inertial Navigation Systems and their Applications – II: Improvements in Radar and Radio Navigation Aids and their Applications – III: Specific Functions and System Concepts – IV: New Major Systems – V: System Improvements and Concepts.

A Technical Evaluation Report on the Symposium is published separately as AGARD Advisory Report No.115.

400 043

AGARD Conference Proceedings No.220 Advisory Group for Aerospace Research and Development, NATO APPLICATIONS OF ADVANCES IN NAVIGATION TO GUIDANCE AND CONTROL Published February 1978 292 pages These Proceedings consist of twenty-two papers contained in the programme of the AGARD Guidance and Control Panel Symposium held in Stuttgart, Germany, 10–13 May 1977. The papers are grouped under the following session titles: Keynote Session – I: Improvements in Inertial Navigation Systems and their Applications – II: Improvements in Radar and Radio Navigation Aids and their Applications – III: Specific P.T.O.	AGARD-CP-220 Inertial navigation Radio navigation All weather navigation	AGARD Conference Proceedings No.220 Advisory Group for Aerospace Research and Development, NATO APPLICATIONS OF ADVANCES IN NAVIGATION TO GUIDANCE AND CONTROL Published February 1978 292 pages These Proceedings consist of twenty-two papers contained in the programme of the AGARD Guidance and Control Panel Symposium held in Stuttgart, Germany, 10–13 May 1977. The papers are grouped under the following session titles: Keynote Session – I: Improvements in Inertial Navigation Systems and their Applications – II: Improvements in Radar and Radio Navigation Aids and their Applications – III: Specific P.T.O.	AGARD-CP-220 Inertial navigation Radio navigation All weather navigation
AGARD Conference Proceedings No.220 Advisory Group for Aerospace Research and Development, NATO APPLICATIONS OF ADVANCES IN NAVIGATION TO GUIDANCE AND CONTROL Published February 1978 292 pages These Proceedings consist of twenty-two papers contained in the programme of the AGARD Guidance and Control Panel Symposium held in Stuttgart, Germany, 10–13 May 1977. The papers are grouped under the following session titles: Keynote Session – I: Improvements in Inertial Navigation Systems and their Applications – II: Improvements in Radar and Radio Navigation Aids and their Applications – III: Specific P.T.O.	AGARD-CP-220 Inertial navigation Radio navigation All weather navigation	AGARD Conference Proceedings No.220 Advisory Group for Aerospace Research and Development, NATO APPLICATIONS OF ADVANCES IN NAVIGATION TO GUIDANCE AND CONTROL Published February 1978 292 pages These Proceedings consist of twenty-two papers contained in the programme of the AGARD Guidance and Control Panel Symposium held in Stuttgart, Germany, 10–13 May 1977. The papers are grouped under the following session titles: Keynote Session – I: Improvements in Inertial Navigation Systems and their Applications – II: Improvements in Radar and Radio Navigation Aids and their Applications – III: Specific P.T.O.	AGARD-CP-220 Inertial navigation Radio navigation All weather navigation

Functions and System Concepts – IV: New Major Systems – V: System Improvements and Concepts.

A Technical Evaluation Report on the Symposium is published separately as AGARD Advisory Report No.115.

ISBN 92-835-0211-6

Functions and System Concepts – IV: New Major Systems – V: System Improvements and Concepts.

A Technical Evaluation Report on the Symposium is published separately as AGARD Advisory Report No.115.

ISBN 92-835-0211-6

Functions and System Concepts – IV: New Major Systems – V: System Improvements and Concepts.

A Technical Evaluation Report on the Symposium is published separately as AGARD Advisory Report No.115.

ISBN 92-835-0211-6

AGARD
NATO OTAN
7 RUE ANCELLE · 92200 NEUILLY-SUR-SEINE
FRANCE
Telephone 745.08.10 · Telex 610176

DISTRIBUTION OF UNCLASSIFIED AGARD PUBLICATIONS

AGARD does NOT hold stocks of AGARD publications at the above address for general distribution. Initial distribution of AGARD publications is made to AGARD Member Nations through the following National Distribution Centres. Further copies are sometimes available from these Centres, but if not may be purchased in Microfiche or Photocopy form from the Purchase Agencies listed below.

NATIONAL DISTRIBUTION CENTRES

BELGIUM
Coordonnateur AGARD – VSL
Etat-Major de la Force Aérienne
Quartier Reine Elisabeth
Rue d'Evere, 1140 Bruxelles

CANADA
Defence Scientific Information Service
Department of National Defence
Ottawa, Ontario K1A OZ2

DENMARK
Danish Defence Research Board
Østerbrogades Kaserne
Copenhagen Ø

FRANCE
O.N.E.R.A. (Direction)
29 Avenue de la Division Leclerc
92 Châtillon sous Bagneux

GERMANY
Zentralstelle für Luft- und Raumfahrt-
dokumentation und -information
Postfach 860880
D-8 München 86

GREECE
Hellenic Armed Forces Command
D Branch, Athens

ICELAND
Director of Aviation
c/o Flugrad
Reykjavik

ITALY
Aeronautica Militare
Ufficio del Delegato Nazionale all'AGARD
3, Piazzale Adenauer
Roma/EUR

LUXEMBOURG
See Belgium

NETHERLANDS
Netherlands Delegation to AGARD
National Aerospace Laboratory, NLR
P.O. Box 126
Delft

NORWAY
Norwegian Defence Research Establishment
Main Library
P.O. Box 25
N-2007 Kjeller

PORTUGAL
Direccao do Servico de Material
da Forca Aerea
Rua de Escola Politecnica 42
Lisboa
Attn: AGARD National Delegate

TURKEY
Department of Research and Development (ARGE)
Ministry of National Defence, Ankara

UNITED KINGDOM
Defence Research Information Centre
Station Square House
St. Mary Cray
Orpington, Kent BR5 3RE

UNITED STATES
National Aeronautics and Space Administration (NASA),
Langley Field, Virginia 23365
Attn: Report Distribution and Storage Unit

THE UNITED STATES NATIONAL DISTRIBUTION CENTRE (NASA) DOES NOT HOLD STOCKS OF AGARD PUBLICATIONS, AND APPLICATIONS FOR COPIES SHOULD BE MADE DIRECT TO THE NATIONAL TECHNICAL INFORMATION SERVICE (NTIS) AT THE ADDRESS BELOW.

PURCHASE AGENCIES

Microfiche or Photocopy
National Technical
Information Service (NTIS)
5285 Port Royal Road
Springfield
Virginia 22151, USA

Microfiche
Space Documentation Service
European Space Agency
10, rue Mario Nikis
75015 Paris, France

Microfiche
Technology Reports
Centre (DTI)
Station Square House
St. Mary Cray
Orpington, Kent BR5 3RF
England

Requests for microfiche or photocopies of AGARD documents should include the AGARD serial number, title, author or editor, and publication date. Requests to NTIS should include the NASA accession report number. Full bibliographical references and abstracts of AGARD publications are given in the following journals:

Scientific and Technical Aerospace Reports (STAR),
published by NASA Scientific and Technical
Information Facility
Post Office Box 8757
Baltimore/Washington International Airport
Maryland 21240, USA

Government Reports Announcements (GRA),
published by the National Technical
Information Services, Springfield
Virginia 22151, USA

Printed by Technical Editing and Reproduction Ltd
Harford House, 7–9 Charlotte St, London W1P 1HD

ISBN 92-835-0211-6